frontiers | Research Topics

Impact of novel omic technologies on biological control against plant pathogens

Edited by
Inmaculada Larena, Eduardo Antonio Espeso and Javier Veloso

Published in
Frontiers in Microbiology

ISSN 1664-8714
ISBN 978-2-8325-2232-5
DOI 10.3389/978-2-8325-2232-5

About Frontiers

Frontiers is more than just an open access publisher of scholarly articles: it is a pioneering approach to the world of academia, radically improving the way scholarly research is managed. The grand vision of Frontiers is a world where all people have an equal opportunity to seek, share and generate knowledge. Frontiers provides immediate and permanent online open access to all its publications, but this alone is not enough to realize our grand goals.

Frontiers journal series

The Frontiers journal series is a multi-tier and interdisciplinary set of open-access, online journals, promising a paradigm shift from the current review, selection and dissemination processes in academic publishing. All Frontiers journals are driven by researchers for researchers; therefore, they constitute a service to the scholarly community. At the same time, the *Frontiers journal series* operates on a revolutionary invention, the tiered publishing system, initially addressing specific communities of scholars, and gradually climbing up to broader public understanding, thus serving the interests of the lay society, too.

Dedication to quality

Each Frontiers article is a landmark of the highest quality, thanks to genuinely collaborative interactions between authors and review editors, who include some of the world's best academicians. Research must be certified by peers before entering a stream of knowledge that may eventually reach the public - and shape society; therefore, Frontiers only applies the most rigorous and unbiased reviews. Frontiers revolutionizes research publishing by freely delivering the most outstanding research, evaluated with no bias from both the academic and social point of view. By applying the most advanced information technologies, Frontiers is catapulting scholarly publishing into a new generation.

What are Frontiers Research Topics?

Frontiers Research Topics are very popular trademarks of the *Frontiers journals series*: they are collections of at least ten articles, all centered on a particular subject. With their unique mix of varied contributions from Original Research to Review Articles, Frontiers Research Topics unify the most influential researchers, the latest key findings and historical advances in a hot research area.

Find out more on how to host your own Frontiers Research Topic or contribute to one as an author by contacting the Frontiers editorial office: frontiersin.org/about/contact

Impact of novel omic technologies on biological control against plant pathogens

Topic editors

Inmaculada Larena — Instituto Nacional de Investigación y Tecnología Agraria y Alimentaria (INIA-CSIC), Spain

Eduardo Antonio Espeso — Spanish National Research Council (CSIC), Spain

Javier Veloso — University of Santiago de Compostela, Spain

Citation

Larena, I., Espeso, E. A., Veloso, J., eds. (2023). *Impact of novel omic technologies on biological control against plant pathogens*. Lausanne: Frontiers Media SA.

doi: 10.3389/978-2-8325-2232-5

Table of contents

frontiers | Frontiers in Microbiology

TYPE Editorial
PUBLISHED 06 April 2023
DOI 10.3389/fmicb.2023.1162422

OPEN ACCESS

EDITED AND REVIEWED BY
Trevor Carlos Charles,
University of Waterloo, Canada

*CORRESPONDENCE
Inmaculada Larena
✉ ilarena@inia.csic.es

SPECIALTY SECTION
This article was submitted to Microbe and Virus Interactions with Plants, a section of the journal Frontiers in Microbiology

RECEIVED 09 February 2023
ACCEPTED 28 March 2023
PUBLISHED 06 April 2023

CITATION
Larena I, Espeso EA and Veloso J (2023) Editorial: Impact of novel omic technologies on biological control against plant pathogens. *Front. Microbiol.* 14:1162422. doi: 10.3389/fmicb.2023.1162422

Editorial: Impact of novel omic technologies on biological control against plant pathogens

Inmaculada Larena[1]*, Eduardo A. Espeso[2] and Javier Veloso[3]

[1]Departamento de Protección Vegetal, Instituto Nacional de Investigación y Tecnología Agraria y Alimentaria-Consejo Superior de Investigaciones Científicas (INIA-CSIC), Madrid, Spain, [2]Departamento de Biología Celular y Molecular, Centro de Investigaciones Biológicas Margarita Salas-Consejo Superior de Investigaciones Científica (CSIC), Madrid, Spain, [3]Departamento de Biología Funcional, Universidad de Santiago de Compostela, Escuela Politécnica Superior de Ingeniería, Lugo, Spain

KEYWORDS

biological control agent (BCA), bio-pesticides, biocontrol, omic-technologies, plant pathogens

Editorial on the Research Topic
Impact of novel omic technologies on biological control against plant pathogens

Control of plant diseases is mainly achieved by applying chemical pesticides to the crops. Although these chemical treatments have greatly contributed to spectacular improvements in food production and crop yields, their indiscriminate use causes significant environmental damage such as water pollution, soil contamination, increased pathogen resistance and loss of biodiversity, among others. Nowadays, strict regulations control the extensive use of chemical pesticides, and there is increasing the public pressure to remove the most hazardous chemicals from the market. Consequently, the use of biological control (BC) through the application of microorganisms as biological control agents (BCA) or bio-pesticides to reduce plant diseases has emerged as a low-cost, environmentally friendly and sustainable alternative to chemical disease control. However, biocontrol approaches are not as widely adapted as chemical pesticides. Thus, it becomes essential to progress, among many other aspects, in a better understanding of the mechanisms governing biocontrol mediated by microorganisms to improve the efficacy and robustness of treatments. A new generation of molecular technologies has recently provided a powerful approach to better understand the relationship of BCA-host plant-pathogen-environment. These new technologies are known under the term "omics" and include techniques such as micro and macroarrays, next generation sequencing (NGS) technology, proteomics, metabolomics, genomics (including its derivatives pangenomics and metagenomics), and transcriptomics, among others. This Research Topic collects different strategies to better understand BCA-host-pathogen-environment interactions. The use of different omics approaches and synthetic biology, and integrating them with traditional technologies, may thus accelerate the development of BCAs against plant pathogens.

This topic includes manuscripts that focus on new approaches leading to a more successful selection of potential BCAs. Microbiome analysis allow for the discovery of new BCAs. In this sense, Ciancio et al. describe a metabarcoding study to examine the soil/root microbiota (bacteria, fungi, and nematodes) of banana, across several farms with different locations and cultivation techniques. The relationship between the microbiota and these factors is highly relevant in the development of pest control strategies. Anguita-Maeso et al. characterized the xylem sap microbial communities in almond trees, identifying

microorganisms that would be good candidates to produce almond plants more resilient to *Xylella fastidiosa* infection. Also, Zhang et al. studied the microbial communities in two cultivars of tea plants, a resistant and a susceptible cultivar. They observed that the relative abundance of *Penicillium* was significantly different between the susceptible and resistant plants, and identified *Penicillium* as a potential biomarker. Zhang et al. analyzed the secondary metabolites produced by resistant and susceptible plants and correlated this with the microbiome. In brief, the authors observed that Penicillium correlated with the secondary metabolite quercetin among others.

Increasing our knowledge of the biocontrol mechanism of BCAs is critical for the subsequent development of appropriate formulations and optimal application timing and methods. Thus, omics disciplines are among the key tools that have significantly improved our understanding of the action mode of BCAs against plant pathogens. Here Ye et al. identified a potential BCA against *Meloidogyne graminicola* which employs multiple anti-nematode mechanisms, including triggering the expression of resistance-related genes and defense enzyme activity to enhance plant resistance. Other works identified the genetic basis of biofilm production based on poly-γ-glutamic acid (γ-PGA) by *Bacillus atrophaeus* NX-12. By generation of a strain lacking the biosynthetic γ-PGA cluster they correlated the formation of biofilm with the colonization of rhizosphere and the biocontrol activity exhibited by this bacteria (Xue et al.).

In the interaction of BCA with the host and the pathogen it is also very important to clarify the mode of action of the target pathogen. Li et al. identified potential genes in the pathogen *Rhizoctonia solani* involved in the production of metabolites and extracellular proteins. This basidiomycete produces a large number of potentially secreted enzymes and small proteins with a putative function as effectors involved in virulence. The reverse genetics and transcriptomic analysis allowed to Lu et al. to explain the role of mating in the virulence of the fungus *Sporisorium scitamineum*. This basidiomycete is the causative agent of sugarcane smut disease in which the formation of dikaryotic strains is essential for filamentous growth and infection in sugarcane plants.

High-throughput analyses are fundamental to the study of the complex tripartite interaction of BCA, host and pathogen. Requena et al. used NGS to compare at the genomic level two strains of *Penicillium rubens*, S27 and PO212. PO212 is an effective BCA against a large number of fungal plant pathogens that infect different horticultural crops while S27 lacks this biocontrol capacity. Comparative genomics showed that PO212 and S27 have a high genomic similarity in gene content. Requena et al. points out the importance to complement this genomic approach with a transcriptomic approach to explain the high similarity in gene sequence but different phenotype. Similarly, Moshe et al. used comparative genomics to study the biocontrol potential of several *Bacillus* strains. The *Bacillus* strains showed different *in-vitro* antagonism against three plant pathogens, *Pythium, Rhizoctonia* and *Fusarium*. The antagonistic effect depended on unique secondary metabolite and chitinase-encoding genes in each Bacillus strain discovered in the comparative genome approach. In this line, Ma et al. use comparative genomic analysis to study two *formae speciales* of *Setosphaeria turcica*. In this regard, some pathogens might act as BCAs in an incompatible host. *S. turcica* f. sp. *zeae* and *S. turcica* f. sp. *sorghi* cause northern leaf blight disease of corn and sorghum, respectively. In this study, *S. turcica* f. sp. *zeae* was predicted to have fewer secreted proteins, pathogen-host interaction (PHI) genes and carbohydrate-active enzymes (CAZys) than *S. turcica* f. sp. *sorghi* but there were eight effector protein-encoding genes specifically in *S. turcica* f. sp. *zeae*, among which cellulase genes had a major role in pathogenicity.

These contributions highlight the progress in the field of BCA research and its potential to bring solutions from the laboratory to the farm. They also highlight the still unanswered questions about BCA-plant-pathogen-environment interactions and thus provide opportunities for continued research. We hope that the information provided in this topic will be helpful to scientists and students.

Author contributions

All authors listed have made a substantial, direct, and intellectual contribution to the work and approved it for publication.

Acknowledgments

We thank the Frontiers editorial team for their help in making this Research Topic possible.

Conflict of interest

The authors declare that the research was conducted in the absence of any commercial or financial relationships that could be construed as a potential conflict of interest.

Publisher's note

frontiers | Frontiers in Microbiology

ORIGINAL RESEARCH
published: 09 June 2022
doi: 10.3389/fmicb.2022.855110

Rhizosphere 16S-ITS Metabarcoding Profiles in Banana Crops Are Affected by Nematodes, Cultivation, and Local Climatic Variations

Aurelio Ciancio[1]*, *Laura Cristina Rosso*[1], *Javier Lopez-Cepero*[2] and *Mariantonietta Colagiero*[1]*

[1] Consiglio Nazionale delle Ricerche, Istituto per la Protezione Sostenibile delle Piante, Bari, Italy, [2] Departamento Técnico de Coplaca S.C., Organización de Productores de Plátanos, Santa Cruz de Tenerife, Spain

OPEN ACCESS

Edited by:
Inmaculada Larena, Instituto Nacional de Investigación y Tecnología Agroalimentaria (INIA), Spain

Reviewed by:
Laith Khalil Tawfeeq Al-Ani, Universiti Sains Malaysia, Malaysia
Antonieta De Cal, Instituto Nacional de Investigación y Tecnología Agroalimentaria (INIA), Spain
Johannes Zimmermann, University of Kiel, Germany

***Correspondence:**
Aurelio Ciancio
aurelio.ciancio@ipsp.cnr.it
Mariantonietta Colagiero
mariantonietta.colagiero@ipsp.cnr.it

Specialty section:
This article was submitted to Microbe and Virus Interactions with Plants, a section of the journal Frontiers in Microbiology

Received: 14 January 2022
Accepted: 13 April 2022
Published: 09 June 2022

Citation:
Ciancio A, Rosso LC, Lopez-Cepero J and Colagiero M (2022) Rhizosphere 16S-ITS Metabarcoding Profiles in Banana Crops Are Affected by Nematodes, Cultivation, and Local Climatic Variations. Front. Microbiol. 13:855110. doi: 10.3389/fmicb.2022.855110

Agriculture affects soil and root microbial communities. However, detailed knowledge is needed on the effects of cropping on rhizosphere, including biological control agents (BCA) of nematodes. A metabarcoding study was carried out on the microbiota associated with plant parasitic and other nematode functional groups present in banana farms in Tenerife (Canary Islands, Spain). Samples included rhizosphere soil from cv Pequeña Enana or Gruesa and controls collected from adjacent sites, with the same agroecological conditions, without banana roots. To characterize the bacterial communities, the V3 and V4 variable regions of the 16S rRNA ribosomal gene were amplified, whereas the internal transcribed spacer (ITS) region was used for the fungi present in the same samples. Libraries were sequenced with an Illumina MiSeq™ in paired ends with a 300-bp read length. For each sample, plant parasitic nematodes (PPN) and other nematodes were extracted from the soil, counted, and identified. Phytoparasitic nematodes were mostly found in banana rhizosphere. They included *Pratylenchus goodeyi*, present in northern farms, and *Helicotylenchus* spp., including *H. multicinctus*, found in both northern and southern farms. Metabarcoding data showed a direct effect of cropping on microbial communities, and latitude-related factors that separated northern and southern controls from banana rizosphere samples. Several fungal taxa known as nematode BCA were identified, with endophytes, mycorrhizal species, and obligate Rozellomycota endoparasites, almost only present in the banana samples. The dominant bacterial phyla were Proteobacteria, Actinobacteria, Planctomycetes, Bacteroidetes, Chloroflexi, and Acidobacteria. The ITS data showed several operational taxonomic units (OTUs) belonging to Sordariomycetes, including biocontrol agents, such as *Beauveria* spp., *Arthrobotrys* spp., *Pochonia chlamydosporia*, and *Metarhizium anisopliae*. Other taxa included *Trichoderma harzianum, Trichoderma longibrachiatum*, *Trichoderma virens*, and *Fusarium* spp., together with mycoparasites such as *Acrostalagmus luteoalbus*. However, only one *Dactylella* spp. showed a correlation with predatory nematodes. Differences among the nematode guilds were found, as phytoparasitic, free-living, and predatory nematode groups were correlated with specific subsets of other bacteria and fungi. Crop cultivation method and soil texture showed differences in taxa

representations when considering other farm and soil variables. The data showed changes in the rhizosphere and soil microbiota related to trophic specialization and specific adaptations, affecting decomposers, beneficial endophytes, mycorrhizae, or BCA, and plant pathogens.

Keywords: 16S rRNA, *Helicotylenchus multicinctus*, ITS, *Pratylenchus goodeyi*, microbiota

INTRODUCTION

Banana (*Musa acuminata*) is an economically important crop in the Canary Islands (Spain), where it represents a source of income for many small holders, with around 50% of cultivated areas and yields that supply around 70% of national consumption. Dwarf Cavendish (Pequeña Enana, AAA) and derived selections represent the most widespread genotype (>90% of plants) due to its productivity and commercial performance. The crop is cultivated in small parcels, with alkaline volcanic soils often proceeding from different sites, amended with organic matter in part originating from old leaves left rotting on the soil surface. The main adversities of this cultivation include nematode pests, banana weevil (*Cosmopolites sordidus*), and Fusarium wilt caused by *Fusarium oxysporum* f. sp. *cubense* (Foc). The latter disease affects 2–12% of plants, with some farms reaching up to 30% prevalence (Gómez-Lama Cabanás et al., 2021). Pest and Foc management include a conventional approach, based on nematicides and insecticides, pheromone traps or products based on cloripirifos, spirodiclofen, and other active components. Alternative organic approaches for pest and disease management include the use of natural products with nematocidal or fungicidal properties, combined with pheromone traps (**Supplementary Table 1**).

PPN found in the Canary Islands banana farms include lesion nematodes *Pratylenchus* spp., spiral nematodes *Helicotylenchus* spp., and occasionally root-knot nematodes, *Meloidogyne* spp. These parasites are widespread in banana cultivated areas of the world (Moens et al., 2006; Coyne et al., 2018). Fusarium wilt is the most severe soil-borne vascular disease encountered in the Canary Islands. Its virulence depends on the race as well as on plant tolerance level (Bubici et al., 2019; Gómez-Lama Cabanás et al., 2021). The races reported in the Canary Islands are the subtropical races 4 (SR4), R2, and R1 (vegetative compatibility group 0120), highly virulent on cv. Gros Michel but not on Grand Naine (Domínguez et al., 2001). The low virulence of those races appears to be related to suppressive soil factors, such as the scarcity of iron and high levels of sodium and clay (Domínguez et al., 2001).

Plant and soil microbiota have an important effect on crop productivity. They include species with a varying degree of specialization, underpinning fundamental services such as nutrient recycling and pest or disease regulation. Is it recognized that many species, including BCA, contribute significantly to crop production by sustaining the rhizosphere and plant health (Bulgarelli et al., 2013; Granzow et al., 2017; Jacoby et al., 2017; Berg et al., 2020). The rhizosphere microbiota may hence represent a natural reservoir of BCA and a possible alternative tool for PPN management (Berg et al., 2017). However, due to the complexity of the rhizosphere environment, natural pest/disease regulation in intensive crops is not as frequent as expected. This often occurs in the case of PPN in intensive cropping systems (Topalović and Heuer, 2019; Topalović et al., 2020). The severity of PPN attacks mostly depends on the changes induced in soil by agriculture, such as the environmental pressure of monocultures and/or the low genetic diversity of crops. These conditions occur, and are particularly evident, in banana crops, in which all plants are usually clones of one or few lineages (mostly Cavendish), selected for commercial or technical reasons including resistance to one or more Foc diseases.

Knowledge of soil and rhizosphere microbial diversity and composition is hence fundamental to implement sustainable crop management, as well as to determine the impact of one or more biological/technical factors on the indigenous BCA. Progress has been achieved in determining the links between Fusarium wilt and banana-associated microorganisms (Effendi et al., 2019; Kaushal et al., 2020; Gómez-Lama Cabanás et al., 2021; Ravi et al., 2021). However, the potential of soil microorganisms to manage plant production in a more sustainable way, relying solely on indigenous species, is not yet fully exploited. Intensive banana crop management still remains highly dependent on frequent applications of synthetic pesticides. In particular, it is unknown if and how co-occurring microbial species, as well as their interactions with the BCA present, act on soil pests such as PPN. Soil-inhabiting organisms form a complex food web system, whose final outcomes may range from the natural regulation of noxious organisms to the insurgence of severe pest attacks (Bardgett et al., 1999; Ram et al., 2008).

Soil microbial communities, including BCA with other cryptic co-occurring species, may reveal undetected but useful interactions with the farm and the local agroenvironment (i.e., soil physical properties and pests), or depending on other external variables (i.e., selection of cropping practices and climate). In this regard, belowground links among species and trophic groups are becoming more and more informative as a huge amount of data is made available through deep sequencing and -omics technologies (Berg et al., 2020; Martínez Arbas et al., 2021). A detailed knowledge of soil microbial profiles may allow the setup of information-based crop management practices, exploiting natural pest/disease regulation, reinforcing or sustaining soil, and rhizosphere health.

Beneficial microorganisms that contribute to plant production include species acting as generalists or, on the contrary, inhabiting specific trophic niches, ranging from endophytes to pathogens or BCA, which affect plant health and thus farm productivity (Bulgarelli et al., 2013; Xue et al., 2015; Granzow

et al., 2017; Kaushal et al., 2020; Zhang et al., 2020; Gómez-Lama Cabanás et al., 2021; Ravi et al., 2021). Apart from plant growth promoters, soil harbors endosymbionts or BCA often specifically associated with their hosts. Some isolates are already exploited as active ingredients in a number of commercial products, worldwide. These include, for example, host-specific PPN antagonists such as the bacteria *Pasteuria* spp. or *Bacillus* spp. (Tian et al., 2007; Mohan et al., 2020), and ubiquitous fungi such as *Pochonia chlamydosporia*, a root endophyte and a parasite of nematode eggs (Manzanilla-López et al., 2013). As a root endophyte, *P. chlamydosporia* also elicits the expression of a wide range of plant defense genes (Larriba et al., 2015; Mingot-Ureta et al., 2020; Tolba et al., 2021; Zhuang et al., 2021).

Other fungi of interest for exploitation as BCA are the members of genera *Metarhizium* and *Trichoderma*. The former, phylogenetically close to *Pochonia*, is characterized by the root endophytism and soil insect parasitism. Within the genus *Trichoderma,* several BCA and/or endophytes are present, including its teleomorph genus *Hypocrea* (Sivan and Chet, 1986; Chaverri and Samuels, 2002). However, data are needed on the competence and persistence of these BCA in the soil and rhizosphere, in particular when they are naturally present, as well as on their interactions with associated bacteria.

A further factor impacting the rhizosphere environment, and thus natural pest or disease regulation, originates from anthropic activities including, i.e., practices adopted by producers through organic or conventional farming, and the related aboveground cover, which also affect belowground microbiota profiles (Leff et al., 2018). Few data are available on the effect of organic and low-impact agriculture, soil properties, climate, on the microbiota diversity and, indirectly, on BCA species distribution, prevalence, and co-occurrence.

Considering the important role played by soil microorganisms in crop production and pest regulation, the focus of this study was to evaluate the interactions of the banana crop with the rhizosphere microbiota and the indigenous BCA of nematodes present in the soil, also to evaluate additional variables. In this study, we produced and analyzed metabarcoding data to: (1) determine the effect of cropping on rhizosphere bacteria and fungi in banana farms, in a subtropical environment, (2) investigate the effect of farm properties on rhizosphere microbial profiles, (3) estimate the impact that factors, such as climate or soil properties, and nematodes have on soil microbiota profiles, and (4) evaluate the crop effects on naturally occurring BCA species as well as their potential for PPN regulation.

MATERIALS AND METHODS

A total of 38 samples were collected in Tenerife (Canary Islands, Spain) from the rhizosphere of *M. acuminata* var. Pequeña Enana or Gruesa (Cavendish clones), on farms applying conventional (only synthetic chemicals), integrated pest management (IPM, using chemical pesticides and natural products), or organic cropping techniques (EU regulation n. 848/2018) (**Supplementary Table 1**). A total of 36 samples were collected in February 2018 (mean month temperature = 18°C, humidity = 65%). Rhizosphere soil samples (ca. 300 ml) were collected at an average depth of 20 cm with banana root fragments. Other local control samples, with mostly grass or weed roots, were collected on the same farms from adjacent, banana root-free sites, within 5–10 m from the sampled banana plants, at the same depth. The three replicate banana samples and corresponding controls (each formed by three or more nearby subsamples, mixed to form a sample) were collected in six farms, located in the northern and southern areas of the island (**Supplementary Table 1**). Two other samples from banana rhizosphere, collected from a northern farm in September 2017 and stored at 4°C, were also included in this study. A subsample (300 g of mixed soil and roots) from each soil bag was stored at −80°C before processing for subsequent analyses. The remaining soil used for nematode and soil analysis was then stored at room temperature.

Samples were classified by latitude (northern or southern coast farm location), farm of origin and cultivation method, soil texture (measured by decanting and weighting of the three soil fractions), pH (Kettler et al., 2001; Schoeneberger et al., 2012) and number of PPNs, free-living, and predatory nematodes. The soil sieving and decanting technique was used for the extraction of nematodes by suspending a 200-ml soil subsample in tap water, followed by filtering and decanting, with a set of 500- and 75-μm sieves. The filtered suspension was then examined for nematode identification and density measurement with light microscopy, using a Hawksley counting chamber at 50×, in three replicates. PPN were identified at the species level using available taxonomic keys (Boag and Jairajpuri, 1985; Handoo and Golden, 1989; Uzma et al., 2015; see **Table 1** for variables considered) with a Leitz Orthoplan light microscope, at 312–500×. Hand-picked nematode specimens were placed on slides in temporary water mounts. We classified the free-living (Rhabditida and Aphelenchoides) and predatory nematodes (Mononchida and non-plant parasitic Dorylaimida) during counts using a Hawksley counting chamber at 40-100× and available nematode descriptions (Goodey, 1963). Free-living (bacterial and fungal feeders) and predatory nematodes (mononchids and dorylaims) were counted as groups. The remaining soil was then used to measure soil texture and pH, for each sample. Spearman's correlations among nematode and soil variables were calculated using PAST (Hammer et al., 2001).

Metabarcoding Analyses

Rhizosphere soil samples were analyzed for the presence of bacteria and fungi using a metabacoding sequencing approach. For metabacoding analyses, 2 g of soil collected from banana roots or from controls were used from each sample. Total RNA was extracted with the RNeasy PowerSoil® Total RNA kit (Qiagen®, UK—MoBio Laboratories, Inc.), following the manufacturer's instructions. RNA concentration was determined with a Nanodrop™ spectrometer at 260 nm. The extracted material was subjected to reverse transcription according to the Illumina™ sequencing protocol, using SuperScript III or IV (Invitrogen, USA), following the manufacturer's protocol. The material obtained was then purified using the QIAquick PCR Purification kit (Qiagen®, UK). The nucleic acid integrity was

TABLE 1 | Variables used for the identification of plant parasitic nematodes.

Nematode taxa	Variables used	References/keys
Helicotylenchus multicinctus	Adults tail and head shape hemispherical; presence of males; spermatheca functional and slightly offset; stylet length < 24 μm; < 5 lip annules; phasmids anterior to anus; lateral fields without striae; habitus = open C; V = 61–76; L = 400–673.	Boag and Jairajpuri, 1985; Uzma et al., 2015
Pratylenchus goodeyi	Presence of males; V = 73–75%; posterior uterine branch short, around one body width at vulva; tapering and almost pointed tail; four lip annules.	Handoo and Golden, 1989

checked by electrophoresis on 1.5% agarose gel. The cDNA was then subjected to PCR amplification of the bacterial 16S ribosomal RNA gene and the fungal internal transcribed spacer (ITS) regions.

16S Data Analysis

Both ends of the V3–V4 hypervariable region were used for the amplification of the 16S rRNA ribosomal gene, which is considered capable of yielding sufficient information for taxonomic classification (Yang et al., 2002; Liu et al., 2007, 2008; Caporaso et al., 2010). The primers 341F (5′-CCTACGGGNGGCWGCAG-3′) and 805R (5′-GACTACHVGGGTATCTAATCC-3′), with affinity for flanking conserved motifs, were used to amplify the V3–V4 of the 16S hypervariable region (Van de Peer et al., 1996; Baker et al., 2003; Clarridge, 2004; Takahashi et al., 2014). MiSeq System Illumina platforms, provided by a commercial service (IGA-Technology Services, Udine, Italy[1]), were used for sequencing. Two amplification steps were used in the library workflow: an initial PCR amplification using locus-specific PCR primers and a subsequent amplification integrating the relevant flow-cell binding domains and unique indices (NexteraXT Index kit FC-131-1001/FC-131-1002), used to amplify the variable V3 and V4 regions of the 16S rRNA gene. Libraries were sequenced on a MiSeq run in paired end features with a 300-bp read length[2].

For the bioinformatic assembly of the single read contigs, raw sequences were processed using the PandaSeq[3] pipeline (Masella et al., 2012). Forward and reverse 16S reads were merged by applying the following PandaSeq parameters: sequences with unidentified nucleotides = filtered; lengths of overlapping region (min–max) = 100–180 nt; contig lengths (min–max) = 200–450 nt (Claesson et al., 2010). For each sample, the single fasta format file of high-quality assembled sequences was obtained by merging data, and then used as the first input for processing with QIIME 1.9 (Caporaso et al., 2010), on a Linux emulator in a Windows® 7 environment. QIIME was applied to filter the chimeras, to assemble the replicate sequences and to analyze the operational taxonomic units (OTUs) assigned through the implementation of UCLUST, applying a 97% identity threshold to discriminate at the species level (Caporaso et al., 2010). Next, an OTU table was constructed using a combined fasta file generated by *add_qiime_labels.py* using labels from a metadata mapping file, and then using *pick_de_novo_otus.py*. An OTUs.biom file was obtained by picking OTUs defined based on 97% sequence similarity, and taxonomy was assigned to individual OTUs through the Greengenes data set (ver._gg 13.5) (McDonald et al., 2012). The HDF5 OTU.biom file with sequence abundance per sample and treatments was converted to JSON.biom format using the BiomCS 1.0.6 online conversion server[4] (ver. 1.0.6). OTUs were filtered using the sum of five sequences per OTU in total (sum of all samples) as minimum threshold, and analyzed with the graphical interface provided by Statistical Analysis of Metagenomic Profiles[5] (STAMP, ver. 2.1.3) (Parks and Beiko, 2010; Parks et al., 2014). To compare sample pairs or samples organized into two or more groups identified by treatment and/or other traits listed in the mapping file (such as farm, crop cultivation method, soil pH or texture, density levels of phytoparasitic, free-living or predatory nematodes, sample latitude, or their combinations), the entire samples were used as the parent level with different profile levels, applying a two-tailed Student's *t*-test, with other comparative statistics. We kept unclassified OTUs and their higher levels in the analyses, by identifying the latter in the hierarchy (and eventually in STAMP plots) using the OTUs codes as tags of the higher, unclassified taxonomic levels. Heatmap plots of only significantly different OTUs [analysis of variance (ANOVA, with a 0.95 *post-hoc* Tuckey–Kramer test, filtering threshold: $p \leq 0.05$)] were produced with the average neighbor UPGMA algorithm and a 0.65 dendrogram clustering threshold. Two-group comparisons were performed by applying a two-sided, equal variance *t*-test ($p \leq 0.05$, effect size as ratio of proportions = 0.8). Principal component analysis for all samples (except the outlier sample N1) was also performed with STAMP.

The .biom OTU table was used for further analyses with the R library *mctoolsr*[6] ver. 0.1.1.2 (R Core Team, 2013) for the production of samples Bray–Curtis dissimilarity matrices and MDS plots, for the whole data set or selected taxonomic lineages or sample groups, and for Kruskal–Wallis *t*-test and permutational multivariate analysis of variance (PERMANOVA). PAST was used to calculate sample α-diversity indices. Further R libraries used included *phyloseq* (McMurdie and Holmes, 2013), *ggplot2* (Wickham, 2016), and *boxplot* for graphics, *psych*, and

[1]www.igatechnology.com

[2]https://www.illumina.com/content/dam/illumina-marketing/documents/products/appnotes/16S-Metagenomic-Library-Prep-Guide.pdf

[3]https://github.com/neufeld/pandaseq

[4]https://biomcs.iimog.org

[5]http://kiwi.cs.dal.ca/Software/STAMP

[6]*Leff J. W. (2016). mctoolsr: Microbial Community Data Analysis Tools. R package version 0.1.0.12.* Available online at: https://github.com/leffj/mctoolsr/.

TABLE 2 | Spearman's rank correlation coefficient (ρ) among nematode population densities and other soil variables*.

	Pratylenchus goodeyi	Predatory nematodes	*Helicotylenchus* spp.	Free living	pH	Sand (%)	Silt (%)	Clay (%)
Pratylenchus goodeyi		*0.59213*	***0.00116***	*0.14411*	*0.55280*	***0.00031***	***0.00735***	***0.00026***
Predatory nematodes	−0.08973		*0.10610*	*0.93726*	*0.30108*	*0.24468*	*0.73659*	***0.00932***
Helicotylenchus spp.	**0.50705**	−0.26628		***0.02984***	*0.18466*	***0.00000***	***0.00364***	***0.00001***
Free living	0.24150	0.01321	**0.35276**		*0.34169*	***0.00077***	***0.00059***	*0.08825*
pH	−0.09937	−0.17225	0.21990	0.15856		*0.47186*	*0.97493*	*0.39637*
Sand (%)	**−0.55431**	0.19339	**−0.67035**	**−0.52229**	−0.12030		***0.00000***	***0.00000***
Loam (%)	**0.42803**	**−0.05641**	**0.46034**	**0.53208**	−0.00527	**−0.87657**		***0.00055***
Clay (%)	**0.55959**	**−0.41634**	**0.66588**	0.28033	0.14162	**−0.81552**	**0.53408**	

*All samples ($n = 37$). Upper matrix shows p levels (italics, significant values at $p \leq 0.05$ are shown in bold). Lower matrix shows ρ values (significant coefficients are shown in bold).

corr.test for correlations. Venn diagrams were produced using an online public service[7] (Heberle et al., 2015).

ITS Data Analysis

Two amplification steps were used in the library workflow: an initial PCR amplification using locus-specific PCR primers and a subsequent amplification, integrating the relevant flow-cell binding domains and unique indices (NexteraXT Index kit FC-131-1001/FC-131-1002), used to amplify the ITS RNA gene. Libraries were sequenced in a MiSeq run in paired end with a 300-bp read length. The primers ITS1 5′-TCCGTAGGTGAACCTGCGG-3′ and ITS4 5′-TCCTCCGCTTATTGATATGC-3′ were used for the ITS locus (White et al., 1990). ITS sequences were processed by the sequencing provider using fast length adjustment of short (FLASH) reads, filtering out the sequences with unidentified nucleotides by applying 15–250 nt (min–max) lengths of the overlapping region (Magoc and Salzberg, 2011). For each sample, the single fasta format file of assembled sequences was obtained by merging data, and then used as the first input for processing with QIIME 1.9 (Caporaso et al., 2010), on a Linux emulator in a Windows® 7 environment. Next, an OTU table was constructed using *pick_otus.py* based on 97% sequence similarity and an OTUs.biom file was obtained. Taxonomy was assigned to individual OTUs using the UNITE data set (ver._7.1) using UCLUST (Edgar, 2010; Tedersoo et al., 2018). The resulting Excel® database was then edited to eliminate redundancies at the species or genus level by summing all reads counts into single representative OTUs or taxa. Unclassified OTUs were kept in the data set by adding the highest taxonomic descriptor to the unclassified, lower level tags. The same statistics and software tools applied for the 16S analysis were then used for the ITS data.

Sequence Data Deposition

All sequence data were deposited in the sequence read archive (SRA) of the National Center for Biotechnology Information (NCBI) under accession number BioProject PRJNA540248.

[7]http://bioinformatics.psb.ugent.be/webtools/Venn/

RESULTS

Nematodes

Plant parasitic nematodes found in the banana rhizosphere included *Pratylenchus goodeyi* Sher and Allen, and *Helicotylenchus* spp. (*H. multicinctus* Cobb, Golden, and *H. abunaamai* Siddiqi), found in 45% (density range: 67–1,750 × 100 cc soil^{-1}) and 70% (60–2,300 × 100 cc soil^{-1}) of samples, respectively. *Pratylenchus goodeyi* is a severe root endoparasite of banana worldwide, with a migratory phase in the soil on or around the roots. This species is considered to have been introduced to the Canary Islands, likely through the infested plant propagation material. *Helicotylenchus multicinctus*, a further severe banana ecto–endoparasite, was more prevalent in banana samples. In control samples, *P. goodeyi* was not detected, whereas *Helicotylenchus* spp. were only found in one sample (**Supplementary Table 2**).

Free-living nematodes included Rhabditidae as bacterial feeders and fungal feeders such as *Aphelenchoides* spp. Microbial feeders were present in 79% of the samples (density range: 120–13,533 nematodes × 100 cc soil^{-1}) (**Supplementary Table 2**). Predatory nematodes belonged to Dorylaimida and Mononchida. They were found in 26% of the samples (60–360 nematodes × 100 cc soil^{-1}) (**Supplementary Table 2**).

Soil profiles showed most prevalent texture class as sandy clay, with a mean pH for all samples around 7.4 (min-max: 6.3–8.8) (**Supplementary Table 2**).

Spearman's correlations of *P. goodeyi* and *Helicotylenchus* densities with soil variables showed a significant inverse relationship with sand and a positive correlation with the other soil fractions. A significant positive correlation also occurred between the density of *P. goodeyi* and the number of *Helicotylenchus* spp., as well as between the latter and the density of free-living nematodes. Predatory nematodes were only negatively correlated with soil clay content (**Table 2**).

16S Data

A total of 4,426,081 single reads of the 16S V3-V4 region were obtained from the 37 samples analyzed (one sample was discarded due to a low number of reads). PandaSeq

produced 1,250,383 contigs that were analyzed with QIIME, yielding a total 469,205 sequences, used for taxonomic assignments in each sample. The 3,938 OTUs obtained after filtering were represented among the different samples with different frequencies, of which only 68 (1.7%) were classified at the species level. The OTUs belonged to 190 classified genera (2,667 OTUs unclassified at this level), 128 families (1,166 unclassified), 400 orders (308 unclassified),

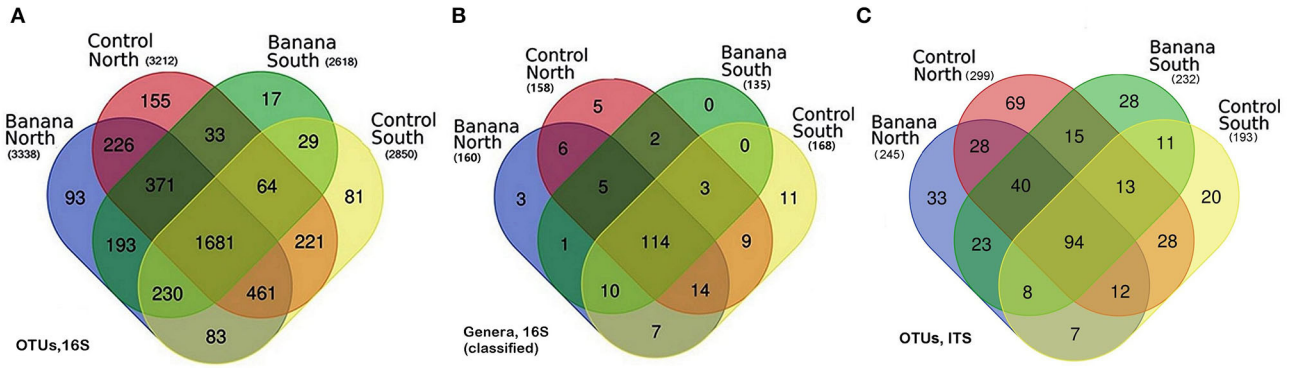

FIGURE 1 | Venn diagrams showing the distribution of bacterial operational taxonomic units (OTUs) **(A)**, classified genera **(B)**, and fungal ITS OTUs **(C)**, among all samples, grouped by crop and latitude.

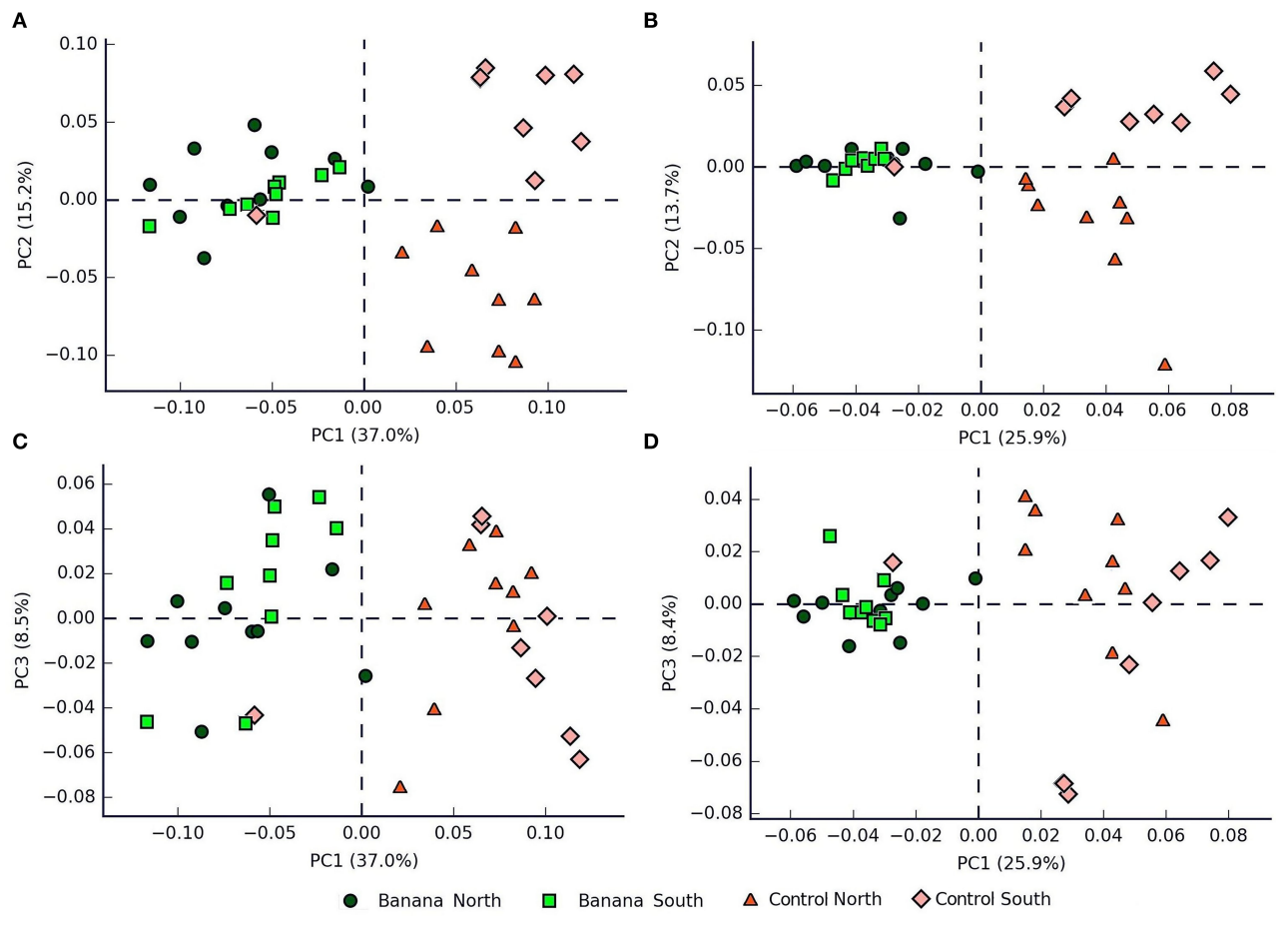

FIGURE 2 | Principal component analysis (PCA) plots (**A,B** = PC1 vs. PC2, **C,D** = PC1 vs. PC3) showing samples classified by crop and latitude, based on 16S sequence data, at the family **(A,C)** and genus **(B,D)** levels (all samples except N1).

97 classes (31 unclassified), and 21 bacterial phyla. Archaea were represented by only 14 OTUs from phyla Crenarcheota and Euryarchaeota.

Venn diagrams showed a core microbiota of 1,681 OTUs, either classified or not, from 190 classified genera, of which 114 were in common for all samples. A higher number of OTUs were observed in northern samples, which also showed the highest number of unique OTUs (**Figures 1A,B**).

Principal component (PCA) plots showed distinct separations among the sample groups (**Figure 2A**) in relation to latitude and presence of banana roots, as did

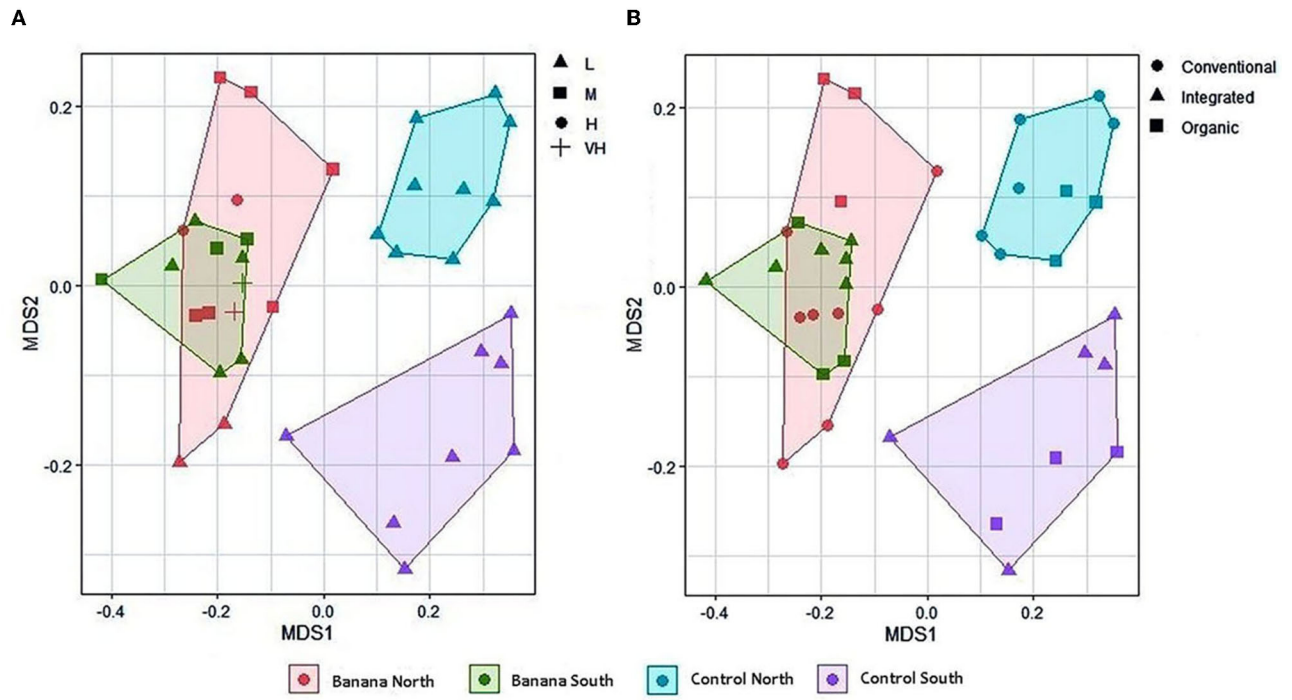

FIGURE 3 | Multidimensional scaling (MDS, stress = 0.14) plots of all samples based on latitude and density of *Helicotylenchus* spp. **(A)**, and crop cultivation method **(B)**. Nematode density levels (expressed as adult and juvenile nematodes × 100 cc soil^{-1}) are: L = low or absent (0–290), M = medium (291–804), H = high (805–1,319), VH = very high (>1,319) (mean density and standard deviation (SD) = 290 ± 514 nematodes × 100 cc soil^{-1}).

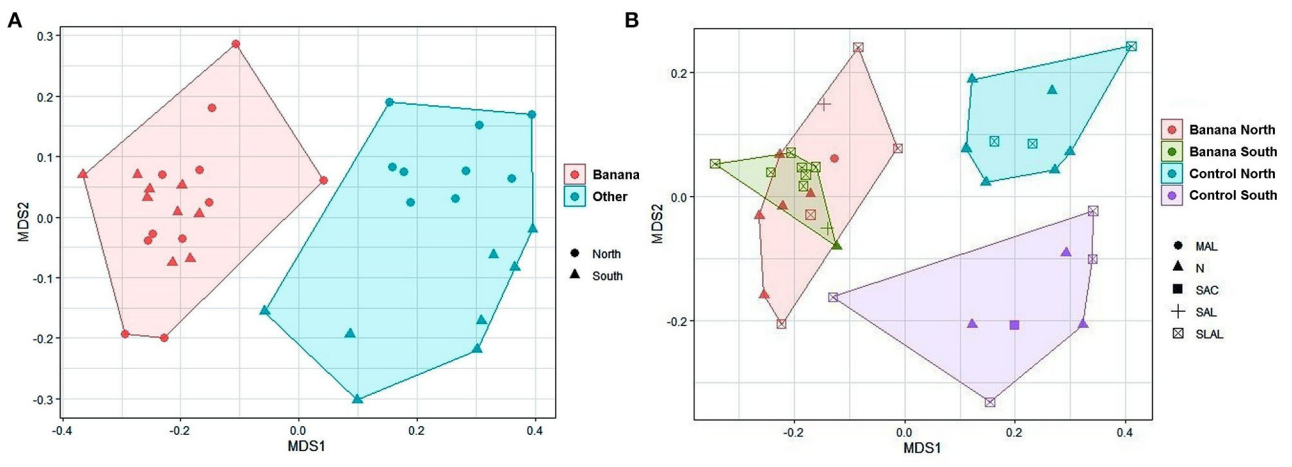

FIGURE 4 | MDS plots (stress = 0.14) of all samples when considering only Proteobacteria (rarefied to 1,800 taxa) and based on latitude and crop **(A)**. MDS plots of only Rhizobiales (**B**, rarefied to 940 taxa, stress = 0.14) with crop, latitude and soil pH. MAL, moderately alcaline; N, neutral; SAC, slightly acid; SLAL, slightly alcaline; SAL, strongly alcaline.

non-metric multidimensional scaling (NMDS) analyses. The clusterings reflected changes in the microbiota, with groups accounting for the presence and density level of *H. multicinctus* and for the effect of the crop cultivation method and latitude (**Figures 3A,B**). A more homogeneous clustering was observed in the PCA plots at the genus level, indicative of a higher similarity among the samples, at a lower taxonomic level (**Figure 2B**). PERMANOVA analysis showed significant differences in false discovery rate (FDR) among groups, mainly related to the presence/absence of banana roots, latitude, and number of *Helicotylenchus* spp. (**Supplementary Table 3**).

Separated sample clusterings were also shown by NMDS when the analysis was limited to specific taxa, such as Proteobacteria, separating samples by crop and latitude (**Figure 4A**), or Rhizobiales, with clusters distinguished by latitude and soil pH (**Figure 4B**).

A higher representation of Proteobacteria, Acidobacteria, and Chloroflexi was observed in the banana rhizosphere, when considering the most abundant taxa by comparing plant and control samples, whereas Actinobacteria were more prevalent in adjacent control sites (**Figure 5A**). This repartition was reflected in a higher prevalence of the classes Alphaproteobacteria, Clostridia, Solibacteres, and Anaerolineae in the banana rhizosphere, with Actinobacteria more represented in control sites (**Figure 5B**). At the order level, a higher frequency of Rhizobiales and Solibacterales characterized the banana rhizosphere samples, with Actinomycetales

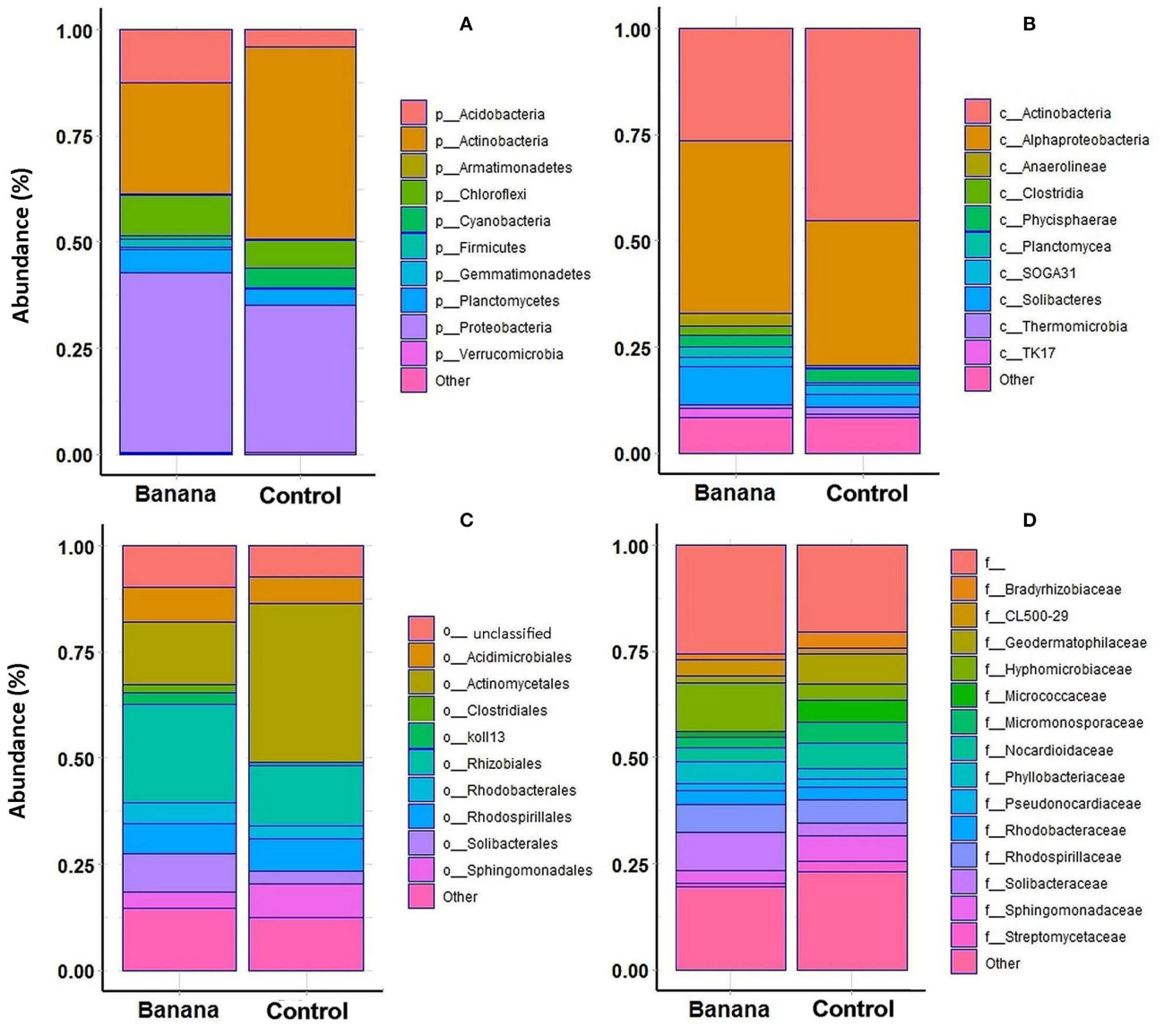

FIGURE 5 | Top 10 more represented phyla **(A)**, classes **(B)**, orders **(C)**, and 15 more represented families **(D)**, in the samples proceeding from *Musa acuminata* rhizosphere vs. adjacent banana root-free control sites.

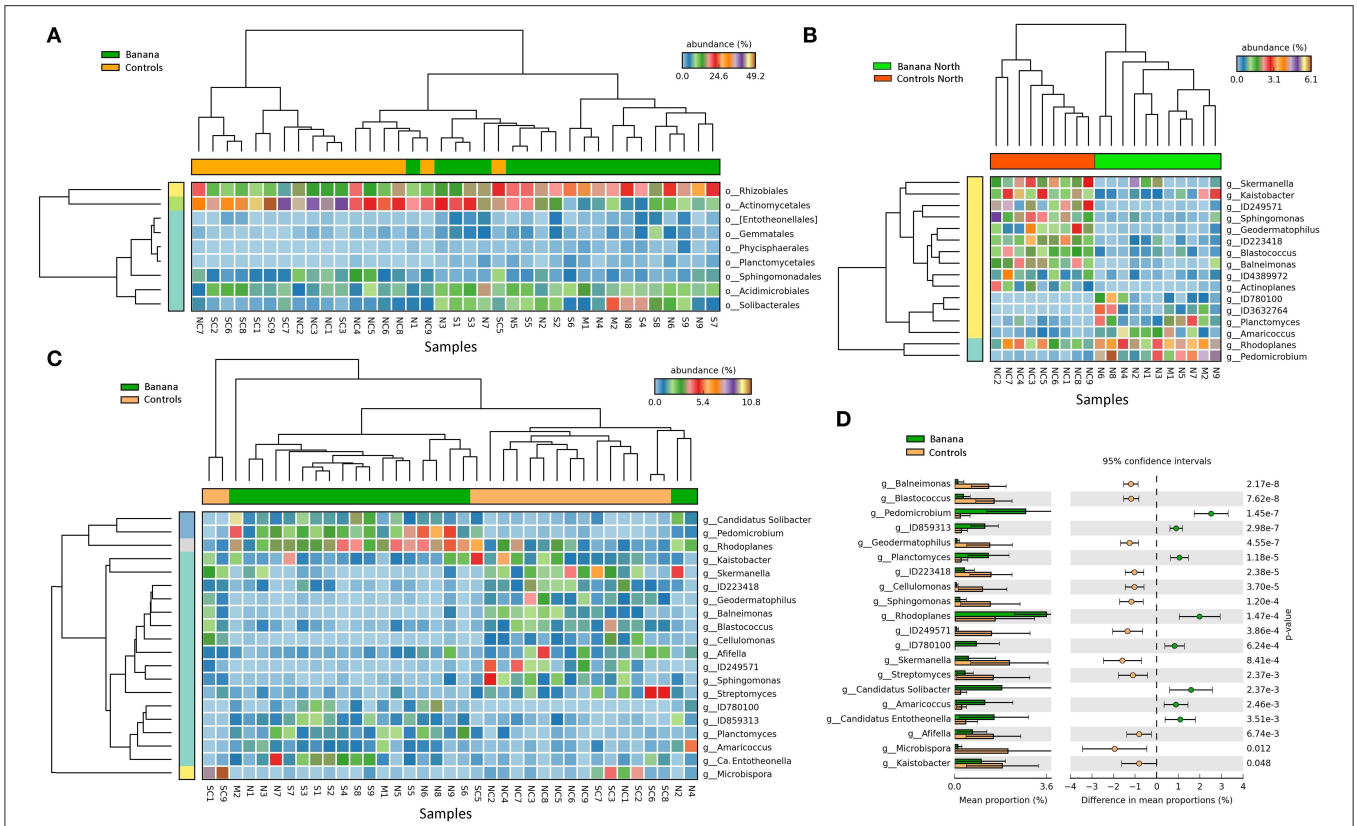

FIGURE 6 | Heatmaps of 16S rRNA sequence abundance among all samples **(A,C)**, and in a subset of northern samples **(B)**, showing the separation of taxa between banana plant rhizosphere and adjacent controls, at the order **(A)** and genus **(B,C)** levels (filtered at $p < 0.05$, effect size filter for difference or proportions = 0.8). Extended error bar plot showing the mean sequence proportions for differentially represented bacterial taxa ($p \leq 0.05$), at the genus level **(D)**.

TABLE 3 | Most represented bacterial families and relative abundance as shown by 16S sequence reads, accounting for differences among banana rhizosphere, and other adjacent, crop-free control sites. Samples were classified by crop and latitude.

	Abundance (%)*						
Families	**Banana North**	**Banana South**	**Control North**	**Control South**	***P***	**Bonferroni P****	**FDR P**
Geodermatophilaceae	0.013	0.018	**0.074**	0.062	2.470368e-05	**0.00027**	**0.00027**
Bradyrhizobiaceae	0.011	0.014	**0.052**	0.023	1.058206e-04	**0.00116**	**0.00058**
Solibacteraceae	**0.092**	0.089	0.035	0.022	1.656480e-04	**0.00182**	**0.00060**
Hyphomicrobiaceae	0.114	**0.116**	0.039	0.036	1.671030e-04	**0.00183**	**0.00045**
Phyllobacteriaceae	**0.056**	0.048	0.015	0.030	2.181649e-04	**0.00239**	**0.00047**
Sphingomonadaceae	0.026	0.031	**0.075**	0.044	5.658774e-04	**0.00622**	**0.00103**
Micromonosporaceae	0.017	0.029	**0.079**	0.018	6.404280e-03	0.07044	**0.01006**
Nocardioidaceae	0.033	0.032	0.045	**0.076**	8.032507e-03	0.08835	**0.01104**

**Min. 5%, in at least one sample group. Most represented families are shown in bold (analyzed with the R library mctoolsr).*

***p-values based on Kruskal–Wallis tests, with Bonferroni and false discovery rate (FDR) corrections (significance at $p \leq 0.05$ is shown in bold; rarefaction level applied = 4,500 sequences per sample; total samples retained = 37).*

more prevalent in the control soils (**Figures 5C**, **6A**). The families Hyphomicrobiaceae and Solibacteraceae were more prevalent in the banana rhizosphere samples, whereas members of Bradyrhizobiaceae were more represented in controls (**Figure 5D**). A similar distribution was observed at the family level when samples were grouped by crop and latitude (**Table 3**). Differences between banana and control samples were also observed at the genus level, with distinct clusterings (**Figure 6C**), more evident when considering only the northern samples (**Figure 6B**). The data showed a higher abundance of *Pedomicrobium*, *Rhodoplanes* with other unclassified taxa in banana rhizosphere, whereas *Microbispora*, *Kaistobacter*, *Ca.*

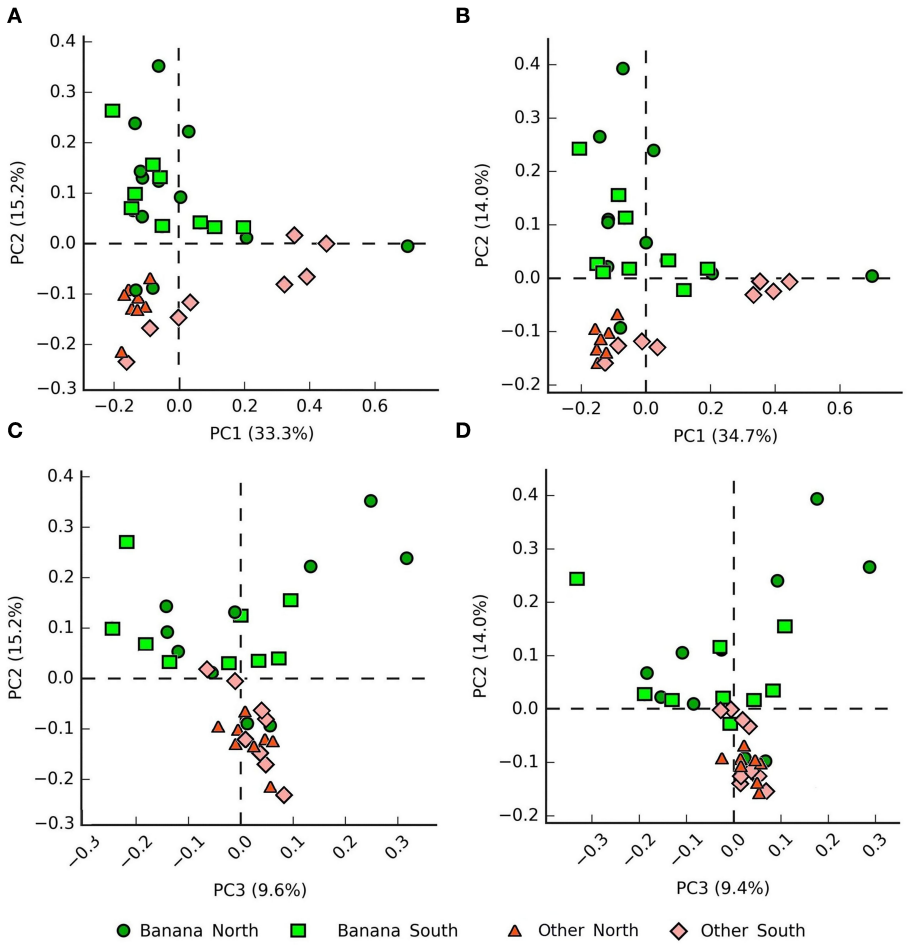

FIGURE 7 | PCA plots (PC1 vs. PC2 and PC1 vs. PC3) by crop and latitude of the samples based on internal transcribed spacer (ITS) data, showing clustering at the family **(A,C)** and genus **(B,D)** levels.

Solibacter, and *Skermanella* were more represented among the controls (**Figure 6D**).

ITS Data

A total of 1,725,692 contigs were obtained from 37 samples analyzed with QIIME, yielding 572,389 ITS sequences. After filtering out sequences from plants and other clades, taxonomic assignments for the Kingdom Fungi across all samples yielded a total of 429 OTUs classified into six phyla and 24 classes. The classification showed fungi in 60 orders (with 15 additional ones unclassified), 106 families (with 48 additional unclassified), and a total of 314 genera (65 of which were unclassified). OTUs classified to the species level were 189, whereas 175 could be only assigned at the genus level, with 65 OTUs also unclassified at the species level.

Venn diagrams showed a common core fungal microbiota of 94 OTUs, either classified or not, including BCA such as *Metarhizium anisopliae* (NCBI accession n. JN377427), *Arthrobotrys oligospora*, and *Acrostalagmus luteoalbus* (AJ292420). A higher frequency of OTUs was observed in the northern control and banana samples, which also showed the highest number of unique OTUs (**Figure 1C**). Several fungal species known as predatory or parasitic on nematodes or other fungi showed, in the banana rhizosphere samples, higher frequencies and/or sequence numbers, including *P. chlamydosporia*, *M. anisopliae*, and species of genera *Arthrobotrys*, *Beauveria*, *Dactylaria*, *Dactylella*, *Lecanicillium*, *Nematoctonus*, and *Trichoderma* (**Supplementary Tables 4, 5**). OTUs also included plant pathogenic fungi such as *Musicillium theobromae* (EF543859; JQ647444), the causal agent of cigar end rot (found in northern and southern banana samples), *Macrophomina phaseolina* (KF766195) (core microbiota), or other pathogens belonging to the genera *Alternaria*, *Cladosporium*, and *Fusarium*. Arbuscular mycorrhizal fungi (AMF) included *Funneliformis* spp. (HF970250) and the ericoid mycorrhiza *Oidiodendron* spp. (KF156313, AF062793 core microbiota). Species reported in the literature as human pathogens, i.e., *Basidiobolus ranarum*, *Lichtheimia corymbifera* (GQ342878), or *Actinomucor elegans,* were also recorded (JN205828) (**Supplementary Table 5**).

Internal transcribed spacer PCA plots showed a clear repartition of samples in relation to the presence/absence of

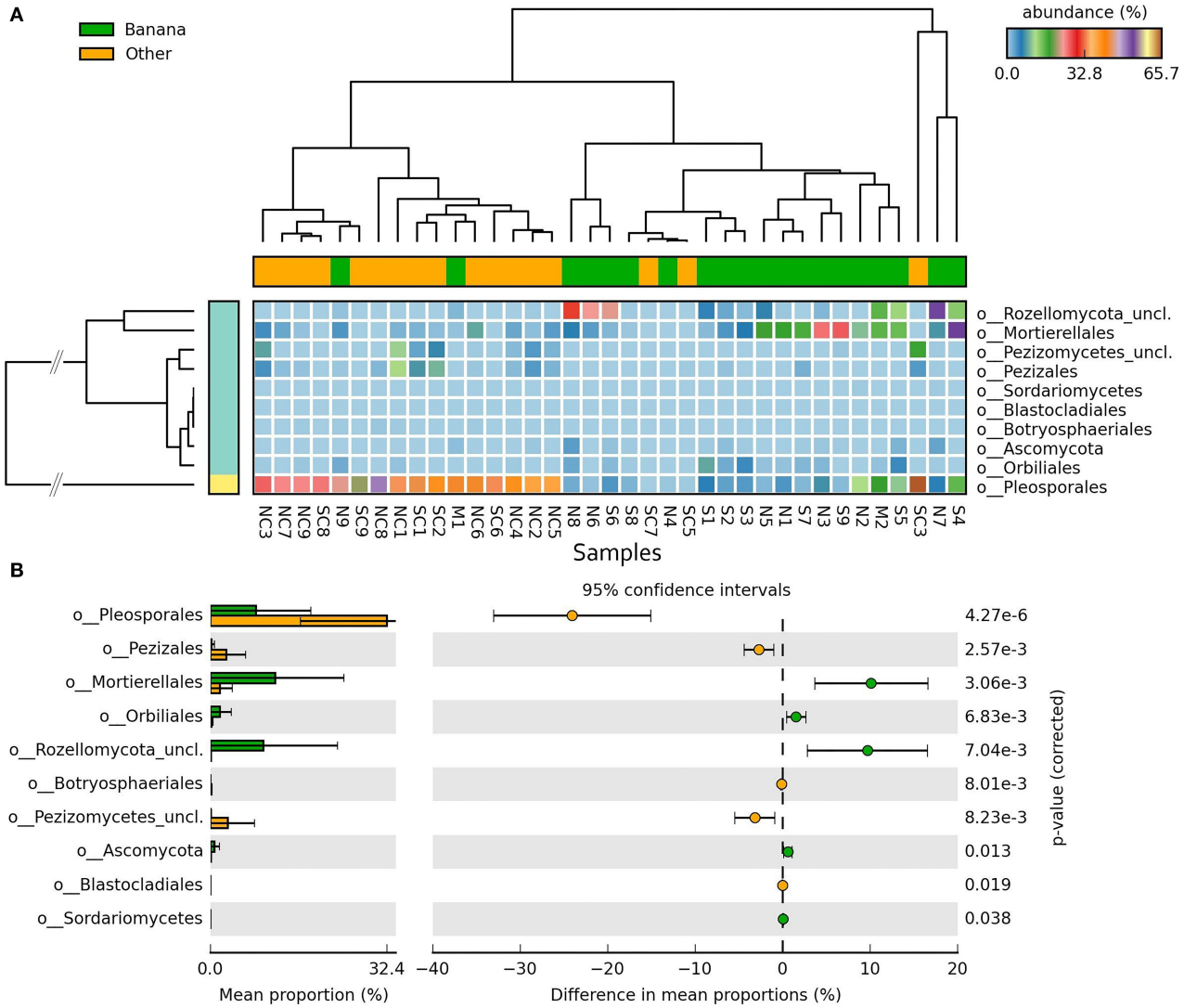

FIGURE 8 | Heatmaps of ITS sequence abundance among all samples showing the differential groupings of fungi between banana plants rhizosphere and adjacent controls, at the order level **(A)**, shown by hierarchical cluster analysis (filtered at $p < 0.05$, effect size filter for difference or proportions = 0.8). Error bar plots of differences in mean proportions among samples **(B)**.

banana plants and latitude, visible at different taxonomic levels (**Figures 7A,B**).

Differences in taxa representation between the banana and control sample groups were observed for mycoparasitic fungi from the phyla Rozellomycota (endoparasites of other fungi) and Zygomycota (i.e., *Mortierella* spp.), which were more represented in the banana rhizosphere, whereas Ascomycota and Basidiomycota were more frequent among adjacent controls (**Figure 8A**; **Supplementary Figures 2A,B**). Hierarchical cluster analysis of samples using ITS sequence abundance showed a major effect of banana plants and, to a lesser extent, of latitude, whereas the crop cultivation method did not appear to affect the clusterings (**Supplementary Figure 2C**). Species of nematophagous fungi within Orbiliales appeared more represented in the banana samples, although with a low proportion, mostly represented by *Arthrobotrys* (**Figures 8B**, **9A,B**; **Supplementary Table 4**), together with Mortierellales and an unclassified order from the phylum Rozellomycota (**Supplementary Figure 3**).

The more represented fungi at the family or genus level were analyzed by comparing sequence representation (%) in samples grouped by crop and latitude, as well as by other classification variables. Differences were found for fungal families in relation to the sample origin (banana rhizosphere vs. controls), age of crops, density levels of predatory or free-living nematodes, plant germplasm, and location of farms (**Supplementary Figure 4**). When comparing banana rhizosphere vs. control samples, the most represented families

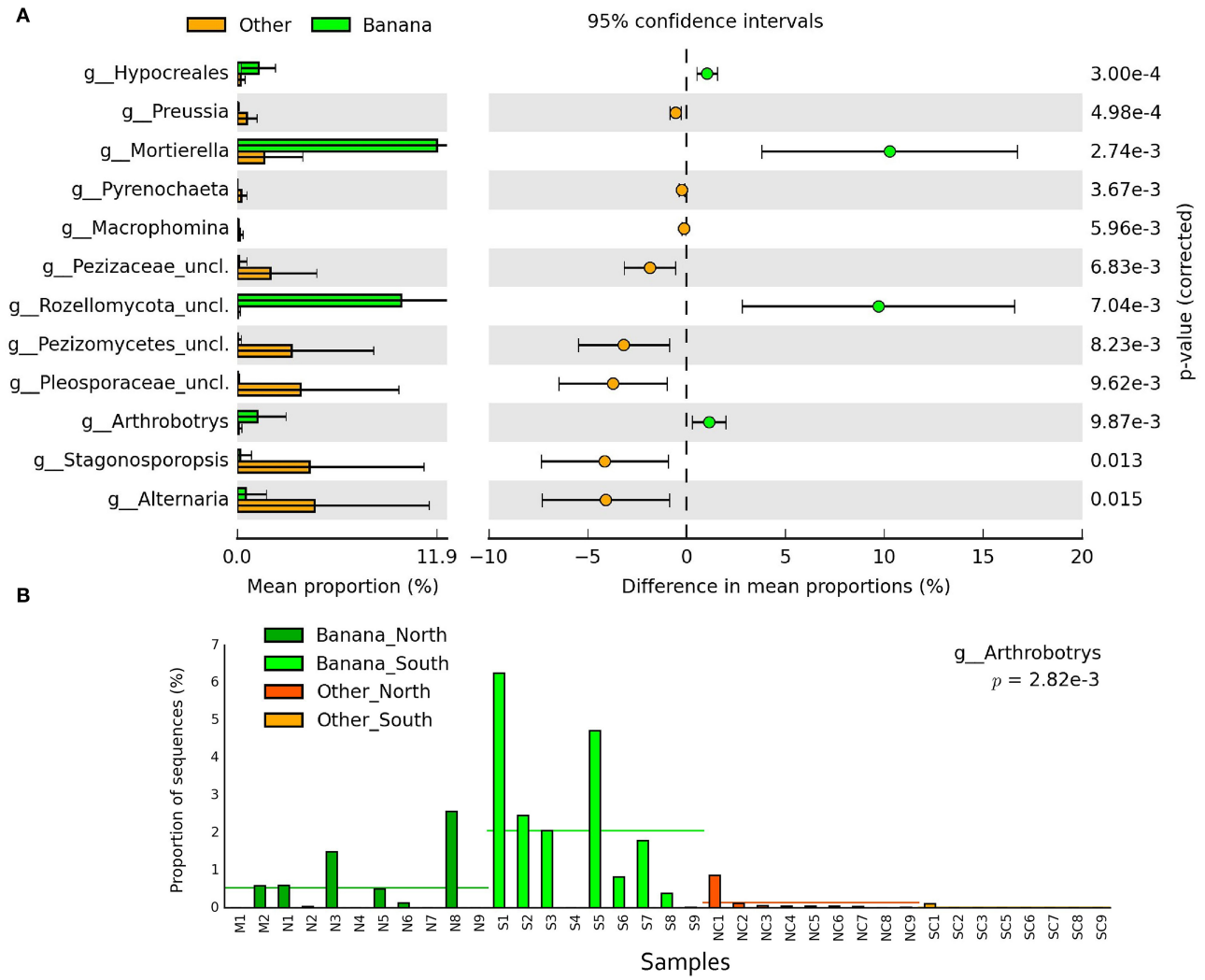

FIGURE 9 | Error bar plots ($p < 0.05$) showing the differences of ITS sequence abundance (mean proportions) among samples at the genus level **(A)**. Bar plot showing the proportion of sequences for the nematophagous genus *Arthrobotrys*, considering rhizosphere and control samples, and latitude **(B)**.

showed a higher abundance of Microascaceae, Wallemiaceae, and Hypocreaceae in the banana rhizosphere, whereas AMF (Glomeraceae and Claroideoglomeraceae) were more abundant in the control soils, as also in younger (<5 years old) plantations (**Supplementary Figures 4A,B**). Considering the location, an effect was shown for fungi associated with organic matter (with a higher abundance of Wallemiaceae in the northern samples, and Trichocomaceae in the southern ones) together with a higher abundance of Glomeraceae and Hypocreaceae in the northern farms (**Supplementary Figure 4E**).

Considering both combined factors, a higher representation was found for *Wallemia* spp. (most represented in the banana northern fields >40 years old), with Hypocreaceae, a *Petriella* sp. and an unclassified member of Claroideoglomeraceae (most frequent in the northern and southern banana samples). Unclassified members of Glomeraceae and Bolbitiaceae were more represented in the northern controls, whereas *Metarhizium* spp. with an unclassified Cystolepiota were most common in the southern controls. An unclassified member of Hypocreaceae was more represented in conventional crops when grouping samples by the cultivation method, whereas *Arthrobotrys* and *Microascus* spp. were more frequent in integrated crops (**Supplementary Table 6**). Banana cv Gruesa showed, when compared to the most prevalent cv Gran Enana and controls, a low abundance of Claroideoglomeraceae and Microascaceae, with a higher content of Vibrisseaceae and an unclassified family within Pezizomycetes (ectomycorrhizae) (**Supplementary Figure 4D**).

Grouping by soil type showed a significantly higher representation of: *Penicillium, Coniochaeta*, and an uncl. Chaetomiaceae in clay soils, *Leucoagaricus* with an uncl. Agaricales in sandy soils, *Phialocephala* and *Wallemia* in

sandy-clay soils, *Sagenomella* in sandy-clay-loamy soils, and *Metarhizium* in sandy-loamy soils. For the effect of pH, *Diaporthe* was more frequent in moderately alkaline soil (pH 7.9–8.4), and an unclassified member of Zygomycota was more represented in slightly acidic soil (pH 6.3–6.5) (**Supplementary Table 6**).

Grouping by nematodes showed a higher representation of *Wallemia*, *Petriella, Phialocephala*, and *Ceratobasidium* with higher densities of *Helicotylenchus* spp., and of *Diaporthe* and *Petriella* with medium densities of *P. goodeyi* (**Supplementary Table 6**). *Phialocephala, Paraconiothyrium, Coniothyrium*, *Meyerozyma*, and *Beauveria*, with unclassified members of Glomerales, Bionectriaceae, and Sordariomycetes, were significantly more represented in samples with high densities of free-living nematodes. An unclassified member of Tulasnellaceae, along with *Zopfiella* spp. and *Cunninghamella* spp., were more represented in samples with medium to highest densities of predatory nematodes (**Supplementary Table 6**). Higher densities of predatory nematodes were associated with a higher abundance of Wallemiaceae and Hypocreaceae, whereas free-living nematodes were associated with an increase in Debaryomycetaceae (budding yeasts), Vibrisseaceae, and an unclassified family within Saccharomycetales (**Supplementary Figures 4C,F**).

Plant pathogenic fungal genera *Alternaria*, *Macrophomina*, and *Pyrenochaeta* along with others were mostly found in control samples, except *Ceratobasidium* and *Chaetomium*, which were more represented in the banana rhizosphere samples (**Supplementary Figure 5**).

A number of diversity indexes were calculated for the ITS data to verify the effects of cropping and latitude on the sample groups examined. Dominance levels in all sample groups were low (0.1–0.2 range), indicating that there were no outstanding taxa (**Supplementary Tables 7A,B**). As shown by the mean comparisons (Student's *t*-test, $p \leq 0.05$, **Supplementary Table 7C**), the α-diversity analysis for the ITS data showed no significant differences between banana samples when they were only grouped by southern vs. northern latitude. On the contrary, most indexes showed significant differences when adjacent, northern, and southern controls were compared. Comparison of northern banana plants vs. adjacent controls showed an effect on the number of taxa, richness (Menhinick, Margalef, and Fisher alpha), and Chao-1 only, indicating that the effect occurred at the level of the rarest taxa. The northern controls also differed significantly from the southern banana and control groups, for the same indexes. Comparison of the southern banana samples vs. adjacent controls showed differences for individuals, Simpson and Shannon indexes, and Menhinick and Margaleff indexes, confirming differences for species richness, as for all sample groups (**Supplementary Table 7C**).

Cooccurrence and Correlations

The correlations between nematodes and fungi or bacteria appeared specific to each nematode species or functional group, when density data and the number of sequences were used. Spearman's correlations showed positive links of *P. goodeyi* densities with bacteria from the genera *Pedomicrobium*, *Afifella, Pilimelia*, *Hyphomicrobium, Rhodoplanes, Microlunatus, Clostridium*, and *Streptomyces,* and unclassified members of Solibacterales and Rhizobiales, Rhodospirillaceae and Ellin329. Significant inverse relationship were found for this nematode with an unclassified member of Rhodobacteraceae and, among fungi, with *Zopfiella* (Sordariomycetes), *Ceratobasidium* (Cantharellales), unclassified Pezizomycetes, *Spiromastix*, *Sordaria*, *Arthrographis*, and *Chaetomium* (**Supplementary Table 8**).

A broader set of taxa was correlated with *Helicotylenchus* spp. Positive correlations included, among fungi, the plant pathogen *Thanatephorus cucumeris* (teleomorph of *Rhizoctonia solani*), *Mortierella oligospora, Cyphellophora*, *Sarocladium*, and unclassified Rozellomycota, Hypocreales, Stramenopiles, Eurotiales, and Onygenales. Among bacteria, positive correlations included members of the genera *Iamia*, *Amaricoccus*, *Planctomyces,* and *Kribbella.* Unclassified taxa positively correlated with *Helicotylenchus* spp. included members of different bacterial lineages, both unclassified (C111, X0319_7L14, S085, WD2101, SAR202, Ellin6529, Ellin6075, and Ellin329) or classified (Nocardioidaceae, Sphingomonadales, Micrococcales, Solibacterales, Hyphomicrobiaceae, Hyphomonadaceae, Erythrobacteraceae, Pseudonocardiaceae, and Acidimicrobiales) (**Supplementary Table 8**). As for *P. goodeyi*, inverse correlations were also found for *Helicotylenchus* spp. with *Zopfiella* and, among the fungi, *Chaetomium and Spiromastix.* Further negative correlations for these nematodes included members of Acidimicrobiales, Rhodobacteraceae, and the fungus *A. luteoalbus*.

Fungi correlated with predatory nematodes (dorylaims and rhabdites) included *Venturia* spp., *A. luteoalbus*, an unclassified member of Mytilinidiaceae and a nematophagous *Dactylella* spp. Negative correlations involved the fungus *Malassezia globosa*, and unclassified bacterial taxa from *Streptomyces,* Caulobacteraceae, Rhodospirillales, and Acidimicrobiales (**Supplementary Table 8**).

Free-living nematodes were positively correlated with a different group of bacteria, including *Cryptococcus randhawii* and members of the genera *Rhodoplanes*, *Roseomonas*, *Sphingomonas, Leptolyngbya*, *Kaistobacter, Streptomyces,* and *Microlunatus*, with further unclassified taxa (members of Caldilineaceae, *WD2101,* Ellin6075, Acidimicrobiales, Bradyrhizobiaceae, and Solibacterales). Fungi positively correlated with free-living nematodes included *Stemphylium herbarum,* species from the genera *Articulospora*, *Westerdykella*, *Stramenopiles*, *Cyphellophora*, *Mortierella*, and members of Olpidiales, Chaetothyriales, and Agaricales. Inverse correlations involved *Streptomyces* spp., *Mesorhizobium* spp., and members of Nocardioidaceae, Rhodospirillaceae, Rhodobacteraceae, S085, and Ellin6529. Among fungi, negative correlations were found with *Spiromastix* sp. and a member of Sordariomycetes (**Supplementary Table 8**).

Arthrobotrys and *Microascus* were significantly more represented on farms applying IPM, whereas an unclassified member of Hypocreaceae was more represented on conventional farms (**Supplementary Table 6**). A plant pathogenic fungus, *Diaporthae* spp., and an organic matter

decomposer, *Petriella* spp., were more represented at medium densities of *P. goodeyi* (151–533 nematodes × 100 cc soil^{-1}). The latter was also more represented, with *Wallemia* and the endophytes *Phialocephala* and *Ceratobasidium* spp., an orchid mycorrhyza and biocontrol agent, respectively (Mosquera-Espinosa et al., 2013), in samples with higher *Helicotylenchus* spp. numbers (**Supplementary Table 6**).

Positive or negative correlations with soil pH were found within the same bacterial lineages (i.e., Acidimicrobiales and Rhodospirillaceae). Taxa most negatively correlated with pH included unclassified members of Ellin329, AKIW874, S085, Alphaproteobacteria, Rhodospirillaceae, Hyphomonadaceae, Rhodospirillaceae, with *Ca.* Solibacter, *Pilimelia* spp. and, among fungi, *Mortierella capitata* (**Supplementary Table 8**).

DISCUSSION

Metabarcoding data showed a clear separation of microbial and fungal samples on the PCA and MDS planes, with clusterings associated with the presence/absence of banana roots, and latitude (**Figures 2–4**, **6**). The representation of the samples hence appears indicative of both anthropogenic effects due to cultivation and, to a lesser extent, farm local climate, which affects a number of microbial taxa. The local climate depends on latitude, differing between northern areas (more humid and cooler, due to exposure to trade winds and ocean currents) and southern zones (arid and more exposed to Sahara heatwaves).

Both climate and aboveground cover have been consistently recognized as key factors influencing soil microbiota profiles. The effect of the aboveground cover on belowground microorganisms has been reported under different agroecological conditions, ranging from pot trials to natural ecosystems. Cropping affects soil microorganisms through many factors including cultivation regimes, plant cover and age, root exudates, and soil types (Berg and Smalla, 2009; Reinhold-Hurek et al., 2015; Compant et al., 2019; Delitte et al., 2021). Experimental data from assays carried out under controlled conditions (with faba bean and wheat plants) for example, showed an effect of the plant species on the soil fungal communities profiles, with differences related to the sample origin (bulk soil or rhizosphere). The tested cropping regimes (monocultures vs. intercroppings) also showed an effect of rhizosphere soil on bacterial diversity and richness (Granzow et al., 2017).

The differences observed between the banana and control samples were also reflected in the different fungal families (Wallemiaceae, Microascaceae, and Agaricaceae) and genera (unclassified member of Claroideoglomeraceae), which were more represented in the banana samples (**Supplementary Table 6**). These changes, including organic matter decomposers and an AMF, appear to be consistent with the introduction and cultivation of the plants. The mechanisms underpinning such an effect are likely related to the farming practices applied, including an enriched organic matter content in the first soil layers, due to the practice of covering the soil surface with banana decaying leaves, adopted locally by farmers. Fertilization, organic matter decomposition, root exudates, and irrigation are likely factors responsible for the observed changes in microbiota structures. Metabarcoding data on banana root endophytes, proceeding from the same environment, showed significant differences between mother plants and suckers, with *Pseudomonas* spp. as the most prevalent endophytic bacteria (Gómez-Lama Cabanás et al., 2021). The microbial community structure originally present in the soil is hence dependent on microenvironmental changes, shifting composition profiles from soil to rhizosphere, up to plants tissues, suggesting a progressive adaptation to the changes that characterize the colonized microhabitats.

The metabarcoding data also showed the presence of several known BCA species of nematodes or fungi. Microbial antagonists of nematodes have a potential to naturally regulate or even suppress PPN numbers, as well as to induce a defense reaction in plants (Oka, 2010; Liang et al., 2019; Topalović and Heuer, 2019). Although correlations may not be considered as a sufficient determinant of an antagonistic or cooperative/exclusion interaction, our data showed specific links of taxa with the variables considered. However, only a limited number of known nematophagous species was directly linked to PPN in the banana samples. Surprisingly, the co-occurrence analysis showed that, apart from the nematode trapping fungus *A. oligospora*, the bacterial and fungal taxa correlated to nematode densities did not include known nematophagous BCA species (**Supplementary Table 8**). The data instead indicated an effect of the nematode guilds as each considered group (two plant parasites, a free-living and a predatory species group) showed significant correlations with a specific subset of unique bacteria and fungi. In particular, the densities of both *P. goodey* and *Helicotylenchus* spp. showed positive correlations with different microbial species. The latter was correlated with a broader range of taxa, different from that of *P. goodeyi*, including, among others, the plant pathogenic fungus *T. cucumeris* (teleomorph of *R. solani*), with other unclassified and poorly studied bacterial lineages (i.e., C111, WD2101, SAR202, and Ellin6529). Moreover, a few significant negative correlations with fungi or bacteria were found for both PPN groups, that included *Spiromastix* spp., a genus of fungi producing antibacterial compounds (Niu et al., 2014), also inversely correlated to free-living nematodes (**Supplementary Table 8**). Negative correlations were found more frequently for free-living, microbiovorous nematodes, likely related to the short life cycle of microbiovorous species, to their direct exposure to fungi or bacteria and possibly to the release of microbial toxic compounds. In this case, a microbial antagonistic activity affects hosts and antagonists almost at the same time, yielding inverse relationships. As the PPN spend part of their cycle in the roots a delay usually occurs between the pathogen and nematode density shifts, affecting correlations. This may be also due to the PPN longer life cycle (4–5 weeks), and to the more complex dispersal and infection strategies of their antagonists.

Data thus indicate that the links between the nematophagous BCA species found and their target PPN hosts are more complex than expected, characterized also by a microbial trophic range and adaptive metabolic capability likely wider than known.

An example of this complexity is given by OTUs classified in the genus *Beauveria*, a fungus usually associated with insects, whose higher frequency in banana samples and higher representation with the highest densities of free-living nematodes (together with other BCA of fungi such as *Paraconiothyrium*) (**Supplementary Tables 4, 6**) is worth further investigation. Despite suggestive of an association, direct assays are needed to establish a dependence of *Beauveria* spp. on nematodes, as both may be correlated to a further, unknown factor (i.e., increased invertebrate densities in the rhizosphere due to higher fertility levels or enhanced freeder roots development). Further assays are hence needed to clarify this aspect. Few data are, moreover, available in the literature for a *Beauveria* nematophagous activity, apart from an isolate of *Beauveria bassiana* obtained from cysts of *Heterodera filipjevi* and successfully tested as a BCA vs. the nematode juvenile stages, in controlled conditions (Zhang et al., 2020).

The data also suggest a probable association of the entomopathogenic fungus *M. anisopliae* with insects other than the banana weevil *C. sordidus*, which may represent a secondary host, as the fungus was more represented, with similar frequency levels, in the control samples. An inverse relationship of this fungus with soil pH was also found (**Supplementary Table 4**). A phylogenetically close species, the endophyte *P. chlamydosporia*, was also found in the banana rhizosphere samples, although with a low frequency (**Supplementary Table 4**). As an endophyte, this species is capable to colonize banana roots, inducing plant growth promotion (Mingot-Ureta et al., 2020). The fungus is also a nematode egg parasite, and is known to activate defense-related genes in endophytically colonized roots (Manzanilla-López et al., 2013), an effect also observed in banana aboveground tissues (Tolba et al., 2021). This fungus may also produce secondary metabolites with insecticidal activities (Lacatena et al., 2019).

The nematode BCA data also showed a number of *Trichoderma* spp., which were found with a higher frequency in the banana samples (**Supplementary Table 4**). Several *Trichoderma* spp. have been reported as an efficient BCA of nematodes, including *Trichoderma harzianum* (Sharon et al., 2001; Sahebani and Hadavi, 2008; Fan et al., 2020). However, no correlation was found for *Trichoderma* spp. with PPN among the samples examined (**Supplementary Table 8**). Moreover, an effective role of *Trichoderma* spp. against plant pathogens, i.e., *Fusarium* spp., has been reported for many hosts, including *Musa* spp. (Sivan and Chet, 1986; Thangavelu and Gopi, 2015; Chaves et al., 2016; Bunbury-Blanchette and Walker, 2019).

The densities of *P. goodeyi* and *Helicotylenchus* spp. in soil varied largely among samples. The endoparasite *P. goodeyi* was only found in the northern banana fields, with a maximum density of 1,100 nematodes × 100 cc soil^{-1}. *Helicotylenchus* spp. were found in 90% of the northern samples and <10% in the southern samples, with a maximum of 2,300 individuals × 100 cc soil^{-1} (**Supplementary Table 2**; **Supplementary Figure 1**). Both nematodes are severe parasites of *Musa* spp., and may reach high densities in roots (Ssango et al., 2004; Roderick et al., 2012). Due to the low amounts of roots collected and required for metabarcoding analyses, nematode densities were preferably assessed in the soil. Density levels appeared, however, sufficient to sustain a severe root infestation, and compatible with the field data reported on other *Musa cvs* from other regions (Talwana et al., 2000; Aguirre et al., 2016). The presence of several BCA and the observed PPN densities appear indicative of complex rhizosphere interactions, based on the BCA host preference, polyphagy, and other interactions that may affect nematode regulation.

The metabarcoding analysis also showed the occurrence of antagonists of fungi, including *A. luteoalbus* and unclassified species of phyla Rozellomycota and Zygomycota (**Supplementary Figures 2A,B**). The former has been reported as an antagonist of *Alternaria*, *Fusarium*, and *Phytophthora* spp. (Lv et al., 2019). It was reported as a causal agent of ginger rhizome rot (Moreira et al., 2013), as an antagonist of fungi and a mushroom pathogen (He et al., 2010; Zhang and Tang, 2015), and as an endophytic plant growth promoter (Khalmuratova et al., 2021). *Rozellomycota* include mostly unclassified zoosporic species characterized by thick-walled resting spores and obligate parasitism on protozoa and fungi (Doweld, 2013). They were found almost uniquely in the banana rhizosphere (**Figures 7**, **8**). Although the biology of these taxa is still poorly investigated, a natural regulatory role may be assigned to members of these clades, which include endoparasitic species in fungi and other eukaryotes. Their density and frequency in banana samples may have been favored by the organic matter applied to plants and by irrigation, providing beneficial services in the rhizosphere such as carbon and nutrients recycling, as well as the regulation of fungal root pathogens.

Finally, the effect of cropping regimes on microbial community structures is considered to be more effective over a longer cultivation period, resulting more evident in older crops or plants (Granzow et al., 2017). Farm age, however, did not show significant differences in the sequence representations (%) of fungi, apart from *Wallemia*, a basidiomycete genus including species inhabiting highly osmotic environments including dry and hypersaline substrates (Zajc and Gunde-Cimerman, 2018), more represented in farms >40 years old (**Supplementary Table 6**).

CONCLUSIONS

The comparison of microbiota composition between banana rhizosphere samples and close, adjacent controls deprived of banana roots showed differences affecting both bacterial and fungal profiles, indicating an effect of cropping. When considering other variables, sample clusterings also reflected latitude effects for both bacteria and fungi. Metabarcoding data showed the occurrence of taxa reported as BCA of nematodes, as well as other endophytes, mycorrhizal species, and obligate endoparasitic taxa (i.e., Rozellomycota), almost only present in the banana samples. However, apart from *a Dactylella* spp., the nematophagous fungi did not show a strict association or correlation with the two PPN species found, *P. goodeyi* and *Helicotylenchus* spp. Instead, differences were found among the nematode guilds as each phytoparasitic, free-living, and predatory nematode group showed correlations with

a specific and different subset of bacteria and fungi. Other factors considered, such as crop cultivation method and soil texture, showed differences in fungal sequence representations as a function of the different variables examined. They were mostly related to trophic specialization and specific biotic requirements or adaptations to a range of decomposers, beneficial endophytes, mycorrhizae, or BCA, as well as plant pathogens. In conclusion, the belowground bacterial and fungal microbiota profiles were affected by plants and latitude, and showed different links to the nematode taxa present. As the impact of microbial species depends not only on their relative but also on their absolute abundance, direct, and specific quantification measurements of the rhizosphere microbial loads for most differential taxa may result informative to exploit the nematode and BCA interactions detected.

DATA AVAILABILITY STATEMENT

The datasets produced in this study can be found in the following online repository: https://www.ncbi.nlm.nih.gov/, SRA BioProject PRJNA540248.

AUTHOR CONTRIBUTIONS

AC, MC, and LR planned and designed the research work. JL-C, MC, and LR performed local samplings. MC performed RNA extraction, bioinformatic work, and the production of sequence data sets. AC and MC interpreted and analyzed the data and wrote this manuscript. All authors critically reviewed, revised, and approved the final version of this manuscript.

FUNDING

Research funded by EU H2020 Project MUSA, Microbial uptakes for sustainable management of major banana pests and diseases, GA n. 727624.

ACKNOWLEDGMENTS

We acknowledge the collaboration provided during sampling by the following producers and technicians of Plátano de Canarias: A. González Benítez, Eudosio, K. Leone, and J. Augusto Mederos. The authors also gratefully thank Colpon Agricola S. L. and Finca Siverio for their support provided during the sampling procedures, N. Centorame for assistance and funds management, and the reviewers for their helpful and constructive suggestions.

SUPPLEMENTARY MATERIAL

The Supplementary Material for this article can be found online at: https://www.frontiersin.org/articles/10.3389/fmicb.2022.855110/full#supplementary-material

REFERENCES

Aguirre, O., Chávez, C., Giraud, A., and Araya, M. (2016). Frequencies and population densities of plant-parasitic nematodes on banana (*Musa* AAA) plantations in Ecuador from 2008 to 2014. *Agron. Col.* 34, 61–73. doi: 10.15446/agron.colomb.v34n1.53915

Baker, G. C., Smith, J. J., and Cowan, D. A. (2003). Review and re-analysis of domain-specific 16S primers. *J. Microbiol. Meth.* 55, 541–555. doi: 10.1016/j.mimet.2003.08.009

Bardgett, R. D., Cook, R., Yeates, G. W., and Denton, C. S. (1999). The influence of nematodes on below-ground processes in grassland ecosystems. *Plant Soil* 212, 23–33. doi: 10.1023/A:1004642218792

Berg, G., Köberl, M., Rybakova, D., Müller, H., Grosch, R., and Smalla, K. (2017). Plant microbial diversity is suggested as the key to future biocontrol and health trends. *FEMS Microbiol. Ecol.* 93, 5. doi: 10.1093/femsec/fix050

Berg, G., Rybakova, D., Fischer, D., Cernava, T., Champomier Vergès, M. C., Charles, T., et al. (2020). Microbiome definition re-visited: old concepts and new challenges. *Microbiome* 8, 103. doi: 10.1186/s40168-020-00875-0

Berg, G., and Smalla, K. (2009). Plant species and soil type cooperatively shape the structure and function of microbial communities in the rhizosphere. *FEMS Microbiol. Ecol.* 68, 1–13. doi: 10.1111/j.1574-6941.2009.00654.x

Boag, B., and Jairajpuri, M. S. (1985). *Helicotylenchus scoticus* n. sp. and a conspectus of the genus *Helicotylenchus* Steiner, 1945 (Tylenchida: Nematoda). *Sys. Parasitol.*7, 47–58. doi: 10.1007/BF00010161

Bubici, G., Kaushal, M., Prigigallo, M. I., Gómez-Lama Cabanás, C., and Mercado-Blanco, J. (2019). Biological control agents against Fusarium wilt of banana. *Front. Microbiol.* 10, 1290. doi: 10.3389/fmicb.2019.01290

Bulgarelli, D., Schlaeppi, K., Spaepen, S., Van Themaat, E. V. L., and Schulze-Lefert, P. (2013). Structure and functions of the bacterial microbiota of plants. *Annu. Rev. Plant Biol.* 64, 807–838. doi: 10.1146/annurev-arplant-050312-120106

Bunbury-Blanchette, A. L., and Walker, A. K. (2019). *Trichoderma* species show biocontrol potential in dual culture and greenhouse bioassays against *Fusarium* basal rot of onion. *Biol. Control.* 130, 127–135. doi: 10.1016/j.biocontrol.2018.11.007

Caporaso, J. G., Kuczynski, J., Stombaugh, J., Bittinger, K., Bushman, F. D., Costello, E. K., et al. (2010). Qiime allows analysis of high throughput community sequence data. *Nature Meth.* 7, 335–336. doi: 10.1038/nmeth.f.303

Chaverri, P., and Samuels, G. J. (2002). *Hypocrea lixii*, the teleomorph of *Trichoderma harzianum*. *Mycol. Progr.* 1, 283–286. doi: 10.1007/s11557-006-0025-8

Chaves, N. P., Staver, C., and Dita, M. A. (2016). Potential of *Trichoderma asperellum* for biocontrol of Fusarium wilt in banana. *Acta Hortic.* 1114, 261–265. doi: 10.17660/ActaHortic.2016.1114.35

Claesson, M. J., Wang, Q., O'Sullivan, O., Greene-Diniz, R., Cole, J. R., Ross, R. P., et al. (2010). Comparison of two next-generation sequencing technologies for resolving highly complex microbiota composition using tandem variable 16S rRNA gene regions. *NAR* 38, e200. doi: 10.1093/nar/gkq873

Clarridge, J. E. (2004). Impact of 16S rRNA gene sequence analysis for identification of bacteria on clinical microbiology and infectious diseases. *Clin. Microbiol. Rev.* 17, 840–862. doi: 10.1128/CMR.17.4.840-862.2004

Compant, S., Samad, A., Faist, H., and Sessitsch, A. (2019). A review on the plant microbiome: ecology, functions, and emerging trends in microbial application. *J. Adv. Res.* 19, 29–37. doi: 10.1016/j.jare.2019.03.004

Coyne, D. L., Cortada, L., Dalzell, J. J., Claudius-Cole, A. O., Haukeland, S., Luambano, N., et al. (2018). Plant-parasitic nematodes and food security in sub-Saharan Africa. *Annu. Rev. Phytopathol.* 56, 381–403. doi: 10.1146/annurev-phyto-080417-045833

Delitte, M., Caulier, S., Bragard, C., and Desoignies, N. (2021). Plant microbiota beyond farming practices: a review. *Front. Sustain. Food Syst.* 5, 624203. doi: 10.3389/fsufs.2021.624203

Domínguez, J., Negrín, M. A., and Rodríguez, C. M. (2001). Aggregate water-stability, particle-size and soil solution properties in conducive and suppressive

soils to Fusarium wilt of banana from Canary Islands (Spain). *Soil Biol Biochem.* 33, 449–455.

Doweld, A. B. (2013). Nomenclatural novelties: Rozellomycota phyl. nov. Index fungorum 43, 1.

Edgar, R. C. (2010). Search and clustering orders of magnitude faster than BLAST. *Bioinformatics* 26, 2460–2461, doi: 10.1093/bioinformatics/btq461

Effendi, Y., Pambudi, A., and Pancoro, A. (2019). Metagenomic analysis of *Fusarium oxysporum* f. sp. *cubense*-infected soil in banana plantation, Sukabumi, Indonesia. *Biodiversitas* 20, 1939–1945. doi: 10.13057/biodiv/d200721

Fan, H., Yao, M., Wang, H., Zhao, D., Zhu, X., Wang, Y., et al. (2020). Isolation and effect of *Trichoderma citrinoviride* Snef1910 for the biological control of root-knot nematode, *Meloidogyne incognita*. *BMC Microbiol.* 20, 299. doi: 10.1186/s12866-020-01984-4

Gómez-Lama Cabanás, C., Fernández-González, A. J., Cardoni, M., Valverde-Corredor, A., López-Cepero, J., Fernández-López, M., et al. (2021). The banana root endophytome: differences between mother plants and suckers and evaluation of selected bacteria to control *Fusarium oxysporum* f. sp. *cubense*. *J. Fungi* 7, 194. doi: 10.3390/jof7030194

Goodey, T. (1963). *Soil and Freshwater Nematodes*. Methuen, MA and London, 544.

Granzow, S., Kaiser, K., Wemheuer, B., Pfeiffer, B., Daniel, R., Vidal, S., et al. (2017). The effects of cropping regimes on fungal and bacterial communities of wheat and faba bean in a greenhouse pot experiment differ between plant species and compartment. *Front. Microbiol.* 8, 902. doi: 10.3389/fmicb.2017.00902

Hammer, Y., Harper, D. A. T., and Ryan, P. D. (2001). PAST: paleontological statistics software package for education and data analysis. *Pal. El.* 4, 4.

Handoo, Z. A., and Golden, A. M. (1989). A key and diagnostic compendium to the species of the genus *Pratylenchus* Filipjev, 1936 (lesion nematodes). *J. Nematol.* 21, 202–218.

He, S., Jin, X., and Wang, S. (2010). Antagonistic activity of *Acrostalagmus luteo-albus* against plant pathogenic fungi. *J. Gansu. Agric. Univ.* 45, 60–65.

Heberle, H., Meirelles, G. V., da Silva, F. R., Telles, G. P., and Minghim, R. (2015). InteractiVenn: a web-based tool for the analysis of sets through Venn diagrams. *BMC Bioinformatics* 16, 169. doi: 10.1186/s12859-015-0611-3

Jacoby, R., Peukert, M., Succurro, A., Koprivova, A., and Kopriva, S. (2017). The role of soil microorganisms in plant mineral nutrition – Current knowledge and future directions. *Front. Plant Sci.* 8, 1617. doi: 10.3389/fpls.2017.01617

Kaushal, M., Swennen, R., and Mahuku, G. (2020). Unlocking the microbiome communities of banana (*Musa* spp.) under disease stressed (Fusarium wilt) and non-stressed conditions. *Microorganisms* 8, 443. doi: 10.3390/microorganisms8030443

Kettler, T. A., Doran, J. W., and Gilbert, T. L. (2001). Simplified method for soil particle-size determination to accompany soil-quality analyses. *Soil Sci. Soc. Am. J.* 65, 849–852. doi: 10.2136/sssaj2001.653849x

Khalmuratova, I., Choi, D. H., Yoon, H. J., Yoon, T. M., and Kim, J. G. (2021). Diversity and plant growth promotion of fungal endophytes in five halophytes from the buan salt marsh. *J. Microbiol. Biotechnol.* 31, 408–418. doi: 10.4014/jmb.2012.12041

Lacatena, F., Marra, R., Mazzei, P., Piccolo, A., Digilio, M. C., Giorgini, M., et al. (2019). Chlamyphilone, a novel *Pochonia chlamydosporia* metabolite with insecticidal activity. *Molecules* 24, 750. doi: 10.3390/molecules24040750

Larriba, E., Jaime, M. D., Nislow, C., Martin-Nieto, J., and Lopez-Llorca, L. V. (2015). Endophytic colonization of barley (*Hordeum vulgare*) roots by the nematophagous fungus *Pochonia chlamydosporia* reveals plant growth promotion and a general defense and stress transcriptomic response. *J. Plant Res.* 128, 665–678. doi: 10.1007/s10265-015-0731-x

Leff, J. W., Bardgett, R. D., Wilkinson, A., Jackson, B. G., Pritchard, W. J., De Long, J. R., et al. (2018). Predicting the structure of soil communities from plant community taxonomy, phylogeny, and traits. *ISME J.* 12, 1794–1805. doi: 10.1038/s41396-018-0089-x

Liang, L. M., Zou, C. G., Xu, J., and Zhang, K. Q. (2019). Signal pathways involved in microbe–nematode interactions provide new insights into the biocontrol of plant-parasitic nematodes. *Phil. Trans. R. Soc. B* 374, 20180317–20180317. doi: 10.1098/rstb.2018.0317

Liu, Z., DeSantis, T. Z., Andersen, G. L., and Knight, R. (2008). Accurate taxonomy assignments from 16S rRNA sequences produced by highly parallel pyrosequencers. *NAR* 36, e120. doi: 10.1093/nar/gkn491

Liu, Z., Lozupone, C., Hamady, M., Bushman, F. D., and Knight, R. (2007). Short pyrosequencing reads suffice for accurate microbial community analysis. *NAR* 35, e120. doi: 10.1093/nar/gkm541

Lv, Y., Shen, Y., Shi, Y., Shen, F., Chen, Y., Zi, S., et al. (2019). Root-endophytic fungi diversity of fuzi (*Aconitum carmichaelii*) and their anti-fungal activity. *Appl. Ecol. Env. Res.* 17, 15289–15300. doi: 10.15666/aeer/1706_1528915300

Magoc, T., and Salzberg, S. (2011). FLASH: fast length adjustment of short reads to improve genome assemblies. *Bioinformatics* 27, 2957–2963. doi: 10.1093/bioinformatics/btr507

Manzanilla-López, R. H., Esteves, I., Finetti-Sialer, M. M., Hirsch, P. R., Ward, E., Devonshire, J., et al. (2013). *Pochonia chlamydosporia*: advances and challenges to improve its performance as a biological control agent of sedentary endo-parasitic nematodes. *J. Nematol.* 45, 1–7.

Martínez Arbas, S., Busi, S. B., Queirós, P., de Nies, L., Herold, M., May, P., et al. (2021). Challenges, strategies, and perspectives for reference-independent longitudinal multi-omic microbiome studies. *Front. Genet.* 12, 666244. doi: 10.3389/fgene.2021.666244

Masella, A. P., Bartram, A. K., Truszkowski, J. M., Brown, D. G., and Neufeld, J. D. (2012). PANDAseq: paired-end assembler for Illumina sequences. *BMC Bioinformat.* 13, 31. doi: 10.1186/1471-2105-13-31

McDonald, D., Price, M. N., Goodrich, J., Nawrocki, E. P., DeSantis, T. Z., Probst, A., et al. (2012). An improved Greengenes taxonomy with explicit ranks for ecological and evolutionary analyses of bacteria and archaea. *ISME J.* 6, 610–618. doi: 10.1038/ismej.2011.139

McMurdie, P. J., and Holmes, S. (2013). Phyloseq: an R package for reproducible interactive analysis and graphics of microbiome census data. *PLoS ONE* 8, e61217. doi: 10.1371/journal.pone.0061217

Mingot-Ureta, C., Lopez-Moya, F., and Lopez-Llorca, L. V. (2020). Isolates of the nematophagous fungus *Pochonia chlamydosporia* are endophytic in banana roots and promote plant growth. *Agronomy* 10, 1299. doi: 10.3390/agronomy10091299

Moens, T., Araya, M., Swennen, R., and De Waele, D. (2006). Reproduction and pathogenicity of *Helicotylenchus multicinctus*, *Meloidogyne incognita* and *Pratylenchus coffeae*, and their interaction with *Radopholus similis* on *Musa*. *Nematology* 8, 45–48. doi: 10.1163/156854106776179999

Mohan, S., Kumar, K. K., Sutar, V., Saha, S., Rowe, J., and Davies, K. G. (2020). Plant root-exudates recruit hyperparasitic bacteria of phytonematodes by altered cuticle aging: implications for biological control strategies. *Front. Plant Sci.* 11, 763. doi: 10.3389/fpls.2020.00763

Moreira, S. I., Dutra, D. C., Rodrigues, A. C., de Oliveira, J. R., Dev Dhingra, O., and Liparini Pereira, O. (2013). Fungi and bacteria associated with post-harvest rot of ginger rhizomes in Espírito Santo, Brazil. *Trop. Plant Pathol.* 38, 218–226. doi: 10.1590/S1982-56762008000300008

Mosquera-Espinosa, A. T., Bayman, P., Prado, G. A., Gómez-Carabal,í, A., and Tupac Otero, J. (2013). The double life of *Ceratobasidium*: orchid mycorrhizal fungi and their potential for biocontrol of *Rhizoctonia solani* sheath blight of rice. *Mycologia* 105, 141–150. doi: 10.3852/12-079

Niu, S., Liu, D., Hu, X., Proksch, P., Shao, Z., and Lin, W. (2014). Spiromastixones A–O, antibacterial chlorodepsidones from a deep-sea-derived *Spiromastix* sp. fungus. *J. Nat. Prod.* 77, 1021–1030. doi: 10.1021/np5000457

Oka, Y. (2010). Mechanisms of nematode suppression by organic soil amendments – A review. *Agric. Ecosyst. Environ. Appl. Soil Ecol.* 44, 101–115. doi: 10.1016/j.apsoil.2009.11.003

Parks, D. H., and Beiko, R. G. (2010). Identifying biologically relevant differences between metagenomic communities. *Bioinformatics* 26, 715–721. doi: 10.1093/bioinformatics/btq041

Parks, D. H., Tyson, G. W., Hugenholtz, P., and Beiko, R. G. (2014). STAMP: statistical analysis of taxonomic and functional profiles. *Bioinformatics* 30, 3123–3124. doi: 10.1093/bioinformatics/btu,494

R Core Team (2013). *R: A Language and Environment for Statistical Computing*. R Foundation for Statistical Computing, Vienna. Available online at: https://www.R-project.org/ (accessed March 31, 2022).

Ram, K., Gruner, D. S., McLaughlin, J. P., Preisser, E. L., and Strong, D. R. (2008). Dynamics of a subterranean trophic cascade in space and time. *J. Nematol.* 40, 85–92.

Ravi, S., Sevugapperumal, N., Nallusamy, S., Shanmugam, H., Mathiyazhagan, K., Rangasamy, A., et al. (2021). Differential bacterial endophytome in

Foc-resistant banana cultivar displays enhanced antagonistic activity against *Fusarium oxysporum* f. sp. *cubense* (Foc). *Env. Microbiol.* 24, 15800. doi: 10.1111/1462-2920.15800

Reinhold-Hurek, B., Bünger, W., Burbano, C. S., Sabale, M., and Hurek, T. (2015). Roots shaping their microbiome: global hotspots for microbial activity. *Annu. Rev. Phytopathol.* 53, 403–424. doi: 10.1146/annurev-phyto-082712-102342

Roderick, H., Mbiru, E., Coyne, D., Tripathi, L., and Atkinson, H. J. (2012). Quantitative digital imaging of banana growth suppression by plant parasitic nematodes. *PLoS ONE* 7, e53355. doi: 10.1371/journal.pone.0053355

Sahebani, N., and Hadavi, N. (2008). Biological control of the root-knot nematode *Meloidogyne javanica* by *Trichoderma harzianum*. *Soil Biol. Biochem*. 40, 2016–2020. doi: 10.1016/j.soilbio.2008.03.011

Schoeneberger, P., Wysocki, D., Benham, E., and Broderson, W. (2012). *Field book for describing and sampling soils, version 2.0. Natural Resources Conservation Service*. Version 3.0. Lincoln, NE: Natural Resources Conservation Service, National Soil Survey Center, 298.

Sharon, E., Bar-Eyal, M., Chet, I., Herrera-Estrella, A., Kleifeld, O., and Spiegel, Y. (2001). Biological control of the root-knot nematode *Meloidogyne javanica* by *Trichoderma harzianum*. *Phytopathology* 91, 687–693. doi: 10.1094/PHYTO.2001.91.7.687

Sivan, A., and Chet, I. (1986). Biological control of *Fusarium* spp. in cotton, wheat and muskmelon by *Trichoderma harzianum. J. Phytopathol*. 116, 39–47. doi: 10.1111/j.1439-0434.1986.tb00892.x

Ssango, F., Speijer, P. R., Coyne, D. L., and De Waele, D. (2004). Path analysis: a novel approach to determine the contribution of nematode damage to East African Highland banana (*Musa* spp., AAA) yield loss under two crop management practices in Uganda. *Field Crops Res.* 90, 177–187. doi: 10.1016/j.fcr.2004.02.018

Takahashi, S., Tomita, J., Nishioka, K., Hisada, T., and Nishijima, M. (2014). Development of a prokaryotic universal primer for simultaneous analysis of bacteria and archaea using Next-Generation Sequencing. *PLoS ONE* 9, e105592. doi: 10.1371/journal.pone.0105592

Talwana, H. A. L., Speijer, P. R., and De Waele, D. (2000). Spatial distribution of nematode population densities and nematode damage in roots of three banana cultivars in Uganda. *Nematropica* 30,19–31.

Tedersoo, L., Sánchez-Ramírez, S., Kõljalg, U., Bahram, M., Döring, M., Schigel, D., et al. (2018). High-level classification of the Fungi and a tool for evolutionary ecological analyses. *Fungal Divers.* 90, 135–159. doi: 10.1007/s13225-018-0401-0

Thangavelu, R., and Gopi, M. (2015). Combined application of native *Trichoderma* isolates possessing multiple functions for the control of Fusarium wilt disease in banana cv. *Grand Naine. Biocontrol Sci. Technol.* 25, 1147–1164. doi: 10.1080/09583157.2015.1036727

Tian, B., Yang, J., and Zhang, K. Q. (2007). Bacteria in the biological control of plant-parasitic nematodes: populations, mechanisms of action, and future prospects. *FEMS Microbiol. Ecol.* 61, 197–213. doi: 10.1111/j.1574-6941.2007.00349.x

Tolba, S. R. T., Rosso, L. C., Pentimone, I., Colagiero, M., Moustafa, M. M. A., Elshawaf, I. I. S., et al. (2021). Root endophytism by *Pochonia chlamydosporia* affects defense-gene expression in leaves of monocot and dicot hosts under multiple biotic interactions. *Plants* 10, 718. doi: 10.3390/plants10040718

Topalović, O., and Heuer, H. (2019). Plant-nematode interactions assisted by microbes in the rhizosphere. *Curr. Issues Mol. Biol.* 30, 75–88. doi: 10.21775/cimb.030.075

Topalović, O., Hussain, M., and Heuer, H. (2020). Plants and associated soil microbiota cooperatively suppress plant-parasitic nematodes. *Front. Microbiol.* 11, 313. doi: 10.3389/fmicb.2020.00313

Uzma, I., Nasira, K., Firoza, K., and Shahina, F. (2015). Review of the genus *Helicotylenchus* Steiner, 1945 (Nematoda: Hoplolaimidae) with updated diagnostic compendium. *Pak. J. Nematol.* 33, 115–160. doi: 10.18681/2015.v33.i02.p01201507310001

Van de Peer, Y., Chapelle, S., and De Wachter, R. (1996). A quantitative map of nucleotide substitution rates in bacterial rRNA. *NAR* 24, 3381–3391. doi: 10.1093/nar/24.17.3381

White, T. J., Bruns, T., Lee, S., and Taylor, J. (1990). "Amplification and direct sequencing of fungal ribosomal RNA genes for phylogenetics," in *PCR Protocols: a Guide to Methods and Applications*, eds M. A. Innis, D. H. Gelfand, J. J. Sninsky, and T. J. White (New York, NY: Academic Press), 315–322.

Wickham, H. (2016). *Ggplot2: Elegant Graphics for Data Analysis*. New York, NY: Springer-Verlag.

Xue, C., Ryan Penton, C., Shen, Z., et al. (2015). Manipulating the banana rhizosphere microbiome for biological control of Panama disease. *Sci. Rep.* 5, 11124. doi: 10.1038/srep11124

Yang, S., Lin, S., Kelen, G. D., Quinn, T. C., Dick, J. D., Gaydos, C. A., et al. (2002). Quantitative multiprobe PCR assay for simultaneous detection and identification to species level of bacterial pathogens. *J. Clin. Microbiol.* 40, 3449–3454. doi: 10.1128/JCM.40.9.3449-3454.2002

Zajc, J., and Gunde-Cimerman, N. (2018). The genus *Wallemia* – from contamination of food to health threat. *Microorganisms* 6, 46. doi: 10.3390/microorganisms6020046

Zhang, G. Z., and Tang, C. Y. (2015). First report of *Acrostalagmus luteo-albus* causing red rust of needle mushroom (*Flammulina velutipes*) in China. *Plant Dis.* 99, 158. doi: 10.1094/PDIS-07-14-0728-PDN

Zhang, J., Fu, B., Lin, Q., Riley, I. T., Ding, S., Chen, L., et al. (2020). Colonization of *Beauveria bassiana* 08F04 in root-zone soil and its biocontrol of cereal cyst nematode (*Heterodera filipjevi*). *PLoS ONE* 15, e0232770. doi: 10.1371/journal.pone.0232770

Zhuang, X., Zhao, J. L., Bai, M., Ping, X. X., Li, Y. L., Yang, Y. H., et al. (2021). *Pochonia chlamydosporia* isolate PC-170-induced expression of marker genes for defense pathways in tomatoes challenged by different pathogens. *Microorganisms* 9, 1882. doi: 10.3390/microorganisms9091882

Conflict of Interest: The authors declare that the research was conducted in the absence of any commercial or financial relationships that could be construed as a potential conflict of interest.

Publisher's Note: All claims expressed in this article are solely those of the authors and do not necessarily represent those of their affiliated organizations, or those of the publisher, the editors and the reviewers. Any product that may be evaluated in this article, or claim that may be made by its manufacturer, is not guaranteed or endorsed by the publisher.

frontiers | Frontiers in Microbiology

ORIGINAL RESEARCH
published: 14 July 2022
doi: 10.3389/fmicb.2022.866085

Xylella fastidiosa Infection Reshapes Microbial Composition and Network Associations in the Xylem of Almond Trees

Manuel Anguita-Maeso[1†], Aitana Ares-Yebra[2,3†], Carmen Haro[1†], Miguel Román-Écija[1], Concepción Olivares-García[1], Joana Costa[2,3], Ester Marco-Noales[4], Amparo Ferrer[5], Juan A. Navas-Cortés[1] and Blanca B. Landa[1*]*

[1] Department of Crop Protection, Institute for Sustainable Agriculture (IAS), Spanish National Research Council (CSIC), Córdoba, Spain, [2] Department of Life Sciences, Centre for Functional Ecology, University of Coimbra, Coimbra, Portugal, [3] Laboratory for Phytopathology, Instituto Pedro Nunes, Coimbra, Portugal, [4] Centro de Protección Vegetal y Biotecnología, Instituto Valenciano de Investigaciones Agrarias, Valencia, Spain, [5] Servicio de Sanidad Vegetal, Generalitat Valenciana, Valencia, Spain

Xylella fastidiosa represents a major threat to important crops worldwide including almond, citrus, grapevine, and olives. Nowadays, there are no efficient control measures for *X. fastidiosa*, and the use of preventive measures and host resistance represent the most practical disease management strategies. Research on vessel-associated microorganisms is gaining special interest as an innate natural defense of plants to cope against infection by xylem-inhabiting pathogens. The objective of this research has been to characterize, by next-generation sequencing (NGS) analysis, the microbial communities residing in the xylem sap of almond trees affected by almond leaf scorch disease (ALSD) in a recent *X. fastidiosa* outbreak occurring in Alicante province, Spain. We also determined community composition changes and network associations occurring between xylem-inhabiting microbial communities and *X. fastidiosa*. For that, a total of 91 trees with or without ALSD symptoms were selected from a total of eight representative orchards located in five municipalities within the *X. fastidiosa*-demarcated area. *X. fastidiosa* infection in each tree was verified by quantitative polymerase chain reaction (qPCR) analysis, with 54% of the trees being tested *X. fastidiosa*-positive. Globally, *Xylella* (27.4%), *Sphingomonas* (13.9%), and *Hymenobacter* (12.7%) were the most abundant bacterial genera, whereas *Diplodia* (30.18%), a member of the family Didymellaceae (10.7%), and *Aureobasidium* (9.9%) were the most predominant fungal taxa. Furthermore, principal coordinate analysis (PCoA) of Bray–Curtis and weighted UniFrac distances differentiated almond xylem bacterial communities mainly according to *X. fastidiosa* infection, in contrast to fungal community structure that was not closely related to the presence of the pathogen. Similar results were obtained when *X. fastidiosa* reads were removed from the bacterial data set although the effect was less pronounced. Co-occurrence network analysis revealed negative associations among

OPEN ACCESS

Edited by:
Inmaculada Larena, Instituto Nacional de Investigación y Tecnología Agroalimentaria (INIA), Spain

Reviewed by:
Shahram Naeimi, Iranian Research Institute of Plant Protection (IRIPP), Iran
Antonio Vicent, Instituto Valenciano de Investigaciones Agrarias, Spain
Ljubica Tasic, State University of Campinas, Brazil

***Correspondence:**
Manuel Anguita-Maeso
manguita@ias.csic.es
Blanca B. Landa
blanca.landa@csic.es

† These authors have contributed equally to this work and share first authorship

Specialty section:
This article was submitted to Microbe and Virus Interactions with Plants, a section of the journal Frontiers in Microbiology

Received: *30 January 2022*
Accepted: *26 May 2022*
Published: *14 July 2022*

Citation:
Anguita-Maeso M, Ares-Yebra A, Haro C, Román-Écija M, Olivares-García C, Costa J, Marco-Noales E, Ferrer A, Navas-Cortés JA and Landa BB (2022) Xylella fastidiosa Infection Reshapes Microbial Composition and Network Associations in the Xylem of Almond Trees. Front. Microbiol. 13:866085. doi: 10.3389/fmicb.2022.866085

four amplicon sequence variants (ASVs) assigned to *X. fastidiosa* with different bacterial ASVs belonging to *1174-901-12*, *Abditibacterium*, *Sphingomonas*, *Methylobacterium–Methylorubrum*, *Modestobacter*, *Xylophilus*, and a non-identified member of the family Solirubrobacteraceae. Determination of the close-fitting associations between xylem-inhabiting microorganisms and *X. fastidiosa* may help to reveal specific microbial players associated with the suppression of ALSD under high *X. fastidiosa* inoculum pressure. These identified microorganisms would be good candidates to be tested in planta, to produce almond plants more resilient to *X. fastidiosa* infection when inoculated by endotherapy, contributing to suppress ALSD.

Keywords: almond leaf scorch (ALS), xylem, microbiome, network associations, *Xylella fastidiosa*, quarantine pathogens

INTRODUCTION

Xylella fastidiosa has been identified as the major transboundary plant pest posing a serious threat to food security and the environment worldwide (Regulation EU, 2019; Regulation EU, 2020; Sanchez et al., 2019). Indeed, *X. fastidiosa* has been identified as the quarantine pathogen with the highest potential impact in the EU, in all economic, social, and environmental domains. Furthermore, it was ranked first in the priority list of quarantine pest/pathogens in the EU in a full spread scenario using a composite indicator (I2P2) developed by the Joint Research Center (Sanchez et al., 2019).

Xylella fastidiosa causes a relevant number of important diseases that induce severe yield losses in highly economic important crops, such as Pierce's disease in grapevines (PD) (Hopkins and Purcell, 2002), citrus variegated chlorosis (CVC) (Coletta-Filho et al., 2020), olive quick decline syndrome (OQDS) (Saponari et al., 2017), and almond leaf scorch disease (ALSD) (Moralejo et al., 2020). *X. fastidiosa* infects not only crops of high economic importance, but also a wide host range of plants including species of cultural/patrimonial importance, ornamental, and landscape plants (EFSA, 2018, 2019b; Delbianco et al., 2022). The overall number of *Xylella* spp. host plants now reach 407 plant species, 185 genera, and 68 families if we consider those reports where the positive infection by the bacterium was determined by at least two different detection methods or with one method only if sequencing or pure culture isolation was used. These numbers rise to 655 plant species, 293 genera, and 88 families if we do not consider the method applied for its detection (Delbianco et al., 2022). This remarkable wide host range is related, in part, to its high efficient natural transmission between plants by diverse xylem sap-feeding insect species. Once inoculated into the plant, the bacterium survives within the xylem vessels of its host plants where its multiplication and biofilm formation result in a detriment of regular sap flow, and a progressive reduction of water and nutrient uptake, causing impairment of plant growth, and eventually, plant death (Chatterjee et al., 2008; Deyett and Rolshausen, 2019).

Xylella fastidiosa is taxonomically divided into three major subspecies (subsp. *fastidiosa*, subsp. *multiplex*, and subsp. *pauca*) (Schaad et al., 2004) although additional subspecies have been proposed (subsp. *sandyi* and subsp. *morus*) (Almeida and Nunney, 2015). Furthermore, each subspecies consists of multiple genetic lineages, grouped as sequence types (ST), each with different host ranges and virulence, although there is some host overlap and most of them infect several hosts (Sicard et al., 2018; Nunney et al., 2019; Landa et al., 2022).

In 2013, *X. fastidiosa* subsp. *pauca* was reported for the first time in Europe and was associated with a lethal disease outbreak affecting olive trees in Apulia, Italy (Saponari et al., 2013). After this detection and following mandatory EU annual surveys (Regulation EU, 2016; Regulation EU, 2020), several *X. fastidiosa* STs belonging to *fastidiosa, pauca, multiplex*, and *sandyi* subspecies have been intercepted and/or detected in Europe, where the bacterium has been detected in open fields and in the natural environment in France (2015, 2016, and 2020), Spain (2016), and Portugal (2018), and an outbreak in the Tuscany region of Italy (2018) (Denancé et al., 2017; EPPO Global Database; Landa et al., 2017; Regulation EU, 2019; Saponari et al., 2019; Olmo et al., 2021). Recent studies indicated that imports of plant material infected by *X. fastidiosa* from the American continent have probably been the origin of outbreaks of this bacterium in the Apulia region (Italy) and on the island of Majorca and in Alicante (Spain) (Jacques et al., 2016; Loconsole et al., 2016; Giampetruzzi et al., 2017; Landa et al., 2020; Moralejo et al., 2020).

In Spain, *X. fastidiosa* is causing severe yield losses in almond crops and the eradication of 1,000 trees. *X. fastidiosa* was first reported in 2016 in Majorca, in the Balearic Islands, infecting cherry (*Prunus avium*) and *Polygala myrtifolia* plants (Olmo et al., 2017). Early after, in 2017, more than 100 almond trees were diagnosed positive for the bacterium. Currently, more than 79% of almond trees in Majorca are estimated to be affected by ALSD (Moralejo et al., 2020). Four STs of *X. fastidiosa* infecting almond trees in the Balearic Islands have been detected: *X. fastidiosa* subsp. *fastidiosa* ST1 and *X. fastidiosa* subsp. *multiplex* ST7 on the island of Majorca, *X. fastidiosa* subsp. *multiplex* ST81 on the islands of Majorca and Menorca, and *X. fastidiosa* subsp. *pauca* ST80 on the island of Ibiza (Delbianco et al., 2022). Simultaneously to the outbreak detected in Majorca, in the summer of 2017, the symptoms of ALSD were also observed for the first time in mainland Spain on 30-year-old almond trees in several orchards in the municipality El Castell de Guadalest of Alicante province, in the Eastern coast of the Iberian

Peninsula (Marco-Noales et al., 2021). Currently, the *X. fastidiosa* demarcated area (DA) in the Valencian Community covers an extension of >136,200 ha (>135,000 in Alicante province and >1,200 in Valencia province). Within the DA, the infected zone (IZ) covers >2,700 ha, of which over 1,100 ha have been already eradicated. This outbreak represents one of the largest eradication campaigns for a plant disease ever carried out in Europe, with around 12,500 orchards and 90,000 trees already destroyed as of November 2021[1] (Vicente Dalmau, Plant Health Service of Valencian Community, personal communication). In this outbreak area, only *X. fastidiosa* subsp. *multiplex* ST6 has been identified in infected almond trees (Marco-Noales et al., 2021).

Nowadays, there are no tools available to cure *X. fastidiosa* once a plant becomes infected in the field (EFSA, 2019a). Consequently, the use of preventive strategies focuses on the eradication of infected host plants, the control of the sap-feeding insect vectors, and restrictions on plant material movements (EFSA, 2019a; Serio et al., 2019; Morelli et al., 2021). Research on plant-associated microorganisms is gaining importance as a key component for the control of plant pathogens by exploiting and using single inoculants or microorganisms consortia that coexist in plant tissues to protect them against pathogen infection (Backman and Sikora, 2008). Plant-associated microorganisms are involved in several biotic and abiotic processes in the host, from the acquisition of nutrients to the increase of plant tolerance to abiotic stresses, without overlooking their role in plant defense against pathogens. In this context, the acquisition and maintenance of an efficient microbiota capable of adapting more rapidly to a changing environment may be undoubtedly a selective advantage (Doty, 2017; Rabiey et al., 2019).

Some studies have described the microbial community structure and composition within xylem vessels and its relationship to plant health and crop productivity (e.g., Deyett et al., 2017; Fausto et al., 2018; Deyett and Rolshausen, 2019; Anguita-Maeso et al., 2020, 2021a,b; Zicca et al., 2020; Haro et al., 2021). However, a very scarce number of studies have focused on the relationships between *X. fastidiosa* and xylem sap microbiota to assess the level of dysbiosis and the potential role of microbial endophytes in protecting host plants from disease development or stimulating plant immunity (Lacava et al., 2004; Azevedo et al., 2016; Deyett et al., 2019; Pacifico et al., 2019; Giampetruzzi et al., 2020; Vergine et al., 2020; Landa et al., 2022). For instance, Lacava et al. (2004) reported *in vitro* growth stimulation of *X. fastidiosa* by *Methylobacterium extorquens* and inhibition by *Curtobacterium flaccumfaciens,* two plant endophytes*;* whereas Deyett et al. (2017) found that the two endophytic bacteria *Pseudomonas fluorescens* and *Achromobacter xylosoxidans* showed significant negative correlations in their abundance with *X. fastidiosa*.

For almond trees, microbiota studies have mainly focused on the epiphytic communities on the phyllosphere (flowers and leaves) using culture-dependent and culture-independent approaches (Fridman et al., 2012; Izhaki et al., 2013; Aleklett et al., 2014), on fungal pathogens associated with almond wood decay based on conventional culture-dependent techniques (Gramaje et al., 2012; Olmo et al., 2016) or *Prunus* replant disease (Khan et al., 2021). However, to our knowledge, no study has addressed the characterization of xylem sap microbial communities in almond trees despite the fact that the microbial profile serves as a basis to identify bacterial and fungal taxa with a potential antagonistic activity that could be used to fight vascular pathogens or as potential biocontrol agents to suppress ALSD.

This study was designed to characterize, for the first time, xylem-inhabiting bacterial and fungal communities from almond trees grown in the *X. fastidiosa*–DA of the Valencian Community (Spain) using a next-generation sequencing (NGS) approach. Next, we determined to what extent the infection of xylem vessels by *X. fastidiosa* affects the composition, diversity, and structure of the xylem microbiota. Finally, we determined the potential existence of tight interactions between specific xylem-inhabiting microorganisms and *X. fastidiosa* by network analysis. Our results could contribute to the development of sustainable and environmentally friendly biocontrol strategies to control ALSD by identifying key microbial players that might contribute to produce almond plants more resilient to infection by *X. fastidiosa*.

MATERIALS AND METHODS

Study Area, Disease Assessment, and Sampling of Almond Trees

The study was conducted in July of 2018 in the DA of the Valencian Community in the province of Alicante (Spain) affected by *X. fastidiosa* subsp. *multiplex* ST6. The incidence and severity of ALSD were assessed in a previous study in 20 almond orchards within the outbreak IZ (Camino et al., 2021). In each plot, ALSD severity (DS) was assessed by visual inspection of each tree for foliar symptoms using a rating scale of 0–4 according to the percentage of foliage with disease symptoms, where 0 corresponds to no visual symptoms (asymptomatic), and 1, 2, and 3 correspond to trees with visual ALSD symptoms between 1% and –25%, 25% and 50%, and 50% and 75% of the tree-crown, respectively, and 4 corresponds to a tree with mostly dead branches (≥75% of the crown canopy; with leaf collapse or leaf scorch) (**Figure 1**) (Camino et al., 2021).

From the 20 almond orchards evaluated by Camino et al. (2021), we selected for sampling and xylem analysis eight orchards within the municipalities of Benifato (two orchards), Benissa (two orchards), La Vall d'Alcala (one orchards), Polop (one orchard), and Xaló (two orchards) (**Table 1**). These plots were selected as the most representative of the 20 evaluated ones covering the geographic area evaluated and a wide range in terms of plot size and disease incidence and severity of ALSD symptoms determined by visual inspection (Camino et al., 2021). **Table 1** shows the disease- and climate-related variables for the eight almond orchards analyzed in this study. Climate variables were selected based on annual temperature and precipitation values, as well as those that were found to be associated with the sensitivity of the bacterium to low winter temperature (Purcell, 1980) and the effects of water stress or warm conditions in the establishment of *X. fastidiosa* (EFSA, 2019b; Martinetti and Soubeyrand, 2019). Bioclimatic variables were obtained from the Chelsa Climatologies database that is based on the downscaled

[1]https://agroambient.gva.es/es/web/agricultura/xylella-fastidiosa

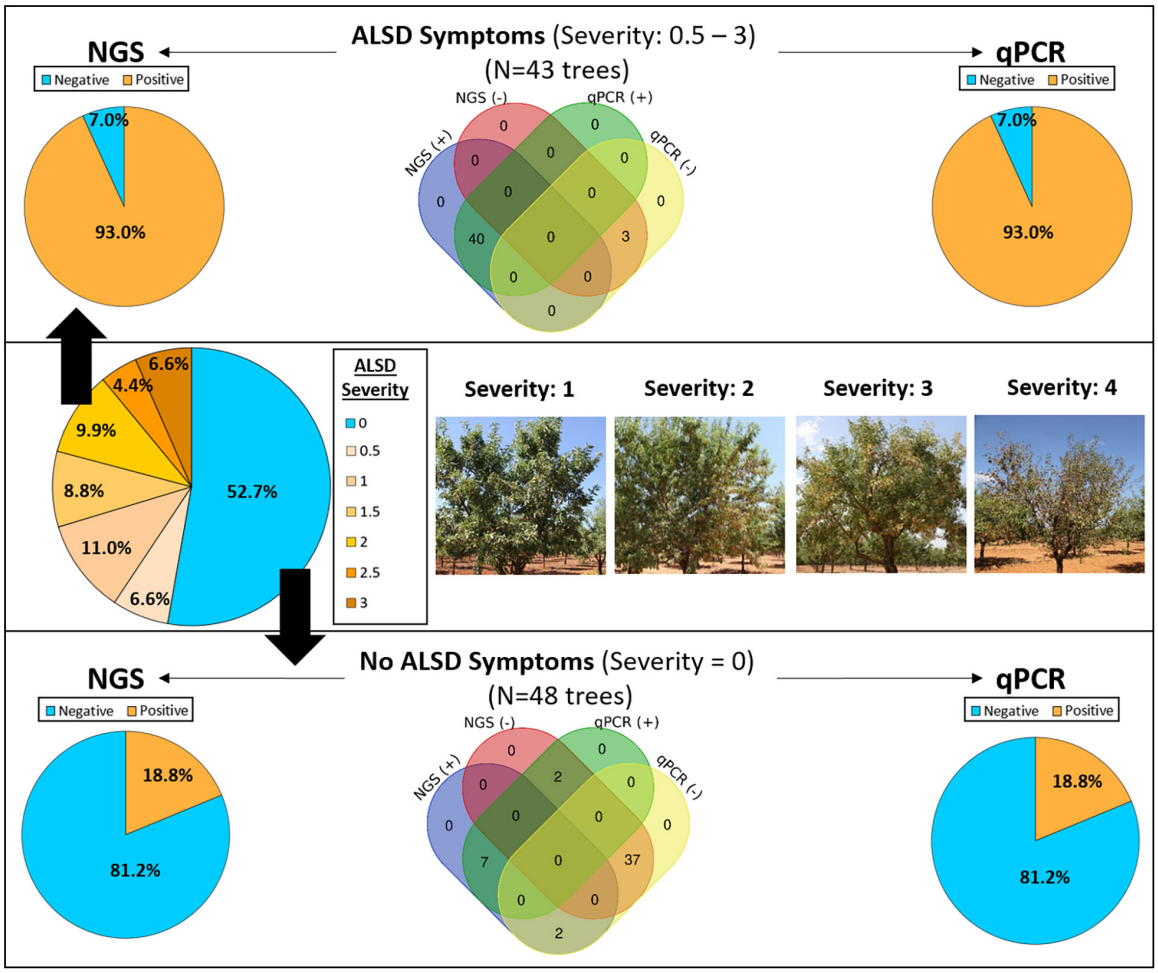

FIGURE 1 | Detection of *Xylella fastidiosa* by next-generation sequencing (NGS) and quantitative polymerase chain reaction (qPCR) from xylem samples obtained from asymptomatic (blue color) and almond leaf scorch disease (ALSD) symptomatic almond trees showing different ALSD severity values (from 0.5 to 3, orange color). No trees showing a disease severity of four were sampled.

ERA-interim global circulation model with Global Precipitation Climatology Centre (GPCC) and Global Historical Climatology Network (GHCM) bias correction, and a resolution of 30 arc s (approximately 1 km) (Karger et al., 2017). Bioclimatic variables were derived from monthly temperature and precipitation values and are intended to approximate climate dimensions meaningful to biological species.

A total of 94 trees were selected for microbiome analysis within the different evaluated plots, with 6–19 trees sampled per plot (**Table 1**). Trees included asymptomatic and symptomatic ALSD trees and were representative of the different disease severity scores present in the plot, from 0 (asymptomatic) to <3 (symptomatic), described above. We discarded those trees with a disease severity of 4 for sampling, as they had most of the canopies showing leaf scorch with dead branches (**Figure 1**). Sampling of the plant material was performed according to the standard protocol of the European and Mediterranean Plant Protection Organization for *X. fastidiosa* (EPPO, 2019). Briefly, samples for laboratory analysis were composed of almond branches/cuttings with attached mature leaves avoiding young growing shoots. Samples were kept refrigerated and shipped to the laboratory within a day. Sampling was supervised by the Plant Health Service of the Regional Ministry of Agriculture of the Valencian Community (Spain) and TRAGSATEC (Grupo TRAGSA) helped in the locations of the selected plots. Prior to sampling, an official permit was requested from the competent Phytosanitary Authority in the Valencian Community to move the plant material from the DA to the IAS-CSIC Laboratory in Córdoba, Spain. Trees could only be sampled once due to the eradication enforcement of the Regulation EU (2019) that is carried out in an IZ in Europe and that obliges to remove all trees tested positive for *X. fastidiosa* immediately after diagnosis.

DNA Extraction From Xylem Tissues and Real-Time PCR Analysis

It is known that, for deciduous plant species (e.g., *Prunus* spp.), a detectable concentration of the bacterium is commonly obtained on leaf petioles at the end of summer for symptomatic

TABLE 1 | Disease incidence and severity of almond leaf scorch disease (ALSD), and climatic characteristics of almond orchards sampled in this study within the demarcated area (DA) for *Xylella fastidiosa* in Alicante province.

Municipality	Plot number	Number of trees in the plot	Number of trees analyzed by NGS	Disease-related variables[a]			Climate-related variables[b]			
				Disease incidence (0–100%)	Disease severity (0–4)	Disease severity range (0–4)	Annual mean temperature (°C)	Mean temperature of the coldest month (°C)	Annual precipitation (mm)	Precipitation of the driest quarter (mm)
Benifato	650	30	10	80.0 ± 40.7	1.43 ± 1.05	0 to 3	13.9	4.9	583.0	40.0
Benifato	652	21	9	61.9 ± 49.8	0.61 ± 0.61	0 to 1.5	13.9	4.9	583.0	40.0
Benissa	75	120	9	71.7 ± 45.3	1.51 ± 1.30	0 to 4	17.0	9.4	529.0	34.0
Benissa	405	69	7	43.5 ± 49.9	0.78 ± 1.24	0 to 4	15.5	7.5	568.0	39.0
Polop	47	456	19	32.5 ± 46.9	0.57 ± 1.04	0 to 4	16.5	7.9	476.0	38.0
Vall d'Alcala	48	43	19	16.3 ± 37.4	0.30 ± 0.80	0 to 3	14.3	5.0	686.0	33.0
Xaló	20A	154	12	94.2 ± 23.5	1.95 ± 1.23	0 to 4	17.1	9.0	487.0	32.0
Xaló	20B	80	6	8.8 ± 2.8	0.11 ± 0.52	0 to 4	17.1	9.0	487.0	32.0

[a]*Disease incidence: Percentage of almond trees showing almond leaf scorch symptoms; Disease severity: mean disease severity assessed by visual inspections of each individual tree using a 0–5 rating scale, where 0 is asymptomatic and 5 is death tree. Data show the mean ± standard deviation (SD).*
[b]*Climate-related variables were estimated using the bioclimatic variables: bio 1 (annual mean temperature), bio 6 (mean temperature of the coldest month), bio 12 (annual precipitation), and bio 17 (precipitation of the driest quarter) obtained from the Chelsa Climatologies database, which is based on the downscaled ERA-interim global circulation model with the Global Precipitation Climatology Centre (GPCC) and the Global Historical Climatology Network (GHCM) bias correction, and a resolution of 30 arcs (approximately 1 km) (Karger et al., 2017). Bioclimatic variables were derived from monthly temperature and precipitation values and are intended to approximate climate dimensions that are meaningful to biological species.*

plants, but asymptomatic leaves collected early in the season during the vegetative period from the same trees can be negative. For this reason, we processed mature branches (i.e., woody cuttings) to maximize the chance of detecting *X. fastidiosa*. Xylem tissue was recovered by obtaining woody chip shavings as previously described by Anguita-Maeso et al. (2020). Shortly, three 6-cm-long pieces from mature almond branches were debarked and disinfested with a sterile paper moistened in ethanol to avoid microbial contamination of the xylem from bark and phloem. Once ethanol had evaporated, xylem chips were obtained by scraping the most external layer of the debarked woody pieces with a sterile scalpel. The xylem chips from the different pieces were mixed, and a 0.5-g sample was placed in a Bioreba bag containing 5 ml of cetyltrimethylammonium bromide (CTAB; 2% hexadecyltrimethylammonium bromide, 0.1 M Tris–HCl pH 8, 20 mM EDTA, and 1.4 M NaCl); the bags were closed with a thermal sealer and the content was macerated with a hand homogenizer (BIOREBA, Reinach, Switzerland). Extracts were stored at −80°C until DNA extraction. All the processes described above were carried out under sterile conditions inside a flow hood chamber.

DNA was extracted from aliquots of xylem sap samples (0.5 ml) obtained from CTAB-macerated xylem chips following the EPPO procedure (2019). DNA was eluted in a final volume of 50 μl of ultrapure, filter-sterilized distilled water, DNA purity (absorbance 260/280 nm ratio) was determined using a NanoDrop®156 ND-1000 UV-Vis spectrophotometer (Thermo Fisher Scientific, Inc., Waltham, MA, United States), and yield concentration was quantified using the Quant-iT^{TM} PicoGreen^{TM} dsDNA Assay kit (Thermo Fisher Scientific).

The quantitative polymerase chain reaction (qPCR) assays of Harper et al. (2010) and Francis et al. (2006) were used to determine the presence of *X. fastidiosa* in the trees with each DNA sample run in duplicate according to EPPO (2019). It should be noted that the analytical sensitivity of the real-time PCR test of Harper et al. (2010) is higher than that of the tests based on Francis et al. (2006). A sample was considered positive if the $Cq \leq 35$ and an exponential amplification curve was obtained for both technical replicates. When a doubtful result was obtained, qPCR reactions were repeated. Appropriate negative and positive isolation controls and negative and positive amplification controls were included during DNA extraction and qPCR assays as described by EPPO (2019).

Bacterial and Fungal rRNA Gene Amplification

For bacteria, the primers 799F (5′-AACMGGATTAGAT ACCCKG-3′) and 1115R (5′-AGGGTTGCGCTCGTTG-3′) targeting V5–V6 of 16S rRNA were used for metabarcoding analysis as previously described (Anguita-Maeso et al., 2020, 2021a,b). Briefly, PCR products were purified using Agencourt Ampere XP (Beckman Coulter) and the barcodes and sequencing adaptors were attached using Fluidigm barcodes (Access Array Barcode Library for Illumina® Sequencers – 384, Single Direction). PCR products were quantified using the Quant-iT^{TM} PicoGreen^{TM} dsDNA Assay kit (Thermo Fisher Scientific) and a Tecan Safire microplate reader (Tecan Group, Männedorf, Switzerland). Equimolecular amounts of each individual sample were combined in 10 mM of Tris, and the pooled library was sequenced by the Genomics Unit of the "Fundación Parque Científico de Madrid," Madrid, Spain, using the Illumina MiSeq platform (V3; PE 2 bp × 300 bp).

For fungal communities, the quantified DNA was sent to the Integrated Microbiome Resource (IMR) at Dalhousie University (Canada) to amplify the ITS2 region of the fungal ITS rRNA

with the primers ITS86F (5′-GTGAATCATCGAATCTTTGAA-3′) and ITS4R (5′-TCCTCCGCTTATTGATATGC-3′) using the Illumina MiSeq platform (V3; PE 2 bp × 300 bp).

In both the cases, the ZymoBIOMICS microbial standard (Zymo Research Corp., Irvine, CA, United States) and water (no template DNA) were used as internal positive and negative controls, respectively, for library construction and sequencing.

Bioinformatics and Statistical Analysis

Quality control and adapter trimming of the demultiplexed raw fastq files of bacterial and fungal sequences were performed with the TrimGalore v.0.6.6 tool[2]. The first 10 pb of all reads were trimmed and a truncation length of 240 and 200 pb was needed in the forward and reverse bacterial reads, respectively, to reach an adequate Phred quality score ($Q > 30$). In contrast, a truncation fixed length was not appropriate in fungal reads due to a variation in ITS biological length and additional quality steps were conducted using the Cutadapt v.3.4 tool (Martin, 2011) to overcome this limitation.

High-quality reads were then analyzed using the DADA2 method for the identification of the amplicon sequence variants (ASVs) present in the samples (Callahan et al., 2016) and taxonomically classified using the Silva SSU v.138 and UNITE v.8.3 databases for bacteria and fungi, respectively. Singletons were discarded for taxonomy assignation and statistical analysis. Differences in bacterial and fungal communities were calculated using α-diversity indexes (Richness and Shannon) at the ASV level. The non-parametric Scheirer–Ray–Hare test ($p < 0.05$) was used to assess the effects of the *X. fastidiosa* infection status of the trees (presence of the pathogen as determined by qPCR), sampled plots, and their interaction on α-diversity indexes, using the package rcompanion v.2.4.1 (Mangiafico, 2020) in R. β-diversity was analyzed using principal coordinate analysis (PCoA) of weighted UniFrac and Bray–Curtis distance matrices and the Permutational multivariate analysis of variance using distance matrices (ADONIS function) within the vegan package in R (999 permutations) was performed to test the effects ($p < 0.05$) of *X. fastidiosa* tree infection, the sampled orchards, and their interaction. α- and β-diversity were conducted after resampling abundance values to the minimum number of reads found to achieve parity in the total number of counts between samples. Furthermore, a negative binomial model approach based on the DESeq2 package in R (Love et al., 2014) was used to find differences in microbiota composition at the genus level among the different treatments ($p < 0.05$). Finally, a 40% prevalence of ASV was fixed before performing a co-occurrence network inference analysis of microbial communities by combining an ensemble of the Pearson and Spearman correlation coefficients, and the Bray–Curtis and Kullback–Leibler dissimilarity indices using CoNet v.1.1.1 (Faust and Raes, 2016) and MCODE (Bader and Hogue, 2003) in Cytoscape v.3.8.2 software to determine key network properties and highly interconnected regions to ascertain the existence of potential differences in microbial interactions occurring in the xylem of almond trees with or without *X. fastidiosa* infection. Statistical significance of co-occurrence and mutual exclusions was computed using edge-specific permutation and bootstrap score distributions with 1,000 iterations (Barberán et al., 2012; Faust et al., 2012). All data analyses were repeated by removing reads assigned to *X. fastidiosa* from the data set.

[2]http://www.bioinformatics.babraham.ac.uk/projects/trim_galore/

RESULTS

Disease Assessment and qPCR

Of the 94 sampled trees, 52.7% were asymptomatic (DS = 0), 17.6% showed initial symptoms ($0 < DS \leq 1$), 18.7% showed low severity symptoms ($1 < DS \leq 2$), and 11.0% showed moderate symptoms ($2 < DS \leq 3$) (**Figure 1**). *X. fastidiosa* infection was analyzed by the qPCR of Harper and Francis (EPPO, 2019) on all sampled trees, obtaining congruent results between the two protocols. The qPCR analysis indicated that 54% of the trees were infected by *X. fastidiosa,* and in the remaining 46%, *X. fastidiosa* could not be detected. After performing library amplification, good-quality reads were not obtained for three of the 94 trees analyzed, and these data were discarded for further analysis. The vast majority of trees showing visual ALSD symptoms were positive for *X. fastidiosa* by qPCR analysis (93.0%) with *Cq* values ranging from 23.2 to 35.7 for Francis qPCR, and from 20.4 to 31.0 for Harper qPCR, respectively. Of the asymptomatic trees, 18.8% were determined to be infected by *X. fastidiosa* by qPCR, with *Cq* values ranging from 25.2 to 34.9 for Francis qPCR, and from 21.3 to 33.2 for Harper qPCR.

For NGS analysis, a sample was considered as *X. fastidiosa* –positive if ≥5 reads were taxonomically assigned to the bacterium. *X. fastidiosa* reads identified by NGS ranged from 1,032 to 21,452, whereas the *Cq* values of same samples ranged from 23.2 to 36.6 for Francis qPCR and from 20.4 to 36.0 for Harper PCR. There was good agreement between the qPCR and NGS analysis, as indicated by the significant linear relationship between the Log(reads) and the *Cq* values of positive samples for both qPCR protocols assessed (**Supplementary Figure 1**). In addition, lower *Cq* values were found for the Harper qPCR protocol compared to the Francis qPCR protocol, when testing the same positive sample, as expected from the higher sensitivity of the former (**Supplementary Figure 1**).

Next-generation sequencing results supported the results obtained by qPCR and allowed the detection of *X. fastidiosa* in 93.0% of the symptomatic trees (**Figure 1**), with *X. fastidiosa* reads per sample between 49 and 21,452, representing between 0.3% and 97.7% of the total reads. A total of 18.8% (9/48) of the asymptomatic trees were found to be positive by NGS (**Figure 1**), with *X. fastidiosa* reads between 51 and 6,709, representing between 3.6 and 74.5% of the total reads. Although a similar proportion of asymptomatic trees were determined to be infected by the bacterium when using qPCR, some differences were found. Thus, in two samples from *X. fastidiosa*–infected asymptomatic trees (i.e., qPCR positive with $Cq > 32$) no reads of *X. fastidiosa* could be detected by NGS. Also, in two asymptomatic trees that were qPCR negative, *X. fastidiosa* reads could be detected, albeit in very low numbers (8 and 18 reads, respectively). Finally, a 7.0%

(3/43) of the trees were found to be negative by both the methods, although those trees showed symptoms (DS < 1) similar to those of the initial ALSD (**Figure 1**). Negative results were obtained for those trees upon repeat qPCR analysis with and without sample dilution.

α- and β-Microbial Diversity Measures

Illumina MiSeq sequencing resulted in a total of 2,360,992 and 8,840,606 raw reads for bacterial and fungal communities, respectively. After removal of chimeras, unassigned, or mitochondrial reads, 928,850 and 6,840,847 good-quality reads were assigned to bacteria and fungi, respectively. No chloroplast reads were detected in our samples.

For bacterial communities, a total of 1,217 ASVs were identified among all treatments, with 776 ASVs being retained for α- and β-diversity analysis after rarefying all data to the minimum number of reads and singleton removal. A total of four ASVs were taxonomically assigned to *X. fastidiosa*. The Scheirer–Ray–Hare test indicated no significant differences ($p > 0.05$) for the Richness α-diversity index according to *X. fastidiosa* infection ($H = 2.57$, $p = 0.108$) whereas orchards were significant ($H = 14.65$, $p = 0.040$) with no significant interaction ($H = 1.67$, $p = 0.892$) between both the factors. Conversely, Shannon α-diversity index showed significant differences for *X. fastidiosa* infection ($H = 5.34$, $p = 0.020$), whereas orchards were not significant ($H = 11.20$, $p = 0.130$) with no significant interaction ($H = 2.11$, $p = 0.833$) (**Figure 2A**). On the contrary, when we removed *X. fastidiosa* ASVs reads from the data set, the Richness and Shannon α-diversity indices presented significant differences according to both orchards ($H > 27.62$, $p < 0.001$) and to the tree infection status ($H < 5.25$, $p < 0.027$) with no significant interaction ($H < 1.99$, $p > 0.850$) (**Figure 2B**).

For fungal communities, a total of 708 ASVs were identified for all treatments, with 356 ASVs retained for α- and β-diversity analysis. Both Richness and Shannon α-diversity indices showed significant differences according to the orchard ($H > 55.16$, $p < 0.001$) with no significant differences according to the tree infection status ($H < 0.92$, $p > 0.342$), nor its interaction ($H < 0.96$, $p > 0.965$) (**Figure 2C**).

Principal coordinate analysis of Bray–Curtis and weighted UniFrac distances differentiated almond xylem bacterial communities mainly according to *X. fastidiosa* infection, in contrast to fungal communities, where the presence of the bacterium had a minor effect on its distribution. Thus, there was a clear tendency to group bacterial communities according to the presence of *X. fastidiosa* on the trees along Axis 1, which explained 22.8 and 18.6% of the variation for Bray–Curtis and weighted UniFrac measures, respectively (**Figure 3A**). Interestingly, this trend was not observed when *X. fastidiosa* ASVs reads were removed from the datasheet indicating the crucial effect that *X. fastidiosa* has in displacing bacterial community composition (**Figure 3B**). These results were also observed when data from each orchard were considered separately (**Supplementary Figures 2A,B**). On the other hand, fungal communities did not show a clear distribution according to *X. fastidiosa* infection, neither when all data were analyzed together (**Figure 3C**) nor by sampled orchard (**Supplementary Figure 2C**).

ADONIS analysis supported the results described above and indicated a significant main effect on *X. fastidiosa* infection in the weighted UniFrac model when the *X. fastidiosa* reads were maintained in the datasheet ($R^2 = 0.211$, $p < 0.001$); and also when *X. fastidiosa* reads were removed from the data set ($R^2 = 0.022$, $p = 0.036$). However, in both cases, the main effect on community composition was due to the orchard for both the Bray–Curtis and weighted UniFrac distance ($R^2 = 0.196$, $p < 0.001$) and ($R^2 = 0.270$, $p < 0.001$), respectively. In addition, fungal communities were mainly affected by the sampled orchard at both dissimilarity distances for Bray–Curtis ($R^2 < 0.358$, $p < 0.001$) and for UniFrac ($R^2 < 0.400$, $p < 0.001$), and to a lesser extent by *X. fastidiosa* infection ($R^2 = 0.014$, $p = 0.033$) at the Bray–Curtis distance, with no significant effect for the weighted UniFrac distance ($R^2 = 0.009$, $p = 0.206$) (**Supplementary Table 1**).

Composition of Xylem Tissue Bacterial and Fungal Communities

A total of 11 phyla, 22 classes, 125 orders, 256 families, and 584 genera of bacteria were taxonomically identified. Globally, the phyla Proteobacteria (68.89%), Bacteroidota (18.53%), and Actinobacteriota (10.83%) and the genus *Xylella* (27.39%), *Sphingomonas* (13.93%), and *Hymenobacter* (12.68%) were the most abundant taxa when analyzing all experimental treatments together (**Figure 4A**). As expected, *Xylella* was the genus with the highest relative abundance in *X. fastidiosa*-infected almond trees (58.23%), reaching maximum frequencies for infected trees sampled in orchard 405 (75.79%). In addition, *Sphingomonas* (with 35.20% in orchard 405 and 34.82% in orchard 20B) and *Hymenobacter* (with 36.13 and 31.31% in orchards 47 and 650, respectively) were the next two predominant genera in the xylem tissue from *X. fastidiosa* non-infected trees. Interestingly, a noticeable lower relative abundance of the main predominant genera was found in *X. fastidiosa*-positive almond trees compared to those with negative detection of the pathogen in each orchard (**Figure 5A**). In fact, when removing the genus *Xylella* from the data, slight differences in microbial relative abundance were found between *X. fastidiosa* qPCR-positive and negative trees (**Figure 5B**). On the contrary, a higher relative abundance of two members of the family Sphingobacteriaceae (ASV7 and ASV9) reached the highest frequencies in orchards 650 and 652 (3.52 and 3.34%, respectively) when compared to the other orchards. Similarly, the genus *Tatumella* presented a high relative abundance in *X. fastidiosa* non-infected trees in orchard 652 (23.86%), *Friedmanniella* in orchard 20B (17.33%), and *Massilia* in orchard 405 in non-infected trees (16.66%) (**Figure 5B**).

Overall, three phyla, 66 classes, 123 orders, 266 families, and 408 genera were taxonomically identified as fungi. Globally, the phyla Ascomycota (98.38%), Basidiomycota (1.61%), and Mucoromycota (0.006%) and the genus *Diplodia* (30.18%), the families Didymellaceae (10.66%) and *Aureobasidium* (9.91%) were the most abundant taxa when exploring all experimental

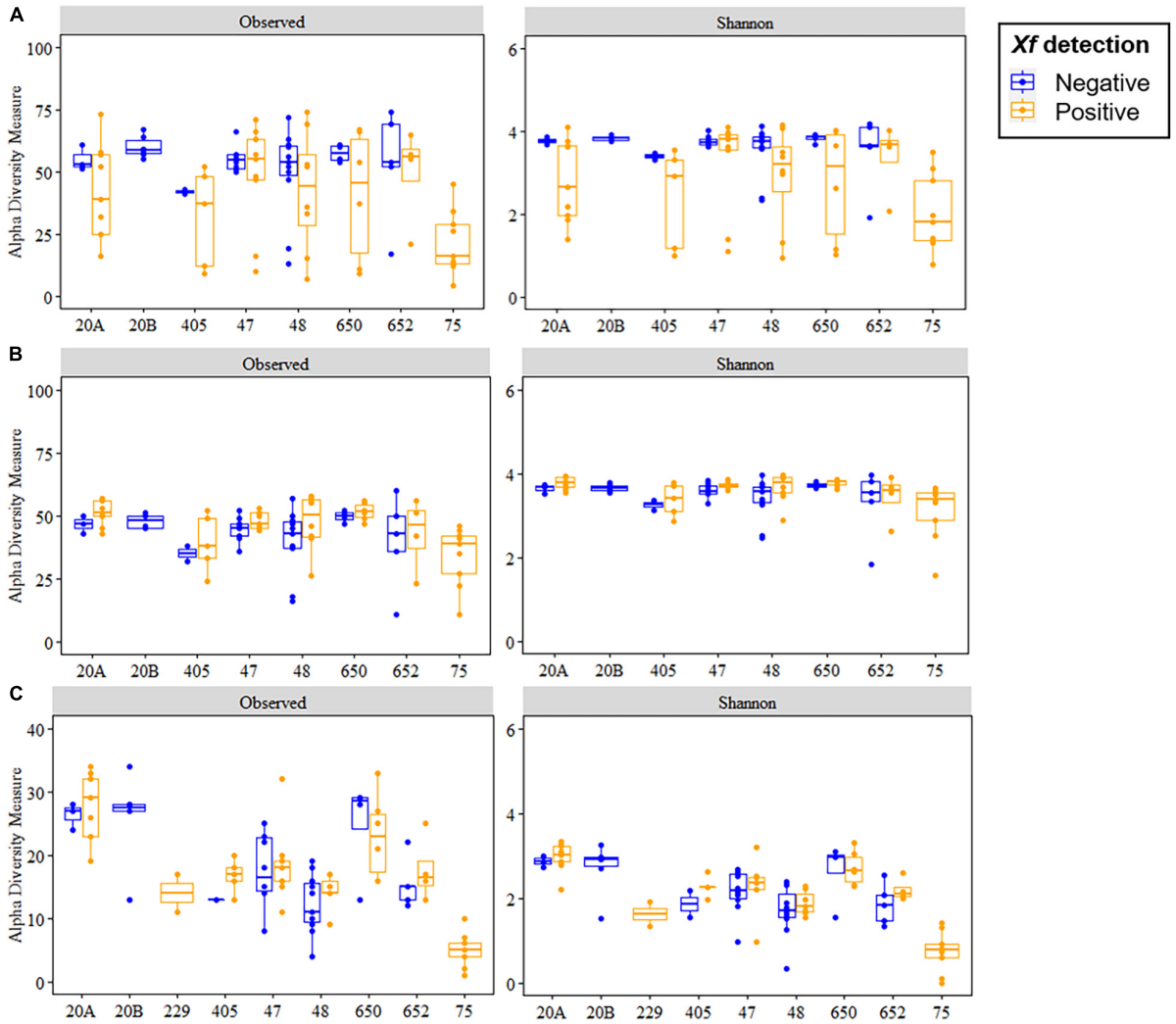

FIGURE 2 | Boxplots of Richness (observed) and Shannon diversity indices for bacterial **(A,B)** and fungal communities **(C)** at the amplicon sequence variant (ASV) taxonomic level in the xylem of *Xylella fastidiosa*-qPCR negative and positive almond trees sampled in different orchards in Alicante province. *X. fastidiosa* ASVs were maintained **(A)** or removed **(B)** from the data set before analysis. The boxes represent the interquartile range, while the horizontal line within the box defines the median and whiskers represent the lowest and highest values of four values for each treatment combination.

treatments together (**Figure 4B**). *Diplodia* and *Neofusicoccum* increased their relative abundance (37.95 and 8.52%, respectively) from non-infected *X. fastidiosa* trees, whereas the genus *Collophora* followed an opposite trend, with a reduction of 3.14% in its relative abundance. When analyzing the data according to orchard, the genus *Diplodia* presented a high relative abundance in *X. fastidiosa*–infected trees in orchard 75 (79.86%), *Neofusicoccum* (24.71%) in orchard 20B, *Lasiodiplodia* (18.02%) in non-infected trees in orchard 48, and *Trichothecium* (29.06%) in infected trees in orchard 650. However, there was no clear pattern of prevalent fungal genera among orchards or *X. fastidiosa* infection. Indeed, *Diplodia* presented the highest relative abundance in *X. fastidiosa*-positive trees in orchard 75 (79.86%), whereas the trend was the opposite in non-infected trees in orchard 47 (43.07%) (**Figure 6**).

Differential Abundance of Bacterial and Fungal Taxa Associated With *Xylella fastidiosa* Infection

In line with these results, DESeq2 analysis was used to identify key genera that could be differentially associated with the presence or absence of *X. fastidiosa* in tree xylem vessels. Globally, a greater number of significant bacterial and fungal genera were found with higher frequencies in *X. fastidiosa*–infected trees (**Figure 7** and **Supplementary Figures 3,4**). Thus, DESeq2 identified a bacterial enrichment (log2 fold change >0) of 50 bacterial members including ASVs from the Class Actinobacteria (two ASVs), family Acetobacteraceae (eight ASVs), and phylum Proteobacteria (two ASVs), and ASVs belonging to the genera *Variovorax*, *Sediminivirga*, *Kineosporia*, and *Erwinia*. On the contrary, *Cupriavidus* and the two unidentified genera from

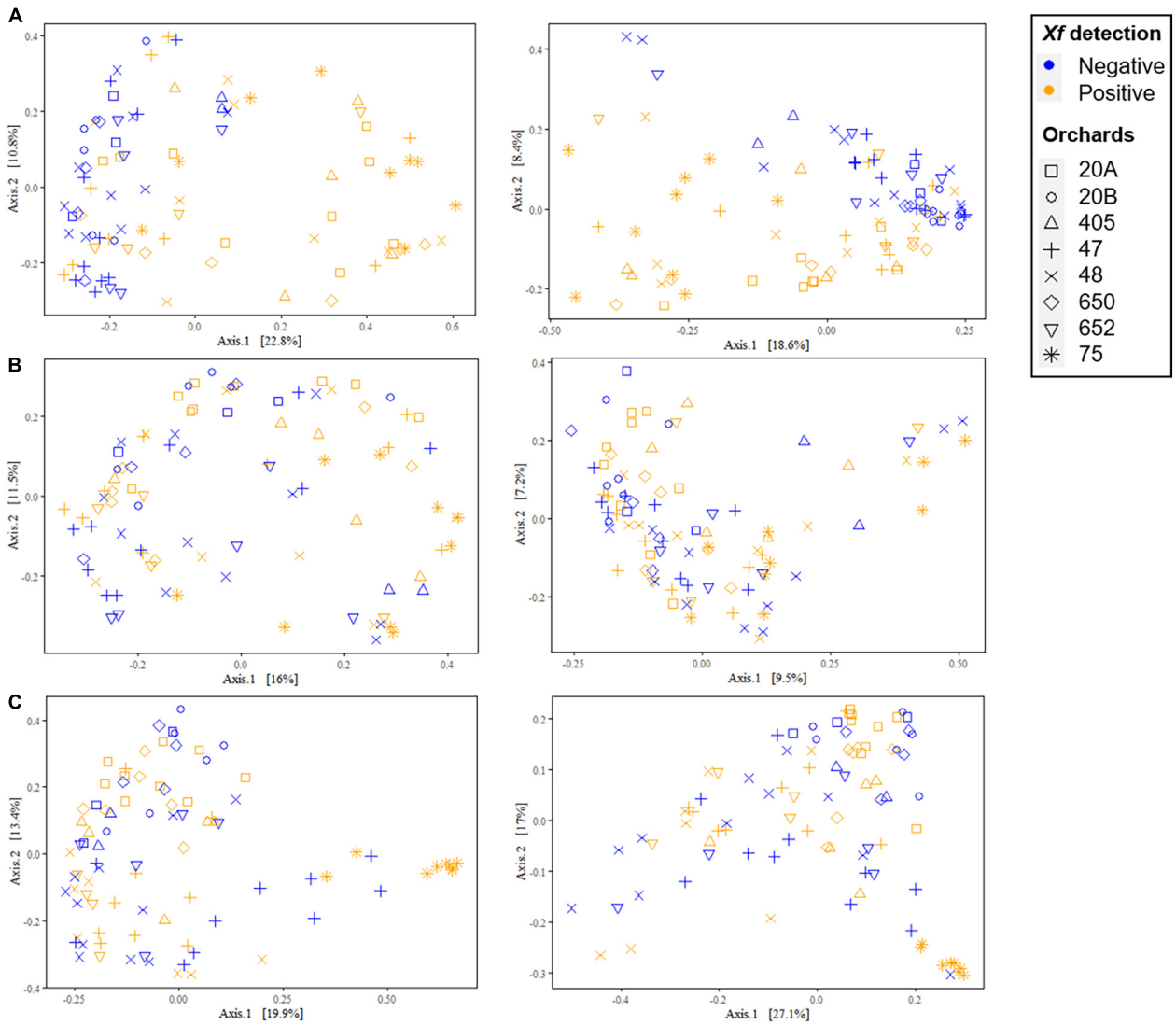

FIGURE 3 | Principal coordinate plots of Bray–Curtis and weighted UniFrac distances of bacterial **(A,B)** and fungal communities **(C)** at the ASV taxonomic level in the xylem of *Xylella fastidiosa*-qPCR negative and positive almond trees sampled in different orchards in Alicante province. *X. fastidiosa* ASVs were maintained **(A)** or removed **(B)** from the data set before analysis. Points are colored by *X. fastidiosa* detection and shaped by municipality.

the families Sphingobacteriaceae (ASV59) and Acetobacteraceae (ASV41) (log2 fold change <0) showed a distinct behavior (**Figure 7A**). Regarding fungal communities, *Neofusicoccum* and *Fitzroyomyces* presented a major enrichment in the xylem when almond trees are infected with the pathogen (log2 fold change >0) whereas the genera *Rosellinia* and *Chaetomium* showed the opposite behavior. In addition, distinct ASVs from the family Didymellaceae showed significantly different enrichment according to the presence of *X. fastidiosa* in the xylem of almond trees (**Figure 7B**).

When analyzing the data by each sampled orchard, DESeq2 identified *Cedecea* in orchard 405, and *Hoyosella* and *Erwinia* in orchard 650, as bacteria with the highest significant enrichment in the xylem of almond trees showing a qPCR *X. fastidiosa*–positive detection. In contrast, Erwiniaceae ASV61 in orchards 652 and 48, and *Pantoea* in orchard 20A were the ASVs with the greatest significant enrichment in the different municipalities in the xylem of almond trees with a negative qPCR detection for *X. fastidiosa* (**Supplementary Figure 3**). Focusing on fungal communities, *Trichothecium* in orchards 405 and 650, and *Diaporthe* in orchard 20A showed the greatest significant enrichment in the xylem of almond trees infected by *X. fastidiosa*, whereas *Cytospora* in orchard 650, ASV248 of the order Tubeufiales in orchard 48, and *Neophaeomoniella* in orchard 652 were enriched in non-infected trees (**Supplementary Figure 4**).

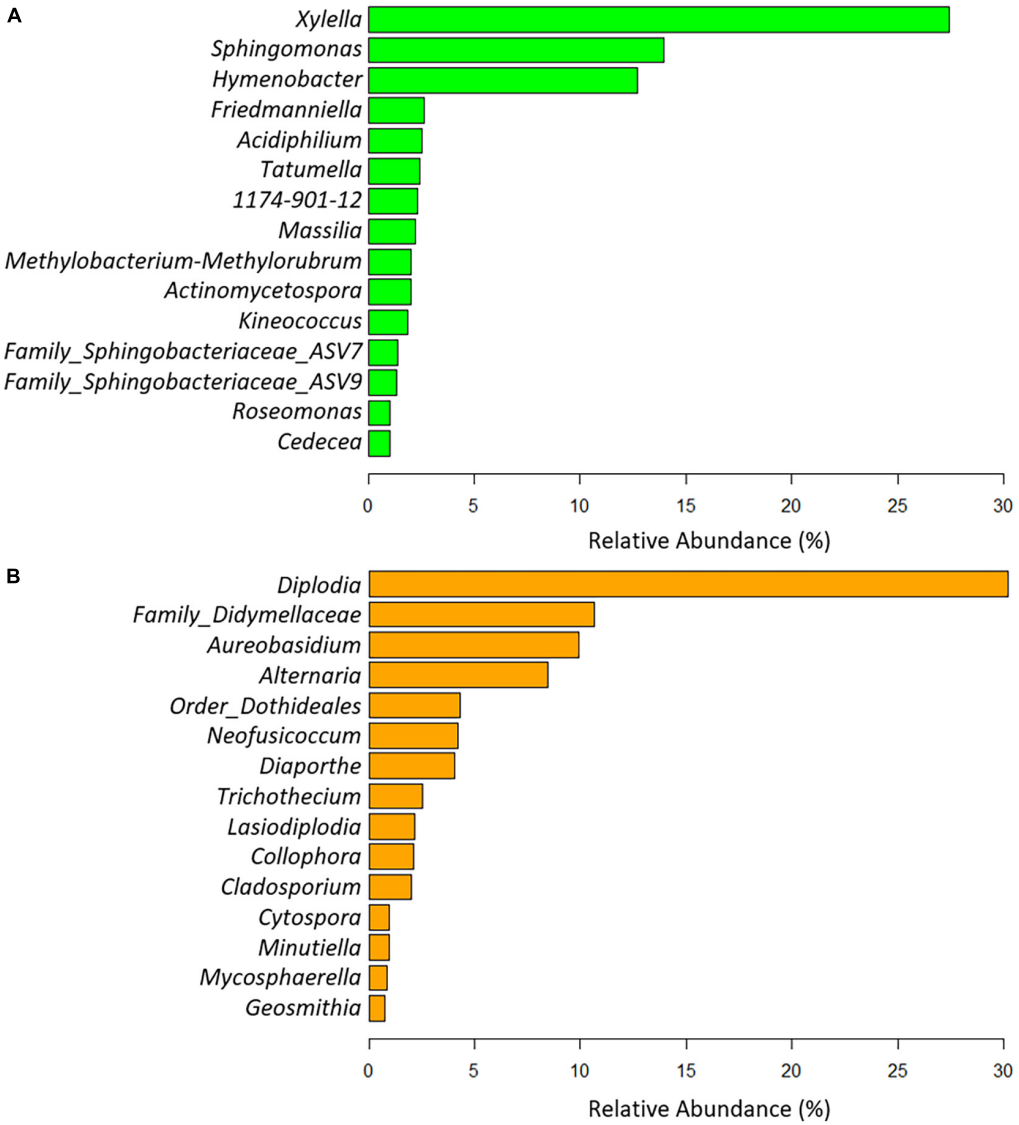

FIGURE 4 | Global relative bacterial **(A)** and fungal **(B)** taxa abundance at the genus level present in the xylem of almond trees for all experimental combinations evaluated in the study.

Co-occurrence Network Inference Analysis

Network analysis indicated aggregation or exclusion interactions between the four ASVs of *X. fastidiosa* identified with the different bacterial and fungal taxa detected in the xylem vessels of almond trees. The fungal phyla Ascomycota and Basidiomycota showed negative interactions within the network, whereas *X. fastidiosa* showed exclusion mainly with the phylum Ascomycota (**Figure 8A**) and a negative interaction mainly with Proteobacteria, and more specifically with *Sphingomonas* (**Supplementary Figure 5A**). Interestingly, the ASVs of *Diplodia* and *Pringsheimia* showed the greatest number of negative interactions (35 and 17, respectively) among all the microorganisms, whereas a member of the Family Acetobacteraceae and *Sphingomonas* showed the greatest number of positive associations (52 and 41, respectively) (data not shown).

On the other hand, when analyzing only bacterial communities, a cluster of positive interactions was found among the four identified *X. fastidiosa* ASVs, and negative interactions were found between *X. fastidiosa* ASVs and a total of 22 ASVs corresponding to the genera *Sphingomonas*, *1174-901-12*, a member of the family Solirubrobacteraceae, *Abditibacterium*, *Methylobacterium–Methylorubrum*, *Modestobacter*, and *Xylophilus* (**Supplementary Figure 5A**), with the four first genera being the most strongly and negatively connected (**Figure 8B**). Remarkably, only positive interactions between different ASVs were found in the network analysis after

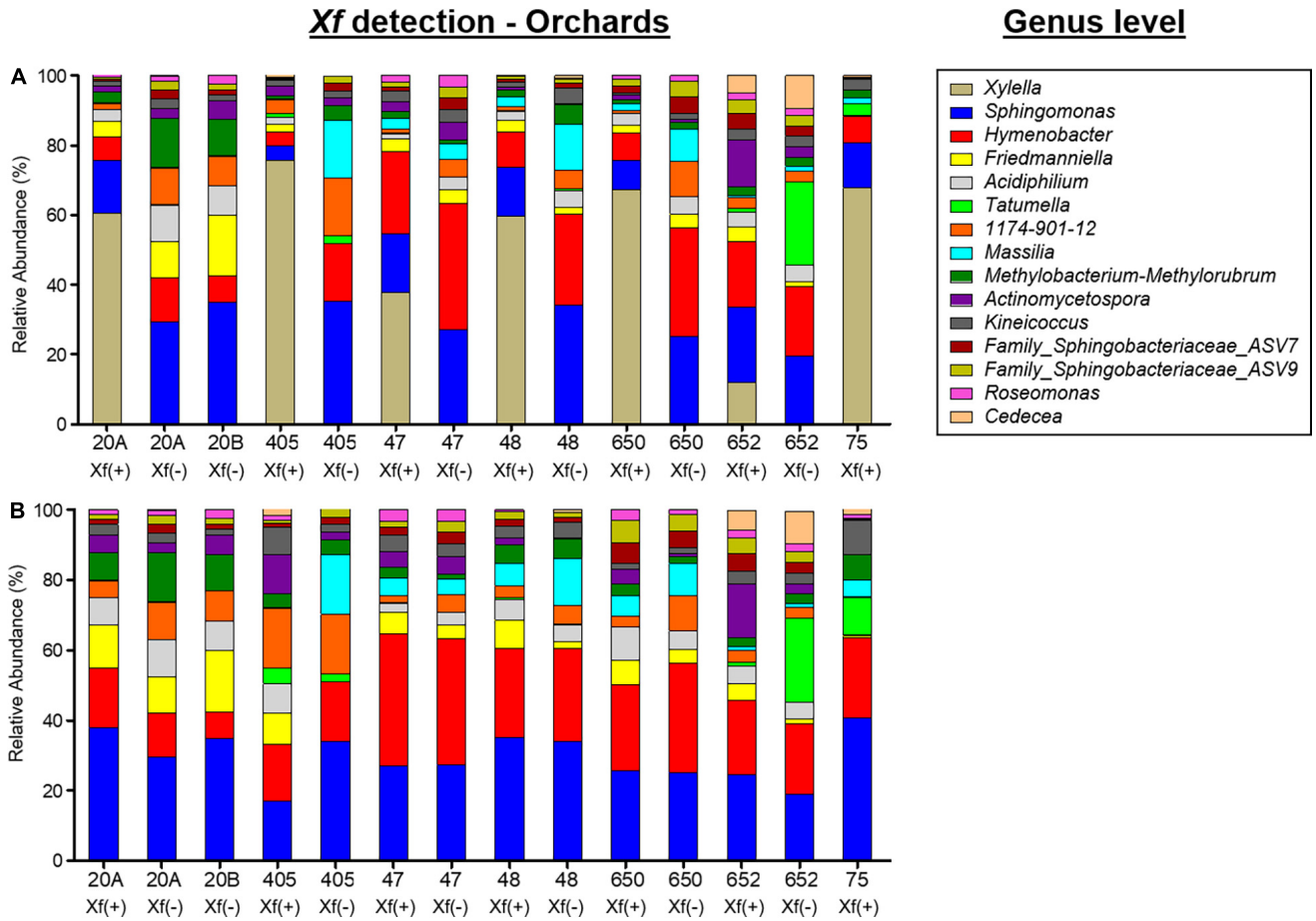

FIGURE 5 | Bar plots showing the relative abundance of bacterial taxa at the genus level in the xylem of almond trees sampled in different orchards in Alicante province before **(A)** or after **(B)** the removal of *Xylella fastidiosa* ASVs from the data set. *X. fastidiosa* (+) and *X. fastidiosa* (–) refer to *X. fastidiosa*-infected or non-infected almond trees, respectively.

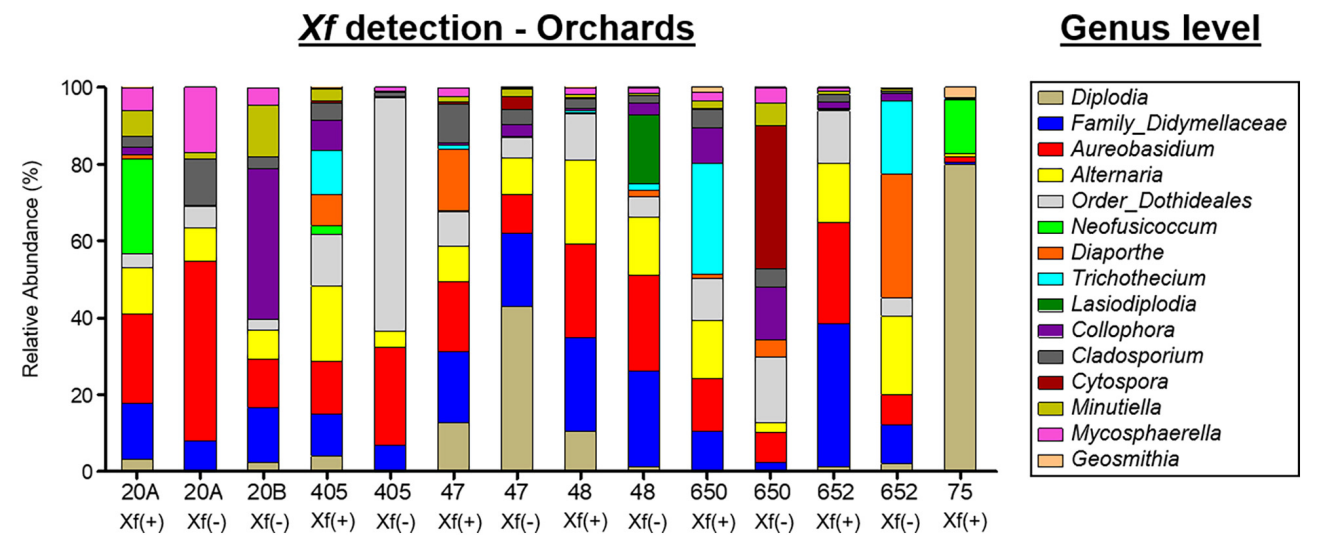

FIGURE 6 | Bar plots showing the relative abundance of fungal taxa at the genus level present in the xylem of almond trees sampled in different orchards in Alicante province. *X. fastidiosa* (+) and *X. fastidiosa* (–) refer to *Xylella fastidiosa*-infected or non-infected almond trees, respectively.

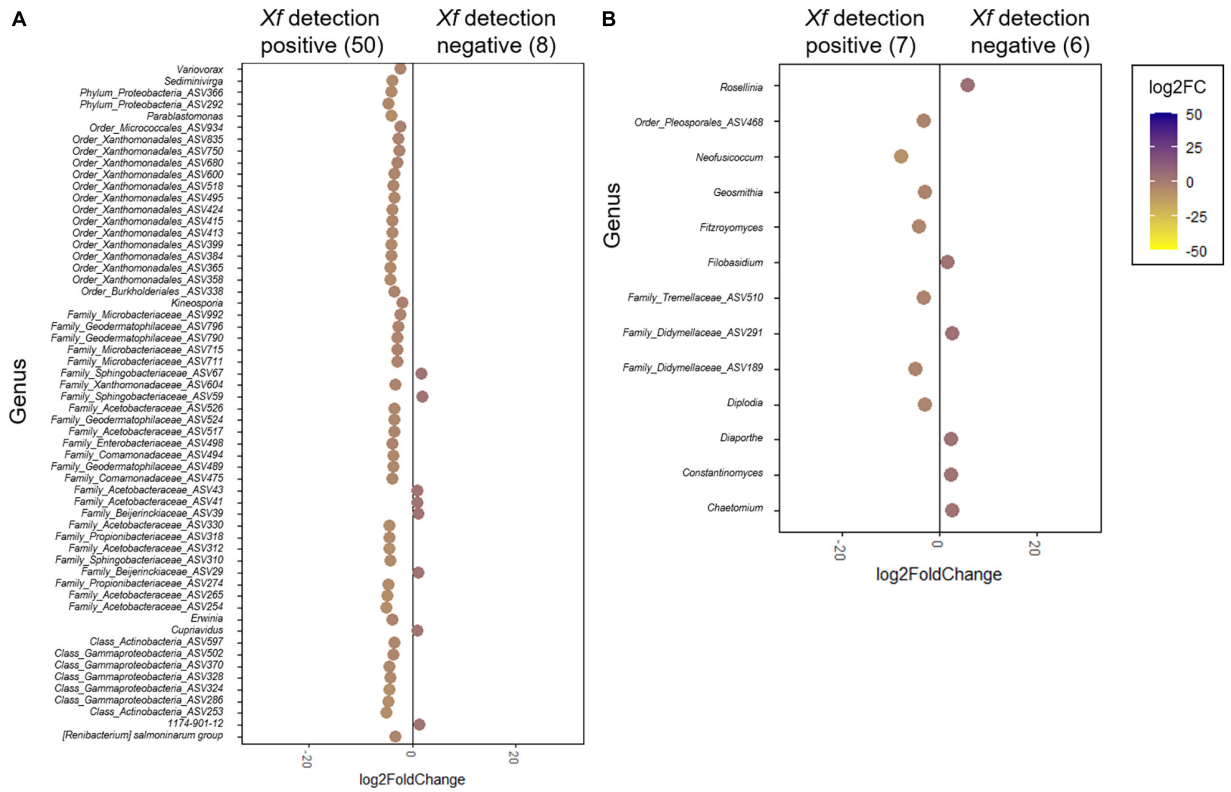

FIGURE 7 | DESeq2 analysis of differentially enriched bacterial **(A)** and fungal **(B)** genera present in the xylem of *Xylella fastidiosa*-qPCR negative and positive almond trees sampled in different orchards in Alicante province. The color scale bar indicates log2 fold change. Only significant genera ($p < 0.05$) are shown.

removing *X. fastidiosa* ASVs from the data set (**Figure 8C** and **Supplementary Figure 5C**). Overall, nine keystone species, the ASV members of the families Acetobacteraceae and Beijerinckiaceae, *Sphingomonas*, *Acidiphilium*, *Friedmaniella*, *Hymenobacter*, and *Methylobacterium–Methylorubrum* with positive interactions and *Diplodia* and *Modestobacter* with negative interactions, were predicted based on the network parameters of high closeness and degree, and low betweenness centrality (**Supplementary Table 2**).

DISCUSSION

This study describes for the first time the endophytic bacterial and fungal communities colonizing the xylem vessels of almond trees using a metabarcoding approach, and describes the changes in the diversity and structural profile of those microbial communities associated with the infection of the tree by *X. fastidiosa.* The study has also revealed the existence of positive and negative associations between xylem-inhabiting microorganisms and the presence of this plant pathogenic bacterium. These results establish the bases to unravel the impacts of *X. fastidiosa* infection on the xylem microbial communities and to identify potential microorganisms that change in response to infection by *X. fastidiosa* or that are predominant in non-infected trees that grow in orchards with high inoculum pressure from the pathogen.

Several studies described the microbial communities inhabiting different ecological niches of almond trees, such as the phyllosphere (Izhaki et al., 2013), flowers (Aleklett et al., 2014), and their nectar (Fridman et al., 2012), or the soil associated to almond roots (Theofel et al., 2021). However, xylem vessels, as a plant niche with very specific characteristics, have been overlooked despite their decisive role in plant growth, as it provides an interconnected route for the circulation and transport of micronutrients and macronutrients (White, 2012) and is an optimal niche for the colonization of microbial endophytes (Malfanova et al., 2013).

As expected, using NGS analysis we identified four different ASVs belonging to *X. fastidiosa* that correspond to the subsp. *multiplex* associated to ALSD in the DA of the Valencian Community, in the province of Alicante (Spain) (Arias-Giraldo et al., 2020; Marco-Noales et al., 2021). Additionally, we found good agreement between *X. fastidiosa* reads obtained by NGS analysis and the *Cq* values obtained by the two qPCR protocols used to detect *X. fastidiosa* infection. The results also indicated that Harper qPCR showed greater sensitivity than Francis qPCR. Besides, we observed similar sensitivity of qPCR as compared with NGS analysis for detecting *X. fastidiosa* in asymptomatic trees. In a study comparing the nanopore amplicon sequencing methodology and the qPCR protocol

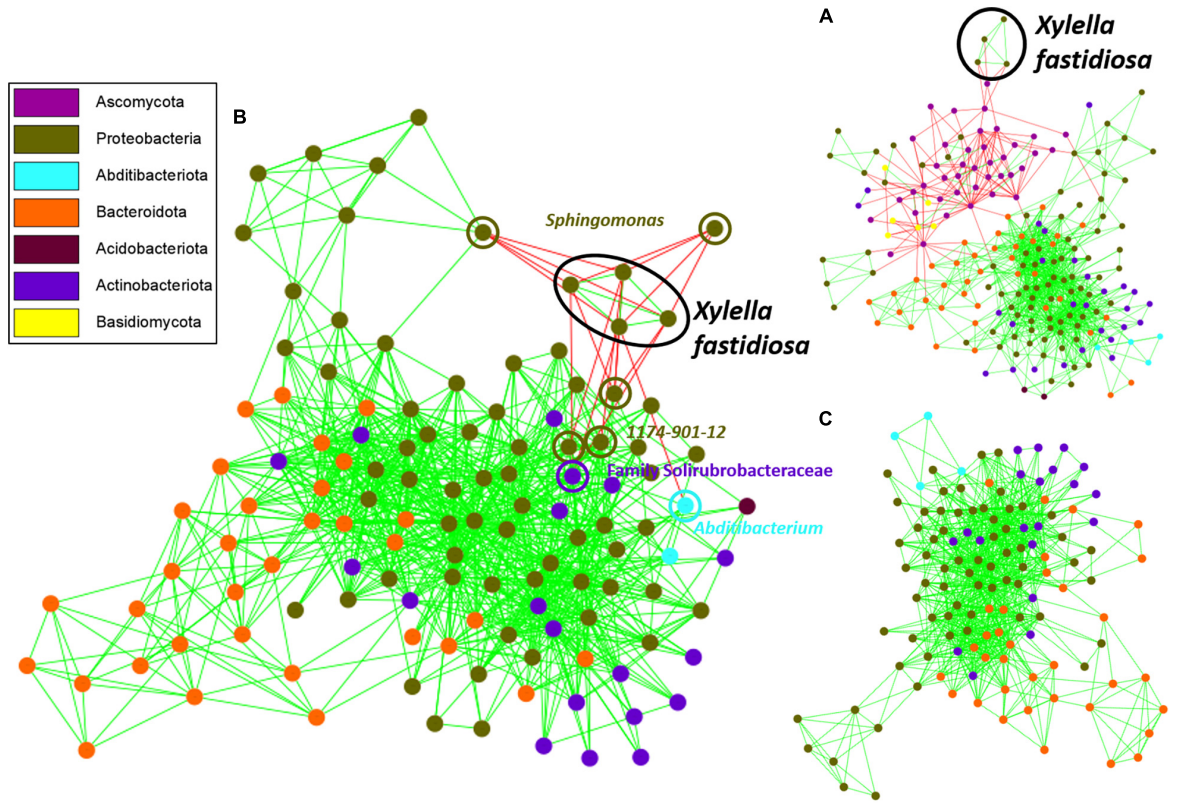

FIGURE 8 | Co-occurrence network inference plot based on the MCODE method showing highly interconnected regions of bacterial and fungal communities **(A)**, or bacteria present in the xylem of almond trees before **(B)** or after **(C)** the removal of *Xylella fastidiosa* ASVs from the data set. Nodes in blue and black represent fungal and bacterial ASVs, respectively, and pink nodes correspond to *X. fastidiosa* ASVs. Copresence (green) and mutual exclusion (red) are shown as the edges between the nodes.

of Francis et al. (2006) on the efficacy of *X. fastidiosa* detection, Faino et al. (2021) found a lower number of samples identified as *X. fastidiosa*-positive using nanopore sequencing, although the percentage of agreement between both approaches was lower than in our study (78.6%). However, they used the whole genome instead of 16S rRNA amplicons for sequencing and a different sequencing platform than those used in our study.

Our metabarcoding results suggest that *X. fastidiosa* infection reshapes almond xylem microbial composition by altering microbial structure and diversity. Thus, *X. fastidiosa* infection was correlated with a reduction in the relative abundance of two of the most predominant bacterial genera inhabiting almond xylem vessels (i.e., *Sphingomonas* and *Hymenobacter*). These bacterial genera have been described as endophytes in other plant species including elm trees (Mocali et al., 2003), maple trees (Wemheuer et al., 2019), rice (Wang et al., 2016), or potato (Tangapo et al., 2018), and more specifically as common xylem inhabitants of woody crops including olive (Anguita-Maeso et al., 2020, 2021a), grapevines (Bruez et al., 2020), and citrus (Ginnan et al., 2020). Additionally, *Sphingomonas* has been described as a bacterium with several functional plant beneficial traits including plant growth promotion and plant protection (Innerebner et al., 2011; Asaf et al., 2020), whereas *Hymenobacter* is a well-known psychrotrophic bacteria involved in plant growth development and bioremediation of heavy metal pollution in natural soils (Dimitrijević et al., 2018; Ubogu and Akponah, 2021).

On the other hand, *X. fastidiosa* infection was also correlated with changes in xylem-associated fungal communities. Thus, *X. fastidiosa* infection was correlated with a general increase of *Diplodia* and *Neofusicoccum,* although this trend was not consistent among the different sampled orchards, which suggest a lower influence of *X. fastidiosa* infection on fungal xylem-associated communities, or that other factors (agronomic practices, climatic conditions, age, or genotype of the tree, etc.) may also play a role. In our study, although we did not have precise information on the age and variety of the sampled trees, we speculated that those factors might have a minor role, since most of orchards sampled were of similar age, and "Marcona" was the most common almond variety grown in the area. Concerning climatic variables, there were small differences among the eight orchards in the study, with annual mean temperature and precipitation ranging from 13.9 to 17.1°C and from 487 to 686 mm, respectively. In the same context within the eight sampled orchards, slight differences in climatic suitability for *X. fastidiosa* establishment have been described (EFSA, 2019b; **Table 1**). Indeed, orchards 20A and

20B, located in Xaló municipality and orchard 75 located in the northeastern part of the municipality of Benissa are classified as highly suitable for the establishment of *X. fastidiosa*, while the remaining five orchards are classified as moderately suitable. Interestingly, the three plots with higher versus moderate suitability for *X. fastidiosa* establishment, present higher values for both mean annual temperature (17–17.1°C vs. 13.9–16.5°C) and the coldest month (9.0–9.4°C vs. 4.9–7.9°C), while they tend to have lower precipitation levels (**Table 1**). This indicated that the environmental conditions in those orchards differ and may affect not only the establishment and further development of *X. fastidiosa*, but also the entire xylem microbiome, and may explain, at least in part, the significant differences in α- and β-diversity measurements found among orchards for both fungal and bacterial communities, which deserves further study.

Diplodia and *Neofusicoccum* have been described as fungal endophytes belonging to the diverse Botryosphaeriaceae family (Slippers et al., 2013; Shetty et al., 2016) and have been found in wood samples of almond trees from Majorca that showed dieback symptoms (Gramaje et al., 2012), as well as in other woody plants, such as olive (Moral et al., 2010), grapevine (Gramaje and Armengol, 2011), mangrove (Osorio et al., 2017), and eucalyptus trees (Barradas et al., 2016). The procedure used for xylem microbiome extraction by macerating structural xylem tissues may explain, in part, why those fungi that are not common inhabitants of the xylem vessels were found. Additionally, although these genera include well-known pathogenic species, members of the genus *Neofusicoccum* are often symbiotically associated with different plant species and are involved in functions related to the response to environmental factors and internal signals that can modulate the production of secondary metabolites by the host (Salvatore et al., 2021). Interestingly, the two orchards sampled in Benissa, although showing an incidence (72 and 44%) and ALSD severity (1.51 and 0.78) similar to other sampled plots, included most of the trees with a higher severity score [i.e., ($2 < DS \leq 3$)], which can be related to a more advanced stage or earlier infection by *X. fastidiosa* in those plots (Moralejo et al., 2020).

In parallel to the results described above, *X. fastidiosa* infection was correlated with a reduction in α-diversity measures estimated by Richness and Shannon indices, although this effect was more pronounced in the α-diversity of xylem-inhabiting bacteria compared to that of fungal populations. The decrease in the relative abundance of specific microbial taxa detected in our study in *X. fastidiosa* trees may be explained by: (i) the displacement of the natural xylem microbiota due to niche exclusion (*X. fastidiosa* colonizes and occludes xylem vessels forming microcolonies); (ii) the secretion by *X. fastidiosa* of specific molecules directly or in outer membrane vesicles with antimicrobial, signaling, and cell wall degrading activity (Feitosa-Junior et al., 2019; de Souza et al., 2020) can induce a direct modification of the xylem microbiome or induce changes if used as nutrient sources; and/or (iii) the triggering of a series of host physiological responses that result in a decrease in the abundance of specific components of the xylem microbiome. Thus, the interaction between *X. fastidiosa* and the plant xylem microbiome is bidirectional and there is still a need to unravel the molecular mechanisms underlying these interactions (Landa et al., 2022). These hypotheses emphasize the need to expand our knowledge on the changes that may take place in xylem microbial communities after infection by vascular plant pathogens (Anguita-Maeso et al., 2021b).

The potential interactions occurring between *X. fastidiosa* and different members of the microbial community into the xylem have been considered by some authors (Deyett et al., 2017; Giampetruzzi et al., 2020; Vergine et al., 2020; Zicca et al., 2020). However, to the best of our knowledge, this study is the first to address interactions between *X. fastidiosa* and microbial composition into the xylem of almond trees *via* network analysis. Among the nine keystone species detected in the co-occurrence network analysis with significant interactions with *X. fastidiosa, Sphingomonas* showed the strongest negative interaction with the pathogen when bacterial and fungal communities were analyzed together. Although this study did not further evaluate the antagonistic activity of *Sphingomonas* against *X. fastidiosa in vitro*, we suggest that it might be worthwhile to assess the biocontrol potential *in planta* of *Sphingonomas* against *X. fastidiosa* covering the major subspecies and STs, because of its determinant position in the network community structure analysis. Although some authors have not found antagonistic activity of *Sphingomonas* against *X. fastidiosa in vitro* (Zicca et al., 2020), it might occur that its antagonistic effect is due to other biocontrol mechanisms rather than antibiosis. Thus, the role of *Sphingomonas* as a biological control agent has been widely studied in other pathosystems, which revealed that substrate competition plays a role in plant protection by *Sphingomonas*. In particular, differences in carbon source profiles have been identified between protecting and non-potecting strains (Innerebner et al., 2011; Wachowska et al., 2013).

This research is pioneering in providing new insights into the characterization of bacterial and fungal communities that colonize the xylem vessels of almond trees. These results can contribute to complement the current knowledge regarding the interaction between *X. fastidiosa* and xylem endophytes to determine the changes correlated with *X. fastidiosa* infection in the xylem-associated microbiome, describing the composition, diversity, and structure of the almond xylem microbial profile in *X. fastidiosa* –infected and non-infected trees. Also, this study provides for the first time the description of significant co-presence and mutual exclusion interactions between *X. fastidiosa* with bacterial and fungal microbial inhabitants of the xylem in almond trees. Some specific limitations can be raised in this study, mainly linked to the sampling of the microbiome in a single season. Thus, for other woody crops, a strong seasonality effect on the diversity and composition of the xylem microbiome has been found for grapes (Deyett and Rolshausen, 2019) and olive (Anguita et al., *unpublished results*). This fact was forced because infected trees were eradicated soon after they were confirmed as positive for *X. fastidiosa* as imposed by legislation (Regulation EU, 2016, 2020). Nevertheless, we consider our results relevant for future studies aimed at identifying xylem-inhabiting microorganisms potentially involved in host tolerance and/or plant defense against xylem-inhabiting pathogens, or may help select key microorganisms that can be tested in planta to determine their ability to suppress ALSD.

DATA AVAILABILITY STATEMENT

The raw sequence data from this study have been submitted to the NCBI database as Sequence Read Archive (SRA) under BioProject accession number: PRJNA800096.

AUTHOR CONTRIBUTIONS

AA-Y, CH, MA-M, and BL: conceived the research and wrote the manuscript. AF, MR-E, and JN-C: selected the field orchards, performed ALSD evaluation, and sampling. MA-M, JN-C, and BL: performed bioinformatics and statistical analyses. AA-Y, CH, CO-G, and MR-E: prepared materials and equipment and performed the qPCR and NGS experiments. JC, EM-N, AF, and JN-C: contributed to reviewing the manuscript and interpreting the results. JC and BL: provided funding. All authors have read and agreed to the published version of the manuscript.

FUNDING

This research was funded by projects AGL2016-75606-R and PID2020-114917RB-I00 (Programa Estatal de I+D Orientado a los Retos de la Sociedad from Spanish Government, the Spanish State Research Agency and FEDER-EU), XF-ACTORS (*X. fastidiosa* Active Containment Through a Multidisciplinary Oriented Research Strategy; grant 727987) and EcoStack (Grant Agreement No. 773554) from the European Union's Horizon 2020 Framework Research Program. AA-Y acknowledges the STM program granted by the COST Action CA16107 EuroXanth, supported by COST (European Cooperation in Science and Technology). Financial support of CYTED network Iber-Xyfas (Ref. 119RT0569) is acknowledged. MA-M is a recipient of a research fellowship BES-2017-082361 from the Spanish Ministry of Economy and Competitiveness and CH is a recipient of a Juan de la Cierva fellowship "Grant IJC2019-040423-I" from the Spanish Ministry of Science and Innovation MCIN/AEI/10.13039/501100011033.

ACKNOWLEDGMENTS

We are grateful for the information provided by the Plant Health Service of the Regional Ministry of Agriculture of the region of Valencia (Spain) on the phytosanitary status of almond orchards in the affected area of Alicante and to TRAGSATEC (Grupo TRAGSA) for their support during the field sampling. M. Montes-Borrego, G. Leon and J.L. Trapero-Casas are also acknowledged for their support during the field sampling. We acknowledge support for the publication fee by the CSIC Open Access Publication Support Initiative through its Unit of Information Resources for Research (URICI).

SUPPLEMENTARY MATERIAL

The Supplementary Material for this article can be found online at: https://www.frontiersin.org/articles/10.3389/fmicb.2022.866085/full#supplementary-material

Supplementary Figure 1 | Linear regression between log [*Xylella fastidiosa* reads] obtained by next-generation sequencing (NGS) sequencing and *Cq* values from the quantitative polymerase chain reaction (qPCR) protocols of Francis et al. (2006) and Harper et al. (2010) obtained from DNA extracted from xylem samples of *X. fastidiosa*-infected almond trees.

Supplementary Figure 2 | Principal coordinate plots of Bray–Curtis and weighted UniFrac distances of bacterial **(A,B)** and fungal communities **(C)** at the amplicon sequence variant (ASV) taxonomic level in the xylem of *Xylella fastidiosa* –qPCR negative and positive almond trees sampled in each orchard in Alicante province. *X. fastidiosa* ASVs were maintained **(A)** or removed **(B)** from the data set before analysis. Points are colored by *X. fastidiosa* detection.

Supplementary Figure 3 | DESeq2 analysis of differentially enriched bacterial genera present in the xylem of *Xylella fastidiosa*–qPCR negative and positive almond trees in the different sampled orchards in Alicante province. The color scale bar indicates log2 fold change. Only significant genera ($p < 0.05$) are shown.

Supplementary Figure 4 | DESeq2 analysis of differentially enriched fungal genera present in the xylem of *Xylella fastidiosa*–qPCR negative and positive almond trees in the different sampled orchards in Alicante province. The color scale bar indicates log2 fold change. Only significant genera ($p < 0.05$) are shown.

Supplementary Figure 5 | Co-occurrence network inference plot of bacterial and fungal communities **(A)** present in the xylem of almond trees with the presence **(B)** or absence **(C)** of *Xylella fastidiosa* ASVs in the data set before analysis. Copresence (green) and mutual exclusion (red) are shown as the edges between the nodes.

REFERENCES

Aleklett, K., Hart, M., and Shade, A. (2014). The microbial ecology of flowers: an emerging frontier in phyllosphere research. *Botany* 92, 253–266. doi: 10.1139/cjb-2013-0166

Almeida, R. P. P., and Nunney, L. (2015). How do plant diseases caused by *Xylella fastidiosa* Emerge? *Plant Dis.* 99, 1457–1467. doi: 10.1094/PDIS-02-15-0159-FE

Anguita-Maeso, M., Haro, C., Montes-Borrego, M., De La Fuente, L., Navas-Cortés, J. A., and Landa, B. B. (2021a). Metabolomic, ionomic and microbial characterization of olive xylem sap reveals differences according to plant age and genotype. *Agronomy* 11:1179. doi: 10.3390/agronomy11061179

Anguita-Maeso, M., Olivares-García, C., Haro, C., Imperial, J., Navas-Cortés, J. A., and Landa, B. B. (2020). Culture-dependent and culture-independent characterization of the olive xylem microbiota: effect of sap extraction methods. *Front. Plant Sci.* 10:1708. doi: 10.3389/fpls.2019.01708

Anguita-Maeso, M., Trapero-Casas, J. L., Olivares-García, C., Ruano-Rosa, D., Palomo-Ríos, E., Jiménez-Díaz, R. M., et al. (2021b). *Verticillium dahliae* inoculation and in vitro propagation modify the xylem microbiome and disease reaction to *Verticillium wilt* in a wild olive genotype. *Front. Plant Sci.* 12:250. doi: 10.3389/fpls.2021.632689

Arias-Giraldo, L. F. F., Giampetruzzi, A., Metsis, M., Marco-Noales, E., Imperial, J., Velasco-Amo, M. P., et al. (2020). Complete circularized genome data of two Spanish strains of *Xylella fastidiosa* (IVIA5235 and IVIA5901) using two hybrid assembly approaches. *Phytopathology* 110, 969–972. doi: 10.1094/PHYTO-01-20-0012-A

Asaf, S., Numan, M., Khan, A. L., and Al-Harrasi, A. (2020). *Sphingomonas*: from diversity and genomics to functional role in environmental remediation and

plant growth. *Crit. Rev. Biotechnol.* 40, 138–152. doi: 10.1080/07388551.2019.1709793

Azevedo, J., Araújo, W. L., and Lacava, P. T. (2016). The diversity of citrus endophytic bacteria and their interactions with *Xylella fastidiosa* and host plants. *Genet. Mol. Biol.* 39, 476–491. doi: 10.1590/1678-4685-GMB-2016-0056

Backman, P. A., and Sikora, R. A. (2008). Endophytes: an emerging tool for biological control. *Biol. Control* 46, 1–3. doi: 10.1016/j.biocontrol.2008.03.009

Bader, G. D., and Hogue, C. W. V. (2003). An automated method for finding molecular complexes in large protein interaction networks. *BMC Bioinform.* 4:2. doi: 10.1186/1471-2105-4-2

Barberán, A., Bates, S. T., Casamayor, E. O., and Fierer, N. (2012). Using network analysis to explore co-occurrence patterns in soil microbial communities. *ISME J.* 6, 343–351. doi: 10.1038/ismej.2011.119

Barradas, C., Phillips, A. J. L., Correia, A., Diogo, E., Bragança, H., and Alves, A. (2016). Diversity and potential impact of Botryosphaeriaceae species associated with *Eucalyptus globulus* plantations in Portugal. *Eur. J. Plant Pathol.* 146, 245–257. doi: 10.1007/s10658-016-0910-1

Bruez, E., Vallance, J., Gautier, A., Laval, V., Compant, S., Maurer, W., et al. (2020). Major changes in grapevine wood microbiota are associated with the onset of esca, a devastating trunk disease. *Environ. Microbiol.* 22, 5189–5206. doi: 10.1111/1462-2920.15180

Callahan, B. J., McMurdie, P. J., Rosen, M. J., Han, A. W., Johnson, A. J. A., and Holmes, S. P. (2016). DADA2: High-resolution sample inference from Illumina amplicon data. *Nat. Methods* 13, 581–583. doi: 10.1038/nmeth.3869

Camino, C., Calderón, R., Parnell, S., Dierkes, H., Chemin, Y., Román-Écija, M., et al. (2021). Detection of *Xylella fastidiosa* in almond orchards by synergic use of an epidemic spread model and remotely sensed plant traits. *Remote Sens. Environ.* 260:112420. doi: 10.1016/j.rse.2021.112420

Chatterjee, S., Almeida, R. P. P., and Lindow, S. (2008). Living in two worlds: the plant and insect lifestyles of *Xylella fastidiosa*. *Annu. Rev. Phytopathol.* 46, 243–271. doi: 10.1146/annurev.phyto.45.062806.094342

Coletta-Filho, H., Castillo, A. I., Laranjeira, F. F., de Andrade, E. C., Silva, N. T., de Souza, A. A., et al. (2020). Citrus variegated chlorosis: an overview of 30 years of research and disease management. *Trop. Plant Pathol.* 45, 175–191. doi: 10.1007/s40858-020-00358-5

Delbianco, A., Gibin, D., Pasinato, L., and Morelli, M. (2022). European Food Safety Authority (EFSA). Update of the *Xylella* spp. host plant database – systematic literature search up to 30 June 2021. *EFSA J.* 20:e07039. doi: 10.2903/j.efsa.2022.7039

Denancé, N., Legendre, B., Briand, M., Olivier, V., de Boisseson, C., Poliakoff, F., et al. (2017). Several subspecies and sequence types are associated with the emergence of *Xylella fastidiosa* in natural settings in France. *Plant Pathol.* 66, 1054–1064. doi: 10.1111/ppa.12695

Deyett, E., Pouzoulet, J., Yang, J. –I., Ashworth, V. E., Castro, C., Roper, M. C., et al. (2019). Assessment of Pierce's disease susceptibility in *Vitis vinifera* cultivars with different pedigrees. *Plant Pathol.* 68, 1079–1087. doi: 10.1111/ppa.13027

Deyett, E., and Rolshausen, P. E. (2019). Temporal dynamics of the Sap microbiome of grapevine under high Pierce's disease pressure. *Front. Plant Sci.* 10:1246. doi: 10.3389/fpls.2019.01246

Deyett, E., Roper, M. C., Ruegger, P., Yang, J.-I., Borneman, J., and Rolshausen, P. E. (2017). Microbial landscape of the grapevine endosphere in the context of Pierce's disease. *Phytobiomes J.* 1, 138–149. doi: 10.1094/PBIOMES-08-17-0033-R

de Souza, J. B., Almeida-Souza, H. O., Zaini, P. A., Alves, M. N., de Souza, A. G., Pierry, P. M., et al. (2020). *Xylella fastidiosa* subsp. *pauca* strains Fb7 and 9a5c from citrus display differential behavior, secretome, and plant virulence. *Int. J. Mol. Sci.* 21:6769. doi: 10.3390/ijms21186769

Dimitrijević, S., Pavlović, M., Maksimović, S., Ristić, M., Filipović, V., Antonović, D., et al. (2018). Plant growth-promoting bacteria elevate the nutritional and functional properties of black cumin and flaxseed fixed oil. *J. Sci. Food Agric.* 98, 1584–1590. doi: 10.1002/jsfa.8631

Doty, S. L. (2017). "Functional importance of the plant microbiome: implications for agriculture, forestry and bioenergy," in *Functional Importance of the Plant Microbiome Implications for Agriculture, Forestry and Bioenergy*, Vol. 178, ed. S. L. Doty (Cham: Springer), 1–111. doi: 10.1007/978-3-319-65897-1

EFSA (2018). Updated pest categorisation of *Xylella fastidiosa*. *EFSA J.* 16:e05357. doi: 10.2903/j.efsa.2018.5357

EFSA (2019a). Effectiveness of in planta control measures for *Xylella fastidiosa*. *EFSA J.* 17:e05666. doi: 10.2903/j.efsa.2019.5666

EFSA (2019b). Update of the scientific opinion on the risks to plant health posed by *Xylella fastidiosa* in the EU territory. *EFSA J.* 17:5665. doi: 10.2903/j.efsa.2019.5665

EPPO (2019). PM 7/24 (4) *Xylella fastidiosa*. *EPPO Bull.* 49, 175–227.

Regulation EU (2016). Regulation (EU) 2016/2031 of the European Parliament of the Council of 26 October 2016 on Protective Measures Against pests of plants, Amending Regulations (EU) No 228/2013, (EU) No 652/2014 and (EU) No 1143/2014 of the European Parliament and of the Council and repealing Council Directives 69/464/EEC, 74/647/EEC, 93/85/EEC, 98/57/EC, 2000/29/EC, 2006/91/EC and 2007/33/EC. Available online at: https://eur-lex.europa.eu/legal-content/EN/TXT/?uri=CELEX%3A32016R2031. (accessed November 9, 2022).

Regulation EU (2019). Commission Delegated Regulation (EU) 2019/1702 of 1 August 2019 Supplementing Regulation (EU) 2016/2031 of the European Parliament and of the Council by Establishing the List of Priority Pests. Available online at: https://eur-lex.europa.eu/legal-content/EN/TXT/?uri=CELEX%3A32019R1702. (accessed November 9, 2022).

Regulation EU (2020). Commission Implementing Regulation (EU) 2020/1201 of 14 August 2020 of the European Parliament and of the Council as Regards Measures to Prevent the Introduction into and the Spread Within the Union of *Xylella fastidiosa* (Wells et al.). Available online at: https://eur-lex.europa.eu/legal-content/en/TXT/?uri=CELEX:32020R1201.

Faino, L., Scala, V., Albanese, A., Modesti, V., Grottoli, A., Pucci, N., et al. (2021). Nanopore sequencing for the detection and identification of *Xylella fastidiosa* subspecies and sequence types from naturally infected plant material. *Plant Pathol.* 70, 1860–1870. doi: 10.1111/ppa.13416

Faust, K., and Raes, J. (2016). CoNet app: inference of biological association networks using Cytoscape. *F1000Res.* 5:1519. doi: 10.12688/f1000research.9050.2

Faust, K., Sathirapongsasuti, J. F., Izard, J., Segata, N., Gevers, D., Raes, J., et al. (2012). Microbial co-occurrence relationships in the human microbiome. *PLoS Comput. Biol.* 8:e1002606. doi: 10.1371/journal.pcbi.1002606

Fausto, C., Mininni, A. N., Sofo, A., Crecchio, C., Scagliola, M., Dichio, B., et al. (2018). Olive orchard microbiome: characterisation of bacterial communities in soil-plant compartments and their comparison between sustainable and conventional soil management systems. *Plant Ecol. Divers.* 11, 597–610. doi: 10.1080/17550874.2019.1596172

Feitosa-Junior, O. R., Stefanello, E., Zaini, P. A., Nascimento, R., Pierry, P. M., Dandekar, A. M., et al. (2019). Proteomic and metabolomic analyses of *Xylella fastidiosa* OMV-enriched fractions reveal association with virulence factors and signaling molecules of the DSF family. *Phytopathology* 109, 1344–1353. doi: 10.1094/PHYTO-03-19-0083-R

Francis, M., Lin, H., Rosa, J. C.-L., Doddapaneni, H., and Civerolo, E. L. (2006). Genome-based PCR primers for specific and sensitive detection and quantification of *Xylella fastidiosa*. *Eur. J. Plant Pathol.* 115, 203–213. doi: 10.1007/s10658-006-9009-4

Fridman, S., Izhaki, I., Gerchman, Y., and Halpern, M. (2012). Bacterial communities in floral nectar: bacterial communities in floral nectar. *Environ. Microbiol. Rep.* 4, 97–104. doi: 10.1111/j.1758-2229.2011.00309.x

Giampetruzzi, A., Baptista, P., Morelli, M., Cameirão, C., Lino Neto, T., Costa, D., et al. (2020). Differences in the endophytic microbiome of olive cultivars infected by *Xylella fastidiosa* across seasons. *Pathogens* 9:723. doi: 10.3390/pathogens9090723

Giampetruzzi, A., Saponari, M., Almeida, R. P. P., Salwa, E., Donato, B., Giuliana, L., et al. (2017). Complete genome sequence of the olive-infecting strain *Xylella fastidiosa* subsp. *pauca* De Donno. *Genome Announc.* 5:e00569–17. doi: 10.1128/genomeA.00569-17

Ginnan, N. A., Dang, T., Bodaghi, S., Ruegger, P. M., McCollum, G., England, G., et al. (2020). Disease-induced microbial shifts in citrus indicate microbiome-derived responses to huanglongbing across the disease severity spectrum. *Phytobiomes J.* 4, 375–387. doi: 10.1094/PBIOMES-04-20-0027-R

Gramaje, D., Agustí-Brisach, C., Pérez-Sierra, A., Moralejo, E., Olmo, D., Mostert, L., et al. (2012). Fungal trunk pathogens associated with wood decay of almond trees on Mallorca (Spain). *Persoonia* 28, 1–13. doi: 10.3767/003158512X626155

Gramaje, D., and Armengol, J. (2011). Fungal trunk pathogens in the grapevine propagation process: potential inoculum sources, detection, identification, and management strategies. *Plant Dis*. 95, 1040–1055. doi: 10.1094/PDIS-01-11-0025

Haro, C., Anguita-Maeso, M., Metsis, M., Navas-Cortés, J. A., and Landa, B. B. (2021). Evaluation of established methods for DNA extraction and primer pairs targeting 16S rRNA gene for bacterial microbiota profiling of olive xylem sap. *Front. Plant Sci.* 12:296. doi: 10.3389/fpls.2021.640829

Harper, S. J., Ward, L. I., and Clover, G. R. G. (2010). Development of LAMP and real-time PCR methods for the rapid detection of *Xylella fastidiosa* for quarantine and field applications. *Phytopathology* 100, 1282–1288. doi: 10.1094/PHYTO-06-10-0168

Hopkins, D. L., and Purcell, A. H. (2002). *Xylella fastidiosa*: cause of Pierce's disease of grapevine and other emergent diseases. *Plant Dis.* 86, 1056–1066. doi: 10.1094/PDIS.2002.86.10.1056

Innerebner, G., Knief, C., and Julia, A. V. (2011). Protection of *Arabidopsis thaliana* against leaf-pathogenic *Pseudomonas syringae* by *Sphingomonas* strains in a controlled model system. *Appl. Environ. Microbiol.* 77, 3202–3210. doi: 10.1128/AEM.00133-11

Izhaki, I., Fridman, S., Gerchman, Y., and Halpern, M. (2013). Variability of bacterial community composition on leaves between and within plant species. *Curr. Microbiol.* 66, 227–235. doi: 10.1007/s00284-012-0261-x

Jacques, M.-A., Denancé, N., Legendre, B., Morel, E., Briand, M., Mississipi, S., et al. (2016). New coffee plant-infecting *Xylella fastidiosa* variants derived via homologous recombination. *Appl. Environ. Microbiol.* 82, 1556–1568. doi: 10.1128/AEM.03299-15

Karger, D. N., Conrad, O., Böhner, J., Kawohl, T., Kreft, H., Soria-Auza, R. W., et al. (2017). Climatologies at high resolution for the earth's land surface areas. *Sci. Data* 4:170122. doi: 10.1038/sdata.2017.122

Khan, A. R., Wicaksono, W. A., Ott, N. J., Poret-Peterson, A. T., and Browne, G. T. (2021). Characterization of soils conducive and non-conducive to *Prunus* replant disease. *PLoS One* 16:e0260394. doi: 10.1371/journal.pone.0260394

Lacava, P. T., Araújo, W. L., Marcon, J., Maccheroni, W., and Azevedo, J. L. (2004). Interaction between endophytic bacteria from citrus plants and the phytopathogenic bacteria *Xylella fastidiosa*, causal agent of citrus-variegated chlorosis. *Lett. Appl. Microbiol.* 39, 55–59. doi: 10.1111/j.1472-765X.2004.01543.x

Landa, B. B., Castillo, A. I., Giampetruzzi, A., Kahn, A., Román-Écija, M., Velasco-Amo, M. P., et al. (2020). Emergence of a plant pathogen in associated with multiple intercontinental introductions. *Appl. Environ. Microbiol* 86:e01521–19, doi: 10.1128/AEM.01521-19

Landa, B. B., Saponari, M., Feitosa-Junior, O. R., Giampetruzzi, A., Vieira, F. J. D., Mor, E., et al. (2022). *Xylella fastidiosa*'s relationships: the bacterium, the host plants and the plant microbiome. *New Phytol* 234, 1598–1605. doi: 10.1111/nph.18089

Landa, B., Marco Noales, E., and López, M. M. (2017). *Enfermedades Causadas por la Bacteria "Xylella fastidiosa*. Almería: Cajamar Caja Rural.

Loconsole, G., Saponari, M., Boscia, D., D'Attoma, G., Morelli, M., Martelli, G. P., et al. (2016). Intercepted isolates of *Xylella fastidiosa* in Europe reveal novel genetic diversity. *Eur. J. Plant Pathol.* 146, 85–94. doi: 10.1007/s10658-016-0894-x

Love, M. I., Huber, W., and Anders, S. (2014). Moderated estimation of fold change and dispersion for RNA-seq data with DESeq2. *Genome Biol.* 15:550. doi: 10.1186/s13059-014-0550-8

Malfanova, N., Lugtenberg, B. J. J., and Berg, G. (2013). "Bacterial endophytes: who and where, and what are they doing there?," in *Molecular Microbial Ecology of the Rhizosphere*, Vol. 2, (Hoboken, NJ: John Wiley & Sons, Inc), 391–403. doi: 10.1002/9781118297674.ch36

Mangiafico, S. (2020). *rcompanion: Functions to Support Extension Education Program Evaluation. R Package Version 2.3.25*, 132. Available online at: https://CRAN.R-project.org/package=rcompanion

Marco-Noales, E., Barbé, S., Monterde, A., Navarro, I., Ferrer, A., Dalmau, V., et al. (2021). Evidence that *Xylella fastidiosa* is the causal agent of almond leaf scorch disease in Alicante, mainland Spain (Iberian Peninsula). *Plant Dis.* 105, 3349–3352. doi: 10.1094/PDIS-03-21-0625-SC

Martin, M. (2011). Cutadapt removes adapter sequences from high-throughput sequencing reads. *EMBnet.journal* 17, 10–12. doi: 10.14806/ej.17.1.200

Martinetti, D., and Soubeyrand, S. (2019). Identifying lookouts for epidemio-surveillance: application to the emergence of *Xylella fastidiosa* in France. *Phytopathology* 109, 265–276. doi: 10.1094/PHYTO-07-18-0237-FI

Mocali, S., Bertelli, E., Di Cello, F., Mengoni, A., Sfalanga, A., Viliani, F., et al. (2003). Fluctuation of bacteria isolated from elm tissues during different seasons and from different plant organs. *Res. Microbiol.* 154, 105–114. doi: 10.1016/S0923-2508(03)00031-7

Moral, J., Muñoz-Díez, C., González, N., Trapero, A., and Michailides, T. J. (2010). Characterization and pathogenicity of Botryosphaeriaceae species collected from olive and other hosts in Spain and California. *Phytopathology* 100, 1340–1351. doi: 10.1094/PHYTO-12-09-0343

Moralejo, E., Gomila, M., Montesinos, M., Borràs, D., Pascual, A., Nieto, A., et al. (2020). Phylogenetic inference enables reconstruction of a long-overlooked outbreak of almond leaf scorch disease (*Xylella fastidiosa*) in Europe. *Commun. Biol.* 3:560. doi: 10.1038/s42003-020-01284-7

Morelli, M., García-Madero, J. M., Jos, Á, Saldarelli, P., Dongiovanni, C., Kovacova, M., et al. (2021). *Xylella fastidiosa* in olive: a review of control attempts and current management. *Microorganisms* 9:1771. doi: 10.3390/microorganisms9081771

Nunney, L., Azad, H., and Stouthamer, R. (2019). An experimental test of the host-plant range of nonrecombinant strains of North American *Xylella fastidiosa* subsp. *multiplex*. *Phytopathology* 109, 294–300. doi: 10.1094/PHYTO-07-18-0252-FI

Olmo, D., Armengol, J., León, M., and Gramaje, D. (2016). Characterization and pathogenicity of Botryosphaeriaceae species isolated from almond trees on the island of Mallorca (Spain). *Plant Dis.* 100, 2483–2491. doi: 10.1094/PDIS-05-16-0676-RE

Olmo, D., Nieto, A., Adrover, F., Urbano, A., Beidas, O., Juan, A., et al. (2017). First Detection of *Xylella fastidiosa* infecting cherry (*Prunus avium*) and *Polygala myrtifolia* Plants, in Mallorca island. *Spain. Plant Dis.* 101:1820. doi: 10.1094/PDIS-04-17-0590-PDN

Olmo, D., Nieto, A., Borràs, D., Montesinos, M., Adrover, F., Pascual, A., et al. (2021). Landscape epidemiology of *Xylella fastidiosa* in the Balearic islands. *Agronomy* 11:473. doi: 10.3390/agronomy11030473

Osorio, J. A., Crous, C. J., de Beer, Z. W., Wingfield, M. J., and Roux, J. (2017). Endophytic Botryosphaeriaceae, including five new species, associated with mangrove trees in South Africa. *Fungal Biol.* 121, 361–393. doi: 10.1016/j.funbio.2016.09.004

Pacifico, D., Squartini, A., Crucitti, D., Barizza, E., Lo Schiavo, F., Muresu, R., et al. (2019). The role of the endophytic microbiome in the grapevine response to environmental triggers. *Front. Plant Sci.* 10:1256. doi: 10.3389/fpls.2019.01256

Purcell, A. H. (1980). Environmental therapy for Pierce's disease of grapevines. *Plant Dis.* 64, 388–390. doi: 10.1094/PD-64-388

Rabiey, M., Hailey, L. E., Roy, S. R., Grenz, K., Al-Zadjali, M. A. S., Barrett, G. A., et al. (2019). Endophytes vs tree pathogens and pests: can they be used as biological control agents to improve tree health? *Eur. J. Plant Pathol.* 155, 711–729. doi: 10.1007/s10658-019-01814-y

Salvatore, M. M., Alves, A., and Andolfi, A. (2021). Secondary metabolites produced by *Neofusicoccum* species associated with plants: a review. *Agriculture* 11:149. doi: 10.3390/agriculture11020149

Sanchez, B., Barreiro, J., Soto, I., and Rodriguez, E. (2019). *The Impact Indicator for Priority Pests (I2P2): a Tool for Ranking Pests According to Regulation (EU) 2016/2031*. Maastricht: Europen Union. doi: 10.2760/585182

Saponari, M., Boscia, D., Altamura, G., Loconsole, G., Zicca, S., D'Attoma, G., et al. (2017). Isolation and pathogenicity of *Xylella fastidiosa* associated to the olive quick decline syndrome in southern Italy. *Sci. Rep.* 7:17723. doi: 10.1038/s41598-017-17957-z

Saponari, M., Boscia, D., Nigro, F., and Martelli, G. P. (2013). Identification of DNA sequences related to *Xylella fastidiosa* in oleander, almond and olive trees exhibiting leaf scorch symptoms in Apulia (Southern Italy). *J. Plant Pathol* 95668.

Saponari, M., D'Attoma, G., Abou Kubaa, R., Loconsole, G., Altamura, G., Zicca, S., et al. (2019). A new variant of *Xylella fastidiosa* subspecies *multiplex* detected in different host plants in the recently emerged outbreak in the region of Tuscany, Italy. *Eur. J. Plant Pathol.* 154, 1195–1200. doi: 10.1007/s10658-019-01736-9

Schaad, N. W., Postnikova, E., Lacy, G., Fatmi, M., and Chang, C.-J. (2004). *Xylella fastidiosa* subspecies: *X. fastidiosa* subsp *piercei*, subsp. nov., *X. fastidiosa* subsp.

multiplex subsp. nov., and *X. fastidiosa* subsp. pauca subsp. nov. *Syst. Appl. Microbiol.* 27:763. doi: 10.1078/0723202042369848

Serio, F. D., Bodino, N., Cavalieri, V., Demichelis, S., Carolo, M. D., Dongiovanni, C., et al. (2019). Collection of data and information on biology and control of vectors of *Xylella fastidiosa*. *EFSA Support. Publ* 16:1628E. doi: 10.2903/sp.efsa.2019.EN-1628

Shetty, K. G., Rivadeneira, D. V., Jayachandran, K., and Walker, D. M. (2016). Isolation and molecular characterization of the fungal endophytic microbiome from conventionally and organically grown avocado trees in South Florida. *Mycol. Prog.* 15, 977–986. doi: 10.1007/s11557-016-1219-3

Sicard, A., Zeilinger, A. R., Vanhove, M., Schartel, T. E., Beal, D. J., Daugherty, M. P., et al. (2018). *Xylella fastidiosa*: insights into an emerging plant pathogen. *Annu. Rev. Phytopathol.* 56, 181–202. doi: 10.1146/annurev-phyto-080417-045849

Slippers, B., Boissin, E., Phillips, A. J. L., Groenewald, J. Z., Lombard, L., Wingfield, M. J., et al. (2013). Phylogenetic lineages in the Botryosphaeriales: a systematic and evolutionary framework. *Stud. Mycol.* 76, 31–49. doi: 10.3114/sim0020

Tangapo, A. M., Astuti, D. I., and Aditiawati, P. (2018). Dynamics and diversity of cultivable rhizospheric and endophytic bacteria during the growth stages of cilembu sweet potato (*Ipomoea batatas* L. var. *cilembu*). *Agric. Nat. Resour* 52, 309–316. doi: 10.1016/j.anres.2018.10.003

Theofel, C. G., Williams, T. R., Gutierrez, E., Davidson, G. R., Jay-Russell, M., and Harris, L. J. (2021). Microorganisms move a short distance into an almond orchard from an adjacent upwind poultry operation. *Appl. Environ. Microbiol.* 86:e00573–20. doi: 10.1128/AEM.00573-20

Ubogu, M., and Akponah, E. (2021). "Plant–microbe interactions in attenuation of toxic waste in ecosystem BT –," in *Rhizobiont in Bioremediation of Hazardous Waste*, eds V. Kumar, R. Prasad, and M. Kumar (Singapore: Springer), 131–150. doi: 10.1007/978-981-16-0602-1_7

Vergine, M., Meyer, J. B., Cardinale, M., Sabella, E., Hartmann, M., Cherubini, P., et al. (2020). The *Xylella fastidiosa*-resistant olive cultivar "Leccino" has stable endophytic microbiota during the olive quick decline syndrome (OQDS). *Pathogens* 9:35. doi: 10.3390/pathogens9010035

Wachowska, U., Irzykowski, W., Jêdryczka, M., Stasiulewicz-Paluch, A. D., and Głowacka, K. (2013). Biological control of winter wheat pathogens with the use of antagonistic *Sphingomonas* bacteria under greenhouse conditions. *Biocontrol Sci. Technol.* 23, 1110–1122. doi: 10.1080/09583157.2013.812185

Wang, W., Zhai, Y., Cao, L., Tan, H., and Zhang, R. (2016). Endophytic bacterial and fungal microbiota in sprouts, roots and stems of rice (*Oryza sativa* L.). *Microbiol. Res* 188–189, 1–8. doi: 10.1016/j.micres.2016.04.009

Wemheuer, F., Wemheuer, B., Daniel, R., and Vidal, S. (2019). Deciphering bacterial and fungal endophyte communities in leaves of two maple trees with green islands. *Sci. Rep.* 9:14183. doi: 10.1038/s41598-019-50540-2

White, P. J. (2012). "Chapter 3 – Long-distance transport in the xylem and phloem," in *Marschner's Mineral Nutrition of Higher Plants*, eds H. Marschner and P. Marschner (San Diego: Academic Press), 49–70. doi: 10.1016/B978-0-12-384905-2.00003-0

Zicca, S., De Bellis, P., Masiello, M., Saponari, M., Saldarelli, P., Boscia, D., et al. (2020). Antagonistic activity of olive endophytic bacteria and of *Bacillus* spp. strains against *Xylella fastidiosa*. *Microbiol. Res.* 236:126467. doi: 10.1016/j.micres.2020.126467

Conflict of Interest: The authors declare that the research was conducted in the absence of any commercial or financial relationships that could be construed as a potential conflict of interest.

The reviewer AV declared a shared affiliation with the author EM-N to the handling editor at the time of review.

Publisher's Note: All claims expressed in this article are solely those of the authors and do not necessarily represent those of their affiliated organizations, or those of the publisher, the editors and the reviewers. Any product that may be evaluated in this article, or claim that may be made by its manufacturer, is not guaranteed or endorsed by the publisher.

frontiers | Frontiers in Microbiology

ORIGINAL RESEARCH
published: 15 July 2022
doi: 10.3389/fmicb.2022.907962

Metabolome and Microbiome Signatures in the Leaves of Wild Tea Plant Resources Resistant to *Pestalotiopsis theae*

Yuqian Zhang[1†], *Jie Zhang*[2†], *Changyu Yan*[1], *Meishan Fang*[1], *Lijie Wang*[1], *Yahui Huang*[1*] *and Feiyan Wang*[1*]

[1] College of Horticulture, South China Agricultural University, Guangzhou, China, [2] Henan Key Laboratory of Tea Plant Comprehensive Utilization in South Henan, College of Tea Science, Xinyang Agriculture and Forestry University, Xinyang, China

OPEN ACCESS

Edited by:
Javier Veloso,
University of A Coruña, Spain

Reviewed by:
Ashutosh Pandey,
National Institute of Plant Genome Research (NIPGR), India
Rupali Gupta,
Agricultural Research Organization, Volcani Center, Israel

***Correspondence:**
Feiyan Wang
wfei08@163.com
Yahui Huang
yahuihuangzz@scau.edu.cn

[†] *These authors have contributed equally to this work*

Specialty section:
This article was submitted to Microbe and Virus Interactions with Plants, a section of the journal Frontiers in Microbiology

Received: *30 March 2022*
Accepted: *23 May 2022*
Published: *15 July 2022*

Citation:
Zhang Y, Zhang J, Yan C, Fang M, Wang L, Huang Y and Wang F (2022) Metabolome and Microbiome Signatures in the Leaves of Wild Tea Plant Resources Resistant to Pestalotiopsis theae. Front. Microbiol. 13:907962. doi: 10.3389/fmicb.2022.907962

Tea (*Camellia sinensis*) is an important crop that is mainly used in the food industry. This study using the metabolome and microbiome investigates the resistance factors of wild tea plant resources against tea gray blight disease, which is caused by *Pestalotiopsis theae* (Sawada) Steyaert. According to the interaction analysis of tea leaves and pathogenic fungus, the resistance of wild tea plant resource "R1" (Resistance 1) to tea gray blight disease was significantly higher than that of wild tea plant resource "S1" (Susceptibility 1). The difference between "R1" and "S1" in the metabolome was obvious. There were 145 metabolites that significantly changed. The phenolic acids and flavonoids were the major increased categories in "R1," and it included 4-O-glucosyl-sinapate and petunidin-3-o-(6"-o-p-coumaroyl) rutinoside. Six metabolic pathways were significantly enriched, including aminoacyl-tRNA biosynthesis, flavone, and flavonol biosynthesis. In terms of bacteria, there was no significant difference between "S1" and "R1" in the principal component analysis (PCA). *Pseudomonas* was the major bacterial genus in "S1" and "R1." In addition, each of the two resources had its own predominant genus: *Cellvibirio* was a predominant bacterial genus in "S1" and *Candidatus_competibacter* was a predominant bacterial genus in "R1." In terms of fungi, the fungal diversity and the abundance of the two tea plant resource samples could be distinguished clearly. The fungal component of "S1" was more abundant than that of "R1" at the genus level. *Toxicocladosporium* was the predominant fungal genus of "S1," and *Filobasidium* was the predominant fungal genus of "R1." The relative abundance of *unclassified-norank-norank-Chloroplast* and *Penicillium* were significantly different between "S1" and "R1." *Penicillium* was identified as a potential biomarker. They correlated with some metabolites enriched in "S1" or "R1," such as L-arginine and quercetin-3-o-(2"-o-rhamnosyl) rutinoside-7-o-glucoside. Overall, phenolic acids, flavonoids, and *Penicillium* could be functional metabolites or microorganisms that contributed to improving the resistance of wild tea plant resources to tea gray blight disease.

Keywords: wild tea plant resource, *Camellia sinensis*, *Pestalotiopsis theae*, microbiome, metabolome

INTRODUCTION

Tea (*Camellia sinensis*) is an important crop that is mainly used in the food industry. Metabolites of polyphenols, alkaloids, theanine, tea saponin, and tea polysaccharides are rich in tea, and they have nutrients and functions in healthcare (Yang et al., 1999; Zheng et al., 2011). Tea gray blight disease, a destructive disease caused by the pathogen *Pestalotiopsis theae* (Sawada) Steyaert, can seriously harm tea leaves and the new shoots of the tea plant. Tea gray blight disease can greatly affect the yield of the tea product (Pallavi et al., 2012). The screening of tea plants' disease-resistance resources plays an important role in the tea industry. It is also important to study the disease-resistance mechanisms in tea.

Previous research has shown that tea plants contain many metabolites with obvious antibacterial properties, such as tea polyphenols and alkaloids (Karou et al., 2006; Ma et al., 2020). Primary and secondary metabolites compose a complex metabolic network in plants. Secondary metabolites can be used as biochemical barriers to resist pathogen invasion and can also be used as signal substances to participate in the transduction of plant-disease resistance response (Escobedo-Martínez et al., 2010; El-Hadidy and El-Ati, 2014). Secondary metabolites that are involved in the plant disease resistance process mainly include lignin, callose, and peroxidase (Luna et al., 2011; Schmelz et al., 2011; Ahuja et al., 2012; Sattler and Funnell-Harris, 2013; Yamane, 2013). Lignin, an important physical antimicrobial substance, causes lignification around the cell wall of the necrotic area to prevent the spread of pathogens (Qiao and Dixon, 2011; Sattler and Funnell-Harris, 2013). When the plant is infected by pathogens, callose can be deposited in a large number of plant cells, which is a response to biological stress such as pathogen invasion. Therefore, the accumulation of callose is an indicator of disease resistance in the study of plant disease resistance (Mt et al., 2003; Luna et al., 2011). Tea polyphenols have various biological activities, such as eliminating free radicals, and antioxidation (Liu et al., 2000). Caffeine also has an inhibitory effect on fungi such as *Hydromycetes*, *Rhizopus serpentonum*, and *Rhizopus piriocephalus* (Zhou et al., 2018; Thangaraj et al., 2020).

Microorganisms are important biological resources in nature and are ubiquitous in plants. Some microorganisms cannot cause disease symptoms when they survive in plant tissues. Some endophytic fungi can produce biochemical substances with insecticidal, antimicrobial, antitumor, immunosuppression, antioxidant, and other biological activities. Endophytic microorganisms can be positively involved in the growth and development of plants, for example, by promoting the ability to defend against biotic stresses. *B. subtilis* strain 330-2 produces lytic enzymes (laminarase, cellulase, and protease) that can degrade the cell walls of pathogenic fungi and inhibit the growth of *Rhizoctonia solani Kühn*. The leaf microbiome is very important for the biological control of leaf diseases (Bruisson et al., 2019; Becker et al., 2020). The special epiphytic bacteria around peach leaves have a great influence on the colonization of pathogenic bacteria (Randhawa, 1986). The endophytic fungus extracted from the leaves and stems of *Nyctanthes arbortristsi* can effectively inhibit pathogenic bacteria and fungus. Thus, these microbiomes have been regarded as potential biological resources to improve plant disease resistance. This present research on the metabolome and microbiome of the disease-resistant wild tea resources can further improve the theory of resistance in tea plants.

This study aimed to investigate the potential microorganisms and metabolites that contribute to disease resistance in tea plants via the metabolome and microbiome. The bacterial and fungal compositions of tea leaves were analyzed using 16S rRNA and ITS high-through sequencing, respectively. Additionally, the quadrupole time of flight mass spectrometry (UPLC–QTOF–MS) was applied to identify the metabolic profiles of the resistance and susceptibility of tea plant resources. The results of this research would provide directions for the mining of functional metabolites and microorganisms of tea tree resources against tea gray blight disease. They can also provide theoretical support for the prevention and control of tea gray blight disease, which would help guide the development of breeding tea plants with improved disease resistance.

MATERIALS AND METHODS

Plant Materials

Fresh disease-free leaves from wild tea plant resources "S1" (Susceptibility 1), "R1" (Resistance 1), and "SR1" (Sub-resistance 1) were used for the analysis of disease resistance. The wild tea plant resources were collected in Yuntai Mountain, Anhua County, Yiyang City, Hunan Province, and non-artificial cultivation. "R1," with obvious resistance to tea gray blight disease, and "S1," with susceptibility to tea gray blight disease, were selected for microbiome and metabolome analysis. The tea leaves for the metabolome and microbiome were collected from nine tea plants, cleaned, and disinfected. This disinfection procedure ensures that there were no other microorganisms on the leaves' surface. The disinfection process was as follows: the leaves were washed 2-3 times with sterile water, soaked in 1% NaClO for 1 min, soaked in 75% alcohol for 1 min, and then washed 2-3 times with sterile water. Finally, the sterile water that was used for the last step of washing was cultured for microorganisms to determine whether the leaves' surface was thoroughly disinfected. Three tea plants were taken as one biological replicate, and three replicates of "S1" and "R1" were used for the microbiome and metabolome analysis.

Resistance Phenotype to *Pestalotiopsis theae*

The third leaves of the three candidate tea plant resources were collected. After surface cleaning and disinfection, they were moisturized and placed in a plastic box. Fungal samples, 5 mm in diameter, were selected from the pathogenic fungus plate, cultivated for 5 days, and inoculated on the leaves. After inoculation for 24 h, the fungal samples were removed and the cultivation of leaves continued, which were observed for the formation of leaf spots. The diameters of the disease spots at different time points were measured with vernier calipers.

Widely Targeted Metabolomics

The tea samples were freeze-dried with a vacuum freeze-dryer (Scientz-100F). The metabolite extraction method was based on Wang et al. (2020). The extracts were filtrated (SCAA-104, 0.22 μm pore size; ANPEL, Shanghai, China) before UPLC-MS/MS analysis.

For UPLC conditions and ESI-Q TRAP-MS/MS processing, the sample extracts were analyzed using the UPLC-ESI-MS/MS system (UPLC, SHIMADZU Nexera X2; MS, Applied Biosystems 4500 Q TRAP) equipped with a C18 column (Agilent SB-C18, 1.8 μm, 2.1 ×100 mm). The mobile phase consisted of solvent A, pure water with 0.1% formic acid, and solvent B, acetonitrile with 0.1% formic acid. The measurement procedure of the tea sample was based on Chen et al. (2013). Linear ion trap (LIT) and triple quadrupole (QQQ) scans were acquired on a triple quadrupole-linear ion trap mass spectrometer, AB4500 Q TRAP UPLC/MS/MS System, equipped with an ESI Turbo Ion-Spray interface, and controlled using Analyst 1.6.3 software (AB Sciex, Framingham, MA, USA). The ESI source operation parameters were based on Wang et al. (2020).

For UPLC-MS/MS baseline data analysis, unsupervised PCA was performed using the prcomp function in R. Data were assessed for unit variance prior to unsupervised PCA. The hierarchical cluster analysis (HCA) results of samples and metabolites were presented as heatmaps with dendrograms, while Pearson correlation coefficients (PCC) between samples were calculated using the cor-function in R and presented only as heatmaps. Significantly changed metabolites between the control ("S1") and treatment ("R1") groups were determined by VIP $\geq$ 1 and absolute Log_2FC (fold change) $\geq$ 1. VIP values were derived from the OPLS-DA result, which also contains score plots and permutation plots. To avoid overfitting, a permutation test (200 permutations) was performed. The identified metabolites were annotated using the KEGG compound database (http://www.kegg.jp/kegg/compound/). The annotated metabolites were subsequently associated with the KEGG pathway database (https://www.kegg.jp/kegg/pathway.html).

Microbiome Profile of Tea Leaf Samples

The genomic DNA of the microbial community was extracted from the tea leaf sample using FastDNA® Spin Kit for Soil (MP Biomedicals, USA) as directed by the manufacturer. The hypervariable region V5-V7 of the bacterial 16S rRNA gene and the fungal ITS gene were amplified with primer pairs 799F (5'-AACMGGATTAGATACCCKG-3') and 1193R (5'-ACGTCATCCCCAC CTTCC-3'), and ITS1F (5'-CTTGGTCATTTAGAGGAAGTAA-3') and ITS2R (5'-GCTGCGTTCTTC ATCGATGC-3'), respectively. The resulting PCR products of the 16S rRNA and ITS gene were extracted and purified. Following standard protocols, the Illumina MiSeq PE300 (Illumina, USA) platform was used for sequencing by Majorbio Bio-Pharm Technology Co. Ltd. (Shanghai, China). The sequenced results were analyzed through the Majorbio Cloud Platform (https://www.majorbio.com). The sequences were demultiplexed and quality-filtered using QIIME (version 1.9.1) with some criteria. The criteria reference was Zhang et al. (2018). The bioinformatics procedure is as follows: in-house Perl scripts were used to analyze the alpha- and beta-diversity. Ribosomal Database Project (RDP) was used to annotate the taxonomic information from OTUs (Cole et al., 2014). Significant differences between the two groups of samples were evaluated using the paired Student's *t*-test in the a-diversity indices. Taxonomical and functional differences between the two groups of samples were analyzed using the STAMP 2.1.3 software (Parks et al., 2014), and the *p*-values were calculated via Welch's *t*-test. LEfSe analysis was performed to identify the most differentially abundant taxa between the two groups of samples (Segata et al., 2011), and the most discriminant taxa were distinguished by linear discriminant analysis (LDA) score > 2 and $p < 0.05$. Differences in relative taxa abundance between the two groups of samples were calculated using a non-parametric Wilcoxon rank-sum test. Taxa-relative abundance in the difference between the two groups of samples was calculated by a non-parametric Wilcoxon rank-sum test. Population differences were analyzed with a unidirectional ANOVA. $p < 0.05$ was deemed statistically significant.

Statistical Analysis

All statistical analyses have been carried out using SPSS 22 statistics. The differences between the control ("S1") and treatment groups ("R1") were analyzed using the Student *t*-tests. Statistical significance was assessed by $p < 0.05$. Correlations between the microbiotas and metabolites were analyzed by Spearman correlation analysis.

RESULTS

Resistance Phenotypes to *Pestalotiopsis theae*

The interaction analysis results of the third tea leaves and the tea gray blight pathogen showed that the wild tea plant resource "R1" had obvious resistance to tea gray blight disease, and no obvious disease spots were found in the leaves during the whole infection cycle (**Figure 1A**). Tea plant resource "S1" was sensitive to tea gray blight disease. On the 6th day of infection, the leaves showed obvious browning (**Figure 1**). On the 12th day, the "S1" leaves were dead (**Figure 1**). The resistance of the tea plant resource "SR1" to tea gray blight disease was between those of "S1" and "R1" (**Figure 1**). Consequently, "S1" and "R1" were selected for subsequent analysis of the microbiome and metabolome to obtain differences in microbial diversity and metabolites between "S1" and "R1."

Metabolism Differences Between the Two Wild Resources

The tea leaf samples were analyzed using UHPLC-MS/MS in positive and negative modes (**Supplementary Figure 1A**). A typical TIC plot of one QC sample and the multipeak detection plot of metabolites in the multiple reaction monitoring (MRM) modes were illustrated in **Supplementary Figures 1B,C**. The TIC plot represents a continuous description of the intensity sum of all ions in the mass spectrum at different time points. The multipeak detection plot of metabolites in the MRM mode

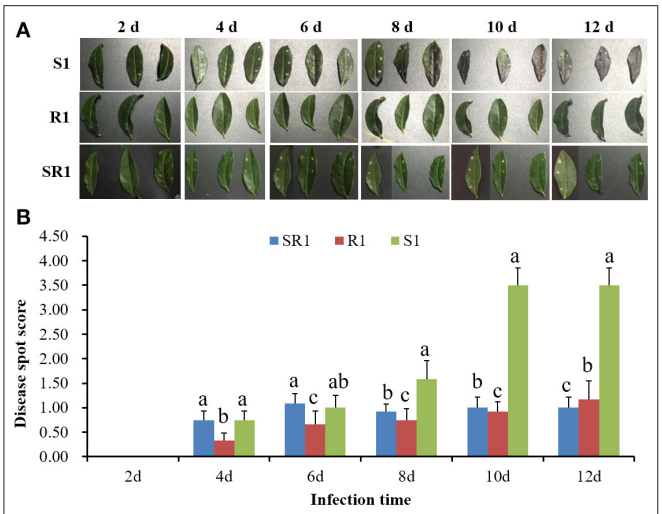

FIGURE 1 | (A) Analysis of the interaction between wild tea leaves and tea gray blight pathogen. **(B)** Disease resistance analysis of wild tea plant resources and tea gray blight pathogen. S1, Susceptibility 1; R1, Resistance 1; SR1, Sub-resistance 1. Different lowercase letters in the histogram indicate significant difference of disease spot score among "S1", "SR1", and "R1" at the same time of infection ($p < 0.05$, SNK-q test).

revealed the substances that were detected in the samples. In the multipeak detection plot, each peak in a different color represents a detected metabolite. Information on metabolite serial numbers, peak integration values, and metabolite names are listed in **Supplementary Table 1**.

In total, 728 metabolites were identified, including 184 flavonoids, 121 phenolic acids, 92 lipids, 76 amino acids and their derivatives, 51 nucleotides and their derivatives, 50 organic acids, 39 alkaloids, 31 tannins, 20 lignans and coumarins, 3 terpenoids, and 61 others (**Figure 2**, **Supplementary Table 1**). The metabolites of class II belong to class I in **Figure 2**. All metabolites were analyzed by ANOVA (**Supplementary Table 1**). As shown in the Venn plot, the most detected and identified metabolites can be found in the two tea leaf samples (**Figure 3A**).

The quality control samples (QC) were prepared by mixing extracts from two tea leaf samples. As shown in the principal component analysis (PCA) plots, there was a large separation of trends between the "S1" and "R1" leaves and little intragroup variation was observed (PC1=50.52% and PC2=10.54%, **Figure 3B**). OPLS-DA modeling can maximize the difference between different groups and can be performed to evaluate the data quality and identify potential biomarkers. As is shown, the values of R^2Y (0.999) were high and the values of Q^2 were >0.5 (**Supplementary Figure 2A**), indicating good reliability and predictability of the model. In the permutation test of the OPLS-DA, the sequential order of categorical variable Y was randomly changed many times (n=200) (**Supplementary Figure 2B**). Three corresponding OPLS-DA models were established on each occasion (**Supplementary Figures 2C,D**). Thus, the R^2 and Q^2 values of the stochastic models were obtained. The results suggested that these methods were of great importance for preventing the test model from overfitting and for evaluating the statistical significance of the model. As shown in **Supplementary Figure 2B**, the original model's R^2Y values were close to 1 in "S1" and "R1," respectively. The results indicate that the established models were an accurate description of the real situation in all sample data. The Q^2 values in "S1" and "R1" were close to 1 (0.966), and these show that a similar distribution would be generated if other new samples were added to the models. As a whole, the original model of the "S1" and "R1" groups can ideally explain the difference between each treatment group and the control group. Furthermore, there was a gradual decrease in the retention degree of the permutation. The R^2Y' and Q^2' values of permutation models are less than those of the R^2Y and Q^2 of the stochastic model shown in **Supplementary Figure 2B**. Therefore, these results indicate that the PCA and OPLS-DA models in the present study demonstrate good repeatability and reliability. The potential biomarkers were screened according to the VIP value (VIP > 1), the absolute value of fold change ≥ 2, and statistical tests $p < 0.05$.

Based on the PCA and OPLS-DA results, the VIP can be used for the preliminary screening of different metabolites between the treatment and the control groups. Moreover, differential metabolites can be further screened by combining the VIP value with the fold-change value. In this study, there were 145 metabolites that significantly changed ($|\text{Log}_2\text{Foldchange}| \geq 1$ and VIP > 1). Among them, compared with "S1," 96 metabolites were significantly decreased and 49 metabolites were significantly increased in "R1" (**Figure 4**, **Supplementary Table 2**). Flavonols, phenolic acids, amino acids and their derivatives, and flavonoids were the main categories of significantly changed metabolites (SCMs). The most increased categories were phenolic acids and flavonoids in "S1" (**Figure 4A**). Among all the differentially enriched metabolites, 21 metabolites were particularly obvious, such as quercetin-7-o-rutinoside-4'-o-glucoside and petunidin-3-o-(6"-o-p-coumaroyl) rutinoside (**Supplementary Figure 3**).

The potential biomarkers were used for pathway analysis using KEGG topology analysis. In this study, 145 SCMs were used for KEGG analysis. The differential metabolites were classified into corresponding pathways according to the information from the pathway database (**Supplementary Table 3**). The pathway analysis of SCMs involved a total of 52 pathways (**Supplementary Figures 4, 5**). Six metabolic pathways (rich factor value > 0, $p < 0.05$) were significantly enriched, including aminoacyl-tRNA biosynthesis (rich factor value = 0.56); glucosinolate biosynthesis (rich factor value = 0.75); tropane, piperidine, and pyridine alkaloid biosynthesis (rich factor value = 0.67); 2-oxocarboxylic acid metabolism (rich factor value = 0.39); flavone and flavonol biosynthesis (rich factor value = 0.42); and valine, leucine, and isoleucine degradation (Rich factor value = 0.50). It should be noted that aminoacyl-tRNA biosynthesis, 2-oxocarboxylic acid metabolism, and flavone and flavonol biosynthesis encompass a large portion of the total metabolites in "S1" and "R1" (**Supplementary Figure 5**).

Microbial Difference Analysis in Tea Leaves

The bacterial and fungal compositions of "S1" and "R1" leaves were analyzed using 16S rRNA and ITS high-throughput

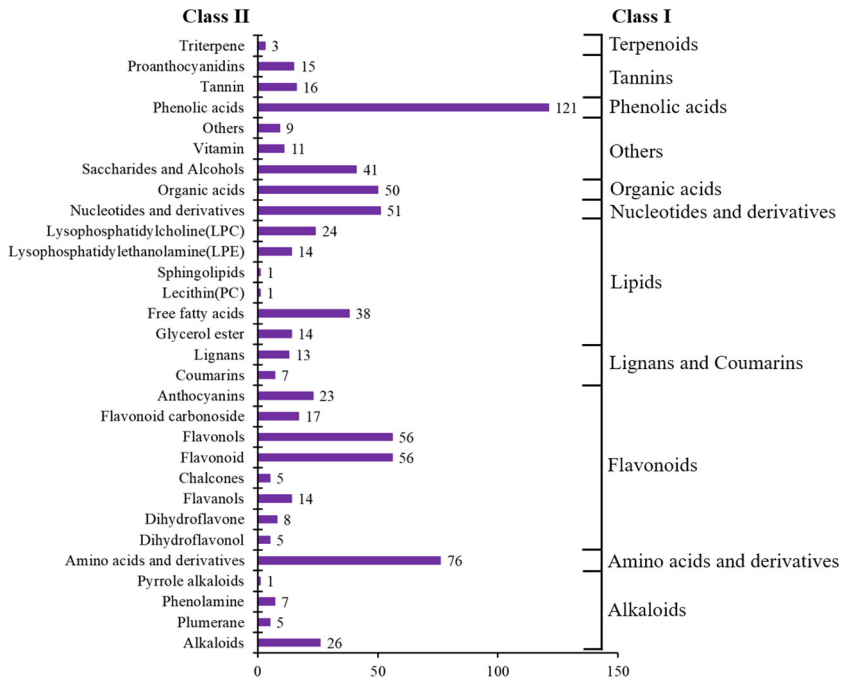

FIGURE 2 | Number of metabolite categories identified in all samples.

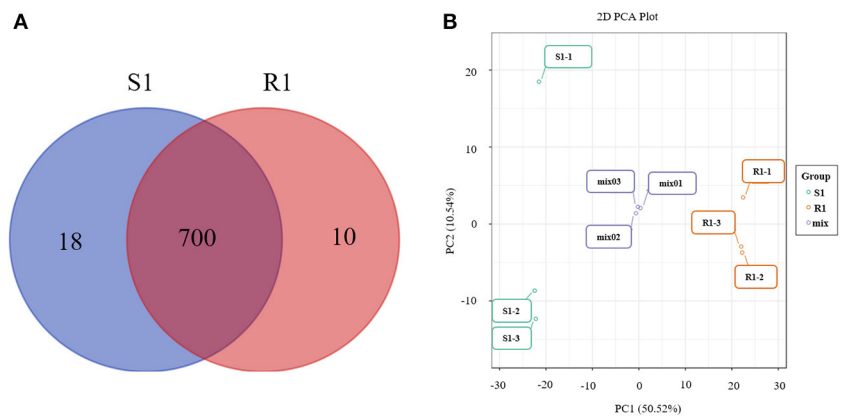

FIGURE 3 | Venn diagrams of metabolites detected in each group **(A)** and principal component analysis (PCA) score plot for mass spectrum data of tea samples and quality control samples **(B)**. The *X*-axis represents the first principal component (PC1) and the *Y*-axis represents the second principal component (PC2) in the PCA score plot.

sequencing, respectively. A total of 69,996 raw reads of 16S rRNA and 4,06,834 raw reads of ITS were obtained from six tea leaves samples ($n = 3$ for each group) with an average of 11,666 reads of bacterial and 67,805 reads of fungi per sample. The average read lengths of 16S rRNA and ITS were 377.18 bp and 232.51 bp, respectively. A total of 207 distinct operational taxonomic units (OTUs) of bacteria and 191 OTUs of fungi were observed in all samples. The Simpson index and Sobs index of bacteria and fungi did not show a significant difference between "S1" and "R1" (**Supplementary Figures 6A,B**). Genus-based principal component analysis (PCA) showed distinct fungal profiles between "S1" and "R1" (**Supplementary Figure 7A**), but the PCA of bacteria did not show distinct bacterial profiles between "S1" and "R1" (**Supplementary Figure 6C**). Also, the results of the hierarchical clustering of fungus and bacteria did not show better separations (**Supplementary Figures 6D, 7B**).

In **Supplementary Figure 6E**, *Proteobacteria* and *Actinobacteria* dominated the leaf microbiota composition at the phylum level of bacteria, contributing to 92 and 7.1% of the leaves' microbiota in "S1," and 91 and 8% of the leaves' microbiota in "R1," respectively. At the genus level, the relative abundance of microbes showed a difference between "S1" and

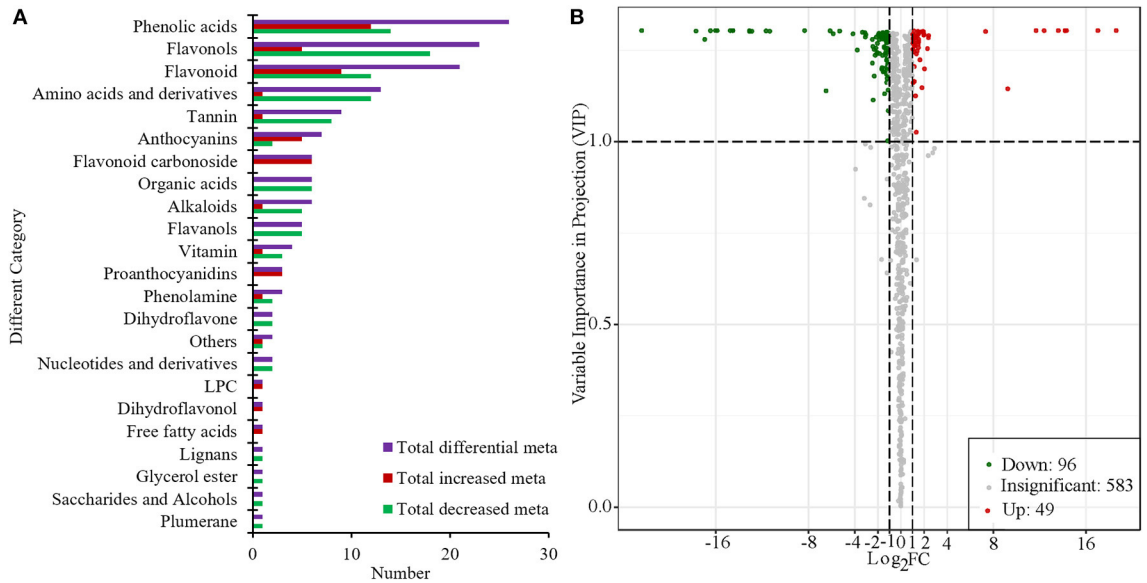

FIGURE 4 | Number of different categories **(A)** and volcano plot of metabolites **(B)** in "R1" vs. "S1."

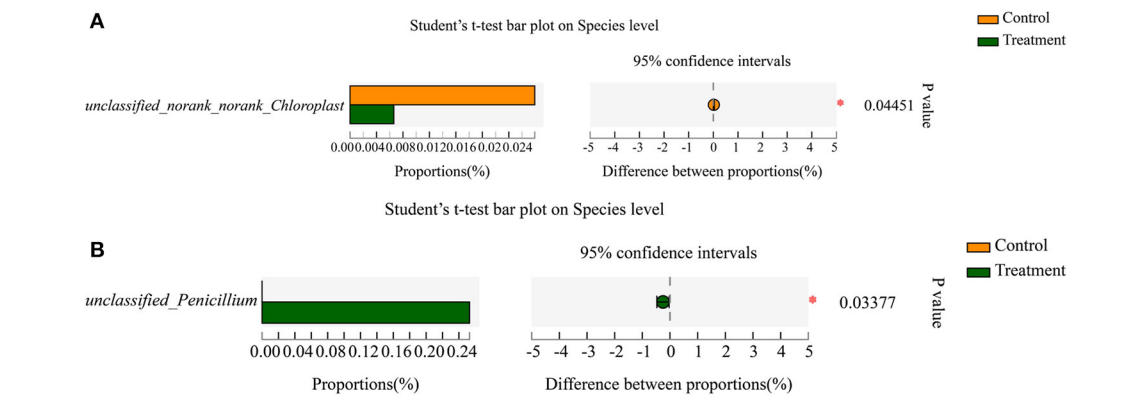

FIGURE 5 | The significantly enriched bacterial and fungal species in "S1" and "R1" samples. **(A)** The significantly enriched bacterial species. **(B)** The significantly enriched fungal species.

"R1" (**Supplementary Figure 6F**). In **Supplementary Figure 7C**, *Ascomycota* and *Basidiomycota* dominated the leaf microbiota composition at the phylum level of fungi, contributing to 83 and 17% of the microbiota in "S1," and 70 and 30% of the microbiota in "R1," respectively. At the genus level, the relative abundance of fungi showed the difference between "S1" and "R1" (**Supplementary Figure 7D**). The differences in leaf microbiota among these groups were also evidenced by linear discriminant analysis effect size (LEfSe), which showed the most different abundant taxon of two tea plant resource samples (**Supplementary Figures 8, 9**). Using a metagenomic biomarker discovery approach, *Cyanobacteria* was found to be significantly enriched in the "S1" samples (LDA score > 3), while *Burkholderia–Caballeronia–Paraburkholderia* (LDA score > 3.5) and *Penicillium*, *Plectosphaerella*, and *Plectosphaerellaceae* (LDA score > 4) were identified as biomarkers of the "R1" group (**Supplementary Figures 8, 9**).

At the genus level of bacteria, 151 genera coexisted in the two tea resources. A total of 40 genera only existed in the "S1" resources and 29 genera only existed in the "R1" resources (**Supplementary Figure 10A**). *Pseudomonas* was the predominant genus, contributing to 79.74% of the common microbiota in the two tea samples (**Supplementary Figure 11A**). *Cellvibirio* was the predominant genus (10.82%) only in "S1," and *Candidatus_competibacter* was the predominant genus (28.90%) only in "R1" (**Supplementary Figures 11B,C**).

At the genus level of fungi, 102 genera coexisted in the two tea resources. A total of 41 genera only existed in the "S1" resources and 27 genera existed in the "R1" resources (**Supplementary Figure 10B**). *Cutaneotrichosporon*

was the predominant genus, contributing to 23.12% of the common microbiota in the two sample groups (**Supplementary Figure 12A**). *Toxicocladosporium* was the predominant genus (18.85%) only in "S1" and *Filobasidium* was the predominant genus (13.30%) only in "R1" (**Supplementary Figures 12B,C**). The results show that the microbiota composition at the genus level of "S1" is more abundant than that in "R1."

Norank_norank_Chloroplast (p=0.04451) was a significantly different enrichment bacterial genera between the two tea resources (**Supplementary Figure 13**). *Penicillium* (p = 0.02156) was a significantly different enrichment fungal genera between the two tea resources (**Supplementary Figure 14**). At the species level of bacteria, the relative abundance of *unclassified_norank_norank_ Chloroplast* (p = 0.04451) showed a significant difference between the two tea resources (**Figure 5A**). At the species level of fungi, the relative abundance of *unclassified_Penicillium* (p = 0.03377) showed a significant difference between the two tea samples (**Figure 5B**).

Correlations Between Microorganisms and Metabolites in Tea Leaves

Correlation analysis between the leaves" microorganisms and metabolites indicates potential mutual contributions. To investigate the contributions of metabolites to leaves' microbiota, we performed RDA on the significantly changed metabolites related to the leaves' microbiota (**Supplementary Figure 15**). The top three high-enrichment or low-enrichment metabolites contributed to the leaves' microbiota. We found that the top three high-enrichment metabolites, namely quercetin-7-o-rutinoside-4'-o-glucoside, 2,3-di-o-galloyl-d-glucose, and L-arginine contributed to the bacteria and fungi of "S1" leaves. However, the top three low-enrichment metabolites, namely luteolin-6-c-glucoside-7-o-(6"-p-coumaroyl) glucoside, isovitexin-2"-o-(6"'-p-coumaroyl) glucoside, and vitexin-7-o-(6"-p-coumaroyl) glucoside contributed to bacteria and fungus of "R1" leaves (**Supplementary Figure 15**).

In addition, the metabolites, and the bacterial and fungal genera in two tea resources were used for Spearman's correlation analysis. In **Supplementary Figures 16, 17**, the relative abundance of *unclassified_Gammaproteobacteria*, *Microbacterium*, *norank_norank_ Gaiellales*, *Aeromonas*, *Bacillus*, *norank_norank_Chloroplast*, *Pseudomonas*, *Ralstonia, unclassified_Enterobacteriaceae*, *Sphingomonas* and *Penicillium*, *Pseudocercospora, Plectosphaerella*, *Cladosporium*, *unclassified_Ascomycota*, *Phyllosticta*, *Strelitziana, Toxicocladosporium*, *Bipolaris*, *Trichoderma,* and *unclassified_Xylariales* were significantly correlated with the top twenty-one metabolites enriched in "S1" or "R1." The positive and negative correlations were as follows: *Microbacterium*, *norank_norank_Gaiellales, Aeromona,* and *unclassified-norank-norank-Chloroplast* were significantly positively correlated with the levels of delphinidin-3-o-(2"'-o-p-coumaroyl) rutinoside and isorhamnetin-3-o-rutinoside-7-o-rhamnoside, but were significantly negatively correlated with some SCMs, such as 1,2,3-tri-o-galloyl-d-glucose and castanoside. *Bacillus*, *norank_norank_Chloroplast*, *Pseudomonas*, *Ralstonia*, *unclassified_ Enterobacteriaceae,* and *Sphingomonas* were significantly positively correlated with the levels of some SCMs, such as 2,3-tri-o-galloyl-d-glucose, 2,3-di-o-galloyl-d-glucose, dicaffeoylquinic acid-o-glucoside, kaempferol-3-o-(2"-p-coumaroyl) galactoside, feruloylmalic acid, feruloyltartaric acid (fertaric acid), and p-coumaroylmalic acid, but were significantly negatively correlated with delphinidin-3-o-(2"'-o-p-coumaroyl)rutinoside, quercetin-3-o-(2"-o-rhamnosyl)rutinoside-7-o-glucoside, petunidin-3-o-(6"-o-p-coumaroyl) rutinoside, isorhamnetin-3-o-rutinoside-7-o-rhamnoside, luteolin-7-o-sophoroside-5-o-arabinoside, etc. *Penicillium*, *Pseudocercospora*, and *Plectosphaerella* were significantly positively correlated with the levels of delphinidin-3-o- (2"'-o-p-coumaroyl) rutinoside, quercetin-3-o- (2"-o-rhamnosyl) rutinoside-7-o-glucoside, petunidin-3-o-(6"-o-p-coumaroyl) rutinoside, and isorhamnetin-3-o-rutinoside-7-o-rhamnoside but were significantly negatively correlated with some metabolites such as L-arginine, eriodictyol-7-o-glucoside, cyanidin-3-o- (6"-o-p-coumaroyl) rutinoside-5-o-glucoside, and 6-c-methylquercetin-3-o-rutinoside. *Strelitziana*, *Toxicocladosporium*, *Bipolaris*, *Trichoderma*, and *unclassified_Xylariales* were significantly positively correlated with the levels of L-arginine and eriodictyol-7-o-glucoside. *Trichoderma* and *unclassified_Xylariales* were significantly negatively correlated with delphinidin-3-o-(2"'-o-p-coumaroyl) rutinoside.

DISCUSSION

Although some secondary metabolites, such as lipids (Lim et al., 2017), flavonoids (Cushnie and Lamb, 2011), alkaloids (Yang et al., 2016), polyphenols (Bazzaz et al., 2016), and glycoside (Escobedo-Martínez et al., 2010), are not directly involved in plant growth and development, they can nonetheless act as a chemical defense. That is, they can be used for defending against the damage caused by plant diseases in specific environments and physiological conditions. Flavonoids, as one of the substances with defense functions, are widely found in plants. In maize, 2,4-dihydroxy-7-methoxy-2H-1,4- benzoxazin-3(4H)-one (DIMBOA) can resist fungus (Frey et al., 1997). The isoflavones also have antimicrobial functions (Undhad et al., 2021). Research has shown that under the stimulation of pathogenic bacterial infection, tea leaves can increase polyphenols as antibacterial factors, and the cortex of roots and stems can also produce antitoxin (Turkmen et al., 2007).

In the present study, the tea plant resource "R1" had obvious resistance to tea gray blight disease, but "S1" was susceptible. Flavonoids, phenolic acids, amino acids, and derivatives were the major differential accumulated categories of SCMs. The major SCMs include kaempferol, luteolin, vitexin, quercetin, and their glycosides. "R1" sample specifically enriched petunidin, luteolin, vitexin, isovitexin, quercetin, and isorhamnetin's glycoside. In *Arabidopsis*, quercetin can protect *Arabidopsis* against *Pseudomonas syringae* pv. Tomato DC3000 infection through

both quercetin-mediated H_2O_2 generation and the involvement of SA and NPR1 (Jia et al., 2010). Isovitexin is a biologically active flavone C-glycosylated derivative of apigenin that possesses anti-inflammatory and antioxidant properties in vegetables and fruits (Zielińska-Pisklak et al., 2015; Lv et al., 2016). Isorhamnetin augments the cellular antioxidant defense capacity by activating the Nrf2/HO-1 pathway (Hyun, 2016). Sinapate helps to improve pathogen resistance for *Botrytis cinerea* by UV-B radiation in *Arabidopsis* (Demkura and Ballaré, 2012). Vitexin has been reported to have inhibitory effects on Gram-negative bacteria, especially *Pseudomonas aeruginosa* and *Bordetella petrii* (Das et al., 2016; Rath et al., 2016; Corrêa et al., 2021), and vitexin's glucoside has a significant antioxidant effect (Fang et al., 2016; Wu et al., 2021). Thus, the enriched metabolites in the "R1" sample may contribute to the disease resistance to tea gray blight disease. These metabolites therefore provided the research directions for analyzing the function of metabolites through the interaction between metabolites and pathogens.

The dominant species and compositions of antimicrobial bacteria are closely related to plants' resistance to disease (Mendes et al., 2011; Lareen et al., 2016). Bacteria can have wide-ranging effects on the host plants. For example, they can affect many plant processes such as disease resistance, drought tolerance, life cycle phenology, and overall vigor (Panke-Buisse et al., 2017). The research on the microorganisms and *Cassava* phenotype shows that *Lactococcus* sp., *Pantoea dispersa,* and *Saccharomyces cerevisiae* are closely associated with cassava disease resistance (Bonito et al., 2014). An antagonistic function has been reported for the pathogen *Pantoea dispersa*, an indigenous endophytic bacterium of rice seeds that can produce auxins to inhibit the pathogen *Fusarium oxysporum*, allowing it to play an important role in the defense against pathogens (Verma et al., 2017). *Pantoea dispersa* has fungicidal properties and was found to significantly inhibit the growth of *Ceratocytis fimbriata* on the leaves and tuberous roots of a susceptible sweet potato cultivar (Jiang et al., 2019). Gu et al. (2020) found that the modulation of siderophore plays an important role in iron competition and biocontrol of the soil-borne pathogen *Ralstonia solanacearum*. In our study, *Proteobacteria*, *Actinobacteria*, *Ascomycota,* and *Basidiomycota* dominated the microbiota composition at the phylum level. At the genus level, *Pseudomonas* and *Cutaneotrichosporon* were the predominant genera in the two sample groups. *Cellvibirio, Toxicocladosporium* or *Candidatus_competibacter,* and *Filobasidium* were the predominant genera only in "S1" or "R1." *Cellvibrio* has been isolated from soil environments; nevertheless, strains belonging to the genus have also been found in aquatic environments (Rhee et al., 2010). The *Cellvibrio* genus, especially *C. japonicus*, has been recognized and studied for its industrial enzymic potential to degrade a variety of polysaccharides, including those present in the plant cell wall (DeBoy et al., 2008). This means that the members of *Cellvibrio* might hurt plant cells. The yeast *Filobasidium* has been described as an important member of the wine consortia for its role in creating specific flavor profiles or reducing final alcohol content (Cureau et al., 2021). At the species level, the relative abundance of *unclassified_norank_norank_Chloroplast* and *unclassified_Penicillium* have shown significant differences between the two groups of samples. Furthermore, we found that the proportional abundance of *Penicillium* in the "R1" group was particularly significantly increased. A high level of *Penicillium* was identified as a potential biomarker of the "R1" group via LEfSe analysis. According to the correlation research between metabolites and microorganisms, the predominant genera, such as *norank_norank_Chloroplast*, *Pseudomonas*, *Penicillium,* and *Toxicocladosporium* are significantly correlated with the top SCMs enriched in "S1" or "R1," including L-arginine, castanoside B, cyanidin-3-o-(6"-o-p-coumaroyl) rutinoside-5-o-glucoside, dicaffeoylquinic acid-o-glucoside, isorhamnetin-3-o-rutinoside-7-o-rhamnoside, luteolin-7-o-sophoroside-5-o-arabinoside, p-coumaroylmalic acid, and quercetin-3-o-(2"-o-rhamnosyl) rutinoside-7-o-glucoside.

Overall, the present study demonstrated an obvious difference between "S1" and "R1" tea plant resources in their metabolomes. The phenolic acids and flavonoids were the categories in "R1" samples with major increases and they included 4-O-glucosyl-sinapate and petunidin-3-o-(6"-o-p-coumaroyl) rutinoside. The major bacterial genus was *Pseudomonas* in "S1" and "R1." *Cellvibirio* was predominant genus in "S1" and *Candidatus_competibacter* was predominant genus in "R1." The microbiota of "S1" is more abundant than that in "R1." *Unclassified_norank_norank_Chloroplast* and *unclassified_Penicillium* showed significant differences between "S1" and "R1." *Penicillium* was identified as a potential biomarker. They were both significantly correlated with some metabolites. Phenolic acids and flavonoids, as well as *Penicillium* can be functional metabolites and microorganisms that may contribute to tea plants' resistance to tea gray blight disease. These will be used for further research on the mechanism of disease resistance.

DATA AVAILABILITY STATEMENT

The datasets presented in this study can be found in online repositories. The names of the repository/repositories and accession number(s) can be found below: NCBI BioProject - PRJNA823872.

AUTHOR CONTRIBUTIONS

YZ and JZ designed and performed the experiments and wrote the manuscript. MF and LW revised the manuscript. YH provided the wild tea plant resources, participated in sample preprocessing, and part of the manuscript writing. FW conceived the experiments and revised the manuscript. All authors contributed to the article and approved the submitted version.

FUNDING

This study was funded by the National Natural Science Foundation of China (No. 31902077), the Open Fund of Henan Key Laboratory of Tea Comprehensive Utilization in South Henan (No. HNKLTOF2020007), and the Guangdong Provincial

Special Fund for Modern Agriculture Industry Technology Innovation Teams (No. 2021KJ120). The funders were not involved in the design of the study, collection, analysis, interpretation of data, and manuscript writing.

ACKNOWLEDGMENTS

We thank Dr. Xiumin Fu of South China Botanical Garden, Chinese Academy of Sciences and MDPI (https://www.mdpi.com/) for linguistic assistance during the preparation and revision of this manuscript.

SUPPLEMENTARY MATERIAL

The Supplementary Material for this article can be found online at: https://www.frontiersin.org/articles/10.3389/fmicb.2022.907962/full#supplementary-material

REFERENCES

Ahuja, I., Kissen, R., and Bones, A. M. (2012). Phytoalexins in defense against pathogens. *Trends Plant Sci.* 17, 73–90. doi: 10.1016/j.tplants.2011.11.002

Bazzaz, B., Sarabandi, S., Khameneh, B., and Hosseinzadeh, H. (2016). Effect of catechins., green tea extract and methylxanthines in combination with gentamicin against *Staphylococcus aureus* and *Pseudomonas aeruginosa*: combination therapy against resistant bacteria. *J. Pharmacopunct.* 19, 312–318. doi: 10.3831/KPI.2016.19.032

Becker, R., Ulrich, K., Behrendt, U., Kube, M., and Ulrich, A. (2020). Analyzing ash leaf-colonizing fungal communities for their biological control of *Hymenoscyphus Fraxineus*. *Front. Microbiol.* 11, 590944. doi: 10.3389/fmicb.2020.590944

Bonito, G., Reynolds, H., Robeson, M. S., Nelson, J., Hodkinson, B. P., and Tuskan, G. (2014). Plant host and soil origin influence fungal and bacterial assemblages in the roots of woody plants. *Mol. Ecol.* 23, 3356–3370. doi: 10.1111/mec.12821

Bruisson, S., Zufferey, M., L'Haridon, F., Trutmann, E., and Anand, A. (2019). Endophytes and epiphytes from the grapevine leaf microbiome as potential biocontrol agents against phytopathogens. *Front. Microbiol.* 10, 2726. doi: 10.3389/fmicb.2019.02726

Chen, W., Gong, L., Guo, Z., Wang, W., Zhang, H., Liu, X., et al. (2013). A novel integrated method for large-scale detection, identification, and quantification of widely targeted metabolites: application in the study of rice metabolomics. *Mol. Plant.* 6, 1769–1780. doi: 10.1093/mp/sst080

Cole, J. R., Wang, Q., Fish, J. A., Chai, B., McGarrell, D. M., Sun, Y., et al. (2014). Ribosomal database project: data and tools for high throughput rRNA analysis. *Nucleic Acids Res.* 42, 633–642. doi: 10.1093/nar/gkt1244

Corrêa, J. G. D. S., Bianchin, M., Lopes, A. P., Silva, E., and Santin, S. (2021). Chemical profile, antioxidant and anti-inflammatory properties of *Miconia Albicans* (Sw.) Triana (melastomataceae) fruits extract. *J. Ethnopharmacol.* 273, 113979. 113979. doi: 10.1016/j.jep.2021.113979

Cureau, N., Threlfall, R., Marasini, D., Lavefve, L., and Carbonero, F. (2021). Year. location, and variety impact on grape-associated mycobiota of arkansas-grown wine grapes for wine production. *Microbial. Ecol.* 82,845–858. doi: 10.1007/s00248-021-01705-y

Cushnie, T., and Lamb, A. J. (2011). Recent advances in understanding the antibacterial properties of flavonoids. *Int. J. Antimicrob. Ag.* 38, 99–107. doi: 10.1016/j.ijantimicag.2011.02.014

Das, M. C., Sandhu, P., Gupta, P., Rudrapaul, P., De, U. C., Tribedi, P., et al. (2016). Attenuation of *Pseudomonas aeruginosa* biofilm formation by vitexin: a combinatorial study with azithromycin and gentamicin. *Sci. Rep.* 6, 23347. doi: 10.1038/srep23347

DeBoy, R. T., Mongodin, E. F., Fouts, D. E., Tailford, L. E., Khouri, H., Emerson, J. B., et al. (2008). Insights into plant cell wall degradation from the genome sequence of the soil bacterium *Cellvibrio japonicus*. *J. Bacteriol.* 190, 5455–5463. doi: 10.1128/JB.01701-07

Demkura, P. V., and Ballaré, C. L. (2012). UVR8 mediates UV-B-induced Arabidopsis defense responses against Botrytis cinerea by controlling sinapate accumulation. *Mol. Plant.* 5, 642–652. doi: 10.1093/mp/sss025

El-Hadidy, A., and El-Ati, A. A. (2014). Efficiency of effective microorganisms (EM) to induce resistance against *chocolate spot disease* and enhance productivity of *Faba Bean* under reclaimed soil conditions. *J. Phytopathol.* 42, 117–142. doi: 10.21608/ejp.2014.96742

Escobedo-Martínez, C., Cruz-Morales, S., Fragoso-Serrano, M., Rahman, M. M., Gibbons, S., and Pereda-Miranda, R. (2010). Characterization of a xylose containing oligosaccharide, an inhibitor of multidrug resistance in *Staphylococcus aureus*, from *Ipomoea Pescaprae*. *Phytochemistry* 71, 1796–1801. doi: 10.1016/j.phytochem.2010.06.018

Fang, A., Cao, X., Qu, H., Wang, S. (2016). Attenuation of oxidative stress of erythrocytes by the plant-derived flavonoids vitexin and apigenin. *Evid Based Compl. Alt.* 70, 724–732. doi: 10.1691/ph.2015.5665

Frey, M., Chomet, P., Glawischnig, E., Stettner, C., Grün, S., and Winklmair, A. (1997). Analysis of a chemical plant defense mechanism in grasses. *Science*. 277, 696–699. doi: 10.1126/science.277.5326.696

Gu, S., Yang, T., Shao, Z., Wang, T., and Pommier, T. (2020). Siderophore-mediated interactions determine the disease suppressiveness of microbial consortia. *Msystems*. 5, e00811–e00819. doi: 10.1128/mSystems.00811-19

Hyun, C. Y. (2016). The cytoprotective effect of isorhamnetin against oxidative stress is mediated by the upregulation of the NrF2-dependent ho-1 expression in C2C12 myoblasts through scavenging reactive oxygen species and ERK inactivation. *Gen. Physiol. Biophys.* 35, 145–154. doi: 10.4149/gpb_2015034

Jia, Z., Zou, B., Wang, X., Qiu, J., Ma, H., and Gou, Z. (2010). Quercetin-induced H_2O_2 mediates the pathogen resistance against *pseudomonas syringae* pv. tomato DC3000 in *Arabidopsis Thaliana*. *Biochem. Bioph. Res. Co.* 396, 522–527. doi: 10.1016/j.bbrc.2010.04.131

Jiang, L., Jeong, J. C., Lee, J. S., Park, J. M., and Lee, J. (2019). Potential of pantoea dispersa as an effective biocontrol agent for black rot in sweet potato. *Sci. Rep.* 9, 16354. doi: 10.1038/s41598-019-52804-3

Karou, D., Savadogo, A., Canini, A., Yameogo, S., and Traore, A. S. (2006). Antibacterial activity of alkaloids from *Sida Acuta*. *Afr. J. Biotechnol.* 5, 195–200. doi: 10.4314/ajb.v4i12.71463

Lareen, A., Burton, F., and Schäfer, P. (2016). Plant root-microbe communication in shaping root microbiomes. *Plant Mol. Biol.* 90, 575–587. doi: 10.1007/s11103-015-0417-8

Lim, G. H., Singhal, R., Kachroo, A., and Kachroo, P. (2017). Fatty acid- and lipid-mediated signaling in plant defense. *Annu. Rev. Phytopathol.* 55, 505–536. doi: 10.1146/annurev-phyto-080516-035406

Liu, Z. Q., Ma, L. P., Zhou, B., Yang, L., and Liu, Z. L. (2000). Antioxidative effects of green tea polyphenols on free radical initiated and photosensitized peroxidation of human low-density lipoprotein. *Chem. Phys. Lipids.* 106, 53–63. doi: 10.1016/S0009-3084(00)00133-X

Luna, E., Pastor, V., Robert, J., Flors, V., Mauch-Mani, B., and Ton, J. (2011). Callose deposition: a multifaceted plant defense response. *Mol. Plant Microbe. Interact.* 24, 183–193. doi: 10.1094/MPMI-07-10-0149

Lv, H., Yu, Z., Zheng, Y., Wang, L., Qin, X., and Cheng, G. (2016). Isovitexin exerts anti-inflammatory and anti-oxidant activities on lipopolysaccharide-induced acute lung injury by inhibiting mapk and NF-?B and activating HO-1/NrF2 pathways. *Int. J. Biol. Sci.* 12, 72–86. doi: 10.7150/ijbs.13188

Ma, T., Peng, W., Liu,Z., and Gao, T., Tian, Y. (2020). Teapolyphenols inhibit the growth and virulence of ETEC K88. *Microb. Pathogenesis*. 152, 104640. doi: 10.1016/j.micpath.2020.104640

Mendes, R., Kruijt, M., Bruijn, I. D., Dekkers, E., and Voort, M. V. D. (2011). Deciphering the rhizosphere microbiome for disease-suppressive bacteria. *Science*. 332, 1097–1100. doi: 10.1126/science.1203980

Mt, N., Stein, M., BH, H., JP, V., Edwards, H., and Sc, S. (2003). Loss of a callose synthase results in salicylic acid-dependent disease resistance. *Science*. 301, 969–972. doi: 10.1126/science.1086716

Pallavi, R. V., Nepolean, P., Balamurugan, A., Jayanthi, R., Beulah, T., and Premkumar, R. (2012). In vitro studies of biocontrol agents and fungicides tolerance against *grey blight disease* in tea. *Asian Pac. J. Trop. Bio*. 12, 435–438. doi: 10.1016/S2221-1691(12)60202-0

Panke-Buisse, K., Lee, S., and Kao-Kniffin, J. (2017). Cultivated sub-populations of soil microbiomes retain early flowering plant trait. *Microb. Ecol*. 73, 394–403. doi: 10.1007/s00248-016-0846-1

Parks, D. H., Tyson, G. W., Philip, H., and Beiko, R. G. (2014). STAMP: statistical analysis of taxonomic and functional profiles. *Bioinformatics* 30, 3123–3124. doi: 10.1093/bioinformatics/btu494

Qiao, Z., and Dixon, R. A. (2011). Transcriptional networks for lignin biosynthesis: more complex than we thought. *Trends Plant Sci*. 16, 227–233. doi: 10.1016/j.tplants.2010.12.005

Randhawa, P. S. (1986). Interaction of *Xanthomonas campestris* pv. *pruni* with pruniphage and epiphytic bacteria on detached peach leaves. *Phytopathology*. 76, 549–553. doi: 10.1094/Phyto-76-549

Rath, S. N., Ray, M., Pattnaik, A., and Pradhan, S. K. (2016). Drug target identification and elucidation of natural inhibitors for *Bordetella petrii*: an *In Silico* study. *Genomics Inform*. 14, 241–254. doi: 10.5808/GI.2016.14.4.241

Rhee, Y. J., Han, C. R., Kim, W. C., Jun, D. Y., Rhee, I. K., and Kim, Y. H. (2010). Isolation of a novel freshwater agarolytic *Cellvibrio* sp. KY-YJ-3 and characterization of its extracellular b-agarase. *J. Microbiol. Biotechnol*. 20, 1378–1385. doi: 10.4014/jmb.1007.07010

Sattler, S. E., and Funnell-Harris, D. L. (2013). Modifying lignin to improve bioenergy feedstocks: strengthening the barrier against pathogens. *Front. Plant Sci*. 4, 70. doi: 10.3389/fpls.2013.00070

Schmelz, E. A., Kaplan, F., Huffaker, A., Dafoe, N. J., Vaughan, M. M., Ni, X., et al. (2011). Identity, regulation, and activity of inducible diterpenoid phytoalexins in maize. *Proc. Natl. Acad. Sci. U. S. A*. 108, 5455–5460. doi: 10.1073/pnas.1014714108

Segata, N., Izard, J., Waldron, L., Gevers, D., Miropolsky, L., and Huttenhower, G. C. (2011). Metagenomic biomarker discovery and explanation. *Genome Biol*. 12, R60. doi: 10.1186/gb-2011-12-6-r60

Thangaraj, K., Deng, C., Cheng, L. L., Deng, W. W., and Zhang, Z. Z. (2020). Inhibition mechanism of caffeine in tea pathogenic fungi *Botryosphaeria Dothidea* and *Colletotrichum Gloeosporioides*. *BMC Microbiol*. 2020, 1–28. doi: 10.21203/rs.3.rs-27631/v1

Turkmen, N., Sedat-Velioglu, Y., Sari, F., and Polat, G. (2007). Effect of extraction conditions on measured total polyphenol contents and antioxidant and antibacterial activities of black tea. *Molecules*. 12, 484–496. doi: 10.3390/12030484

Undhad, T., Hati, S., and Makwana, S. (2021). Significance of storage study on ace inhibitory, antioxidative, antimicrobial Activities and biotransformation of isoflavones of functional fermented soy-based beverage. *J. Food Process. Pres.* 45, e15062. doi: 10.1111/jfpp.15062

Verma, S. K., Kingsley, K., Irizarry, I., Bergen, M., Kharwar, R. N., and White, JF. Jr. (2017). Seed-vectored endophytic bacteria modulate development of rice seedlings. *J. Appl. Microbiol.* 122, 1680–1691. doi: 10.1111/jam.13463

Wang, F. Y., Huang, Y. J., Wu, W., Zhu, C. Y., Zeng, J. W., and Chen, J. Z. (2020). Metabolomics analysis of the peels of different colored citrus fruits (*Citrus reticulata* cv. 'Shatangju') during the maturation period based on UHPLC-QQQ-MS. *Molecules*. 25, 396-411. doi: 10.3390/molecules25020396

Wu, S. T., Shen, D. Y., Wang, R. H., Li, Q. Y., Mo, R. H., Zheng, Y. W., et al. (2021). Phenolic profiles and antioxidant activities of free, esterified and bound phenolic compounds in *Walnut Kernel*. *Food Chem*. 350, 129217. doi: 10.1016/j.foodchem.2021.129217

Yamane, H. (2013). Biosynthesis of phytoalexins and regulatory mechanisms of it in rice. *Bioscience Biosci. Biotech. Bioch*. 77, 1141–1148. doi: 10.1271/bbb.130109

Yang, C., Kim, S., Yang, G., Mao, L., Liao, J., Chung, J., et al. (1999). Inhibition of carcinogenesis by tea: bioavailability of tea polyphenols and mechanisms of actions. *Proc. Soc. Exp. Biol. Med*. 220, 213–7. doi: 10.3181/00379727-220-44368

Yang, P. S., Zhang, W., Shen, X. F., Wang, X. L., Li, C., and Gong, X. W. (2016). Two new alkaloids from the seeds of *Cassia alata* and their bioactivities. *Heterocycles*. 92, 1706–1712. doi: 10.3987/COM-16-13511

Zhang, F., Sun, X. X., Zhang, X. C., Zhang, S., Lu, J., Xia, Y. M., et al. (2018). The interactions between gut microbiota and entomopathogenic fungi: a potential approach for biological control of Blattella germanica (L.). *Pest Manag. Sci*. 74, 438–447. doi: 10.1002/ps.4726

Zheng, R., Chen, T. S., and Lu, T. (2011). A comparative reverse docking strategy to identify potential antineoplastic targets of tea functional components and binding mode. *Int. J. Mol. Sci.* 12, 5200–5212. doi: 10.3390/ijms12085200

Zhou, B., Ma, C., Wang, H., and Tao, X. (2018). Biodegradation of caffeine by whole cells of tea-derived fungi *Aspergillus sydowii*, *Aspergillus niger* and optimization for caffeine degradation. *BMC Microbiol*. 18, 53–63. doi: 10.1186/s12866-018-1194-8

Zielińska-Pisklak, M. A., Kaliszewska, D., Stolarczyk, M., and Kiss, A. K. (2015). Activity-guided isolation, identification and quantification of biologically active isomeric compounds from folk medicinal plant desmodium adscendens using high performance liquid chromatography with diode array detector, mass spectrometry and multidimentional nuclear magnetic resonance spectroscopy. *J. Pharmaceut. Biomed*. 102, 54–63. doi: 10.1016/j.jpba.2014.08.033

Conflict of Interest: The authors declare that the research was conducted in the absence of any commercial or financial relationships that could be construed as a potential conflict of interest.

Publisher's Note: All claims expressed in this article are solely those of the authors and do not necessarily represent those of their affiliated organizations, or those of the publisher, the editors and the reviewers. Any product that may be evaluated in this article, or claim that may be made by its manufacturer, is not guaranteed or endorsed by the publisher.

frontiers | Frontiers in Microbiology

TYPE Original Research
PUBLISHED 22 July 2022
DOI 10.3389/fmicb.2022.925355

OPEN ACCESS

EDITED BY
Boqiang Li,
Institute of Botany (CAS), China

REVIEWED BY
Yuli Dai,
Fujian Academy of Agricultural Sciences, China
Wenxing Liang,
Qingdao Agricultural University, China
Roshni R. Kharadi,
Michigan State University, United States

*CORRESPONDENCE
Bo Liu
liubo4552@126.com
Zenggui Gao
gaozenggui@outlook.com

SPECIALTY SECTION
This article was submitted to Microbe and Virus Interactions With Plants, a section of the journal Frontiers in Microbiology

RECEIVED 26 May 2022
ACCEPTED 29 June 2022
PUBLISHED 22 July 2022

CITATION
Ma Z, Huang Y, Zhang Z, Liu X, Xuan Y, Liu B and Gao Z (2022) Comparative genomic analysis reveals cellulase plays an important role in the pathogenicity of *Setosphaeria turcica* f. sp. *zeae*. *Front. Microbiol.* 13:925355. doi: 10.3389/fmicb.2022.925355

Comparative genomic analysis reveals cellulase plays an important role in the pathogenicity of *Setosphaeria turcica* f. sp. *zeae*

Zhoujie Ma[1], Yufei Huang[1], Zhaoran Zhang[1], Xiaodi Liu[1], Yuanhu Xuan[1], Bo Liu[2]* and Zenggui Gao[1]*

[1]Institute of Plant Immunology, College of Plant Protection, Shenyang Agricultural University, Shenyang, China, [2]College of Life Sciences, Yan'an University, Yan'an, China

Setosphaeria turcica f. sp. *zeae* and *S. turcica* f. sp. *sorghi*, the two formae speciales of *S. turcica*, cause northern leaf blight disease of corn and sorghum, respectively, and often cause serious economic losses. They have obvious physiological differentiation and show complete host specificity. Host specificity is often closely related to pathogen virulence factors, including secreted protein effectors and secondary metabolites. Genomic sequencing can provide more information for understanding the virulence mechanisms of pathogens. However, the complete genomic sequence of *S. turcica* f. sp. *sorghi* has not yet been reported, and no comparative genomic information is available for the two formae speciales. In this study, *S. turcica* f. sp. *zeae* was predicted to have fewer secreted proteins, pathogen-host interaction (PHI) genes and carbohydrate-active enzymes (CAZys) than *S. turcica* f. sp. *sorghi*. Fifteen and 20 polyketide synthase (PKS) genes were identified in *S. turcica* f. sp. *zeae* and *S. turcica* f. sp. *sorghi*, respectively, which maintained high homology. There were eight functionally annotated effector protein-encoding genes specifically in *S. turcica* f. sp. *zeae*, among which the encoding gene *StCEL2* of endo-1, 4-β-D-glucanase, an important component of cellulase, was significantly up-regulated during the interaction process. Finally, gluconolactone inhibited cellulase activity and decreased infection rate and pathogenicity, which indicates that cellulase is essential for maintaining virulence. These findings demonstrate that cellulase plays an important role in the pathogenicity of *S. turcica* f. sp. *zeae*. Our results also provide a theoretical basis for future research on the molecular mechanisms underlying the pathogenicity of the two formae speciales and for identifying any associated genes.

KEYWORDS

***Setosphaeria turcica*, formae speciales, pathogenicity, genome sequencing, gene function, comparative genome, cellulase activity**

Introduction

Northern leaf blight caused by *Setosphaeria turcica* is a major disease of gramineous crops and leads to serious yield losses of cereal crops in the world, especially during the growing season when the temperature is moderate (15°C–25°C) and the dew is heavy (Ramathani et al., 2011; Galiano-carneiro and Miedaner, 2017). Under natural conditions, *S. turcica* infects a broad range of plants, including corn, sorghum, Sudan grasses, and other sorghum species (Robert, 1960; Bhowmik and Prasada, 1970; Martin et al., 2011). Mitra (1923) first reported a clear physiological differentiation of *S. turcica*, with different formae speciales. *S. turcica* is classified as *S. turcica* f. sp. *zeae*, *S. turcica* f. sp. *Sorghi*, and *S. turcica* f. sp. *complexa*, based on the pathogen infecting a specific host or group of hosts and producing the typical spots. *S. turcica* f. sp. *zeae* can only infect corn, *S. turcica* f. sp. *sorghi* is virulent to sorghum and Sudan grasses, whereas *S. turcica* f. sp. *complexa* infects more plants (Bergquist and Masias, 1974).

Previous studies on *S. turcica* mainly focused on strains isolated from corn (*S. turcica* f. sp. *zeae*). With the completion of the genome sequencing of *S. turcica* f. sp. *zeae* in recent years (Ohm et al., 2012), considerable genetic information became available to understand its infection mechanism and its interaction with corn. At present, molecular-level studies on the pathogenicity of *S. turcica* f. sp. *zeae* mainly focus on signal transduction pathways and extracellular secretions of pathogens, such as cell wall degrading enzymes, host-specific toxin, and melanin (Cuq et al., 1993; Degefu et al., 2004; Ni, 2004). Previous studies have shown that HT (from *Helminthosporium turcicum*) toxin can induce typical symptoms of northern leaf blight in corn. Further, 1, 8-dihydroxynaphthalene (DHN) melanin has been shown to be closely related to pathogenicity (Butler et al., 2001; Nosanchuk and Casadevall, 2003). The secretion of melanin promotes the production of adhesive cells and increases the turgor pressure, which enhances the penetration of *S. turcica* into the corn tissue (Lagunas-Muñoz et al., 2006). Many genes (*StLAC2*, *StPKS* and *St4HNR*) have been proved to play important roles in the melanin synthesis pathway (Wen et al., 2008; Zhang et al., 2011; Ma et al., 2017). Some oxidoreductases are involved in various physiological metabolic activities of pathogens. Deletion of peroxisomes might interfere with the development of pathogenic fungi, reduce virulence, and decrease the ability to resist plant defense enzymes (Segmüller et al., 2008). However, the virulence factors of *S. turcica* f. sp. *sorghi* have not yet been investigated at the molecular level.

The two formae speciales of *S. turcica* could not be distinguished by morphology and internal transcribed spacer (ITS), but inoculation results showed that *S. turcica* f. sp. *zeae* and *S. turcica* f. sp. *sorghi* have high specificity on host and have no obvious cross-infection (Tang et al., 2014). Meanwhile, microsatellites had also been used to distinguish *S. turcica* from corn and sorghum (Nieuwoudt et al., 2018). With the advent of new molecular research techniques, the study of pathogens has remarkably benefited from the information of the genome and the analysis of comparative genomics. A comparative genomic study was conducted on the two pathogens in corn, *Ustilago mayais* and *Sporisorium reilianum*; 43 variant regions were identified in the two species. These regions mainly encode secretory effectors and some virulence clusters (Schirawski et al., 2010). The specialized secondary metabolites and small secretory protein effectors of pathogens are closely related to host specificity (Buiate et al., 2017). *Alternaria longipes* and *A. alternata* can also cause tobacco brown spot disease, but comparative genomic analysis revealed that *A. longipes* has more plant-pathogen-associated genes, carbohydrate-active enzymes (CAZys), secreted protein genes and conditionally dispensable chromosomes (Hou et al., 2016). Therefore, exploring the differences in pathogenicity mechanism between the formae speciales of *S. turcica* and host interaction requires the genomic information of the two formae speciales.

It was reported that pathogens can secrete a large amount of cellulase during the pathogenesis process, which softens the host cell wall leading to faster infection rates and longer disease duration (Wanjiru et al., 2002). In cellulase-inhibited mutants of *Erwinia carotovora* subsp. *carotovora*, this process of cell wall softening was significantly reduced in potato tissues (Walker et al., 1994). Owing to the secretion of other cell wall degrading enzymes, the pathogenicity of *Cochliobolus carbonum* was not affected by the destruction of the *CEL1* gene (Sposato et al., 1995). Furthermore, a highly aggressive strain of *Phaeosphaeria nodorum* secreted more cellulase than a weakly aggressive strain (Lalaoui et al., 2008). The cellulase activity of *S. turcica* f. sp. *zeae* was slightly higher than that of *S. turcica* f. sp. *sorghi*, and the cellulase genes of *S. turcica* f. sp. *zeae* and *S. turcica* f. sp. *sorghi* were significantly upregulated at 72 and 36 h after inoculation, respectively (Tang et al., 2015). D-glucono-l, 5-lactone, a mixed inhibitor of cellulase activity in *Trichoderma reesei*, mainly affects the activity of glucosidase, but also has a inhibitory effect on the activity of exoglucanase, endoglucanase, and related enzymes, and it can induce cellulase gene expression (Reese et al., 1971; Kou et al., 2014).

Obvious host specializations are noted in *S. turcica* f. sp. *zeae* and *S. turcica* f. sp. *sorghi*. The whole genome sequencing and comparative genomic analysis of the two formae speciales of *S. turcica* can help in the identification of the relevant pathogenic genes that help in host-specific interactions; the whole genome sequence of *S. turcica* f. sp. *zeae* has been published in 2012 (Ohm et al., 2012). In the present study, a strain named GD003 was isolated from sorghum leaves infected with northern leaf blight by using the monospore separation method, and then identified using Koch's postulates and ITS sequencing of *S. turcica* f. sp. *sorghi*. Whole-genome sequencing and gene function annotations revealed important genomic information about *S. turcica*. Comparative genomic analysis revealed differences in the genomes between the two formae speciales, including secreted proteins, pathogen-host interaction (PHI) genes, CAZys and secondary metabolic pathways. Furthermore, we used gluconolactone to alter the pathogenicity of *S. turcica* f. sp. *zeae* and speculated that the cellulase was one of the important reasons

for its pathogenicity. The study findings might provide important theoretical information for the pathogenic differentiation mechanism of the formae speciales of *S. turcica* and provide an effective reference for the prevention of northern leaf blight and genetic breeding of resistant varieties.

Materials and methods

Fungal isolation and identification

Strain GD003 was isolated from sorghum leaves infected with northern leaf blight by using the single-spore isolation method (Gao et al., 2010). The spores were transferred to water agar (WA: 17 g agar and 1 L ddH_2O) by tapping the leaves, and then the single spore was directly picked up under low magnification and transferred to potato dextrose agar (PDA: 200 g potato, 20 g glucose, and 17 g agar, and 1 L ddH_2O) by using a simple homemade needle. The strain GD003 was deposited in the Institute of Plant Immunology, Shenyang Agricultural University and used to study pathogenic mechanism of the pathogen for 5 years. The strain was incubated under continuous darkness at 25°C.

ITS sequences and the inoculation and were used for the identification of strain GD003. Mycelia were collected from potato dextrose broth, the DNA was separated using the modified CTAB method, and the ITS sequences were amplified using PCR by using primers ITS1 and ITS4 (Gardes and Bruns, 1993; Okori et al., 2004). The amplified product was sequenced, and phylogenetic relationships were analyzed using MEGA4.0 (Tamura et al., 2007) as well as the neighbor-joining (NJ) model. Bootstrap replication was set to 1,000, and the bootstrap value was at the branch node. Sweet sorghum variety LR115 and corn variety Huobai susceptible to northern leaf blight were obtained from Dr. Jiang (Liaoning Academy of Agricultural Sciences, China). Three germinated seeds were sown in pots having 15 cm diameter and cultivated in a greenhouse with a temperature of 21/18°C day/night and light intensities of 35–50 Klux. When the plants grew to the V6 stage, the strain incubated for 2 weeks was added to a small amount of sterile water and filtered through a double-layered gauze to form a suspension of 1×10^6 conidia per milliliters. Tween-20 was added to the prepared spore suspension to a final concentration of 0.1%, and the seedlings were inoculated the spore suspension by using a sprayer; after inoculation, the seedlings were transferred to a plastic shed for 48 h for moistening, and then transferred to a greenhouse. The leaves of plants were inspected for symptoms of infection at 14 days after inoculation.

Genome sequencing and assembly

The improved CTAB method was used to extract genomic DNA from GD003, a sorghum-specific strain of *S. turcica*. After DNA was qualified by electrophoresis, two DNA libraries were constructed, of which 350 bp small fragment library was sequenced at paired-end by HiSeq PE150 and 20 kb SMRT Bell library was sequenced at single-molecule by PacBio RSII. Sequencing was performed at the Beijing Novogene Bioinformatics Technology Co., Ltd. (Beijing, China). The low quality reads were filtered by the SMRT Link v5.0.1 (Li et al., 2010) and the filtered reads were assemblied to generate contigs. The relationship between the contigs were determined by SOAPdenovo2 (Luo et al., 2012) to obtain the final assembly results that reflecting the basic conditions of the sample genome, including total data, GC content, read coverage depth, and mass value distribution.

Comparative genomic analysis

The genome sequences of *S. turcica* f. sp. *zeae* Et28A was deposited at joint genome institute (JGI) with project ID 401988. The open reading frames across the genome were predicted and filtered using Augustus software (Stanke et al., 2006), and the number, total length, average length, and proportion of encoding genes were recorded. The gene function annotation was mainly based on the comparison of protein sequences, and the local comparison tool BlastP (Gao et al., 2011) was used for homology matching with the annotation results on GenBank, gene ontology (GO; Ashburner et al., 2000), kyoto encyclopedia of genes and genomes (KEGG; Kanehisa et al., 2004), cluster of orthologous groups (COG; Tatusov et al., 2003), non-redundant protein sequence (NR; Li et al., 2002), transporter classification database (TCDB; Milton et al., 2009), Swiss-Prot (Bairoch and Apweiler, 2000), PHI (Urban et al., 2015) and CAZy (Cantarel et al., 2009) databases to obtain the corresponding functional annotation information. SignalP (Petersen et al., 2011) was used to analyze the N-terminal signal peptide of encoded proteins, TMHMM (Krogh et al., 2001) was used for transmembrane structure prediction, and TargetP (Emanuelsson et al., 2007) was used to predict the subcellular localization of encoded proteins. Proteins located extracellularly, with signal peptide and lacking transmembrane domains, were defined as secreted proteins. Further, effectors in secreted proteins were screened by EffectorP (Sperschneider et al., 2016).

The key genes for secondary metabolite syntheses were identified using antiSMASH v4.0.2 program (Medema et al., 2011), especially polyketide synthase (PKS) coding genes. The MEGA4.0 (Tamura et al., 2007) was used to compare the protein domains encoded by PKSs of two formae speciales and other plant pathogenic fungi, and to construct phylogenetic tree, including *Bipolaris maydis* T-toxin synthesis related to PKS1 (GenBank accession number: AAB08104), *Fusarium graminearum* zearalenone synthesis related to PKS4 (GenBank accession number: ABB90283), *Aspergillus nidulans* locastatin synthesis related to LovF (GenBank accession number: AAD34559), *F. verticillioides* fumonisin synthesis related to Fum1p (GenBank accession number: AAD43562), *A. steynii* ochratoxin synthesis

related to PKS (GenBank accession number: AHZ61902), and *A. alternate* ACT-toxin synthesis related to ACTTS3 (GenBank accession number: BAJ14522), as well as genes closely related to melanin synthesis such as *B. oryzae* PKS1 (GenBank accession number: BAD22832), *S. turcicia* PKS (GenBank accession number: AEE68981), *Ascochyta rabiei* PKS1 (GenBank accession number: ACS74449), *Podospora anserine* PKS1 (GenBank accession number: CDP25014), *Colletotrichum lagenarium* PKS1 (GenBank accession number: BAA18956), *A. fumigatus* A1b1p (GenBank accession number: ACJ13039), *Ceratocystis resinifera* PKS1 (GenBank accession number: AAO60166).

Real-time PCR analysis of genes encoding the specific effectors of *Setosphaeria turcica* f. sp. *zeae*

The mycelium disk of strain Et28A with diameter of 1 cm was inoculated onto corn leaves *in vitro*, and 50–100 mg of the leaves under the disk were cut with RNA-free scissors at different infection periods (0, 24, 48, 72, and 96 h), wrapped in tin foil and immediately frozen in liquid nitrogen for 10 min, transferred to −80°C for storage. Total cellular RNA was isolated using an Ultrapure RNA Kit (CWBIO, Beijing, China), and then cDNA was synthesized using the PrimeScript™ RT reagent Kit with gDNA Eraser (Perfect Real Time; TaKaRa, Tokyo, Japan). The reaction mixture contained 10 μl of TB Green Premix Ex Taq II (Tli RhaseH Plus; TaKaRa, Tokyo, Japan), 1 μl of forward primer, 1 μl of reverse primer, 2 μl of cDNA, and 6 μl of ddH_2O. The reactions were performed in the CFX-96 system (BioRad, Hercules, CA, United States), and all samples were tested in triplicate and repeated twice. All reaction conditions were performed as follows: initial denaturation at 95°C for 30 s, followed by 40 cycles of denaturation at 95°C for 5 s and annealing at 60°C for 30 s. The cycle threshold (Ct) values were analyzed using CFX Manager and relative expression levels of functionally annotated effector protein-coding genes specific for *S. turcica* f. sp. *zeae* were calculated at each period according to the $2^{-\triangle\triangle Ct}$ method.

Effect of gluconolactone on *Setosphaeria turcica* f. sp. *zeae*

The gluconolactone solution was sterilized and cooled, and then added to a PDA medium under sterile conditions to final concentrations of 0.2, 0.4, and 0.8% (w/v). Five millimeter agar disks containing mycelium of strain Et28A were transferred to the medium with an inoculation needle. Then the side of the hyphae was pressed down to the medium and one agar disk was placed in the center of each dish. Each treatment was repeated five times and cultured at 25°C for 5 days. The gluconolactone solution was replaced by sterile water for the control group. For each treatment group, the colony diameter was measured then the growth inhibition rate was calculated (Quiroga et al., 2001).

To analyze the effect of gluconolactone on cellulase activity, preparation of the crude enzyme solution was slightly modified based on the methods of Lee and Blackburn (1975). The agar disks containing mycelium of strain Et28A that were cultured on the PDA were added to Czaper liquid culture medium (2 g KNO_3, 0.5 g KCl, 0.01 g $FeSO_4$, 1 g K_2HPO_4, 0.5 g $MgSO_4$, 10 g sodium carboxymethyl cellulose, and 1 L ddH_2O) both with and without gluconolactone (0.2, 0.4, and 0.8%; w/v). Then, nine disks were inoculated in 150 ml medium and were shaken for 1 h per day (120 rpm), incubated for 15 days at 25°C in the dark, and then filtered through sterile double gauze (22 mesh). The filtrate was centrifuged at 4°C and 10,000 g for 20 min and the crude enzyme solution was the supernatant. Cellulase activity was determined based on the method described by Eveleigh et al. (2009). Briefly, 1 ml of 1% sodium carboxymethyl cellulose in 0.1 M citrate buffer (pH 4.5) and 0.5 ml extracted crude enzyme solution were placed in a test tube and then incubated in a 50°C water bath for 30 min. After the reaction mixture was cooled, 3 ml of 3, 5-dinitrosalicylic acid reagent was added, and the solution was heated to 100°C for 5 min. The absorbance at 540 nm of the reaction mixture after appropriate dilution was measured with a spectrophotometer. A cellulase activity unit (U) was defined as the amount of enzyme required to catalyze the reaction to produce 1 μmol of reducing sugar per min under specific conditions. All enzyme activity assays were repeated three times. The protein content was determined using the Coomassie brilliant blue G250 staining method (Bradford, 1976).

Analysis of expression levels was used to measure the effect of gluconolactone on endo-1, 4-β-D-glucanohydrolase encoding gene A2464. The agar disks containing the mycelium of *S. turcica* f. sp. *zeae* Et28A that were cultured on the PDA were inoculated *in vitro* on corn leaves at the 6–8 leaf stage. One hundred microliter gluconolactone solutions (0.2 and 0.4%, w/v) were added to the edge of the disks each day, and the control group was treated with sterile water. The expression levels of A2464 were determined at different infection periods (0, 6, 12, 24, 36, 48, 72, and 96 h). All samples were tested in triplicate and repeated twice. Finally, the infection rate and pathogenicity were determined and the inoculation method was described above. Pathogenicity was determined after culturing for 72 h in the dark at 25°C for moistening. Then it was stained with trypan blue, dehydrated with saturated chloral hydrate, and rinsed with sterile water before being placed under a microscope to observe the infection efficiency of *S. turcica* f. sp. *zeae* Et28A. Each treatment was repeated three times.

Statistical analysis

All statistical tests were calculated in SPSS Statistics 19 software. Data were represented as means ± standard error of at least three repeated experiments. $p < 0.05$ was defined as a statistically significant difference.

Results

Identification of *Setosphaeria turcica* f. sp. *sorghi* GD003

Phylogenetic tree of the ITS sequences showed that GD003, *S. turcica* f. sp. *zeae* strain QDY1307 (GenBank accession number: KJ922736.1) and *S. turcica* f. sp. *sorghi* strain LLG1302 (GenBank accession number: KJ922728.1) were in the same branch (only four differential bases; Figure 1A). The ITS sequences do not distinguish the two formae speciales of *S. turcica*. Within 14 days after inoculation, this GD003 strain formed a typical long spindle lesion on sorghum leaves, while no visible reaction was evident on corn leaves (Figure 1B), so the pathogenicity tests identified strain GD003 as *S. turcica* f. sp. *sorghi*.

Genomic sequencing and assembly of *Setosphaeria turcica* f. sp. *sorghi* GD003

After electrophoresis, 159.60 ng/ml DNA yielded OD260/280 of 1.87 and OD260/230 of 2.24; the fragment size was mainly distributed above 30 K, and the genome was slightly broken, which met the requirements for single-sequencing database creation. A total of 7.82 Gb of reads were obtained by sequencing the genome of *S. turcica* f. sp. *sorghi* GD003 (depth: 177×), including 938,546 reads. The length of the sequence N50 was 11,965 bp, and the average sequencing quality value was 0.86. The genome assembly revealed 22 contigs (Supplementary Fasta 1) with a total length of 44,063,561 bp and a GC content of 50.7%. The scatter diagram of *S. turcica* f. sp. *sorghi* GD003 genomic GC-depth was mostly concentrated in the range of 40%–60% (Supplementary Figure 1).

Genome comparison of two formae speciales of *Setosphaeria turcica*

A total of 10,428 protein-coding genes (Supplementary Fasta 2) were predicted in the genome of *S. turcica* f. sp. *sorghi* GD003, accounting for 35.47% of the total length of the genome sequence, and the average length of the coding genes was 1,499 bp. In contrast, only 8,276 protein-coding genes (Supplementary Fasta 3) were found in the genome of *S. turcica* f. sp. *zeae* Et28A, accounting for 26.86% of the total length of the genomic sequence, and the average length of the coding genes was 1,396 bp (Table 1). From the gene distribution map, the most abundant *S. turcica* f. sp. *sorghi* GD003 and *S. turcica* f. sp. *zeae* Et28A genes were found to be concentrated in the region of 2,500 bp or more, including 1,431 and 882 genes, respectively.

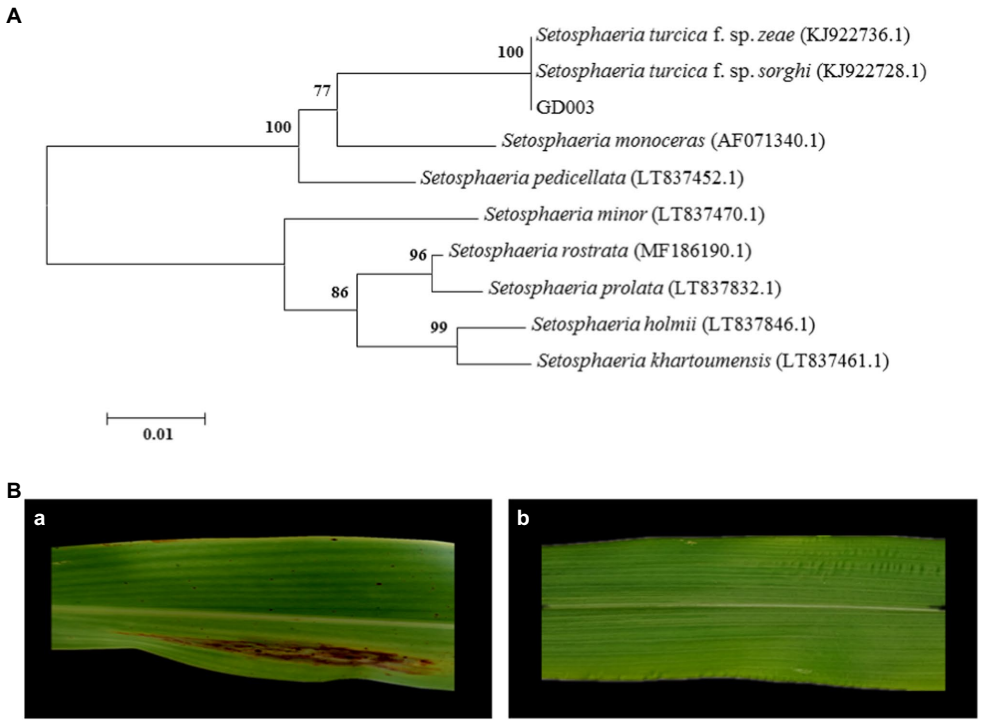

FIGURE 1
Identification of GD003 based on ITS sequences and pathogenicity. **(A)** Phylogenetic analysis of ITS sequences of GD003. The numbers in parentheses indicate the accession numbers of ITS sequences of the species in GenBank. **(B)** Pathogenicity of GD003 strain on sorghum and corn. **(a)** Typical lesions of GD003 on sorghum. **(b)** No visible reaction of GD003 on corn.

TABLE 1 *Setosphaeria turcica* f. sp. *sorghi* GD003 and *S. turcica* f. sp. *zeae* Et28A genome features.

Features	*S. turcica* f. sp. *sorghi* GD003	*S. turcica* f. sp. *zeae* Et28A
Genome size (bp)	44,063,561	43,014,577
Gene number	10,428	8,276
Gene length (bp)	15,630,591	11,553,107
Gene GC content (%)	55.94	56.52
% of genome (genes)	35.47	26.86
Gene average length (bp)	1,499	1,396
Gene internal length (bp)	28,432,970	31,461,470
Gene internal GC content (%)	47.83	49.57
% of genome (internal)	64.53	73.14

TABLE 2 Number of genes annotated by different functional databases in *Setosphaeria turcica* f. sp. *sorghi* GD003 and *S. turcica* f. sp. *zeae* Et28A genomes.

Database type	*S. turcica* f. sp. *sorghi* GD003		*S. turcica* f. sp. *zeae* Et28A	
	Number	Percent (%)	Number	Percent (%)
GO	7,000	67.13	5,708	68.97
KEGG	9,570	91.77	7,762	93.79
COG	2048	19.64	2043	24.69
NR	10,161	97.44	8,013	96.82
TCDB	428	4.10	411	4.97
SwissProf	3,039	29.14	2,952	35.67
PHI	796	7.63	673	8.13
CAZy	480	4.60	442	5.34
Secretory protein	704	6.75	521	6.30

Different numbers of genes in the two formae speciales genomes were annotated in each functional database (Table 2). By comparing *S. turcica* f. sp. *sorghi* GD003 and *S. turcica* f. sp. *zeae* Et28A, 704 and 521 secreted proteins were predicted, respectively (Supplementary Figure 2), containing 161 and 137 effectors, which were required for the pathogens to act directly or indirectly on the hosts. The findings suggested that the *S. turcica* f. sp. *sorghi* GD003 and *S. turcica* f. sp. *zeae* Et28A could directly secrete 42 and 33 small cysteine-rich proteins (SCRPs; the number of amino acids is less than or equal to 200, and cysteine content is 4% or more), respectively, of which 30 SCRPs existed in both formae speciales.

In the present study, 796 and 673 PHI genes were detected in *S. turcica* f. sp. *sorghi* GD003 and *S. turcica* f. sp. *zeae* Et28A, covering 609 and 539 PHI accessions, respectively, but they had seven types of phenotypic mutations (Supplementary Table 1). The PHI information of 655 genes was identical in the two formae speciales. Among 141 PHI genes unique to *S. turcica* f. sp. *sorghi* GD003, excluding 81 genes that did not affect the pathogenicity, phenotypic mutants of 45 genes (accession number: PHI139, PHI323, PHI339, PHI3837, PHI3865, PHI4992, etc.) had reduced virulence. Further searches revealed that the secreted proteins of *S. turcica* f. sp. *sorghi* GD003 and *S. turcica* f. sp. *zeae* Et28A contained 62 and 54 PHI related genes, respectively, of which 51 PHI genes were homologous and 11 PHI genes were specific in *S. turcica* f. sp. *sorghi* GD003.

Blastp alignment was performed using the genomically encoded proteins and CAZy database, and 480 and 442 CAZys were identified from *S. turcica* f. sp. *sorghi* GD003 and *S. turcica* f. sp. *zeae* Et28A, respectively; the related CAZys were mainly involved in carbohydrate degradation, modification, and biosynthesis (Figure 2). The most common CAZys were glycoside hydrolases (GHs) containing 224 and 216 genes, respectively, and the remaining were auxiliary activities (AAs), glycosyltransferases (GTs), carbohydrate binding modules (CBMs), carbohydrate esterases (CEs) and polysaccharide lyases (PLs). Further analysis found that 216 (30.68%) and 178 (34.17%) CAZy genes were identified in the secreted proteins of *S. turcica* f. sp. *sorghi* GD003 and *S. turcica* f. sp. *zeae* Et28A, respectively, and most of these genes were associated with GHs in the subfamily classification (Supplementary Table 2).

Further, 20 and 15 PKSs were predicted for secondary metabolic gene clusters in *S. turcica* f. sp. *sorghi* GD003 and *S. turcica* f. sp. *zeae* Et28A genomes, respectively (Supplementary Table 3). The PKS genes of the two formae speciales were mainly divided into two types (Figure 3A). The core domain of type I consisted of ketoacyl synthase (KS), acyltransferase (AT) and dehydratase (DH), including 16 *S. turcica* f. sp. *sorghi* GD003 PKSs, 12 *S. turcica* f. sp. *zeae* Et28A PKSs, and 6 other PKSs related to the synthesis of phytopathogenic mycotoxins. The other type of core domain was KS + AT, including 4 *S. turcica* f. sp. *sorghi* GD003 PKSs, 3 *S. turcica* f. sp. *zeae* Et28A PKSs, and 7 known melanin synthesis-related PKSs from phytopathogenic fungi. Further analysis of PKSs associated with melanin synthesis revealed that the two formae speciales shared the same core domain, including one KS, one AT, two acyl carrier proteins (ACPs) and one thioesterase (TE), and both coding sequences were 99.48% similar to the known *S. turcica* PKS (GenBank accession number: AEE68981; Figure 3B).

Analysis of the expression levels of *Setosphaeria turcica* f. sp. *zeae* specific effector coding genes

In our study, 21 effector protein-coding genes were found specifically in *S. turcica* f. sp. *zeae* Et28A, and 13 of them were defined as encoding hypothetical proteins. 18S rRNA was used as a reference gene, primer sequences of eight functionally annotated effector protein-encoding genes specific to *S. turcica* f. sp. *zeae* were designed (Table 3). Compared with the 0 h control, only A1078 was downregulated after inoculation, while the expression levels of A0353, A2199, A2464, A3017, A6166, and A8125 were significantly upregulated. The expression level of

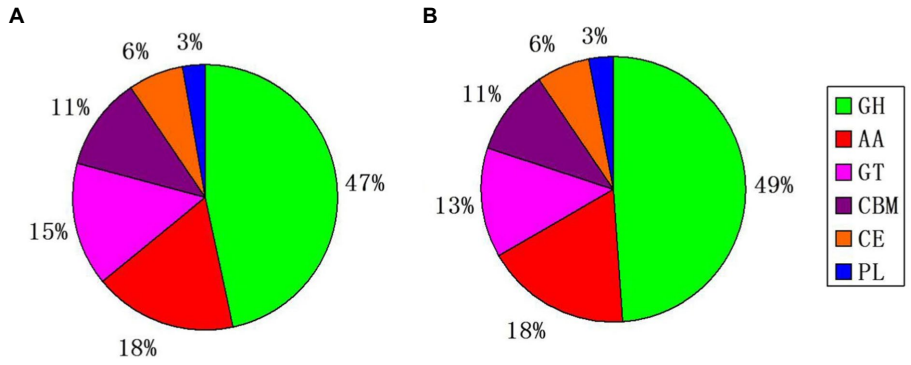

FIGURE 2
Classification and comparison of the two formae speciales by using whole genome CAZy database. **(A)** *Setosphaeria turcica* f. sp. *sorghi* GD003. **(B)** *S. turcica* f. sp. *zeae* Et28A. GH, glycoside hydrolase; AA, auxiliary activity; GT, glycosyltransferase; CBM, carbohydrate-binding module; CE, carbohydrate esterase, and PL, polysaccharide lyase.

A2464 after 72 h of inoculation increased by more than 150-fold compared with that before (Figure 4).

Inhibition effect of gluconolactone on cellulase activity and pathogenicity of *Setosphaeria turcica* f. sp. *zeae*

At a concentration of 0.4% (w/v), hyphal growth was significantly inhibited. When the concentration increased to 0.8% (w/v), the inhibition rate reached 46.12%, which indicated that gluconolactone inhibited the hyphal growth of *S. turcica* f. sp. *zeae* Et28A (Figure 5A). The cellulase activity of *S. turcica* f. sp. *zeae* Et28A was significantly inhibited by different concentrations of gluconolactone ($p < 0.05$), and the effect increased with increasing concentration (Figure 5B). Despite different gluconolactone concentrations (0.2 and 0.4%, w/v), *StCEL2* gene expression showed a consistent trend, all peaked at 72 h. *StCEL2* gene expression level increased with increasing gluconolactone concentration during the same infection period (Figure 5C). Differently-treated pathogens could invade the host and caused corn leaf lesions after 72 h of inoculation. However, the number of invasion sites observed in the control group was significantly higher than that in the gluconolactone treatment group. Furthermore, the number of invasion sites decreased with increasing concentration (Figure 5D), indicating that gluconolactone affected the infection and pathogenicity of *S. turcica* f. sp. *zeae* Et28A.

Discussion

Previous studies have shown that the variability of ITS sequences among different formae speciales of the same fungus is limited. For example, the ITS and EF-alpha elongation factor analyses cannot identify the formae speciales of *F. oxysporum* (Zhang et al., 2013). Since the ITS information of GD003, *S. turcica* f. sp. *zeae* strain QDY1307 (GenBank accession number: KJ922736.1), and *S. turcica* f. sp. *sorghi* strain LLG1302 (GenBank accession number: KJ922728.1) reveal a difference of only four bases, it proves once again that ITS could not identify the formae speciales of *S. turcica*. Because of the obvious host-specificity between the formae speciales (Mitra, 1923), the inoculation of sorghum leaves showed a clear feature of northern leaf blight. Finally, GD003 was identified as *S. turcica* f. sp. *sorghi* and named *S. turcica* f. sp. *sorghi* GD003.

In this study, we comprehensively reported the first genome information of *S. turcica* f. sp. *sorghi* and compared it with the published genomic data of *S. turcica* f. sp. *zeae* Et28A (JGI ID: 401988), which can provide a reference for revealing the pathogenic mechanism of *S. turcica*. Different strains of the same species also have large differences in genomic structure and encoded proteins (Condon et al., 2013). Several random amplified polymorphic DNA haplotypes uniquely present in sorghum strains of *S. turcica* were not observed in strains collected from corn (Borchardt et al., 1998; Ferguson and Carson, 2004). Genetic differences were confirmed in two formae speciales of *S. turcica* by universally primed polymerase chain reaction (Tang et al., 2014). The genome size of *S. turcica* f. sp. *zeae* GD003 (44.06 Mb) is greater than that of *S. turcica* f. sp. *sorghi* Et28A (43.01 Mb), which may be caused by the pressure of host selection (Thrall et al., 2002). Changes of GC content were speculated to prompt *Curvularia lunata* to mutate more frequently in virulence differentiation (Gao et al., 2014). The GC content of the same species shows a concentrated distribution in the sequencing depth profile (Forsdyke, 1996). Concentration of most of the points in the distribution map in a narrow range (40%–60%) indicates no pollution in the assembly results.

Secreted protein is a generic term for a class of proteins that are produced by cells at specific times and conditions and transported extracellularly, which is often directly related to PHI, is a candidate effector, and is more likely to exhibit population differences during natural selection (Klein et al., 1996). Therefore, studies on secreted proteins might help understand host specificity issues in PHIs. The

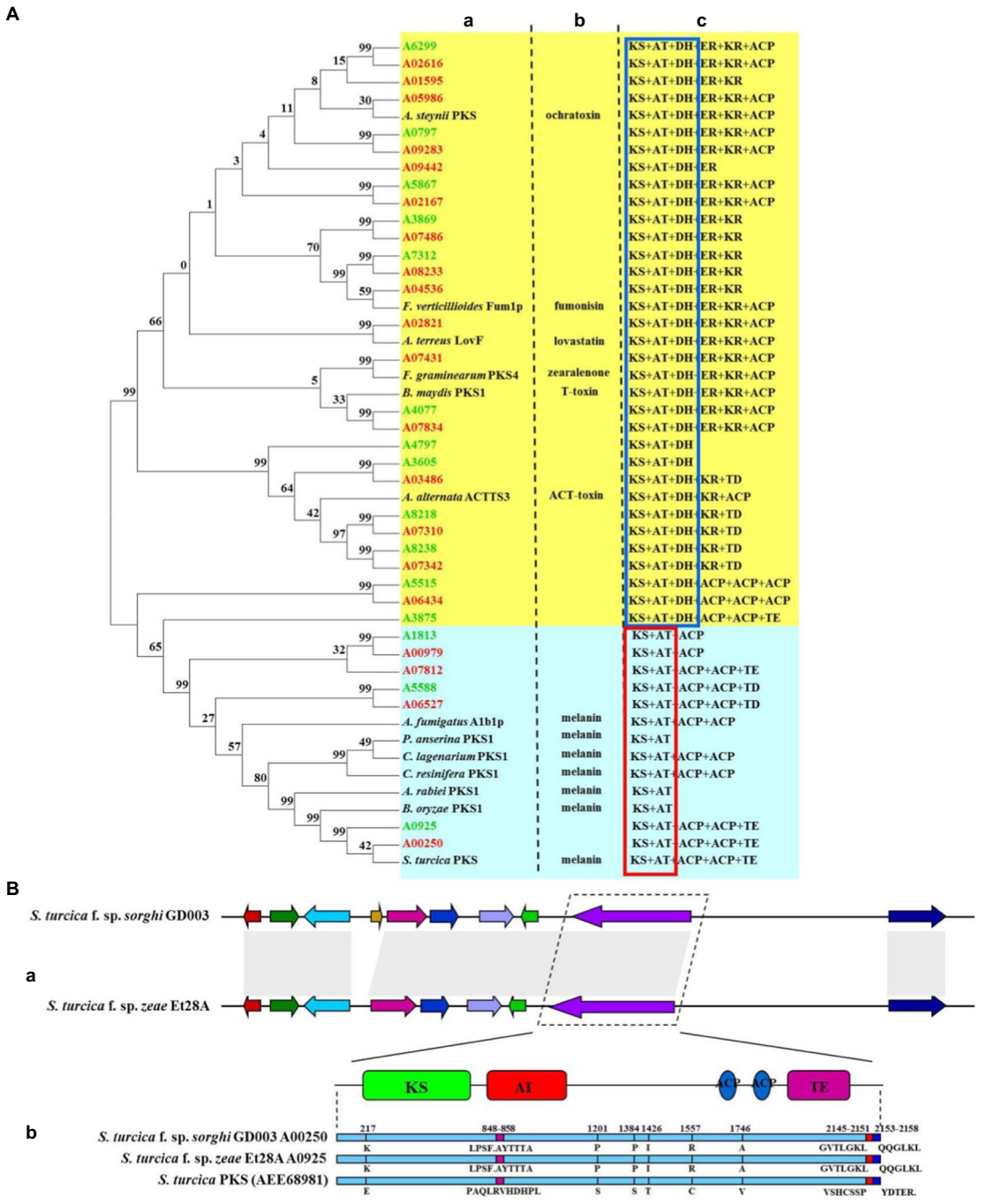

FIGURE 3
Comparative analysis of polyketide synthase (PKS) key genes of two formae speciales of *Setosphaeria turcica*. **(A)** Phylogeny and domain comparison of PKSs from *Setosphaeria turcica* f. sp. *sorghi* GD003 and *S. turcica* f. sp. *zeae* Et28A with that from other known plant pathogenic fungi. (a) Phylogenetic analysis of proteins encoded by PKS genes. (b) PKS-related toxin and melanin from other known phytopathogenic fungi. (c) PKS-associated protein domains. KS, ketoacyl synthase; AT, acyltransferase; DH, dehydratase; ER, enoylreductase; KR, ketoacyl reductase; ACP, acyl carrier protein; TE, thioesterase; and TD, tudor domain. Words marked in green and red indicate gene names for *S. turcica* f. sp. *zeae* Et28A and *S. turcica* f. sp. *sorghi* GD003, respectively. The red and blue boxes indicate common domains. **(B)** Comparison of gene clusters and core gene-coding sequences of melanin synthesis in *S. turcica* f. sp. *sorghi* GD003 and *S. turcica* f. sp. *zeae* Et28A genomes. (a) Melanin synthesis gene clusters of the two formae speciales. (b) Differences in protein sequence of the melanin synthesis core gene from known *S. turcica*.

secreted proteins related to pathogenicity are mainly avirulence genes of pathogens, products of pathogenic genes, and related regulatory proteins (Rep, 2005), such as cell wall degrading enzymes can reduce or even overcome the host's barrier to pathogen infection (Brito et al., 2006), elicitor substances can induce pathogenic responses in host plants (Kamoun et al., 1998), and some of the

TABLE 3 Primer sequences and amplification lengths of functionally annotated effector protein-coding genes in *Setosphaeria turcica* f. sp. *zeae*.

Gene ID	Accession number	Functional description	Primer	Seq (5'to3')	Amplification length (bp)
A0353	XP_008021443.1	Carbohydrate-binding module family 18 protein	CBM18-F	CCAAGAACGACATCCAGGACCAG	138
			CBM18-R	GACCGCAGCTCTCGCCATTC	
A1078	XP_008022422.1	Glycoside hydrolase family 20 protein	GH20-F	CGCACTGGCAACGGTCCTTAC	178
			GH20-R	GCGGTTGAAGGCGTTGGAGAC	
A2199	XP_008024103.1	Carbohydrate esterase family 1 protein	CE1-F	CAGGCGACAAGGCAGAAGTGG	153
			CE1-R	CTCACGGTTGCCTGGCTGTATC	
A2464	XP_008024638.1	Glycoside hydrolase family 7 protein	GH7-F	GGTGGTCGCTCCAAGCTCAAC	144
			GH7-R	AATCTGAGTCGCCTGGCTGTTG	
A3017	EKG13298.1	Argonaute/Dicer protein PAZ	PAZ-F	GCAACGCCTACGACTTCTTCCTC	121
			PAZ-R	GTCATGGCCTGCATCTGGTCTG	
A3531	XP_008025955.1	Glycoside hydrolase family 62 protein	GH62-F	TACCTGCGAACCTCCGTCCATC	111
			GH62-R	GGTTGCGGCTGTCCTTCTTGG	
A6616	XP_008029324.1	Glycoside hydrolase family 16 protein	GH16-F	AAGTCACGGCAGGAAGCATCAAC	173
			GH16-R	GGATTGGAGAATGGCAGACGACAC	
A8125	XP_008031550.1	Glycoside hydrolase family 10 protein	GH10-F	GCACTGACAATCCGCAATGACAAC	121
			GH10-R	CTTGACTTGGTTCCGTGGCATCC	

secreted proteins can also degrade the antifungal toxin produced by host plants to facilitate the progression of infection (Sperschneider et al., 2016). In this study, more secreted proteins were predicted in *S. turcica* f. sp. *sorghi* GD003. Many phytopathogenic fungi can also directly secrete SCRPs, which have a close relationship with the mechanism of pathogenesis (Rep et al., 2004). These small molecular proteins can act as virulence effector proteins and have carbohydrate-binding activity; they can directly play a role by interfering with host cell signal transduction or inhibiting host PAMP-triggered immunity responses (Marcet-Houben et al., 2012). Twelve SCRPs unique to *S. turcica* f. sp. *sorghi* GD003 were all uncharacterized proteins, and further studies are warranted to determine the function of SCRPs specific to the two formae speciales in PHI.

The genes involved in the interaction between pathogens and hosts play a crucial role in pathogenesis; their products are directly involved in the adaptation and response of pathogens to the host-infecting environment, and the secreted elicitors can directly induce the host plants to express the symptom (Barrett et al., 2009). The PHI database integrates pathogen-related genes to different hosts such as animals, plants, and microorganisms and is widely used to investigate plant pathogen genomes and genes implicated in virulence (Winnenburg et al., 2006; Urban et al., 2015). In this study, 45 genes with phenotypic mutations with reduced pathogenicity were specifically present in *S. turcica* f. sp. *sorghi* GD003, such as PHI139 was required for *Cryptococcus neoformans* to maintain virulence (Chang and Kwon-chung, 1999), the loss of PHI339 significantly reduced the pathogenicity of *C. lindemuthianum* (Siriputthaiwan et al., 2005), and PHI4992 was required for *Candida albicans* biofilm formation *in vitro* and *in vivo* (Desai et al., 2015). Differences in these PHI-related genes might lead to differences in pathogenicity between the two formae speciales. Significantly, there were 11 PHI genes specific for the secreted protein encoding genes of *S. turcica* f. sp. *sorghi* GD003, the knockout of PHI323 significantly reduced the virulence of *Verticillium fungicola* (Amey et al., 2003), and PHI3865 was required for *Penicillium expansum* to cause blue mold rot (Barad et al., 2012), while the related genes PHI569, PHI2849, and PHI6126 reported in *Fusarium* did not affect their pathogenicity.

The plant pathogenic fungi CAZys play a crucial role in degrading plant cell walls, breaking through host passive defense systems, and establishing PHI relationships (Cantarel et al., 2009). The enzymes encoded by the GH, CE, and PL family genes play a role in depolymerizing cell walls (Walton, 1994), and they had only slight differences between the two formae speciales. Considering the errors in gene sequencing and energy prediction, the CAZy species and quantity of the two formae speciales could basically be thought to be consistent at the genome level. Further, 32 and 26 CBM family genes were found in the *S. turcica* f. sp. *sorghi* GD003 and *S. turcica* f. sp. *zeae* Et28A genomes, respectively; the modules of approximately 40 residues in the family genes were unique to the fungi and played a key role in cellulose degradation in plant cell walls (Quentin et al., 2002). Comparison of CAZy annotation results in secreted proteins of the two formae speciales revealed that the content of GHs in *S. turcica* f. sp. *sorghi* GD003 was significantly higher than that in *S. turcica* f. sp. *zeae* Et28A, which might suggest that the former has stronger pathogenic ability than the latter.

Among the secondary metabolites of plant pathogens, melanin and toxin are the two key pathogenic factors in *S. turcica*. The synthesis of these two virulence substances is mainly mediated by PKSs. *PKS1* had been successfully cloned in *B. oryzae* and *C. resinifera* and was found to affect the synthesis of melanin and reduce pathogenicity (Moriwaki et al., 2004; Tanguay et al., 2006). *StPKS* of *S. turcica* f. sp. *zeae* was shown to play a role in the DHN melanin synthesis pathway, and its decreased expression reduced melanin production (Zhang et al., 2011). Moreover, *S. turcica* f. sp. *zeae* Et28A had an additional betaenone biosynthetic gene cluster unlike in *S. turcica* f. sp. *sorghi* GD003; this cluster acted as a

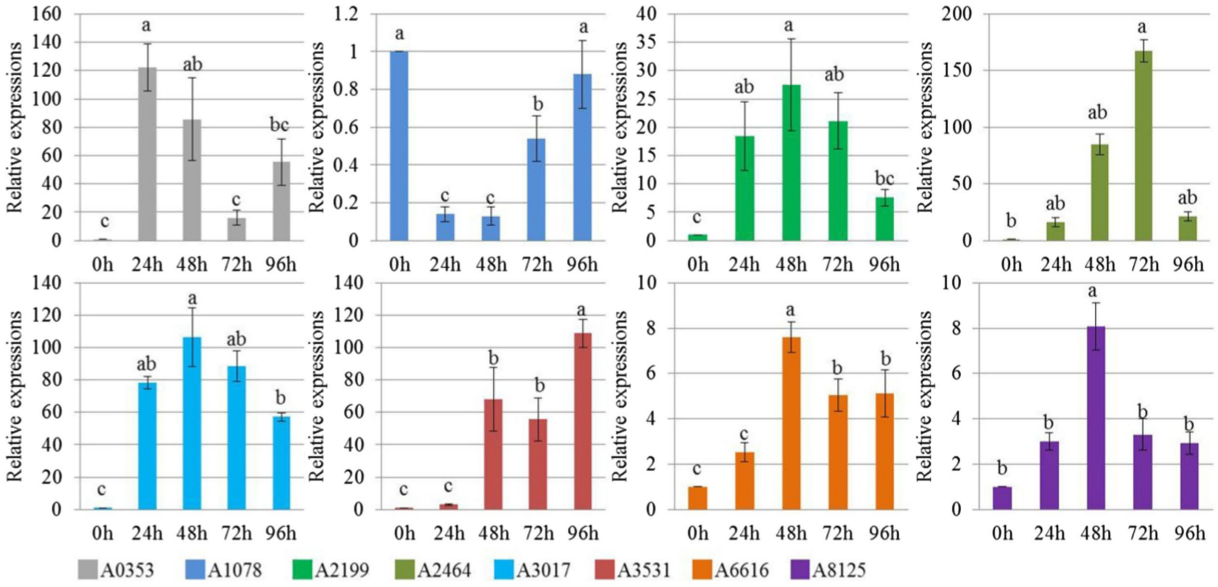

FIGURE 4
Relative expression level of *Setosphaeria turcica* f. sp. *zeae* specific effector coding genes at different infection periods postinoculation. Error bars represent means±SE of three repeated experiments (n=3). Different letters indicate significant differences (p<0.05). A0353 encodes carbohydrate binding module family 18 protein; A1078 encodes glycoside hydrolase family 20 protein; A2199 encodes carbohydrate esterase family 1 protein; A2464 encodes glycoside hydrolase family 7 protein; A3017 encodes Argonaute/Dicer protein PAZ; A3531 encodes glycoside hydrolase family 62 protein; A6616 encodes glycoside hydrolase family 16 protein; A8125 encodes glycoside hydrolase family 10 protein.

phytotoxin that inhibited multiple protein kinases (Patrick and Heimbrook, 1996) and caused significant growth inhibition of *Beta vulgaris* (Haraguchi et al., 1983). This study was the first to identify the core domain of the PKS genes related to melanin and toxin biosynthesis of the two formae speciales of *S. turcica*, and it was found that they had high homology with PKS genes of other pathogenic fungi (common domain of toxin-synthesized PKS genes: KS + AT + DH; common domain of melanin-synthesized PKS genes: KS + AT). Differences in key genes involved in secondary metabolite synthesis have less effect on pathogenic differentiation of the two formae speciales of *S. turcica*.

The determination of the host range in plant pathogens is often closely related to the fungal effectors (Baroncelli et al., 2016). A total of 346 candidate effectors in *S. turcica* were identified by time-course RNAseq, and SIX13-like proteins of *S. turcica* isolated from corn and sorghum were demonstrated to have host-specific polymorphisms (Human et al., 2020). In this study, we first excluded the influence of shared effector protein coding genes of pathogens on host specificity, and only analyzed the expression of specific effector protein-coding genes in *S. turcica* f. sp. *zeae* during the interaction with corn. In the future, further verification of the functions of differential genes is required. During the interaction between plants and pathogens, the activity of hydrolase is conducive to the invasion of the pathogen and the expansion of the disease course. The hydrolytic enzymes related to pathogenicity mainly include cellulase, hemicellulase, pectinase, xylanase, etc. (van den Brink and de Vries, 2011). The significant up-regulation of α-L-arabinofuranosidase encoding gene-A3531 (targeting xylan in plant fibers) during the infection process once again proves that many pathogenic related genes are simultaneously expressed in the interaction, and the time and level of expression determine the pathogenic level of the pathogen to the host (Kim et al., 2016).

Cellulose, an important component of plant cell walls, has a stable structure, which functions effectively to resist pathogen invasion and exogenous stress (Hu et al., 2018). Many cell wall degrading enzymes produced by pathogens cooperate to degrade host cell walls and infect the host (Cooper et al., 1988). Novo et al. (2006) found high levels of activity for endo-1, 4-β-D-glucanase, and β-1, 4-D-glucosidase in invasive *V. dahliae* strains. Furthermore, highly invasive *P. nodorum* strains can produce more cellulase (Lalaoui et al., 2008). The cellulase activity of *S. turcica* f. sp. *zeae* was previously reported to be slightly higher than that of *S. turcica* f. sp. *sorghi*, and it was noted that differences in cell wall degrading enzymes might be one of the reasons for its pathogenic specialization (Tang et al., 2015). The protein encoded by A2464 was annotated as a member of the seventh family of GHs with endo-1, 4-β-D-glucanohydrolase activity (EC 3.2.1.4). This is an important component of cellulase gene and might be a cause of the pathogenicity of *S. turcica* f. sp. *zeae* Et28A. Therefore, we selected the highest expressed *S. turcica* f. sp. *zeae* specific cellulase gene (*StCEL2*) for analysis. In this study, we used gluconolactone to treat *S. turcica* f. sp. *zeae* and analyzed its inhibitory effect on cellulase activity, and our results are consistent with those of Holtzapple et al. (1990). Interestingly, the expression of *StCEL2*, an endo-1, 4-β-D-glucanase coding gene, was upregulated, and increased with

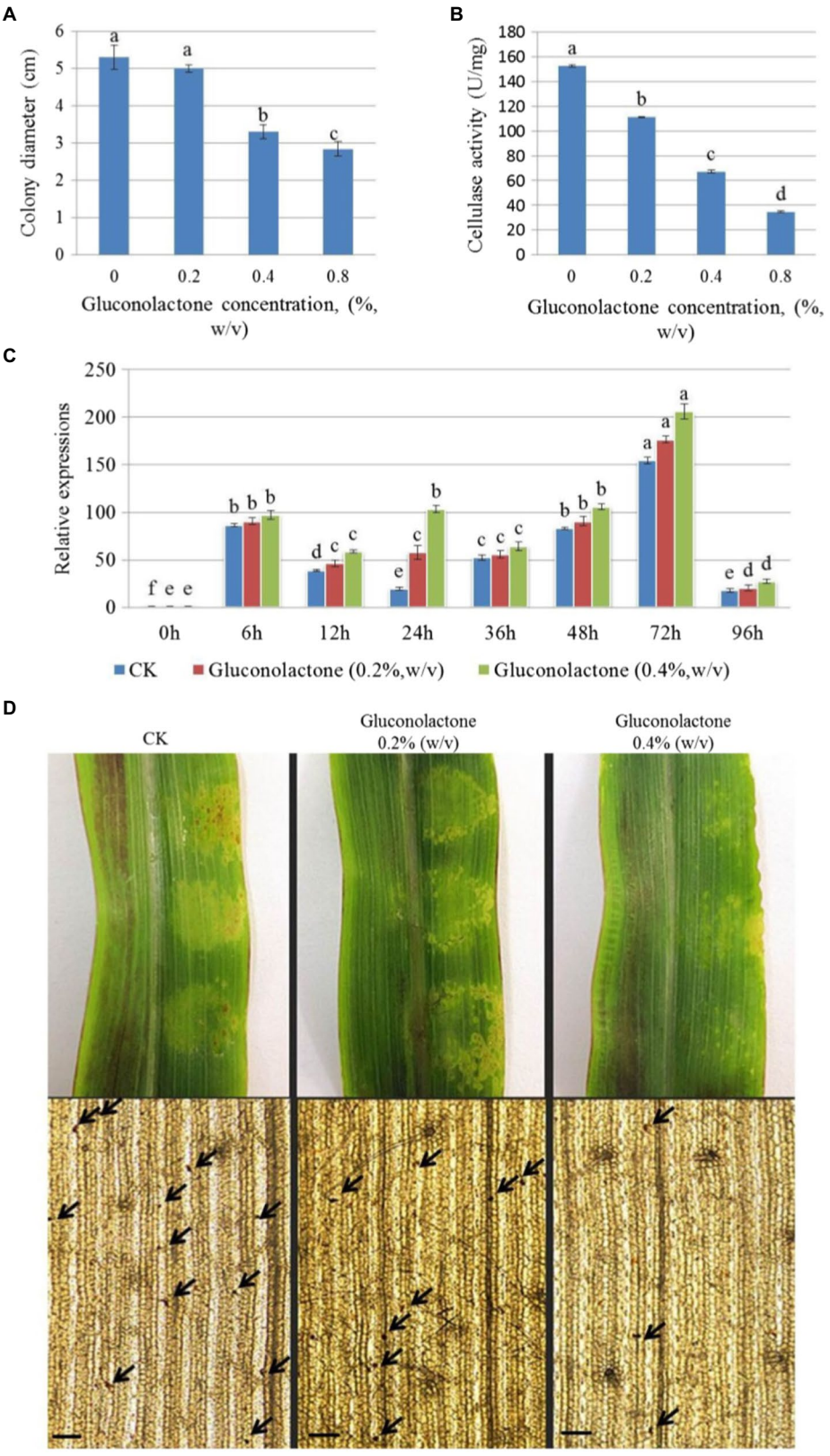

FIGURE 5
Effect of gluconolactone on *Setosphaeria turcica* f. sp. *zeae*. **(A)** Effect of gluconolactone on colony diameter. Error bars are presented as means±SE (n=5). Different letters indicate significant differences (p<0.05). **(B)** Effect of gluconolactone on cellulase activity. Error bars indicate means±SE (n=3). **(C)** Effect of glucolactone on the expression level of endo-1, 4-β-D-glucanase encoding gene *StCEL2*. Data represent means±SE (n=3). **(D)** Effect of gluconolactone on the pathogenicity and infection rate. Arrow positions are the infection dots. Scale bars are equal to 50μm.

increasing concentration of gluconolactone. This is probably due to gluconolactone inhibiting cellulase activity, and the pathogen taking advantage of this stress to invade the host, inducing the expression of related genes (Kou et al., 2014). In summary, gluconolactone can reduce infection rate and pathogenicity by inhibiting the cellulase activity of *S. turcica* f. sp. *zeae*. Furthermore, methods such as gene knockout will be applied to reveal the reasons of two formae speciales infect specific hosts. These results provide useful information for understanding the mechanism of infection and pathogenic differentiation of *S. turcica* f. sp. *zeae*.

Conclusion

In this study, we reported the genome sequence of *S. turcica* f. sp. *sorghi* and compared it with the number of genes of *S. turcica* f. sp. *zeae* in each functional database. Because of the obvious host specificity of the two formae speciales, we focused on the differences in the coding genes of secreted proteins and secondary metabolites, and pointed out the expression levels of specific effector protein-coding genes in *S. turcica* f. sp. *zeae* at different infection periods. Furthermore, the close relationship between cellulase and pathogenicity of *S. turcica* f. sp. *zeae* was determined by the inhibitory effect of enzyme activity, and it was clear that cellulase was one of the important factors of its pathogenicity. In summary, our results provide a novel ideas for studying the interaction between pathogens and the host, and lay a strong foundation for further knockout of cellulase genes and mining of pathogenicity-related genes. Obviously, our data improve the understanding of important pathogens of *S. turcica*, increase the genomic information of *S. turcica* f. sp. *sorghi*, and contribute to the study of pathogenic mechanisms.

Data availability statement

The raw sequence reads of *Setosphaeria turcica* f. sp. *sorghi* have been deposited in GeneBank under the accession number PRJNA860778.

Author contributions

ZM, BL, and ZG conceived and designed the experiments. ZM, YH, ZZ, and XL performed the experiments and analyzed the data. ZM drafted the manuscript, which was critically revised by YX. All authors contributed to the article and approved the submitted version.

Funding

This project was supported by the National Key Technology Research and Development Program of China (2018YFD0300307, 2017YFD0300704, and 2016YFD0300704).

Conflict of interest

The authors declare that the research was conducted in the absence of any commercial or financial relationships that could be construed as a potential conflict of interest.

Publisher's note

All claims expressed in this article are solely those of the authors and do not necessarily represent those of their affiliated organizations, or those of the publisher, the editors and the reviewers. Any product that may be evaluated in this article, or claim that may be made by its manufacturer, is not guaranteed or endorsed by the publisher.

Supplementary material

The Supplementary Material for this article can be found online at: https://www.frontiersin.org/articles/10.3389/fmicb.2022.925355/full#supplementary-material

References

Amey, R. C., Mills, P. R., Bailey, A., and Foster, G. D. (2003). Investigating the role of a *Verticillium fungicola* β-1, 6-glucanase during infection of *Agaricus bisporus* using targeted gene disruption. *Fungal Genet. Biol.* 39, 264–275. doi: 10.1016/S1087-1845(03)00061-6

Ashburner, M., Ball, C. A., Blake, J. A., Botstein, D., Butler, H., Cherry, J. M., et al. (2000). Gene ontology: tool for the unification of biology. *Nat. Genet.* 25, 25–29. doi: 10.1038/75556

Bairoch, A., and Apweiler, R. (2000). The SWISS-PROT protein sequence database and its supplement TrEMBL in 2000. *Nucleic Acids Res.* 28, 45–48. doi: 10.1093/nar/28.1.45

Barad, S., Horowitz, S. B., Moscovitz, O., Lichter, A., Sherman, A., and Prusky, D. (2012). A *Penicillium expansum* glucose oxidase-encoding gene, *GOX2*, is essential for gluconic acid production and acidification during colonization of deciduous fruit. *Mol. Plant Microbe Interact.* 25, 779–788. doi: 10.1094/MPMI-01-12-0002

Baroncelli, R., Amby, D. B., Zapparata, A., Sarrocco, S., Vannacci, G., Le Floch, G., et al. (2016). Gene family expansions and contractions are associated with host range in plant pathogens of the genus *Colletotrichum*. *BMC Genomics* 17:555. doi: 10.1186/s12864-016-2917-6

Barrett, L. G., Kniskern, J. M., Bodenhausen, N., Zhang, W., and Bergelson, J. (2009). Continua of specificity and virulence in plant host-pathogen interactions: causes and consequences. *New Phytol.* 183, 513–529. doi: 10.1111/j.1469-8137.2009.02927.x

Bergquist, R. R., and Masias, O. R. (1974). Physiologic specialization in *Trichometasphaeria turcica* f. sp. *zeae* and *Trichometasphaeria turcica* f. sp. *sorghi* in Hawaii. *Phytopathology* 64, 645–649. doi: 10.1094/Phyto-64-645

Bhowmik, T. P., and Prasada, R. (1970). Physiologic specialization in *Helminthosporium turcicum* Pass. from India. *J. Phytopathol.* 68, 84–87. doi: 10.1111/j.1439-0434.1970.tb02491.x

Borchardt, D. S., Welz, H. G., and Geiger, H. H. (1998). Molecular marker analysis of European *Setosphaeria turcica* populations. *Eur. J. Plant Pathol.* 104, 611–617. doi: 10.1023/A:1008641920356

Bradford, M. M. (1976). A rapid method for the quantitation of microgram quantities of protein utilizing the principle of protein-dye binding. *Anal. Biochem.* 72, 248–254. doi: 10.1016/0003-2697(76)90527-3

Brito, N., Espino, J. J., and Gonzalez, C. (2006). Endo-β-1, 4-xylanase xyn11A required for virulence in *Botrytis cinerea*. *Mol. Plant Microbe Interact.* 19, 25–32. doi: 10.1094/MPMI-19-0025

Buiate, E. A. S., Xavier, K. V., Moore, N., Torres, M. F., Farman, M. L., Schardl, C. L., et al. (2017). A comparative genomic analysis of putative pathogenicity genes in the host-specific sibling species *Colletotrichum graminicola* and *Colletotrichum sublineola*. *BMC Genomics* 18:67. doi: 10.1186/s12864-016-3457-9

Butler, M. J., Day, A. W., Henson, J. M., and Money, N. P. (2001). Pathogenic properties of fungal melanins. *Mycologia* 93, 1–8. doi: 10.1080/00275514.2001.12061273

Cantarel, B. L., Coutinho, P. M., Rancurel, C., Bernard, T., Lombard, V., and Henrissat, B. (2009). The carbohydrate-active EnZymes database (CAZy): an expert resource for glycogenomics. *Nucleic Acids Res.* 37, 233–238. doi: 10.1093/nar/gkn663

Chang, Y. C., and Kwon-chung, K. J. (1999). Isolation, characterization, and localization of a capsule-associated gene, *CAP10*, of *Cryptococcus neoformans*. *J. Bacteriol.* 181, 5636–5643. doi: 10.1128/JB.181.18.5636-5643.1999

Condon, B. J., Leng, Y., Wu, D., Bushley, K. E., Ohm, R. A., Otillar, R., et al. (2013). Comparative genome structure, secondary metabolite, and effector coding capacity across *Cochliobolus pathogens*. *PLoS Genet.* 9:e1003233. doi: 10.1371/journal.pgen.1003233

Cooper, R. M., Longman, D., Campbell, A., Henry, M., and Lees, P. E. (1988). Enzymatic adaptation of cereal pathogens to monocotyledonous primary wall. *Physiol. Mol. Plant Pathol.* 32, 33–47. doi: 10.1016/S0885-5765(88)80004-3

Cuq, F., Herrmanngorline, S., Klaebe, A., Rossignol, M., and Petitprez, M. (1993). Monocerin in *Exserohilum turcicum* isolates from maize and a study of its phytotoxicity. *Phytochemistry* 34, 1265–1270. doi: 10.1016/0031-9422(91)80013-Q

Degefu, Y., Lohtander, K., and Paulin, L. (2004). Expression patterns and phylogenetic analysis of two xylanase genes (*htxyl1* and *htxyl2*) from *Helminthosporium turcicum*, the cause of northern leaf blight of maize. *Biochimie* 86, 83–90. doi: 10.1016/j.biochi.2004.01.001

Desai, J. V., Cheng, S. J., Ying, T., Nguyen, M. H., Clancy, C. J., Lanni, F., et al. (2015). Coordination of *Candida albicans* invasion and infection functions by phosphoglycerol phosphatase Rhr2. *Pathogens* 4, 573–589. doi: 10.3390/pathogens4030573

Emanuelsson, O., Brunak, S., Von, H. G., and Nielsen, H. (2007). Locating proteins in the cell using TargetP, SignalP and related tools. *Nat. Protoc.* 2, 953–971. doi: 10.1038/nprot.2007.131

Eveleigh, D. E., Mandels, M., Androtti, R., and Roche, C. (2009). Mesurement of saccharifying cellulases. *Biotechnol. Biofuels* 6, 21–23. doi: 10.1186/1754-6834-2-21

Ferguson, L. M., and Carson, M. L. (2004). Spatial diversity of *Setosphaeria turcica* sampled from the eastern United States. *Phytopathology* 94, 892–900. doi: 10.1094/PHYTO.2004.94.8.892

Forsdyke, D. R. (1996). Different biological species "broadcast" their DNAs at different (G+C)% "wavelengths". *J. Theor. Biol.* 178, 405–417. doi: 10.1006/jtbi.1996.0038

Galiano-carneiro, A. L., and Miedaner, T. (2017). Genetics of resistance and pathogenicity in the maize/*Setosphaeria turcica* pathosystem and implications for breeding. *Front. Plant Sci.* 8, 1490. doi: 10.3389/fpls.2017.01490

Gao, J. X., Gao, Z. G., Zhang, X. F., Zhang, S., and Chen, L. (2010). A simple and feasible method for single-spore isolation of *Exserohilum turcicum*. *Microbiology* 37, 1548–1550. doi: 10.13344/j.microbiol.china.2010.10.023

Gao, Q., Jin, K., Ying, S. H., Zhang, Y., Xiao, G., Shang, Y., et al. (2011). Genome sequencing and comparative transcriptomics of the model entomopathogenic fungi *Metarhizium anisopliae* and *M. acridum*. *PLoS Genet.* 7:e1001264. doi: 10.1371/journal.pgen.1001264

Gao, S. G., Li, Y. Q., Gao, J. X., Suo, Y. J., Fu, K. H., Li, Y. Y., et al. (2014). Genome sequence and virulence variation-related transcriptome profiles of *Curvularia lunata*, an important maize pathogenic fungus. *BMC Genomics* 15:627. doi: 10.1186/1471-2164-15-627

Gardes, M., and Bruns, T. D. (1993). ITS primers with enhanced specificity of basidiomycetes–application to the identification of mycorrhizae and rusts. *Mol. Ecol.* 2, 113–118. doi: 10.1111/j.1365-294X.1993.tb00005.x

Haraguchi, T., Oguro, M., Nagano, H., Ichihara, A., and Sakamura, S. (1983). Specific inhibitors of eukaryotic DNA synthesis and DNA polymerase α, 3-deoxyaphidicolin and aphidicolin-17-monoacetate. *Nucleic Acids Res.* 11, 1197–1209. doi: 10.1093/nar/11.4.1197

Holtzapple, M., Cognata, M., Shu, Y., and Hendrickson, C. (1990). Inhibition of *Trichoderma reesei* cellulase by sugars and solvents. *Biotechnol. Bioeng.* 36, 275–287. doi: 10.1002/bit.260360310

Hou, Y. J., Ma, X., Wan, W. T., Long, N., Zhang, J., Tan, Y. T., et al. (2016). Comparative genomics of pathogens causing brown spot disease of tobacco: *Alternaria longipes* and *Alternaria alternata*. *PLoS One* 11:e0155258. doi: 10.1371/journal.pone.0155258

Hu, H. Z., Zhang, R., Tao, Z. S., Li, X. K., Li, Y. Y., Huang, J. F., et al. (2018). Cellulose synthase mutants distinctively affect cell growth and cell wall integrity for plant biomass production in *Arabidopsis*. *Plant Cell Physiol.* 59, 1144–1157. doi: 10.1093/pcp/pcy050

Human, M. P., Berger, D. K., and Crampton, B. G. (2020). Time-course RNAseq reveals *Exserohilum turcicum* effectors and pathogenicity determinants. *Front. Microbiol.* 11:360. doi: 10.3389/fmicb.2020.00360

Kamoun, S., van West, P., Vleeshouwers, V. G., de Groot, K. E., and Govers, F. (1998). Resistance of *Nicotiana benthamiana* to *Phytophthora infestans* is mediated by the recognition of the elicitor protein INF1. *Plant Cell* 10, 1413–1426. doi: 10.1105/tpc.10.9.1413

Kanehisa, M., Goto, S., Kawashima, S., Okuno, Y., and Hattori, M. (2004). The KEGG resource for deciphering the genome. *Nucleic Acids Res.* 32, 277–280. doi: 10.1093/nar/gkh063

Kim, S., Cho, Y. J., Song, E. S., Lee, S. H., Kim, J. G., and Kang, L. W. (2016). Time-resolved pathogenic gene expression analysis of the plant pathogen *Xanthomonas oryzae* pv. *Oryzae*. *BMC Genomics* 17:345. doi: 10.1186/s12864-016-2657-7

Klein, R. D., Gu, Q., Goddard, A., and Rosenthal, A. (1996). Selection for genes encoding secreted proteins and receptors. *Proc. Natl. Acad. Sci. U. S. A.* 93, 7108–7113. doi: 10.1073/pnas.93.14.7108

Kou, Y. B., Xu, J. T., Cao, Y. L., Lv, X. X., Zhao, G. L., Chen, G. J., et al. (2014). Gluconolactone induces cellulase gene expression in cellulolytic filamentous fungus *Trichoderma reesei*. *RSC Adv.* 4, 36057. doi: 10.1039/C4RA06731B

Krogh, A., Larsson, B., Von, H. G., and Sonnhammer, E. L. L. (2001). Predicting transmembrane protein topology with a hidden Markov model: application to complete genomes. *J. Mol. Biol.* 305, 567–580. doi: 10.1006/jmbi.2000.4315

Lagunas-Muñoz, V. H., Cabrera-Valladares, N., Bolívar, F., Gosset, G., and Martínez, A. (2006). Optimum melanin production using recombinant *Escherichia coli*. *J. Appl. Microbiol.* 101, 1002–1008. doi: 10.1111/j.1365-2672.2006.03013.x

Lalaoui, F., Halama, P., Dumortier, V., and Paul, B. (2008). Cell wall-degrading enzymes produced *in vitro* by isolates of *Phaeosphaeria nodorum* differing in aggressiveness. *Plant Pathol.* 49, 727–733. doi: 10.1046/j.1365-3059.2000.00491.x

Lee, B. H., and Blackburn, T. H. (1975). Cellulase production by a thermophilic *Clostridium* species. *Appl. Microbiol.* 30, 346–353. doi: 10.1128/am.30.3.346-353.1975

Li, W. Z., Jaroszewski, L., and Godzik, A. (2002). Tolerating some redundancy significantly speeds up clustering of large protein databases. *Bioinformatics* 18, 77–82. doi: 10.1093/bioinformatics/18.1.77

Li, R. Q., Zhu, H. M., Ruan, J., Qian, W. B., Fang, X. D., Shi, Z. B., et al. (2010). De novo assembly of human genomes with massively parallel short read sequencing. *Genome Res.* 20, 265–272. doi: 10.1101/gr.097261.109

Luo, R., Liu, B., Xie, Y., Li, Z., Huang, W., Yuan, J., et al. (2012). SOAPdenovo2: an empirically improved memory-efficient short-read *de novo* assembler. *GigaScience* 1:18. doi: 10.1186/2047-217x-1-18

Ma, S. X., Cao, K. K., Liu, N., Meng, C., Cao, Z. Y., Dai, D. Q., et al. (2017). The *StLAC2* gene is required for cell wall integrity, DHN-melanin synthesis and the pathogenicity of *Setosphaeria turcica*. *Fungal Biol.* 121, 6–7. doi: 10.1016/j.funbio.2017.04.003

Marcet-Houben, M., Ballester, A. R., de la Fuente, B., Harries, E., Marcos, J. F., González-Candelas, L., et al. (2012). Genome sequence of the necrotrophic fungus *Penicillium digitatum*, the main postharvest pathogen of citrus. *BMC Genomics* 13, 646. doi: 10.1186/1471-2164-13-646

Martin, T., Biruma, M., Fridborg, I., Okori, P., and Dixelius, C. (2011). A highly conserved NB-LRR encoding gene cluster effective against *Setosphaeria turcica* in sorghum. *BMC Plant Biol.* 11, 151. doi: 10.1186/1471-2229-11-151

Medema, M. H., Blin, K., Cimermancic, P., de Jager, V., Zakrzewski, P., Fischbach, M. A., et al. (2011). antiSMASH: rapid identification, annotation and analysis of secondary metabolite biosynthesis gene clusters in bacterial and fungal genome sequences. *Nucleic Acids Res.* 39, W339–W346. doi: 10.1093/nar/gkr466

Milton, H. S. Jr., Yen, M. R., Noto, K., Tamang, D. G., and Elkan, C. (2009). The transporter classification database: recent advances. *Nucleic Acids Res.* 37, 274–278. doi: 10.1093/nar/gkn862

Mitra, M. (1923).*Helminthosporium spp. on cereals and sugarcane in India*. Part I. Diseases of Zeamays and Sorghum vulgare caused by species of Helminthosporium. *India Dep. Agric. Mem. Bot. Ser.* 11, 219–242.

Moriwaki, A., Kihara, J., Kobayashi, T., Tokunaga, T., Arase, S., and Honda, Y. (2004). Insertional mutagenesis and characterization of a polyketide synthase gene (*PKS1*) required for melanin biosynthesis in *Bipolaris oryzae*. *FEMS Microbiol. Lett.* 238, 1–8. doi: 10.1016/j.femsle.2004.07.007

Ni, L. N. (2004). Isolation and identification of a high-melanin-producting bacterium. *Microbiology* 31, 55–59. doi: 10.13344/j.microbiol.china.2004.01.013

Nieuwoudt, A., Human, M. P., Craven, M., and Crampton, B. G. (2018). Genetic differentiation in populations of *Exserohilum turcicum* from maize and sorghum in South Africa. *Plant Pathol.* 67, 1483–1491. doi: 10.1111/ppa.12858

Nosanchuk, J. D., and Casadevall, A. (2003). The contribution of melanin to microbial pathogenesis. *Cell. Microbiol.* 5, 203–223. doi: 10.1046/j.1462-5814.2003.00268.x

Novo, M., Pomar, F., Gayoso, C., and Merino, F. (2006). Cellulase activity in isolates of *Verticillium dahliae* differing in aggressiveness. *Plant Dis.* 90, 155–160. doi: 10.1094/PD-90-0155

Ohm, R. A., Feau, N., Henrissat, B., Schoch, C. L., Horwitz, B. A., Barry, K. W., et al. (2012). Diverse lifestyles and strategies of plant pathogenesis encoded in the genomes of eighteen *Dothideomycetes* fungi. *PLoS Genet.* 8:e1003037. doi: 10.1371/journal.ppat.1003037

Okori, P., Rubaihayo, P. R., Ekwamu, A., Fahleson, J., and Dixelius, C. (2004). Genetic characterization of *Cercospora sorghi* from cultivated and wild sorghum and its relationship to other *Cercospora* fungi. *Phytopathology* 94, 743–750. doi: 10.1094/PHYTO.2004.94.7.743

Patrick, D. R., and Heimbrook, D. C. (1996). Protein kinase inhibitors for the treatment of cancer. *Drug Discov. Today* 1, 325–330. doi: 10.1016/1359-6446(96)10030-1

Petersen, T. N., Brunak, S., Von, H. G., and Nielsen, H. (2011). SignalP 4.0: discriminating signal peptides from transmembrane regions. *Nat. Methods* 8, 785–786. doi: 10.1038/nmeth.1701

Quentin, M., Ebbelaar, M., Derksen, J., Mariani, C., and van der Valk, H. (2002). Description of a cellulose-binding domain and a linker sequence from *aspergillus* fungi. *Appl. Microbiol. Biotechnol.* 58, 658–662. doi: 10.1007/s00253-002-0937-4

Quiroga, E. N., Sampietro, A. R., and Vattuone, M. A. (2001). Screening antifungal activities of selected medicinal plants. *J. Ethnopharmacol.* 74, 89–96. doi: 10.1016/S0378-8741(00)00350-0

Ramathani, I., Biruma, M., Martin, T., Dixelius, C., and Okari, P. (2011). Disease severity, incidence and races of *Setosphaeria turcica* on sorghum in Uganda. *Eur. J. Plant Pathol.* 131, 383–392. doi: 10.1007/s10658-011-9815-1

Reese, E. T., Parrish, F. W., and Ettlinger, M. (1971). Nojirimycin and D-glucono-l, 5-lactone as inhibitors of carbohydrases. *Carbohydr. Res.* 18, 381–388. doi: 10.1016/S0008-6215(00)80274-8

Rep, M. (2005). Small proteins of plant-pathogenic fungi secreted during host colonization. *FEMS Microbiol. Lett.* 253, 19–27. doi: 10.1016/j.femsle.2005.09.014

Rep, M., van der Does, H. C., Meiger, M., van Wijk, R., Houterman, P. M., Dekker, H. L., et al. (2004). A small, cysteine-rich protein secreted by *Fusarium oxysporum* during colonization of xylem vessels is required for *I-3*-mediated resistance in tomato. *Mol. Microbiol.* 53, 1373–1383. doi: 10.1111/j.1365-2958.2004.04177.x

Robert, A. L. (1960). Physiologic specialization in *Helminthosporium turcicum*. *Phytopathology* 50, 217–220. doi: 10.1111/j.1399-3054.1960.tb08108.x

Schirawski, J., Mannhaupt, G., Münch, K., Breport, T., Schipper, K., Doehlemann, G., et al. (2010). Pathogenicity determinants in smut fungi revealed by genome comparison. *Science* 330, 1546–1548. doi: 10.1126/science.1195330

Segmüller, N., Kokkelink, L., Giesbert, S., Odinius, D., Kan, J. V., and Tudzynski, P. (2008). NADPH oxidases are involved in differentiation and pathogenicity in *Botrytis cinerea*. *Mol. Plant Microbe Interact.* 21, 808–819. doi: 10.1094/MPMI-21-6-0808

Siriputthaiwan, P., Jauneau, A., Herbert, C., Garcin, D., and Dumas, B. (2005). Functional analysis of *CLPT1*, a Rab/GTPase required for protein secretion and pathogenesis in the plant fungal pathogen *Colletotrichum lindemuthianum*. *J. Cell Sci.* 118, 323–329. doi: 10.1242/jcs.01616

Sperschneider, J., Gardiner, D. M., Dodds, P. N., Tini, F., Covarelli, L., Singh, K. B., et al. (2016). EffectorP: predicting fungal effector proteins from secretomes using machine learning. *New Phytol.* 210, 743–761. doi: 10.1111/nph.13794

Sposato, P., Ahn, J. H., and Walton, J. D. (1995). Characterization and disruption of a gene in the maize pathogen *Cochliobolus carbonum* encoding a cellulase lacking a cellulose binding domain and hinge region. *Mol. Plant Microbe Interact.* 8, 602–609. doi: 10.1094/MPMI-8-0602

Stanke, M., Tzvetkova, A., and Morgenstern, B. (2006). AUGUSTUS at EGASP: using EST, protein and genomic alignments for improved gene prediction in the human genome. *Genome Biol.* 7, 1–8. doi: 10.1186/gb-2006-7-s1-s11

Tamura, K., Dudley, J., Nei, M., and Kumar, S. (2007). MEGA4: molecular evolutionary genetics analysis (MEGA) software version 4.0. *Mol. Biol. Evol.* 24, 1596–1599. doi: 10.1093/molbev/msm092

Tang, L., Gao, Z. G., Yang, R. X., Yao, Y., and Liu, X. (2015). Activity analysis and gene expression of cell wall degradation enzymes in *Setosphaeria turcica* f. sp. *zeae* and *S. turcica* f. sp. *sorghi*. *Acta Phytophylacica Sin.* 42, 935–941. doi: 10.13802/j.cnki.zwbhxb.2015.06.011

Tang, L., Gao, Z. G., Yao, Y., and Liu, X. (2014). Identification and genetic diversity of formae speciales of *Setosphaeria turcica* in China. *Plant Dis.* 99, 482–487. doi: 10.1094/pdis-06-14-0570-re

Tanguay, P., Loppnau, P., Morin, C., Bernier, L., and Breuil, C. (2006). A spontaneous albino mutant of *Ceratocystis resinifera* results from a point mutation in the polyketide synthase gene, *PKS1*. *Can. J. Microbiol.* 52, 501–507. doi: 10.1139/w05-150

Tatusov, R. L., Fedorova, N. D., Jackson, J. D., Jacobs, A. R., Eiryutin, B., Koonin, E. V., et al. (2003). The COG database: an updated version includes eukaryotes. *BMC Bioinf.* 4, 41. doi: 10.1186/1471-2105-4-41

Thrall, P. H., Burdon, J. J., and Young, A. (2002). Variation in resistance and virulence among demes of a plant host–pathogen metapopulation. *J. Ecol.* 89, 736–748. doi: 10.1046/j.0022-0477.2001.00597.x

Urban, M., Irvine, A. G., Cuzick, A., and Hammond-Kosack, K. E. (2015). Using the pathogen-host interactions database (PHI-base) to investigate plant pathogen genomes and genes implicated in virulence. *Front. Plant Sci.* 6, 605. doi: 10.3389/fpls.2015.00605

van den Brink, J., and de Vries, R. P. (2011). Fungal enzyme sets for plant polysaccharide degradation. *Appl. Microbiol. Biotechnol.* 91, 1477–1492. doi: 10.1007/s00253-011-3473-2

Walker, D. S., Reeves, P. J., and Salmond, G. P. C. (1994). The major secreted cellulase, CelV, of *Erwinia carotovora* subsp. *carotovora* is an improtant soft rot virulence factor. *Mol. Plant Microbe Interact.* 7, 425–431. doi: 10.1094/MPMI-7-0425

Walton, J. D. (1994). Deconstructing the cell wall. *Plant Physiol.* 104, 1113–1118. doi: 10.1104/pp.104.4.1113

Wanjiru, W. M., Kang, Z. S., and Buchenauer, H. (2002). Importance of cell wall degrading enzymes produced by *Fusarium graminearum* during infection of wheat heads. *Eur. J. Plant Pathol.* 108, 803–810. doi: 10.1023/A:1020847216155

Wen, L. L., Cao, Z. Y., and Dong, J. G. (2008). Cloning and promoter prediction of melanin biosynthesis gene *4HNR* in *Setosphaeria turcica*. *Acta Phytopathol. Sin.* 38, 641–644. doi: 10.13926/j.cnki.apps.2008.06.008

Winnenburg, R., Baldwin, T. K., Urban, M., Rawlings, C., Köhler, J., and Hammond-Kosack, K. E. (2006). PHI-base: a new database for pathogen host interactions. *Nucleic Acids Res.* 34, D459–D464. doi: 10.1093/nar/gkj047

Zhang, X., Cao, Z. Y., Liu, S. W., Guo, L. Y., and Dong, J. G. (2011). Functional analysis of polyketide synthase gene *StPKS* in *Setosphaeria turcica*. *Sci. Agric. Sin.* 44, 1603–1609. doi: 10.3864/j.issn.0578-1752.2011.08.008

Zhang, S., Zhao, B. X., Liu, X., Li, J. B., Gao, Z. G., and Huang, X. Y. (2013). DNA sequencing and UP-PCR characterization of *Fusarium oxysporum* isolates from three cucurbit species. *Plant Pathol. J.* 12, 78–84. doi: 10.3923/ppj.2013.78.84

frontiers | Frontiers in Microbiology

TYPE Original Research
PUBLISHED 29 July 2022
DOI 10.3389/fmicb.2022.972393

OPEN ACCESS

EDITED BY
Motaher Hossain,
Bangabandhu Sheikh Mujibur Rahman Agricultural University, Bangladesh

REVIEWED BY
Xingang Zhou,
Northeast Agricultural University, China
Dongbo Cai,
Hubei University, China

*CORRESPONDENCE
Liang Sun
sunl@njtech.edu.cn
Hong Xu
xuh@njtech.edu.cn
Peng Lei
lei-peng@njtech.edu.cn

SPECIALTY SECTION
This article was submitted to Microbe and Virus Interactions With Plants, a section of the journal Frontiers in Microbiology

RECEIVED 18 June 2022
ACCEPTED 04 July 2022
PUBLISHED 29 July 2022

CITATION
Xue J, Tong T, Wang R, Qiu Y, Gu Y, Sun L, Xu H and Lei P (2022) Secretion of poly-γ-glutamic acid by *Bacillus atrophaeus* NX-12 enhanced its root colonization and biocontrol activity.
Front. Microbiol. 13:972393.
doi: 10.3389/fmicb.2022.972393

Secretion of poly-γ-glutamic acid by *Bacillus atrophaeus* NX-12 enhanced its root colonization and biocontrol activity

Jian Xue, Tong Tong, Rui Wang, Yibin Qiu, Yian Gu, Liang Sun*, Hong Xu* and Peng Lei*

State Key Laboratory of Materials-Oriented Chemical Engineering, College of Food Science and Light Industry, Nanjing Tech University, Nanjing, China

Bacilli are used as biocontrol agents (BCAs) against phytopathogens and most of them can produce poly-γ-glutamic acid (γ-PGA) as one of the major extracellular polymeric substances (EPSs). However, the role of γ-PGA in plant biocontrol is still unclear. In this study, *Bacillus atrophaeus* NX-12 (γ-PGA yield: 16.8g/l) was screened, which formed a strong biofilm and has been proved to be a promising BCA against Cucumber *Fusarium* wilt. Then, the γ-PGA synthesis gene cluster *pgsBCA* was knocked out by CRISPR-Cas9n. Interestingly, the antifungal ability of γ-PGA synthetase-deficient strain NX-12Δ*pgs* (γ-PGA yield: 1.65g/l) was improved *in vitro*, while the biocontrol ability of NX-12Δ*pgs* was greatly diminished *in situ*. Data proved that γ-PGA produced by NX-12 contributes to the biofilm formation and rhizosphere colonization, which effectively improved biocontrol capability. Taken together, these findings prove that the mechanism of γ-PGA promotes the colonization of NX-12 and thus assists in controlling plant diseases, which highlight the key role of γ-PGA produced by BCA in biocontrol.

KEYWORDS

***Bacillus atrophaeus*, antifungal, biocontrol, poly-γ-glutamic acid, rhizosphere colonization**

Introduction

Fusarium wilt is a very serious disease and it is caused by *Fusarium oxysporum* (Dr et al., 2003; Dean et al., 2012). This disease has become one of the main factors restricting cucumber production worldwide as the fungus is present in all types of soil worldwide (Cao et al., 2011). Because of the lack of effective chemical control methods, biological control has become a potential alternative to chemical pesticides and other conventional control methods (Compant et al., 2005; Raza et al., 2016). Biocontrol agents (BCAs) can colonize plant rhizosphere or tissues and therefore resist plant root pathogens through direct action (including the secretion of antibiotics and production of various

hydrolases) or indirect action (including nutritional or space competition with pathogenic microorganisms and induction of systemic resistance; Backer et al., 2018). Reducing the use of chemical fertilizers and pesticides in agriculture is slowly becoming a reality (Olanrewaju et al., 2017). However, after BCAs are applied in the field, they cannot successfully occupy favorable competition spaces and achieve effective colonization and survival in the rhizosphere native microbial community, which is one of the main bottlenecks limiting their function (Rilling et al., 2019). In recent years, evidence has suggested that the colonization of plant roots by BCAs and the formation of root-related biofilms are key to their use as a method of biocontrol (Kolter and Greenberg, 2006; Compant et al., 2010; Chen et al., 2012; Santoyo et al., 2021).

As an important member of the BCAs family, *Bacillus* has attracted the attention of researchers (Brannen and Kenney, 1997; Ngugi et al., 2005). How this bacterium uses its advantages to colonize the roots and establish beneficial interactions with the roots of the plants is not clearly understood. In recent years, it has been found that some microorganisms with the ability to produce strong extracellular polymeric substances (EPSs) can form a biofilm adhesion structure, which makes it easier to occupy a favorable space in the competition for rhizosphere colonization space (Jayathilake et al., 2017; Karygianni et al., 2020). EPSs are mainly composed of extracellular polysaccharides, nucleic acids (eDNA and eRNA), proteins, lipids, and other biomolecules (Flemming et al., 2016). Because of the physical and chemical properties of EPSs, such as stability, viscosity, gelation, suspension ability, chelation, film formation, and water-holding capacity, biofilms can bind a large number of cells together. In this way, information exchange and interactions can occur to form a microenvironment that cooperates and co-exists with plants (Costa et al., 2018). Studies have shown that the knockout of genes related to EPSs synthesis often leads to the loss of EPS secretion ability of the strain, which makes it unable to form a biofilm structure and eventually leads to the failure of its colonization in the rhizosphere or plant tissue (Wang et al., 2008; Meneses et al., 2011).

Many reports have found that in some *Bacillus* spp. strains with the ability of EPSs secretion, γ-polyglutamic acid (γ-PGA) is the main component of its EPS (Yiyang et al., 2016; Maruzani et al., 2019). The γ-PGA biosynthesis genes are highly conserved in various *Bacillus* species. In *B. subtilis*, the biosynthesis of γ-PGA relies on the conserved operon *pgsB-pgsC-pgsA-pgsE* (Ashiuchi and Misono, 2002). In recent years, research on γ-PGA in agriculture has mainly focused on its biological functions, such as water retention, chelation of heavy metals, fertilizer synergism, antioxidant effect, stress resistance, and growth promotion (Wang et al., 2022). However, little is known about how γ-PGA affects biofilm formation and how it can control plant diseases. Although γ-PGA is similar to other biofilm matrix components, it is not clear whether γ-PGA plays a structural role in biofilm matrix assembly. One study showed that the *pgs*-deletion mutant of the *B. subtilis* model strain NCIB 3610 had no differences in the biofilm phenotype (Branda et al., 2006). Another study showed that γ-PGA had an effect on the biofilm phenotype when different medium conditions were used (Stanley and Lazazzera, 2005).

In this study, we screened a strain of *B. atrophaeus*, NX-12, from the rhizosphere of a cotton plant as a potential BCA. The biocontrol effect, biofilm-forming ability, and antagonistic activity of this strain against various plant pathogens were characterized. The main component of the EPS was identified as γ-PGA through the extraction and identification of the EPS. Based on the technology of CRISPR-Cas9n, we constructed a *pgsBCA*-deletion mutant (NX-12Δ*pgs*). We have demonstrated that a lack of γ-PGA led to a decrease in the biofilm formation and colonization ability of the strain, which, in turn, significantly reduced the biocontrol effect of the strain in cucumber *Fusarium* wilt. Our findings are consistent with those of a previous study that reported an inseparable relationship between biofilm formation and plant protection (Bais et al., 2004). We further showed that the extracellular matrix secreted by bacteria, especially γ-PGA, is an important factor that affects bacterial rhizosphere colonization and plant protection.

Materials and methods

Strain isolation

Samples were collected from the Juxin cotton farm in Hutubi County, Xinjiang, China. They were divided into four parts (root, stem, leaves, and rhizosphere soil). The rhizosphere soil samples were collected at a depth of 20 cm from the cotton planting fields. Bacterial isolation was performed using modified methods based on a previous study (Saravana Kumar et al., 2014). Tissues (root, stem, and leaves 0.2 g each) were sterilized with 75% (v/v) ethanol and 0.3% (m/v) mercuric chloride solution. The tissues were then thoroughly crushed in liquid nitrogen-containing glass beads to make them completely uniform, and they were then resuspended in a 0.9% (m/v) sterile NaCl solution. The rhizosphere soil sample (0.2 g) was mixed with a 0.9% (m/v) sterile NaCl solution, followed by shaking and mixing well for 30 min. The mixture was diluted 10 folds and plated onto Luria-Bertani (LB) agar plates. After incubation at 30°C for 24 h, colonies were picked and further purified by repeated streaking onto LB medium. The pure isolates were preserved in sterile glycerol (20% v/v) at −80°C. Subsequently, the antifungal activity was tested on PDA plates. Briefly, a 6-mm-diameter plug containing mycelium was plated at the center of the PDA plates, and 5 μl of the bacterial suspension ($OD_{600} = 1.0$) was patched 3 cm away from the fungus. After incubation at 28°C for 72 h, the strain with the largest antibacterial circle was selected and named NX-12 for use in further experiments.

Characteristics of the strain NX-12

The characteristics of strain NX-12 were determined according to Bergey's Manual of Systematic Bacteriology. The

NX-12 genome was extracted using a genomic DNA purification kit and used for a polymerase chain reaction (PCR) amplification of the 16S ribosomal DNA (rDNA) gene using the primers *27F* (5′-AGAGTTTGATCMTGGCTCAG-3′) and *1492R* (5′-TACG GYTACCTTGTTACGACTT-3′). The sequences were compared to the reference sequences of other bacterial isolates deposited in the NCBI nucleotide database using the BlastN algorithm.

Plant growth conditions

Cucumber seeds ("Jinchun No. 4") were purchased from the Tianjin Kerun Cucumber Research Institute and surface-sterilized (Li et al., 2015). The seeds were surface-sterilized for 10 min in 30% sodium hypochlorite and rinsed three times with distilled water. The seeds were then incubated at 28°C for 48 h on a sterile wet filter paper. The sprouted seeds were then planted in sterilized soil (Laoshan National Forest Park, Nanjing, China). The initial moisture content of the soil was 30%. After 7 days of cultivation, the uniform cucumber seedlings were randomly divided into three groups: group CK, uninoculated group; group FOC, inoculated with spores of *Fusarium. oxysporum* f. sp. *cucumber* (FOC) up to a final concentration of 1×10^5 CFU/g soil; and group NX-12 + FOC, which was inoculated with strain NX-12 up to a final concentration of 1×10^7 CFU/g soil and spores of FOC up to a final concentration of 1×10^5 CFU/g soil. The plants were then cultured for 4 weeks. The samples were then harvested. All cucumber seedlings were cultivated in a growth chamber with a 16-h photoperiod (26°C, 4,000 lx) at 65% relative humidity and fertilized twice a week with 1/4 MS liquid fertilizer.

Plant growth measurements and physiological indices

Four weeks after inoculation with FOC, the disease severity was assessed for each plant on a 0–4 rating scale according to the percentage of defoliation (0 = healthy plant, 1 = 1–33%, 2 = 34–66%, 3 = 67–97%, and 4 = dead plant; Huang et al., 2006), and was calculated according to the following formulas: leaf wilt index (LWI) = Σ(disease score × the number of plants with that score)/(the total number of plants investigated × 4; Li et al., 2012), and biocontrol efficacy = [(LWI of control plants–LWI of treated plants)/disease incidence of control] × 100% (Chen et al., 2019). For each treatment, there were three replicates with six seedlings each. The height of cucumber plants was measured using a measuring tape. The leaf area of fully expanded leaves was recorded before flowering using a ScanMaker (i800 plus, Microtek, China). Stomatal conductance, net photosynthetic rate, transpiration rate, and intercellular carbon dioxide concentration were measured using a portable photosynthetic system (LI-800, LI-COR, United States). The MDA and POD indices were elucidated using previously described methods (Bilal et al., 2018). The quantity of FOC in the cucumber rhizosphere soil was determined as described previously (Faheem et al., 2014).

Identification of extracellular polymers

Strain NX-12 was incubated in an LB medium at 37°C and 200 rpm for 8 h. It was then transferred into the selected medium, which contained (per liter) glucose, 30 g, sodium glutamate 30 g, $(NH_4)_2SO_4$ 5 g, K_2HPO_4 2 g, $MgSO_4$ 0.1 g, and $MnSO_4$ 0.03 g at an inoculum volume of 5% (v/v). The fermentation was carried out at 30°C and 200 rpm for 48 h. The EPS was purified using a previously described method (Qiu et al., 2017). The total carbohydrate content was determined by the phenol–sulfuric acid method. Simultaneously, the prepared extracellular polymer was scanned at wavelengths between 200 and 600 nm, and γ-PGA was used as a control. The amino acid composition was determined according to the procedure recommended by Amino Acid Analysis (AAA; AdvanceBio, Agilent, United States).

Construction of the γ-PGA-deficient strain NX-12Δ*pgs* and the complementary strain NX-12Δ*pgs* (pMA5-*pgs*)

The strains and plasmids used in the present study are listed in Supplementary Table S1. The construction of mutants was based on the CRISPR-Cas9n system, as described previously (Qiu et al., 2020), and this procedure was modified appropriately. The strain was cultured overnight in a fresh NA medium at 37°C and 200 rpm, and it was then transferred into an SPI medium until the OD_{600} reached 1.5. The solution was then transferred into an SPII medium at 37°C and 100 rpm. When the OD_{600} reached 0.6, EGTA solution was added at a final concentration of 0.1 mM and incubated for 10 min. The culture broth (50 ml) was centrifuged at 6,000 × *g* for 15 min at 4°C. The cells were washed twice with ice-cold deionized water (15 ml) and then washed twice again with an equal volume of cold 10% glycerol (v/v). Finally, the cells were suspended in 10% sterile glycerol (v/v) so that the cell density was 1×10^{10} CFU/ml. Precooled plasmid DNA (100 ng) and competent cells (100 μl) were mixed gently and then transferred into pre-cooled 2-mm electroporation cuvettes. The sample was then exposed to a single electrical pulse (2 kV, 4 ms). Next, an NA medium (800 μl) was immediately added. After growth at 30°C and 200 rpm for 3 h, the cells were plated onto LB agar (Spec, 25 μg/ml; Kar, 50 μg/ml; Cm, 10 μg/ml if necessary). The PCR primers listed in Supplementary Table S2 were used to screen and identify positive colonies. Specifically, overnight cultured cells were transferred to a new resistant LB medium containing 1% of the inoculum. When the OD_{600} reached 0.8, IPTG was added at a final concentration of 1 mM. After induction at 30°C and 200 rpm for 10 h, the positive clones were grown at 30°C for 12 h in LB medium containing

spectinomycin and then subcultured for more than 20 generations. A single colony with a dry morphology was selected for culture. The results were verified by PCR and synchronized with the sequencing results.

The *pgsBCA* gene was amplified using the primers pMA5-*pgsBCA*-F and pMA5-*pgsBCA*-R from the NX-12 genome, and a fragment of the plasmid pMA5 was used to construct the recombinant plasmid pMA5-*pgsBCA* by In-Fusion cloning. The mutant NX-12Δ*pgs* was complemented with pMA5-*pgsBCA*. Analysis of the EPS from NX-12Δ*pgs* (pMA5-*pgs*) was performed as described above.

Comparison of the antibacterial activity and biocontrol abilities of NX-12 and NX-12Δ*pgs*

The antibacterial activity of the wild isolate toward five important types of *Fusarium oxysporum* (FO; f. sp. *cucumerium, strawberry, cotton, lotus root,* and *watermelon*) was measured. Strains were cultured in an LB medium for 12 h at 30°C and 200 rpm. The culture broth's pellets were then washed with a PBS buffer (pH 7.0) and resuspended to $OD_{600} = 1.0$. A suspension of the wild isolate of NX-12 was placed around the fungal inocula at a distance of 3 cm. After incubation at 28°C for 72 h, the zones of inhibition were measured, as described previously (Berg et al., 2005). The fungus FOC with the best inhibition effect was used for the comparison of the antibacterial activities between NX-12 and NX-12Δ*pgs*, and the experimental steps were consistent with those described above.

The plants were grown under the same conditions as those described in Plant growth conditions, with some modifications. Uniform seedlings were randomly divided into four groups. Group CK was the uninoculated group; group FOC was inoculated with spores of the FOC up to a final concentration of 1×10^5 CFU/g soil; group NX-12 + FOC was inoculated with strain NX-12 up to a final concentration of 1×10^7 CFU/g soil; and group NX-12Δ*pgs* + FOC was inoculated with strain NX-12Δ*pgs* up to a final concentration of 1×10^7 CFU/g soil. After 4 weeks of cultivation, the samples were collected, and the LWI, dry weight, and height were measured.

qPCR analysis

The prediction and analysis of the secondary metabolite genes of the strain were analyzed using antiSMASH (https://antismash.secondarymetabolites.org/). The complete genome sequence of NX-12 was determined using Novogene (Beijing, China). According to the standard protocol, bacterial RNA was extracted using an RNA isolation kit (RC112-01, Vazyme). It was necessary to lyse the cell wall with lysozyme at a final concentration of 20 mg /mL before extraction. The primer sequences used for qPCR are listed in Supplementary Table S2. qPCR was performed according to the recommended protocol (R323-01/Q711-02/Q711-03, Vazyme). The $2^{-\Delta\Delta CT}$ method was used to analyze the qPCR data (Kenneth and Thomas, 2002).

Biofilm formation assay

Biofilm formation was determined by crystal violet staining (Hsueh et al., 2006) with some modifications. NX-12 and NX-12Δ*pgs* were grown in LB broth at 30°C and 200 rpm overnight to generate inoculum cultures. They were then adjusted to an optical density at 600 nm (OD_{600}) of 0.01. Specifically, the modified Msgg medium (0.005 M potassium phosphate buffer, 0.1 M Mops, 0.002 M $MgCl_2$, 0.7 M $CaCl_2$, 0.05 M $MnCl_2$, 0.05 M $FeCl_3$, 0.002 M VB_1, 1.2% (m/v) glucose, and 1.2% (m/v) sodium glutamate) was pre-formulated. Next, 2 ml of modified Msgg medium was added to the wells of polystyrene 24-well plates, followed by incubation at 30°C for 24 h. The planktonic bacteria were removed and the wells were washed with distilled water and air-dried. The remaining biofilm cells were stained with 2 ml of 0.3% crystal violet for 10 min, then washed with distilled water, and were finally air-dried. The crystal violet in the biofilm cells was solubilized with 2 ml of 70% ethanol, and the optical density at 570 nm (OD_{570}) was measured.

Rhizosphere colonization assay

The general methods for the rhizosphere colonization assay followed published protocols (Tian et al., 2021) with some modifications. NX-12-gfp, NX-12Δ*pgs*-gfp, and NX-12Δ*pgs*-gfp (PMA5-*pgsBCA*) were constructed according to the protocol described in Construction of the γ-PGA deficient strain NX-12Δ*pgs* and the complementary strain NX-12Δ*pgs* (pMA5-*pgs*). The uniform seedlings were divided into four groups: NX-12, NX-12Δ*pgs*, NX-12Δ*pgs* + γ-PGA, and NX-12Δ*pgs* (PMA5-*pgsBCA*). The cucumber seeds were cultured in plastic pots (70 mm × 70 mm × 75 mm) containing 15 g sterilized vermiculite, and the pots were incubated in moist chambers (26°C/23°C day/night temperatures, 4,000 Lux light for 16 h/day, and 65% relative humidity). The pots were watered weekly with 1/4 MS. After 15 days of incubation, 5 ml of cell suspension containing freshly cultivated *B. atrophaeus* cells (1.0×10^8 CFU/ml) supplemented with γ-PGA (0.1 mg/ml) was added to the pot by pouring onto the surrounding root. After another 3 days of incubation, the roots of the seedlings were removed and rinsed with sterilized water. A 0.2-g root ripening zone for each sample was collected and immediately stored in a sterile Eppendorf tube for fluorescence microscopy (FM) and plate recovery counting.

The green fluorescent protein (GFP) gene was biosynthesized using GenScript (Nanjing, China) and amplified using the primer pairs pM-GFP-F and pM-GFP-R. pMA5-GFP was constructed using In-Fusion cloning as described above. Next, pMA5-GFP was electroporated into NX-12 and NX-12Δ*pgs*. The cucumber seedlings were treated as described above, and the roots were observed under a fluorescence microscope to detect the presence of the bacteria.

Results

Isolation and identification of *Bacillus atrophaeus* NX-12

The initial purpose of this work was to screen candidate strains for BCAs. We isolated strains from both four parts (root, stem, leaves, and rhizosphere soil) of samples and the strains co-existing in the four parts were selected as the target strains. Supplementary Figure S1 shows the microbiological of the strain NX-12. This strain is a Gram-positive, motile, spore-forming, rod-like bacterium. A partial 16S rRNA gene sequence analysis (1,416 bp) demonstrated that strain NX-12 was most likely *B. atrophaeus* strain JCM9070 (98%), indicating that strain NX-12 belongs to the species *B. atrophaeus* (Supplementary Figure S1). Therefore, we designated this strain as *B. atrophaeus* NX-12.

Strain NX-12 exhibits high biocontrol efficacy against *Fusarium* wilt on cucumber

To evaluate the inhibition ability of the strain to the pathogen of *Fusarium* wilt, five *Fusarium* wilt Pathogens from different plant specialization types were used to test, in which NX-12 had the strongest effect on FOC (Figure 1A). The biocontrol efficacy of *Fusarium* wilt on cucumber seedlings was also verified. *Fusarium* wilt in cucumber plants peaks 4 weeks after the challenging inoculation with FOC. The stomatal conductance, net photosynthetic rate, and transpiration rate of cucumber seedlings in the pathogen treatment group were the lowest among the three treatments, which were decreased by 65.05, 41.73, and 64.74%, respectively, when compared with the control group. At the same time, the intercellular carbon dioxide concentration was 21.91% lower than that in the control group. However, the above conditions were significantly changed by the treatment with NX-12 + FOC, which meant that the above values changed to be 56.75, 103.14, and 55.12% of the control group, respectively (Supplementary Figure S1). The leaf wilt index (LWI) value obtained in the seedlings treated with FOC was 51.39%, which was significantly higher than the LWI of the NX-12 + FOC group (26.39%; Figure 1B). The contents of MDA (8.91 μmol mg^{-1} for FOC versus 5.11 μmol mg^{-1} for NX-12 + FOC) and POD (5.42 U mg^{-1} protein min^{-1} for FOC versus 2.81 U mg^{-1} protein min^{-1} for NX-12 + FOC) indicated that strain NX-12 exhibits great biocontrol efficacy against *Fusarium* wilt in terms of the physiological indicators (Figure 1C).

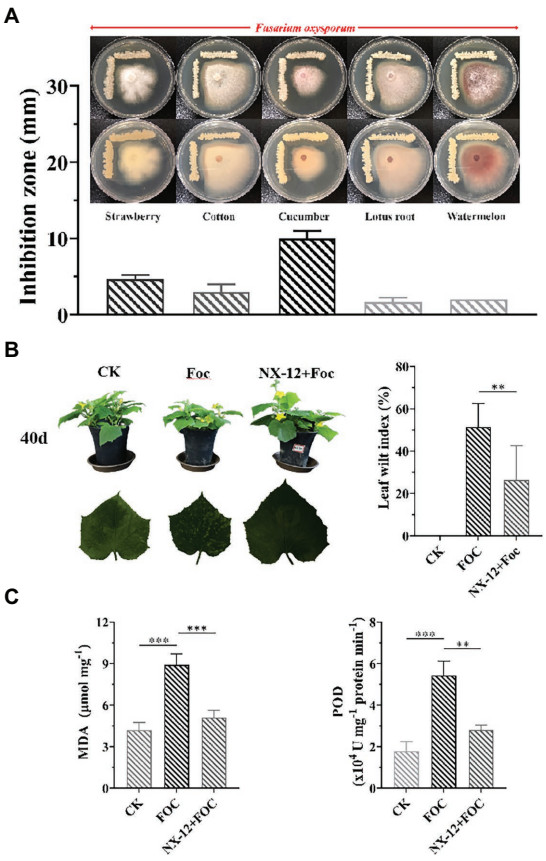

FIGURE 1
Antifungal activity and biocontrol efficacy of *Bacillus atrophaeus* NX-12. **(A)** The inhibitory effect of NX-12 on *Fusarium oxysporum* of different plant specialization types; **(B)** Biocontrol efficacy of strain NX-12 against *Fusarium* wilt in cucumber; **(C)** Activities of MDA and POD in Cucumber Leaves. Error bars represent standard deviations. ** indicated value of p <0.01; *** indicated value of p <0.001.

Main component of the extracellular polymeric substances is γ-PGA

Because strain NX-12 is a robust biofilm-forming strain, it can form a strong biofilm on the surface of solid and liquid (Supplementary Figure S2). The formation of biofilm is closely related to the secretion of extracellular matrix. We then measured the yield of its EPSs, the yield of which reached 16.8 g/l in the selected medium. At the same time, it was also proved that the effect of nitrogen source on yield was greater than that of carbon source (Figure 2A). However, there was no significant difference in the polysaccharide content of the EPS, regardless of the medium (Figure 2B). This also prompted us to think about polypeptides rather than polysaccharides. Spectral analysis revealed that EPS and γ-PGA had a consistent maximum absorption peak at 209 nm (Figure 2C). Subsequently, the results of High-Performance Liquid Chromatography (HPLC) analysis verified that the content of glutamate after hydrolysis reached 89.5% of the EPSs (Figure 2D).

Knockout of *pgsBCA* significantly reduced the yield of the EPS

To better understand the function of γ-PGA, the γ-PGA synthase gene *pgsBCA* of NX-12 was knocked out using the

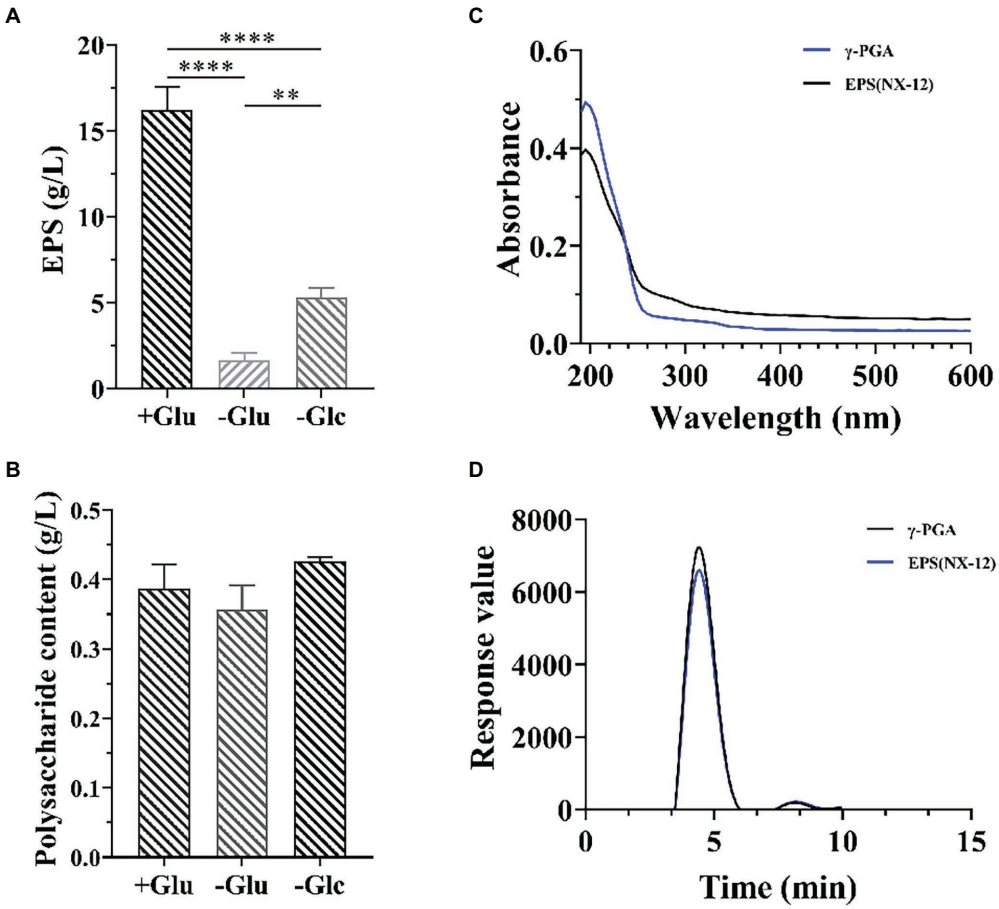

FIGURE 2
Isolation and Identification of EPS from NX-12. **(A)** Comparison of the production of EPSs by fermentation; **(B)** Comparison of the production of extracellular polysaccharide by fermentation; **(C)** Spectral analysis of EPS from NX-12 and γ-PGA. **(D)** Comparison of monomer liquid phase analysis after hydrolysis of EPS and γ-PGA; Error bars represent standard deviations. ** indicated value of $p<0.01$; **** indicated value of $p<0.0001$.

Crispr-Cas9n system (Figure 3A). It can be clearly seen that the colony morphology on the plate changed from wet to dry. PCR screening was used to verify whether the target gene fragment (*pgsBCA*) had been effectively deleted. A 2048-bp PCR product was amplified using the mutant chromosome DNA as a template, which was 2,813 bp less than the PCR product using the NX-12 chromosome DNA as a template (Figure 3B). The mutant strain was designated *B. atrophaeus* NX-12Δ*pgs*. The EPS yield of NX-12Δ*pgs* was 90.2% lower than that of NX-12 (Figure 3C). There was no significant difference between the wild-type and mutant bacteria in the LB medium (Figure 3D).

The transcription levels of genes related to antimicrobial peptide synthesis and glutamate metabolism were different between wild and the mutant strain

In order to confirm whether the knockout of *pgsBCA* has an effect on the antifungal ability of the strain, we verified the antifungal ability of wild bacteria and mutant bacteria by punching holes on the plate. Contrary to our expectations, it can be clearly seen that NX-12Δ*pgs* had significantly improved inhibition activity against pathogenic fungi when compared with NX-12 (Figure 4A; Supplementary Figure S3). However, the growth curve of NX-12 and NX-12Δ*pgs* in the PDA liquid medium showed no significant difference within 48 h (Figure 4B). We therefore tested the transcription of genes related to antimicrobial peptide synthesis as well as glutamate transferase. Six lipopeptide antibiotics were predicted according to the antiSMASH website, and key synthetic genes were identified using the NCBI comparison database. The results of qPCR showed that when compared with NX-12, the synthesis of fengycin, rhizocticin A, bacillibactin, and bacillaene genes of NX-12Δ*pgs* was significantly upregulated. No significant differences were observed between surfactin and subtilisin A. The transcription level of the glutamate dehydrogenase gene *rocG*, which is related to nitrogen metabolism (Feng et al., 2015), was significantly decreased (Figure 4C). These results suggest the enhancement of antifungal ability *in vitro*.

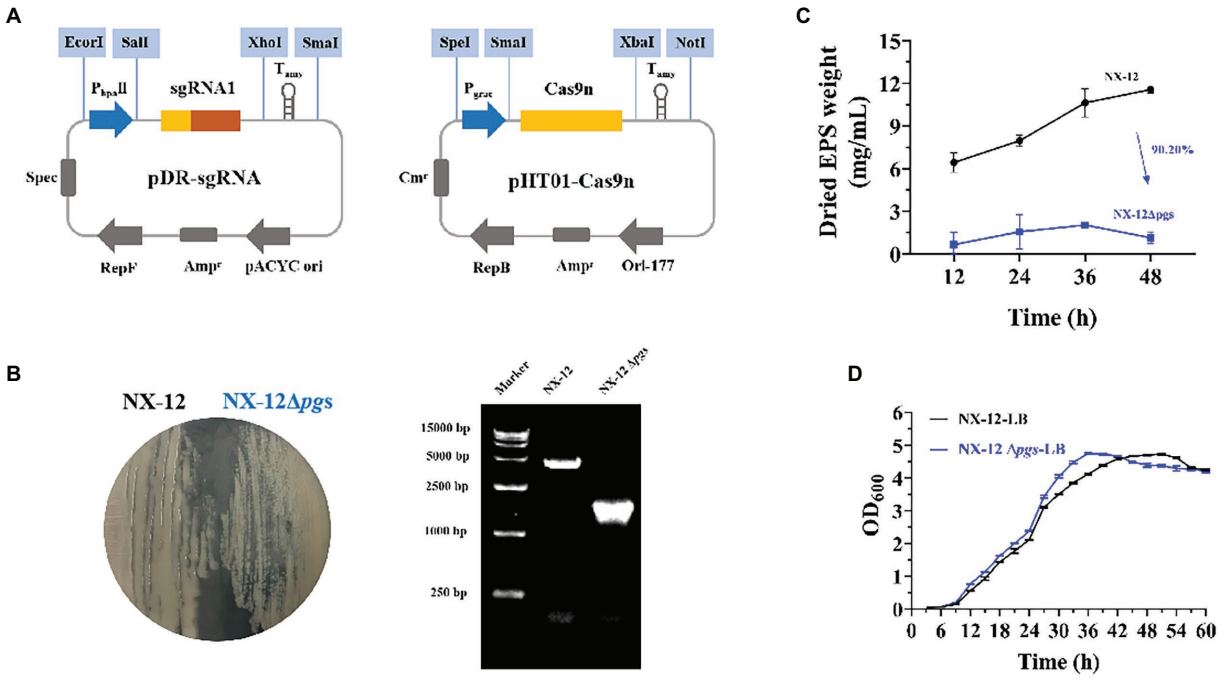

FIGURE 3
Knockout of *pgsBCA* based on CRISPR-Cas9n system. **(A)** Construction of double plasmid system; **(B)** Comparison of colony morphology and verification by PCR after knockout; **(C)** Yield of EPS between NX-12 and NX-12Δ*pgs*; **(D)** Growth curves of NX-12 and NX-12Δ*pgs* in LB medium.

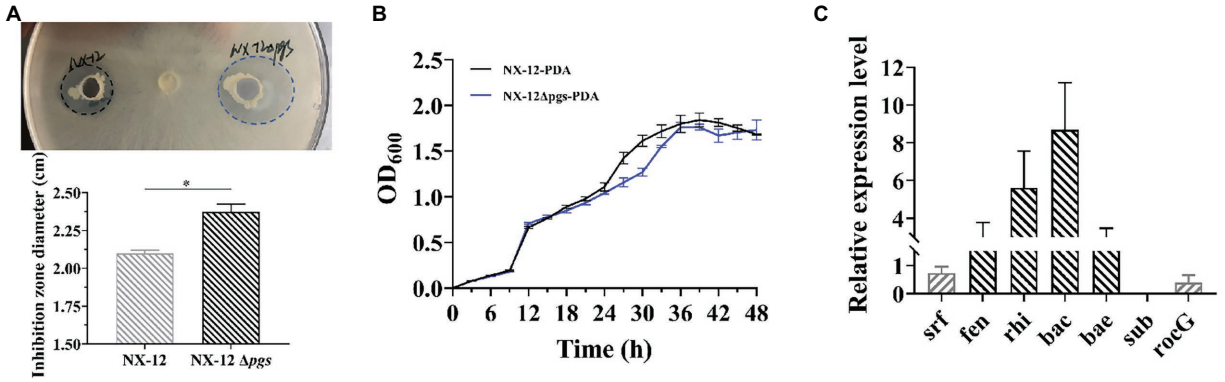

FIGURE 4
Comparison of the transcription levels of genes related to antimicrobial peptide synthesis between NX-12 and NX-12Δ*pgs*. **(A)** Comparison of antibacterial ability of NX-12 and NX-12Δ*pgs* against FOC *in vitro*; **(B)** Growth curves of NX-12 and NX-12Δ*pgs* in PDB medium; **(C)** Transcription levels of synthetic genes related to antimicrobial peptides in NX-12 and NX-12Δ*pgs*. Error bars represent standard deviations. * indicated value of $p<0.05$.

The biocontrol ability of NX-12Δ*pgs* against Cucumber *Fusarium* wilt decreased significantly

As described above, the deletion of *pgsBCA* led to the enhancement of antifungal activities. Therefore, we wondered whether wild bacteria and mutant bacteria have the same effect in plant biocontrol as *in vitro*. The biocontrol abilities of NX-12 and NX-12Δ*pgs* in cucumber seedlings were tested. Contrary to the antibacterial effect *in vitro*, the leaf wilt index (LWI) value obtained in the seedlings treated with strain NX-12Δ*pgs* was 50%, which was significantly higher than the LWI of the NX-12 group (33.3%). Whether the seedlings were treated with NX-12 or NX-12Δ*pgs*, the LWI of cucumbers after treatment was significantly lower than that of the FOC group (90.3%; Figure 5A). In addition, the height and dry weight of the cucumber seedlings were measured. Compared to the NX-12Δ*pgs* + FOC group, both the height and dry weight were significantly increased in the

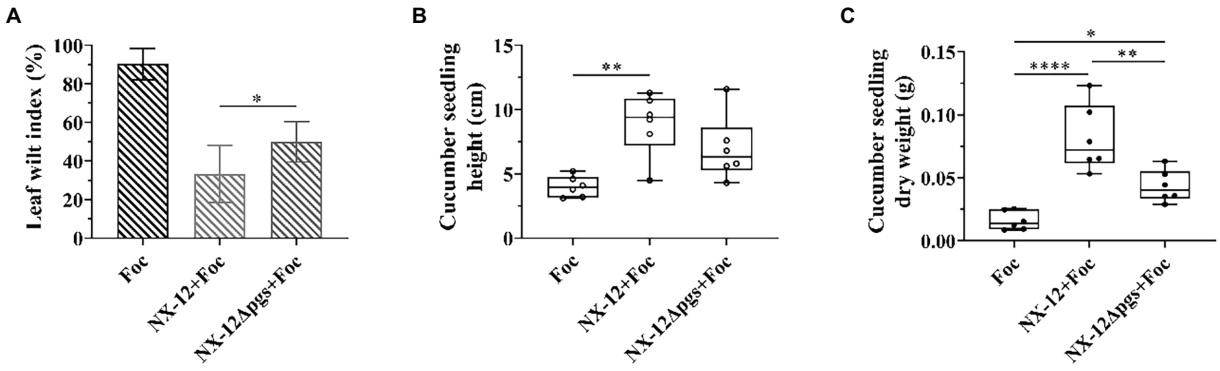

FIGURE 5
The biological control ability of NX-12Δ*pgs* decreased significantly. **(A)** The leaf wilt index (LWI) under different treatments; **(B)** Seeding height of cucumber treated by NX-12 and NX-12Δ*pgs* in controlling Fusarium wilt; **(C)** Seeding dry weight of cucumber treated by NX-12 and NX-12Δ*pgs* in controlling Fusarium wilt. Error bars represent standard deviations. * indicated value of $p<0.05$; ** indicates value of $p<0.01$; **** indicates value of $p<0.0001$.

NX-12 + FOC group (Figures 5B,C). This indicated that strain NX-12 was more effective than strain NX-12Δ*pgs* at suppressing cucumber *Fusarium* wilt.

Synergistic action between γ-PGA and NX-12 to enhance the ability of colonization and biocontrol

Since the function of BCA is related to the interaction between host plants, we further hypothesized that NX-12 could realize the function of biological control by enhancing the formation of biofilm and promoting its colonization in the rhizosphere with the help of secreted γ-PGA. The biofilm-forming ability of NX-12 was significantly higher than that of NX-12Δ*pgs* (Figure 6A). NX-12 could form a clear thick layer of biofilm ($OD_{570} = 20.44$), whereas the biofilm formation ability of NX-12Δ*pgs* ($OD_{570} = 2.57$) was significantly diminished, which was only 12.6% when compared to NX-12. Under pot soil conditions, colonization of NX-12 and NX-12Δ*pgs* in the rhizosphere was determined by plate counting and fluorescence observation. It was found that NX-12Δ*pgs* (0.98×10^7 CFU/g root) failed to colonize roots as effectively when compared to NX-12 (1.66×10^7 CFU/g root). To further support the idea that γ-PGA plays a key role in rhizosphere colonization, the mutant NX-12Δ*pgs* was complemented with pMA5-*pgsBCA* and we named NX-12Δ*pgs* (pMA5-*pgs*). The EPS yield of NX-12Δ*pgs* (pMA5-*pgs*; 11.17 mg/ml) recovered significantly compared to that of NX-12Δ*pgs* (2.77 mg/ml; Supplementary Figure S4). As expected, NX-12Δ*pgs* (pMA5-*pgs*) restored most of its biofilm formation (Figure 6A) and colonization ability. At the same time, the exogenous addition of γ-PGA improved the colonization ability of NX-12Δ*pgs* (1.23×10^7 CFU/g root), although it did not reach the level of NX-12Δ*pgs* (pMA5-*pgs*; 1.51×10^7 CFU/g root; Figure 6B). The FOC population was monitored using plate counting and remained high (28.83×10^3 CFU/g soil) in the NX-12Δ*pgs* group compared to that in the NX-12 group (2.67×10^3 CFU/g soil). However, the FOC population in the rhizosphere was significantly reduced by the application of NX-12Δ*pgs* (pMA5-*pgs*; 7.8×10^3 CFU/g soil). Exogenous addition of γ-PGA also slightly reduced the FOC population to 22.33×10^3 CFU/g soil (Figure 6C).

Fluorescence microscopy images also confirmed that γ-PGA significantly affected the colonization ability of NX-12 (Figure 6D).

Discussion

Rhizosphere bacteria play a key role in protecting plants and promoting plant growth and health (Berendsen et al., 2012). *Bacillus subtilis*, as well as other *Bacilli*, have been used as important BCAs in agriculture (Nagórska et al., 2007; Ongena and Jacques, 2008; Liu et al., 2021). The newly isolated strain, *B. atrophaeus* NX-12, demonstrated strong antifungal efficacy toward FOC *in vitro* and biocontrol activities *in situ*. The mechanism by which *B. atrophaeus* exerts a strong biocontrol activity in the rhizosphere is not well understood. Previous studies have provided evidence that the production of antimicrobial agents, biofilm formation, and triggering host systemic resistance can contribute to the biocontrol activities of *Bacillus* (Bais et al., 2004; Chen et al., 2019). Here, we have focused on the role of biofilm formation in plant biocontrol, and we have provided several types of evidence documenting its importance.

In view of the high yield of γ-PGA in NX-12, which is not common in most *Bacillus* sp. strains, we first knocked out the key genes for γ-PGA synthesis, *pgsBCA*, through CRISPR-Cas9n. A strain NX-12Δ*pgs* with low γ-PGA yield was obtained and used to study the differences between NX-12Δ*pgs* and wild strains. Interestingly, NX-12Δ*pgs* showed better antifungal activity against the pathogen than NX-12, which was not as expected. Previous studies have found that *Bacillus* species have become the most successfully commercialized biocontrol agents

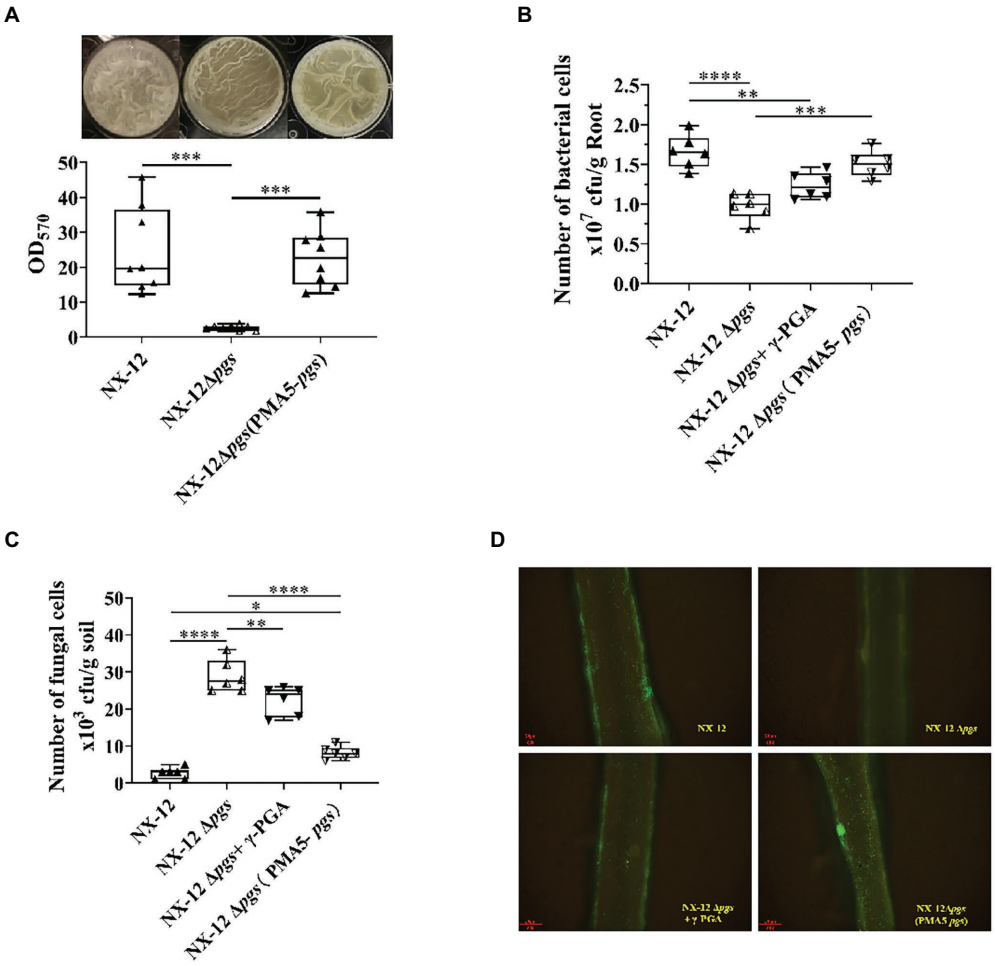

FIGURE 6
γ-PGA helps colonize and control pathogens. **(A)** Difference in biofilm formation between NX-12 and NX-12Δ*pgs in vitro*; **(B)** Number of bacteria cells colonized on the root surface of cucumber under the treatments of NX-12, NX-12Δ*pgs*, NX-12Δ*pgs*+γ-PGA, and NX-12Δ*pgs* (pMA5-*pgs*); **(C)** Number of fungal cells colonized on the root surface of cucumber under the treatments of NX-12, NX-12Δ*pgs*, NX-12Δ*pgs*+γ-PGA, and NX-12Δ*pgs* (pMA5-*pgs*); **(D)** Colonization of fluorescent strains in the rhizosphere. Error bars represent standard deviations. * indicates value of $p<0.05$; ** indicates value of $p<0.01$; *** indicated value of $p<0.001$; **** indicates value of $p<0.0001$.

owing to their ability to produce a broad spectrum of antimicrobial secondary metabolites (Koumoutsi et al., 2004; Sansinenea and Ortiz, 2011; Xingshan et al., 2021). These substances can inhibit many phytopathogens, including fungi and bacteria (Bais et al., 2004; Koumoutsi et al., 2004; Sansinenea and Ortiz, 2011; Liu et al., 2021). We predicted some secondary metabolites that NX-12 might produce according to the secondary metabolite prediction analysis website antiSMASH and mined its key genes using NCBI. qPCR analysis showed that genes related to antimicrobial peptide synthesis (*fen, rhi, bac, and bae*) were significantly upregulated in the mutants, while *rocG*, a gene related to glutamate synthesis (Feng et al., 2015), was significantly downregulated. Therefore, we hypothesized that the increased antifungal ability of mutant bacteria was due to the fact that more nitrogen was used for the synthesis of antimicrobial substances, while in wild bacteria, more nitrogen was used for the synthesis of γ-PGA.

On the contrary, the biocontrol effect of NX-12Δ*pgs* was significantly decreased *in situ*. This showed that antifungal ability was not the only criterion for considering biocontrol ability. Many studies have shown that the effective colonization of microorganisms in plant rhizosphere determines whether they can play the corresponding biological functions. Biofilm formation is critical for bacterial rhizosphere colonization (Cao et al., 2011; Allard-Massicotte et al., 2016). Here, we found that the biofilm-forming capacity of NX-12Δ*pgs* was significantly lower than that of NX-12. Although extracellular polysaccharides are thought to be the main component of biofilms; in fact, in some strains with high yield of γ-PGA, it is the main component of biofilms (Stanley and Lazazzera, 2005). In addition, we found that the number of rhizosphere colonization of NX-12 was significantly higher than that of NX-12Δ*pgs* due to its strong biofilm-forming ability. Interestingly, we also found that FOC colonization in

rhizosphere in NX-12 group was significantly less than that in NX-12Δ*pgs* group. These results indicated that γ-PGA enhanced the biofilms formation of NX-12, promoted the colonization of NX-12 in the rhizosphere, and occupied the dominant ecological niche, thus enhancing the resistance of plants to biological stress through this indirect way.

In conclusion, our research shows that the newly isolated *B. atrophaeus* NX-12 with high yield of γ-PGA owns strong antifungal ability against FOC *in vitro* and biocontrol effects *in situ*. It is found that γ-PGA enhances plant tolerance to biotic stress by promoting the formation of NX-12 biofilm and rhizosphere colonization ability. Our results reveal that the effective colonization of BCAs in the rhizosphere is very important for its function. Our work broadens the research direction of biofilms and has enhanced our knowledge of the application of γ-PGA in biocontrol.

Data availability statement

Strain Bacillus atrophaeus NX-12 presented in the study is deposited in the CGMCC repository, accession number 22125.

Author contributions

JX, YG, LS, HX, and PL conceived and designed study. JX and YQ contributed to the new methods or models. JX and TT performed the experiments. JX performed the data collection and analysis and the first draft of the manuscript. RW, YG, LS, HX, and PL assisted JX in revising the previous versions of the manuscript. All authors contributed to the article and approved the submitted version.

Funding

The research was funded by the National Key Research and Development Program of China (2021YFC2101700), the National Natural Science Foundation of China (42177271), the Jiangsu Agricultural Science and Technology Innovation Fund [CX (21) 3158], the Key Research and Development Project of Jiangsu Province (BE2019390), and the Jiangsu Synergetic Innovation Center for Advanced Bio-Manufacture (XTB2202).

Conflict of interest

The authors declare that the research was conducted in the absence of any commercial or financial relationships that could be construed as a potential conflict of interest.

Publisher's note

Supplementary material

The Supplementary materials for this article can be found online at: https://www.frontiersin.org/articles/10.3389/fmicb.2022.972393/full#supplementary-material

References

Allard-Massicotte, R., Tessier, L., Lécuyer, F., Lakshmanan, V., Lucier, J., Garneau, D., et al. (2016). *Bacillus subtilis* early colonization of *arabidopsis thaliana* roots involves multiple chemotaxis receptors. *MBio* 7, e01664–e01616. doi: 10.1128/mBio.01664-16

Ashiuchi, M., and Misono, H. (2002). Biochemistry and molecular genetics of poly-γ-glutamate synthesis. *Appl. Microbiol. Biotechnol.* 59, 9–14. doi: 10.1007/s00253-002-0984-x

Backer, R., Rokem, J., Ilangumaran, G., Lamont, J., Praslickova, D., Ricci, E., et al. (2018). Plant growth-promoting rhizobacteria: context, mechanisms of action, and roadmap to commercialization of biostimulants for sustainable agriculture. *Front. Plant Sci.* 9:1473. doi: 10.3389/fpls.2018.01473

Bais, H. P., Fall, R., and Vivanco, J. M. (2004). Biocontrol of *Bacillus subtilis* against infection of arabidopsis roots by *pseudomonas syringae* is facilitated by biofilm formation and surfactin production. *Plant Physiol.* 134, 307–319. doi: 10.1104/pp.103.028712

Berendsen, R. L., Pieterse, C. M. J., and Bakker, P. A. H. M. (2012). The rhizosphere microbiome and plant health. *Trends Plant Sci.* 17, 478–486. doi: 10.1016/j.tplants.2012.04.001

Berg, G., Krechel, A., Ditz, M., Sikora, R., Ulrich, A., and Hallmann, J. (2005). Endophytic and ectophytic potato-associated bacterial communities differ in structure and antagonistic function against plant pathogenic fungi. *FEMS Microbiol. Ecol.* 51, 215–229. doi: 10.1016/j.femsec.2004.08.006

Bilal, S., Shahzad, R., Kang, S.-M., Imran, Q., Al-Harrasi, A., Yun, B.-W., et al. (2018). Endophytic microbial consortia of phytohormones-producing fungus *Paecilomyces formosus* lhl10 and bacteria *Sphingomonas* sp. lk11 to glycine max l. regulates physio-hormonal changes to attenuate aluminum and zinc stresses. *Front. Plant Sci.* 9:1273. doi: 10.3389/fpls.2018.01273

Branda, S., Chu, F., Kearns, D., Losick, R., and Kolter, R. (2006). A major protein component of the *bacillus* biofilm matrix. *Mol. Microbiol.* 59, 1229–1238. doi: 10.1111/j.1365-2958.2005.05020.x

Brannen, P., and Kenney, D. (1997). Kodiak® - A successful biological-control product for suppression of soil-borne plant pathogens of cotton. *J. Ind. Microbiol. Biotechnol.* 19, 169–171. doi: 10.1038/sj.jim.2900439

Cao, Y., Zhang, Z., Ling, N., Yuan, Y., Zheng, X., Shen, B., et al. (2011). *Bacillus subtilis* SQR 9 can control *Fusarium* wilt in cucumber by colonizing plant roots. *Biol. Fertil. Soils* 47, 495–506. doi: 10.1007/s00374-011-0556-2

Chen, Y., Cao, S., Chai, Y., Clardy, J., Kolter, R., Guo, J.-H., et al. (2012). A *Bacillus subtilis* sensor kinase involved in triggering biofilm formation on the roots of tomato plants. *Mol. Microbiol.* 85, 418–430. doi: 10.1111/j.1365-2958.2012.08109.x

Chen, Y., Yan, F., Chai, Y., Liu, H., Kolter, R., Losick, R., et al. (2019). Biocontrol of tomato wilt disease by *Bacillus subtilis* isolates from natural environments depends on conserved genes mediating biofilm formation. *Environ. Microbiol.* 15, 848–864. doi: 10.1111/j.1462-2920.2012.02860.x

Compant, S., Clément, C., and Sessitsch, A. (2010). Plant growth-promoting bacteria in the rhizo- and endosphere of plants: their role, colonization, mechanisms involved and prospects for utilization. *Soil. Boil. Biochem.* 42, 669–678. doi: 10.1016/j.soilbio.2009.11.024

Compant, S., Duffy, B., Nowak, J., Clément, C., and Ait Barka, E. (2005). Use of plant growth-promoting bacteria for biocontrol of plant diseases: principles, mechanisms of action, and future prospects. *Appl. Environ. Microbiol.* 71, 4951–4959. doi: 10.1128/AEM.71.9.4951-4959.2005

Costa, O. Y. A., Raaijmakers, J. M., and Kuramae, E. E. (2018). Microbial extracellular polymeric substances: ecological function and impact on soil aggregation. *Front. Microbiol.* 9:1636. doi: 10.3389/fmicb.2018.01636

Dean, R., Kan, J., Pretorius, Z., Hammond-Kosack, K., Pietro, A., Spanu, P., et al. (2012). The top 10 fungal pathogens in molecular plant pathology. *Mol. Plant Pathol.* 13, 414–430. doi: 10.1111/j.1364-3703.2011.00783.x

Dr, F., Olivain, C., and Alabouvette, C. (2003). *Fusarium oxysporum* and its biocontrol. *New Phytol.* 157, 493–502. doi: 10.1046/j.1469-8137.2003.00700.x

Faheem, M., Raza, W., Wei, Z., Zhang, N., Shen, Q., and Xu, Y. (2014). Evaluation of the biocontrol potential of *Streptomyces goshikiensis* YCXU against *Fusarium oxysporum* f. sp. niveum. *Biol. Control* 81, 101–110. doi: 10.1016/j.biocontrol.2014.11.012

Feng, J., Gu, Y., Quan, Y., Cao, M., Gao, W., Zhang, W., et al. (2015). Improved poly-γ-glutamic acid production in *Bacillus amyloliquefaciens* by modular pathway engineering. *Metab. Eng.* 32, 106–115. doi: 10.1016/j.ymben.2015.09.011

Flemming, H.-C., Wingender, J., Szewzyk, U., Steinberg, P., Rice, S., and Kjelleberg, S. (2016). Biofilms: An emergent form of bacterial life. *Nat. Rev. Microbiol.* 14, 563–575. doi: 10.1038/nrmicro.2016.94

Hsueh, Y.-H., Somers, E., Lereclus, D., and Wong, A. (2006). Biofilm formation by *Bacillus cereus* is influenced by plcr, a pleiotropic regulator. *Appl. Environ. Microbiol.* 72, 5089–5092. doi: 10.1128/AEM.00573-06

Huang, J., Li, H., and Yuan, H. (2006). Effect of organic amendments on *Verticillium* wilt of cotton. *Crop Prot.* 25, 1167–1173. doi: 10.1016/j.cropro.2006.02.014

Jayathilake, P. G., Rushton, S., Curtis, T., Chen, J., Pg, J., Jana, S., et al. (2017). Extracellular polymeric substance production and aggregated bacteria colonization influence the competition of microbes in biofilms. *Front. Microbiol.* 8:1. doi: 10.3389/fmicb.2017.01865

Karygianni, L., Ren, Z., Koo, H., and Thurnheer, T. (2020). Biofilm matrixome: extracellular components in structured microbial communities. *Trends Microbiol.* 28, 668–681. doi: 10.1016/j.tim.2020.03.016

Kenneth, J. L., and Thomas, D. S. (2002). Analysis of relative gene expression data using real-time quantitative PCR and the 2-ΔΔCT method. *Methods* 25, 402–408. doi: 10.1006/meth.2001.1262

Kolter, R., and Greenberg, E. P. (2006). The superficial life of microbes. *Nature* 441, 300–302. doi: 10.1038/441300a

Koumoutsi, A., Chen, X.-H., Henne, A., Liesegang, H., Hitzeroth, G., Franke, P., et al. (2004). Structural and functional characterization of gene clusters directing nonribosomal synthesis of bioactive cyclic lipopeptides in *Bacillus amyloliquefaciens* strain FZB42. *J. Bacteriol.* 186, 1084–1096. doi: 10.1128/JB.186.4.1084-1096.2004

Li, Y., Gu, Y.-L., Li, J., Xu, M., Wei, Q., and Wang, Y. (2015). Biocontrol agent *Bacillus amyloliquefaciens* LJ02 induces systemic resistance against cucurbits powdery mildew. *Front. Microbiol.* 6:883. doi: 10.3389/fmicb.2015.00883

Li, C. H., Shi, L., Han, Q., Hu, H. L., Zhao, M., Tang, C. M., et al. (2012). Biocontrol of *Verticillium* wilt and colonization of cotton plants by an endophytic bacterial isolate. *J. Appl. Microbiol.* 113, 641–651. doi: 10.1111/j.1365-2672.2012.05371.x

Liu, R., Li, J., Zhang, F., Zheng, D., Chang, Y., Xu, L., et al. (2021). Biocontrol activity of *Bacillus velezensis* D4 against apple Valsa canker. *Biol. Control* 163:104760. doi: 10.1016/j.biocontrol.2021.104760

Maruzani, R., Sutton, G., Nocerino, P., and Marvasi, M. (2019). Exopolymeric substances (EPS) from *Salmonella enterica*: polymers, proteins and their interactions with plants and abiotic surfaces. *J. Microbiol.* 57, 1–8. doi: 10.1007/s12275-019-8353-y

Meneses, C., Rouws, L., Simoes-Araujo, J., Vidal, M., and Baldani, J. (2011). Exopolysaccharide production is required for biofilm formation and plant colonization by the nitrogen-fixing endophyte gluconacetobacter diazotrophicus. *Mol. Plant. Microbe. In.* 24, 1448–1458. doi: 10.1094/MPMI-05-11-0127

Nagórska, K., Bikowski, M., and Obuchowski, M. (2007). Multicellular behaviour and production of a wide variety of toxic substances support usage of *Bacillus subtilis* as a powerful biocontrol agent. *Acta Biochim. Pol.* 54, 495–508. doi: 10.18388/abp.2007_3224

Ngugi, H. K., Dedej, S., Delaplane, K. S., Savelle, A. T., and Scherm, H. (2005). Effect of flower-applied serenade biofungicide (*Bacillus subtilis*) on pollination-related variables in rabbiteye blueberry. *Biol. Control* 33, 32–38. doi: 10.1016/j.biocontrol.2005.01.002

Olanrewaju, O., Glick, B., and Babalola, O. (2017). Mechanisms of action of plant growth promoting bacteria. *World J. Microbiol. Biotechnol.* 33, 197–116. doi: 10.1007/s11274-017-2364-9

Ongena, M., and Jacques, P. (2008). *Bacillus lipopeptides*: versatile weapons for plant disease biocontrol. *Trends Microbiol.* 16, 115–125. doi: 10.1016/j.tim.2007.12.009

Qiu, Y., Sha, Y., Zhang, Y., Xu, Z., Li, S., Lei, P., et al. (2017). Development of Jerusalem artichoke resource for efficient one-step fermentation of poly-(γ-glutamic acid) using a novel strain *Bacillus amyloliquefaciens* NX-2S. *Bioresour. Technol.* 239, 197–203. doi: 10.1016/j.biortech.2017.05.005

Qiu, Y., Zhu, Y., Sha, Y., Lei, P., Zhengshan, L., Feng, X., et al. (2020). Development of a robust *Bacillus amyloliquefaciens* cell factory for efficient poly(γ-glutamic acid) production from Jerusalem artichoke. *ACS Sustain. Chem. Eng.* 8, 9763–9774. doi: 10.1021/acssuschemeng.0c02107

Raza, W., Ling, N., Zhang, R., Huang, Q., Xu, Y., and Shen, Q. (2016). Success evaluation of the biological control of *Fusarium* wilts of cucumber, banana, and tomato since 2000 and future research strategies. *Crit. Rev. Biotechnol.* 37, 202–212. doi: 10.3109/07388551.2015.1130683

Rilling, J. I., Acuña, J. J., Nannipieri, P., Cassan, F., Maruyama, F., and Jorquera, M. A. (2019). Current opinion and perspectives on the methods for tracking and monitoring plant growth–promoting bacteria. *Soil. Boil. Biochem.* 130, 205–219. doi: 10.1016/j.soilbio.2018.12.012

Sansinenea, E., and Ortiz, A. (2011). Secondary metabolites of soil *bacillus* spp. *Biotechnol. Lett.* 33, 1523–1538. doi: 10.1007/s10529-011-0617-5

Santoyo, G., Urtis-Flores, C. A., Loeza-Lara, P. D., Orozco-Mosqueda, M. D. C., and Glick, B. R. (2021). Rhizosphere colonization determinants by plant growth-promoting rhizobacteria (PGPR). *Biology* 10, 475. doi: 10.3390/biology10060475

Saravana Kumar, P., Duraipandiyan, V., and Ignacimuthu, S. (2014). Isolation, screening and partial purification of antimicrobial antibiotics from soil *Streptomyces* sp. SCA 7. *Kaohsiung J. Med. Sci.* 30, 435–446. doi: 10.1016/j.kjms.2014.05.006

Stanley, N., and Lazazzera, B. (2005). Defining the genetic differences between wild and domestic strains of *Bacillus subtilis* that affect poly-γ-DL-glutamic acid production and biofilm formation. *Mol. Microbiol.* 57, 1143–1158. doi: 10.1111/j.1365-2958.2005.04746.x

Tian, T., Sun, B., Shi, H., Gao, T., He, Y., Liu, Y., et al. (2021). Sucrose triggers a novel signaling cascade promoting *Bacillus subtilis* rhizosphere colonization. *ISME J.* 15, 2723–2737. doi: 10.1038/s41396-021-00966-2

Wang, L., Chen, S., and Yu, B. (2022). Poly-γ-glutamic acid: recent achievements, diverse applications and future perspectives. *Trends Food Sci. Technol.* 119, 1–12. doi: 10.1016/j.tifs.2021.11.009

Wang, P., Zhong, Z., Cai, T., and Zhu, J. (2008). Exopolysaccharide biosynthesis is important for *Mesorhizobium tianshanense*: plant host interaction. *Arch. Microbiol.* 189, 525–530. doi: 10.1007/s00203-007-0345-3

Xingshan, H., Dongxia, S., Xiong, Q., Bao, B., Zhang, W., Dai, C.-F., et al. (2021). The plant-beneficial rhizobacterium *Bacillus velezensis* FZB42 controls the soybean pathogen *Phytophthora sojae* due to bacilysin production. *Appl. Environ. Microbiol.* 87:e0160121. doi: 10.1128/AEM.01601-21

Yiyang, Y., Yan, F., Chen, Y., and Jin, C., Guo, J-H., Chai, Y. (2016). Poly-γ-glutamic acids contribute to biofilm formation and plant root colonization in selected environmental isolates of *Bacillus subtilis*. *Front. Microbiol.* 7:1811. doi: 10.3389/fmicb.2016.01811

frontiers | Frontiers in Microbiology

TYPE Original Research
PUBLISHED 20 September 2022
DOI 10.3389/fmicb.2022.954767

OPEN ACCESS

EDITED BY
Masamichi Nishiguchi,
Ehime University, Japan

REVIEWED BY
Shin-Yi Lee Marzano,
Agricultural Research Service (USDA), United States
Kunal Singh,
Institute of Himalayan Bioresource Technology (CSIR), India

*CORRESPONDENCE
Baoshan Chen
chenyaoj@gxu.edu.cn

†These authors share first authorship

SPECIALTY SECTION
This article was submitted to Microbe and Virus Interactions with Plants, a section of the journal Frontiers in Microbiology

RECEIVED 27 May 2022
ACCEPTED 29 August 2022
PUBLISHED 20 September 2022

CITATION
Lu S, Zhang H, Guo F, Yang Y, Shen X and Chen B (2022) SsUbc2, a determinant of pathogenicity, functions as a key coordinator controlling global transcriptomic reprogramming during mating in sugarcane smut fungus. *Front. Microbiol.* 13:954767. doi: 10.3389/fmicb.2022.954767

SsUbc2, a determinant of pathogenicity, functions as a key coordinator controlling global transcriptomic reprogramming during mating in sugarcane smut fungus

Shan Lu[1,2†], Haoyang Zhang[2†], Feng Guo[3], Yanfang Yang[2], Xiaorui Shen[3] and Baoshan Chen[1,2*]

[1]State Key Laboratory for Conservation and Utilization of Subtropical Agro-Bioresources, Ministry and Province Co-sponsored Collaborative Innovation Center for Sugarcane and Sugar Industry, Nanning, China, [2]Guangxi Key Laboratory of Sugarcane Biology, College of Agriculture, Guangxi University, Nanning, China, [3]College of Life Science and Technology, Guangxi University, Nanning, China

The basidiomycete fungus *Sporisorium scitamineum* is the causative agent of sugarcane smut disease. Mating between two strains of the opposite mating type is essential for filamentous growth and infection in sugarcane plants. However, the mechanisms underlying mating and pathogenicity are still not well understood. In this work we used gene disruption to investigate the role of *Ssubc2*, the gene encoding a kinase regulator in *S. scitamineum*. Deletion of *Ssubc2* did not alter the haploid cell morphology or growth rate *in vitro* or tolerance to stress, but mutants with both alleles deleted lost mating ability and infectivity. Deletion of one *Ssubc2* allele in a pair with a wild-type strain resulted in impaired mating and reduced virulence. Transcriptome profiling revealed that about a third of genes underwent reprogramming in the wild types during mating. Although gene expression reprogramming occurred in the pairing of *Ssubc2*-null mutants, their transcriptomic profile differed significantly from that of the wild types, in which 625 genes differed from those present in the wild types that seemed to be among the required genes for a successful mating. These genes include those known to regulate mating and pathogenicity, such as components of the MAPK pathway and *hgl1*. Additionally, a total of 908 genes were differentially expressed in an out-of-control manner in the mutants. We conclude that SsUbc2 functions as a key factor to coordinate the reprogramming of gene expression at the global level and is essential for the transition from monokaryotic basidial growth to dikaryotic hyphal growth through mating.

KEYWORDS

kinase regulator, sexual mating, smut, pathogenicity, *Sporisorium scitamineum*

Introduction

Sugarcane smut, first reported in Natal, South Africa, in 1877, is a fungal disease with enormous economic impact on the sugarcane industry worldwide (McMartin, 1945; Ershad and Bani-Abbassi, 1971; Leu and Teng, 1974; Akalach and Touil, 1996; Ramesh Sundar et al., 2012). A whip-like structure composed of plant tissue, fungal hyphae, and teliospores in the apex of the plant in the late stage of infection is a hallmark of sugarcane smut (Ramesh Sundar et al., 2012). *Sporisorium scitamineum*, the causative agent of sugarcane smut, has three distinct phenotypes during its life cycle: yeast-like haploid basidiospore, dikaryotic hypha, and diploid teliospore (Pombert et al., 2015). The formation of dikaryotic hyphae through the fusion of two non-pathogenic haploid basidiospores from strains of opposite mating types (MAT-1 and MAT-2) via sexual mating is required for the fungus to infect host sugarcane plants (Yan et al., 2016). Previous studies have revealed that certain genes (e.g., *Sskpp2*, *SsSln1*, *Ssprf1*, *SsAgc1*, and *SsSln1*) and cAMP-dependent protein kinase A pathways are involved in the regulation of mating/filamentation and pathogenicity (Deng et al., 2018; Chang et al., 2019; Wang et al., 2019; Zhu et al., 2019; Cai et al., 2021). However, the mechanisms underlying the regulation of mating and virulence in this fungus are still far from clear.

In the yeast *Saccharomyces cerevisiae*, the adaptor protein Ste50p, a protein kinase regulator, is necessary for pheromone-induced signal transduction and hormone-induced differentiation of cells. Ste50 bridges the downstream α-pheromone receptor (Ste2) and upstream Ste11 and Ste7 kinase cascades (Xu et al., 1996). It is also involved in regulating pseudohyphal development by regulating the kinase function of mitogen extracellular signal-regulated kinase kinase (MEKK) Ste11 (Wu et al., 1999, 2006; Grimshaw et al., 2004), a protein that also functions in hypertonicity and pheromone response (Ekiel et al., 2009; Sharmeen et al., 2019). In the human pathogen *Cryptococcus neoformans*, Ste50p is required for monokaryotic fruiting and sexual reproduction (Fu et al., 2011). In the maize smut fungus *Ustilago maydis*, a homolog of yeast Ste50, designated Ubc2, is essential for filamentous growth and virulence (Mayorga and Gold, 2001; Klosterman et al., 2008).

In this work, we used gene disruption to investigate the role of a *U. maydis* Ubc2 homolog called SsUbc2 in *S. scitamineum*. *Ssubc2* deletion mutants did not alter the morphology, growth, or response to stress in haploid basidiospores but had an adverse impact on mating and pathogenicity. Comparative transcriptome analysis revealed that SsUbc2 functioned as a master to coordinate gene reprogramming at the global level. Deletion of *Ssubc2* resulted in extensive change in gene expression patterns in monokaryotic basidiospores and in the mating process and impairment of mating, filamentation, and pathogenicity with a dose-response effect.

Results

Identification of *Ssubc2* in *Sporisorium scitamineum*

By blasting the nucleotide database of *S. scitamineum*[1] using the sequence of *Ubc2* of *U. maydis* (accession no. taxid:49012) as a query, we identified a deduced protein (accession no. ON164841) with 76.3% similarity to Ubc2. The gene encoding this protein, designated *Ssubc2*, encodes a protein of 837 amino acids without any introns. Alignment with selected Ubc2 homologs from other fungi showed that SsUbc2 possesses all three domains [Sterile Alpha Motif (SAM), Ras-Association (RA), Src Homology 3 (SH3); **Figure 1A**]. Phylogenetic analysis revealed that Ubc2 of the basidiomycetous fungi formed a unique clade separate from Ubc2 of the ascomycetous fungi (**Figure 1B**).

Phenotypic characterization and gene expression profile of *Ssubc2* deletion mutants

Mutation of the *Ssubc2* gene in both mating types, JG36 (MAT-1) and JG35 (MAT-2), was achieved by the transformation of wild-type strains with the CRISPR-Cas9/T-DNA system for *S. scitamineum* (Lu et al., 2017; **Figure 2A**). We screened *Ssubc2* disruptants using PCR (**Figure 2B**). A total of six mutants (three for JG35 and three for JG36) were obtained. Complementation of the *Ssubc2* disruptants was achieved through the introduction of a copy of *Ssubc2* with a modified target sequence to avoid recognition by the CRISPR-Cas9 system carried by the disruptants (**Figure 2C**). Quantification of transcript accumulation confirmed that no *Ssubc2* expression was detected in the disruptants; *Ssubc2* expression was fully restored in the complemented Δ35-*ubc2*-C and restored up to 55% of the wild-type level in complemented Δ36-*ubc2*-C (**Figure 2D**). When haploid *Ssubc2*-null mutants were grown in liquid YEPS medium, no obvious defects in cell morphology, growth rate, or tolerance to stress were detected (**Figures 2E–G**). These results indicate that *Ssubc2* is not involved in basidial growth and may not play an essential role in hyperosmotic or oxidative stress response or in cell wall integrity.

Filamentous growth is a simple indicator of successful mating between strains of smut fungi of opposite mating types. As shown in **Figure 3A**, co-spotting of JG35 and JG36 resulted in a fluffy white colony after 48 h of growth, whereas colonies developed from co-spotting of Δ35-*ubc2* and JG36 or of JG35 and Δ36-*ubc2* were significantly less fluffy and delayed in filamentous growth. No dikaryotic hyphae were observed

1 https://www.ncbi.nlm.nih.gov/assembly/GCA_900002365.1

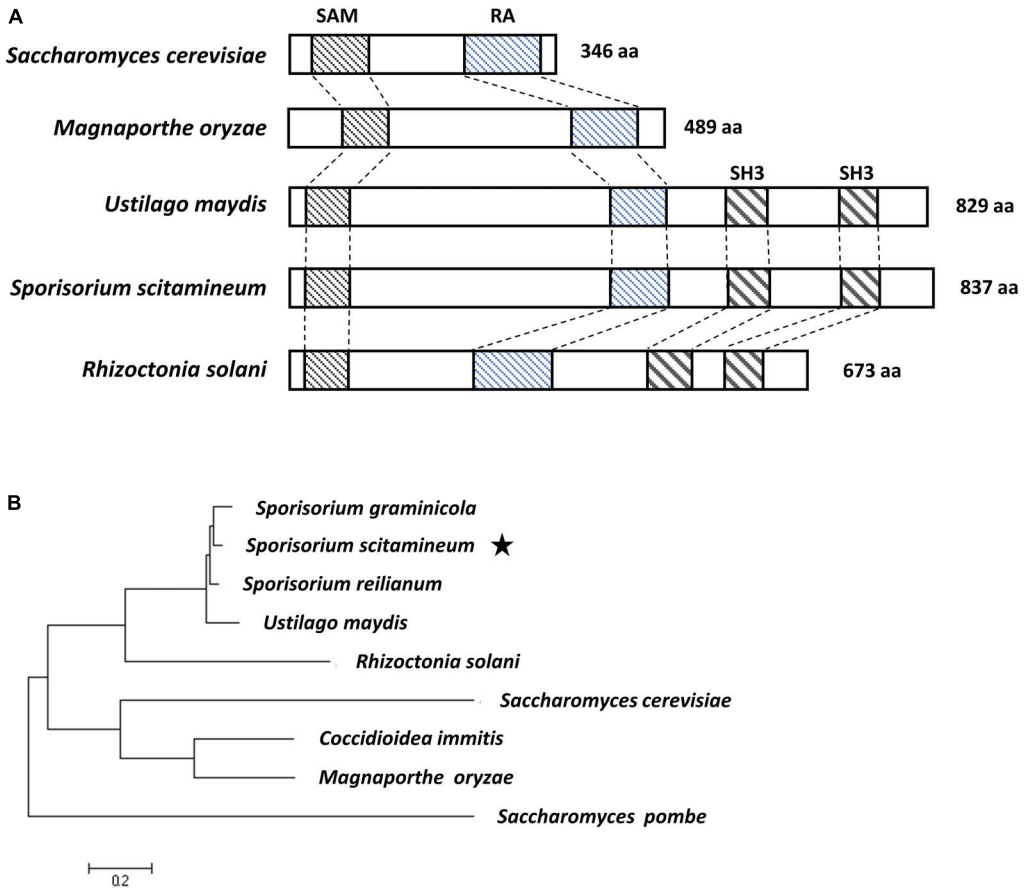

FIGURE 1
Sequence analysis of *S. scitamineum* adaptor protein SsUbc2. **(A)** Structure of the Ste50 and Ubc2 proteins. Conserved domains of Sterile Alpha Motif (SAM), Ras-Association (RA), and Src Homology 3 (SH3) are in boxes. **(B)** Phylogenetic tree constructed with amino acid sequences of Ste50 and Ubc2 proteins from ascomycetous and basidiomycetous species. The evolutionary history was inferred using the maximum likelihood method based on the JTT matrix-based model (Jones et al., 1992). Evolutionary analyses were conducted in MEGA7 (Kumar et al., 2016). Accession numbers are CBQ70036.1 for *S. reilianum*, XP_011391983.1 for *U. maydis*, XP_029739906.1 for *S. graminicola*, ELU43665 for *Rhizoctonia solani*, XP_001239789.2 for *Coccidioidea immitis*, XP_003712743.1 for *M. oryzae*, NP_009898.1 for *Saccharomyces cerevisiae*, and NP_596828.1 for *Saccharomyces pombe*. The star indicates the position of Ubc2 from *Sporisorium scitamineum*.

from mating the two *Ssubc2* disruptants (Δ35-*ubc2* × Δ36-*ubc2*), even after 96 h (**Figures 3A,B** and **Supplementary Table 1**). However, the reintroduction of a copy of the wild-type *Ssubc2* into the Δ*Ssubc2* mutants (Δ35-*ubc2*-C and Δ36-*ubc2*-C) fully restored the mating phenotype of the Δ*Ssubc2* mutants (**Figure 3A**). Indeed, microscopic examination and statistical data in three independent biological replicates confirmed that *Ssubc2* deletion in both mating types prevented the mutants from mating (**Figure 3B** and **Supplementary Table 1**).

Loci *a* and *b* are known to regulate sexual mating process of *S. scitamineum*. The *mfa* and *pra* genes in the *a* locus encode pheromone and pheromone receptor that are responsible for recognition and fusion of the opposite haploid sporidia. The *b* locus harbors *bE* and *bW* genes which encode a heterodimeric transcription factor involved in dikaryotic filamentation and invasion of host plants (Zhu et al., 2019). To identify the reasons for the mating defect in the *Ssubc2* mutants, we used RT-qPCR to quantify the expression of genes in *a* and *b* loci known to be involved in the pheromone and filamentation pathway. All genes investigated were expressed at the same or higher level in the *Ssubc2* mutant strains before mating compared to the wild-type strains (**Figure 3C**). However, after mating, *mfa2*, *pra2*, *bE2*, and *bW2* were significantly downregulated in the mating pair Δ35-*ubc2* × Δ36-*ubc2* compared to the wild-type pair of JG35 and JG36 (**Figure 3D**). These results suggest that the low accumulation of pheromone, pheromone receptor, and the heterodimer transcription factor likely contributes to the lost or weak mating ability of *Ssubc2*-null mutants.

Ssubc2 is essential for pathogenicity

To determine whether *Ssubc2* is required for the development of smut disease in sugarcane, we conducted

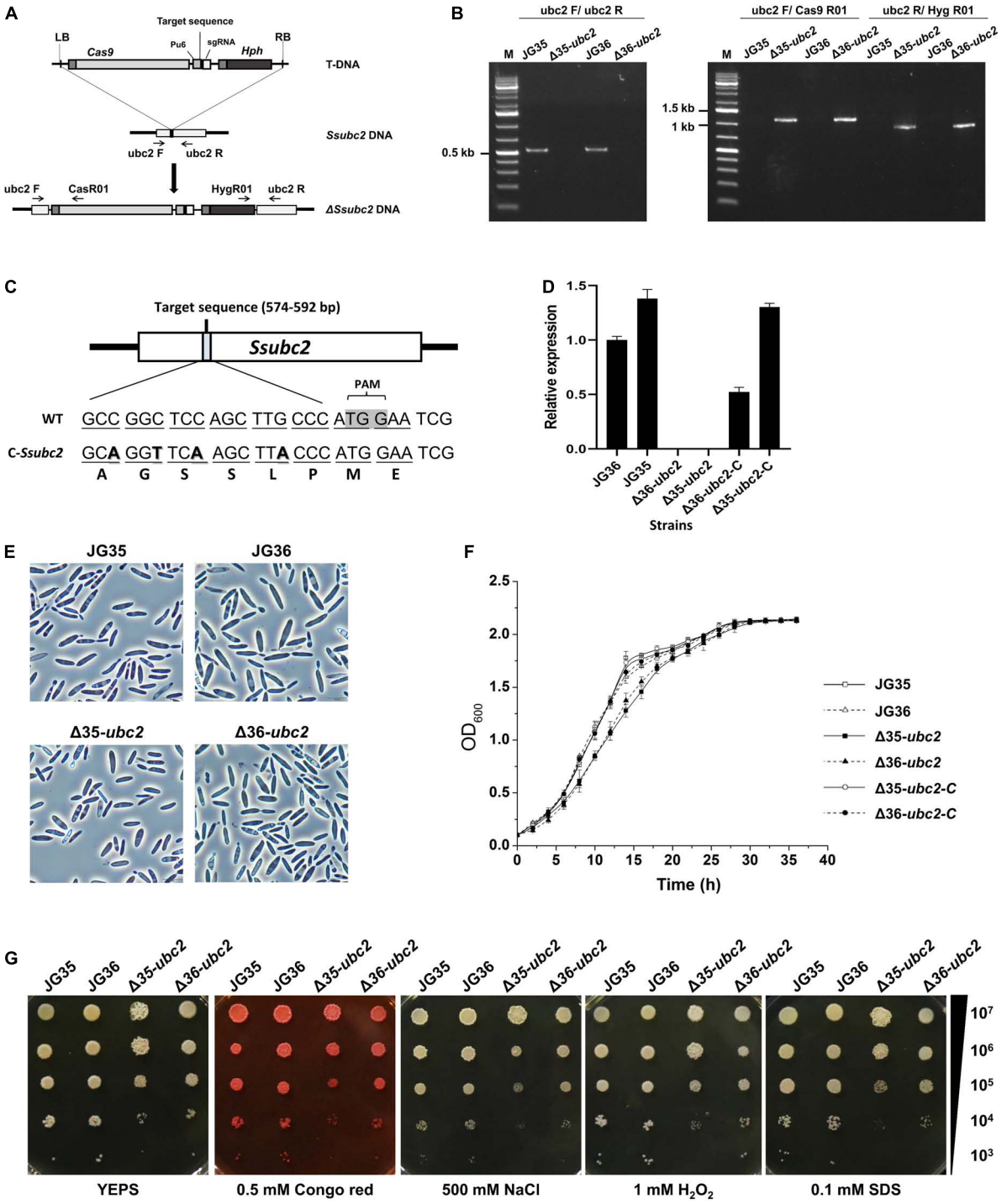

FIGURE 2
Characterization of *S. scitamineum Ssubc2* deletion and complementation strains. **(A)** Schematic representation of the *Ssubc2* gene disruption strategy. **(B)** PCR verification of insertion fragments. The primer pair ubc2F/ubc2R was used to amplify the S*subc2* gene (538 bp). The primer pairs ubc2F/Cas9R01 and ubc2R/Hyg9R01 were used to amplify the left (1,087 bp) and right (878 bp) ends of the disrupted insertion fragments, respectively. **(C)** Nucleotide and amino acid sequences of wild-type and base-modified *Ssubc2* targets. **(D)** Quantification of the *Ssubc2* gene transcript in Δ*Ssubc2* mutants and complementation strains. **(E)** Microscopic images of basidiospores of wild-type strains and Δ*Ssubc2* mutants. Bar, 20 μm. **(F)** Growth rates of wild-type strains and Δ*Ssubc2* mutants. The strains were cultured in liquid YEPS medium with an initial inoculum of 1×10^5 cells mL^{-1} at 28°C with shaking at 200 rpm. Data shown are an average of three independent cultures for each strain, and error bars represent standard deviations. **(G)** Stress assays for osmolarity, ROS, and cell wall integrity. Cell concentrations are indicated at the right. Test strains were spotted onto YEPS medium supplemented with stressors and incubated at 28°C for 72 h.

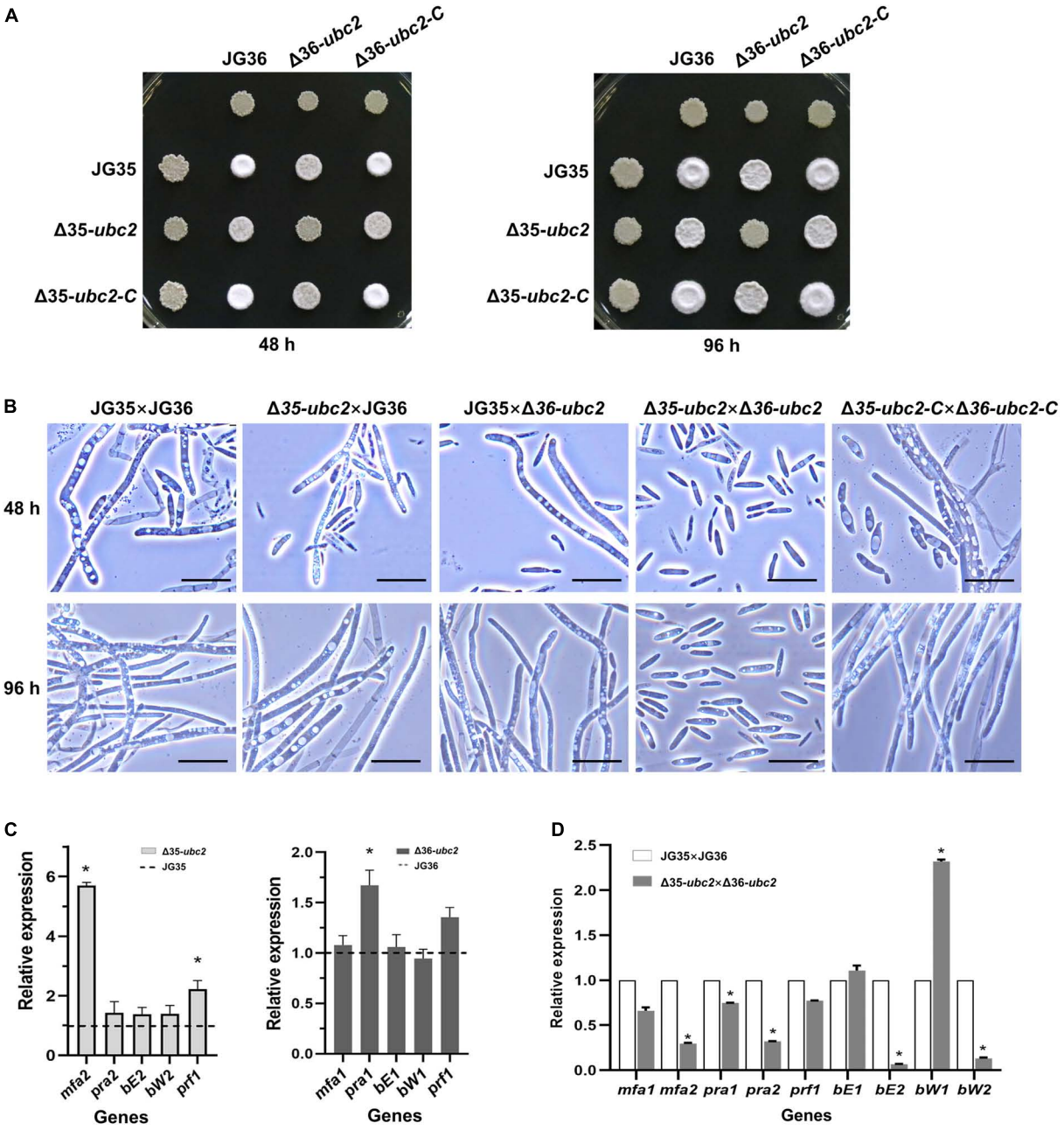

FIGURE 3
Sexual mating is attenuated in *Ssubc2* deletion mutants. **(A)** Wild-type strains, Δ*Ssubc2* mutants, and complementation strains were co-spotted on YEPS plates and incubated at 28°C for 48 h (left) or 96 h (right). Dikaryotic filaments formed colonies with a characteristic fuzzy white appearance. **(B)** Cells from a region of the colony were placed on a glass slide for observation under a microscope. Bar, 20 μm. **(C,D)** Quantification of gene transcript accumulation by quantitative real-time PCR. The relative gene expression fold change was calculated with the $2^{-\Delta\Delta Ct}$ method. The *actin* gene of *S. scitamineum* was used as a control. Gene expression in the wild-type haploid strains or pairs of wild-type strains was set as 1.0. *$p < 0.05$.

virulence assays using tissue culture seedlings derived from the smut-susceptible sugarcane variety ROC22 (Lu et al., 2021). An average of 85.7% of whip development was recorded for the wild-type strain JG35 × JG36 within 90 days of inoculation, whereas only 7.1–8.7% of whip-producing seedlings were observed for Δ35-*ubc2* × JG36 and JG35 × Δ36-*ubc2* in the same period of time, and no whips were observed for Δ35-*ubc2* × Δ36-*ubc2* up to 120 days after inoculation (**Figure 4A**). Teliospores harvested from the whips induced by the different inoculum sources did not differ in their

morphology. Histopathological examination revealed that a fraction of the inoculated plantlets was infected by Δ35-*ubc2* × JG36 (28 out of 65) or JG35 × Δ36-*ubc2* (22 out of 63), but none were infected by Δ35-*ubc2* × Δ36-*ubc2* or the control H_2O (**Figure 4B** and **Table 1**). No obvious difference in the morphology of teliospores from whips induced by the wild-type strains or Δ35-*ubc2* × JG36 or JG35 × Δ36-*ubc2* was found. The teliospores germinated at a similar rate, with spores from Δ35-*ubc2* × JG36 and JG35 × Δ36-*ubc2* reaching 85–90% that of the wild types or the complementation strains.

Ssubc2 influences a large number of gene expression in haploid cells

To obtain a better understanding of Ssubc2 function in haploid growth, we performed a transcriptome analysis by comparing the Δ*Ssubc2* and corresponding wild type strains under haploid condition. In total, 2,555 differentially expressed genes (DEGs) were identified in the Mat-2 strain comparison group (Δ35-*ubc2* vs. JG35) and 583 DEGs were identified in the Mat-1 strain comparison group (Δ36-*ubc2* vs. JG36), in the three biological replicates (**Supplementary Figure 1**). Although there was no detectable difference in haploid phenotype between the disruptants and the mutants, there were still a large number of genes whose transcription were altered, and these DEGs were mainly enriched in the cell cycle, peroxisome related pathway (peroxisomal transport, protein targeting to peroxisome, protein localization to peroxisome), membrane, catalytic activity, and G protein-coupled receptor signaling pathway (**Supplementary Tables 2**, **3**).

Ssubc2 regulates gene expression at the global level and coordinates the massive change in gene expression during mating

To probe the mechanisms by which SsUbc2 regulates mating and pathogenicity in the fungus, we compared the transcriptomes of the wild types and the mutants in a time course manner. Profound changes in the transcription profile at time 0 were observed in the mutants compared to the wild types, with a total of 1,540 DEGs, 560 upregulated and 980 downregulated (**Figures 5A,B**). In terms of function, the most enriched genes were involved in cell cycle and chromosome organization in the upregulated DEGs, and the most enriched genes were involved in the rRNA and ribosome process in the downregulated DEGs (**Figures 5C,D**).

Comparing transcriptomes at different time points after mating might give a complete picture of the change in gene expression. Impressive gene expression reprogramming was observed during the first 24 h of co-spoting for all three mating pairs, the wild types (WT × WT), JG35 × Δ36-*ubc2* (WT × Δ), and Δ35-*ubc2* × Δ36-*ubc2* (Δ × Δ; **Figure 6A**). In the case of WT × WT, 2,405 genes representing more than one third of the total genes annotated were reprogrammed compared to time 0, and much fewer DEGs were seen afterward (**Supplementary Figure 1**). Similar trends in gene expression reprogramming were observed in WT × Δ and Δ × Δ (**Figure 6B** and **Supplementary Figure 2**). The first sign of filamentous growth appeared 24 h after mating for the wild types, vigorous growth of the mycelium was observed at 48 h, and a steady colony was observed at 72 h. Thus, we speculate that the fungal cells experience a massive change in gene expression to respond to and cope with the mating event in the first 24 h of pairing.

We then performed a transcriptome correlation analysis of WT × WT, WT × Δ, and Δ × Δ at 0, 24, 48, and 72 h. At time 0, all three pairs clustered together, but at 24 h, the wild-type pair distanced itself from the other pairs. It is intriguing that WT × Δ (48 h) and WT × Δ (72 h) clustered around WT × WT (24 h), whereas Δ × Δ mostly maintained a distance from the wild types at 24 h and onward (**Figure 7A**). Because 24 h after mating is considered crucial for reprogramming gene expression to make the transition from yeast-type growth to filamentous growth, we further analyzed the reprogrammed genes (DEGs) by comparing their expression with expression at time 0. Venn analysis of DEGs identified a set of 1,813 genes shared by both WT × WT and WT × Δ at 24 h, representing 68.88% of the DEGs in WT × Δ (designated as DEGs/WT × Δ/24). However, 82.38% of the DEGs/WT × Δ/48 and 79.45% of the DEGs/WT × Δ/72 were shared with the DEGs/WT × WT/24 (**Figure 7B**), which suggests a delay in the change in gene expression during sexual mating in WT × Δ. The shifts of DEGs in WT × Δ were in accordance with the transcriptome profiles shown in **Figure 7A**. In contrast, the mating-defect

TABLE 1 Phenotypic characterization of sugarcane plantlets inoculated with wild-type or *Ssubc2* mutant strains of *S. scitamineum*[a].

Inoculum	No. plantlets inoculated	No. whips (rate)	No. whip-less infections	Total infection rate
JG35 × JG36	70	59 (84.2%)	1	85.7%
JG35 × Δ36-*ubc2*	69	6 (8.7%)	22	40.6%
Δ35-*ubc2* × JG36	70	5 (7.1%)	28	47.1%
Δ35-*ubc2* × Δ36-*ubc2*	88	0	0	0%
JG35 × Δ36-*ubc2-C*	20	17 (85%)	1	90%
Δ35-*ubc2-C* × JG36	20	18 (90%)	0	90%
Δ35-*ubc2-C* × Δ36-*ubc2-C*	40	38 (95%)	0	95%
H_2O	30	0	0	0%

[a]Recorded up to 120 days after inoculation.

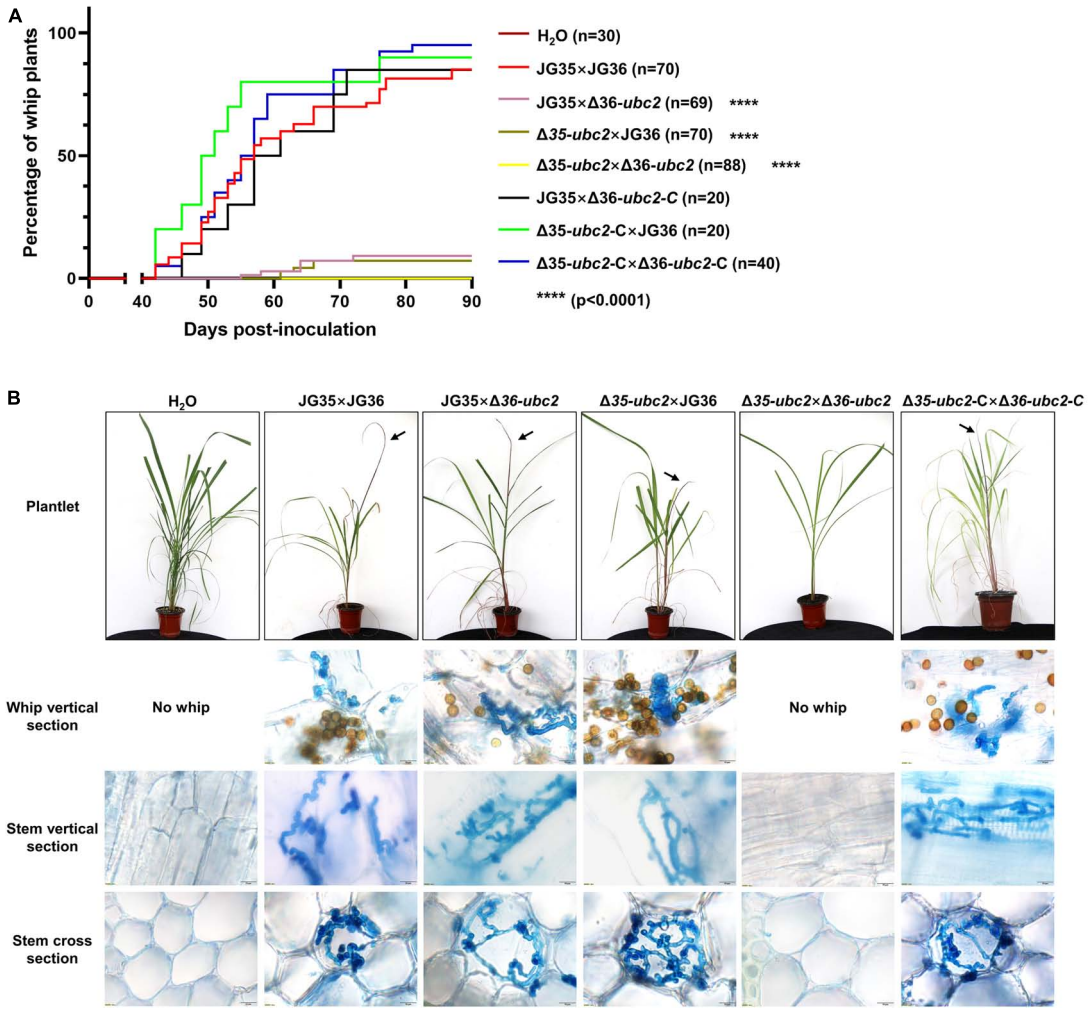

FIGURE 4
The influence of *Ssubc2* deletion on pathogenicity. **(A)** Progression of whip development induced by *Ssubc2* deletion mutants and complementation strains. Sugarcane culture tissue-derived plantlets were inoculated with combinations of wild-type strains, Δ*Ssubc2* mutants, and/or complementation strains at a concentration of OD_{600} = 1.0. Significance was set at $p = 0.05$. ****$p < 0.0001$. **(B)** Symptoms of plantlets inoculated with Δ*Ssubc2* mutants or wild-type strains. Arrows indicate whips. Histopathology of the plantlets was performed by dissecting the plantlets and staining them with 0.4% trypan blue. No hyphae were detected in plantlets inoculated with H_2O or Δ35-*ubc2* × Δ36-*ubc2*. Scale bar, 20 μm.

mutant pair Δ × Δ shared only a relatively constant portion of DEGs with WT × WT: 53.04, 50.56, and 47.32% at 24, 48, and 72 h (Figure 7B). Although only a single sample at a time point was taken for the analysis, multiple time points at the mating course unveiled a specific set of genes that were responding in WT × WT and WT × Δ, but never in Δ × Δ, suggesting that these genes are regulated by SsUbc2.

As both DEGs/WT × Δ/48 and DEGs/Δ × Δ/48 had the highest match with DEGs/WT × WT/24, we then looked into the nature of the set of 625 DEGs shared only by WT × WT and WT × Δ but not Δ × Δ (Supplementary Table 4). GO enrichment analysis showed that all 26 kinase activity–associated genes, all nine signal transduction–associated genes, and 21 out of the 32 transcription-associated genes were upregulated, whereas 11 out of the 32 transcription-associated genes were downregulated (Table 2). KEGG pathway enrichment analysis showed that all seven genes in MAPK signaling and 11 genes involved in PI3K-AK signaling, calcium signaling, AMPK signaling, and other signaling pathways were upregulated; all five genes in PPAR signaling, one gene in cAMP signaling, and one gene in the adipocytokine signaling pathway were downregulated (Table 3).

Discussion

Protein kinases play vital roles in the cell by phosphorylating target proteins to activate or suppress their cellular activity.

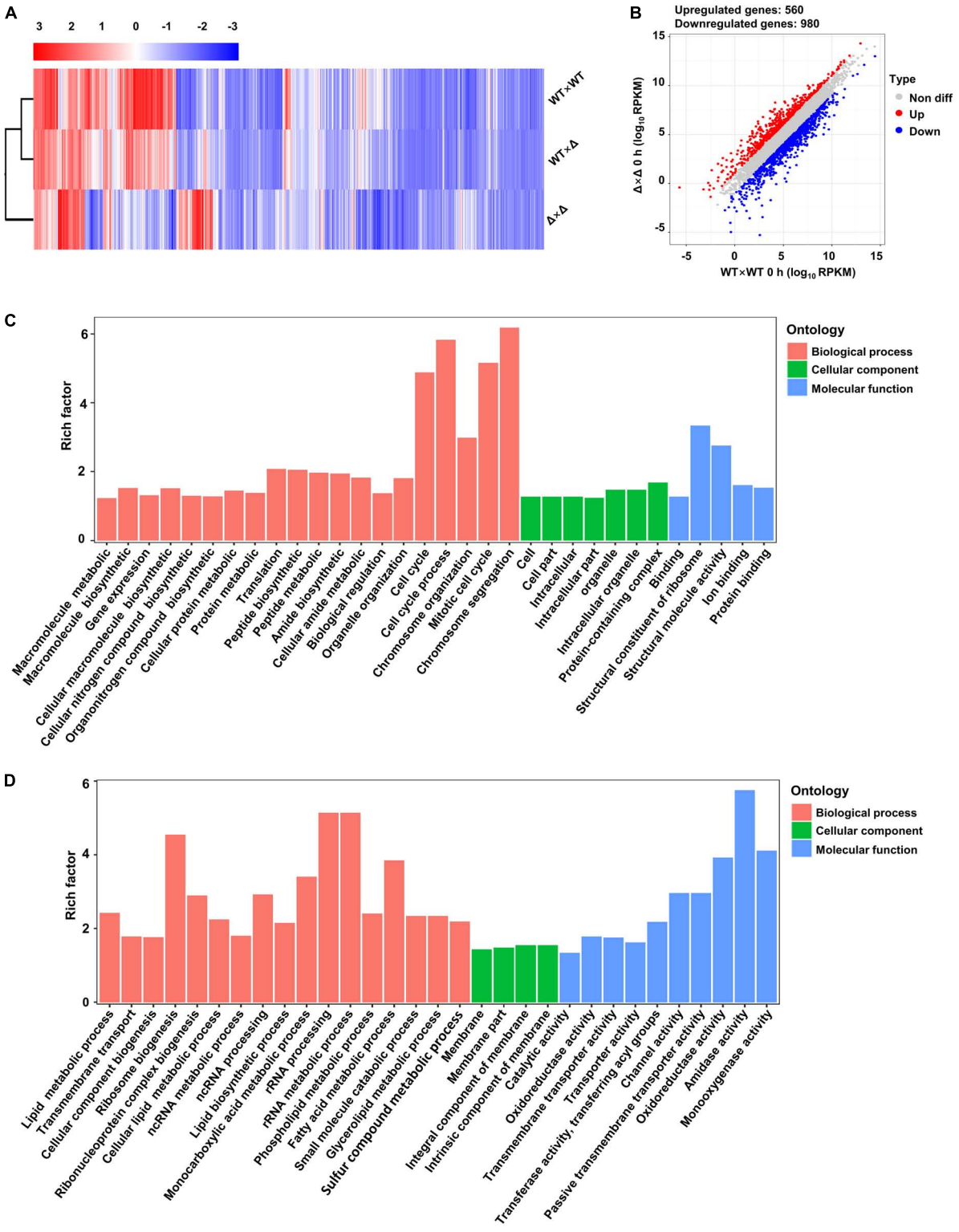

FIGURE 5
Ssubc2 regulates the expression of a wide range of genes in the basidiospore stage. **(A)** Heat map of the RPKM values of differentially expressed genes (DEGs) of WT × WT, WT × Δ, and Δ × Δ combinations at time 0. Red indicates high expression, and blue indicates low expression. **(B)** Scatter plot of DEGs in Δ × Δ compared to WT × WT at time 0. Red dots indicate upregulated genes, and blue dots indicate downregulated genes. **(C)** Go enrichment analysis of upregulated genes in Δ × Δ compared to WT × WT at time 0. **(D)** Go enrichment analysis of upregulated genes in Δ × Δ compared to WT × WT at time 0.

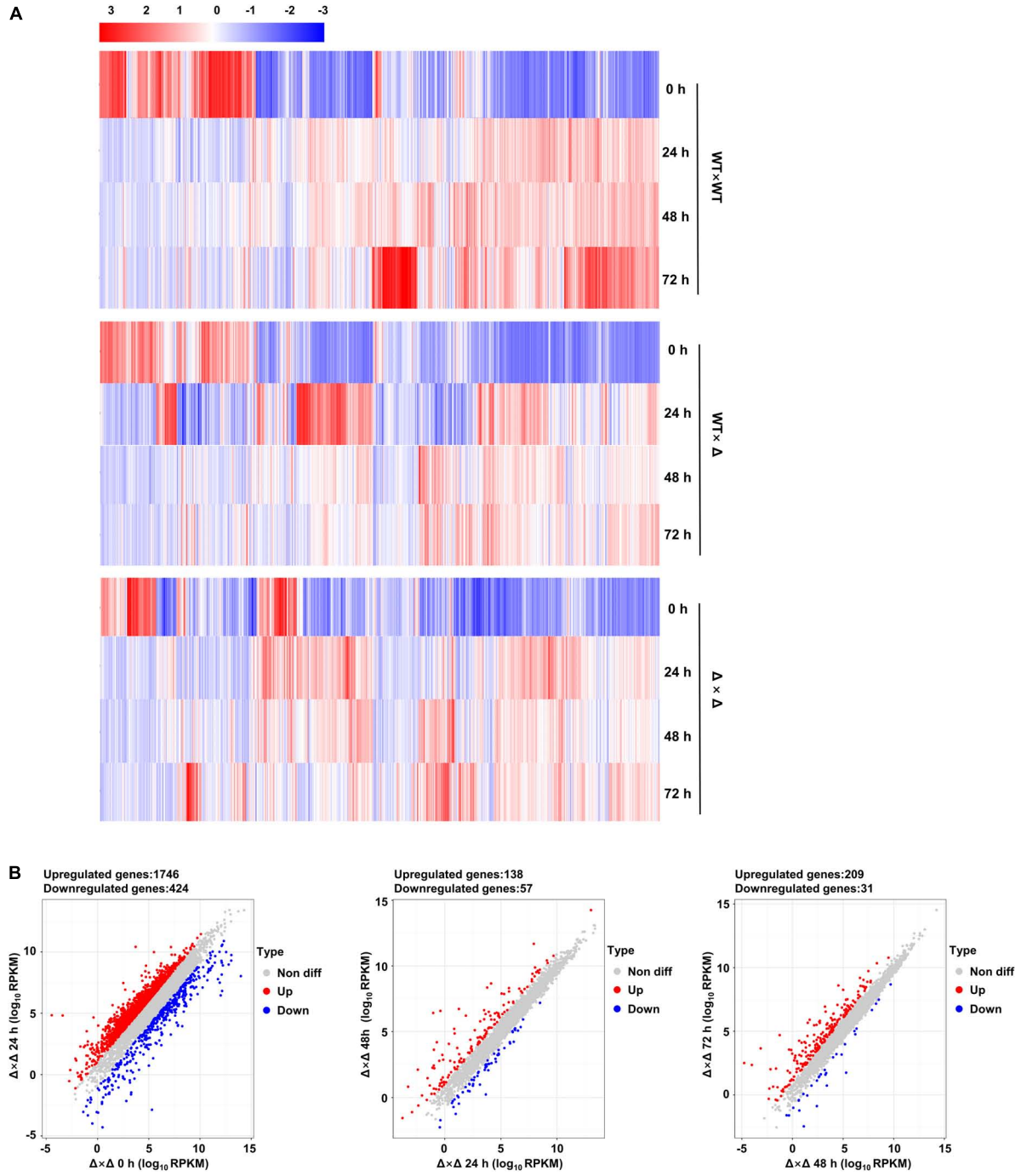

FIGURE 6
Time course of transcriptional reprogramming during mating. **(A)** Heat maps generated on the basis of RPKM values. Red indicates high expression, and blue indicates low expression. Samples were taken at 0, 24, 48, and 72 h. **(B)** Scatter plots of differentially expressed genes (DEGs) of Δ × Δ with 0 h as a reference.

Likewise, the regulation of kinase activity by kinase regulators is essential for keeping biological processes in the cell in order. Since the first kinase regulator in yeast, Ste50, was reported, many kinase regulators have been identified and demonstrated to function in the regulation of various aspects of growth and/or development—such as the osmolarity response, mating, filamentous growth, and pathogenicity—in fungi ranging from single-cell yeast to multicellular ascomycetes and basidiomycetes (Schamber et al., 2010; Yamamoto et al., 2010; Jung et al., 2011; Bayram et al., 2012; Gu et al., 2015). Ubc2,

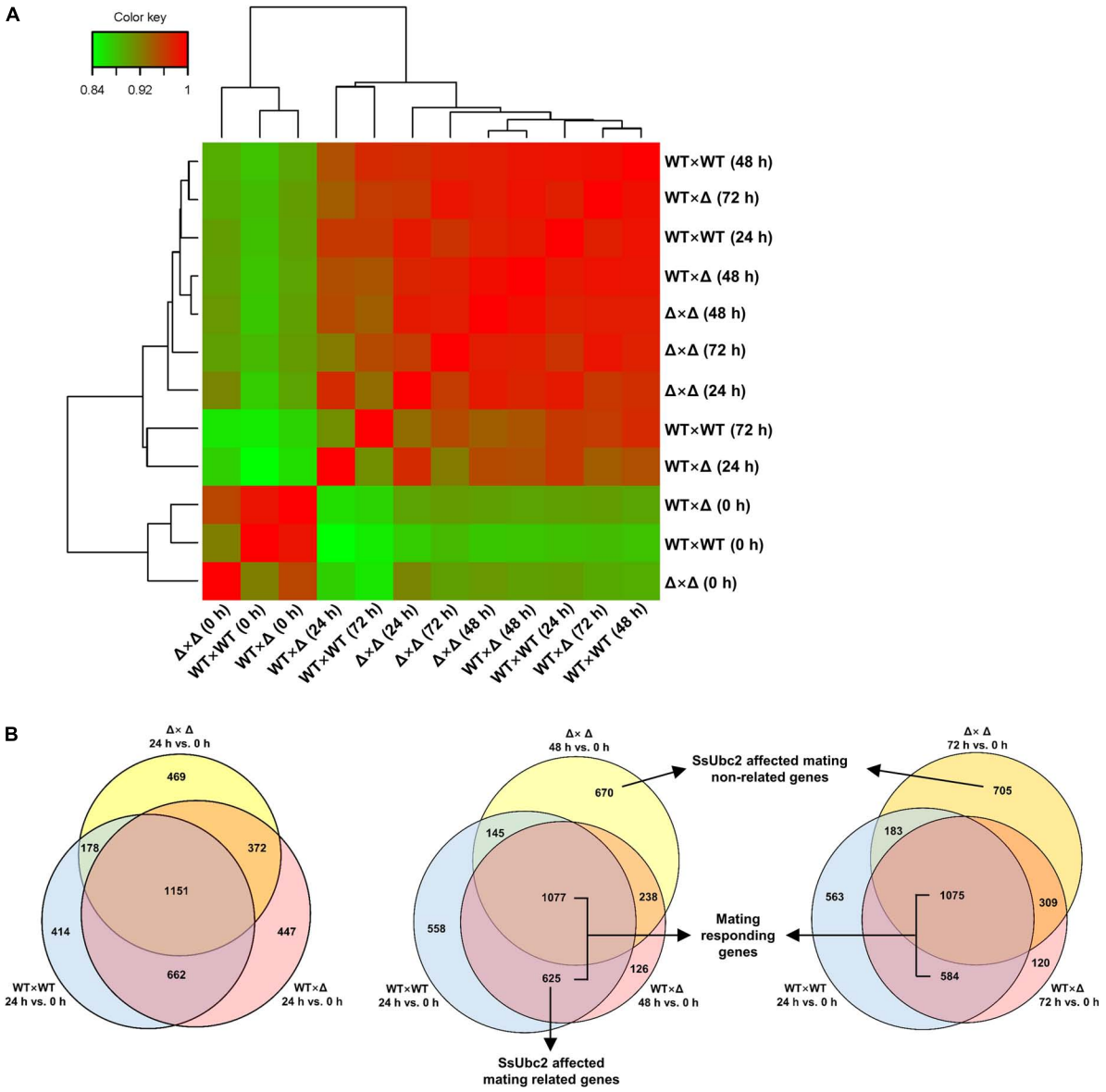

FIGURE 7
Comparison of transcriptional reprogramming during sexual mating among pairing strains. **(A)** Hierarchical cluster diagram of transcriptomes. The color scale from green to red represents lower to higher sample correlations based on gene expression. Branch lines generated by the same node indicate that the corresponding samples can be grouped into one cluster, and the length of the branch represents the similarity of the samples: the shorter the branch, the greater the similarity between samples. **(B)** Comparison of reprogrammed genes (DEGs) at different time points. DEGs were defined by reference to time 0 for each of the samples, respectively.

the homolog of Ste50 in the basidiomycetous fungus *U. maydis*, differs from Ste50 homologs in that it possesses two extra SH3 domains (Mayorga and Gold, 2001). Because SsUbc2 of the sugarcane smut fungus *S. scitamineum* is highly homologous to Ubc2 of *U. maydis* (**Figure 1**), it is assumed that these two proteins may have similar biochemical and biological functions in their respective fungi. Indeed, characterization of *Ssubc2*-disrupted mutants revealed that SsUbc2 is essential for mating, filamentation, and pathogenicity. Interestingly, there seems to be a dosage effect for SsUbc2, in that half dosage (one out of two alleles) resulted in weaker and delayed mating and filamentation and reduced virulence to the sugarcane plants, and the loss of both alleles totally abolished the ability of the fungus to mate or infect sugarcane plants (**Figures 3**, **4**). However, unlike STE50 of *Saccharomyces cerevisiae*, SsUbc2 does not seem to be involved in the stress response in *S. scitamineum* (**Figure 2**).

The mechanisms by which STE50/Ubc2 regulates the cellular process have been investigated using molecular

TABLE 2 Functional categories of DEGs that do not respond to mating in *Ssubc2*-null mutants.

Function		Shared only by WT × WT and WT × Δ				
GO term		**No. of DEGs**	**Upregulated**	**Gene ID**	**Downregulated**	**Gene ID**
Kinase associated	Kinase activity	16	16	g_000815, g_001439, g_001470, g_001476, g_001588, g_002441, g_003156, g_003450, g_003664, g_003976, g_004071, g_004156, g_004192, g_004306, g_005858, g_006323	0	
	GTPase activity; GTP binding	10	10	g_000645, g_001368, g_001950, g_001986, g_001993, g_002305, g_003162, g_005322, g_005401, g_006652	0	
Transcription associated	Transcription cofactor activity	4	3	g_002196, g_003047, g_001330	1	g_001238
	Cofactor binding	1	1	g_004423	0	
	Transcription corepressor activity	1	0		1	g_001238
	DNA binding transcription factor activity	4	3	g_004499, g_004877, g_006179	1	g_004566
	Zinc ion binding; RNA polymerase II transcription factor activity	12	6	g_006181, g_005758, g_000133, g_004877, g_002445, g_003128	6	g_001515, g_002926, g_000570, g_002497, g_006705, g_002297
	Transcription factor TFIID complex	1	1	g_002332	0	
	CCAAT-binding factor complex	1	0		1	g_004566
	Regulation of transcription	5	4	g_002233, g_005138, g_005226, g_005715	1	g_000657
	Regulation of transcription by RNA polymerase II	2	2	g_002196, g_003047	0	
	Transcription	1	1	g_001119	0	
Signal transduction associated	Small GTPase-mediated signal transduction	4	4	g_001950, g_002795, g_003162, g_005202	0	
	Intracellular signal transduction	2	2	g_003664, g_005963	0	
	Signal transduction	1	1	g_005322	0	
	Regulation of ARF protein signal transduction	1	1	g_005213	0	
	Phosphorelay signal transduction	1	1	g_006179	0	

genetics. Through its RA domain, STE50 conducts cell signal transduction between activated G protein and STE11 and is also an essential component of three MAPK signaling pathways that control mating reaction, invasion/filament growth, and the HOG pathway, respectively (Sharmeen et al., 2019). This domain interacts with the small GTPase Cdc42 to activate the Ste11p/Ste7p/Kss1p MAP kinase cascade to control filamentous growth (Truckses et al., 2006). SH3 of Ubc2 acts as a modular component and has been implicated in mediating protein–protein interactions in receptor signaling processes, regulating enzyme activity, facilitating complex formation, and changing the subcellular localization of signaling pathway components (Bar-Sagi et al., 1993; Li, 2005; Sharmeen et al., 2019). However, one question remains: On what scale does Ubc2 influence the cellular function of a fungus?

By taking advantage of *Ssubc2*-null mutants and the half dosage mating pair (one out of two alleles) and RNA-seq technology, it could be possible to estimate the scale of the impact of SsUbc2. To our surprise, deletion of *Ssubc2* resulted in a change in expression of more than 2,000 genes, some of

TABLE 3 Signaling-involved DEGs that do not respond to mating in *Ssubc2*-null mutants.

Function	Shared only by WT × WT and WT × Δ				
KEGG term	**No. of DEGs**	**Upregulated**	**Gene ID**	**Downregulated**	**Gene ID**
PI3K-AKT signaling pathway	1	1	g_005988	0	
MAPK signaling pathway	7	7	g_004248, g_005322, g_004192, g_005202, g_002642, g_004306, g_001939	0	
PPAR signaling pathway	5	0		5	g_005724, g_002970, g_006649, g_004876, g_000462
cAMP signaling pathway	1	0		1	g_000462
Calcium signaling pathway	1	1	g_005963	0	
AMPK signaling pathway	1	1	g_005988	0	
Ras signaling pathway	1	1	g_005322	0	
Phosphatidylinositol signaling pathway	2	2	g_003685, g_005963	0	
Sphingolipid signaling pathway	1	1	g_005988	0	
FOX0 signaling pathway	1	1	g_003086	0	
mTOR signaling pathway	2	2	g_003665, g_002639	0	
Adipocytokine signaling pathway	1	0		1	g_002970
TGF-beta signaling pathway	1	1	g_005988	0	

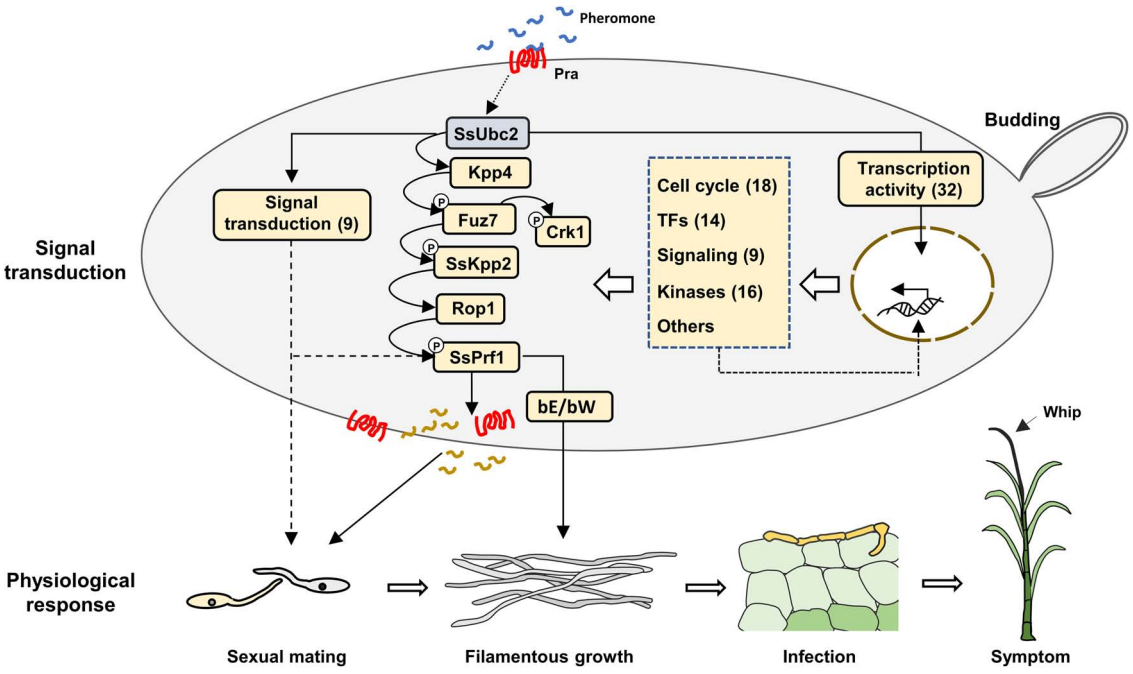

FIGURE 8
Proposed working model of SsUbc2 in *S. scitamineum*. SsUbc2 functions as a coordinator to orchestrate the transcriptome of the fungus by regulating key transcription factors that have a global impact on the transcriptome. More secondary transcription factors, protein kinases, signaling components, and other essential genes initially regulated may further exert their influence on transcription to refine gene regulation and cell function, including responses to mating and infection. Loss of SsUbc2 causes chaos in the regulation of gene expression, resulting in impairment in key signaling transduction pathways such as the MAPK pathway and dysfunction in the cell that further results in failed mating/filamentation and pathogenicity (Brefort et al., 2009). TFs, transcription factors. Arabic numerals indicate the number of DEGs.

which are essential for the fate of the cell (e.g., cell cycle, rRNA processing and ribosome biogenesis, and nitrogen metabolism) at the basidial stage (**Figure 5**). Thus, we speculate that SsUbc2 may function at a top level of the kinase regulation hierarchy. Despite its extensive impact on the transcriptome, deletion of *Ssubc2* does not seem to have an apparent impact on the yeast-type growth of basidiospores (**Figure 3**). We further investigated the behavior of *Ssubc2*-null mutants in mating. With time 0 as a reference, the number of DEGs at 24, 48, and 72 h was 2,530, 2,130, and 2,272, respectively (**Figures 6**, **7B**), which suggests that the mutants can detect signals from the opposite strains and respond at the transcription level accordingly. However, this transcriptional response was not in accordance with the wild-type strains or with the mating pair involving a mutant and a wild-type strain. With the DEGs of the wild types 24 h after mating as a reference, just about 50% of the DEGs of the mutants matched those of the wild types. It is interesting that about 80% of the DEGs from the pair with a half dose of SsUbc2 (WT × Δ) matched those of the wild types. Because a positive mating could be achieved in WT × Δ, we assumed that some of the genes shared by WT × WT and WT × Δ were required for mating. In this regard, the mutants failed to orchestrate some 600 genes that appear to be required for mating, although some 1,000 genes did respond (**Figure 7B** and **Supplementary Table 4**). An inspection of these 625 genes revealed many kinases, transcription factors, and signal transduction components—including hgl1 (g_003889), Rho (g_00195), Mck1 (g_004306), and Ssk2 (g_0041932)—which are required for hyphal growth, the stress response, and sporulation in other pathogenic fungi (Durrenberger et al., 2001; Bahn et al., 2007; Jeon et al., 2008; Levin, 2011).

The impairment of the MAPK pathway and kinases caused by the lack of the *Ssubc2* gene not only affects the sexual mating of mutants but also attenuates their pathogenicity to the host plant. Deletion of one *Ssubc2* allele in the pairing strains significantly reduced the virulence to sugarcane, with only 7.1–8.7% of the plantlets developing whip symptoms, even if the ability to mate was not much affected. Furthermore, when both alleles were deleted in both mating partners, the pathogenicity to sugarcane plantlets was completely abolished (**Figure 4**). This is distinct from the genes *Sskpp2* and *Ssprf1* and component genes of cAMP pathway, which reduce pathogenicity possibly by impairing mating/filamentation (Deng et al., 2018; Zhu et al., 2019), suggesting that the influence of *Ssubc2* deletion on pathogenicity is not entirely due to the weakened ability to form dikaryotic hyphae.

Because Ubc2 does not seem to possess a nuclear translocation signal (**Figure 1**), its direct involvement in gene transcription could be largely ruled out. A more likely possibility is that high-level transcription factor(s) in the transcription regulation hierarchy is activated by a kinase with Ubc2 as an adaptor to exert its broad-spectrum effect on the fungal transcriptome. Atf1 orthologs, bZIP-type transcription factors, play an important role in vegetative growth, sexual and asexual development, the stress response, secondary metabolite production, and virulence in both human and plant fungal pathogens (Leiter et al., 2021). We noticed that many genes that encode transcription factors or transcription-related proteins and protein kinases were among the DEGs regulated by SsUbc2 upon mating (**Tables 2**, **3**). These DEGs likely represent events downstream of the initial SsUbc2 function, but they could amplify the effect of SsUbc2. Thus, we propose that SsUbc2 functions as a coordinator to orchestrate the global transcriptome of the fungus by regulating phosphorylation of key substrate proteins in the core of the transcription regulation network. The broad and extensive impact on the transcriptome observed in *Ssubc2*-null mutants may result from the exaggeration of many downstream regulators, such as kinases and transcription factors (**Figure 8**).

Because *Ssubc2* is required in pathogenicity and functions at the core of the regulation of gene expression in the pathogen, it appears that this gene could be an ideal target for antifungal strategies. Of importance is that the sugarcane genome does not seem to have significant sequence homology to *Ssubc2*. Given the conserved SAM and RA domains in both ascomycetes and basidiomycetes, a broad spectrum of resistance against many plant fungal diseases caused by ascomycetous pathogens (e.g., rice blast pathogen *Magnaporthe oryzea*, cotton blight pathogen *Verticillium dahlia*, and sugarcane Pokkah boeng pathogen *Fusarium* species complex) and basidiomycetes pathogens (e.g., maize smut pathogen *U. maydis*, rice sheath blight pathogen *Rhizoctonia solani*, and sugarcane smut pathogen *S. scitamineum*) could be developed by using host-induced gene silencing (HIGS) to target *Ubc2* transcripts (Hua et al., 2018; Koch and Wassenegger, 2021). In this regard, a current report showed that HIGS was highly efficient for developing transgenic lines in rice resistant to sheath blight caused by *R. solani* (Zhao et al., 2021). In fact, recombinant microRNAs expressed by cotton plant could inhibit virulent gene expression in *V. dahlia*, and the transgenic plants showed elevated resistance to cotton blight (Zhang et al., 2016). In summary, *Ssubc2* may serve as a potentially valuable target for the control of sugarcane smut.

Experimental procedures

Strains, plasmids, and growth conditions

Wild-type strains JG36 (MAT-1) and JG35 (MAT-2) of the sugarcane smut fungus *S. scitamineum* are haploid basidiospores that represent opposite mating types (Zhu et al., 2019). *S. scitamineum* basidiospores were cultured in liquid YEPS medium at 28°C on a rotary shaker at 220 rpm for 1 day or were plated on solid YEPS plates for 3 days (Brachmann et al., 2001). *Escherichia coli* strain DH5α (Vazyme, Nanjing, China)

was plated on Luria Agar (LA) plates or in Luria Broth (LB) at 37°C and shaken in a rotary shaker at 220 rpm. *Agrobacterium tumefaciens* strain Agl1 (Sun et al., 2014) was used for fungal transformation and was grown on LA plates at 28°C or cultured in LB liquid medium with shaking at 220 rpm.

Generation of gene deletion and complementation mutants

The *Ssubc2* gene was deleted with the CRISPR/Cas9/T-DNA system of *S. scitamineum* as described previously (Lu et al., 2017). In brief, the target sequence (5'-ggcaagctggagccggcag-3') of *Ssubc2* was inserted between the Pu6 promotor and the sgRNA sequence by PCR with pSgRNA-SsU6 as the template and four primers, U-F and gR-R and gRT ubc2 + and U6T ubc2–, for 30 cycles. This PCR product served as a template to amplify the sgRNA expression cassette with primer pair U-Fs-*Bam*HI/gR-R-*Hin*dIII. The sequences of primers used in this study are listed in **Supplementary Table 5**. The sgRNA expression cassette was cloned into the *Bam*HI and *Hin*dIII restriction sites of binary vector pLS-HCas9 to yield the disruption construct pLS-ubc2. *A. tumefaciens* strain Agl1 carrying pLS-ubc2 was used to transform *S. scitamineum* JG35 and JG36 basidiospores as described previously (Sun et al., 2014).

For complementation, the target sequence of *Ssubc2* was modified by base substitution without changing the amino acid sequence to avoid it being recognized and cleaved by Cas9 in the Δ*Ssubc2* genome. Then the modified *Ssubc2* and its promoter were amplified with wild-type *S. scitamineum* genomic DNA as the template and primer pairs ubc2-pst1-F/ubc2-com-R and ubc2-com-F/ubc2-pst1-R. The products were cloned into the *Pst*I restriction site of pLS-Ncom to yield complementation construct pUbc2-com. *A. tumefaciens* strain Agl1 carrying pUbc2-com was transformed into basidiospores of *Ssubc2* deletion strains.

Quantification of gene expression

S. scitamineum cells for DNA and RNA isolation were grown on solid YEPS plates at 28°C for 3 days. DNA and RNA were extracted from fungal cells with a MiniBEST Plant Genomic DNA Extraction Kit and a MiniBEST Plant RNA Extraction Kit (TaKaRa, Beijing, China) following the protocols. A PrimeScript RT Reagent Kit was used for cDNA synthesis. Gene expression was determined with TaKaRa TB Green Premix Ex Taq II on a LightCycler® 480 II. The sequences of primers used for qRT-PCR are listed in **Supplementary Table 5**. Relative gene expression was calculated with the $2^{-\Delta\Delta CT}$ method with the *S. scitamineum* actin gene as an endogenous control.

Phenotypic characterization

S. scitamineum cells for stress assay were cultured in liquid YEPS medium at 28°C on a rotary shaker at 220 rpm until they reached an OD_{600} of 1.0. Ten-fold serial dilutions were made, and 1 μL of each dilution was spotted onto YEPSA medium with or without 0.5 M NaCl, 2.0 mM H_2O_2, 0.5 M Congo red, or 0.1 mM SDS, respectively, and incubated at 28°C for 3 days before observation.

Haploid basidiospores of *S. scitamineum* for mating assay were grown in liquid YEPS until they reached an OD_{600} of 1.0. A volume of 0.5 μL of mixture of compatible basidiospores was co-spotted onto solid YEPS medium and incubated at 28°C. Images were taken on days 2 and 4 after cultivation (Lu et al., 2021).

RNA isolation and sequencing

S. scitamineum cells were collected for RNA extraction after 0, 24, 48, and 72 h of co-spotted for mating on solid YEPS plates, respectively. Total RNA was extracted from fungal cells with TRIzol reagent, and DNA was then digested with DNase I following the manufacturer's instructions. Construction of the cDNA library, UID (Unique Identifier) RNA sequencing, and data analysis were conducted by Wuhan SeqHealth Technology (Wuhan, China). Clean reads were aligned to reference genome sequences of *S. scitamineum* JG36 (unpublished data). The expression of each gene was calculated and normalized by corresponding reads per kilobase of transcript per million mapped reads (RPKM). DEGs between samples were selected on the basis of their fold change ($|\log_2[\text{fold change}]| > 1$) and p-value (< 0.05).

Pathogenicity assay

The pathogenicity assay was performed with the root-dipping method as described previously (Lu et al., 2021).

Microscopy

Tissue samples were harvested from sugarcane seedlings and stained with 0.4% trypan blue according to the protocol described previously (Lu et al., 2021). Samples were visualized with an Olympus CX33 microscope operated with CellSens Dimension software.

Data availability statement

The datasets presented in this study can be found in online repositories. The names of the repository/repositories

and accession number(s) can be found below: NCBI—BioProject ID PRJNA855015.

Author contributions

SL, HZ, and BC conceived and designed the experiments. SL, HZ, FG, YY, and XS performed the experiments. SL and HZ analyzed the data. SL and BC wrote the manuscript. All authors contributed to the article and approved the submitted version.

Funding

This work was supported in part by grants from the National Natural Science Foundation of China (31872635), Guangxi Key Laboratory of Sugarcane Biology (2018-266-Z01), State Key Laboratory of Conservation and Utilization of Subtropical Agro-Bioresources (SKLCUSA-a201909), and Department of Science and Technology of Guangxi Zhuang Autonomous Region (AD17129002).

Acknowledgments

We are grateful to J. R. Meng for technical assistance with the sugarcane tissue culture. SL was sponsored by a fellowship from the Ministry and Province Co-sponsored Collaborative Innovation Center for Sugarcane and Sugar Industry.

Conflict of interest

The authors declare that the research was conducted in the absence of any commercial or financial relationships that could be construed as a potential conflict of interest.

Publisher's note

All claims expressed in this article are solely those of the authors and do not necessarily represent those of their affiliated organizations, or those of the publisher, the editors and the reviewers. Any product that may be evaluated in this article, or claim that may be made by its manufacturer, is not guaranteed or endorsed by the publisher.

Supplementary material

The Supplementary Material for this article can be found online at: https://www.frontiersin.org/articles/10.3389/fmicb.2022.954767/full#supplementary-material

References

Akalach, M., and Touil, B. (1996). Occurrence and spread of sugarcane smut caused by *Ustilago scitaminea* in Morocco. *Plant Dis.* 80, 1363–1366. doi: 10.1094/Pd-80-1363

Bahn, Y. S., Geunes-Boyer, S., and Heitman, J. (2007). Ssk2 mitogen-activated protein kinase kinase kinase governs divergent patterns of the stress-activated Hog1 signaling pathway in *Cryptococcus neoformans*. *Eukaryot. Cell* 6, 2278–2289. doi: 10.1128/EC.00349-07

Bar-Sagi, D., Rotin, D., Batzer, A., Mandiyan, V., and Schlessinger, J. (1993). SH3 domains direct cellular localization of signaling molecules. *Cell* 74, 83–91. doi: 10.1016/0092-8674(93)90296-3

Bayram, O., Bayram, O. S., Ahmed, Y. L., Maruyama, J., Valerius, O., Rizzoli, S. O., et al. (2012). The *Aspergillus nidulans* MAPK module AnSte11-Ste50-Ste7-Fus3 controls development and secondary metabolism. *PLoS Genet.* 8:e1002816. doi: 10.1371/journal.pgen.1002816

Brachmann, A., Weinzierl, G., Kamper, J., and Kahmann, R. (2001). Identification of genes in the bW/bE regulatory cascade in *Ustilago maydis*. *Mol. Microbiol.* 42, 1047–1063. doi: 10.1046/j.1365-2958.2001.02699.x

Brefort, T., Doehlemann, G., Mendoza-Mendoza, A., Reissmann, S., Djamei, A., and Kahmann, R. (2009). *Ustilago maydis* as a pathogen. *Annu. Rev. Phytopathol.* 47, 423–445. doi: 10.1146/annurev-phyto-080508-081923

Cai, E., Sun, S., Deng, Y., Huang, P., Sun, X., Wang, Y., et al. (2021). Histidine kinase Sln1 and cAMP/PKA signaling pathways antagonistically regulate *Sporisorium scitamineum* mating and virulence via transcription factor Prf1. *J. Fungi* 7:610. doi: 10.3390/jof7080610

Chang, C., Cai, E., Deng, Y. Z., Mei, D., Qiu, S., Chen, B., et al. (2019). cAMP/PKA signalling pathway regulates redox homeostasis essential for *Sporisorium scitamineum* mating/filamentation and virulence. *Environ. Microbiol.* 21, 959–971. doi: 10.1111/1462-2920.14496

Deng, Y. Z., Zhang, B., Chang, C., Wang, Y., Lu, S., Sun, S., et al. (2018). The MAP kinase SsKpp2 is required for mating/filamentation in *Sporisorium scitamineum*. *Front. Microbiol.* 9:2555. doi: 10.3389/fmicb.2018.02555

Durrenberger, F., Laidlaw, R. D., and Kronstad, J. W. (2001). The *hgl1* gene is required for dimorphism and teliospore formation in the fungal pathogen *Ustilago maydis*. *Mol. Microbiol.* 41, 337–348. doi: 10.1046/j.1365-2958.2001.02528.x

Ekiel, I., Sulea, T., Jansen, G., Kowalik, M., Minailiuc, O., Cheng, J., et al. (2009). Binding the atypical RA domain of Ste50p to the unfolded Opy2p cytoplasmic tail is essential for the high-osmolarity glycerol pathway. *Mol. Biol. Cell* 20, 5117–5126. doi: 10.1091/mbc.E09-07-0645

Ershad, D., and Bani-Abbassi, N. (1971). The occurrence of sugarcane smut *Ustilago scitaminea* in Iran. *Iran. J. Plant Pathol.* 7, 19–22.

Fu, J., Mares, C., Lizcano, A., Liu, Y., and Wickes, B. L. (2011). Insertional mutagenesis combined with an inducible filamentation phenotype reveals a conserved STE50 homologue in *Cryptococcus neoformans* that is required for monokaryotic fruiting and sexual reproduction. *Mol. Microbiol.* 79, 990–1007. doi: 10.1111/j.1365-2958.2010.07501.x

Grimshaw, S. J., Mott, H. R., Stott, K. M., Nielsen, P. R., Evetts, K. A., Hopkins, L. J., et al. (2004). Structure of the sterile alpha motif (SAM) domain of the *Saccharomyces cerevisiae* mitogen-activated protein kinase pathway-modulating protein STE50 and analysis of its interaction with the STE11 SAM. *J. Biol. Chem.* 279, 2192–2201. doi: 10.1074/jbc.M305605200

Gu, Q., Chen, Y., Liu, Y., Zhang, C., and Ma, Z. (2015). The transmembrane protein FgSho1 regulates fungal development and pathogenicity via the MAPK module Ste50-Ste11-Ste7 in *Fusarium graminearum*. *New Phytol.* 206, 315–328. doi: 10.1111/nph.13158

Hua, C., Zhao, J. H., and Guo, H. S. (2018). Trans-kingdom RNA silencing in plant-fungal pathogen interactions. *Mol. Plant* 11, 235–244. doi: 10.1016/j.molp.2017.12.001

Jeon, J., Goh, J., Yoo, S., Chi, M. H., Choi, J., Rho, H. S., et al. (2008). A putative MAP kinase kinase kinase, MCK1, is required for cell wall integrity and pathogenicity of the rice blast fungus, *Magnaporthe oryzae*. *Mol. Plant Microbe Interact.* 21, 525–534. doi: 10.1094/MPMI-21-5-0525

Jones, D. T., Taylor, W. R., and Thornton, J. M. (1992). The rapid generation of mutation data matrices from protein sequences. *Comput. Appl. Biosci.* 8, 275–282. doi: 10.1093/bioinformatics/8.3.275

Jung, K. W., Kim, S. Y., Okagaki, L. H., Nielsen, K., and Bahn, Y. S. (2011). Ste50 adaptor protein governs sexual differentiation of *Cryptococcus neoformans* via the pheromone-response MAPK signaling pathway. *Fungal Genet. Biol.* 48, 154–165. doi: 10.1016/j.fgb.2010.10.006

Klosterman, S. J., Martinez-Espinoza, A. D., Andrews, D. L., Seay, J. R., and Gold, S. E. (2008). Ubc2, an ortholog of the yeast Ste50p adaptor, possesses a basidiomycete-specific carboxy terminal extension essential for pathogenicity independent of pheromone response. *Mol. Plant Microbe Interact.* 21, 110–121. doi: 10.1094/MPMI-21-1-0110

Koch, A., and Wassenegger, M. (2021). Host-induced gene silencing–mechanisms and applications. *New Phytol.* 231, 54–59. doi: 10.1111/nph.17364

Kumar, S., Stecher, G., and Tamura, K. (2016). MEGA7: Molecular evolutionary genetics analysis version 7.0 for bigger datasets. *Mol. Biol. Evol.* 33, 1870–1874. doi: 10.1093/molbev/msw054

Leiter, E., Emri, T., Pakozdi, K., Hornok, L., and Pocsi, I. (2021). The impact of bZIP Atf1ortholog global regulators in fungi. *Appl. Microbiol. Biotechnol.* 105, 5769–5783. doi: 10.1007/s00253-021-11431-7

Leu, L. S., and Teng, W. S. (1974). Culmicolous smut of sugarcane in Taiwan (v): Two pathogenic strains of *U. scitaminea* Sydow. *Proc. Int. Soc. Sugarcane Technol.* 15, 275–279.

Levin, D. E. (2011). Regulation of cell wall biogenesis in *Saccharomyces cerevisiae*: The cell wall integrity signaling pathway. *Genetics* 189, 1145–1175. doi: 10.1534/genetics.111.128264

Li, S. S. (2005). Specificity and versatility of SH3 and other proline-recognition domains: Structural basis and implications for cellular signal transduction. *Biochem. J.* 390(Pt 3), 641–653. doi: 10.1042/BJ20050411

Lu, S., Guo, F., Wang, Z., Shen, X., Deng, Y., Meng, J., et al. (2021). Genetic dissection of T-DNA insertional mutants reveals uncoupling of dikaryotic filamentation and virulence in sugarcane smut fungus. *Phytopathology* 111, 2303–2308. doi: 10.1094/PHYTO-03-21-0114-R

Lu, S., Shen, X., and Chen, B. (2017). Development of an efficient vector system for gene knock-out and near in-cis gene complementation in the sugarcane smut fungus. *Sci. Rep.* 7:3113. doi: 10.1038/s41598-017-03233-7

Mayorga, M. E., and Gold, S. E. (2001). The *ubc2* gene of *Ustilago maydis* encodes a putative novel adaptor protein required for filamentous growth, pheromone response and virulence. *Mol. Microbiol.* 41, 1365–1379. doi: 10.1046/j.1365-2958.2001.02606.x

McMartin, A. (1945). Sugar-cane smut reappearance in Natal. *S. Afr. Sugar J.* 29, 55–57.

Pombert, J.-F., Taniguti, L. M., Schaker, P. D. C., Benevenuto, J., Peters, L. P., Carvalho, G., et al. (2015). Complete genome sequence of *Sporisorium scitamineum* and biotrophic interaction transcriptome with sugarcane. *PLoS One* 10:e0129318. doi: 10.1371/journal.pone.0129318

Ramesh Sundar, E. L. B., Malathi, P., and Viswanathan, R. (2012). "A mini review on smut disease of sugarcane caused by *Sporisorium scitamineum*," in *Botany*, ed. K. M. John (Rijeka: IntechOpen), 107–128.

Schamber, A., Leroch, M., Diwo, J., Mendgen, K., and Hahn, M. (2010). The role of mitogen-activated protein (MAP) kinase signalling components and the Ste12 transcription factor in germination and pathogenicity of *Botrytis cinerea*. *Mol. Plant Pathol.* 11, 105–119. doi: 10.1111/j.1364-3703.2009.00579.x

Sharmeen, N., Sulea, T., Whiteway, M., and Wu, C. (2019). The adaptor protein Ste50 directly modulates yeast MAPK signaling specificity through differential connections of its RA domain. *Mol. Biol. Cell* 30, 794–807. doi: 10.1091/mbc.E18-11-0708

Sun, L., Yan, M., Ding, Z., Liu, Y., Du, M., Xi, P., et al. (2014). Improved dominant selection markers and co-culturing conditions for efficient *Agrobacterium tumefaciens*-mediated transformation of *Ustilago scitaminea*. *Biotechnol. Lett.* 36, 1309–1314. doi: 10.1007/s10529-014-1486-5

Truckses, D. M., Bloomekatz, J. E., and Thorner, J. (2006). The RA domain of Ste50 adaptor protein is required for delivery of Ste11 to the plasma membrane in the filamentous growth signaling pathway of the yeast *Saccharomyces cerevisiae*. *Mol. Cell. Biol.* 26, 912–928. doi: 10.1128/MCB.26.3.912-928.2006

Wang, Y., Deng, Y. Z., Cui, G., Huang, C., Zhang, B., Chang, C., et al. (2019). The AGC kinase SsAgc1 regulates *Sporisorium scitamineum* mating/filamentation and pathogenicity. *mSphere* 4:e00259-19. doi: 10.1128/mSphere.00259-19

Wu, C., Jansen, G., Zhang, J., Thomas, D. Y., and Whiteway, M. (2006). Adaptor protein Ste50p links the Ste11p MEKK to the HOG pathway through plasma membrane association. *Genes Dev.* 20, 734–746. doi: 10.1101/gad.1375706

Wu, C., Leberer, E., Thomas, D. Y., and Whiteway, M. (1999). Functional characterization of the interaction of Ste50p with Ste11p MAPKKK in *Saccharomyces cerevisiae*. *Mol. Biol. Cell* 10, 2425–2440. doi: 10.1091/mbc.10.7.2425

Xu, G., Jansen, G., Thomas, D. Y., Hollenberg, C. P., and Ramezani Rad, M. (1996). Ste50p sustains mating pheromone-induced signal transduction in the yeast *Saccharomyces cerevisiae*. *Mol. Microbiol.* 20, 773–783. doi: 10.1111/j.1365-2958.1996.tb02516.x

Yamamoto, K., Tatebayashi, K., Tanaka, K., and Saito, H. (2010). Dynamic control of yeast MAP kinase network by induced association and dissociation between the Ste50 scaffold and the Opy2 membrane anchor. *Mol. Cell* 40, 87–98. doi: 10.1016/j.molcel.2010.09.011

Yan, M., Zhu, G., Lin, S., Xian, X., Chang, C., Xi, P., et al. (2016). The mating-type locus *b* of the sugarcane smut *Sporisorium scitamineum* is essential for mating, filamentous growth and pathogenicity. *Fungal Genet. Biol.* 86, 1–8. doi: 10.1016/j.fgb.2015.11.005

Zhang, T., Zhao, Y. L., Zhao, J. H., Wang, S., Jin, Y., Chen, Z. Q., et al. (2016). Cotton plants export microRNAs to inhibit virulence gene expression in a fungal pathogen. *Nat. Plants* 2:16153. doi: 10.1038/nplants.2016.153

Zhao, M., Wang, C., Wan, J., Li, Z., Liu, D., Yamamoto, N., et al. (2021). Functional validation of pathogenicity genes in rice sheath blight pathogen *Rhizoctonia solani* by a novel host-induced gene silencing system. *Mol. Plant Pathol.* 22, 1587–1598. doi: 10.1111/mpp.13130

Zhu, G., Deng, Y., Cai, E., Yan, M., Cui, G., Wang, Z., et al. (2019). Identification and functional analysis of the pheromone response factor gene of *Sporisorium scitamineum*. *Front. Microbiol.* 10:2115. doi: 10.3389/fmicb.2019.02115

frontiers | Frontiers in Microbiology

TYPE Original Research
PUBLISHED 11 October 2022
DOI 10.3389/fmicb.2022.1001327

OPEN ACCESS

EDITED BY
Martin Filion,
Agriculture and Agri-Food Canada (AAFC), Canada

REVIEWED BY
Srayan Ghosh,
University of Warwick, United Kingdom
Runmao Lin,
Hainan University, China

*CORRESPONDENCE
Chong Zhang
zhangchong0816@syau.edu.cn
Yuanhua Wu
wuyh09@syau.edu.cn

SPECIALTY SECTION
This article was submitted to Microbe and Virus Interactions with Plants, a section of the journal Frontiers in Microbiology

RECEIVED 23 July 2022
ACCEPTED 16 September 2022
PUBLISHED 11 October 2022

CITATION
Li X, An M, Xu C, Jiang L, Yan F, Yang Y, Zhang C and Wu Y (2022) Integrative transcriptome analysis revealed the pathogenic molecular basis of *Rhizoctonia solani* AG-3 TB at three progressive stages of infection. *Front. Microbiol.* 13:1001327. doi: 10.3389/fmicb.2022.1001327

Integrative transcriptome analysis revealed the pathogenic molecular basis of *Rhizoctonia solani* AG-3 TB at three progressive stages of infection

Xinchun Li[1], Mengnan An[1], Chuantao Xu[1,2], Lianqiang Jiang[3], Fangfang Yan[4], Yang Yang[5], Chong Zhang[1]* and Yuanhua Wu[1]*

[1]Liaoning Key Laboratory of Plant Pathology, College of Plant Protection, Shenyang Agricultural University, Shenyang, China, [2]Luzhou Branch of Sichuan Province Tobacco Company, Luzhou, China, [3]Liangshan Branch of Sichuan Province Tobacco Company, Xichang, China, [4]Panzhihua Branch of Sichuan Province Tobacco Company, Panzhihua, China, [5]Yibin Branch of Sichuan Province Tobacco Company, Yibin, China

Rhizoctonia solani has a broad host range and results in significant losses in agricultural production. Here, an integrated transcriptomic analysis was performed to reveal the critical genes responsible for the pathogenesis of *R. solani* AG-3 TB on *Nicotiana tabacum* at different infection stages. The results showed that various differential expressed genes (DEGs) were enriched in fatty acid metabolism, amino sugar, carbon metabolism, and cellular carbohydrate biosynthetic process at the early (6–12 hpi), middle (24–36 hpi), and late stage (48–72 hpi) of infection. Specifically, several critical genes such as shikimate kinase that were involved in the biosynthesis of an important fungal toxin, phenylacetic acid (PAA) showed markedly increase at 24 hpi. Additionally, the genes expression levels of carbohydrate-active enzymes (CAZymes) and cell wall degrading enzymes (CWDEs) were significantly increased at the late infection stage. Furthermore, we identified 807 potential secreted proteins and 78 small cysteine-rich proteins, which may function as fungal effectors and involved in the pathogenicity. These results provide valuable insights into critical and potential genes as well as the pathways involved in the pathogenesis of *R. solani* AG-3 TB.

KEYWORDS

***Rhizoctonia solani* AG-3 TB, pathogenic molecular mechanism, secondary metabolites, carbohydrate-active enzymes, cell wall degrading enzymes, effector**

Introduction

Rhizoctonia solani kühn (teleomorph: *Thanatephorus cucumeris*) belongs to the soil-borne basidiomycete and ubiquitously causes diseases on roots, stem and leaves of plant (Ogoshi, 1987; Vidhyasekaran et al., 1997; Yang et al., 2008). *R. solani* can be classified into at least 14 different anastomosis groups (AG-1 to AG-13 and a bridging isolate AG-BI) based on its morphological diversity, physiological diversity, host specificity and pathogenic diversity (Taheri and Tarighi, 2011). For instance, *R. solani* AG-3 PT is the main causal agent of potato black scurf which causes wilt and stalk rot on potato seedlings (Kuninaga et al., 1997, 2000). While *R. solani* AG-3 TB is the main pathogen of tobacco target spot, which induces necrosis and perforation lesions on the leaves that significantly reduced the economic quality of the plants (Lucas, 1975; Sneh et al., 1996; Gonzalez et al., 2001). *R. solani* AG-3 TB was first recorded in tobacco fields in the United States in the early 20th century (Lucas, 1975). This disease spread quickly and caused considerable losses nearly $ 20 million in Carolina (Shew and Main, 1985). In China, the tobacco target spot caused by *R. solani* AG-3 TB was first reported in 2006 in the tobacco fields of Liaoning province (Wu et al., 2012), and successively reported in Yunnan, Guangxi, and Sichuan province (Xu et al., 2018, 2021). The losses caused by the tobacco target spot are serious. In 2018, the tobacco yield in Gulin and Xuyong County of Luzhou, Sichuan Province was reduced by 20%, and the yield of serious fields was reduced by up to 90% (Xu et al., 2021). Due to its rapid transmission and genetic diversity, it is an urgent issue to clarify the pathogenesis of the fungus and explore effective disease resistance genes in the host plant.

Bioactive molecules such as toxins, enzymes and secreted proteins play important roles during *R. solani* infection (Yamamoto et al., 2019). Typical fungal pathogenic toxins such as succinic acid, PAA, furancarboxylic acid are isolated from *R. solani* AG-1IA, among which, PAA significantly inhibits the growth of roots of sugar beet (Aoki et al., 1963). A recent integrated study revealed that PAA and 3-Methylthiopropionic Acid (MTPA) produced by *R. solani* AG-3 PT, can cause degradation of the cell membrane, rough mitochondrial and cell walls, change of the shape of chloroplasts, and swollen endoplasmic reticulum (Kankam et al., 2016; Yamamoto et al., 2019). In addition to the toxins, enzymes involved in the production of secondary metabolites such as the non-ribosomal peptide synthases (NRPSs), polyketide synthases (PKSs), hybrid NRPS-PKS enzymes, prenyltransferases (DMATSs), and terpene cyclases (TCs) play the pathogenic role in fungi (Slot and Rokas, 2010). Moreover, a study demonstrated that the saprophytic nature of fungi has a close relation to their type and quantity of carbohydrate-active enzymes (CAZymes) (Cantarel et al., 2009). Currently, an array of CAZymes produced by *R. solani* was reported to degrade the cell wall of plants and express significantly during disease development (Lakshman et al., 2012). A total of 223 CAZymes and an expanded set of other cell wall degrading enzymes (CWDEs) genes, including those of *pectinase*, *xylanase* and *laccase* were secreted by *R. solani* AG-1 IA, which was associated with the pathogenicity and had a connection to the saprophytic lifestyle of fungi (Zheng et al., 2013). Furthermore, secreted proteins have been reported in many pathogenic fungi and play various roles in pathogenesis (Dutheil et al., 2016; Anderson et al., 2017; Fang et al., 2019). Some of the secreted proteins serve as 'effectors' that facilitate the infection of the pathogen as well as suppress host immunity responses (Dickman and de Figueiredo, 2013), while the reported numbers of the effectors differ between various fungi (Zheng et al., 2013; Anderson et al., 2017). A total of 1546 and 949 secretory proteins were predicted in *Magnaporthe grisea* and *A. laibachii*, respectively, and these proteins include the unusual carbohydrate-binding domains (Dean et al., 2005). In contrast, 965 secretory proteins have been predicted in *R. solani* AG-1 IA and most of their functions generally remain unclear (Zheng et al., 2013). Some of the effectors, such as AGLIP1, is a possible effector in *R. solani* AG-1 IA which inhibits basal defenses and promote disease development in plants (Li et al., 2019).

Until now, effective fungicides and highly resistant cultivars for *R. solani* are still very limited. Therefore, research in the molecular pathogenic mechanism of *R. solani* will provide valuable theoretical basis for disease control. Here, we analyzed the transcriptomes of *R. solani* AG-3 TB infecting leaves of *Nicotiana tabacum* at different time points, which were designated as early (6–12 h post inoculation, hpi), middle (24–36 hpi), and late (48–72 hpi) infection stage. The results of RNA-seq showed that several crucial genes involved in PAA synthesis of *R. solani* AG-3 TB were significantly increased, especially at the middle infection stage. And the expression of CAZymes and CWDEs genes gradually increased and peaked at the late infection stage. We also predicted 807 secretory proteins which may play a key pathogenic role during infection. These results provide extensive molecular basis for the pathogenic mechanisms of pathogen *R. solani* AG-3 TB during its infection in the host plants.

Materials and methods

Rhizoctonia solani AG-3 TB isolates and inoculation of tobacco

The *R. solani* AG-3 TB (YC-9) strain was isolated from severely infected tobacco plants in Kuandian County, Dandong City, Liaoning province of China (Wu et al., 2012). The YC-9 strain was activated in potato dextrose agar medium at 28°C for 3 days in the dark. The potato dextrose agar (PDA) medium with *R. solani* AG-3 TB (6 mm diameter) were inoculated on the acupuncture point and the cotton with sterile water was

used for moisturizing. A time course study was performed by acupuncture inoculating *R. solani* YC-9 on the 5th and 6th leaf of tobacco variety Yunyan 87 (one of the commonly cultivated susceptible variety) at the 9th leaf stage, and harvested at 0, 6, 12, 24, 36, 48, 72 hpi. The center of the acupuncture part was taken, which was drilled with a 1.5 cm diameter punch, then the inoculated leaves were collected and frozen with liquid nitrogen. Four leaves were inoculated per tobacco and each leaf was inoculated four acupuncture points. A total of 105 tobacco plants were inoculated at 0, 6, 12, 24, 36, 48, 72 hpi, among which, 15 tobacco plants were inoculated at each time point and five of them were measured once as one biological replicate. Tobacco leaves inoculated with PDA medium serve at 0, 6, 12, 24, 36, 48, 72 hpi as mock treatment, the method of sample collection was the same as above. At the same time, the fungi were cultivated at PDA (0, 6, 12, 24, 36, 48, and 72 h), which were taken as the fungal control group for subsequent analysis.

RNA extraction, library preparation, and sequencing

Total RNAs were extracted from the fungus inoculated leaf tissues at each time point using TRIzol Reagent (Invitrogen cat. NO.15596026). All the RNA samples were treated with DNase prior to mRNA isolation and sequencing, then the quality was determined using NanodropTM One Cspectrophotometer. And the 1.5% agarose gel electrophoresis using to determine the RNA integrity and using the Qubit 3.0 to quantify the final qualified RNAs. The total RNAs were subjected to stranded RNA sequencing library preparation. Each sample mentioned above was measured one time as one biological replicate. The generation sequencing library was constructed followed the Illumina's recommendations. Oligo (dT) was used to purify poly (A)-containing mRNA from total RNA. Then the purified mRNA was fragmented and reverse transcribed to cDNAs. The short fragments were connected with adapters at both ends. Thereafter, the adaptor-ligated cDNA was performed using AxyPrep Mag PCR clean-up (Axygen) and recovered the fragments of ∼360 bp. The products were purified and enriched by PCR (11 cycles), and generated the indexed double-stranded cDNA library. The cDNA libraries were analyzed by Agilent 2100 Bioanalyzer and quantified by a Qubit 3.0 Fluorometer (Invitrogen, Carlsbad, CA, USA). Subsequently, the libraries were sequenced by paired-end sequencing under the platform of an Illumina HiSeq 6000 (SeqHealth Co., Ltd, Wuhan, China).

RNA-seq data analysis and gene annotation

For transcriptomic analysis of *R. solani* AG-3 TB, raw sequencing data was first filtered by fastp (version 0.23.0) (Chen S. et al., 2018), low-quality reads were removed and the reads with adaptor sequences were trimmed. Then clean and deduplicated data were mapped to the reference genomes of *Nicotiana tabacum* from https://ftp.ncbi.nlm.nih.gov/genomes/all/GCF/000/715/135/GCF_000715135.1_Ntab-TN90/using STAR software (version 2.5.3a) with default parameters (Dobin et al., 2013) to remove the host transcripts. Then unmapped reads were *de novo* assembled by Trinity with the default parameters (Grabherr et al., 2011). Sequencing reads were mapped back to the assembled transcripts for assessing the quality of the transcriptome assembly using the Bowtie2 (Langmead and Salzberg, 2012). The longest transcripts of the same genes were screened as the unigenes for annotation and DEG analysis. For functional annotations of the unigenes, the protein databases Nr (NCBI non-redundant protein database), UniProt (universal protein database), Pfam (homologous protein family), eggNog (orthologous groups of genes), GO (Gene Onotology), and KEGG (Kyoto encyclopedia of genes and genomes) were used to infer the amino acid sequences.

Differentially expressed gene analysis

The reads per kilobase per million mapped reads (RPKM) were used to compare the levels of differentially expressed genes (DEGs). Each sample in different time points (0, 6, 12, 24, 36, 48, and 72 hpi) was compared with the control. The tool of the EdgeR package (version 3.12.1) was utilized to identify the expression of DEGs (Robinson et al., 2010; McCarthy et al., 2012). The p value cut-off of 0.05 and a fold-change cut-off of 2 was used to determine the statistical significance of gene expression differences. The gene ontology (GO) analysis and Kyoto encyclopedia of genes and genomes (KEGG) enrichment for DEGs were analyzed by KOBAS software (version: 2.1.1) with a p value cut-off of 0.05 to determine the statistically significant enrichment (Wu et al., 2006).

Secretory protein prediction

The screening of secretory proteins was performed based on the presence or absence of the predicted coding sequence of the signal peptide, transmembrane domain, ω-sites for glycosylphosphatidylinositol (GPI) anchor, transit peptides to mitochondrion and nuclear localization signal (Zheng et al., 2013). SignalP6.0[1] was used to perform signal peptide cleavage site prediction. Transmembrane helices in the proteins were predicted using TMHMM.[2] GPI-anchored proteins were identified using PredGPI.[3] Proteins located in the mitochondria

1 https://services.healthtech.dtu.dk/service.php?SignalP-6.0

2 http://www.cbs.dtu.dk/services/TMHMM-2.0/

3 http://gpcr.biocomp.unibo.it/predgpi/pred.htm

were determined by TargetP.[4] Nuclear localization signal was predicted using NetNES.[5] The proteins that comprise signal peptide cleavage sites and nuclear localization signal, helices without transmembrane domain together with the GPI-anchored proteins were retrieved as secreted proteins. Effector candidates were searched from among the predicted coding sequences of the transcriptome contigs using effectorP.[6] Localization of probable effectors was predicted using the apoplastP.[7]

Real-time quantitative PCR of candidate differentially expressed genes

To analyze the gene expression of the selected DEGs from each time point, Real-time quantitative PCR (qRT-PCR) was performed using a real-time PCR system Q711 (Vazyme Biotechnology, Nanjing, China) according to the manufacturer's instruction. The quantitative PCR reaction was carried out in a 20 μl volume containing 1 μl of reverse transcription product, 10 μl of ChamQ Universal SYBR qRCR Master Mix, 0.4 μl of each primer (10 μM) and 8.2 μl of dd H_2O. The reaction conditions for RT-qPCR including three steps (Step 1: 95°C, 30s, Reps1; Step 2: 95°C, 10s, 60°C, 30s, Reps40; Step 3: 60–95°C, increment 0.5°C/5s, Reps1). To verify gene expression of *R. solani* AG-3 TB during the growth and invasion stage, total cDNA was extracted from total RNA by time course (0, 6, 12, 24, 36, 48, and 72 hpi). The primers were designed by Primer Premier 5 (**Supplementary Table 1**).

Results

Tissue infection, transcriptome sequencing, *de novo* assembly and differentially expressed genes analysis

A time course observation and sampling were conducted to clarify the induction of host symptoms and gene expression of pathogenic fungus *R. solani* AG-3 TB at different infection stages. The results indicated that tobacco leaves with pathogen did not show observable symptoms at 6 and 12 hpi, while the obvious yellow halo can be observed at the inoculated site at 24 hpi. The symptom aggravated with the appearance of wheel pattern after 72 hpi (**Figure 1A**). The diameters of the necrotic lesions were 0.0036, 0.0152, 0.1709, 0.2633, 0.3939, 0.6434 cm at 6, 12, 24, 36, 48, 72 hpi, respectively (**Figure 1B**).

Thereafter, an integrated transcriptomic analysis was conducted to globally reveal the crucial genes and pathways involved in *R. solani* AG-3 TB infection on *N. tabacum* at different stages, specifically at 6, 12, 24, 36, 48, and 72h after pathogen inoculation. The assembly statistics of *R. solani* AG-3 TB infection showed a total of 35,415,039 contigs, lengths of N50 and N90 with 1487 and 321 bp, respectively, with 49.06% GC content, of which the GC content maximum was 87.07% and the GC content minimum was 22.52% (**Table 1**).

The six time points were designated as the early stage (6–12 hpi), middle stage (24–36 hpi), and late stage (48–72 hpi) after *R. solani* AG-3 TB inoculation. The DEGs change showed that 37,999 DEGs were detected in the early stage, including 18,317 up-regulated genes and 19,682 down-regulated genes after *R. solani* AG3 TB inoculation. In contrast, the number of DEGs were 43,371, including 28,133 up-regulated and 15,238 down-regulated genes in the middle stage, which comprised largest amounts of DEGs (**Supplementary Figure 1** and **Supplementary Table 2**). These results suggested that the number change of DEGs have the difference during in various hours post inoculation, which may be related to pathogenic factors secreted of *R. solani* AG-3 TB.

Enrichment analysis of differential gene pathway

Functional enrichment analysis is an important way to retrieve some significant DEGs for organisms. The Gene Ontology related to three items including biological processes, molecular function and cellular components was analyzed. The results showed that DEGs involved in biological processes including the fatty acid metabolism process, pyridine-containing compound metabolic process and cellular components including proton-transporting V-type ATPase complex and cytosolic were significantly enriched compared with other items in the early infection stage of *R. solani* AG-3 TB (6–12 hpi) (**Supplementary Figure 2A**). At 24 hpi after the fungus inoculation, the critical items such as biological processes involved in cellular carbohydrate biosynthetic process, response to stress were enriched, and cell periphery related to cellular components was enriched (**Supplementary Figure 2B**). In addition, the MAPK cascades involved in biological processes was significantly enriched in the late stage of infection (48 –72 hpi) (**Supplementary Figure 2C**).

The KEGG pathway analysis indicated that the enrichment pathways of *R. solani* AG-3 TB were diverse in different infection stages. The results showed that amino sugar and nucleotide sugar metabolism, carbon metabolism, biosynthesis of amino acids and other pathway were significantly enriched in the early infection stage (6 –12 hpi) (**Figure 2A**). In

4 https://services.healthtech.dtu.dk/service.php?TargetP-2.0

5 https://services.healthtech.dtu.dk/service.php?NetNES-1.1

6 http://effectorp.csiro.au/

7 http://apoplastp.csiro.au/data.html

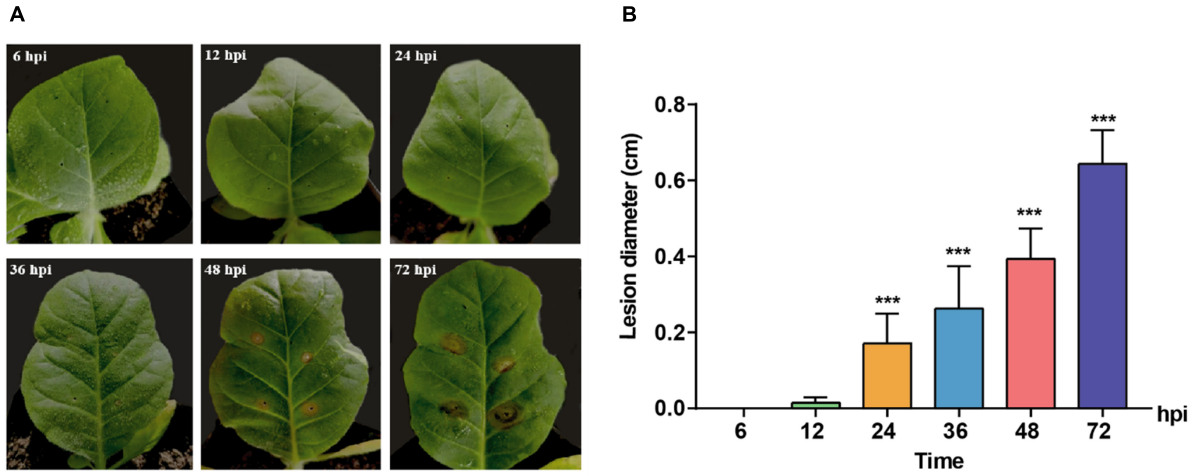

FIGURE 1
Symptoms change of *Nicotiana tabacum* inoculated with *R solani* AG-3 TB strain at different infection stages. **(A)** The symptoms on the Yunyan 87 leaf at 6, 12, 24, 36, 48, 72 hours post inoculation (hpi), respectively. **(B)** Measurement of the lesion diameter (cm) at 6 (control), 12, 24, 36, 48, 72 hpi. The asterisks show the statistical significances using the two-tailed *t*-test (*$p < 0.05$, **$p < 0.01$, ***$p < 0.001$).

contrast, the ubiquitin mediated proteolysis pathway was the most significantly enriched item in the middle stage (**Figure 2B**). Specifically, pyrimidine metabolism pathway was only enriched in the middle infection stage (24 hpi). Furthermore, the amino sugar and nucleotide sugar metabolism, and biosynthesis of amino acid pathways were enriched, while the carbon metabolism pathway was not enriched at 72 hpi stage (**Figure 2C**).

Gene expression involved in the biosynthesis of fungal toxin

The synthesis of fungal toxin PAA requires five important enzymes, including shikimate kinase, 3-phosphoshikimate 1-carboxyvinyltransferase (EPSP synthase), chorismate synthase, prephenate dehydrogenase and prephenate dehydratase, of which, shikimate is used as the initial material and the phenylpyruvate is the precursor of PAA (Cook et al., 2016; **Figure 3A**). In the DEGs during *R. solani* AG-3TB infection, the critical enzymes required for PAA synthesis were retrieved, and their expression levels were gradually increased in different infection stages. A total of 10 DEGs were selected and the expression levels of chorismate synthase, prephenate dehydrogenase were increased in the early and middle stage, while those of shikimate kinase, EPSP synthase and prephenate dehydratase were up-regulated in the middle and late stage of infection (**Figure 3B**). Specifically, the expression of five enzyme genes in PAA synthesis pathway increased to the highest levels in the middle infection (24 hpi).

Prenyltransferases (DMATSs) and polyketide synthases (PKSs) are two important enzymes involved in the production of secondary metabolites (Slot and Rokas, 2010). The number of DMATSs and PKSs were 11 and 2, and those DMATSs and PKSs genes expression continuously increased from 24 to 48 hpi stage (**Figure 3C**). The expression levels of most DMATSs were increased at 24 hpi and peaked at 48 hpi. As for PKSs, the expression of DN1756_c0_g1_i1 was increased in the early stage, while the expression of DN14539_c0_g1_i2 increased significantly at 48 hpi (**Figure 3C**).

TABLE 1 Data statistics of the transcriptome sequencing in *R solani* AG-3 TB subgroups.

Type	Trinity	Unigene
N50	2126	1487
N90	554	321
average length	1293.52	826.3
Max length	17497	17497
Min length	201	201
Total base	108235063	35415039
Total contigs	83675	42860
GC content (%)	49.36	49.06
GC content max	87.07	87.07
GC content min	22.52	22.52

Gene expression of *Rhizoctonia solani* AG-3 pathogenic related enzymes

Carbohydrate-active enzymes (CAZymes) is a large gene family involved in the construction and breakdown of complex carbohydrates and glycoconjugates, and mainly comprise

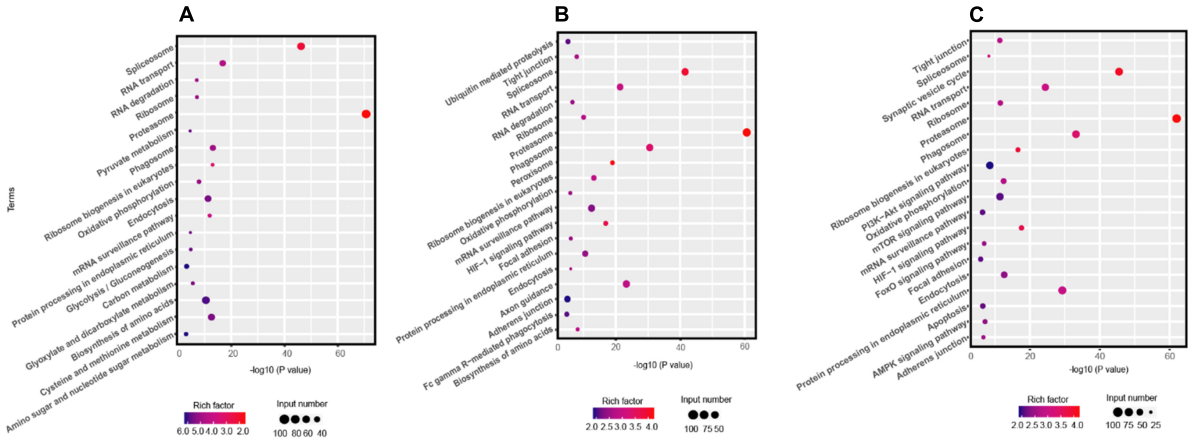

FIGURE 2
KEGG pathway analysis the DEGs of *R solani* AG-3 TB at different stage. **(A)** KEGG pathway analysis at 6 hpi stage. **(B)** KEGG pathway analysis at 24 hpi stage. **(C)** KEGG pathway analysis at 72 hpi stage.

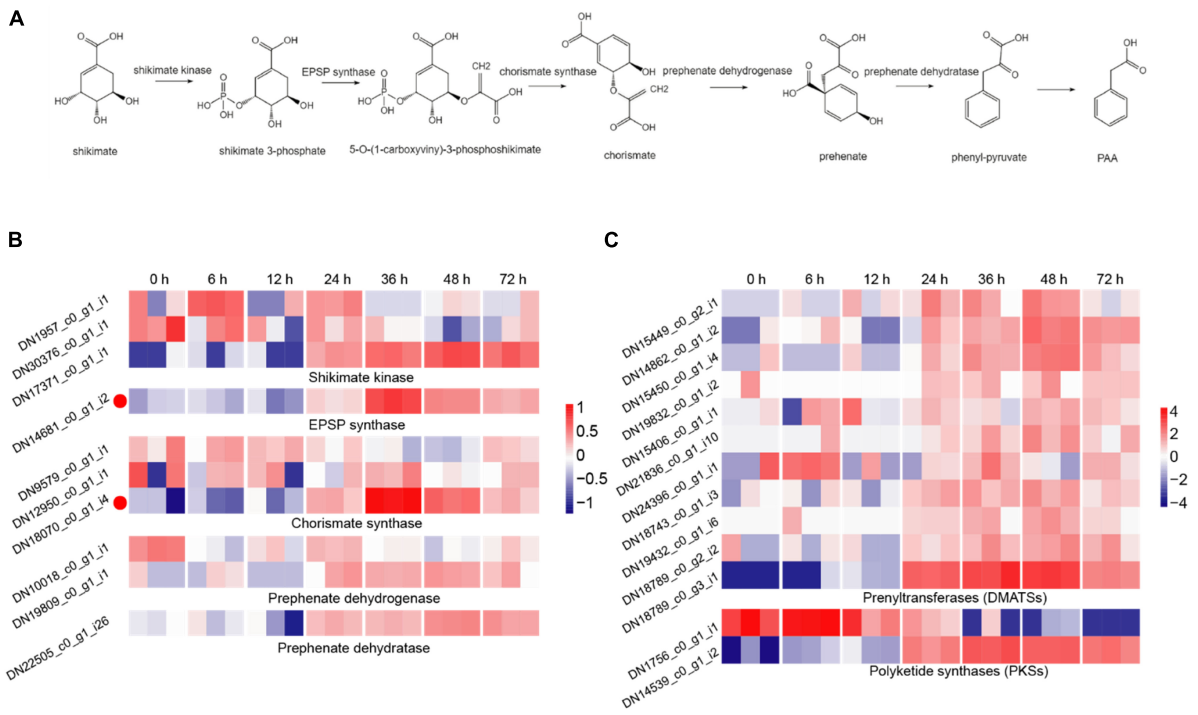

FIGURE 3
The DEGs for secondary metabolites production. **(A)** The biosynthetic pathway for PAA production, including the five key synthetases (shikimate kinase, EPSP synthase, chorismate synthase, prephenate dehydrogenase, and prephenate dehydratase) of PAA and six synthetic compounds associated with shikimate 3-phosphate, 5-O-(1-carboxyviny)-3-phosphoshikimate, chorismite, prehenate, phenyl-pyruvate, PAA. **(B)** The expression patterns of candidate genes on the five key synthetases of PAA biosynthetic pathway. The heatmap describes the expression of candidate genes (RPKM in log2-scale) associated with shikimate kinase, EPSP synthase, chorismate synthase, prephenate dehydrogenase, and prephenate dehydratase. The red circles next to the heatmap were candidate genes tested by qRT-PCR. **(C)** The expression patterns of candidate genes on DMATSs and PKSs. The heatmap describes candidate gene expression of DMATSs and PKSs.

Glycoside hydrolases (GHs), Glycosyl transferases (GTs), Polysaccharide lyases (PLs), Carbohydrate esterases (CEs) and Carbohydrate-binding modules (CBMs) (Cantarel et al., 2009).

The transcriptomic results showed that the gene expression levels of 12, 13, 51, 55, 69, and 53 CAZyme families were gradually up-regulated from the 6 to 72 hpi (**Figure 4A**). In

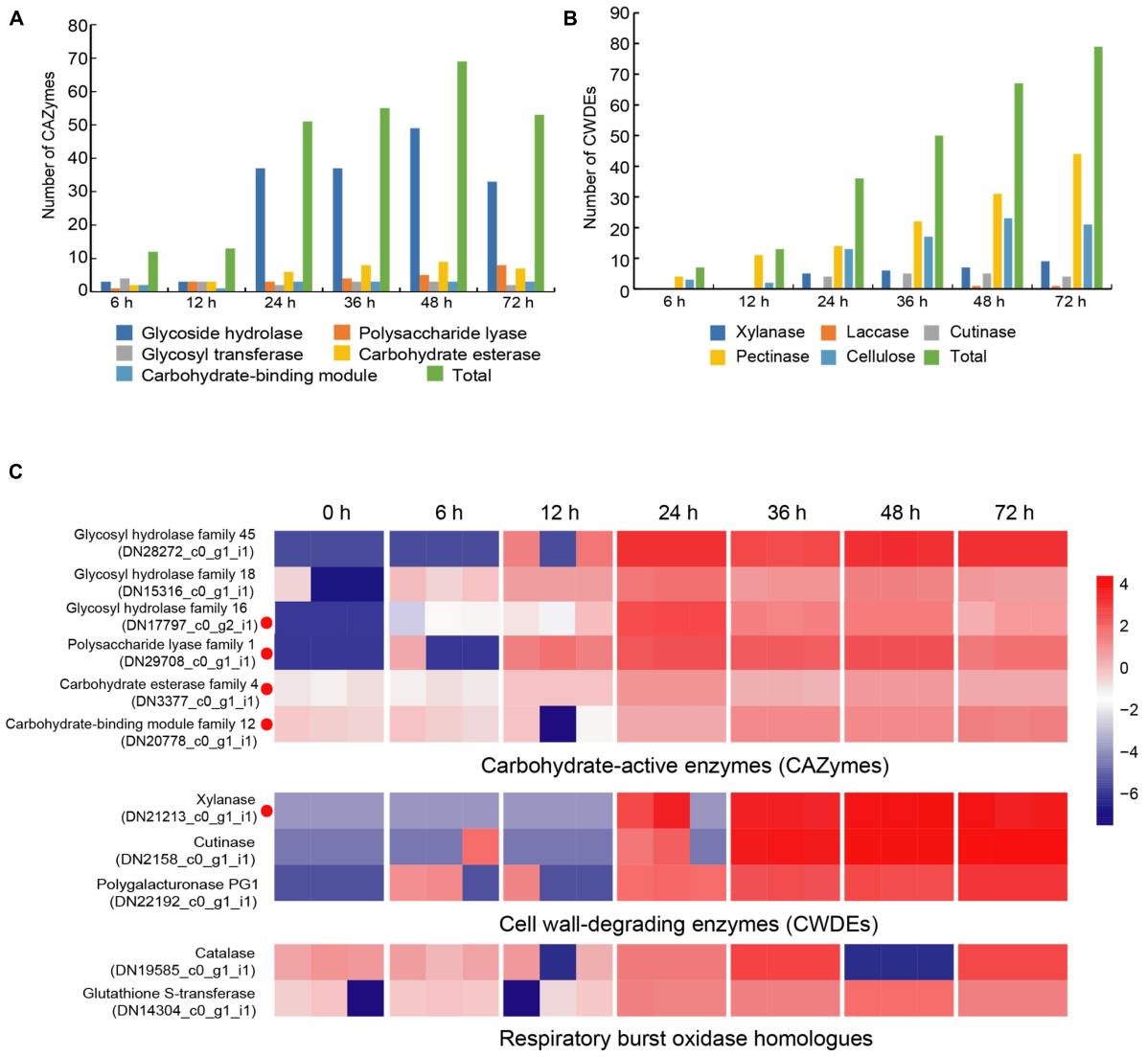

FIGURE 4
Changes of different enzyme genes during various infection stages. **(A)** The number of CAZymes at different infection stage. **(B)** The number of CWDEs at different infection stages. **(C)** Expression patterns of candidate genes on CAZymes (*glycosy hydrolase family 45*, *glycosy hydrolase family 18*, *glycosy hydrolase family 16*, *polysaccharide lysae family 1*, *carbohydrate esterase family 4*, *carbohydrate-binding module family 12*), CWDEs (*xylanase*, *cutinase*, *polygalacturonase PG1*) and respiratory burst oxidase homologs (*catalase*, *glutathione S-transferase*). The heatmap describes the enzyme gene expression at different stages (RPKM in log10-scale). The red circles next to the heatmap were candidate genes tested by qRT-PCR.

the early infection stage (6–12 hpi), the secretion of CAZymes was low. Then, the number of CAZymes related DEGs rapidly increased at 24 hpi and peaked at 48 hpi (**Figure 5**). The quantities of *GHs* and *PLs* were slightly higher than other components during *R. solani* AG-3 TB infection. Results of the heatmap indicated that expression levels of *GH45*, *GH18* and *GH16* genes were progressively increased in the early infection stage, while those of *PL1*, *CE4* and *CBM12* genes were increased in the middle and late infection stages, respectively (**Figure 4C**).

Cell wall-degrading enzymes (CWDEs) produced by plant pathogenic fungi, especially those without special penetration, can damage the cell wall polymers (Kubicek et al., 2014). Among these fungi, *R. solani* can produce CWDEs including pectinase, xylanase, laccase, cutinase and cellulase (Zheng et al., 2013). Here, the pectinase, xylanase, laccase, cutinase and cellulase of *R. solani* AG-3 TB were retrieved from the RNA-seq (**Supplementary Figure 3**). The result indicated that expression of 7 CWDEs genes (pectinase and cellulose) were increased in the initial stage of infection (6 hpi), while 79 total genes including pectinase, xylanase, laccase, cutinase and cellulase were significantly increased at 72 hpi (**Figure 4B**). According to the expression levels of

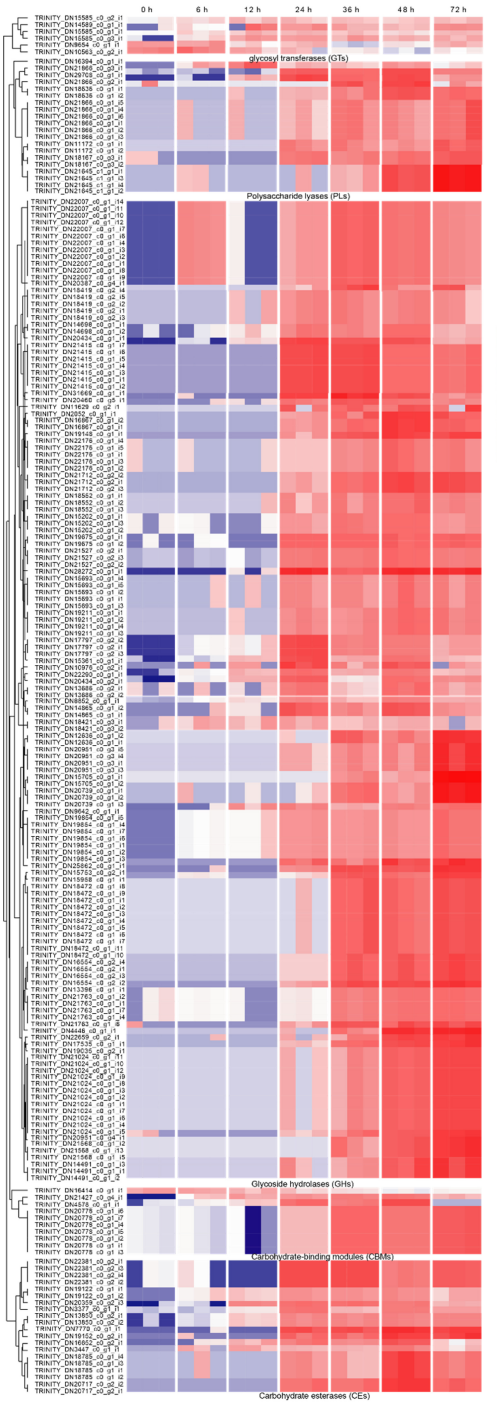

FIGURE 5
The heatmap of the expression levels of CAZymes genes in different stages expression patterns of candidate genes (RPKM in log10-scale) for CAZymes were represented in heatmaps (numerals indicate hours after inoculation onto tobacco).

CWDEs, *xylanase* (TRINITY_DN21213_c0_g1_i1) and *cutinase* (TRINITY_DN2158_c0_g1_i1) were increased at 24 hpi, while those of the *PG1* (TRINITY_DN22192_c0_g1_i1) were up-regulated at 6 hpi (**Figure 4C**).

When pathogenic fungi infect plants, the respiratory burst oxidase homologs play an important role to increase their pathogenicity (Ghosh et al., 2014). To clarify the gene change involved in respiratory burst oxidase homologs during the interaction between *R. solani* AG-3 TB and tobacco, the catalase, glutaredoxin, glutathione peroxidase, glutathione S-transferase, copper/zinc superoxide dismutase, and iron/manganese superoxide dismutase were retrieved for further analysis. The results showed that the expression of respiratory burst oxidase homologs increased exponentially in the middle and late stages of infection (**Supplementary Figure 4**). Additionally, the expression of *catalase* (TRINITY_DN19585_c0_g1) was significantly up-regulated in the middle stage of infection (36 hpi), and the expression of *glutathione S-transferase* (TRINITY_DN14304_c0_g1) was increased in the late stage of infection (48 hpi) (**Figure 4C**).

The gene sequences of *Rhizoctonia solani* AG-3 TB for the secretomes

The secretion of biologically active proteins is a fundamental infection strategy during the interaction between plants and fungi (Lo Presti et al., 2015). Secretomes of fungi play important roles in infection, colonization and pathogenicity (Xia et al., 2020). We adopted the classical secretion pathway (searching protein domains) as well as the apoplastic and cytoplasmic effectors (Effectrop 2.050 and ApoplastP) to retrieve the secreted proteases during the *R. solani* AG-3 TB infection. A total of 807 potential secretomes were retrieved, and 124 apoplastic effectors and 236 cytoplasmic effectors were predicted. There are few reports on apoplastic and cytoplasmic effectors of fungus, but some report had revealed that cytoplasmic effectors in *phytophthora sojae* encoding conservative sequences such as *RxLR* can cause tissue necrosis of plants (Zhang et al., 2015; Sperschneider et al., 2018). A total of 13 cytoplasmic effectors and 28 apoplastic effectors were retrieved, and most of these effectors can be classified in to serine protease (TRINITY_DN17844_c0_g3_i1), eukaryotic metallothionein (TRINITY_DN22450_c1_g5_i2), polysaccharide deacetylase (TRINITY_DN3377_c0_g1_i1), acetylxylan esterase (TRINITY_DN7106_c0_g1_i1), extracellular metalloproteinases (TRINITY_DN18673_c0_g3_i1), and deuterolysin metalloprotease (TRINITY_DN19525_c0_g1_i1) families (**Supplementary Table 3**). The expression analysis of pathogenic protease genes showed that the candidate cytoplasmic effector genes were significantly up-regulated at the late infection stage (48 hpi), while the genes of apoplastic effector were enriched significantly in the middle and late infection stages (24, 48 hpi) (**Figure 6**).

Small cysteine-rich proteins play functional roles in the molecular interaction between fungi and plant (Stergiopoulos and de Wit, 2009), and generally have a classical structural

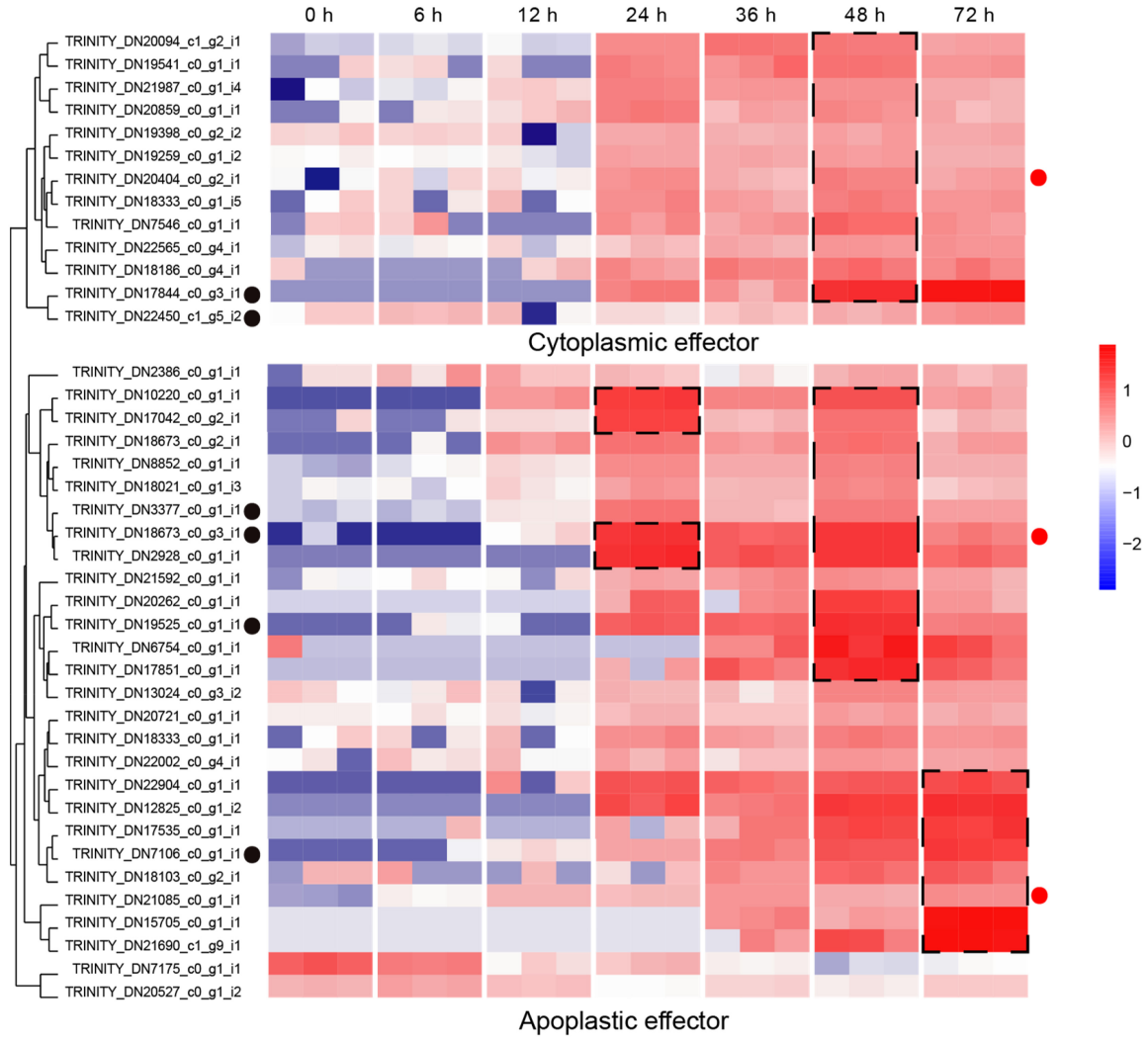

FIGURE 6
Expression patterns of candidate apoplastic and cytoplasmic effectors The heatmap represents apoplastic and cytoplasmic effectors genes expression (RPKM in log10-scale). The genes retrieved from Pfam, Blast and reads counts (>50). The up-regulated clusters were showed in dot black boxes. The red circles next to the heatmap were candidate genes tested by qRT-PCR.

characteristic with a less than 300aa protein and more than 4% cysteine (Yamamoto et al., 2019). Here, a total of 78 potential small cysteine-rich proteins were retrieved from *R. solani* AG-3 TB data (**Supplementary Table 4**). It should be noted that most of the small cysteine-rich proteins are unnamed protein products, which still require further investigation for clarification of their functions.

qPCR verification of transcriptome up-regulated genes

We chose the DEGs with large difference expression and revealed the potential critical roles (CAZymes, toxins and effectors) during *R. solani* AG-3 TB infection in different infection stages (6 hpi, 12 hpi, 24 hpi, 36 hpi, 48 hpi, 72 hpi). The expression levels of DN3377 (TRINITY_DN3377_c0_g1_i1), DN14681 (TRINITY_DN14681_c0_g1_i2), DN17797 (TRINITY_DN17797_c0_g2_i1), DN18673 (TRINITY_DN18673_c0_g3_i1), DN20404 (TRINITY_DN20404_c0_g2_i1), DN20778 (TRINITY_DN20778_c0_g1_i1), DN29708 (TRINITY_DN29708_c0_g1_i1), DN21213 (TRINITY_DN21213_c0_g1_i1), DN18070 (TRINITY_DN18070_c0_g1_i4), DN21085(TRINITY_DN21085_c0_g1_i1) were verified by qRT-PCR. The result indicated that CAZymes (DN29708, DN3377, DN20778, DN21213, and DN17797) expression were diverse, but increased levels were found for those five genes in the middle and late infection stages. EPSP synthase (DN14681) and chorismite synthase (DN18070) were two important genes involved in PAA synthesis pathway, and their expression started increasing at 24

hpi. The 36 hpi and 48hpi were important infection stages for *secretory protein* (DN20404, DN18673, and DN21085). These results indicated that the pathogenic genes expression obviously changed and also proved the reliability of transcriptomics during *R. solani* AG-3 TB infection (**Figure 7**).

Discussion

Rhizoctonia solani is an important group of saprophytic soilborne basidiomycetes that causes significant losses to a variety of crops. The complex multiple AGs and multi-nuclear nature of *R. solani* make it difficult to thoroughly understand its pathogenesis and development mechanism. Therefore, clarification of gene expression patterns in the development and infection of *R. solani* is crucial for the following research on the pathogenic mechanism and effective control of the fungus.

Before doing transcriptomic analysis, the AG3-T5[8] (Kaushik et al., 2020) as the reference genomes was mapped with the sequencing data of AG-3 TB. But the mapped rates of reads were low (<41%) (**Supplementary Table 5**). The low mapping rates may suggest that the reported strains with genetic data is quite distinct from AG-3 TB. Therefore, we used the transcriptome assembly from RNA-Seq data without reference genome. And according to the way of RNA-Seq data analysis without a reference genome, the quantity of DEGs was large than other *R. solani*. The reason for this result related to the fragmented genes and isoform genes were produced caused an increase in the number of DEGs.

In this study, many lines of critical DEGs in different stages of *R. solani* AG-3 TB infection were investigated, and showed various enrichment of the pathways. In the early infection stage, fatty acid metabolism, amino sugar, nucleotide sugar metabolism, carbon metabolism and biosynthesis of amino acids were significantly enriched. Such metabolisms have been indicated to correlate with branching, initiation and elongation, cell wall and biofilm matrix of fungal hyphae (Chen et al., 2020; Liboro et al., 2021). In the middle stage of infection, the cellular carbohydrate biosynthetic process of *R. solani* AG-3 TB began to be enriched. One gene in cellular carbohydrate biosynthetic process was predicted as *trehalose-phosphate phosphatase* (TRINITY_DN20403_c0_g1), and it associated with the development of sclerotia, stress response, and protection of cells from hydrogen peroxide in some pathogenic fungi (Jiang et al., 2017; Wang et al., 2018). Furthermore, ubiquitin-proteasome mediated protein turnover and the pyrimidine metabolic pathway was significantly enriched in the middle stage, which have a close relation to stress response, host adaptation and fungal pathogenesis (Qin et al., 2020). Herein, the detailed results of DEGs variation and pathway analysis indicated that mycelial growth and development should occur in the early stage of infection (6–12 hpi), while the crucial pathogenic stage of *R. solani* AG-3 TB may occur in the middle and late stages of infection.

8 https://ftp.ncbi.nlm.nih.gov/genomes/all/GCA/905/219/615/GCA_905219615.1_AG3-T5/

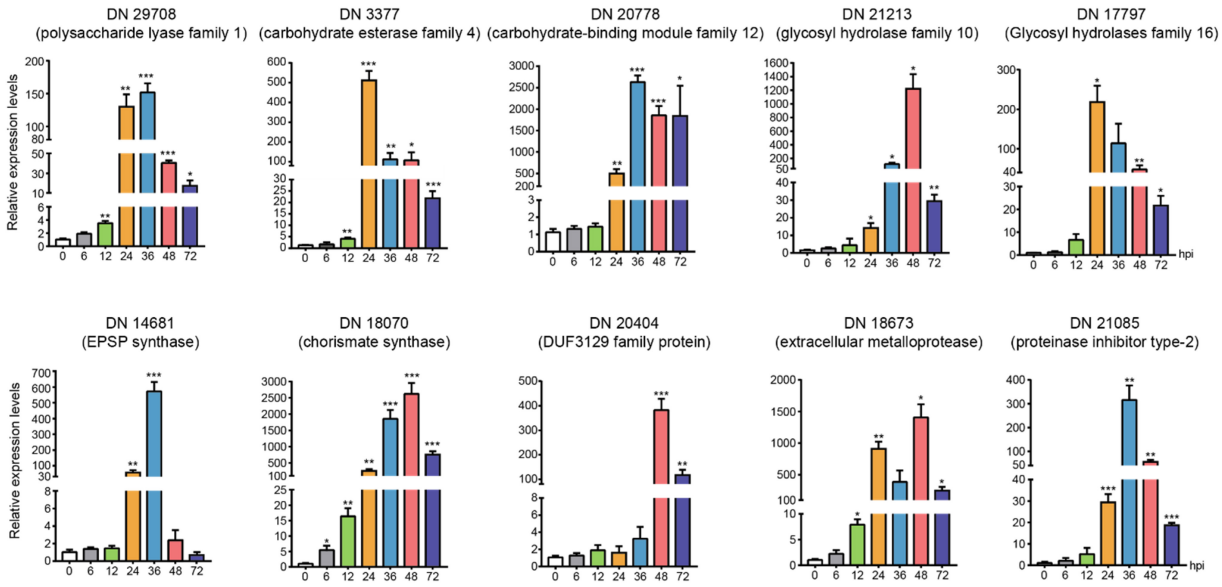

FIGURE 7
The expression levels of candidate genes expression patterns of candidate genes associated with toxins, enzymes, and secreted proteins using quantitative real time RT-PCR verification at 0, 6(control), 12, 24, 36, 48, and 72 hours after inoculation. The asterisks showed the statistical significances using the two-tailed t-test (*$p < 0.05$, **$p < 0.01$ ***$p < 0.001$).

Phenylacetic acid is an organic compound that can be produced by many kinds of fungi with various functions (Moore and Towers, 1967; Moore et al., 1968; Siddiqui and Shaukat, 2005). For example, PAA is the side chain precursor in the biosynthesis of penicillin (Mohammad-Saeid et al., 2018), and the catabolism of PAA is closely related to the virulence of *Burkholderia cenocepacia* (Lightly et al., 2019). PAA was also indicated to be an important signal molecule during microbial interactions with their hosts (Lightly et al., 2017). In a previous study, we isolated and purified a PAA derivative, namely 3-methoxyphenylacetic acid ($C_9H_{10}O_3$) from *R. solani* AG-3 TB, and confirmed its structure using thin layer chromatography (TLC), high performance liquid chromatography (HPLC), IR and NMR spectra (Hou, 2018). Importantly, five enzymes including shikimate kinase, EPSP synthase, chorismate synthase, prephenate dehydrogenase and prephenate dehydratase were considered to play crucial roles in the synthesis of PAA (Cook et al., 2016). Among those genes, prephenate dehydrogenase is an important enzyme associated with virulence and defense in fungi (Lopez-Nieves et al., 2019). A study showed that the expression of *prephenate dehydratase* of *R. solani* AG-1 IA was markedly increased at 18 h after infection (Zheng et al., 2013). In this study, we investigated the time-course expression of the five genes involved in PAA synthesis of *R. solani* AG-3 TB, and noted most of these genes were rapidly up-regulated at 24 hpi, which may be a critical time point for toxin production of the fungus. While precise detection of PAA at each infection stage should be conducted in the following study to clarify this hypothesis. In addition, many lines of secondary metabolites may also play roles in *R. solani* AG-3 TB infection. We herein investigated several 'backbone' enzymes for the synthesis of secondary metabolites from *R. solani* AG-3 TB, including prenyltransferases (DMATSs) and polyketide synthases (PKSs) (Slot and Rokas, 2010). Studies have indicated that DMATSs are involved in the production and secretion of indole alkaloids secondary metabolites (Julia et al., 2016; Arndt et al., 2017), while the PKSs are required for pigment production in fungi, which have a central role in the pathogenicity of fungi (Chen X. et al., 2018; Liu et al., 2021). In this study, our results showed that expression levels of DMATSs and PKSs genes significantly increased in the early and middle infection stage. These results collectively suggested that *R. solani* AG-3 TB may produce secondary metabolite classes or complex compounds to damage the plant or play the function of parasite life cycle.

Cell wall degrading enzymes (CWDEs) secreted by pathogenic fungi are advantageous to the colonization, expansion and spread of fungi. Furthermore, the amount and species of CWDEs produced by the pathogenic fungi during infection differ between monocot or dicot host plants (Cuomo et al., 2007; King et al., 2011). The fungus *Macrophomina phaseolina* was reported to secrete 49 kinds of CWDEs involved in cellulose and homogalacturonan degradation when infecting sorghum (Bandara et al., 2018). In the study of genome analysis interaction between *R. solani* AG-1 IA and rice, the pectinase genes, xylanase genes, and laccase genes can be produced by *R. solani* AG-1 IA, among which the laccase genes, pectinase genes may play specific roles to necrotrophic life cycle (Zheng et al., 2013). In addition, treatment *in vitro* expressed pectinase PG2 of *R. solani* AG-1 IA can cause necrosis symptoms in the rice tissue (Chen et al., 2020). In the previous study, we have shown that the pectinase (PG, PMG, PGTE, and PMTE) and cellulase (Cx, β-Glucosidase) of *R. solani* AG-3 TB have the highest activity in the culture medium of Marcus in 18 hpi during *R.solani* AG-3 TB infection (Fu, 2011). In this study, the results of RNA-seq and qRT-PCR demonstrated that expression levels of 7 CWDEs in *R. solani* AG-3 TB were increased in 6 hpi, while those of 79 CWDEs (pectinase, xylanase, laccase, cutinase, and cellulase) were significantly up-regulated in 48-72 hpi. These results systemically investigated the expression of these critical CWDEs at each infection stages, and suggested their possible functions in the pathogenesis of *R. solani* AG-3 TB as well as the induction of necrotic symptoms of the host.

Moreover, we also found that respiratory burst oxidase homologs genes including catalase, glutaredoxin, glutathione peroxidase, glutathione S-transferase, copper/zinc superoxide dismutase, and iron/manganese superoxide dismutase were differentially regulated in the transcriptome of *R. solani* AG-3 TB infection. The respiratory burst oxidase homologs were reported to detoxify ROS produced by plant (Ghosh et al., 2014). Studies have shown that the fungal respiratory burst oxidase homologs were involved in the colonization of necrotrophic fungi as well as the induction of host necrotic symptoms (Kámán-Tóth et al., 2018). An RNA-seq study indicated that the expression levels of two respiratory burst oxidase homologs genes of *R. solani* AG-1 IA were increased during ROS production (Zhang et al., 2017), and the oxidases were reported to be associated with the colonization of this fungus (Pauly, 2012). In this study, the expressions of respiratory burst oxidase homologs genes were increased in the middle and late infection stage, which indicated that these critical genes may be associated with the detoxification and oxidative stress for the pathogen of tobacco target spot.

Generally, pathogens can produce many kinds of effectors that are particularly important in promoting pathogen expansion and inhibiting host defense (Giraldo and Valent, 2013; Lo Presti et al., 2015). *R. solani* has become one of the most devastating plant fungal pathogens in the past decade and it is difficult to clarify its genetic characteristics and pathogenicity because of anastomosis groups and multinuclear nature (Yamamoto et al., 2019). During genomic analysis of *R. solani* AG-1 IA, a total of 965 secreted proteins were predicted, including 103 potential small cysteine-rich proteins (Zheng et al., 2013). In contrast, little is known about the secreted proteins as well as the effectors produced by *R. solani*

AG-3 TB. In this study, 807 possible secretory proteins were predicted from *R. solani* AG-3 TB, which comprise possible 124 apoplastic effectors and 236 cytoplasmic effectors. In addition, 41 genes were predicted as deuterolysin metalloprotease, serine protease, and extracellular metalloproteinases. The fungal deuterolysin metalloprotease (M35) family was reported to be involved in cell wall degradation, epidermal growth inhibition, and cell activity of insects (Huang et al., 2020). The serine protease is an important pathogenic marker for *Alternaria solani* (Chandrasekaran et al., 2014). We presumed that these deduced secreted proteins in pathogen of tobacco target spot may serve as potential effectors that may play important roles in the pathogenicity of fungus, and remains to be further investigated in the following work.

In this study, we conducted integrated transcriptomic analysis and revealed many lines of potentially critical genes involved in the pathogenesis of *R. solani* AG-3 TB on *Nicotiana tabacum* at different infection stages. The results showed that various enzymes, toxins as well as effectors may play different, but critical roles in the interaction between pathogen and plant. Based on the results of systemic analysis of RNA-seq, we proposed the pathogenic mechanisms of *R. solani* AG-3 TB infecting plants. The hypha of *R. solani* AG-3 TB should begin to develop and grow in the leaves during the early infection stage (6–12 hpi). Then, the critical toxins and effectors may synergistically suppress plant defense response and regulate the infection of *R. solani* AG-3 TB in the middle stage (24–36 hpi). At the late stage (48–72 hpi), the plant cell structure and tissue were continuously eroded by toxins and CWDEs, which resulted in necrosis in leaves (**Supplementary Figure 5**). These results collectively provide critical insights into many lines of potentially functional genes as well as the pathways involved in the pathogenesis of tobacco target spot, and provide valuable theoretical basis for the accurate prevention and control of the disease. This is the first time to predict potentially functional genes for AG-3 TB, the agent of tobacco target spot by the transcriptome analyses. According to our results, the functional genes between AG-1 IA and AG-3 TB have big difference, for instance, the number of enzymes and effectors in AG-1 IA is larger than AG-3 TB (Zheng et al., 2013). Moreover, the PAA is a potential pathogenicity toxin in AG-1 IA, AG-3 TB, and AG-3 PT (Kankam et al., 2016; Yamamoto et al., 2019). Therefore, comparison the difference in candidate effectors or toxin genes from different AG strains will be an important aspect to investigate the genetic characteristics and pathogenic differences.

Data availability statement

The datasets presented in this study can be found in online repositories. The names of the repository/repositories and accession number(s) can be found below: https://www.ncbi.nlm.nih.gov/, PRJNA853492.

Author contributions

CZ and YW: conceptualization and project administration. XL, CX, LJ, FY, and YY: methodology and software. XL: formal analysis and data curation. XL and MA: resources and writing—original draft preparation. YW: supervision and funding acquisition. All authors read and agreed to the published version of the manuscript.

Funding

This work was financially supported by the National Natural Science Foundation of China (No. 32172454), the Key Scientific and Technological Projects of Sichuan Branch of China National Tobacco (SCYC202113), and the Tobacco Pests and Diseases Green Prevention and Control Major Special Project [110202101045(LS-05)].

Conflict of interest

Author CX was employed by Luzhou Branch of Sichuan Province Tobacco Company. Author LJ was employed by Liangshan Branch of Sichuan Province Tobacco Company. Author FY was employed by Panzhihua Branch of Sichuan Province Tobacco Company. Author YY was employed by Yibin Branch of Sichuan Province Tobacco Company.

The remaining authors declare that the research was conducted in the absence of any commercial or financial relationships that could be construed as a potential conflict of interest.

Publisher's note

Supplementary material

The Supplementary Material for this article can be found online at: https://www.frontiersin.org/articles/10.3389/fmicb.2022.1001327/full#supplementary-material

References

Anderson, J. P., Sperschneider, J., Win, J., Kidd, B., Yoshida, K., Hane, J., et al. (2017). Comparative secretome analysis of *Rhizoctonia solani* isolates with different host ranges reveals unique secretomes and cell death inducing effectors. *Sci. Rep.* 7:10410. doi: 10.1038/s41598-017-10405-y

Aoki, H., Sassa, T., and Tamura, T. (1963). Phytotoxic Metabolites of *Rhizoctonia solani*. *Nature* 20, 575–575. doi: 10.1038/200575a0

Arndt, B., Janevska, S., Schmid, R., Hübner, F., and Humpf, H. U. (2017). A fungal N-dimethylallyltryptophan metabolite from *Fusarium fujikuroi*. *Communication* 18, 899–904. doi: 10.1002/cbic.201600691

Bandara, Y. M. A. Y., Weerasooriya, D. K., Liu, S., and Little, C. R. (2018). The necrotrophic fungus *Macrophomina phaseolina* promotes charcoal rot susceptibility in grain sorghum through induced host cell wall-degrading enzymes. *Phytopathology* 108, 948–956. doi: 10.1094/PHYTO-12-17-0404-R

Cantarel, B. L., Coutinho, P. M., Corinne, R., Thomas, B., Vincent, L., and Bernard, H. (2009). The Carbohydrate-Active EnZymes database (CAZy): An expert resource for Glycogenomics. *Nucleic Acids Res.* 37, 233–238. doi: 10.1093/nar/gkn663

Chandrasekaran, M., Chandrasekar, R., Sa, T., and Sathiyabama, M. (2014). Serine protease identification (*in vitro*) and molecular structure predictions (*in silico*) from a phytopathogenic fungus, *Alternaria solani*. *J. Basic Microbiol.* 54(Suppl. 1), S210–S218. doi: 10.1002/jobm.201300433

Chen, S., Zhou, Y., Chen, Y., and Gu, J. (2018). fastp: An ultra-fast all-in-one FASTQ preprocessor. *Bioinformatics* 34, 884–890. doi: 10.1101/274100

Chen, X., Meng, X., Cheng, F., and Hu, C. (2018). Progress in fungal polyketide biosynthesis. *Chin. J. Biotechnol.* 34, 151–164. doi: 10.13345/j.cjb.170219

Chen, Y., Mauff, F. L., Wang, Y., Lu, R., and Zhang, S. (2020). The transcription factor soma synchronously regulates biofilm formation and cell wall homeostasis in *Aspergillus fumigatus*. *mBio* 11:e02329-20. doi: 10.1128/mBio.02329-20

Cook, S. D., Nichols, D. S., Smith, J., Chourey, P. S., and Ross, J. J. (2016). Auxin biosynthesis: Are the Indole-3-acetic acid and phenylacetic acid biosynthesis pathways mirror images? *Plant Physiol.* 171, 1230–1241. doi: 10.1104/pp.16.00454

Cuomo, C. A., Guldener, U., Xu, J. R., Trail, F., and Turgeon, B. G. (2007). The *Fusarium graminearum* genome reveals a link between localized polymorphism and pathogen specialization. *Science* 317, 1400–1402. doi: 10.1126/science.1143708

Dean, R. A., Talbot, N. J., Ebbole, D. J., Farman, M. L., Mitchell, T. K., Orbach, M. J., et al. (2005). The genome sequence of the rice blast fungus *Magnaporthe grisea*. *Nature* 434, 980–986. doi: 10.1038/nature03449

Dickman, M. B., and de Figueiredo, P. (2013). Death be not proud-cell death control in plant fungal interactions. *PLoS Pathog.* 9:e1003542. doi: 10.1371/journal.ppat.1003542

Dobin, A., Davis, C. A., and Schlesinger, F. (2013). STAR: Ultrafast universal RNA-seq aligner. *Bioinformatics* 29, 15–21. doi: 10.1093/bioinformatics/bts635

Dutheil, J. Y., Mannhaupt, G., Schweizer, G., Sieber, C. M. K., Münsterkötter, M., Güldener, U., et al. (2016). A tale of genome compartmentalization: The evolution of virulence clusters in smut fungi. *Genome Biol. Evol.* 8, 681–704. doi: 10.1093/gbe/evw026

Fang, A., Gao, H., Zhang, N., Zheng, X., and Sun, X. (2019). A novel effector gene *SCRE2* contributes to full virulence of *Ustilaginoidea virens* to Rice. *Front. Microbiol.* 10:845. doi: 10.3389/fmicb.2019.00845

Fu, Y. (2011). *Study on the genetic differentiation, infection characteristics and pathogenic mechanism of Rhizoctonia solani*. Shenyang: Shenyang Agriculture University.

Ghosh, S., Gupta, S. K., and Jha, G. (2014). Identifcation and functional analysis of AG1-IA specifc genes of *Rhizoctonia solani*. *Curr. Genet.* 60, 327–341. doi: 10.1007/s00294-014-0438-x

Giraldo, M. C., and Valent, B. (2013). Filamentous plant pathogen effectors in action. *Nat. Rev. Microbiol.* 11, 800–814. doi: 10.1038/nrmicro3119

Gonzalez, D., Carling, D. E., Kuninaga, S., Vilgalys, R., and Cubeta, M. A. (2001). Ribosomal DNA systematics of *Ceratobasidium* and *Thanatephorus* with *Rhizoctonia anamorphs*. *Mycologia* 93:1138. doi: 10.2307/3761674

Grabherr, M. G., Haas, B. J., Yassour, M., Levin, J. Z., Thompson, D. A., Amit, I., et al. (2011). Full-length transcriptome assembly from RNA-Seq data without a reference genome. *Nat. Biotechnol.* 29, 644–652. doi: 10.1038/nbt.1883

Hou, H. H. (2018). *The active components and their pathogenic mechanism of toxins produced by Rhizoctonia solani from tobacco target spot disease*. Shenyang: Shenyang Agriculture University.

Huang, A., Lu, M., Ling, E., Li, P., and Wang, C. S. (2020). A M35 family metalloprotease is required for fungal virulence against insects by inactivating host prophenoloxidases and beyond. *Virulence* 11, 222–237. doi: 10.1080/21505594.2020.1731126

Jiang, H., Liu, G. L., Chi, Z., Hu, Z., and Chi, Z. M. (2017). Genetics of trehalose biosynthesis in desert-derived *Aureobasidium melanogenum* and role of trehalose in the adaptation of the yeast to extreme environments. *Curr. Genet.* 64, 479–491. doi: 10.1007/s00294-017-0762-z

Julia, W., Xie, X. L., and Li, S. M. (2016). Characterisation of 6-DMATS_(Mo) from *Micromonospora olivasterospora* leading to identification of the divergence in enantio-selectivity, regioselectivity and multiple prenyla-tion of tryptophan prenyltransferases. *Org. Biomol. Chem.* 14, 9883–9895. doi: 10.1039/c6ob01803c

Kámán-Tóth, E., Dankó, T., Gullner, G., Bozsó, Z., Palkovics, L., and Pogány, M. (2018). Contribution of cell wall peroxidase- and NADPH oxidase -derived reactive oxygen species to *Alternaria brassicicola*-induced oxidative burst in *Arabidopsis*. *Mol. Plant Pathol.* 20, 485–499. doi: 10.1111/mpp.12769

Kankam, F., Long, H. T., He, J., Zhang, C. H., and Qiu, H. (2016). 3-Methylthiopropionic Acid of *Rhizoctonia solani* AG-3 and its role in the pathogenicity of the fungus. *Plant Pathol. J.* 32, 85–94. doi: 10.5423/PPJ.OA.08.2015.0159

Kaushik, A., Roberts, D. P., Ramaprasad, A., Mfarrej, S., Nair, M. B., Lakshman, D., et al. (2020). The pangenome analysis of the soil-borne fungal phytopathogen *Rhizoctonia solani* and development of a comprehensive web resource: *Rsolani*DB. *biorxiv* [Preprint]. doi: 10.1101/2020.12.18.423518

King, B. C., Waxman, K. D., Nenni, N. V., Walker, L. P., Bergstrom, G. C., and Gibson, D. M. (2011). Arsenal of plant cell wall degrading enzymes reflects host preference among plant pathogenic fungi. *Biotechnol. Biofuels* 4:4. doi: 10.1186/1754-6834-4-4

Kubicek, C. P., Starr, T. L., and Glass, N. L. (2014). Plant cell wall–degrading enzymes and their secretion in plant-pathogenic fungi. *Annu. Rev. Phytopathol.* 52, 427–451. doi: 10.1146/annurev-phyto-102313-045831

Kuninaga, S., Carling, D. E., Takeuchi, T., and Yokosawa, R. (2000). Comparison of rDNA ITS sequences between potato and tobacco strains in *Rhizoctonia solani* AG-3. *J. Gen. Plant Pathol.* 66, 2–11. doi: 10.1007/PL00012917

Kuninaga, S., Natsuaki, T., Takeuchi, T., and Yokosawa, R. (1997). Sequence variation of the rDNA ITS regions with between anastomosis groups in *Rhizoctonia solani*. *Curr. Genet.* 32, 237–243. doi: 10.1007/s002940050272

Lakshman, D. K., Alkharouf, N., Roberts, D. P., Natarajan, S. S., and Mitra, A. (2012). Gene expression profling of the plant pathogenic basidiomycetous fungus *Rhizoctonia solani* AG-4 reveals putative virulence factors. *Mycologia* 104, 1020–1035. doi: 10.3852/11-226

Langmead, B., and Salzberg, S. (2012). Fast gapped-read alignment with Bowtie 2. *Nat. Methods* 9, 357–359. doi: 10.1038/nmeth.1923

Li, S., Peng, X., Wang, Y., Hua, K. Y., Xing, F., Zheng, Y. Y., et al. (2019). The effector *AGLIP1* in *Rhizoctonia solani* AG1 IA triggers cell death in plants and promotes disease development through inhibiting PAMP-triggered immunity in *Arabidopsis thaliana*. *Front. Microbiol.* 10:2228. doi: 10.3389/fmicb.2019.02228

Liboro, K., Yu, S.-R., Lim, J., So, Y.-S., Bahn, Y.-S., Eoh, H., et al. (2021). Transcriptomic and metabolomic analysis revealed roles of Yck2 in Carbon metabolism and morphogenesis of *Candida albicans*. *Front. Cell. Infect. Microbiol.* 16:636834. doi: 10.3389/fcimb.2021.636834

Lightly, T. J., Frejuk, K. L., Groleau, C., Chiarelli, L. R., and Cardona, S. T. (2019). Phenylacetyl-CoA, not phenylacetic acid, attenuates CepIR-regulated virulence in *Burkholderia cenocepacia*. *Appl. Environ. Microbiol.* 85:e01594-19. doi: 10.1128/AEM.01594-19

Lightly, T. J., Phung, R. R., Sorensen, J. L., and Cardona, S. T. (2017). Synthetic cystic fibrosis sputum medium diminishes *Burkholderia cenocepacia* antifungal activity against *Aspergillus fumigatus* independently of phenylacetic acid production. *Can. J. Microbiol.* 63, 427–438. doi: 10.1139/cjm-2016-0705

Liu, M., Hu, J., Zhang, A., Dai, Y., Chen, W., He, Y., et al. (2021). Auxilin-like protein *MoSwa2* promotes effector secretion and virulence as a clathrin uncoating factor in the rice blast fungus *Magnaporthe oryzae*. *New Phytol.* 230, 720–736. doi: 10.1111/nph.17181

Lo Presti, L., Lanver, D., Schweizer, G., Tanaka, S., Liang, L., Tollot, M., et al. (2015). Fungal effectors and plant susceptibility. *Annu. Rev. Plant Biol.* 66, 513–545. doi: 10.1146/annurev-arplant-043014-114623

Lopez-Nieves, S., Pringle, A., and Maeda, H. A. (2019). Biochemical characterization of TyrA dehydrogenases from *Saccharomyces cerevisiae* (Ascomycota) and *Pleurotus ostreatus* (Basidiomycota). *Arch. Biochem. Biophys.* 665, 12–19. doi: 10.1016/j.abb.2019.02.005

Lucas, G. B. (1975). *Diseases of tobacco*, 3rd Edn. Raleigh, NC: Biological Consulting Associates. doi: 10.1038/1781421a0

McCarthy, J. D., Chen, Y. S., and Smyth, K. G. (2012). Differential expression analysis of multifactor RNA-Seq experiments with respect to biological variation. *Nucleic Acids Res.* 40, 4288–4297. doi: 10.1093/nar/gks042

Mohammad-Saeid, J., Juan-Francisco, M., Carlos, B., Rebeca, D. S., María-Fernanda, V. C., María, P., et al. (2018). Catabolism of phenylacetic acid in *Penicillium rubens*. Proteome-wide analysis in response to the benzylpenicillin side chain precursor. *J. Proteomics* 187, 243–259. doi: 10.1016/j.jprot.2018.08.006

Moore, K., Rao, P. V., and Towers, G. H. N. (1968). Degradation of Phenylalanine and Tyrosine by *Sporobolomyces roseus*. *Biochem. J.* 106, 507–514. doi: 10.1042/bj1060507

Moore, K., and Towers, G. H. N. (1967). Degradation of Aromatic Amino Acids By Fungi I. Fate of L-Phenylalanine in *Schizophyllum* commune. *Can. J. Biochem.* 45, 1659–1665. doi: 10.1139/o67-196

Ogoshi, A. (1987). Ecology and pathogenicity of anastomosis and intraspecifc groups of *Rhizoctonia Solani* Kühn. *Annu. Rev. Phytopathol.* 25, 125–143. doi: 10.1146/annurev.py.25.090187.001013

Pauly, P. N. (2012). A burst of plant NADPH oxidases. *Trends Plant Sci.* 17, 9–15. doi: 10.1016/j.tplants.2011.10.001

Qin, T. F., Hao, W., Sun, R. R., and Li, Y. Q. (2020). *Verticillium dahliae* VdTHI20, involved in pyrimidine biosynthesis, is required for DNA repair functions and pathogenicity. *Int. J. Mol. Sci.* 20:1378. doi: 10.3390/ijms21041378

Robinson, M. D., McCarthy, D. J., and Smyth, G. K. (2010). edgeR: A Bioconductor package for differential expression analysis of digital gene expression data. *Bioinformatics* 26, 139–140. doi: 10.1093/bioinformatics/btp616

Shew, H. D., and Main, C. E. (1985). *Rhizoctonia* leaf spot of flue-cured tobacco in North Carolina. *Plant Dis.* 69, 901–903.

Siddiqui, I. A., and Shaukat, S. S. (2005). Phenylacetic acid-producing *Rhizoctonia solani* represses the biosynthesis of nematicidal compounds in vitro and influences biocontrol of meloidogyne incognita in tomato by *Pseudomonas fluorescens* Strain CHA0 and its GM Derivatives. *J. Appl. Microbiol.* 98, 43–55. doi: 10.1111/j.1365-2672.2004.02457.x

Slot, J. C., and Rokas, A. (2010). Multiple GAL pathway gene clusters evolved independently and by different mechanisms in fungi. *Proc. Natl. Acad. Sci. U.S.A.* 107, 10136–10141. doi: 10.1073/pnas.0914418107

Sneh, B., Jajabi-Hare, S., Neate, S., and Dijst, G. (1996). *Rhizoctonia species: Taxonomy, molecular biology, ecology, pathology and disease control*. Dordrecht: Kluwer Academic Publishers.

Sperschneider, J., Dodds, P. N., Gardiner, D. M., Singh, K. B., and Taylor, J. M. (2018). Improved prediction of fungal efector proteins from secretomes with EfectorP 2.0. *Mol. Plant Pathol.* 19, 2094–2110. doi: 10.1111/mpp.12682

Stergiopoulos, I., and de Wit, P. J. (2009). Fungal effector proteins. *Annu. Rev. Phytopathol.* 47, 233–263. doi: 10.1146/annurev.phyto.112408.132637

Taheri, P., and Tarighi, S. (2011). Cytomolecular aspects of rice sheath blight caused by *Rhizoctonia solani*. *Eur. J. Plant Pathol.* 129, 511–528. doi: 10.1007/s10658-010-9725-7

Vidhyasekaran, P., Ponmalar, T. R., Samiyappan, R., Velazhahan, R., and Muthukrishnan, S. (1997). Host-specifc toxin production by *Rhizoctonia solani*, the Rice Sheath Blight Pathogen. *Phytopathology* 87, 1258–1263. doi: 10.1094/PHYTO.1997.87.12.1258

Wang, C., Pi, L., Jiang, S., Yang, M., Shu, C., and Zhou, E. (2018). ROS and trehalose regulate sclerotial development in *Rhizoctonia solani* AG-1 IA. *Fungal Biol.* 122, 322–332. doi: 10.1016/j.funbio.2018.02.003

Wu, J., Mao, X., Cai, T., Luo, J., and Wei, L. (2006). KOBAS server: A web-based platform for automated annotation and pathway identification. *Nucleic Acids Res.* 34, 720–724. doi: 10.1093/nar/gkl167

Wu, Y. H., Zhao, Y. Q., Fu, Y., Zhao, X. X., and Chen, J. G. (2012). First report of target spot of flue-cured Tobacco Caused by *Rhizoctonia solani* AG-3 in China. *Plant Dis.* 96, 1824–1824. doi: 10.1094/PDIS-06-12-0551-PDN

Xia, Y., Ma, Z., Qiu, M., Guo, B., and Wang, Y. (2020). N-glycosylation shields *Phytophthora sojae* apoplastic effector *PsXEG1* from a specific host aspartic protease. *Proc. Natl. Acad. Sci. U.S.A.* 117, 27685–27693. doi: 10.1073/pnas.2012149117

Xu, C. T., Zhang, C., and Zhang, M. J. (2021). The study on pathogen identification and biological control of tobacco target spot in Sichuan Province. *Hubei Agric. Sci. China* 60:4. doi: 10.14088/j.cnki.issn0439-8114.2021.08.016

Xu, M. L., Hao, K. Q., Yang, J. G., Wang, F. L., Xiao, Z. X., and Li, W. (2018). First Report of *Rhizoctonia solani* AG-3 Causing Tobacco Target Spot in Yunnan, China. *Plant Dis.* 102:2038. doi: 10.1094/PDIS-02-18-0249-PDN

Yamamoto, N., Wang, Y., Lin, R., Liang, Y., Liu, Y., Zhu, J., et al. (2019). Integrative transcriptome analysis discloses the molecular basis of a heterogeneous fungal phytopathogen complex, *Rhizoctonia solani* AG-1 subgroups. *Sci. Rep.* 9:19626. doi: 10.1038/S41598-019-55734-2

Yang, G. H., Conner, R. L., Chen, Y. Y., Chen, J. Y., and Wang, Y. G. (2008). Frequency and pathogenicity distribution of *Rhizoctona* spp. causing sheath blight on rice and banded leaf disease on Maize in Yunnan, China. *J. Plant Pathol.* 90, 387–392. doi: 10.4454/jpp.v90i2.679

Zhang, J., Chen, L., Fu, C., Wang, L., Liu, H., Cheng, Y., et al. (2017). Comparative transcriptome analyses of gene expression changes triggered by *Rhizoctonia solani* AG1 IA infection in resistant and susceptible rice varieties. *Front. Plant Sci.* 8:1422. doi: 10.3389/fpls.2017.01422

Zhang, M., Rajput, N. A., Shen, D., Peng, S., Zeng, W., Liu, T., et al. (2015). A Phytophthora sojae cytoplasmic effector mediates disease resistance and abiotic stress tolerance in *Nicotiana benthamiana*. *Sci. Rep.* 5:10837. doi: 10.1038/srep10837

Zheng, A., Lin, R., Zhang, D., Qin, P., Xu, L., Ai, P., et al. (2013). The evolution and pathogenic mechanisms of the rice sheath blight pathogen. *Nat. Commun.* 4:1424. doi: 10.1038/ncomms2427

frontiers | Frontiers in Microbiology

TYPE Original Research
PUBLISHED 13 October 2022
DOI 10.3389/fmicb.2022.1025727

OPEN ACCESS

EDITED BY
Md. Motaher Hossain,
Bangabandhu Sheikh Mujibur Rahman Agricultural University, Bangladesh

REVIEWED BY
Richard Singh,
Ghent University,
Belgium
Narayan Chandra Paul,
Chonnam National University,
South Korea
Ziaul Haque,
Aligarh Muslim University,
India
Ma. Teodora Cabasan,
University of Southern Mindanao,
Philippines

*CORRESPONDENCE
Zhong Ding
dingzh@hunau.net

SPECIALTY SECTION
This article was submitted to Microbe and Virus Interactions With Plants, a section of the journal Frontiers in Microbiology

RECEIVED 23 August 2022
ACCEPTED 23 September 2022
PUBLISHED 13 October 2022

CITATION
Ye S, Yan R, Li X, Lin Y, Yang Z, Ma Y and Ding Z (2022) Biocontrol potential of *Pseudomonas rhodesiae* GC-7 against the root-knot nematode *Meloidogyne graminicola* through both antagonistic effects and induced plant resistance. *Front. Microbiol.* 13:1025727. doi: 10.3389/fmicb.2022.1025727

Biocontrol potential of *Pseudomonas rhodesiae* GC-7 against the root-knot nematode *Meloidogyne graminicola* through both antagonistic effects and induced plant resistance

Shan Ye[1,2], Rui Yan[1], Xinwen Li[3], Yufeng Lin[3], Zhuhong Yang[1,2], Yihang Ma[4] and Zhong Ding[1,2]

[1]College of Plant Protection, Hunan Agricultural University, Changsha, Hunan, China, [2]Hunan Provincial Engineering & Technology Research Center for Biopesticide and Formulation Processing, Changsha, Hunan, China, [3]Agriculture and Rural Department of Hunan Province, Plant Protection and Inspection Station, Changsha, Hunan, China, [4]Department of Chemical Metrology and Reference Materials, Hunan Institute of Metrology and Test, Changsha, Hunan, China

Plant-parasitic nematodes (PPNs) cause serious damage to agricultural production worldwide. Currently, because of a lack of effective and environmental-friendly chemical nematicides, the use of microbial nematicides has been proposed as an eco-friendly management strategy to control PPNs. A nematicidal bacterium GC-7 was originally isolated from the rice rhizosphere, and was identified as *Pseudomonas rhodesiae*. Treatment with the fermentation supernatant of GC-7 *in vitro* showed a highly lethal effect on second-stage juveniles of *Meloidogyne graminicola*, with the mortality rate increasing to 95.82% at 24h and egg hatching significantly inhibited, with a hatch inhibition rate of 60.65% at 96h. The bacterium significantly reduced the level of damage caused by *M. graminicola* infestations to rice (*Oryza sativa*) in greenhouse and field experiments. Under greenhouse conditions, the GC-7 culture efficiently reduced the gall index and nematode population in rice roots and soils, as well as inhibited nematode development compared to the control. Under field conditions, application of the GC-7 consistently showed a high biocontrol efficacy against *M. graminicola* (with a control efficiency of 58.85%) and promoted plant growth. In addition, the inoculation of GC-7 in *M. graminicola*-infested rice plant fields significantly suppressed final nematode populations in soil under natural conditions. Furthermore, activities of plant defense-related enzymes, peroxidase, polyphenol oxidase, and phenylalanine ammonia-lyase were remarkably increased in plant roots treated with GC-7 compared with roots that were challenge to *M. graminicola*. Moreover, quantitative real-time PCR analysis showed that GC-7 significantly enhanced the expression of defense genes (*PR1a*, *WRKY45*, *JaMYB*, *AOS2*, *ERF1*, and *ACS1*) related to salicylic acid, jasmonic acid, and ethylene signaling pathways in rice roots after inoculation with GC-7 at different levels. The

results indicated that GC-7 could be an effective biological component in the integrated management of *M. graminicola* infecting rice.

KEYWORDS

***Meloidogyne graminicola*, biological control, nematicidal activity, defense enzyme, systemic resistance**

Introduction

Plant-parasitic nematodes (PPNs) are one of the most destructive groups of soilborne pathogens and are responsible for annual agricultural losses estimated at USD 358.24 billion worldwide in past years (Abad et al., 2008; Abd-Elgawad, 2022). The most damaging and yield-limiting group among PPNs are the root-knot nematodes (RKNs), which have a broad host range, including many economically important crops (Abad et al., 2003; Forghani and Hajihassani, 2020). The rice RKN *Meloidogyne graminicola* is one of the most devastating pests of rice, causing substantial yield losses in rice-producing areas, especially in Asia (De Waele and Elsen, 2007; Kyndt et al., 2012; Mantelin et al., 2017). *M. graminicola* is an obligate, sedentary endoparasite that occurs across a range of different rice ecosystems. Although it cannot penetrate rice roots in flooded soils, this RKN can survive long periods in anoxic environments and rapidly reinvade roots whenever soils are drained (Bridge and Page, 1982). The infective second-stage juvenile (J2) of *M. graminicola* penetrates rice roots and induces the formation of giant cells as nutrition resource throughout its life cycle. The infection is characterized by hook-shaped galls (root-knots) mainly on the root tips (Kyndt et al., 2013). Once established in the roots, J2s become sedentary and undergo three molts to become third (J3) and fourth stages (J4) and adult stage. Females remain in the galled roots, and laying eggs inside the root. On average, *M. graminicola* complete life cycle in about 19 to 27 days during the early summer, but the period can extend by 5 to 12 days (Khan et al., 2021; Rusinque et al., 2021). *M. graminicola* is difficult to control because it has a short generation and high reproduction rate (Jang et al., 2016). At present, the main strategy for controlling PPNs relies on chemical nematicides; however, they are often highly toxic to human health and the environment, causing multi-drug resistance in nematodes (Medina-Canales et al., 2019; Rajasekharan et al., 2020). Therefore, environmentally-friendly treatments targeted towards nematodes are urgently needed.

Microorganisms have shown great potential as biological agents for controlling nematode infections. Bacteria, in particular, have received considerable attention (Abd-Elgawad, 2021; Khanna et al., 2021; Migunova and Sasanelli, 2021; Zhao et al., 2021). In recent years, studies have shown the efficacy of several bacteria to control nematodes, and the use of plant growth-promoting rhizobacteria (PGPR) is considered as the most applicable and promising strategy for PPN biocontrol (Hu et al., 2017; Zhao et al., 2018; Liu et al., 2020). Previous studies have shown that *Bacillus cereus* and *Burkholderia arboris* isolated from the plants' rhizosphere significantly induced mortality in J2s of *Meloidogyne incognita*, and markedly reduced nematode infection in host plant roots (Yin et al., 2021; Zhang et al., 2022). Similarly, *Bacillus altitudinis* can promote plant growth and showed high nematicidal activity against *Meloidogyne javanica* (Antil et al., 2022). Moreover, *Bacillus megaterium* and *Klebsiella pneumoniae* significantly inhibit the invasion, development, and reproduction of *Heterodera glycines* by inducing systemic resistance, promoting soybean growth (Liu et al., 2018; Zhou et al., 2021). So far, there are few microbial biological based nematicides, *Bacillus subtilis* and *B. amyloliquefaciens* are prevalent in the market of products used to promote plant growth and biological control (Migunova and Sasanelli, 2021). However, there was some limitations, including their relative low efficiency and high inconsistency in agricultural environments (Liang et al., 2019).

Biocontrol bacteria inhibit nematode infection *via* various mechanisms, including direct antagonisms (e.g., predation, competition for nutrients, and release of toxic metabolites) and indirect antagonisms through the induction of host systemic resistance (Bukhat et al., 2020; Forghani and Hajihassani, 2020). Typically, plants have two types of induced resistance, termed induced systemic resistance (ISR) and systemic acquired resistance (SAR) (Vallad and Goodman, 2004). ISR is activated by nonpathogenic rhizobacteria such as specific PGPR and relies on the jasmonic acid (JA)/ethylene (ET) signaling pathways in plants (Subedi et al., 2020). Generally, SAR is caused by different necrotizing pathogens and is dependent on the signaling molecule salicylic acid (SA; Conn et al., 2008). A previous study indicated that *B. cereus* Bc-cm103 activated the defense-responsive genes related to the SA, JA, and ET signaling pathways in host plants in response to *M. incognita* (Yin et al., 2021). Ghahremani et al. (2020) reported that *Bacillus firmus* I-1582 can degrade *M. incognita* eggs by inducing systemic resistance in tomato. The expression of JA and SA pathway-related genes were upregulated at different times in plants inoculated with I-1582 (Ghahremani et al., 2020). In addition, the development of inducible resistance in host plants is associated with enhanced activities of plant enzymes, including phenylalanine ammonia lyase (PAL), polyphenol oxidase (PPO), and peroxidase (POD) (Amil-Ruiz et al., 2011). Several studies show the ability of beneficial microbes to stimulate the activity of defense enzymes in host plants in response to pathogen infection (Narendra Babu et al., 2015;

Salla et al., 2016; de Oliveira et al., 2021; Yan et al., 2021). The PGPR *Bacillus* spp. suppressed *Pyricularia oryzae* infection in rice by elevating the activity of antioxidant enzymes (PAL, PPO, and POD) (Rais et al., 2017). Similarly, *Pseudomonas* spp. effectively improved the growth parameters and inhibited the nematode infection by upregulating the activities of defense enzymes (SOD, POD, and PPO) (Sharma and Sharma, 2016; Khanna et al., 2019). *Streptomyces* spp. have also been reported to markedly increase PPO activity in RKN-exposed tomato plants (Ma et al., 2017).

Despite *M. graminicola*'s widespread occurrence in Asian rice production systems, the research carried out on its biological control remains limited. To date, only a few fungi and bacteria have been reported to possess antagonistic potential against *M. graminicola* and reduce the number of root knots (Padgham and Sikora, 2007; Le et al., 2016; Haque et al., 2018; Liu et al., 2019; Yang et al., 2020; Khan et al., 2021). Identifying novel nematicidal microorganisms and investigating their underlying mechanism are necessary for the biological control of *M. graminicola* and are of vital practical and economic significance. The *Pseudomonas* is one of the most frequently studied groups of bacteria used for biological control agents. The genus *Pseudomonas* is gram-negative, rod-shaped straight or slightly curved cells with polar flagella (Sah et al., 2021). Researchers have indicated that biological control by *Pseudomonas* spp. involves a variety of mechanisms, including antibiosis, nutrient competition, and induction of host systemic resistance (Walsh et al., 2001). *Pseudomonas rhodesiae* is a strain that promotes plant growth and biocontrol of tomato and rice diseases (Romero et al., 2016; Forghani and Hajihassani, 2020). However, reports of *P. rhodesiae* antagonistic against *M. graminicola* are still lacking.

The objectives of the present study were to screen for a novel effective bacterial isolate against *M. graminicola,* and investigate the effects of *P. rhodesiae* GC-7 on *M. graminicola* eggs and J2s through *in vitro* experiments. The study also evaluated the biocontrol potential of GC-7 under greenhouse and field conditions and assessed the effect of GC-7 inoculation on plant growth and on nematode infestation and development. In addition, the expression levels of defense genes related to the SA, JA, and ET pathways and the enzymatic activities of PAL, POD, and PPO in the roots of rice induced by isolate GC-7 were examined to explore the mechanism by which GC-7 suppressed *M. graminicola*.

Materials and methods

Isolation and identification of isolate GC-7

Isolate GC-7 was isolated from the rhizosphere soil of a rice field in Changsha city, Hunan Province, China using the serial dilution technique (up to 10^{-7}-fold). A single bacterial colony was selected, streaked on beef extract-peptone medium (NA) (1% tryptone, 0.3% beef extract, 0.5% NaCl, 1.5% agar), and incubated for 24 h at 30°C to obtain the pure isolate. The bacteria were then cultured in beef extract-peptone broth (NB) at 30°C, with shaking at 200 rpm for 48 h (approximately 2×10^9 cfu/ml) for further experiments.

Routine physiological and biochemical tests of isolate GC-7 were performed according to Bergey's Manual of Determinative Bacteriology (8th Ed.). They included gram staining, the methyl red (MR) Voges-Proskauer (VP), and indole tests, testing for oxidase and catalase activity, nitrate reduction, citrate utilization, starch and gelatin hydrolysis, as well as utilization of carbon sources. The identity of GC-7 was further confirmed through 16S rRNA and *gyrB* gene sequencing. Bacterial genomic DNA was extracted using the Bacteria Genomic DNA Extraction Kit (Takara, Dalian, China) according to the manufacturer's instructions. The 16S rRNA gene fragment of this isolate was amplified *via* PCR using the universal bacterial primers 27F (AGAGTTTGAT CCTGGCTCAG) and 1492R (GGTTACCTTG TTACGACTT). The *gyrB* gene was amplified by using the primers UP-f 5′-AGCAGGGTACGGATGTGCGAGCCRTCNACRTCN GCRTCNGTCAT-3′ and UP-r 5′-GAAGTCATCATGACCG TTCTGCAYGCNGGNGGNAARTTYGA-3′ (Yamamoto and Harayama, 1995). The PCR products were sequenced by Shenggong Biotechnology Co. Ltd., Shanghai, China. The GC-7 sequence was analyzed *via* a BLASTN search in the National Center for Biotechnology Information (NCBI)[1] database. The partial 16S rRNA and *gyrB* sequences were submitted to GenBank (NCBI) to obtain the accession number. The alignment of sequences and construction of the phylogenetic tree were performed using Clustal X 2.1 (Thompson et al., 1997) and MEGA 7.0 (Kumar et al., 2016), respectively.

Cultivation of rice plants and preparation of nematode inoculum

Rice (*Oryza sativa* variety Nipponbare) seeds were obtained from the United States Department of Agriculture (GSOR-100). Seeds were germinated on wet filter paper for 4 days at 30°C, and seedlings were transferred to synthetic absorbent polymer SAP-substrate and further grown in a greenhouse at 28 ± 2°C under a 14-h photoperiod and 70–75% relative humidity (Reversat et al., 1999). Plants were watered with distilled water twice per week and fertilized once per week with 10 ml of Hoagland solution. A population of *M. graminicola* isolated from lowland rice in Pingjiang County, Hunan Province, China was maintained on susceptible *O. sativa* variety Nipponbare in a greenhouse in ChangSha. Infected roots and root galls were cut into pieces, and nematode eggs were isolated from the root galls. The egg masses were surface-sterilized with 1% sodium hypochlorite for 1 min and placed on double-layered tissue paper in a Baermann funnel containing distilled water for 3–5 days at 25°C to obtain

1 http://www.ncbi.nlm.nih.gov/

second-stage juveniles (J2s). The freshly hatched J2s were used for *in vitro* assays and pot-based experiments.

Nematicidal activity of *Pseudomonas rhodesiae* GC-7 *in vitro*

Pseudomonas rhodesiae isolate GC-7 was cultured in NB at 30°C on a shaker at 200 rpm for 48 h. The bacterial fermentation broth (2×10^9 cfu/ml) was centrifuged at 10,000 rpm for 10 min, and the crude supernatant was passed through a 0.22-μm nitrocellulose filter to obtain the cell-free supernatant. The GC-7 fermentation supernatant was diluted with sterile water to 10, 20, and 50% (v/v) concentrations. The NB medium was diluted to a concentration of 10, 20, and 50% with sterile water.

Lethal activity assay of isolate GC-7 against J2s of *Meloidogyne graminicola*

The lethal activity of isolate GC-7 to J2s of *M. graminicola* was determined. The assay of mortality was performed in a 24-well plate. Each well contained approximately 100 J2s of *M. graminicola* and 1 ml of the different concentrations of GC-7 supernatant, separately. Treatments with different concentrations of NB medium were included as the control. The plates were incubated at 28°C. After 24 h, the dead and living nematodes were counted using an inverted microscope (Olympus, Tokyo, Japan). A nematode that was malformed, immobile, or motionless even when probed with a fine needle was deemed dead (Cayrol et al., 1989). Each treatment had six replicates and was performed three times independently. Mortality was calculated according to the following formula:

$$\text{J2s mortality}(\%) = \left(\text{The number of dead J2s} \,/\, \text{The Number of total J2s}\right) \times 100$$

Inhibition of egg hatching by isolate GC-7 *in vitro*

The effect of isolate GC-7 on egg hatching was tested in 24-well plates, using a method similar to the J2 mortality test described previously. One hundred sterilized eggs were mixed with 1 ml of the 50% GC-7 fermentation supernatant. Eggs mixed in 1 ml of 50% NB medium were used as control. The plates were covered and incubated at 28°C. The number of unhatched eggs was counted using a microscope at 24 h, 48 h, 72 h, and 96 h after incubation. The experiment had six replicates and the test was repeated three times. The egg hatching rate and hatch inhibition rate were calculated using the following formulae:

$$\text{Egg hatching rate}(\%) = \left(\text{Number of hatched eggs} \,/\, \text{Total number of eggs}\right) \times 100$$

$$\begin{aligned}&\text{Hatching inhibition rate}(\%)\\ &= (\text{The number of hatched eggs in the control}\\ &\quad - \text{The number of hatched eggs}\\ &\qquad \text{in the bacteria-treated group})\\ &\quad / \text{The number of hatched eggs in the control} \times 100\end{aligned}$$

Effect of isolate GC-7 on infection by *Meloidogyne graminicola* J2s

Meloidogyne graminicola were inocubated on rice seedlings (*Oryza sativa* variety Nipponbare) treated with GC-7 to determine the direct effect of isolate GC-7 on the infectivity of nematodes. The roots of rice seedlings were immersed in a 50% GC-7 isolate fermentation culture (1×10^9 cfu/ml) for 8 h. Roots soaked in NB medium for 8 h were used as controls. Pluronic F-127 powder (Sigma Aldrich, St Louis, United States) was added to sterile water and allowed to dissolve with stirring at 4°C for 24 h. Next, treated rice seedlings were placed in F127 gel plot, then 100 μl of *M. graminicola* suspension (1,000 vigorous J2s/mL) was added surrounding to each seedling. The F127 plot was incubated in greenhouse previously described. At 5 and 14 days post inoculation (dpi), the plant roots were carefully collected and stained using the NaOCl-acid fuchsin method (Bridge and Page, 1982). The total number of nematodes inside root galls per rice seedling was counted using a stereomicroscope (Nikon, Tokyo, Japan). The number of nematodes at different life stages was determined using a stereomicroscope to calculate their ratio and analyze the effect of GC-7 on nematode development. Each treatment had four replicates and was performed three times independently.

Biocontrol efficacy of isolate GC-7 against *Meloidogyne graminicola* and the biomass changes of rice plants in the greenhouse

A pot-based validation experiment was conducted under greenhouse conditions at Hunan Agricultural University, China. Bacteria was prepared as described above. The bacterial fermentation broth was cultured to approximately 2×10^9 cfu/ml, then diluted to obtain concentrations of 50% (1×10^9 cfu/ml), 20% (4×10^8 cfu/ml), and 10% (2×10^8 cfu/ml). Seeds were treated as described previously. Five two-leaf stage rice seedings were transplanted into sterile soil in each pot (15 cm in diameter and 10 cm in height), it is about 1 kg of soil per pot. Different concentrations of the bacterial fermentation broth (40 ml each) and fluopyram (0.33 g a.i./L, Lufta, Bayer Crop Science, China) were added to each pot. An equal amount of sterile water was added to the pots as a control. Two days after inoculation with the bacterial fermentation broth, 2 ml of *M. graminicola* suspension (750 vigorous J2s/mL) was drenched into each pot. All pots were arranged in a completely randomized block design on a bench in

the greenhouse, and each treatment consisted of four replicates. The rice plants were uprooted and washed free of adhering soil 21 days post inoculation. The number of root galls on the rice plants were examined to assess nematode penetration. The disease index of the roots was confirmed using the 0–10 scale described by Bridge and Page (Bridge and Page, 1980). Gall indices and biocontrol efficacy were calculated as follows:

$$\begin{aligned}&\text{Gall index}(\%)\\&=[\sum(\text{The number of diseased plants in each grade})\\&\quad/(\text{Total number of plants investigated}\\&\quad\times\text{The highest grade})]\times 100\end{aligned}$$

$$\begin{aligned}&\text{Bio - control efficiency}(\%)\\&=(\text{Gall index in the control}-\text{Gall index in the treated group})\\&\quad/(\text{Gall index in the control})\times 100\end{aligned}$$

Soil samples from each pot were examined to obtain the actual frequency and relative number of nematodes and eggs in the soil. The soil was mixed, and the sucrose solution-elutriation-centrifugation method was used to extract soil nematodes and eggs from approximately 100 g of fresh soil (Li et al., 2016). The total number of nematodes and eggs in each soil sample was counted under a dissecting microscope, and a statistical analysis was performed. Biomass values, including total length, root length, and fresh weight of the entire plants and roots, were measured to survey the promotion of plant growth.

Biocontrol efficiency of isolate GC-7 against *Meloidogyne graminicola* in the field

Field trials were carried out in a field infested with *M. graminicola* in Pingjiang County City, Hunan Province, China (113.67 E, 28.57 N) in 2021. The soil in the field was a sandy loam containing 55.6% sand, 9.2% silt and 36.4% clay, with a pH of 5.0, a water holding capacity of 30%, and an organic matter content of 1.0%. The initial *M. graminicola* population consisted of 393 ± 32 J2/100g soil. The experiment consisted of three treatments: fermentation broth GC-7 (2×10^9 cfu/ml), 41.7% fluopyram SC (250.2 g a.i/ha; Lufta, Bayer Crop Science, China), and water (as control). Sprouted seeds of the rice variety HuangHuaZhan were sown in the fields and irrigated with different treatments (750 l/ha). The experiment was set up in a completely randomized block design, and each treatment was applied to four replicated plots 5.0 m long and 3.0 m wide. The trial was fertilized with 375 kg/ha carbamide and 750 kg/ha diammonium phosphate 2 days before sowing, and with 75 kg/ha carbamide and 75 kg/ha potassium chloride at the middle tillering stage. After 60 days, 15 seedlings were randomly selected (using the Z-shaped sampling method) from each plot, a total of 60 seedlings were obtained from each treatment.

The rice plants were observed and disease index of the roots was recorded as described above. The plants were also used to record the effect of the GC-7 isolate on the following growth parameters: shoot and root length (cm), shoot and root fresh weight (g), and total chlorophyll content (Konica Minolta, Inc., SPAD-502 Plus, Japan). At the time of harvest (4 months after planting), the grain yield was recorded and the rhizosphere soil samples randomly selected from each plot were returned to the laboratory. The nematodes and eggs in each 100 g soil sample were isolated and counted as described above.

Resistance-related enzymes assays

Rice seedlings were treated with different concentrations of isolate GC-7 and grown as described for the pot-based experiment to detect resistance-related enzymes. The experiment consisted of five treatments: rice seedlings treated with (1) sterile water (CK), (2) sterile water and inoculated with *M. graminicola* J2 (J2), (3) 50% GC-7 and inoculated with *M. graminicola* (50% GC-7 + J2), (4) 20% GC-7 and inoculated with *M. graminicola* (20% GC-7 + J2), and (5) 10% GC-7 and inoculated with *M. graminicola* (10% GC-7 + J2).

Defense-related enzymes, including PAL, PPO, and POD, were quantified from rice plants grown under pot conditions after 2 days, 4 days, 6 days, and 8 days of nematode inoculation. Plants were carefully uprooted, causing no damage to root tissues. The activities of PAL, PPO, and POD were extracted and measured from fresh rice root samples using commercial assay kits (Nanjing Jiancheng Bioengineering Institute, China).

PPO activity was measured using the assay kit based on the principle that PPO can catalyze quinone production from the substrate phenol, which is characterized by light absorption at 420 nm. PPO activity was calculated by the decrease in absorbance at 420 nm; one unit (U) of PPO activity was defined as a change in absorbance by 0.01 for 1 g fresh weight (FW) per minute in the 1-mL reaction system.

PAL catalyzes the decomposition of L-phenylalanine into trans-cinnamic acid and ammonia. The maximum absorption value for trans-cinnamic acid was obtained at 290 nm, and PAL activity was calculated by measuring the change in absorbance value at 290 nm. One unit of PAL activity was defined as a change in absorbance by 0.1 for 1 g FW per minute in the 1-mL reaction system. The obtained values for absorbance were converted into enzyme activity according to the formula used for assay kits.

POD activity was measured based on the change of absorbance at 420 nm by catalyzing H_2O_2. One unit was defined as the amount of enzyme which was catalyzed and generated 1 μg substrate by 1 g fresh weight tissues in the reaction system at 37°C. POD activity was calculated as the formula according to POD assay kit. The

enzymes were expressed as U/g FW, and the experiment was performed in three replicates.

RNA extraction and gene expression analysis

Rice seedlings were treated with isolate GC-7 and grown as previously described, with sterile water used as control. The seedlings were carefully drenched with 40 ml of *P. rhodesiae* GC-7 (1×10^9 cfu/ml). Each individual pot was inoculated with approximately 1,500 freshly hatched *M. graminicola* J2s 2 days later and it is about 1 kg of soil per pot. The experiment consisted of four treatments: rice seedlings treated with (1) sterile water as the non-treated control (CK), (2) sterile water and inoculated with J2 (J2), (3) GC-7 (GC-7), and (4) GC-7 and inoculated with *M. graminicola* (GC-7 + J2). To measure the transcript levels of defense-related genes in real time, whole rice roots were collected at 1 d and 4 d after nematode inoculation, frozen immediately in liquid nitrogen, and stored at −80°C until further use. Total RNA was extracted from the rice roots using the MiniBEST Universal RNA Extraction kit (TaKaRa, Dalian, China). Total RNA from each sample (1 μg) was reverse-transcribed using the PrimeScript RT Reagent kit (TaKaRa, Dalian, China). Quantitative real-time RT-PCR assays were performed using gene-specific primers for the genes Pathogenesis-related 1a (*PR1a*), WRKY TF 45 (*WRKY45*), Allene oxide synthase2 (*AOS2),* JA-inducible Myb TF (*JaMYB*), Aminocyclopropane-1-carboxylic acid synthase 1 (*ACS1*) and Ethylene-responsive factor 1 (*ERF1*) (Takaki et al., 2015; Leonetti et al., 2017; Salman et al., 2022), described in Supplementary Table S1. Quantitative real-time PCR (qRT-PCR) was performed in a CFX Connect Real-Time PCR Detection System (Bio-Rad, California, United States) using a SYBR green I quantitative PCR master mix (TaKaRa, Dalian, China). The reaction conditions were 95°C for 30 s followed by 40 cycles at 95°C for 5 s, and 60°C for 30 s. A melting curve analysis was performed after 40 cycles to confirm that a single product was present for each reaction. qRT-PCR was performed on three biological replicates and each reaction was replicated three times. Expression of the rice gene actin was used as an internal reference gene, and the data were quantified using the $2^{-\Delta\Delta ct}$ method (Livak and Schmittgen, 2001).

Statistical analysis

Statistical analysis was performed with SPSS Statistics version 20.0.0 (International Business Machines Corporation, United States). Both data normality and homogeneity of variances were assessed. Ninety-five percent fiducial limits of the experiment data were determined *via* probit analysis. For multiple-group comparison, ANOVA was performed followed by Tukey's multiple comparison test. Statistical differences were considered significant at $p \leq 0.05$. Different lowercase letters indicate significant differences between treatments ($p < 0.05$).

Results

Isolation and characterization of bacterium *Pseudomonas rhodesiae* isolate GC-7

GC-7 colonies grown on nutrient agar were round, white, and non-transparent, with a smooth surface. The bacterium had Gram-negative staining reaction with a rod-shaped structure. The detailed morphological and physiological characteristics are summarized in Table 1.

Furthermore, identification was confirmed using 16S rRNA and *gryB* analysis. The nucleotide sequences of 16S rRNA (accession number OP160002.1) and *gryB* (accession number OP429596) deposited in GenBank of NCBI. According to a phylogenetic tree constructed using the neighbor-joining method, isolate GC-7 was found most closely related to *P. rhodesiae* (Figure 1). Based on the phylogenetic trees and morphological features, isolate GC-7 was identified as *P. rhodesiae* and was deposited at the China Center for Type Culture Collection (CCTCC) under accession number CCTCC M 2020346.

Evaluation of the nematicidal activity of isolate GC-7 *in vitro*

To determine whether *P. rhodesiae* GC-7 has nematicidal activity against *M. graminicola*, a mortality assay was carried out using a direct contact method *in vitro*. Following incubation in a suspension of GC-7 for 24 h, all treatments at different concentrations exhibited significant larvicidal potential. The collected mortality at concentrations of 50, 20, and 10% GC-7 was 95.82, 87.86, and 58.79%, respectively, which were significantly

TABLE 1 Morphological and physiological characteristics of isolate GC-7.

Characteristics	Reaction	Characteristics	Reaction
Colony color	White	Citrate utilization	+
shape	Rod shaped	Indole experiment	−
Gram-stain	−	Hydrolysis of starch	+
Oxidase activity	+	Decomposition of casein	+
Catalase activity	+	Gelatin liquefaction	+
Nitrate reduction	+	Carbohydrate utilization	
Methyl red test	+	D-Glucose	+
Voges-Proskauer test	−	Lactose	−
Anaerobic growth	−	Sucrose	+

+, positive reaction; −, negative reaction.

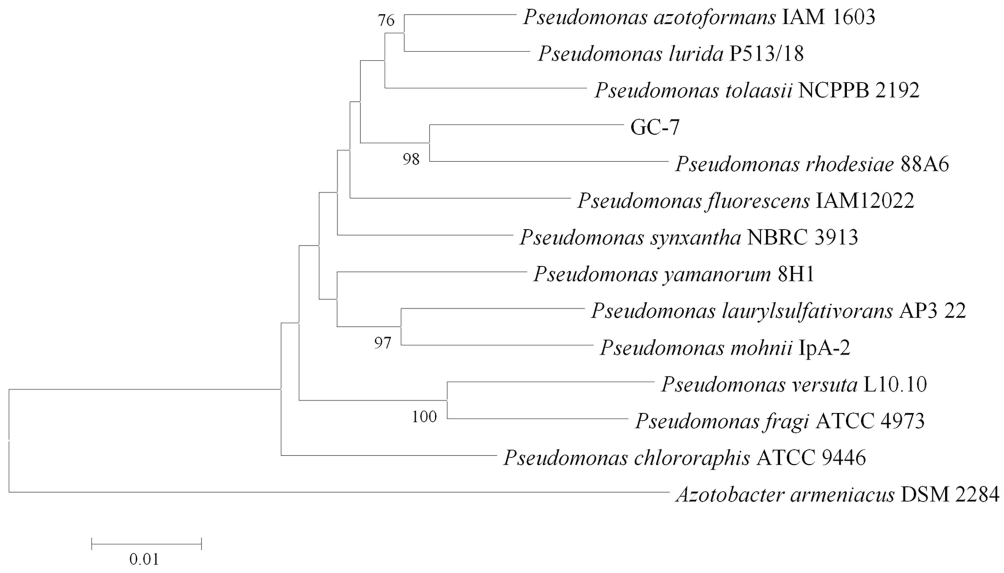

FIGURE 1
Phylogenetic tree of isolate GC-7 based on 16S rRNA and *gyrB* gene sequences. The neighbor-joining method was used to construct the tree, which shows the relationships between isolate GC-7 and closely related species. Only values greater than 50% are provided. The scale bar indicates 0.01 nucleotide substitutions per nucleotide position. The numbers at the nodes represent percentages after 1,000 bootstrap replicates.

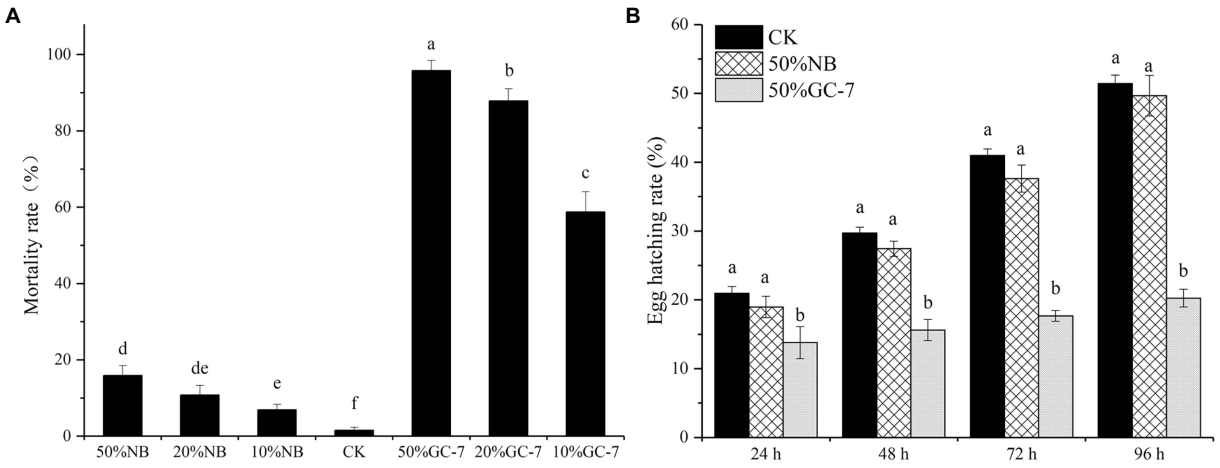

FIGURE 2
Evaluation of the nematicidal activity of *Pseudomonas rhodesiae* GC-7 *in vitro*. **(A)** Effects of isolate GC-7 on second stage juveniles (J2s) mortality of *M. graminicola in vitro*. Mortality rates were assessed by *M. graminicola* J2 incubated in fermentation cell-free supernatant of GC-7 at different concentrations in 24-well plates at 28°C for 24h. J2 suspension mixed with different concentrations of NB medium, and sterilized water was used as control (CK). **(B)** The egg hatching rate of *M. graminicola* exposed to *Pseudomonas* sp. GC-7 cell-free supernatant *in vitro*. The egg hatching rate was evaluated by treating approximately 100 eggs with 50% GC-7 supernatant for 24h, 48h, 72h, and 96h at 28°C. The negative control was sterilized water. The results are from three independent experiments, each containing four replicates. The data were analyzed by Tukey's multiple range test ($p< 0.05$) using SPSS software. Error bars represent standard deviation, different letters represent a significant difference at $p< 0.05$.

higher than that in the controls (Figure 2A). The results indicated that the cell-free culture filtrate of *P. rhodesiae* GC-7 was highly antagonistic to *M. graminicola*.

Moreover, the effect of GC-7 on *M. graminicola* egg hatching is shown in Figure 2B. The GC-7 suspension significantly reduced nematode egg hatching compared with CK at each stage of incubation. After incubation for 48 h, percentage egg hatching in the GC-7-treated and control sample was 15.61 and 29.73%, respectively, and the hatch inhibition rate was up to 47.48% in GC-7 compared to the control treatment (Figure 2B). The hatch

inhibition rate of isolate GC-7 was 60.65% at 96 h after treatment. These results indicated that isolate GC-7 could significantly inhibit the hatching of *M. graminicola* eggs.

Effect of isolate GC-7 on infection by *Meloidogyne graminicola* J2s

The nematode penetration recorded at 5 and 14 days post inoculation (dpi) is shown in Figure 3. Nematode observation in roots after staining showed that the total number of nematodes was significantly lower in GC-7-treated plants compared to the untreated controls. The reduction in the number of nematodes inside GC-7-treated roots was 64.58 and 48.50% at 5 dpi and 14 dpi, respectively (Figure 3A).

The development of nematodes in GC-7-treated plants was slightly delayed compared with that in untreated control plants. At 5 dpi, the percentage of third-stage juvenile (J3) in GC-7-treated plants (64.36%) was significantly lower than that in untreated plants (83.93%). At 14 dpi, the ratio of fourth-stage juvenile (J4) and adult females was higher in untreated plants (77.01%) than in GC-7-treated roots (58.42%). By contrast, the percentage of J3s was lower in untreated plants (22.99%) than in GC-7-treated plants (41.58%) (Figures 3B–D). These data showed that isolate GC-7 not only lowered infection by *M. graminicola* but also slightly inhibited nematode development in rice roots.

Biocontrol of *Meloidogyne graminicola* in pot-based experiments

Pot-based experiments were carried out to further evaluate the biocontrol efficiency of isolate GC-7 *in vivo* using a soil drenching method. Here, *M. graminicola* infection was severe, forming numerous large root galls on the roots of control rice plants. By contrast, fewer and smaller galls were observed on rice roots following treatment with GC-7 fermentation broth. The average root gall index of the control group was 53.56, and the average root gall index with all dilutions (50, 20, 10%) of isolate GC-7 were 23.44, 27.81, and 29.36, respectively (Figure 4A). All concentrations of the GC-7 fermentation broth showed a high control effect on *M. graminicola* with a control efficiency of 45.19 to 56.23% (Figure 4B), However, application of different concentrations of GC-7 did not show dose effect on gall index and control efficacy. In addition, the final nematode density in soil treated with GC-7 was also significantly lower than that of the CK. Inhibition rates for treatment with 20 and 10% GC-7 fermentation broth reaching 75.84 and 82.84%, respectively, higher than treatment with fluopyram (70.42%; Figure 4C). Moreover, the number of eggs in soil treated with isolate GC-7 was lower than in the control soil, with inhibition rates reaching 72.52 to 78.18% (Figure 4D).

In addition, the effect of different dilutions of GC-7 fermentation broth on the growth of rice parasitized by *M. graminicola* showed a significant improvement in all plant growth parameters compared to the control (Table 2). Rice treated with 50% GC-7 showed the highest average total length (53.83 cm), root length (15.22 cm), and total fresh weight (1.70 g), corresponding to increases of 17.89, 22.41, and 68.98%, respectively, above control treatments. The control samples exhibited the lowest plant growth.

Efficacy in controlling nematodes in the field experiment

The field experiment was carried out using the GC-7 fermentation broth. The average root gall index corresponding to the GC-7 treatment against *M. graminicola* was 18.63 (Table 3), which was significantly lower than that of the control (45.27). GC-7 culture showed a high control effect on *M. graminicola* with a control efficiency of 58.85%. In addition, the inoculation of isolate GC-7 in *M. graminicola* infested rice fields significantly suppressed the nematode and egg populations under natural conditions (Figure 5). The final nematode population in 100 g of GC-7-treated soil and chemical nematicide fluopyram-treated soil was much lower than CK soil (Figure 5A). The number of eggs in GC-7-treated soil reduced by 77.67% compared to CK soil (Figure 5B). Concurrently, the application of GC-7 displayed a better effect on the promotion of root weight and stem base width than CK and fluopyram. At harvest, the rice yield increased by 31.98% in GC-7 treated plants compared with control (Table 3).

Enhancement of resistance-related enzyme activities

The quantitative changes in the defense-related enzyme activities of POD, PPO, and PAL in rice roots were investigated. Supplementation of GC-7 resulted in significant enhancement of the PAL activities in nematode-infected plants compared to CK plants and challenged with the nematode-treated (J2) plants at all times. The highest PAL activity was recorded in plants treated with 50% GC-7 + J2 at 2 dpi, which was elevated by 4.33-fold and 2.02-fold compared to CK and nematode-treated plants, respectively (Figure 6A). Rice plants inoculated with nematodes only had slightly higher PAL activity compared to the untreated control. PPO activity from 2 dpi was induced by the GC-7 fermentation broth and plants treated with almost all concentrations of bacteria showed the highest levels of PPO activity at 4 dpi. The maximum level of PPO activity was observed in plants treated with a 20% dilution of GC-7 (20% GC + J2), increasing 6.34-fold and 3.23-fold compared to CK and nematode-treated plants, respectively (Figure 6B). Untreated control plants showed the lowest enzyme activity among all treatments. A similar pattern of increased POD activity was found in bacterized plants

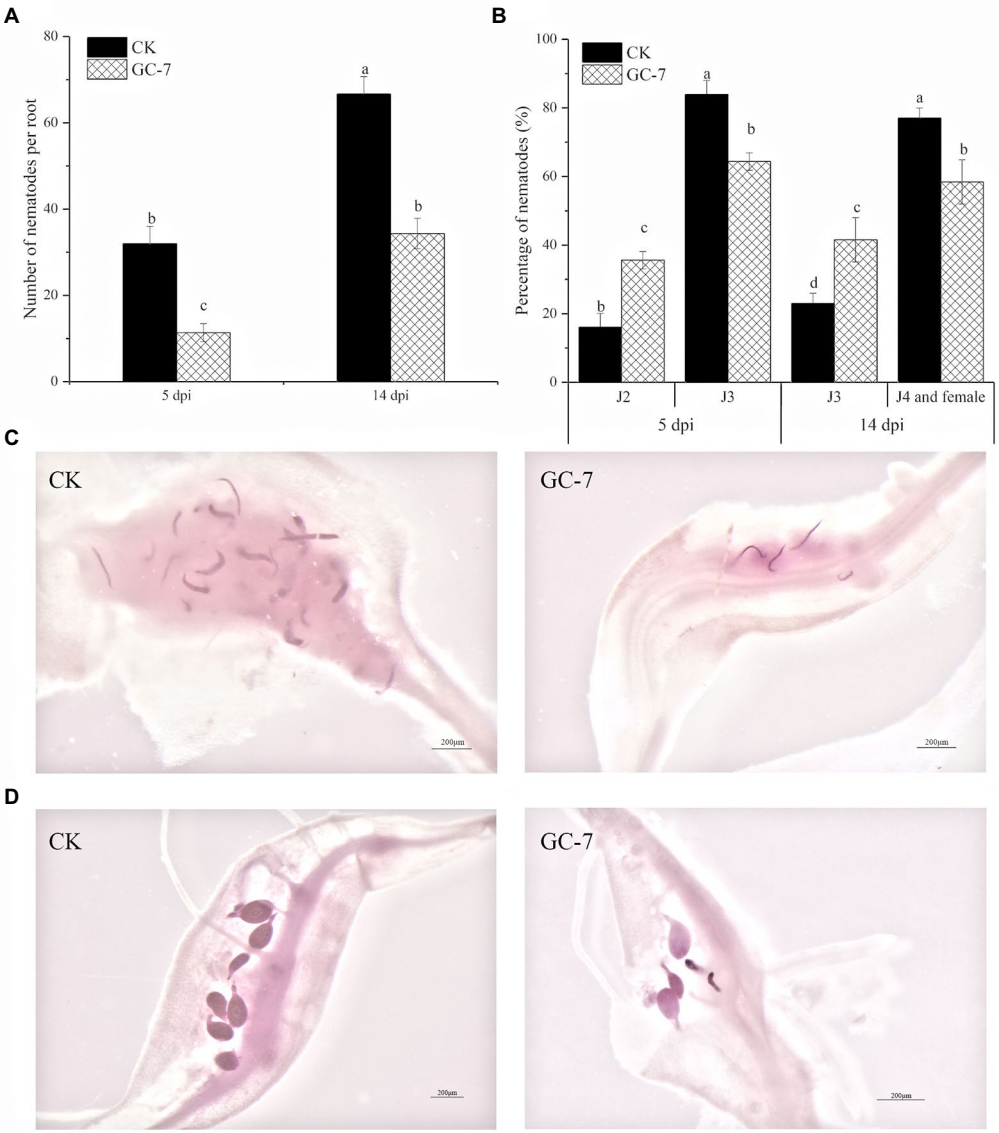

FIGURE 3
Infection and development of *M. graminicola* inside rice roots at 5 dpi and 14 dpi. **(A)** Penetration of *M. graminicola* in GC-7- and NB medium-treated (CK) rice roots. **(B)** The ratio of nematodes in rice roots at different developmental stages at 5 dpi and 14 dpi. **(C)** Nematodes in CK and GC-7-treated plants were photographed at 5 dpi. **(D)** Nematodes in CK and GC-7-treated plants were photographed at 14 dpi. The roots of rice seedlings were immersed in a 50% GC-7 strain fermentation culture (1x10^{9}cfu/ml) for 8h, and roots soaked in 50% NB medium for 8h were used as controls. Each plant was inoculated with about 100 J2s. Scale bar=200μm. The bars in the different graphs represent the mean±SE of data from three independent biological replicates, each containing eight individual plants. Different letters indicate statistically significant differences (Tukey's multiple range test at $p \leq 0.05$).

treated with the challenge inoculation. Plants treated with each concentration of GC-7 + J2 expressed higher POD activity compared to untreated control and nematode-infected (J2) plants (Figure 6C). The enzyme activities peaked at approximately 4 dpi, then slowly decreased. The highest activity was observed in plants treated with 50% GC-7 + J2 at 4 dpi, which increased by 4.31-fold and 2.27-fold compared to CK and nematode-treated plants, respectively.

Transcriptional levels of defense-related genes

We studied the relative expression levels of defense linked genes *PR1a* and *WRKY45* associated with the SA pathway, ET responsive transacting factors *ERF1* and *ACS1*, as well as JA-dependent gene markers *JaMYB* and *AOS2*, to obtain an insight into the GC-7-induced rice defense response against

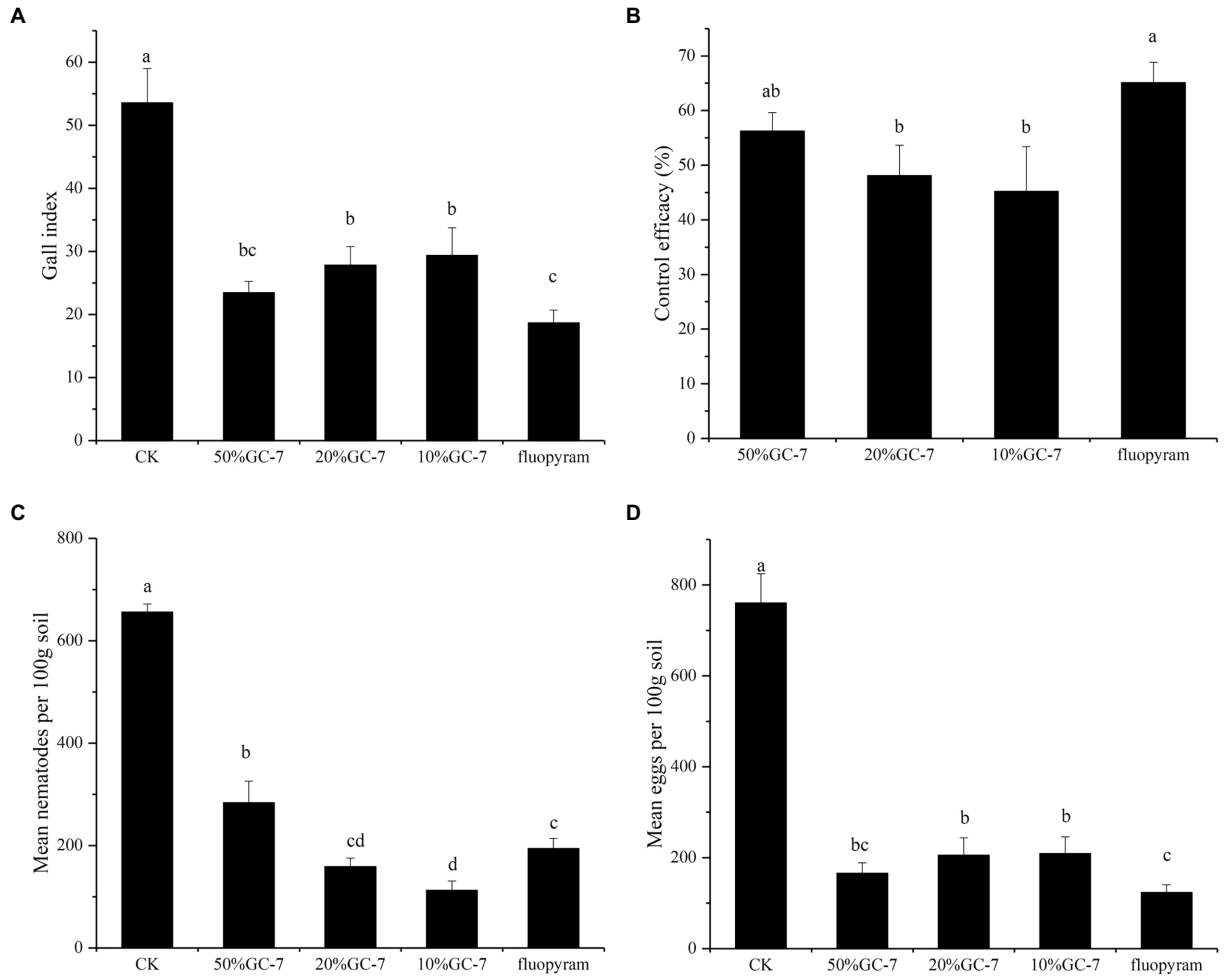

FIGURE 4
Biocontrol of *M. graminicola* in the pot-based experiment. **(A)** Gall index of GC-7 against *M. graminicola* in the pot-based experiment. **(B)** The control efficacy in different treatments. **(C)** Effects of the application of GC-7 on the final nematodes in soil. **(D)** Suppression of *M. graminicola* eggs by GC-7 in soil of pot-based experiment under greenhouse conditions. Each pot contains five two-leaf stage rice seedings, fourty millilitre of the different concentrations of the bacterial fermentation broth was applied as irrigation to each pot. The control were treated with sterilized water or fluopyram. Two days after inoculation with the bacterial fermentation broth, 2ml of *M. graminicola* suspension (750 vigorous J2s/mL) was drenched into each pot. Vertical bars represent standard deviation of the mean values. Tukey's multiple range test was employed to test for significant differences between treatments at $p<0.05$. Different lowercase letters indicate significant difference between treatments ($p<0.05$).

M. graminicola. The relative expression level of *PR1a* at 1 dpi decreased by 33.48% in GC-7-treated plants, 30.28% in GC-7 + J2 plants, and 12.09% in J2 plants, compared with that in CK plants. However, at 4 dpi, a significant upregulation of *PR1a* was observed for all treatments. The highest relative expression level (3.48-fold higher than in the control) was reported in plants treated with GC-7, followed by GC-7 + J2 and J2, with expression levels that were 2.12- and 1.43-fold higher, respectively (Figure 7A). A significant upregulation of *WRKY45* was observed in all treated plants at 1 dpi compared to the control. However, no differences were observed in plants treated with GC-7 and GC-7 + J2 compared with CK plants at 4 dpi (Figure 7B).

At 1 dpi, significant increases in the relative expression levels of the *JaMYB* and *AOS2* were observed in plants treated with GC-7 and GC-7 + J2 compared with control and J2-treated plants. The expression level of *JaMYB* was most notably higher in GC-7-treated plants (5.75-fold), followed by GC-7 + J2- (3.03-fold) and J2- (1.15-fold) treated plants, than in control plants (Figure 7C). In a similar pattern, *AOS2* expression level was upregulated in plants from all treatments compared to the control at 1 dpi. The highest transcriptional level was observed with GC-7 (4.59-fold), while the levels for the GC-7 + J2 and J2 treatments were 2.69- and 0.89-fold higher, respectively. At 4 dpi, the JA gene expression level in plants from the GC-7 and GC-7 + J2 treatments was slightly higher than in the CK plants (Figure 7D).

A significantly and consistently enhanced transcription of *ERF1* was induced by GC-7 in GC-7 + J2 at 1 dpi and 4 dpi, compared with that induced by the CK and J2 treatments. By contrast, the transcript level in J2-treated plants was repressed at 4 dpi compared to CK plants (Figure 7E). Transcription of *ACS1*

in plants treated with GC-7, GC-7 + J2, and J2 was 2.14-fold, 1.73-fold, and 0.87-fold higher, respectively, than the control at 1 dpi (Figure 7F).

Discussion

RKNs are a severe threat to world agriculture. Many nematicidal biocontrol agents have been discovered from microorganisms, and the application of bacteria, especially PGPR, have received increasing attention (Hu et al., 2017; Liang et al., 2019). However, the microorganisms used for controlling the rice RKN *M. graminicola* are limited. In the present study, the novel *P. rhodesiae* isolate GC-7 was isolated from the rhizosphere soil of rice plants. This isolate could efficiently kill *M. graminicola* J2s directly, as well as suppress egg hatching *in vitro*. Microorganisms can inhibit growth of PPNs through diverse processes. Production of various antagonistic compounds with inhibiting effects against PPNs is a direct mode of action. Many bacteria produce nematicidal bioactive hydrolytic enzymes, antibiotics and toxins that directly kill nematodes or inhibit proliferation (Yang et al., 2013; Mnif and Ghribi, 2015; Migunova and Sasanelli, 2021). In addition, some bacterial strains also produce nematicidal volatile organic compounds (VOC) against *Meloidogyne* (Zhao et al., 2018). The underlying mechanisms by which GC-7 restrains *M. graminicola* can be complicated. Further research is needed to determine primary nematicidal compounds of *P. rhodesiae* GC-7. Greenhouse and field tests demonstrated that GC-7 effectively controlled *M. graminicola* and promoted rice plant growth. The biocontrol effects of GC-7 might be because the isolate adheres to the rhizospheric zone and increases plant biomass to secrete stronger substances that kill nematode J2s and inhibit egg hatching (Khanna et al., 2019; Zhao et al., 2021). In addition, our data demonstrated a significant reduction in *M. graminicola* penetration in rice plants and their population densities in GC-7-treated soil. Moreover, nematode development was inhibited in GC-7-treated plants compared with that in non-treated plants. These results are consistent with previous reports of PGPR and other beneficial microbes (Liu et al., 2018, 2019; Zhou et al., 2021). The number of egg masses was considered as the infective ability of the nematode as it shows the number of J2s that were able to penetrate and infect the root tissue and develop into egg-laying females (Ghareeb et al., 2020). Here, the egg populations in soil treated with GC-7 under greenhouse and natural conditions were significantly decreased compared with control. Therefore, our study aligns with the three key principles of biological control proposed by Stenberg et al. (2021), and indicates that *P. rhodesiae* isolate GC-7 could be used as a potential biological nematicide against *M. graminicola*.

Several rhizobacteria can enhance plant resistance against pathogens by activating defense-related enzymes (Chen et al., 2009; Fatma et al., 2014; Narendra Babu et al., 2015; Salla et al., 2016; Rais et al., 2017). PAL has been reported to be involved in plant defense mechanisms as it is the first enzyme in phenylpropanoid metabolism and related to the biosynthesis of phenolics and SA (Jain and Choudhary, 2014; Di Lelio et al., 2021). PPO plays an important role in phenol metabolism related to the synthesis of lignin and quinone compounds, which can inhibit the invasion of pests and diseases (Ju et al., 2013). POD activity is important in lignin accumulation and ROS production, both important components of a plant's active defense response against pathogens (de Oliveira et al., 2021). Our data indicated that, following *M. graminicola* infection, POD, PPO, and PAL activities showed more rapid and greater increases in the rice roots of GC-7-treated plants than in the controls, further revealing the mechanism underlying nematode control by GC-7. The highest PAL activity in GC-7 fermentation broth-treated plants were observed at 2 dpi, whereas POD and PPO activities peaked at 4 dpi. The results suggest that isolate GC-7 can significantly enhance such defense enzymes and probably other defense compounds, leading to systemic resistance in plants. These findings are consistent with those of previous studies, which showed increasing

TABLE 2 Effects of biocontrol agents (isolate GC-7) on the growth parameters of rice plants infected with *Meloidogyne graminicola* in pot-based experiments.

Treatments	Total length (cm)	Root length (cm)	Total fresh weight (g)
GC-7 (50%)	53.83 ± 2.65a	15.22 ± 0.60a	1.70 ± 0.16ab
GC-7 (20%)	52.63 ± 2.47a	14.74 ± 0.58a	1.59 ± 0.10bc
GC-7 (10%)	49.86 ± 1.60ab	14.21 ± 0.37a	1.44 ± 0.08c
CK	45.67 ± 1.55b	12.43 ± 0.90b	1.01 ± 0.19d
Fluopyram	53.27 ± 2.74a	15.39 ± 0.49a	1.89 ± 0.05a

The data are mean ± SE from four replicates per treatment. Means followed by the same letter in the same column are not considered statistically different following Tukey's multiple range test ($p < 0.05$).

TABLE 3 Effects of biocontrol agents (isolate GC-7) on the growth parameters and protection of rice plants infected with *M. graminicola* under natural field conditions in 2021.

Treatments	Shoot length (cm)	Root length (cm)	Shoot fresh weight (g)	Root fresh weight (g)	Stem base width (cm)	Chlorophyll (SPAD)	Gall index	Control effect (%)	Yield(kg/ha)
CK	34.06 ± 0.94a	12.30 ± 0.10c	3.38 ± 0.20b	2.15 ± 0.17c	0.47 ± 0.03c	38.56 ± 0.59b	45.27 ± 6.41a	–	4,384 ± 863b
Fluopyram	41.10 ± 2.05a	15.20 ± 0.27a	8.85 ± 0.66a	3.69 ± 0.09b	0.53 ± 0.03b	41.03 ± 0.45a	12.34 ± 3.49b	72.73 ± 7.71a	6,084 ± 606a
GC-7	39.33 ± 1.48b	13.40 ± 0.44b	8.72 ± 0.40a	4.07 ± 0.19a	0.61 ± 0.05a	40.83 ± 0.66a	18.63 ± 3.25b	58.85 ± 7.20b	5,787 ± 462a

Data are mean ± SE for four replicates per treatment. Means followed by the same letter in the same column are not considered statistically different following Tukey's multiple range test ($p < 0.05$).

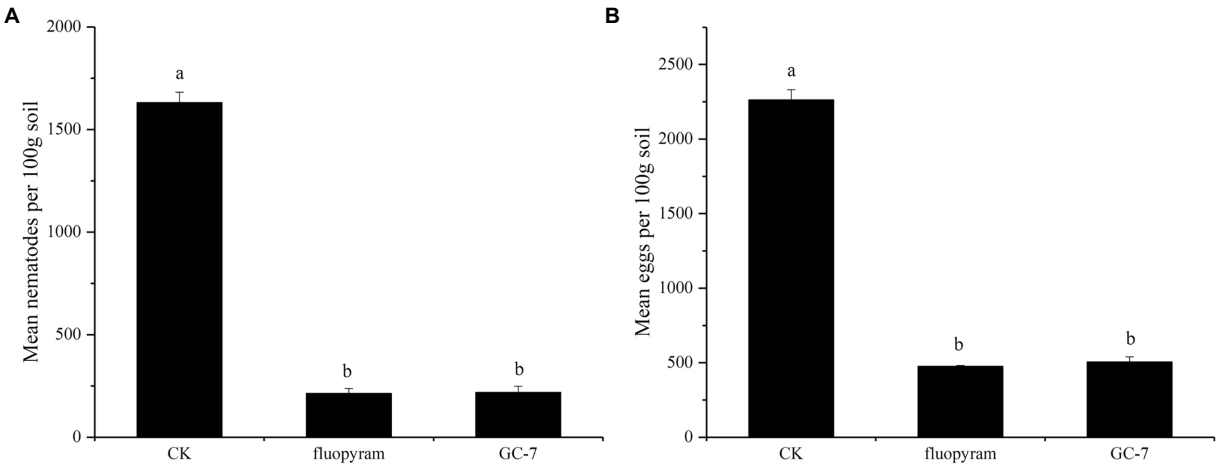

FIGURE 5
Biocontrol of *M. graminicola* in the field. **(A)** GC-7 isolate decreased the nematodes in soil. **(B)** Suppression of *M. graminicola* eggs by GC-7 in soil under field conditions. At the time of harvest (4months after planting), the nematodes and eggs in each 100g soil sample were isolated and counted. Vertical bars represent standard deviation of the mean values. Tukey's multiple range test was employed to test for significant differences between treatments at $p<0.05$. Different lowercase letters indicate significant difference between treatments ($p<0.05$).

levels of defense enzymes during the early stages of defense, thus playing a crucial role in plant host resistance (Jain and Choudhary, 2014; Kurth et al., 2014). In addition, PAL, PPO, and POD activities in non-bacterized plants increased slightly after the nematode challenge, indicating that some increased enzyme activity is a natural response of infected plants susceptible to nematode attack. This finding is similar to those of previous studies, in which plants subjected to pathogen control showed higher enzyme activities of PAL, POX, and PPO than the untreated control (Jetiyanon, 2007; Chen et al., 2009). However, the level of the increase was too low to overcome nematode invasion.

The major defense mechanisms of plants are regulated through SA, JA, or ET signaling pathways (Shoresh et al., 2005; Rasool et al., 2021). Certain related defense genes are activated by various factors, consequently inducing systemic resistance against disease. ISR often relies on pathways regulated by JA/ET. *JaMYB* and *AOS2* are marker genes for JA-dependent signaling pathways, whereas *ERF1* and *ACS1* are markers of the ET signaling pathway (Leonetti et al., 2017; Salman et al., 2022). Previous studies on rice have also shown that the exogenous application of plant hormones and antioxidants induces systemic defense against *M. graminicola,* and that the JA pathway plays a pivotal role in the induction of defense against RKN (Nahar et al., 2011; Singh et al., 2020; Chavan et al., 2022). Conversely, abscisic acid (ABA), brassinosteroids (BRs), gibberellic acid, and strigolactones promote the susceptibility of rice to *M. graminicola* infection by interacting antagonistically with the JA pathway (Nahar et al., 2012; Yimer et al., 2018; Lahari et al., 2019). Rhizobacteria may act against nematodes through ISR in plants (Ryan et al., 2015; Migunova and Sasanelli, 2021); however, little is known about the role of bacteria in the interaction between rice plants and *M. graminicola.* We studied the influence of isolate GC-7 on defense-associated gene expression in rice plants either challenged with *M. graminicola* or free from infection. The qRT-PCR results indicated that rice seedlings treated with isolate GC-7 only greatly enhanced the subsequent expression of *JaMYB*, *AOS2, ERF1*, and *ACS1* (especially JA signaling pathway genes *JaMYB* and *AOS2*) at 1 dpi. The JA pathway, in particular, may play an important role in inducing defense against *M. graminicola*. Moreover, nematode infection provoked a marked increase of these gene transcript levels in the roots of plants pre-treated with isolate GC-7 compared with uninoculated (J2-treated) plants at 1 dpi. *JaMYB* and *ERF1* transcript levels remain high, whereas *AOS2* transcript levels show a slight increase at 4 dpi. The high expression of defense-related genes in GC-7 treated roots suggests that rice seedlings respond rapidly to *M. graminicola* infection, indicating GC-7 ISR and the JA- and ET- dependent ISR pathways are involved in root resistance to nematode infection by isolate GC-7 at an early stage.

PR1a and *WRKY45* are markers of the SA signaling pathway and are major characteristic proteins of SAR (Salman et al., 2022). *WRKY45* and *PR1a* expression were increased in GC-7- and J2 + GC-7-treated plants compared to control and J2-treated plants at 1 dpi and 4 dpi, respectively, indicating that the defense response of rice to *M. graminicola* mediated by the SA signaling pathway was also activated. Our result is similar to a previous finding, where certain PGPRs, including *Bacillus* spp., *Pseudomonas* spp., and fungi such as *Trichoderma*, can activate SAR and facilitate the expression of characteristic *SAR* genes in plants, thereby enhancing plant systemic resistance (Subedi et al., 2020; Rasool et al., 2021; TariqJaveed et al., 2021). Previous reports have shown that *Trichoderma* could reduce *Meloidogyne* by triggering host defense, which was attributed first to SA-regulated defense that limited the root invasion of nematodes, then to enhanced JA-regulated defense (Martinez-Medina et al., 2017; Medeiros et al., 2017). Similarly, it has been reported that

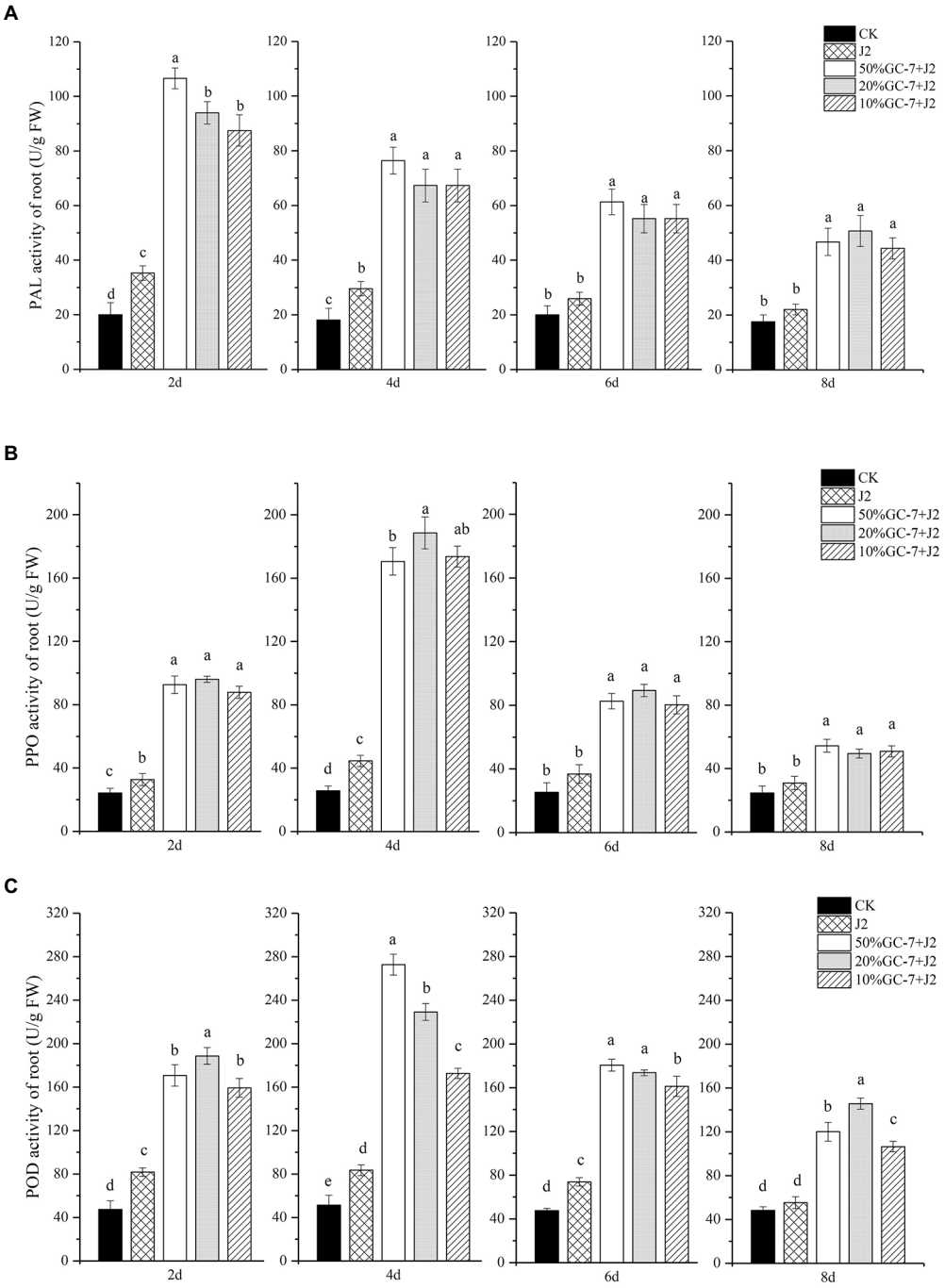

FIGURE 6
Changes of defense enzyme (PAL, PPO, POD) activities in roots of rice plants subjected to different treatments and *M. graminicola*. **(A)** PAL activity (U/g FW). **(B)** POD activity (U/g FW). **(C)** PPO activity (U/g FW) in rice roots inoculated with GC-7 fermentation broth at different dilutions and *M. graminicola*. Each pot contains five two-leaf stage rice seedings, fourty millilitre of the different concentrations of the bacterial fermentation broth was applied as irrigation to each pot. The control rice seedlings were treated with sterilized water. Each individual pot was inoculated with approximately 1,500 freshly hatched *M. graminicola* J2s 2days later. Values are means of three replicates and vertical bars represent the standard error. All treatments are significantly different from each other at $p<0.05$.

Microbacterium maritypicum Sneb159 induced an interaction between the SA-dependent SAR pathway and JA-dependent ISR pathway to defend against *H. glycines* (Zhao et al., 2019). In addition, treatment with isolate GC-7 suppressed the expression of *PR1a* at 1 dpi compared to CK plants, which may be to allow the colonization of rice roots at the early stage. Our finding was similar to SA-mediated plant defense, which is generally inhibited by certain microorganisms to achieve a compatible interaction

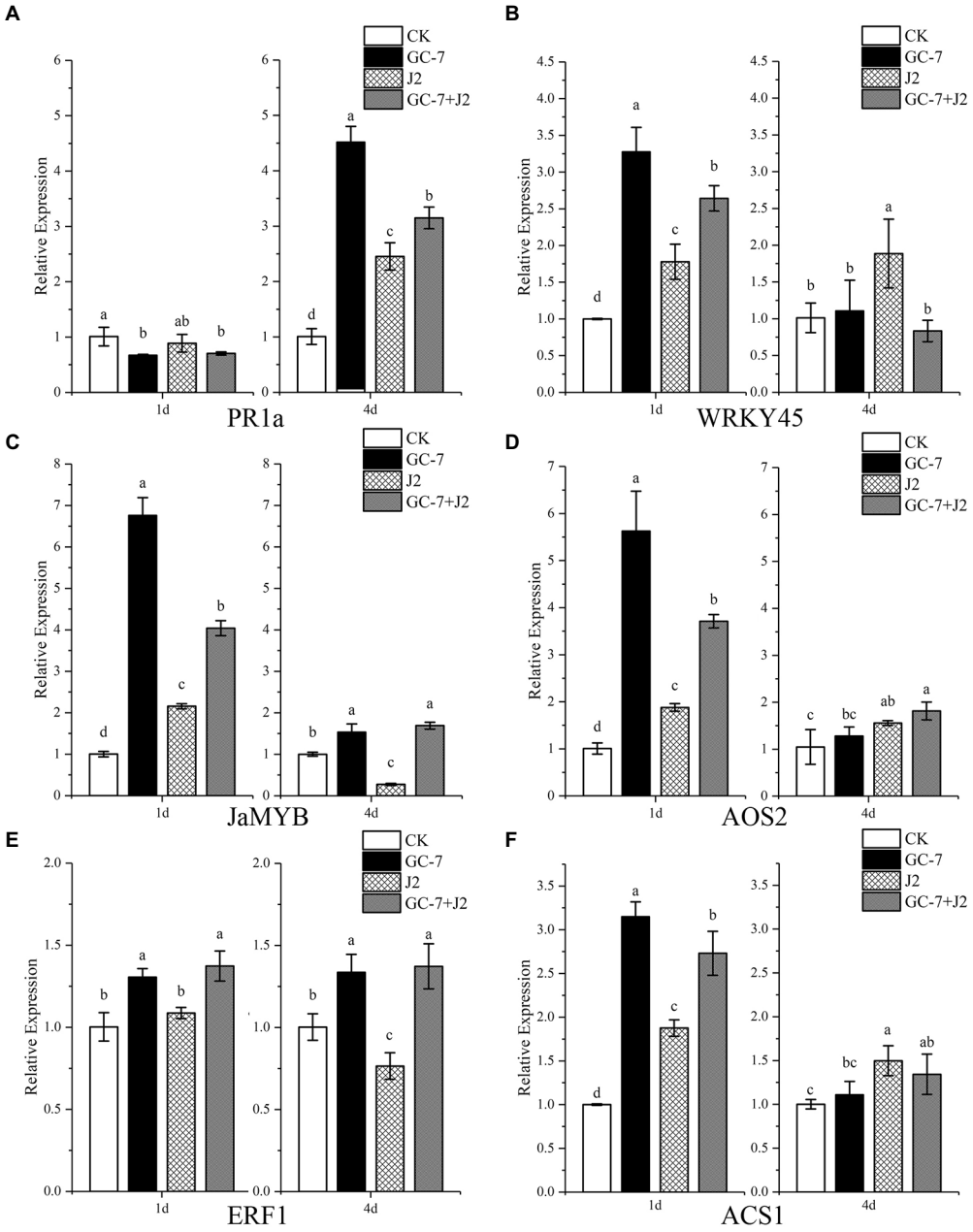

FIGURE 7
Quantitative RT-PCR analysis of genes involved in the salicylic acid, jasmonic acid, and ethylene pathways in rice roots. **(A)** Relative expression of *PR1a*. **(B)** Relative expression of *WRKY45*. **(C)** Relative expression of *JaMYB*. **(D)** Relative expression of *AOS2*. **(E)** Relative expression of *ERF1*. **(F)** Relative expression of *ACS1*. Gene expression levels were analyzed from four treatments: CK, GC-7, J2, GC-7+J2 at 1 and 4days after *M. graminicola* infection. Each pot contains five two-leaf stage rice seedings and was drenched with 40ml of 50% GC-7 ($1x10^9$cfu/ml) or sterilized water. The individual pot was inoculated with approximately 1,500 freshly hatched *M. graminicola* J2s 2days later. Rice seedlings were treated with sterile water as the non-treated control Error bars represent standard error of the mean values of three independent replicates from four biological replicates. All treatments are significantly different from each other at $p<0.05$. For each gene and time point, bars with different letters indicate statistically significant differences between treatments.

and host colonization (Leonetti et al., 2017; Zhao et al., 2019). The results implied that GC-7 might also activate the SA signaling pathways to induce plant defense against *M. graminicola*. Our report is the first to suggest that *P. rhodesiae* as a PGPR inducing protection against *M. graminicola* of rice plants involves both ISR and SAR mechanisms.

In conclusion, we isolated the novel *P. rhodesiae* isolate GC-7 from the rhizoplane of rice plants. Isolate GC-7 exhibited direct nematicidal and egg inhibition against *M. graminicola*, as well as effectively prevented nematode invasion and delayed the development of *M. graminicola* in rice roots. Pot- and field-based tests showed that isolate GC-7 significantly reduced the gall index

and presented remarkable growth-promoting properties in rice plants. In addition, GC-7 also activated resistance-related gene expression and defense enzyme activity to enhance plant resistance against *M. graminicola*. Our results suggest that isolate GC-7 employs multiple anti-nematode mechanisms and could be a potential biocontrol agent for *M. graminicola*.

Data availability statement

All datasets generated for this study are included in the article/Supplementary material, further inquiries can be directed to the corresponding author.

Author contributions

ZD and SY: conception of the work. SY, RY, XL, YL, and ZY: collection of data. SY, RY, ZD, and YM: analysis of data. SY, ZD, and YM: writing of manuscript. All authors have read and agreed to the published version of the manuscript.

Funding

This work was supported by the National Natural Science Foundation of China (grant nos. 32001879 and 31872038) and Natural Science Foundation of Hunan Province (grant no. 2022JJ30302).

Conflict of interest

The authors declare that the research was conducted in the absence of any commercial or financial relationships that could be construed as a potential conflict of interest.

Publisher's note

All claims expressed in this article are solely those of the authors and do not necessarily represent those of their affiliated organizations, or those of the publisher, the editors and the reviewers. Any product that may be evaluated in this article, or claim that may be made by its manufacturer, is not guaranteed or endorsed by the publisher.

Supplementary material

The Supplementary material for this article can be found online at: https://www.frontiersin.org/articles/10.3389/fmicb.2022.1025727/full#supplementary-material

References

Abad, P., Favery, B., Rosso, M. N., and Castagnone-Sereno, P. (2003). Root-knot nematode parasitism and host response: molecular basis of a sophisticated interaction. *Mol. Plant Pathol.* 4, 217–224. doi: 10.1046/j.1364-3703.2003.00170.x

Abad, P., Gouzy, J., Aury, J. M., Castagnone-Sereno, P., Danchin, E. G., Deleury, E., et al. (2008). Genome sequence of the metazoan plant-parasitic nematode *Meloidogyne incognita*. *Nat. Biotechnol.* 26, 909–915. doi: 10.1038/nbt.1482

Abd-Elgawad, M. M. M. (2021). Optimizing safe approaches to manage plant-parasitic nematodes. *Plants (Basel)* 10:1911. doi: 10.3390/plants10091911

Abd-Elgawad, M. M. M. (2022). Understanding molecular plant-nematode interactions to develop alternative approaches for nematode control. *Plants (Basel)* 11:2141. doi: 10.3390/plants11162141

Amil-Ruiz, F., Blanco-Portales, R., Munoz-Blanco, J., and Caballero, J. L. (2011). The strawberry plant defense mechanism: a molecular review. *Plant Cell Physiol.* 52, 1873–1903. doi: 10.1093/pcp/pcr136

Antil, S., Kumar, R., Pathak, D. V., Kumar, A., Panwar, A., Kumari, A., et al. (2022). Potential of *Bacillus altitudinis* KMS-6 as a biocontrol agent of *Meloidogyne javanica*. *J. Pest. Sci.* 95, 1443–1452. doi: 10.1007/s10340-021-01469-x

Bridge, J., and Page, S. L. J. (1980). Estimation of root-knot nematode infestation levels on roots using a rating chart. *Trop. Pest Manage.* 26, 296–298. doi: 10.1080/09670878009414416

Bridge, J., and Page, S. L. J. (1982). The rice root-knot nematode, *Meloidogyne graminicola*, on deep water rice (*Oryza sativa* subsp. *indica*). *Revue Nématol* 5, 225–232.

Bukhat, S., Imran, A., Javaid, S., Shahid, M., Majeed, A., and Naqqash, T. (2020). Communication of plants with microbial world: exploring the regulatory networks for PGPR mediated defense signaling. *Microbiol. Res.* 238:126486. doi: 10.1016/j.micres.2020.126486

Cayrol, J.-C., Djian, C., and Pijarowski, L. (1989). Study of the nematocidal properties of the culture filtrate of the nematophagous fungus *Paecilomyces lilacimus*. *Revue Nématol* 12, 331–336.

Chavan, S. N., De Kesel, J., Desmedt, W., Degroote, E., Singh, R. R., Nguyen, G. T., et al. (2022). Dehydroascorbate induces plant resistance in rice against root-knot nematode *Meloidogyne graminicola*. *Mol. Plant Pathol.* 23, 1303–1319. doi: 10.1111/mpp.13230

Chen, F., Wang, M., Zheng, Y., Luo, J., Yang, X., and Wang, X. (2009). Quantitative changes of plant defense enzymes and phytohormone in biocontrol of cucumber *Fusarium* wilt by *Bacillus subtilis* B579. *World J. Microbiol. Biotechnol.* 26, 675–684. doi: 10.1007/s11274-009-0222-0

Conn, V. M., Walker, A. R., and Franco, C. M. (2008). Endophytic actinobacteria induce defense pathways in *Arabidopsis thaliana*. *Mol. Plant-Microbe Interact.* 21, 208–218. doi: 10.1094/MPMI-21-2-0208

de Oliveira, C. M., Almeida, N. O., Côrtes, M. V. D. C. B., Júnior, M. L., Da Rocha, M. R., and Ulhoa, C. J. (2021). Biological control of *Pratylenchus brachyurus* with isolates of *Trichoderma* spp. on soybean. *Biol. Control* 152:104425. doi: 10.1016/j.biocontrol.2020.104425

De Waele, D., and Elsen, A. (2007). Challenges in tropical plant nematology. *Annu. Rev. Phytopathol.* 45, 457–485. doi: 10.1146/annurev.phyto.45.062806.094438

Di Lelio, I., Coppola, M., Comite, E., Molisso, D., Lorito, M., Woo, S. L., et al. (2021). Temperature differentially influences the capacity of *Trichoderma* species to induce plant defense responses in tomato against insect pests. *Front. Plant Sci.* 12:678830. doi: 10.3389/fpls.2021.678830

Fatma, A. M., K, A. E., Deen Ah, N. E., Ibrahim, , and D, S. (2014). Induction of systemic resistance in sugar- beet against root-knot nematode with commercial products. *J. Plant Pathol. Microbiol.* 5:236. doi: 10.4172/2157-7471.1000236

Forghani, F., and Hajihassani, A. (2020). Recent advances in the development of environmentally benign treatments to control root-knot nematodes. *Front. Plant Sci.* 11:1125. doi: 10.3389/fpls.2020.01125

Ghahremani, Z., Escudero, N., Beltran-Anadon, D., Saus, E., Cunquero, M., Andilla, J., et al. (2020). *Bacillus firmus* strain I-1582, a nematode antagonist by itself and through the plant. *Front. Plant Sci.* 11:796. doi: 10.3389/fpls.2020.00796

Ghareeb, R. Y., Alfy, H., Fahmy, A. A., Ali, H. M., and Abdelsalam, N. R. (2020). Utilization of *Cladophora glomerata* extract nanoparticles as eco-nematicide and

enhancing the defense responses of tomato plants infected by *Meloidogyne javanica*. *Sci. Rep.* 10:19968. doi: 10.1038/s41598-020-77005-1

Haque, Z., Khan, M. R., and Ahamad, F. (2018). Relative antagonistic potential of some rhizosphere biocontrol agents for the management of rice root-knot nematode, *Meloidogyne graminicola*. *Biol. Control* 126, 109–116. doi: 10.1016/j.biocontrol.2018.07.018

Hu, H. J., Chen, Y. L., Wang, Y. F., Tang, Y. Y., Chen, S. L., and Yan, S. Z. (2017). Endophytic *Bacillus cereus* effectively controls *Meloidogyne incognita* on tomato plants through rapid Rhizosphere occupation and repellent action. *Plant Dis.* 101, 448–455. doi: 10.1094/PDIS-06-16-0871-RE

Jain, S., and Choudhary, D. K. (2014). Induced defense-related proteins in soybean (*Glycine max* L. Merrill) plants by *Carnobacterium* sp. SJ-5 upon challenge inoculation of *Fusarium oxysporum*. *Planta* 239, 1027–1040. doi: 10.1007/s00425-014-2032-3

Jang, J. Y., Choi, Y. H., Shin, T. S., Kim, T. H., Shin, K. S., Park, H. W., et al. (2016). Biological control of *Meloidogyne incognita* by *Aspergillus* Niger F22 producing oxalic acid. *PLoS One* 11:e0156230. doi: 10.1371/journal.pone.0156230

Jetiyanon, K. (2007). Defensive-related enzyme response in plants treated with a mixture of bacillus strains (IN937a and IN937b) against different pathogens. *Biol. Control* 42, 178–185. doi: 10.1016/j.biocontrol.2007.05.008

Ju, R., Zhao, Y., Li, J., Jiang, H., Liu, P., Yang, T., et al. (2013). Identification and evaluation of a potential biocontrol agent, *Bacillus subtilis*, against *Fusarium* sp. in apple seedlings. *Ann. Microbiol.* 64, 377–383. doi: 10.1007/s13213-013-0672-3

Khan, M. R., Haque, Z., Ahamad, F., and Zaidi, B. (2021). Biomanagement of rice root-knot nematode *Meloidogyne graminicola* using five indigenous microbial isolates under pot and field trials. *J. Appl. Microbiol.* 130, 424–438. doi: 10.1111/jam.14788

Khanna, K., Jamwal, V. L., Kohli, S. K., Gandhi, S. G., Ohri, P., Bhardwaj, R., et al. (2019). Role of plant growth promoting bacteria (PGPRs) as biocontrol agents of *Meloidogyne incognita* through improved plant defense of *Lycopersicon esculentum*. *Plant Soil* 436, 325–345. doi: 10.1007/s11104-019-03932-2

Khanna, K., Kohli, S. K., Ohri, P., and Bhardwaj, R. (2021). Plants-nematodes-microbes crosstalk within soil: a trade-off among friends or foes. *Microbiol. Res.* 248:126755. doi: 10.1016/j.micres.2021.126755

Kumar, S., Stecher, G., and Tamura, K. (2016). MEGA7: molecular evolutionary genetics analysis version 7.0 for bigger datasets. *Mol. Biol. Evol.* 33, 1870–1874. doi: 10.1093/molbev/msw054

Kurth, F., Mailander, S., Bonn, M., Feldhahn, L., Herrmann, S., Grosse, I., et al. (2014). *Streptomyces*-induced resistance against oak powdery mildew involves host plant responses in defense, photosynthesis, and secondary metabolism pathways. *Mol. Plant-Microbe Interact.* 27, 891–900. doi: 10.1094/MPMI-10-13-0296-R

Kyndt, T., Denil, S., Haegeman, A., Trooskens, G., Bauters, L., Van Criekinge, W., et al. (2012). Transcriptional reprogramming by root knot and migratory nematode infection in rice. *New Phytol.* 196, 887–900. doi: 10.1111/j.1469-8137.2012.04311.x

Kyndt, T., Vieira, P., Gheysen, G., and de Almeida-Engler, J. (2013). Nematode feeding sites: unique organs in plant roots. *Planta* 238, 807–818. doi: 10.1007/s00425-013-1923-z

Lahari, Z., Ullah, C., Kyndt, T., Gershenzon, J., and Gheysen, G. (2019). Strigolactones enhance root-knot nematode (*Meloidogyne graminicola*) infection in rice by antagonizing the jasmonate pathway. *New Phytol.* 224, 454–465. doi: 10.1111/nph.15953

Le, H. T. T., Padgham, J. L., Hagemann, M. H., Sikora, R. A., and Schouten, A. (2016). Developmental and behavioural effects of the endophytic *Fusarium moniliforme* Fe14 towards *Meloidogyne graminicola* in rice. *Ann. Appl. Biol.* 169, 134–143. doi: 10.1111/aab.12287

Leonetti, P., Zonno, M. C., Molinari, S., and Altomare, C. (2017). Induction of SA-signaling pathway and ethylene biosynthesis in *Trichoderma harzianum*-treated tomato plants after infection of the root-knot nematode *Meloidogyne incognita*. *Plant Cell Rep.* 36, 621–631. doi: 10.1007/s00299-017-2109-0

Li, X., Geng, Y., Ma, J., Gao, B., Wang, R., and Chen, S. (2016). An accurate method for estimating the number of root-knot nematodes in soil. *J. Plant Prot.* 43, 768–773. doi: 10.13802/j.cnki.zwbhxb.2016.05.009

Liang, L. M., Zou, C. G., Xu, J., and Zhang, K. Q. (2019). Signal pathways involved in microbe-nematode interactions provide new insights into the biocontrol of plant-parasitic nematodes. *Philos. Trans. R. Soc. Lond. Ser. B Biol. Sci.* 374:20180317. doi: 10.1098/rstb.2018.0317

Liu, D., Chen, L., Zhu, X., Wang, Y., Xuan, Y., Liu, X., et al. (2018). *Klebsiella pneumoniae* SnebYK mediates resistance against *Heterodera glycines* and promotes soybean growth. *Front. Microbiol.* 9:1134. doi: 10.3389/fmicb.2018.01134

Liu, Y., Ding, Z., Peng, D.-L., Liu, S.-M., Kong, L.-A., Peng, H., et al. (2019). Evaluation of the biocontrol potential of *Aspergillus welwitschiae* against the root-knot nematode *Meloidogyne graminicola* in rice (*Oryza sativa* L.). *J. Integr. Agricu.* 18, 2561–2570. doi: 10.1016/S2095-3119(19)62610-9

Liu, G., Lin, X., Xu, S., Liu, G., Liu, F., and Mu, W. (2020). Screening, identification and application of soil bacteria with nematicidal activity against root-knot nematode (*Meloidogyne incognita*) on tomato. *Pest Manag. Sci.* 76, 2217–2224. doi: 10.1002/ps.5759

Livak, K. J., and Schmittgen, T. D. (2001). Analysis of relative gene expression data using real-time quantitative PCR and the 2(-Delta Delta C(T)) method. *Methods* 25, 402–408. doi: 10.1006/meth.2001.1262

Ma, Y.-Y., Li, Y.-L., Lai, H.-X., Guo, Q., and Xue, Q.-H. (2017). Effects of two strains of *Streptomyces* on root-zone microbes and nematodes for biocontrol of root-knot nematode disease in tomato. *Appl. Soil Ecol.* 112, 34–41. doi: 10.1016/j.apsoil.2017.01.004

Mantelin, S., Bellafiore, S., and Kyndt, T. (2017). *Meloidogyne graminicola*: a major threat to rice agriculture. *Mol. Plant Pathol.* 18, 3–15. doi: 10.1111/mpp.12394

Martinez-Medina, A., Fernandez, I., Lok, G. B., Pozo, M. J., Pieterse, C. M., and Van Wees, S. C. (2017). Shifting from priming of salicylic acid- to jasmonic acid-regulated defences by *Trichoderma* protects tomato against the root knot nematode *Meloidogyne incognita*. *New Phytol.* 213, 1363–1377. doi: 10.1111/nph.14251

Medeiros, H. A., Araujo Filho, J. V., Freitas, L. G., Castillo, P., Rubio, M. B., Hermosa, R., et al. (2017). Tomato progeny inherit resistance to the nematode *Meloidogyne javanica* linked to plant growth induced by the biocontrol fungus *Trichoderma* atroviride. *Sci. Rep.* 7:40216. doi: 10.1038/srep40216

Medina-Canales, M. G., Terroba-Escalante, P., Manzanilla-López, R. H., and Tovar-Soto, A. (2019). Assessment of three strategies for the management of *Meloidogyne arenaria* on carrot in Mexico using *Pochonia chlamydosporia* var. *mexicana* under greenhouse conditions. *Biocontrol Sci. Tech.* 29, 671–685. doi: 10.1080/09583157.2019.1582267

Migunova, V. D., and Sasanelli, N. (2021). Bacteria as biocontrol tool against phytoparasitic nematodes. *Plants (Basel)* 10:389. doi: 10.3390/plants10020389

Mnif, I., and Ghribi, D. (2015). Potential of bacterial derived biopesticides in pest management. *Crop Prot.* 77, 52–64. doi: 10.1016/j.cropro.2015.07.017

Nahar, K., Kyndt, T., De Vleesschauwer, D., Hofte, M., and Gheysen, G. (2011). The jasmonate pathway is a key player in systemically induced defense against root knot nematodes in rice. *Plant Physiol.* 157, 305–316. doi: 10.1104/pp.111.177576

Nahar, K., Kyndt, T., Nzogela, Y. B., and Gheysen, G. (2012). Abscisic acid interacts antagonistically with classical defense pathways in rice-migratory nematode interaction. *New Phytol.* 196, 901–913. doi: 10.1111/j.1469-8137.2012.04310.x

Narendra Babu, A., Jogaiah, S., Ito, S., Kestur Nagaraj, A., and Tran, L. S. (2015). Improvement of growth, fruit weight and early blight disease protection of tomato plants by rhizosphere bacteria is correlated with their beneficial traits and induced biosynthesis of antioxidant peroxidase and polyphenol oxidase. *Plant Sci.* 231, 62–73. doi: 10.1016/j.plantsci.2014.11.006

Padgham, J. L., and Sikora, R. A. (2007). Biological control potential and modes of action of *Bacillus megaterium* against *Meloidogyne graminicola* on rice. *Crop Prot.* 26, 971–977. doi: 10.1016/j.cropro.2006.09.004

Rais, A., Jabeen, Z., Shair, F., Hafeez, F. Y., and Hassan, M. N. (2017). *Bacillus* spp., a bio-control agent enhances the activity of antioxidant defense enzymes in rice against *Pyricularia oryzae*. *PLoS One* 12:e0187412. doi: 10.1371/journal.pone.0187412

Rajasekharan, S. K., Kim, S., Kim, J. C., and Lee, J. (2020). Nematicidal activity of 5-iodoindole against root-knot nematodes. *Pestic. Biochem. Physiol.* 163, 76–83. doi: 10.1016/j.pestbp.2019.10.012

Rasool, M., Akhter, A., and Haider, M. S. (2021). Molecular and biochemical insight into biochar and *Bacillus subtilis* induced defense in tomatoes against *Alternaria solani*. *Sci. Hortic.* 285:110203. doi: 10.1016/j.scienta.2021.110203

Reversat, G., Boyer, J., Sannier, C., and Pando-Bahuon, A. (1999). Use of a mixture of sand and water-absorbent synthetic polymer as substrate for the xenic culturing of plant-parasitic nematodes in the laboratory. *Nematology* 1, 209–212. doi: 10.1163/156854199508027

Romero, F. M., Marina, M., and Pieckenstain, F. L. (2016). Novel components of leaf bacterial communities of field-grown tomato plants and their potential for plant growth promotion and biocontrol of tomato diseases. *Res. Microbiol.* 167, 222–233. doi: 10.1016/j.resmic.2015.11.001

Rusinque, L., Maleita, C., Abrantes, I., Palomares-Rius, J. E., and Inacio, M. L. (2021). *Meloidogyne graminicola* – a threat to rice production: review update on distribution, biology, identification, and management. *Biology (Basel)* 10:1163. doi: 10.3390/biology10111163

Ryan, R. P., An, S. Q., Allan, J. H., McCarthy, Y., and Dow, J. M. (2015). The DSF family of cell-cell signals: An expanding class of bacterial virulence regulators. *PLoS Pathog.* 11:e1004986. doi: 10.1371/journal.ppat.1004986

Sah, S., Krishnani, S., and Singh, R. (2021). *Pseudomonas* mediated nutritional and growth promotional activities for sustainable food security. *Curr Res Microb Sci* 2:100084. doi: 10.1016/j.crmicr.2021.100084

Salla, T. D., Astarita, L. V., and Santarem, E. R. (2016). Defense responses in plants of eucalyptus elicited by *Streptomyces* and challenged with *Botrytis cinerea*. *Planta* 243, 1055–1070. doi: 10.1007/s00425-015-2460-8

Salman, E. K., Ghoniem, K. E., Badr, E. S., and Emeran, A. A. (2022). The potential of dimetindene maleate inducing resistance to blast fungus *Magnaporthe oryzae* through activating the salicylic acid signaling pathway in rice plants. *Pest Manag. Sci.* 78, 633–642. doi: 10.1002/ps.6673

Sharma, I. P., and Sharma, A. K. (2016). Physiological and biochemical changes in tomato cultivar PT-3 with dual inoculation of mycorrhiza and PGPR against root-knot nematode. *Symbiosis* 71, 175–183. doi: 10.1007/s13199-016-0423-x

Shoresh, M., Yedidia, I., and Chet, I. (2005). Involvement of Jasmonic acid/ethylene signaling pathway in the systemic resistance induced in cucumber by *Trichoderma asperellum* T203. *Phytopathology* 95, 76–84. doi: 10.1094/PHYTO-95-0076

Singh, R. R., Verstraeten, B., Siddique, S., Tegene, A. M., Tenhaken, R., Frei, M., et al. (2020). Ascorbate oxidation activates systemic defence against root-knot nematode *Meloidogyne graminicola* in rice. *J. Exp. Bot.* 71, 4271–4284. doi: 10.1093/jxb/eraa171

Stenberg, J. A., Sundh, I., Becher, P. G., Björkman, C., Dubey, M., Egan, P. A., et al. (2021). When is it biological control? A framework of definitions, mechanisms, and classifications. *J. Pest. Sci.* 94, 665–676. doi: 10.1007/s10340-021-01354-7

Subedi, P., Gattoni, K., Liu, W., Lawrence, K. S., and Park, S. W. (2020). Current utility of plant growth-promoting rhizobacteria as biological control agents towards plant-parasitic nematodes. *Plants (Basel)* 9:1167. doi: 10.3390/plants9091167

Takaki, Y., Katsuhiro, S., Minoru, N., Aya, F., Miho, A., Itsuro, T., et al. (2015). Ethylene biosynthesis is promoted by very-long-chain fatty acids during lysigenous aerenchyma formation in rice roots. *Plant Physiol.* 169, 180–193. doi: 10.1104/pp.15.00106

TariqJaveed, M., Farooq, T., Al-Hazmi, A. S., Hussain, M. D., and Rehman, A. U. (2021). Role of *Trichoderma* as a biocontrol agent (BCA) of phytoparasitic nematodes and plant growth inducer. *J. Invertebr. Pathol.* 183:107626. doi: 10.1016/j.jip.2021.107626

Thompson, J. D., Gibson, T. J., Plewniak, F., Jeanmougin, F., and Higgins, D. G. (1997). The CLUSTAL_X windows interface: flexible strategies for multiple sequence alignment aided by quality analysis tools. *Nucleic Acids Res.* 25, 4876–4882. doi: 10.1093/nar/25.24.4876

Vallad, G. E., and Goodman, R. M. (2004). Systemic acquired resistance and induced systemic resistance in conventional agriculture. *Crop Sci.* 44, 1920–1934. doi: 10.2135/cropsci2004.1920

Walsh, U. F., Morrissey, J. P., and O'Gara, F. (2001). *Pseudomonas* for biocontrol of phytopathogens: from functional genomics to commercial exploitation. *Curr. Opin. Biotechnol.* 12, 289–295. doi: 10.1016/S0958-1669(00)00212-3

Yamamoto, S., and Harayama, S. (1995). PCR amplification and direct sequencing of gyrB genes with universal primers and their application to the detection and taxonomic analysis of *Pseudomonas* putida strains. *Appl. Environ. Microbiol.* 61, 1104–1109. doi: 10.1128/aem.61.3.1104-1109.1995

Yan, Y., Mao, Q., Wang, Y., Zhao, J., Fu, Y., Yang, Z., et al. (2021). *Trichoderma harzianum* induces resistance to root-knot nematodes by increasing secondary metabolite synthesis and defense-related enzyme activity in *Solanum lycopersicum* L. *Biol. Control* 158:104609. doi: 10.1016/j.biocontrol.2021.104609

Yang, J., Liang, L., Li, J., and Zhang, K. Q. (2013). Nematicidal enzymes from microorganisms and their applications. *Appl. Microbiol. Biotechnol.* 97, 7081–7095. doi: 10.1007/s00253-013-5045-0

Yang, J. I., Stadler, M., Chuang, W.-Y., Wu, S., and Ariyawansa, H. A. (2020). In vitro inferred interactions of selected entomopathogenic fungi from Taiwan and eggs of *Meloidogyne graminicola*. *Mycol. Prog.* 19, 97–109. doi: 10.1007/s11557-019-01546-7

Yimer, H. Z., Nahar, K., Kyndt, T., Haeck, A., Van Meulebroek, L., Vanhaecke, L., et al. (2018). Gibberellin antagonizes jasmonate-induced defense against *Meloidogyne graminicola* in rice. *New Phytol.* 218, 646–660. doi: 10.1111/nph.15046

Yin, N., Zhao, J. L., Liu, R., Li, Y., Ling, J., Yang, Y. H., et al. (2021). Biocontrol efficacy of *Bacillus cereus* strain Bc-cm103 against *Meloidogyne incognita*. *Plant Dis.* 105, 2061–2070. doi: 10.1094/PDIS-03-20-0648-RE

Zhang, R., Ouyang, J., Xu, X., Li, J., Rehman, M., Deng, G., et al. (2022). Nematicidal activity of *Burkholderia arboris* J211 against *Meloidogyne incognita* on tobacco. *Front. Microbiol.* 13:915546. doi: 10.3389/fmicb.2022.915546

Zhao, J., Liu, D., Wang, Y., Zhu, X., Xuan, Y., Liu, X., et al. (2019). Biocontrol potential of *Microbacterium maritypicum* Sneb159 against *Heterodera glycines*. *Pest Manag. Sci.* 75, 3381–3391. doi: 10.1002/ps.5546

Zhao, J., Wang, S., Zhu, X., Wang, Y., Liu, X., Duan, Y., et al. (2021). Isolation and characterization of nodules endophytic bacteria *Pseudomonas* protegens Sneb1997 and Serratia plymuthica Sneb 2001 for the biological control of root-knot nematode. *Appl. Soil Ecol.* 164:103924. doi: 10.1016/j.apsoil.2021.103924

Zhao, D., Zhao, H., Zhao, D., Zhu, X., Wang, Y., Duan, Y., et al. (2018). Isolation and identification of bacteria from rhizosphere soil and their effect on plant growth promotion and root-knot nematode disease. *Biol. Control* 119, 12–19. doi: 10.1016/j.biocontrol.2018.01.004

Zhou, Y., Chen, J., Zhu, X., Wang, Y., Liu, X., Fan, H., et al. (2021). Efficacy of *Bacillus megaterium* strain Sneb207 against soybean cyst nematode (*Heterodera glycines*) in soybean. *Pest Manag. Sci.* 77, 568–576. doi: 10.1002/ps.6057

frontiers | Frontiers in Microbiology

TYPE Original Research
PUBLISHED 13 January 2023
DOI 10.3389/fmicb.2022.1075327

OPEN ACCESS

EDITED BY
Vinay Kumar,
ICAR-National Institute of Biotic Stress Management, India

REVIEWED BY
Mehi Lal,
ICAR-Central Potato Research Institute, Regional Station, India
Malkhan Singh Gurjar,
Indian Agricultural Research Institute (ICAR), India

*CORRESPONDENCE
Inmaculada Larena
✉ ilarena@inia.csic.es

SPECIALTY SECTION
This article was submitted to Microbe and Virus Interactions With Plants, a section of the journal Frontiers in Microbiology

RECEIVED 20 October 2022
ACCEPTED 06 December 2022
PUBLISHED 13 January 2023

CITATION
Requena E, Alonso-Guirado L, Veloso J, Villarino M, Melgarejo P, Espeso EA and Larena I (2023) Comparative analysis of *Penicillium* genomes reveals the absence of a specific genetic basis for biocontrol in *Penicillium rubens* strain 212. *Front. Microbiol.* 13:1075327. doi: 10.3389/fmicb.2022.1075327

Comparative analysis of *Penicillium* genomes reveals the absence of a specific genetic basis for biocontrol in *Penicillium rubens* strain 212

Elena Requena[1], Lola Alonso-Guirado[2], Javier Veloso[3], María Villarino[1], Paloma Melgarejo[1], Eduardo Antonio Espeso[4] and Inmaculada Larena[1]*

[1]Grupo Hongos Fitopatógenos, Departamento de Protección Vegetal, Instituto Nacional de Investigación y Tecnología Agraria y Alimentaria, Consejo Superior de Investigaciones Científicas (INIA-CSIC), Madrid, Spain, [2]Grupo de Epidemiología Genética y Molecular, Centro Nacional de Investigaciones Oncológicas (CNIO), Madrid, Spain, [3]Departamento de Biología Funcional, Escuela Politécnica Superior de Ingeniería, Universidad de Santiago de Compostela, Lugo, Spain, [4]Laboratorio de Biología Celular de Aspergillus, Departamento de Biología Celular y Molecular, Centro de Investigaciones Biológicas Margarita Salas, CSIC (CIB-CSIC), Madrid, Spain

Penicillium rubens strain 212 (PO212) is a filamentous fungus belonging to the division Ascomycete. PO212 acts as an effective biocontrol agent against several pathogens in a variety of horticultural crops including *Fusarium oxysporum* f.sp. *lycopersici*, causing vascular wilt disease in tomato plants. We assembled draft genomes of two P. rubens strains, the biocontrol agent PO212 and the soil isolate S27, which lacks biocontrol activity. We also performed comparative analyses of the genomic sequence of PO212 with that of the other *P. rubens* and *P. chrysogenum* strains. This is the first *Penicillium* strain with biocontrol activity whose genome has been sequenced and compared. PO212 genome size is 2,982 Mb, which is currently organized into 65 scaffolds and a total of 10,164 predicted Open Reading Frames (ORFs). Sequencing confirmed that PO212 belongs to *P. rubens* clade. The comparative analysis of the PO212 genome with the genomes of other *P. rubens* and *Penicillium chrysogenum* strains available in databases showed strong conservation among genomes, but a correlation was not found between these genomic data and the biocontrol phenotype displayed by PO212. Finally, the comparative analysis between PO212 and S27 genomes showed high sequence conservation and a low number of variations mainly located in ORF regions. These differences found in coding regions between PO212 and S27 genomes can explain neither the biocontrol activity of PO212 nor the absence of such activity in S27, opening a possible avenue toward transcriptomic and epigenetic studies that may shed light on this mechanism for fighting plant diseases caused by fungal pathogens. The genome sequences described in this study provide a useful novel resource for future research into the biology, ecology, and evolution of biological control agents.

KEYWORDS

PO212, biocontrol agent, *Penicillium rubens*, genome, comparative genomics

Introduction

Penicillium rubens strain 212 (PO212, ATCC201888), formerly known *Penicillium oxalicum* (Villarino et al., 2016), is a filamentous fungus belonging to the division Ascomycete. PO212 is a strain that mainly attracts agricultural and biotechnological interest because it is an effective biocontrol agent (BCA) against several pathogens in a variety of horticultural crops (Larena et al., 2003b; De Cal et al., 2008, 2009; Martinez-Beringola et al., 2013). Among the fungal pathogens, PO212 acts against *Fusarium oxysporum* f.sp. *lycopersici* (FOL; Sacc.) W. C. Snyder and H. N. Hans, causing vascular wilt disease in tomato plants (De Cal et al., 1995). The effective control of tomato wilt is based on the application of PO212 conidia (Pascual et al., 2000) and conidial contact with roots (De Cal et al., 2000). Plant–fungus contact is achieved by watering seedlings 7 days before transplanting, in seedbeds with a conidial suspension of PO212, at a final conidial density in the seedbed substrate and rhizosphere between 10^6 and 10^7 conidia per gram (De Cal et al., 1999, 2000; Larena et al., 2003b). PO212 acts against Fusarium wilt primarily through a mechanism of induced resistance in tomato plants (De Cal et al., 1997b, 1999, 2000). Nevertheless, a previous study showed that the competition for space and nutrients (Sabuquillo et al., 2009) and the promotion of plant growth have been demonstrated (De Cal et al., 1995).

Genome sequencing is currently on the rise due to new and faster procedures and reduced sequencing costs. This allows for expanded comparative studies of the genomes of organisms with key roles in health, biotechnology, or agriculture. Among these interesting organisms are species of the genus *Penicillium*, especially *Penicillium chrysogenum* and *P. rubens*. However, controversy remains about the true existence of these two separate species (Houbraken et al., 2011). Genome sequences of several *P. chrysogenum* and/or *P. rubens* strains have been reported. In genome databases, the following strains are classified as *P. chrysogenum*: P2niaD18 (Specht et al., 2014), HKF42 (Gujar et al., 2018), KF-25 (Peng et al., 2014), NCPC10086 (PENC1.0 0; Wang et al., 2014), and v1.0 (de Vries et al., 2017). Meanwhile, the strains PrWis (*P. rubens* Wisconsin 54-1255; Van Den Berg et al., 2008) and Biourge 1923 (IMI 15378; Pathak et al., 2020) are classified as *P. rubens*. PrWis was the first strain of *P. rubens* to be sequenced (Van Den Berg et al., 2008). The strains P2niaD18 and PrWis were interesting from a sanitary point of view because of their high penicillin-producing capacity. Notably, these two strains are descendants from the natural isolate NRRL 1951 which was classified as *P. chrysogenum* (Martín, 2020). Both strains have undergone various mutagenesis procedures and screening methods to improve their respective penicillin yields. This implies that the presence of sequence modifications and reorganizations in the genomes of these strains is highly expected.

Penicillium rubens strain 212 was initially misclassified as *P. oxalicum* based on morphological characteristics, such as the color of the spore layer on the colony surface, the size and shape of the colony, conidial size, and conidiophore morphology (Ramírez, 1982). Subsequent sequencing of internal transcribed spacers (ITS) regions and the isolation and identification of 5-fluoroorotic acid (5-FOA)-resistant mutants showed that PO212 was a *P. rubens* strain (Villarino et al., 2016). The first study to understand the genetic basis of PO212 biocontrol activity (BA) focused on the analysis of genes involved in nitrate assimilation since PO212, and other *P. rubens* strains showing a BA against Fusarium wilt lacked the ability to use nitrate as the main nitrogen source (Espeso et al., 2019). This nitrate assimilation-deficient phenotype was due to the presence of mutations in the NirA regulator or the nitrate transporter CrnA. However, the complementation of these mutations did not help to understand the BA of PO212 (Espeso et al., 2019).

Genome-wide analyses proved to be a good method to determine the genetic basis behind the biocontrol process in several organisms (Pattemore et al., 2014; Sharma et al., 2017; Piombo et al., 2018). Moreover, comparative genomics allowed the identification of pathways or mutations between the genomes of different organisms that may be specific to organisms with BA (Massart et al., 2015). Comparative analyses of *Trichoderma* spp. genomes revealed notable differences in contrast to the genomes of other multicellular ascomycetes in comparison to publicly available genomes (Kubicek et al., 2011). These analyses of *Trichoderma* spp. represent a useful new resource for the further development of improved and research-driven strategies to select and improve *Trichoderma* species as BCA (Kubicek et al., 2011). However, the comparative genomics of two biocontrol strains of *Metschnikowia fructicola* revealed a very high mutation rate, which may suggest that *M. fructicola* could undergo genomic changes to adapt to plant surfaces, tolerate a variety of environmental stresses, and survive under nutritional restrictions (Piombo et al., 2018). Major efforts in technology and bioinformatics tools have significantly increased our knowledge of BCA and their properties (Massart et al., 2015).

In this study, we conducted a comparative genomic approach to understand the genetic basis of BA in *P. rubens*. We assembled draft genomes of two *P. rubens* strains, the BCA PO212 and the soil isolate S27, which lacks BA. We also performed comparative analyses of the genomic sequence of PO212 with that of the other *P. rubens* and *P. chrysogenum* strains. These analyses revealed significant conservation of genomic sequences among all strains compared and evidenced the absence of any specific genes related to biocontrol in PO212.

Materials and methods

Strains and growth conditions

Penicillium rubens strain 212 and other *P. rubens* strains, isolated from diverse agricultural soils and plant samples in Spain, are listed in Table 1. Conidia from these strains were stored in 20% glycerol for a long term at −20°C except for PO212, which was stored at 4°C as dried conidia. Dried conidia of PO212 were

TABLE 1 List of *Penicillium rubens* strains used in this work.

Strain	Origin	Host	BCA[a]	References
PO212	Spain	Soil	+	De Cal et al. (1995)
S27	Spain (Ávila)	Soil	–	Villarino et al. (2016)
S17	Spain (Segovia)	Soil	–	Villarino et al. (2016)
S71	Spain (Segovia)	Soil	–	Villarino et al. (2016)
S73	Spain (Segovia)	Soil	+	Villarino et al. (2016)
CH2	Spain (Madrid)	Leaf of a perennial plant	–[b]	This work
CH5	Spain (Madrid)	Shoot of a perennial plant in a field of peach trees	–[b]	This work
CH6	Spain (Madrid)	A deep soil sample in the field of peach trees	+[b]	This work
CH8	Spain (Madrid)	A shoot of a perennial plant in a pine forest	+[b]	Espeso et al. (2019)
CH16	Spain (Lérida)	Outbreak of pruning	+[b]	This work

[a]BCA: Biological Control Agent.
[b]Unpublished results, general screenings of BCA strains INIA-CSIC. The symbol + indicates biocontrol activity. The symbol – indicates no biocontrol activity.

produced in a solid-state fermentation system and dried as previously described by Larena et al. (2003a). *Penicillium* strains were grown on potato dextrose agar (PDA) or minimal medium (MM; Espeso et al., 2019) with 5 mM ammonium tartrate and D-glucose 1% (w/v) as nitrogen and carbon source, respectively, and incubated at 25°C for 5 days. For short-term storage, strains were kept at 4°C on solid media.

The biocontrol activity of *P. rubens* strains was tested using the pathogenic isolate 1A of FOL, provided by Dr. Cristina Moyano from the Laboratory for Assessment of Variety, Seed and Nursery Plants, INIA-CSIC (Madrid, Spain). FOL was stored at 4°C in tubes containing sterile sand. For mycelial production, conidia from FOL stored in sterile sand were germinated on Czapek Dox agar (CDA; Difco Laboratories, Detroit, MI, United States) and cultivated in darkness at 25°C for 7 days. Microconidial inoculum of FOL was produced in 250 ml flasks containing 150 ml of sterile Czapek Dox broth (Difco). Each flask was inoculated with three mycelial plugs (1 cm diameter) from the 7-day-old cultures on CDA (De Cal et al., 1995) and incubated for 5 days at 25°C in a rotary shaker (model 3527; Lab-Line Instruments, Inc.) at 150 rpm. Microconidia were separated from the mycelial mass by filtration through glass wool. The conidial concentration was determined using a hematocytometer and adjusted to 10^6 microconidia/ml.

Efficacy assays

At least two growth chamber experiments were carried out on tomato plants to evaluate the biocontrol efficacy of S27 against FOL as described by Villarino et al. (2018). Seeds of tomato cultivar "San Pedro", which is susceptible to races 1 and 2 of FOL, were used in all experiments. Tomato seeds were sown in sterile trays (27 cm × 42 cm × 7 cm) that contained an autoclaved (for 1 h at pressure of 1 kg cm^{-2} and temperature of 121°C, during 3 consecutive days) mixture of vermiculite (Termita; Asfaltex, S.A., Barcelona, Spain) and peat (Gebr. BRILL substrate GmbH & Co. KG; 1:1, *v:v*). The trays were maintained in a growth chamber at 25°C with fluorescent lighting (100 µE m^{-2} s^{-1}, 16-h photoperiod) and 80–100% relative humidity for 3–4 weeks. Tomato seedlings (with at least two true leaves) were treated 7 days before transplanting with an aqueous conidial suspension (6×10^6 conidia per gram of substrate) of S27 or PO212. Conidial suspensions of PO212 and S27 were prepared as follows: Dried conidia of PO212 were rehydrated in sterile distilled water (SDW) using a rotatory shaker at 150 rpm for 2 h (CERTOMAT® RM). Conidia of S27 were harvested from colonies grown on PDA and incubated in the dark at 25°C for 7 days. The day before treatment, the viability of PO212 and S27 conidia were estimated by measuring their germination as previously described (Larena et al., 2003a). For each replicate (three by sample type), the germination of 50 randomly selected conidia was counted and viability was calculated and expressed as a percentage (De Cal et al., 1990). Seven days after treatment, tomato seedlings were transplanted from seedbeds into 100-ml flasks containing 100 ml of Hoagland solution (Hoagland and Arnon, 1950) so that the roots were in contact with the solution, as described by De Cal et al. (1997a). An aliquot of an aqueous (SDW) conidial suspension of FOL was added to the flasks just before transplanting so that the final conidial concentration in the flasks was 1×10^5 conidia/ml. Plants that had been inoculated with the pathogen but not treated with any strain of *P. rubens*, were used as the control. Five replicate flasks, each containing four plants, were used per treatment. The flasks were placed in a randomized complete block design in a growth chamber for 4 weeks under the conditions described earlier in this subsection. The complete experiment was done two times. Disease severity was graded on days 7, 14, 21, and 28 after the transplant. Disease severity followed a 1–5 index scale: 1, healthy plants (0–24%); 2, yellow lower leaves (25–49%); 3, dead lower leaves and some yellow upper leaves (50–74%); 4, dead lower leaves and wilted upper leaves (75–99%); and 5, dead plants (100%; De Cal et al., 1995). All plant roots were placed in humidity chambers at the end of

each experiment, and the presence or absence of the pathogen in the crown after 5 days of incubation at 25°C was recorded.

Data of disease severity and incidence were analyzed by ANOVA with the STATGRAPHICS program (XVII Centurion. v. 17.2.00). When the *F* test was significant at a value of p of < 0.05, means were compared using the Student–Newman–Keul's multiple range test (Snedecor and Cochran, 1980).

Genomic DNA extraction, sequencing, and PCR

Genomic DNA (gDNA) was extracted from the mycelia of *Penicillium* strains (Table 1) grown in liquid MM at 25°C for 2 days. Mycelia were harvested by filtration using Miracloth (Calbiochem, Merck-Millipore, Darmstadt, Germany). Samples were lyophilized for at least 6 h. For each sample, mycelium was pulverized using a ceramic bead in a FastPrep-24 homogenizer (MP Biomedicals™), one pulse for 20 s at minimum speed. A sample of 100 mg of powdered mycelium was mixed with 1 ml of DNA extraction solution (25 mM Tris–HCl pH 8.0, 250 mM sucrose, and 20 mM EDTA pH 8.0). Before incubation for 15 min at 65°C, 100 µl of 10% SDS were added to each sample. Next, proteins and cellular debris were removed by adding 1 ml of Phenol/Chloroform/Isoamyl alcohol mixture per sample and further mixing on a rotary shaker (Rotator Multi Bio RS-24) for 15 min at room temperature (RT). Organic and aqueous phases were separated by centrifugation on a benchtop centrifuge at maximum speed for 5 min. gDNA was precipitated from the aqueous phase by the addition of 1/10 vol of sodium acetate pH 6 and 0.6 vol of 2-propanol, followed by incubation for 15 min at RT and centrifugation for 5 min at RT. To wash the gDNA pellet, 1 ml ethanol (80%) was added, followed by centrifugation at max. Speed for 5 min at RT. After drying the ethanol in samples, pellets were dissolved in 500 µl sterile water, and samples were treated with DNase-free RNase A (5 mg/ml; 37°C, 60 min). gDNA was newly precipitated and washed as described before. Finally, gDNA was dissolved in 200 µl nuclease-free water and stored at −20°C until use.

Sequencing of PO212 gDNA was performed on an Illumina MiSeq 500 cycles at the "FPCM, Fundación Parque Científico de Madrid" sequencing facility using 150 bp and 250 bp paired-end sequencing reads. For S27 gDNA, Stab Vida (Portugal) performed the construction and sequencing of DNA libraries. DNA libraries were sequenced on the lllumina Hiseq 4000 platform, using 150 bp paired-end sequencing reads.

Standard PCR protocols were used: initial denaturation at 95°C for 2 min, 30 cycles of denaturation at 95°C for 10 s, annealing at 55°C for 30 s, and extension at 72°C for 1 min/kb. After 30 cycles, an extension at 72°C for 10 min and storage at 4°C. The polymerase Takara (TaKaRa Taq™) was used for amplification. Oligonucleotides were designed using Vector NTI™ Suite 8 and are listed in Table 2. The oligonucleotides for the amplification of MAT1-1 and MAT1-2 were previously described in Espeso et al. (2019). PCR products were analyzed in 0.8% agarose-TAE electrophoresis and when required, they were purified using the PCR clean-Up kit (Macherey-Nagel), following the manufacturer's instructions. Sequencing of DNA fragments was done by Stab Vida's (Portugal) sequencing service.

TABLE 2 List and nucleotide sequence of the oligonucleotides used in this work.

Primer code	5′-3′ Sequence
g196 F	GGACAGTACGGCATTGGATATTACGGACACC
g196 R	CCAGATTGTGTCCCATAGACGTTGTCCG
g1339 F	CCACACCGTCAGACTTTGGAATCCTATACC
g1339 R	CGACTTGCACGACAAGATGAGTTGGTTTCC
g3160 F	GCTCCGCTGGGAATGTATTATACACCTACG
g3160 R	CTCGCAATTCCTCTTGAGATGGAAGCTCG
g3741 F	GGATCGAACACGAGGGAAGATTCCTTGCC
g3741 R	CCAACACTGTTACAGAAAGCCTCGATGG
g3975 F	GCCAAAGCTCAACCAATACCCAGAGTACC
g3975 R	CGACTATGTCGCTAATTCGCAGGGTCGTGTC
g4471 F	CCAAGATCACCTCAACTTGTCTGCCTCACC
g4471 R	CGTATGGAGGAGCAACGATGAAAGAGGATCG
MAT1-1_fw	TGCAGCTCAAGTTCTACG
MAT1-1_rv[a]	AGGAGTACATCTCATCAACC
MAT1-2_fw	ATGGTGAAGTCTTCCTGCC
MAT1-2_rv[a]	AGAGAGTGGCTCGACACC
nirA 1	CACTAGGCATGCGAAGAGG
nirA 2	TACATCGCTGCTGATCTCGC

[a]These sequences correct the sequences previously published in Espeso et al. (2019).

Assemblies and comparative analyses of genomes

For sequencing of the PO212 genome, two libraries of 150 and 250 bp paired-end fragments were produced and raw sequencing reads were subjected to quality control using the FastQC program.[1] A Q > 28 along the read length and the *k*-mers and nucleotide distribution were homogeneous in both libraries. An A5-miseq pipeline was used (Coil et al., 2015) to assemble the PO212 genome. The nuclear reads were extended using FLASH (Magoč and Salzberg, 2011) and were assembled using the A5-miseq pipeline, until the output, named final.scaffolds.fasta, was obtained. The previously aligned mitochondrial reads were assembled to obtain a single mitochondrial contig of ~28 kbp.

De novo assembly of the S27 genome was performed using the A5-miseq pipeline (Coil et al., 2015) and further revised with Gapcloser from the Soapdenovo assembler (Luo et al., 2015). The

1 https://www.bioinformatics.babraham.ac.uk/projects/fastqc/

aligned S27 mitochondrial reads were assembled apart from the genome in 13 contigs of ~34 kbp.

Completeness of the genome assemblies was assessed by the Benchmarking Universal Single-Copy Orthologs (BUSCO) v.2.0.1 software tool (Simão et al., 2015). The assembled genomes were annotated using the MAKER (v.2.31.9) pipeline (Campbell et al., 2014). Before annotation, a species-specific repeat library was constructed using RepeatModeler (v.1.0.8) to mask repeats (Tempel, 2012). Gene models were predicted with AUGUSTUS (Stanke et al., 2006) using two strategies, *ab initio* gene predictors and training with *Aspergillus nidulans* as a model genome.

Gene models of the PO212 and S27 genomes were manually curated using the P2niaD18 (GCA_000710275) and PrWis (GCA_000226395) strain proteins available in the EnsemblFungi and the National Center of Biotechnology Information (NCBI) database as evidence for gene prediction using Apollo (Dunn et al., 2019). Predicted proteins were functionally annotated using BLASTp (Altschul et al., 1990) against the non-redundant database of the NCBI and classified using InterProScan and Pfam analysis (Jones et al., 2014).

The comparison of the PO212 genome with genomes from other strains of *P. rubens* and *P. chrysogenum*, which are available in the database and listed in Table 3, was performed through the Quast bioinformatics tool (Gurevich et al., 2013). To visualize the genomes of the *P. rubens* and *P. chrysogenum* strains, Icarus, a genome visualizer based on the Quast tool, was used (Mikheenko et al., 2016). These genomes are divided into two groups according to the literature: *P. chrysogenum* (P2niaD18, KF-25, HKF42, NCPC10086, and v1.0) and *P. rubens* (PrWis and Biourge 1923; Table 3).

Due to the current controversy in the classification of *P. chrysogenum* and *P. rubens*, in this study, all these strains have been classified as belonging to the *P. chrysogenum or P. rubens* clade, based on the barcodes of three genes encoding proteins: β-tubulin (BenA), RNA polymerase II second largest subunit (RPB2), and calmodulin (CaM). The barcodes used were JF909949 (BenA), JX996658 (RPB2), and JX996263 (CaM) to *P. rubens* and AY495981 (BenA), JN121487 (RPB2), and JX996273 (CaM) to *P. chrysogenum* (Visagie et al., 2014). The sequences of *P. rubens* and *P. chrysogenum* were aligned to the barcodes with the Multiple Sequence Alignment tool of Clustal Omega (EMBL-EBI).

MUMmer4 software package (Marçais et al., 2018) was used for pairwise alignment of PO212 and S27 assemblies by setting PO212 as the reference; the minimum length of a matched group to 20 bp and the distance an alignment extension will attempt to extend to poor scoring regions before yielding to 100 bp. Comparative analysis was performed using Circos tools (Krzywinski et al., 2009). Moreover, CLC Genomics Workbench 12 (QIAGEN Bioinformatics; https://digitalinsights.qiagen.com/products-overview/discovery-insightsportfolio/analysis-and-visualization/qiagen-clc-genomics-workbench/) was used to align the reads of S27 to the assembled genome of PO212. The CLC alignment workflow was used to map the raw reads to a reference genome and to detect variants. Default values were used, except for the minimum coverage and minimum count, which were set to 10 and 2, respectively, to avoid loss of information. Of all the variations found, homozygous variations were selected. Only variations with 100% of frequency were taken into account for manual verification by PCR amplification using specific primers and sequencing. To visualize amino acid changes in genes between PO212 and S27 strains, we used Integrative Genome Viewer (IGV version 2.9.4; Robinson et al., 2011).

Phylogenetic analysis

A phylogenetic tree was constructed based on nucleotide sequence from assemblies of genomes from PO212, S27, and other strains of *P. rubens* and *P. chrysogenum* available in the database and listed in Table 3. For this purpose, *Aspergillus nidulans* strain FGSC-A4 genome (Wortman et al., 2009) and *P. oxalicum* strain HP7-1 genome (Zhao et al., 2016) were used as outgroups. The phylogenetic tree was generated using the software JolyTree (Criscuolo, 2019). The algorithm uses an alignment-free distance-based procedure for inferring phylogenetic trees from genome contig sequences. The pairwise dissimilarity between each pair of genomes was estimated using the Mash method (Ondov et al., 2016). Balanced Minimum-Evolution (BME) was used to optimize the evolutionary distances calculated in the first step. Finally, the rate of elementary quartets (REQ) was used for assessing the

TABLE 3 List of fungal strains whose genomes have been used in this work.

Strain	Species	Assembly	References
PO212	*Penicillium rubens*	JAPDLE000000000	This work
S27	*P. rubens*	JAPDLD000000000	This work
PrWis	*P. rubens*	GCA_000226395.1	Van Den Berg et al. (2008)
Biourge 1923	*P. rubens*	GCA_902636305.1	Pathak et al. (2020)
P2niaD18	*Penicillium chrysogenum*	GCA_000710275.1	Specht et al. (2014)
NCPC10086	*P. chrysogenum*	GCA_000523475.1	Wang et al. (2014)
HKF42	*P. chrysogenum*	GCA_002080375.1	Gujar et al. (2018)
KF-25	*P. chrysogenum*	GCA_000816005.1	Peng et al. (2014)
v1.0	*P. chrysogenum*	JGI Mycocosm	de Vries et al. (2017)
HP7-1	*Penicillium oxalicum*	GCA_001723175.3	Zhao et al. (2016)
FGSC-A4	*Aspergillus nidulans*	GCA_000011425.1	Wortman et al. (2009)

branch confidence values to construct the final tree (Criscuolo, 2019).

In addition, a tree obtained with the concatenated sequences *benA, caM*, and *RPB2* barcodes was generated using the maximum likelihood method with 1,000 bootstrap replications. The tree was drawn to scale, with branch lengths representing the inferred evolutionary distances. Between 1,879 and 1,931 bp were presented in the final data set. Sequences of *P. oxalicum* barcodes were used as an outgroup. Multiple sequence alignments were performed using the ClustalW algorithm (Thompson et al., 1994). The Tamura-Nei model and MEGA11 software were used for the phylogenetic analysis of sequence data (Tamura and Nei, 1993; Tamura et al., 2021).

Results

Genome sequencing of PO212, assembly, and general characteristics

The genome of PO212 was sequenced *via* paired-end Illumina MiSeq technology, providing two DNA-seq libraries: one paired-end small fragment library and a second obtained from long-range DNA fragments. The resulting assembly was performed *de novo* and evaluated in terms of N50 and L50 using Quast. Automated assembly and manual sequence verification yielded an estimated PO212 genome size of 29.82 Mb at ~200× coverage. PO212 genome was organized into 65 scaffolds with an N50 scaffold length of 1.88 Mb, comprising the first six longest scaffolds and reaching an N90 scaffold length of 0.38 Mb, corresponding to the first 18 scaffolds (Table 4 and Supplementary Table S1). PO212 genome had a GC content of 49.07%, similar to that of other *Penicillium* genomes. After the manual curation of automated ORF predictions by AUGUSTUS, we determined at least 10,164 ORFs in the PO212 genome.

The data presented in the study are deposited in the GenBank repository, accession number JAPDLE000000000.

Comparative analysis of PO212 assembly and genomic data from *Penicillium rubens* and *Penicillium chrysogenum* strains

To perform a comparison of PO212 with other genomes, we chose those genomes deposited in databases of *Penicillium* species classified as *P. rubens* or *P. chrysogenum*. Given the controversy in the current classification of *P. rubens* and *P. chrysogenum*, we first analyzed the barcode sequences corresponding to *benA*, *caM*, and *RPB2* in these deposited genomes and the newly sequenced PO212 to determine which strains corresponded to each species.

Using the Clustal Omega Multiple Sequence Alignment tool (EMBL-EBI), we generated multiple alignments with each of the three barcode sequences (Supplementary Figure S1). These alignments indicated that all strains share the same sequence changes characteristic of *P. rubens* barcodes (indicated as pink boxes in Supplementary Figure S1). In the genomes of strains KF-25 and v1.0, *benA*, *caM*, and *RPB2* barcodes displayed a mixture of sequence changes between those of *P. rubens* and *P. chrysogenum*. This analysis indicated that most probably all strains, including PO212 and with the exception of KF-25 and v1.0, may belong to the *P. rubens* clade, as the nucleotide sequences of the barcodes were identical to those described as *P. rubens* as compared to the sequence described as *P. chrysogenum* (Supplementary Figure S1). Supplementary Figure S2 shows the tree generated for all studied strains of *Penicillium* spp. by concatenating the sequences of *benA, caM*, and *RPB2* gene fragments (between 1,879 and 1,931 bp). This tree clustered the multilocus sequence of *P. rubens* strain DTO 98E8 and all multilocus sequences from previously described *P. rubens* strains and differentiated those from *P. chrysogenum* strains KF-25 and v1.0. This cluster of *P. rubens* strains included PO212 multilocus. Consistent with the multilocus analysis shown in Supplementary Figure S2, a genome-based phylogenetic tree constructed using nucleotide sequence from assemblies of all studied strains showed the identical distribution of strains into two clusters (Figure 1).

For a more detailed comparison, multiple comparative analyses of these genomes were conducted using the Quast tool and the PO212 genome as a reference genome (Supplementary Table S1). The genomes of strains KF-25 and v1.0 were included as distant members of the *P. rubens* and *P. chrysogenum* clades. All genomes used in this comparison contained similar GC content (Supplementary Figure S3). The percentage of the genome represented relative to the PO212 genome ranged from 92.91 (KF-25) to 98.579% (HKF42). The duplication ratio was low (1.001–1.007), indicating high sequence conservation and the absence of major duplication events in the BCA PO212. In terms of mismatches, the greatest differences were found, as expected, with those that presented the greatest differences in barcode alignments (KF-25 and v1.0). However, the most similar strains to PO212 in the number of mismatches were HKF42 and Biourge 1923. The best-assembled genome, organized

TABLE 4 Assembly and gene prediction summary of PO212 and S27 genomes.

Strain	Scaffolds	Assembly Size (Mb)	Largest Scaffold (Mb)	N50 (Mb)	BUSCO completeness (%)	Predicted genes
PO212	65	29.82	3.49	1.88	98.5	10,164
S27	414	29.89	1.65	0.42	98.3	10,164

into five scaffolds, is P2niaD18 and the comparison with PO212 assembly showed the presence of 98.46 mismatches per 100 kbp, probably indicating the distant origins of both strains.

Quast analysis also showed the differences between the PO212 assembly and the other selected *Penicillium* genomes, suggesting the presence of numerous variations that could prevent immediate identification of those causing the BCA phenotype. Figure 2 provides an overview of the distinctive organization of the assemblies used in this comparison with respect to PO212. The excessive number of variations and the difficulties in testing biocontrol characteristics of the strains with a sequenced genome prompted us to choose for sequencing and detailed genomic analysis an alternative *P. rubens* strain that lacked the BA but was close to the PO212 strain.

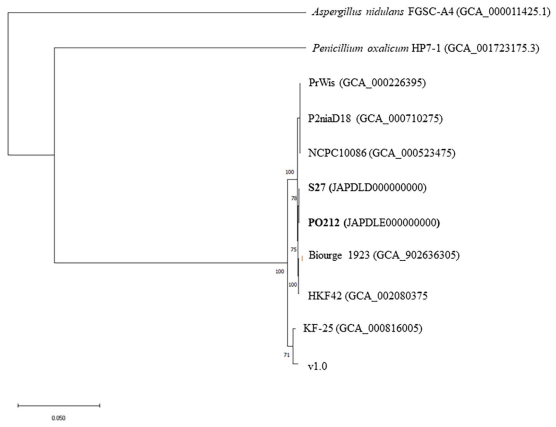

FIGURE 1
Genome-based phylogenetic tree among *Penicillium rubens* strains studied in this work. The phylogenetic tree was generated using the software JolyTree. The *Aspergillus nidulans* strain FGSC-A4 genome and *Penicillium oxalicum* strain HP7-1 genome were used as outgroups.

S27 lacks efficacy against Fusarium wilt

The S27 strain was isolated from the soil and was primarily classified as a non-BA strain (Villarino et al., 2016). Notably, S27 displayed similar colonial morphology to PO212 (Figure 3). Sequencing of ITS1-5.8S-ITS2 regions classified S27 as a *P. rubens* strain, and a dendrogram based on BOX and repetitive extragenic palindromic (REP) DNA fingerprints placed S27 close to the isolate PO212 (Villarino et al., 2016).

The efficacy of S27 against Fusarium wilt in tomato plants was recently determined. In contrast to PO212, strain S27 did not significantly ($p \leq 0.05$) reduce either the disease severity or incidence caused by FOL in tomato plants. FOL-inoculated and S27-treated plants showed similar symptoms to FOL-inoculated and untreated control plants (control +, Figure 3). Thus, we chose S27 for genomic sequencing as the best tool for a comparative genomic analysis with PO212 to target genes potentially related to PO212 BA.

Comparative of PO212 and S27 genomes

The genome of the S27 strain was sequenced using the Illumina Hiseq 4000 platform by 150 bp paired-end sequencing reads that generated 2,345 Mbp (15,532,752 sequence reads). These reads showed coverage of ~82.3× over PO212 assembly. *De novo* assembly of the S27 genome was performed and evaluated in terms of N50 and L50 using Quast. Automated assembly and manual sequence verification allowed estimating for the S27 strain

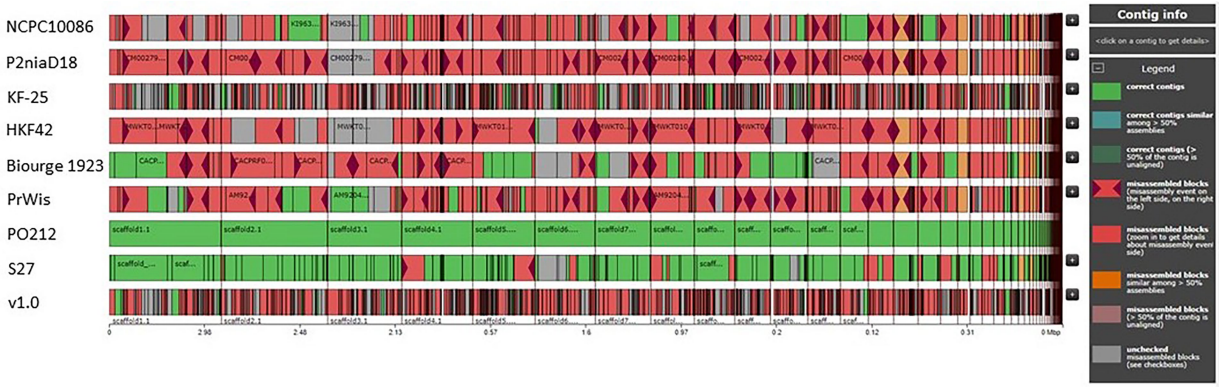

FIGURE 2
Comparative graphs of P2niaD18, PrWis, Biourge 1923, NCPC10086, KF-25, HKF42, v1.0, S27, and PO212 genomes. Contig alignment viewer, showing the organization of the genomes with reference to PO212. Green regions are right contigs, blue regions are correct contigs similar among >50% assemblies, and in dark green are the contigs referring to correct contigs (>50% of the contigs are unaligned). Pink regions with garnet triangles refer to misassembled blocks (misassemblies events on the left side or the right side), whole pink regions refer to misassembled blocks, orange regions are misassembled blocks (similar among >50% assemblies), brown regions are misassembled blocks (>50% of the contigs are unaligned), and gray regions are unchecked misassembled blocks (Visualized with Icarus).

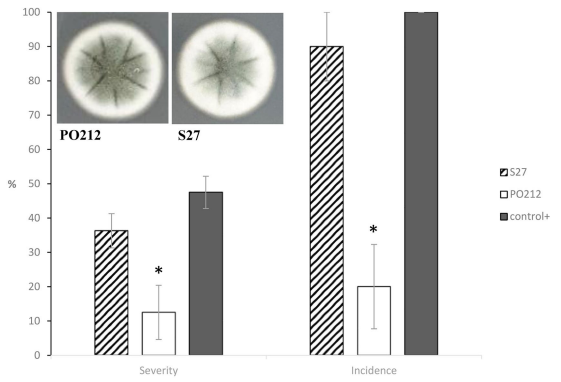

FIGURE 3
Cultures of 7-day-old *Penicillium rubens* strains 212 and S27 growing on potato dextrose agar (PDA) at 25°C (front). The graph shows the effect of PO212- and S27-treatment on percentage of disease severity and incidence caused by *Fusarium oxysporum* f.sp. *lycopersici* (FOL) in tomato plants cv. "San Pedro" at 28days after FOL-inoculation under controlled growth chamber conditions. PO212 and S27 treatments were applied to seedlings 7days before transplanting by watering with a conidial suspension to a final concentration of 6×10^6 conidia g^{-1}. Control+, untreated and FOL-inoculated plants. Data are the mean value of five replicates (flasks) per treatment and four plants per replicate. Asterisks in each parameter are significantly different from each other ($p<0.05$) according to the Student–Newman–Keuls multiple range test. Vertical bars represent the standard error of the mean of five replicates. MSE is the mean squared error of ANOVA. SME 182.292 (Severity) and 416.667 (Incidence).

a genome size of 29.89 Mb. S27 genomic assembly was organized into 414 scaffolds with an N50 scaffold length of 0.42 Mb. At least 10,164 coding sequences were estimated after manual curation of ORF prediction by AUGUSTUS.[2] Barcode analyses of *P. rubens* and *P. chrysogenum* showed that S27 was also a *P. rubens* strain (Supplementary Figure S1). Table 4 shows a summary of the two genomes. The data presented in the study are deposited in the GenBank repository, accession number JAPDLD000000000.

Genome wide alignment showed the strong conservation of PO212 and S27 genomic sequences (Figure 4). MUMmer plot showed that 99.95% of the PO212 genome assembly matched that of the S27 strain with identity equal to or greater than 75%. Only 0.05% of the genomic sequence seemed to be unique to PO212 but did not contain any predicted gene model.

Quast analysis (Supplementary Table S1) also revealed the high similarity between PO212 and S27 genomes. Comparisons of the S27 and PO212 assemblies showed that up to 99.81% of the S27 genome was represented in PO212 and a duplication ratio of 1.002. In this comparison 1,890 mismatches were found, a rate of 6.34 changes per 100 kbp of genomic sequence, which was significantly lower than the previous genomic comparison (Supplementary Table S1). The phylogenetic trees using either multilocus or genomic analysis also confirmed the proximity of

2 http://bioinf.uni-greifswald.de/augustus/

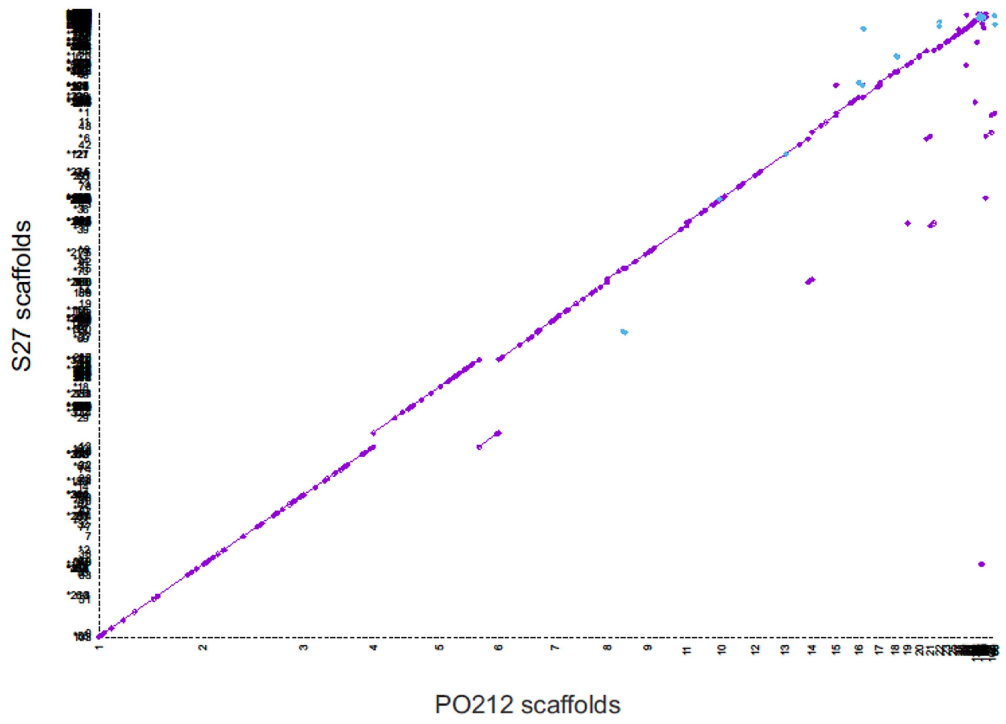

FIGURE 4
Whole-genome dot-plot showing regions of forward alignment (in purple), translocations (displacements from the diagonal), inversions (in blue), and duplications (parallel diagonal lines) between *Penicillium rubens* strains 212 (PO212) and S27. The PO212 assembly (*X* axis) was used as a reference.

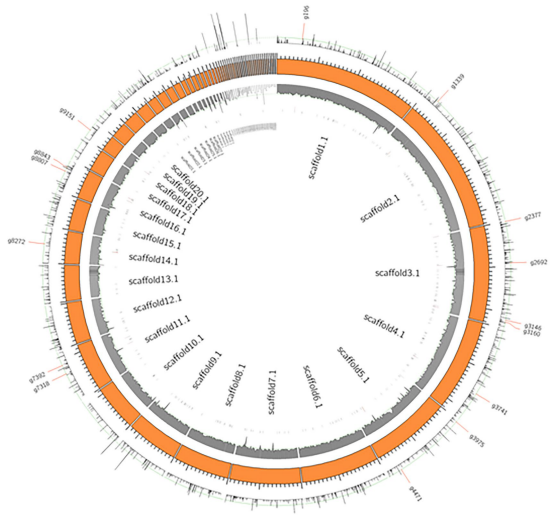

FIGURE 5
Genome wide SNVs of PO212 genome against S27. Orange boxes present scaffolds of the PO212 genome. The first inner track, the gray histogram, shows the coverage of the S27 reads aligned against the PO212 genome. The data show full coverage of the PO212 genome. The outermost track represents the SNV density of the PO212 genome against the aligned S27 reads. The innermost track, black ticks, represents genes containing SNVs in their coding region. 15 genes are highlighted with longer ticks in the innermost track and labeled in the outermost track. These 15 genes showed 100% allelic variation on the SNV loci of PO212 when compared with S27.

the two strains PO212 and S27 and other *P. rubens* strains by joining them in a clade (Figure 1 and Supplementary Figure S2).

Figure 5 shows a circos ideogram representing a comparison between the assembly of PO212 and S27 raw reads. S27 sequencing data present full coverage of the PO212 genome. Figure 6A shows that 97.86% of S27 reads mapped over the 65 scaffolds PO212 genomic assembly. The remaining 2.14% of S27 reads mapped to the mitochondrial genome. With the aid of Circos analysis and CLC software, we searched for those Single Nucleotide Variants (SNVs) displaying 100% allelic variation between S27 and PO212 genome. We detected at least 104 variations between both genomic sequences. Most of this low number of variations was classified as SNVs (Figures 5, 6B). In addition to 71 nucleotide changes found in coding or intergenic regions, we found seven Multi-Nucleotide Variants (MNVs), 14 insertions, nine deletions, and three replacements (Figure 6B). Only 15 of these variations were found in coding regions (Figures 5, 6C). However, manual curation still reduced the number of variations to six with amino acid change (see Figure 7 and Table 5) and two silent mutations (Supplementary Table S2).

We focused on six genes that carried an SNV causing an amino acid change. Only one SNV caused an early stop in the coding sequence. In g4471.t1 gene (orthologue of Pc16g08360 in PrWis), the CGA codon for arginine 327 was changed to a TGA stop codon. This SNV caused the truncation of the hypothetical protein S27g3229.t1 at amino acid 326, missing 3/4 of the ORF compared to the predicted PO212 protein (g4471.t1; Table 5). The

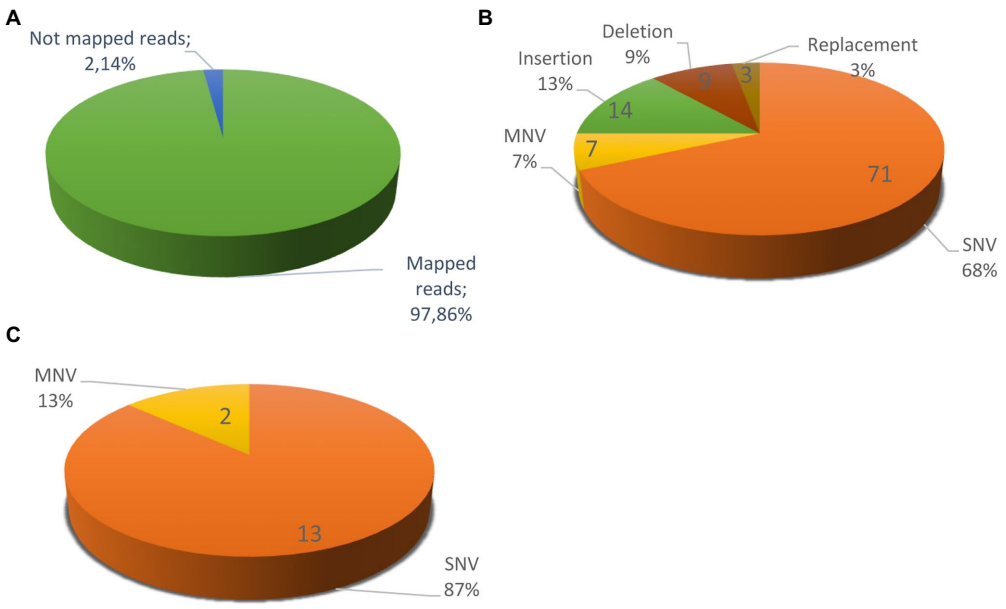

FIGURE 6
Variations between *Penicillium rubens* strains 212 (PO212) and S27 genomes. **(A)** S27 mapped reads vs. the un-mapped reads using PO212 as a reference genome. **(B)** Differences between two strains classified according the type of mutation: 71 SNVs, 7 MNVs, 14 Insertions, 9 Deletions, and 3 Replacements. **(C)** Differences between the two strains in the coding regions with 100% of frequency: 13 SNVs and 2 MNVs. After a review with preliminary RNA-Seq data support, we discarded seven variations, considered them as mistakes, and classified two as silent variations, since they did not cause an amino acid change (Supplementary Table S2).

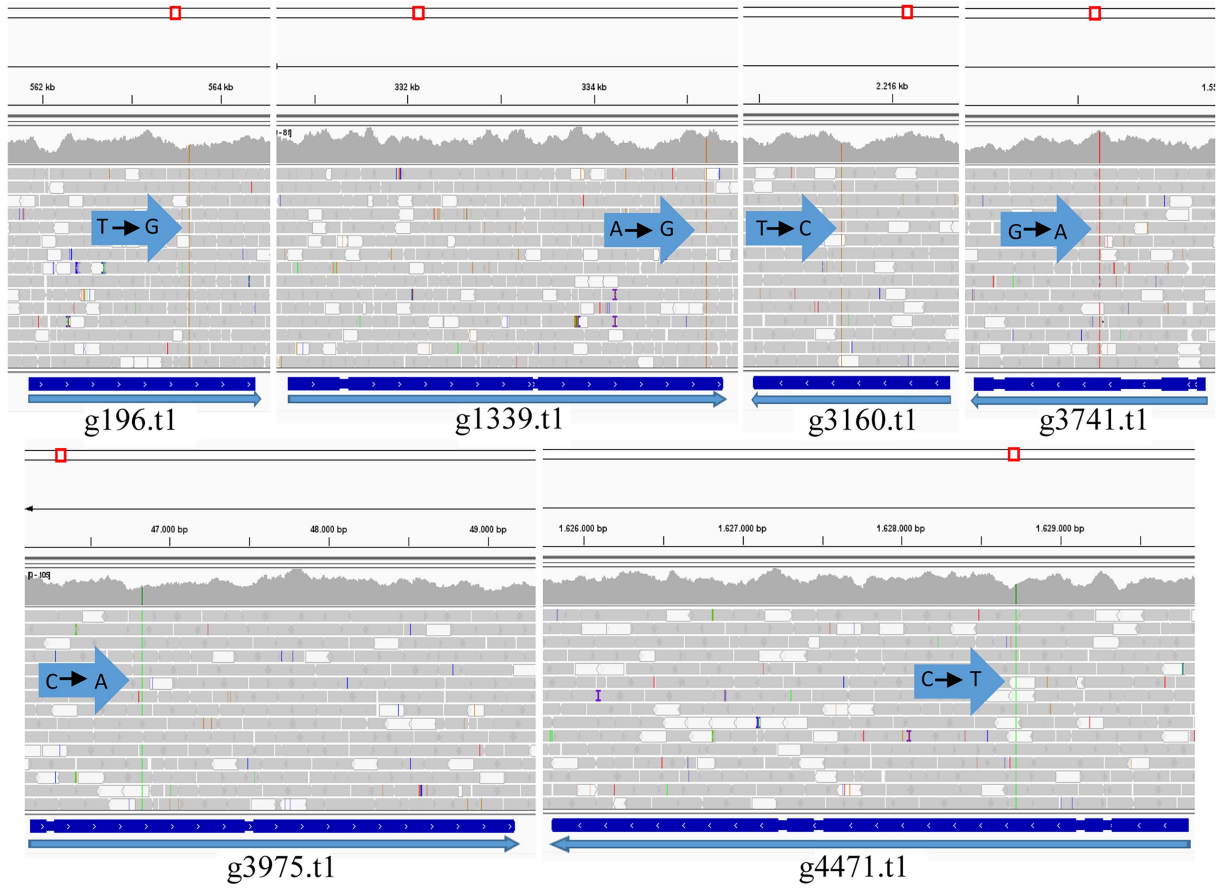

FIGURE 7
Graph mapping the S27 reads against the PO212 reference genome in the genes containing the variation (PO212 genes): g196.t1 (Dimethylglycine oxidase), g1339.t1 (Vegetative incompatibility protein HET-E-1), g3160.t1 (Putative mitochondrial chaperone), g3741.t1 (Hypothetical protein), g3975.t1 (RNA polymerase I specific TF), and g4471.t1 (Hypothetical protein). Arrows indicate the point of variation and nucleotide change (Visualized with IGV).

remaining SNVs described in Table 5 caused punctual amino acid substitutions (Figure 7). Notably, these SNVs were found only in S27. The orthologues of PO212 showed the same nucleotide sequences as in the PrWis and P2niaD18 reference genomes.

We then confirmed the presence of these variations between S27 and PO212 genomes by PCR amplification of these regions and subsequent sequencing (Table 6). To investigate whether any of these variations were specific to the biocontrol phenotype, we chose eight strains from our collection of *P. rubens* strains classified accordingly to their BA. We sequenced the regions where those SNVs were mapped. We found that SNVs are present in g196.t1, g1339.t1, and g3169.t1 genes (nomenclature as in PO212 genome) specific to S27 (Table 6). For the remaining genes, it was feasible to establish two well-differentiated groups based on specific changes in g3741.t1, g3975.t1, and g4471.t1 (Table 6).

Given the absence of specific mutations or genes that could explain the BA of PO212, we performed a search for putative homologs of 13 genes involved in biocontrol in *Trichoderma* species (Table 7; Sharma et al., 2011). Twelve were found in the genomes of PO212 and S27 without any difference in nucleotide sequences.

Discussion

Penicillium rubens strain 212 is a BCA not only capable of reducing the vascular wilt of tomatoes caused by FOL but also other diseases in a variety of horticultural crops (Larena et al., 2003a; De Cal et al., 2008, 2009; Martinez-Beringola et al., 2013). The main mode of action for the control of Fusarium wilt by PO212 is the induction of resistance in tomato plants (De Cal et al., 1997b, 1999, 2000), although plant growth promotion and competition for space and nutrients are also described (De Cal et al., 1995; Sabuquillo et al., 2009). Despite these numerous studies, the molecular basis of PO212 BA remains unexplored. Therefore, the main objective of this study was to understand the genetic components governing the biocontrol mechanism. For this purpose, we sequenced and assembled the PO212 genome for comparison with other *Penicillium* genomes deposited in databases.

A *de novo* assembly of the PO212 genome was performed, yielding a genomic sequence organized into 65 scaffolds. The estimated size of the PO212 genome (29.82 Mb) is consistent with the predicted genome size from other strains such as KF-25 (29.91

TABLE 5 List of the genes whose sequences present variations between PO212 and S27 strains and the affected amino acid.

Coding region change PO212/S27	Scaffold in PO212 genome	Triplet PO212/S27 (5′➔ 3′)	Amino acid change	Protein	*P. rubens* Wisconsin 54-1255
g196.t1/S27g134.t1	1.1	TGC/GGC	Cys605Gly	Dimethylglycine oxidase	Pc13g04270
g1339.t1/S27g7851.t1	2.1	GAT/GGT	Asp1447Gly	Vegetative incompatibility protein HET-E-1	Pc12g06410
g3160.t1/S27g8511.t1	3.1	TCC/CCC	Ser271Pro	Putative mitochondrial chaperone	Pc21g18720
g3741.t1/S27g3030.t1	4.1	GGT/AGT	Gly135Ser	Hypothetical protein	Pc06g00910
g3975.t1/S27g4439.t1	5.1	CCT/CAT	Pro219His	RNA polymerase I specific TF	E8E15_002124
g4471.t1/S27g3229.t1	5.1	CGA/TGA	Arg327*	Hypothetical protein	Pc16g08360

TABLE 6 Nucleotide variations and alleles in loci of *Penicillium rubens* strains from INIA, CSIC collection.

Strain	BCA[a]	MAT alleles	*nirA* alleles	g196.t1	g1339.t1	g3160.t1	g3741.t1	g3975.t1	g4471.t1
PO212	+	MAT1-1	*nirA1*	T	A	T	G	C	C
S27	–	MAT1-1	*nirA1*	G	G	C	A	A	T
S17	–	MAT1-1	*nirA1*	T	A	T	A	A	T
S71	–	MAT1-1	*nirA1*	T	A	T	A	A	T
S73	+	MAT1-1	*nirA1*	T	A	T	A	A	T
CH2	–	MAT1-2	WT	T	A	T	G	C	C
CH5	–	MAT1-2	WT	T	A	T	G	C	C
CH6	+	MAT1-1	*nirA1*	T	A	T	G	C	C
CH8*	+	MAT1-1	WT	T	A	T	G	C	C
CH16	+	MAT1-1	*nirA1*	T	A	T	G	C	C

BCA[a], biological control agent. The symbol + indicates biocontrol activity. The symbol – indicates no biocontrol activity. *CH8 carries the crnA1 mutation. The name of the genes corresponds to PO212.

Mb; Peng et al., 2014) and Biourge 1923 (30.45 Mb; Pathak et al., 2020). However, other *Penicillium* genomes have a larger genome, as it is the case of P2niaD18 and NCPC10086 with 32.5 and 32.3 Mb, respectively (Specht et al., 2014; Wang et al., 2014).

With the assembled genome of PO212 and the barcodes of the *benA*, *caM*, and *RPB2* genes (Visagie et al., 2014), we confirmed that PO212 belongs to the *P. rubens* clade, as previously described by Villarino et al. (2016). In addition, the PO212 genome was compared with the genomes of other *P. rubens* and *P. chrysogenum* strains to assess the quality of the PO212 assembly. These comparisons pointed to KF-25 and v1.0 as distant relatives of the other *Penicillium* strains, which were easily included in the *P. rubens* clade. *P. chrysogenum* and *P. rubens* are morphologically very similar, making it difficult to classify them into these clades without the aid of molecular data (Houbraken et al., 2011). Genome comparisons using the Quast tool allowed us to establish the strains most similar to PO212, but the lack of knowledge of whether the strains whose genomes are compared are BCAs and the differences between strains do not help us to delve deeper into the genetic basis that governs the biocontrol mechanism. Therefore, we considered the sequencing and comparison of a local strain more similar and geographically close to strain PO212 but lacking BA, so we selected isolate S27 (Villarino et al., 2016).

Similar studies comparing biocontrol microorganisms with non-biocontrol microorganisms of the same species (Hernández-Salmerón et al., 2017) and different species (Kubicek et al., 2011) have found notable differences and thus provide a genetic basis for understanding the biocontrol process. Following that strategy, Wang et al. (2014), through a comparison of the genomes of NCPC10086 and PrWis, identified 69 genes located in different scaffolds of strain NCPC10086. However, comparative analysis of the PO212 and S27 genomes showed strong conservation of their genomic sequences. Only six variants, causing an amino acid change, were found in the coding regions between PO212 and S27. Sequencing of these ORFs in eight other strains from our stock collection, previously classified according to their BA, showed the presence of specific variations in soil isolates and those taken from plants, but no correlation was found with their BAs. We also took advantage of these strains to determine whether the presence of known mutations or variations was the cause of BA. First,

TABLE 7 List of genes described in *Trichoderma* spp. as genes related to biocontrol (Sharma et al., 2011).

Genbank number	Gene	Function	PrWis code	PO212 code	S27 code
AM050097	Squalene epoxidase (*erg1* gene)	Silencing of the *erg1* gene enhances resistance to terbinafine that shows antifungal activity	Pc22g15550	g7259.t1	S27g7219.t1
EU124654	Putative acetyltransferase and monooxygenase	Antagonist activity against *S. sclerotiorum*, *S. minor*, and *S. cepivorum*	Pc21g05060	g8955.t1	S27g5480.t1
EU311400	Heat shock protein 70 kDa (*hsp70* gene)	Increases fungal resistance to heat and abiotic stresses	Pc22g11240	g9809.t1	S27g8859.t1
AJ605116	mRNA for endochitinase (*ech42* gene).	Antifungal activity in transgenic tobacco	Pc13g09520	g648.t1	S27g7976.t1
EF407410	Carotenoid cleavage dioxygenase 1 (*ccd*1 gene)	Helps in hyphal growth, conidiospore development and carotenoid pigment production	Pc12g09530	g1595.t1	S27g829.t1
EU551672	Transcription factor CTF1 (*ctf1* gene)	Antifungal activity against *R. solani*, *Fusarium oxysporum*, and *B. cinerea* and production of 6-pentyl-2H-pyran-2	Pc21g11250	g5805.t1	S27g1152.t1
DQ910533	Protease gene SL41	Biocontrol activity against pathogens	AAG44693	g5366.t1	S27g8455.t1
AM421521	Endopolygalacturonase (*pg1* gene) exons 1–5	Secretion of plant cell wall degrading enzymes against *R. solani* and *P. ultimum*	Pc22g20290	g9752.t1	S27g1693.t1
EU399786	Hypothetical kelch domain containing protein (*Thkel1*)	Expression of this gene in *A. thaliana* modulates glucosidase activity, and enhances tolerance to salt and osmotic stresses	Pc13g04170	g188.t1	S27g126.t1
AY156910	Xylanase (*xyl* gene)	Helps in breakdown of hemicellulose	Pc12g01520	g7689.t1	S27g1384.t1
Accession number not available	*tmkA* gene	Induction of plant systemic resistance and biocontrol activity against *R. solani*. (Tested in green house condition)	Pc22g01670	g7951.t1	S27g4744.t1
Accession number not available	*qid74* gene	Involved in cell protection and adherence to hydrophobic surfaces that helps in antagonism against *R. solani*	not located	not located	not located
Accession number not available	*Sm1* gene	A small cysteine-rich protein that induces defense responses in dicot and monocot plants and in protecting crop diseases	Pc20g15140	g6346.t1	S27g2607.t1

The GenBank number, the gene name, and the function are detailed. In addition, the code in PrWis, PO212, and S27 if the gene is present in these strains.

we determined the presence of MAT1-1, which is believed to play an important role in several biotechnological traits (Böhm et al., 2013) or MAT1-2. This analysis yielded no correlation between these loci and BA; in fact, both PO212 and S27 carry the MAT1-1 locus. Second, we had previously studied the complementation of the *nirA1* mutation causing a nitrate-assimilation deficient phenotype in PO212 (Espeso et al., 2019). Although complementation of *nirA1* mutation in PO212 transformants caused a reduction in their biocontrol phenotype, the S27 and other non-biocontrol strains carried the same *nirA1* mutation, indicating that the loss of NirA activity has no role in BA. In conclusion, PO212 and S27 are two strains very similar in sequence, with one important difference, the biocontrol capacity of PO212. However, current data do not suggest any correlation between the presence of the SNVs found and the biocontrol capacity of PO212 nor the absence or presence of extra genes specifically related to this phenotype.

Genome comparisons of *Postia placenta* strains evidenced high similarity between their genomes while showing important differences in phenotypes (Kölle et al., 2020). Hence, the high conservation of PO212 and S27 genomic sequences points to the presence of specific variants located in non-coding regions as candidates for a role in biocontrol. When located in putative promoter sequences, these variations could cause changes in gene expression patterns. Transcriptomic analyses are a convenient approach to studying the expression patterns of candidate genes with a potential role in biocontrol as previous works have shown (Jiang et al., 2019; Morán-Diez et al., 2019). Future lines of research will find the basis of the biocontrol phenotype in *Penicillium* focusing on epigenetics or the presence of RNA-based mycoviruses.

Data availability statement

The datasets presented in this study can be found in online repositories. The names of the repository/repositories and accession number(s) can be found in the article/supplementary material.

Author contributions

EE and IL conceived and designed the experiments. ER and MV performed the experiments. ER, LA, and JV carried out trimming and mapping of sequencing reads. ER and JV analyzed the data. ER, EE, and IL wrote the original draft manuscript. All authors contributed to the article and approved the submitted version.

Funding

The work at the INIA-CSIC laboratory was supported by the RTA2013-00060-C05-01 (Plan Nacional de Ministerio de Economía y Competitividad), RTA2017-00019-C03-01 (Plan Nacional de I+D, MICIU, Spain), and PID2021-123594OR-C21 (MCIN/AEI/10.13039/501100011033/FEDER, UE). ER received a scholarship from the MICIU.

Acknowledgments

The authors wish to thank Y. Herranz for their support and collaboration at the INIA-CSIC. The computation has been carried out in the node Centro de Supercomputación de Galicia (CESGA) of the Red Española de Supercomputación (RES).

Conflict of interest

The authors declare that the research was conducted in the absence of any commercial or financial relationships that could be construed as a potential conflict of interest.

Publisher's note

Supplementary material

The Supplementary material for this article can be found online at: https://www.frontiersin.org/articles/10.3389/fmicb.2022.1075327/full#supplementary-material

References

Altschul, S. F., Gish, W., Miller, W., Myers, E. W., and Lipman, D. J. (1990). Basic local alignment search tool. *J. Mol. Biol.* 215, 403–410. doi: 10.1016/S0022-2836(05)80360-2

Böhm, J., Hoff, B., O'Gorman, C. M., Wolfers, S., Klix, V., Binger, D., et al. (2013). Sexual reproduction and mating-type-mediated strain development in the penicillin-producing fungus *Penicillium chrysogenum*. *Proc. Natl. Acad. Sci. U. S. A.* 110, 1476–1481. doi: 10.1073/pnas.1217943110

Campbell, M. S., Holt, C., Moore, B., and Yandell, M. (2014). Genome annotation and curation using MAKER and MAKER-P. *Curr. Protoc. Bioinformatics* 48, 4.11.1–4.1139. doi: 10.1002/0471250953.bi0411s48

Coil, D., Jospin, G., and Darling, A. E. (2015). A5-miseq: an updated pipeline to assemble microbial genomes from Illumina MiSeq data. *Bioinformatics* 31, 587–589. doi: 10.1093/bioinformatics/btu661

Criscuolo, A. (2019). A fast alignment-free bioinformatics procedure to infer accurate distance-based phylogenetic trees from genome assemblies. *Res. Ideas Outcomes* 5:e36178. doi: 10.3897/rio.5.e36178

De Cal, A., Garcia-Lepe, R., and Melgarejo, P. (2000). Induced resistance by *Penicillium oxalicum* against *fusarium oxysporum* f. sp. *lycopersici*: histological studies of infected and induced tomato stems. *Phytopathology* 90, 260–268. doi: 10.1094/PHYTO.2000.90.3.260

De Cal, A., García-Lepe, R., Pascual, S., and Melgarejo, P. (1999). Effects of timing and method of application of *Penicillium oxalicum* on efficacy and duration of control of fusarium wilt of tomato. *Plant Pathol.* 48, 260–266. doi: 10.1046/j.1365-3059.1999.00324.x

De Cal, A., Pascual, S., Larena, I., and Melgarejo, P. (1995). Biological control of *fusarium oxysporum* f. sp. *lycopersici*. *Plant Pathol.* 44, 909–917. doi: 10.1111/j.1365-3059.1995.tb02750.x

De Cal, A., Pascual, S., and Melgarejo, P. (1997a). A rapid laboratory method for assessing the biological control potential of *Penicillium oxalicum* against fusarium wilt of tomato. *Plant Pathol.* 46, 699–707. doi: 10.1046/j.1365-3059.1997.d01-55.x

De Cal, A., Pascual, S., and Melgarejo, P. (1997b). Involvement of resistance induction by *Penicillum oxalicum* in the biocontrol of tomato wilt. *Plant Pathol.* 46, 72–79. doi: 10.1046/j.1365-3059.1997.d01-204.x

De Cal, A., Redondo, C., Sztejnberg, A., and Melgarejo, P. (2008). Biocontrol of powdery mildew by *Penicillium oxalicum* in open-field nurseries of strawberries. *Biol. Control* 47, 103–107. doi: 10.1016/j.biocontrol.2008.07.010

De Cal, A., Sagasta, E. M., and Melgarejo, P. (1990). Antifungal substances produced by *Penicillium frequentans* and their relationship to the biocontrol of *Monilinia laxa*. *Dis. Aquat. Org.* 8, 157–163. doi: 10.3354/dao008157

De Cal, A., Sztejnberg, A., Sabuquillo, P., and Melgarejo, P. (2009). Management fusarium wilt on melon and watermelon by *Penicillium oxalicum*. *Biol. Control* 51, 480–486. doi: 10.1016/j.biocontrol.2009.08.011

de Vries, R. P., Riley, R., Wiebenga, A., Aguilar-Osorio, G., Amillis, S., Uchima, C. A., et al. (2017). Comparative genomics reveals high biological diversity and specific adaptations in the industrially and medically important fungal genus *aspergillus*. *Genome Biol.* 18:28. doi: 10.1186/s13059-017-1151-0

Dunn, N. A., Unni, D. R., Diesh, C., Munoz-Torres, M., Harris, N. L., Yao, E., et al. (2019). Apollo: Democratizing genome annotation. *PLoS Comput. Biol.* 15:e1006790. doi: 10.1371/journal.pcbi.1006790

Espeso, E. A., Villarino, M., Carreras, M., Alonso-Guirado, L., Alonso, J. M., Melgarejo, P., et al. (2019). Altered nitrogen metabolism in biocontrol strains of Penicillium rubens. *Fungal Genet. Biol.* 132:103263. doi: 10.1016/j.fgb.2019.103263

Gujar, V. V., Fuke, P., Khardenavis, A. A., and Purohit, H. J. (2018). Annotation and De novo sequence characterization of extracellular β-Fructofuranosidase from *Penicillium chrysogenum* strain HKF42. *Indian J. Microbiol.* 58, 227–233. doi: 10.1007/s12088-017-0704-y

Gurevich, A., Saveliev, V., Vyahhi, N., and Tesler, G. (2013). QUAST: quality assessment tool for genome assemblies. *Bioinformatics* 29, 1072–1075. doi: 10.1093/bioinformatics/btt086

Hernández-Salmerón, J. E., Moreno-Hagelsieb, G., and Santoyo, G. (2017). Genome comparison of *Pseudomonas fluorescens* UM270 with related fluorescent strains unveils genes involved in rhizosphere competence and colonization. *J. Genom.* 5, 91–98. doi: 10.7150/jgen.21588

Hoagland, D. R., and Arnon, D. I. (1950). Preparing the nutrient solution. the water-culture method for growing plants without soil. *Circ. Calif. Agric. Exp. Stat.* 347, 29–31.

Houbraken, J., Frisvad, J. C., and Samson, R. A. (2011). Fleming's penicillin producing strain is not *Penicillium chrysogenum* but *P. rubens*. *IMA Fungus* 2, 87–95. doi: 10.5598/imafungus.2011.02.01.12

Jiang, C. H., Yao, X. F., Mi, D. D., Li, Z. J., Yang, B. Y., Zheng, Y., et al. (2019). Comparative transcriptome analysis reveals the biocontrol mechanism of *bacillus velezensis* F21 against fusarium wilt on watermelon. *Front. Microbiol.* 10:652. doi: 10.3389/fmicb.2019.00652

Jones, P., Binns, D., Chang, H. Y., Fraser, M., Li, W., McAnulla, C., et al. (2014). InterProScan 5: genome-scale protein function classification. *Bioinformatics* 30, 1236–1240. doi: 10.1093/bioinformatics/btu031

Kölle, M., Horta, M. A. C., Nowrousian, M., Ohm, R. A., Benz, J. P., and Pilgård, A. (2020). Degradative capacity of two strains of *Rhodonia placenta*: from phenotype to genotype. *Front. Microbiol.* 11:1338. doi: 10.3389/fmicb.2020.01338

Krzywinski, M., Schein, J., Birol, I., Connors, J., Gascoyne, R., Horsman, D., et al. (2009). Circos: an information aesthetic for comparative genomics. *Genome Res.* 19, 1639–1645. doi: 10.1101/gr.092759.109

Kubicek, C. P., Herrera-Estrella, A., Seidl-Seiboth, V., Martinez, D. A., Druzhinina, I. S., Thon, M., et al. (2011). Comparative genome sequence analysis underscores mycoparasitism as the ancestral life style of *Trichoderma*. *Genome Biol.* 12:R40. doi: 10.1186/gb-2011-12-4-r40

Larena, I., Melgarejo, P., and De Cal, A. (2003a). Drying of conidia of Penicillium oxalicum, a biological control agent against fusarium wilt of tomato. *Journal of Phytopathology.* 151, 600–606. doi: 10.1046/j.0931-1785.2003.00772.x

Larena, I., Sabuquillo, P., Melgarejo, P., and De Cal, A. (2003b). Biocontrol of fusarium and verticillium wilt of tomato by *Penicillium oxalicum* under greenhouse and field conditions. *J. Phytopathol.* 151, 507–512. doi: 10.1046/j.1439-0434.2003.00762.x

Luo, R., Liu, B., Xie, Y., Li, Z., Huang, W., Yuan, J., et al. (2015). Erratum to "SOAPdenovo2: an empirically improved memory-efficient short-read de novo assembler" [GigaScience, (2012), 1, 18]. *GigaScience* 4:30. doi: 10.1186/s13742-015-0069-2

Magoč, T., and Salzberg, S. L. (2011). FLASH: fast length adjustment of short reads to improve genome assemblies. *Bioinformatics* 27, 2957–2963. doi: 10.1093/bioinformatics/btr507

Marçais, G., Delcher, A. L., Phillippy, A. M., Coston, R., Salzberg, S. L., and Zimin, A. (2018). MUMmer4: A fast and versatile genome alignment system. *PLoS Comput. Biol.* 14:e1005944. doi: 10.1371/journal.pcbi.1005944

Martín, J. F. (2020). Insight into the genome of diverse *Penicillium chrysogenum* strains: specific genes, cluster duplications and DNA fragment translocations. *Int. J. Mol. Sci.* 21:3936. doi: 10.3390/ijms21113936

Martinez-Beringola, M. L., Salto, T., Vázquez, G., Larena, I., Melgarejo, P., and De Cal, A. (2013). *Penicillium oxalicum* reduces the number of cysts and juveniles of potato cyst nematodes. *J. Appl. Microbiol.* 115, 199–206. doi: 10.1111/jam.12213

Massart, S., Perazzolli, M., Höfte, M., Pertot, I., and Jijakli, M. H. (2015). Impact of the omic technologies for understanding the modes of action of biological control agents against plant pathogens. *BioControl* 60, 725–746. doi: 10.1007/s10526-015-9686-z

Mikheenko, A., Valin, G., Prjibelski, A., Saveliev, V., and Gurevich, A. (2016). Icarus: visualizer for de novo assembly evaluation. *Bioinformatics* 32, 3321–3323. doi: 10.1093/bioinformatics/btw379

Morán-Diez, M. E., Carrero-Carrón, I., Belén Rubio, M., Jiménez-Díaz, R. M., Monte, E., and Hermosa, R. (2019). Transcriptomic analysis of *Trichoderma atroviride* overgrowing plant-wilting *Verticillium dahliae* reveals the role of a new m14 metallocarboxypeptidase CPA1 in biocontrol. *Front. Microbiol.* 10:1120. doi: 10.3389/fmicb.2019.01120

Ondov, B. D., Treangen, T. J., Melsted, P., Mallonee, A. B., Bergman, N. H., Koren, S., et al. (2016). Mash: fast genome and metagenome distance estimation using MinHash. *Genome Biol.* 17:132. doi: 10.1186/s13059-016-0997-x

Pascual, S., De Cal, A., Magan, N., and Melgarejo, P. (2000). Surface hydrophobicity, viability and efficacy in biological control of *Penicillium oxalicum* spores produced in aerial and submerged culture. *J. Appl. Microbiol.* 89, 847–853. doi: 10.1046/j.1365-2672.2000.01189.x

Pathak, A., Nowell, R. W., Wilson, C. G., Ryan, M. J., and Barraclough, T. G. (2020). Comparative genomics of Alexander Fleming's original *Penicillium* isolate (IMI 15378) reveals sequence divergence of penicillin synthesis genes. *Sci. Rep.* 10, 15705–15710. doi: 10.1038/s41598-020-72584-5

Pattemore, J. A., Hane, J. K., Williams, A. H., Wilson, B. A. L., Stodart, B. J., and Ash, G. J. (2014). The genome sequence of the biocontrol fungus *Metarhizium anisopliae* and comparative genomics of *Metarhizium* species. *BMC Genomics* 15, 660–675. doi: 10.1186/1471-2164-15-660

Peng, Q., Yuan, Y., Gao, M., Chen, X., Liu, B., Liu, P., et al. (2014). Genomic characteristics and comparative genomics analysis of *Penicillium chrysogenum* KF-25. *BMC Genomics* 15:144. doi: 10.1186/1471-2164-15-144

Piombo, E., Sela, N., Wisniewski, M., Hoffmann, M., Gullino, M. L., Allard, M. W., et al. (2018). Genome sequence, assembly and characterization of two *Metschnikowia fructicola* strains used as biocontrol agents of postharvest diseases. *Front. Microbiol.* 9:593. doi: 10.3389/fmicb.2018.00593

Ramírez, C. (1982). *Manual and Atlas of the Penicillia 76*. Amsterdam: Elsevier Biomedical Press, 381

Robinson, J. T., Thorvaldsdóttir, H., Winckler, W., Guttman, M., Lander, E. S., Getz, G., et al. (2011). Integrative genome viewer. *Nat. Biotechnol.* 29, 24–26. doi: 10.1038/nbt.1754.Integrative

Sabuquillo, P., Sztejnberg, A., De Cal, A., and Melgarejo, P. (2009). Relationship between number and type of adhesions of *Penicillium oxalicum* conidia to tomato roots and biological control of tomato wilt. *Biol. Control* 48, 244–251. doi: 10.1016/j.biocontrol.2008.11.001

Sharma, V., Salwan, R., Sharma, P. N., and Gulati, A. (2017). Integrated translatome and proteome: approach for accurate portraying of widespread multifunctional aspects of *Trichoderma*. *Front. Microbiol.* 8:1602. doi: 10.3389/fmicb.2017.01602

Sharma, P., Vignesh Kumar, P., Ramesh, R., Saravanan, K., Deep, S., Sharma, M., et al. (2011). Biocontrol genes from *Trichoderma* species: a review. *Afr. J. Biotechnol.* 10, 19898–19907. doi: 10.5897/AJBX11.041

Simão, F. A., Waterhouse, R. M., Ioannidis, P., Kriventseva, E. V., and Zdobnov, E. M. (2015). BUSCO: assessing genome assembly and annotation completeness with single-copy orthologs. *Bioinformatics* 31, 3210–3212. doi: 10.1093/bioinformatics/btv351

Snedecor, G.W., and Cochran, W.G., (1980). *Statistical Methods 7th Edn.* Iowa State, USA: University Press

Specht, T., Dahlmann, T. A., Zadra, I., Kürnsteiner, H., and Kück, U. (2014). Complete sequencing and chromosome-scale genome assembly of the industrial progenitor strain P2niaD18 from the penicillin producer *Penicillium chrysogenum*. *Genome Announc.* 2, 4–5. doi: 10.1128/genomeA.00577-14

Stanke, M., Schöffmann, O., Morgenstern, B., and Waack, S. (2006). Gene prediction in eukaryotes with a generalized hidden Markov model that uses hints from external sources. *BMC Bioinformatics* 7, 1–11. doi: 10.1186/1471-2105-7-62

Tamura, K., and Nei, M. (1993). Estimation of the number of nucleotide substitutions in the control region of mitochondrial DNA in humans and chimpanzees. *Mol. Biol. Evol.* 10, 512–526. doi: 10.1093/oxfordjournals.molbev.a040023

Tamura, K., Stecher, G., and Kumar, S. (2021). MEGA11: molecular evolutionary genetics analysis version 11. *Mol. Biol. Evol.* 38, 3022–3027. doi: 10.1093/molbev/msab120

Tempel, S. (2012). Using and understanding repeat masker. *Methods Mol. Biol.* 859, 29–51. doi: 10.1007/978-1-61779-603-6_2

Thompson, J. D., Higgins, D. G., and Gibson, T. J. (1994). CLUSTAL W: improving the sensitivity of progressive multiple sequence alignment through sequence weighting, position-specific gap penalties and weight matrix choice. *Nucleic Acids Res.* 22, 4673–4680. doi: 10.1093/nar/22.22.4673

Van Den Berg, M. A., Albang, R., Albermann, K., Badger, J. H., Daran, J. M., Driessen, M. A. J., et al. (2008). Genome sequencing and analysis of the filamentous fungus *Penicillium chrysogenum*. *Nat. Biotechnol.* 26, 1161–1168. doi: 10.1038/nbt.1498

Villarino, M., De Cal, A., Melgarejo, P., Larena, I., and Espeso, E. A. (2016). The development of genetic and molecular markers to register and commercialize *Penicillium rubens* (formerly *Penicillium oxalicum*) strain 212 as a biocontrol agent. *Microb. Biotechnol.* 9, 89–99. doi: 10.1111/1751-7915.12325

Villarino, M., Espeso, E. A., Melgarejo, P., and Larena, I. (2018). Transformation of *Penicillium rubens* 212 and expression of GFP and DsRED coding genes for visualization of plant-biocontrol agent interaction. *Front. Microbiol.* 9:1653. doi: 10.3389/fmicb.2018.01653

Visagie, C. M., Houbraken, J., Frisvad, J. C., Hong, S. B., Klaassen, C. H. W., Perrone, G., et al. (2014). Identification and nomenclature of the genus *Penicillium*. *Stud. Mycol.* 78, 343–371. doi: 10.1016/j.simyco.2014.09.001

Wang, F. Q., Zhong, J., Zhao, Y., Xiao, J., Liu, J., Dai, M., et al. (2014). Genome sequencing of high-penicillin producing industrial strain of *Penicillium chrysogenum*. *BMC Genomics* 15, 1–12. doi: 10.1186/1471-2164-15-S1-S11

Wortman, J. R., Gilsenan, J. M., Joardar, V., Deegan, J., Clutterbuck, J., Andersen, M. R., et al. (2009). The 2008 update of the *aspergillus nidulans* genome annotation: a community effort. *Fungal Genet. Biol.* 46, S2–S13. doi: 10.1016/j.fgb.2008.12.003

Zhao, S., Yan, Y. S., He, Q. P., Yang, L., Yin, X., Li, C. X., et al. (2016). Comparative genomic, transcriptomic and secretomic profiling of *Penicillium oxalicum* HP7-1 and its cellulase and xylanase hyper-producing mutant EU2106, and identification of two novel regulatory genes of cellulase and xylanase gene expression. *Biotechnol. Biofuels* 9, 203–217. doi: 10.1186/s13068-016-0616-9

frontiers | Frontiers in Microbiology

TYPE Original Research
PUBLISHED 09 February 2023
DOI 10.3389/fmicb.2023.996287

OPEN ACCESS

EDITED BY
Javier Veloso,
University of Santiago de Compostela, Spain

REVIEWED BY
Malek Marian,
University of Trento,
Italy
Harish Sankarasubramanian,
Tamil Nadu Agricultural University,
India
Artur Pinski,
University of Silesia in Katowice, Poland

*CORRESPONDENCE
Eddie Cytryn
✉ eddie@volcani.agri.gov.il

†PRESENT ADDRESS
Chhedi L. Gupta,
Department of Medicine,
The Benioff Center for Microbiome Medicine,
University of California,
San Francisco,
CA, United States

SPECIALTY SECTION
This article was submitted to
Microbe and Virus Interactions with Plants,
a section of the journal
Frontiers in Microbiology

RECEIVED 17 July 2022
ACCEPTED 12 January 2023
PUBLISHED 09 February 2023

CITATION
Moshe M, Gupta CL, Sela N, Minz D, Banin E, Frenkel O and Cytryn E (2023) Comparative genomics of *Bacillus cereus sensu lato* spp. biocontrol strains in correlation to *in-vitro* phenotypes and plant pathogen antagonistic capacity.
Front. Microbiol. 14:996287.
doi: 10.3389/fmicb.2023.996287

Comparative genomics of *Bacillus cereus sensu lato* spp. biocontrol strains in correlation to *in-vitro* phenotypes and plant pathogen antagonistic capacity

Maya Moshe[1,2,3], Chhedi Lal Gupta[1†], Noa Sela[2], Dror Minz[1], Ehud Banin[3], Omer Frenkel[2] and Eddie Cytryn[1*]

[1]Institute of Soil, Water and Environmental Sciences, Agricultural Research Organization, Rishon-Lezion, Israel, [2]Institute of Plant Pathology and Weed Research, Agricultural Research Organization, Rishon-Lezion, Israel, [3]The Mina and Everard Goodman Faculty of Life Sciences, Bar-Ilan University, Ramat Gan, Israel

Bacillus cereus sensu lato (Bcsl) strains are widely explored due to their capacity to antagonize a broad range of plant pathogens. These include *B. cereus* sp. UW85, whose antagonistic capacity is attributed to the secondary metabolite Zwittermicin A (ZwA). We recently isolated four soil and root-associated Bcsl strains (MO2, S–10, S-25, LSTW-24) that displayed different growth profiles and *in-vitro* antagonistic effects against three soilborne plant pathogens models: *Pythium aphanidermatum* (oomycete) *Rhizoctonia solani* (basidiomycete), and *Fusarium oxysporum* (ascomycete). To identify genetic mechanisms potentially responsible for the differences in growth and antagonistic phenotypes of these Bcsl strains, we sequenced and compared their genomes, and that of strain UW85 using a hybrid sequencing pipeline. Despite similarities, specific Bcsl strains had unique secondary metabolite and chitinase-encoding genes that could potentially explain observed differences in *in-vitro* chitinolytic potential and anti-fungal activity. Strains UW85, S-10 and S-25 contained a (~500 Kbp) mega-plasmid that harbored the ZwA biosynthetic gene cluster. The UW85 mega-plasmid contained more ABC transporters than the other two strains, whereas the S-25 mega-plasmid carried a unique cluster containing cellulose and chitin degrading genes. Collectively, comparative genomics revealed several mechanisms that can potentially explain differences in *in-vitro* antagonism of Bcsl strains toward fungal plant pathogens.

KEYWORDS

biocontrol agent, chitinase, comparative genomics, phytopathogen, secondary metabolites, zwittermicin

1. Introduction

The ban on many chemical pesticides has facilitated interest in discovery and application of bacteria (termed biocontrol agents) that antagonize soilborne plant pathogens. These bacteria protect plants from pathogens through a variety mechanisms that include niche exclusion (Wang et al., 2021), metabolic competition (Spadaro et al., 2010), production of siderophores (Yu et al., 2010; Li et al., 2014), secretion of chitinases that target the chitin components of fungal cell walls (Veliz et al., 2017), antibacterial and antifungal compounds (Raaijmakers et al., 2002; Ongena and Jacques, 2008), and induction of plant resistance (Pieterse et al., 2014). Secondary metabolites (SM),

which include siderophores and antibiotics play a pivotal role in the antagonistic capacities of biocontrol agents, but the scope and the specific role of these compounds in different strains are not well understood (Braga et al., 2016).

Bacillus cereus sensu lato (Bcsl) is a phylogenetically related group that includes the well-studied member's *B. cereus sensu stricto* (*s.s.*), *B. anthracis*, and *B. thuringiensis* (Stenfors Arnesen et al., 2008; Ehling-Schulz et al., 2019; Bianco et al., 2021; Carroll et al., 2021). Several of these strains produce a variety of biologically active plant-pathogen antagonizing molecules, and have thus been explored as potential biocontrol agents (Silo-Suh et al., 1994; Kumar et al., 2014a). *Bacillus cereus s.l.* strain UW85 (ATCC 53522) has been extensively explored as a biocontrol agent due to its *in-vitro* and *in-planta* capacity to antagonize various fungal and oomycetes pathogens, which is at least partially facilitated by the antimicrobials ZwA and kanosamine (Silo-Suh et al., 1994).

Bcsl strains frequently harbor multiple plasmids, including mega-plasmids larger than 100 kb (Zheng et al., 2013). These mega-plasmids have been primarily explored in obligatory and opportunistic *B. anthracis* and other *B. cereus s.l.* strains that carry genes and operons encoding for virulence factors (i.e., *cya*, *lef*, *pagA*, haemolysin BL, *capABCDE* and *cesABCD*; Okinaka et al., 1999; Hoton et al., 2005). In addition, certain *B. thuringiensis* strains harbor mega-plasmids with genes encoding insecticidal (Cry and Cyt) toxins that are used commercially to control different insect pests (Gillis et al., 2018). Recently, whole-genome sequencing revealed that the biosynthetic gene cluster encoding ZwA and Kanosamine in certain Bcsl strains is also situated on a mega-plasmid (Kevany et al., 2009; Lozano et al., 2016; Lechuga et al., 2020), suggesting that Bcsl strain mega-plasmids play a role in ecological adaptation and antagonism of plant pathogens.

The objective of this study was to identify Bcsl strain mechanisms potentially involved in antagonizing soilborne phytopathogens and pinpoint specific mechanisms that are unique to individual strains that may explain differences in their *in-vitro* antagonistic capacity. This was achieved by combining long-and short-read (i.e., Oxford Nanopore Minion and Illumina) whole genome sequencing, which enables assembly of complete chromosomes and plasmids (Arredondo-Alonso et al., 2017; George et al., 2017). Concomitant to whole genome sequencing, the five Bcsl strains (four isolated in our lab from different soils around Israel, and *B. cereus* strain UW85) were screened against the soilborne pathogens *Pythium aphanidermatum* (oomycetes), *Rhizoctonia solani* (basidiomycetes) and *Fusarium oxysporum* (ascomycetes) using both whole cell and cell extract antagonistic assays.

2. Materials and methods

2.1. Bacterial and fungal strains and growth conditions

Bacillus cereus s.l. UW85 (coined UW85), originally isolated from alfalfa roots in Wisconsin, USA, was purchased from the American Type Culture Collection (serial number ATCC 53522). *Bacillus cereus s.l.* S-25 (coined S-25) and *B. cereus s.l.* S-10 (coined S-10) were isolated from a clay-rich wheat field soil, and *B. cereus s.l.* MO2 (coined MO2) was isolated from the roots of a *Moringa oleifera* tree within the Volcani Institute campus of the Agricultural Research Organization (ARO) in Rishon Lezion, Israel. *Bacillus cereus s.l.* LSTW-24 (coined LSTW-24) was isolated from a sandy soil from the coastal plain of Israel. The studied Bcsl strains were grown on Luria-Bertani (LB) broth or agar and incubated at 30°C overnight, with or without shaking at 180 rpm. Their antagonistic effects was tested against three model soilborne pathogens: *R. solani* anastomosis group AG4, isolated from a tomato plant in the Western Negev, Israel, whereas *P. aphanidermatum* strain P88 and *F. oxysporum* f.sp. *radicis cucumerinum* strain Hazera were isolated from cucumber plants in the Hefer Valley, Israel. The three model pathogens were routinely grown on Potato Dextrose Agar (PDA, DIFCO, France), which was amended with 250 mg/l chloramphenicol (PDA+, Sigma, Israel) for growth of *R. solani* and *F. oxysporum*.

2.2. Evaluation of *in-vitro* antifungal activity

The *in-vitro* antagonistic activity of the five Bcsl group strains against the three model soilborne phytopathogens was evaluated using a standard dual culture assay. Briefly, we streaked an overnight bacterial suspension in the middle of a 9 cm Petri dish containing 50% LB agar, and incubated it at 30°C for 3 days in a temperature controlled incubator (Tuttnauer, Israel). Subsequently, a 5 mm diameter mycelial disk from the actively growing margin of one of the three pathogens described above was placed on opposite sides of the Petri dish and further incubated at 25°C. The inhibition zone between the bacteria and the pathogen, and the area of the pathogen mycelium were measured daily for 3 to 14 days after initial inoculation, depending on the rate of pathogen growth. Two criteria were considered when evaluating the *in-vitro* antagonistic capacity:

(1) Mycelia area - calculated as the proximal area of an ellipse according to the following formula:

$$\pi * \left(\frac{D1}{2} * \frac{D2}{2} \right)$$

where $D1$ is the long diameter and $D2$ is the short diameter.

(2) Inhibition zone - calculated as the minimal distance between the pathogen and the bacteria. A schematic diagram of both criteria is shown in Supplementary Figure S1.

2.3. Evaluation of *in-vitro* cell free supernatant antifungal activity

The five Bcsl strains were inoculated in 100 mL of 50% LB medium in 250 mL Erlenmeyer flasks and incubated at 30°C with shaking at 130 rpm for 6 days in a Witeg model WIS-30R shaking incubator (Witeg Labortechnik GMBH, Germany). Starting from the third day, 1 mL of culture from each flask was centrifuged and filtered through 0.22 µm, 22mm membranes and the cell-free supernatants (CFS) were stored at 4°C. PDA plates were inoculated with 4 mm diameter agar plugs containing one of the three model pathogens, and 50 µL of CFS (or 50% LB medium used as a control) was pipeted into aseptically created holes in the agar placed at a distance of 0.5 cm from *F. oxysporum* plug, 1 cm from *R. solani* plug and 1.5 cm from *P. aphanidermatum* plug. The plates were incubated at 25°C and inhibition was inspected after 1–3 days, depending on the pathogen growth rate. The experiment was conducted three times.

2.4. Evaluation of *in-vitro* chitinase and cellulase activities and genome screening for associated genes

Approximately 15 µL of an overnight culture of the five Bcsl strains was pipetted onto agar plates containing M9 minimal medium mixed with 0.4% colloidal chitin as a sole carbon source (Kuddus and Ahmad, 2013), and subsequently incubated for 20 days at 30°C. Chitinase activity was estimated by measuring the clearing zone around the bacterial colonies, calculated by subtracting the halo area from the area of the bacterial colony.

In tandem, we mined the five Bcsl genomes for genes associated with chitin metabolism (chitinases and chitin binding proteins) using RAST and BLASTX together with the web server dbCAN2, for carbohydrate-active enzyme (CAZyme) annotation (Zhang et al., 2018; Drula et al., 2022). The chitinase-associated genes sequences of the five Bcsl strains are shown in Supplementary Table S3.

The cellulose-degrading capacity of the five Bcsl strains was estimated by plating the strains on cellulose-amended Congo-Red agar media composed of: KH_2PO_4 0.5 g, $MgSO_4$ 0.25 g, cellulose 2 g, agar 15 g, Congo-Red 0.2 g, and gelatin 2 g, distilled water 1 l and at pH 6.8–7.2 (Gupta et al., 2011). Approximately 15 µL of an overnight culture normalized to 0.5 O.D. of the five Bcsl strains were pipetted onto the cellulose Congo-Red agar and incubated for 6 days at 30°C. Cellulytic activity was calculated by measuring the clearing zone around the bacterial colonies (Supplementary Figure S5). In addition, we mined the five Bcsl genomes for genes encoding for celluloses enzymes using RAST and the web server dbCAN.

2.5. DNA extraction and genome sequencing

Bcsl strains were inoculated in LB medium and incubated overnight at 30°C with shaking at 180 rpm. The overnight culture was diluted and incubated for an additional 3 h before harvesting 2 mL for genomic DNA (gDNA) isolation using the Wizard Genomic DNA Purification Kit (Promega, Madison, WI) according to the manufacturer's instructions with slight modifications to minimize pipetting and vortex steps. gDNA yield and quality was examined using a Qubit flurometer (Thermo Fisher Scientific Inc., Waltham, MA) and a Nanodrop ND1000 spectrophotometer (NanoDrop Technologies, Wilmington, DE), and its integrity was verified by gel electrophoresis (1% agarose w/v). The gDNA was sequenced using short (Illumina MiSeq) and long (Oxford Nanopore Minion) read sequencing technologies at Genotypic Technologies, (Bengaluru, India) as described below.

A volume of 1 µg of DNA from each isolate was used for Nextra XT DNA library preparation using the manufacturers protocol (Cat#FC-131-1,024), and libraries were sequenced on an Illumina HiSeq X Ten sequencer (Illumina, San Diego, USA). In tandem, sequencing was performed on an Oxford Nanopore GridON X5 sequencing (Oxford, UK) using a SpotON flow cell R9.4 (FLO-MIN106) in a 48 h sequencing protocol. The quality of the genomes was analyzed using BUSCO (Manni et al., 2021).

2.6. Genome assembly and annotation

Trimmomatic software version 0.39 (Bolger et al., 2014) was used for removal of adaptors and low quality sequences using the following parameters: ILLUMINACLIP:adapters.fa:2:30:10 LEADING:3 TRAILING:3 SLIDINGWINDOW:4:15 MINLEN:36. Subsequently, Unicycler version 0.4.8 (Wick et al., 2017) was used for hybrid assembly of the trimmed Illumina paired-end and Nanopore reads using defaults parameters. The RAST server version 2 (Aziz et al., 2008; Overbeek et al., 2014; Brettin et al., 2015) was applied for the annotation of the assembled genomes using default parameters. OAT software was applied for genome comparisons of the five Bcsl strains and representative reference strains from the *Bacillus* group (*B. pumilus* NCTC10337, *B. velezensis* FZB42 and *B. subtilis* HJ5), based on OrthoANI (Average Nucleotide Identity) values (Lee et al., 2015). The online service OrthoVenn2 was used for genome wide comparisons and visualization of orthologous clusters based on protein sequences generated by RAST annotation tool (Xu et al., 2019). The pantoate-b-alanine ligase gene (*panC*) was used to identify the Bcsl strains lineage within the group (Guinebretière et al., 2008) using MEGA11 alignment of the five Bcsl strains and representative reference strains from the *B. cereus* group (*B. cereus* ATCC 14579 T, *B. thuringiensis* CIP 53137 T and *B. weihenstephanensis* INRA1). The *B. subtilis*-associated strain NYG5 was included as an outlier for rooting the tree (Supplementary Figure S3). The JSpeciesWS tool was used for calculating identity using tetra correlation of our five Bcsl strains against an updated published genome reference database (Richter et al., 2015).

The webserver antiSMASH (RRID:SCR_022060) version 5.1.2 (Blin et al., 2019) was applied for identification and annotation of secondary metabolite encoding biosynthetic gene clusters (BGC) using the default parameters. Comparative analysis of ZwA BGCs was performed and visualized with EasyFig (Sullivan et al., 2011), using the UW85 ZwA BGC as a template. The extrachromosomal plasmids were visualized using BLAST Ring Image Generator (BRIG) version 0.95 (Alikhan et al., 2011).

3. Results

3.1. Colony expansion and *in-vitro* antagonism of model phytopathogens by Bcsl strains

Dual culture assays revealed substantial differences in colony expansion and *in-vitro* mycelial growth inhibition by the five tested Bcsl isolates (Figure 1; Supplementary Figures S1, S2). S-10 spread rapidly and covered approximately two-thirds of the agar (resulting in substantial inhibition of *F. oxysporum*, *P. aphanidermatum* and *R. solani* mycelial expansion), whereas the other Bcsl strains grew much slower. Strain LSTW-24 did not inhibit *P. aphanidermatum* but moderately inhibited *R. solani* (~67% mycelial inhibition), while MO2 strongly inhibited *R. solani* (~92%), and moderately inhibited *P. aphanidermatum* (~54%). S-25 did not substantially inhibit *P. aphanidermatum* (~47%) and *R. solani* (~58%) mycelial growth, but caused a clear inhibition zone in dual culture assays with *P. aphanidermatum* and *R. solani* (0.5 and 0.8 cm, respectively).

3.2. Effect of Bcsl strain cell-free supernatant on model phytopathogen mycelial growth

We tested the antagonistic effect of cell-free supernatants (CFS) of the five Bcsl strains against the three model pathogens (Figure 2).

10.3389/fmicb.2023.996287

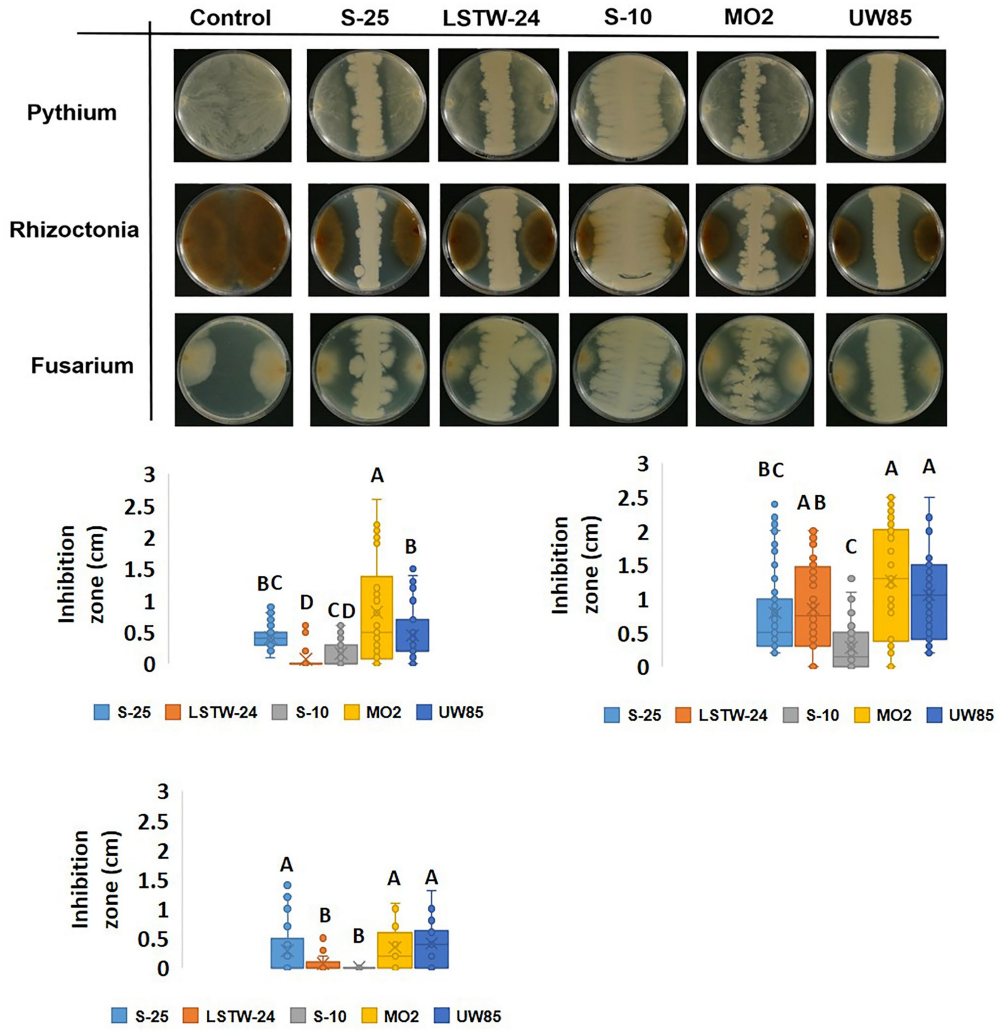

FIGURE 1
Dual culture inhibition assay of the five Bcsl strains against soilborne phytopathogens. Images of dual culture experiments (A); and inhibition zones measurements in dual cultures of 3days old Bcsl strains with *Pythium aphanidermatum* (B); *Rhizoctonia solani* (C); and *Fusarium oxysporum* (D) on 50% LB agar at 25°C. Images are shown following 3days of incubation for *P. aphanidermatum* and *R. solani* and 16days of incubation for *F. oxysporum*. Box plots represent data from three independent experiments with five replicates each. The lines in the box plot represent the median while the *x* symbols represent the mean. Different letters indicate statistically significant differences ($p<0.05$) based on the ANOVA Tukey–Kramer *post hoc* test ($\alpha=0.05$).

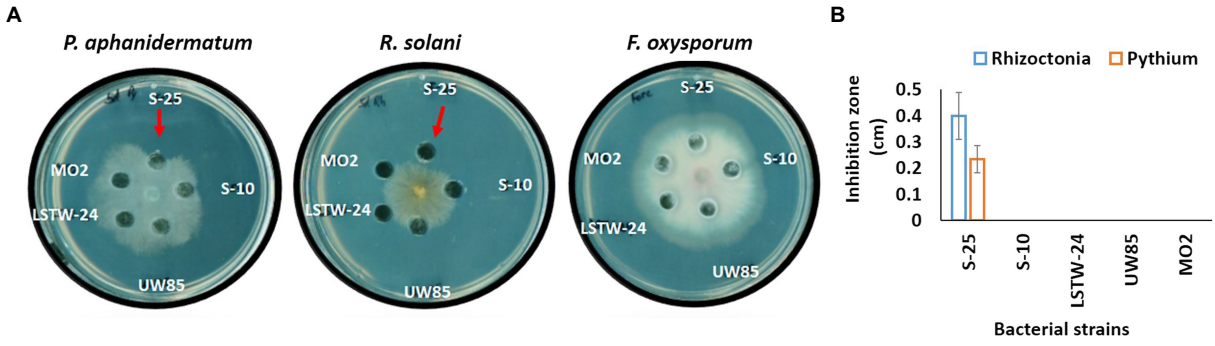

FIGURE 2
Antagonistic effect of cell-free supernatant (CFS) of the five Bcsl strains against the three model phytopathogens. Images showing antagonistic effect on mycelial growth of the three phytopathogen, *F. oxysporum*, *R. solani*, and *P. aphanidermatum* inoculated in the center of 9cm PDA plates, mediated by CFS of 5days old Bcsl strains grown on 50% LB medium **(A)**; Inhibition zone measurments of *R. solani* and *P. aphanidermatum* mycelia by the CFS of the five Bcsl strains **(B)**. The graph represents data from three independent experiments, and the vertical line shows standard deviations between replicates.

10.3389/fmicb.2023.996287

The CFS from S-25 had a clear inhibitory effect against *P. aphanidermatum* and *R. solani* mycelia (suggesting that it secretes compounds that antagonize these phytopathogens), but not against *F. oxysporum*. In contrast, the other four strains did not show a clear antagonistic phenotype against any of the screened model phytopathogens.

3.3. Comparative genomic analysis of Bcsl strains

Genome characteristics and sequencing metadata are summarized in Table 1. The genome sizes ranged from 5.3 to 6.3 Mbp with a mean GC-content of 35%, which is typical for members of the Bcsl group. Collectively, the genome size of Bcsl strains is larger than genomes of other *Bacillus* species used for biocontrol such as *B. Pumilus*, *B. velezensis* and *B. subtilis* (Shafi et al., 2017), whose average genome size is 3.7 Mbp, 4 Mbp and 4.1 Mbp, respectively. The total number of Open Reading Frames (ORFs) varied from 5,755 to 6,564, and the number of identified RNA genes from 107 to 138. Except for LSTW-24, all the sequenced Bcsl strains contained plasmids.

Average Nucleotide Identity (ANI) comparisons revealed a high level of similarity (>95%) between the Bcsl strains, with the exception of MO2 (91%, Figure 3A). Nevertheless, phylogenetic characterization of the strains based on the *pan*C housekeeping gene (involved in pantothenate biosynthesis), which has been used for phylogenetic characterization of *B. cereus* strains (Guinebretière et al., 2008), indicated that MO2 is a closely related lineage within the Bcsl group (Supplementary Figure S3). Furthermore, comparing MO2 tetra-nucleotide signatures (Tetra) to those of Bcsl strains from a large and continuously updated genome reference database using the JSpeciesWS tool, revealed a high level of identity with a correlation coefficient above 0.99. The pangenome comparisons of the five Bcsl strains identify 4,257 shared clusters out of 6,195, with 2, 17, 17, 35, and 26 clusters that were unique to LSTW-24, S-25, S-10, UW85 and MO2, respectively (Figure 3B). UW85 and MO2 accessory genes included: i) ABC transporter encoding genes, ii) genes encoding toxin and antibiotic synthesis; iii) genes linked to quorum sensing and biofilm formation, iv) genes encoding for siderophores and surfactants; v) genes encoding for carbohydrate and phosphate metabolism; and vi) genes associated with utilization of sulfur and nitrogen (Supplementary Table S1).

TABLE 1 Characteristics of the five Bcsl strain genomes used in this study.

Isolate name	Genome size (Mbp)	Total number of contigs[a]	Genome quality (% of completeness)	GC content (%)	N50[b]	Total open reading frames (ORFs[c])	RNA genes	Plasmids detected
LSTW-24	5.3	46 (14)	98.7	35.2	1,355,660	5809	107	0
MO2	5.7	6 (6)	99.8	35.2	5,250,910	5755	134	5
S-25	5.9	20 (4)	99.6	35.0	5,281,513	5795	138	2
S-10	6.0	3 (3)	99.8	34.9	5,391,120	5894	134	1
UW-85	6.3	23 (6)	99.1	34.8	2,521,153	6564	129	3

[a]Brackets show number of contigs larger than 2,500 bp.
[b]Sequence length of the shortest contig at 50% of the total genome length.
[c]ORFs predicted by Prodigal software.

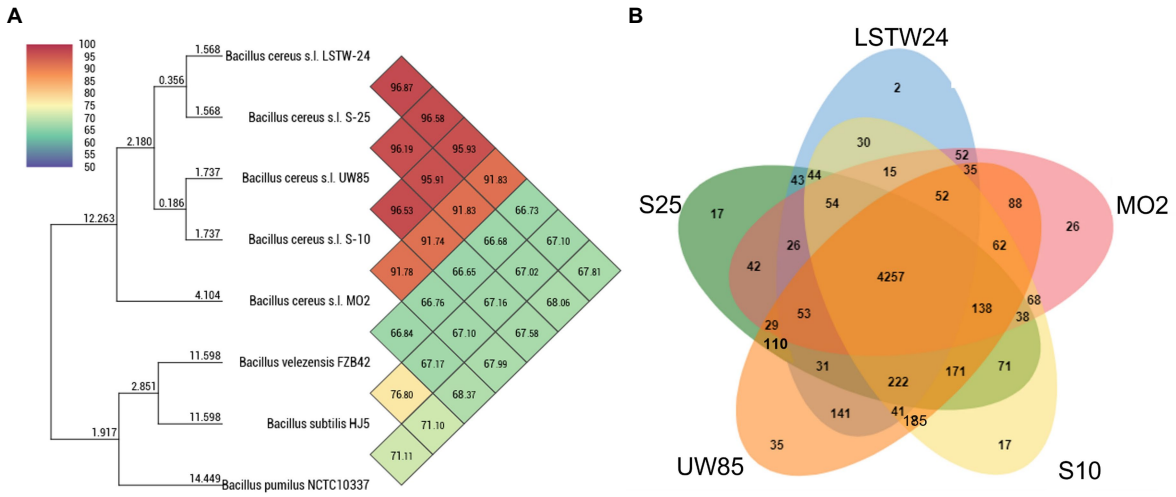

FIGURE 3
Heatmap and phylogenomic tree **(A)** showing similarity of the five-targeted Bcsl strain genomes relative to other species of *Bacillus*, based on average nucleotide identity (ANI) values, calculated using the Orthologous Average Nucleotide Identity Tool (OAT); Venn diagrams constructed using the OrthoVenn 2 online service displaying the distribution of shared and unique orthologous clusters among the five Bcsl strains **(B)**.

3.4. Evaluation of chitonolytic and cellulytic activity and associated metabolic genes in the Bcsl strains

We mined the five genomes for genes associated with chitin metabolism concomitant to evaluation of extracellular *in-vitro* chitinolytic activity. Two chitinase encoding genes were identified in S-25, S-10 and MO2, three in strain UW85, and four in strain LSTW-24. Furthermore, three chitin binding protein (CBP) encoding genes were detected in the five Bcsl, an additional CBP was found in S-25, LSTW-24, and MO2, whereas four additional CBP encoding genes were detected in UW85. A single endoglucanase gene potentially involved in chitin/cellulose degradation was also detected in S-25 but not in the other four Bcsl genomes. Based on blastx, each of the five isolates harbor chitinase genes belonging to subfamily A (ChiA) and subfamily B (ChiB) of the glycoside hydrolase GH18 family while only strains LSTW-24 and UW85 harbored additional chitinase genes. ChiA and ChiB were also ubiquitous in 20 additional Bcsl genomes that we screened. More than that, while additional genes associated with chitin degradation were only detected in some of the strains, the chitinases and CBPs genes found in LSTW-24 and UW85 strains were not detected in any of the other 20 analyzed Bcsl genomes (Supplementary Figure S4). The extracellular chitinolytic activity was generally proportional to the scope of genes associated with chitin degradation, with UW85 and LSTW-24 showing higher chitinolytic activity than the three other strains and S-25 showing the lowest activity (Figure 4). Similarly, we tested the five Bcsl strains for their *in vitro* cellulose-degrading capacity on cellulose-amended Congo Red agar plates (Supplementary Figure S5). Two strains (UW85 and LSTW-24) showed slightly higher cellulolytic activity than the three other strains, while MO2 showed the lowest activity. Nevertheless, despite the differences in the cellulolytic activity, we could not detect any correlation between the cellulolytic activity and the *in vitro* antagonistic activity against the oomycetes *P. aphanidermatum*, whose cell wall is composed of cellulose instead of chitin.

Screening the five Bcsl genomes did not reveal significant differences in genes encoding for cellulolytic enzymes that could explain the variances in *in-vitro* cellulolytic activity. We identified a gene encoding for 6-phospho-beta-glucosidase (EC:3.2.1.86), and the PTS transporter homologs CelC, CelB, and CelA in all of the strains. An additional gene encoding for beta-glucosidase (EC:3.2.1.21) was only identified in strains S-25, UW85 and LSTW-24. We did not identify genes encoding for endoglucanase (EC:3.2.1.4) in any of the strains except for a putative endoglucanase detected in the plasmid of the S-25 strain.

3.5. Annotation and comparative analysis of secondary metabolite encoding genes in Bcsl strains

The Bcsl genomes were screened for documented and potentially novel secondary metabolite encoding BGCs using Antismash (Medema et al., 2011), which ranks gene clusters by similarity to a queried gene cluster of known function, presenting the percentage of genes in the queried cluster that show similarity to the known BGC (Figure 5). All five genomes harbored BGCs encoding for the catecholate siderophores petrobactin and bacillibactin (100 and 46% similarity, respectively) (Lee et al., 2011). LSTW-24 harbored an additional BGC with 55% similarity to the siderophore fuscachelin. All genomes harbored a BGC with 40% similarity to fengycin, a biologically active lipopeptide produced by several *B. subtilis* strains known to antagonize filamentous fungi (Deleu et al., 2008). A BGC similar to Locillomycin was detected in UW85 (21%) and two such clusters (28 and 42% identity, respectively) were identified in LSTW-24. Another BGC similar to the lipopeptide Puwainaphycin was detected in UW85 (50% identity) and S-10 (60% identity). Each of the five genomes contained unique secondary metabolite encoding BGCs. For example, S-25 carried a lassopeptide-encoding BGC, MO2 harbored a BGC encoding for a sophorolipid (100% identity), a group of amphiphilic biosurfactants, and UW85 carried a BGC predicted to encode for an unknown cyclodipeptide. In addition, S-25 and S-10 harbored BGCs putatively encoding for the hybrid NRPS/PKS metabolite ZwA (81 and 100% similarity, respectively), which was first characterized in UW85 (Silo-Suh et al., 1994). This metabolite has been extensively explored in UW85 and other prospective Bcsl biocontrol strains, due to its antagonistic effect against oomycetes and other soilborne pathogens

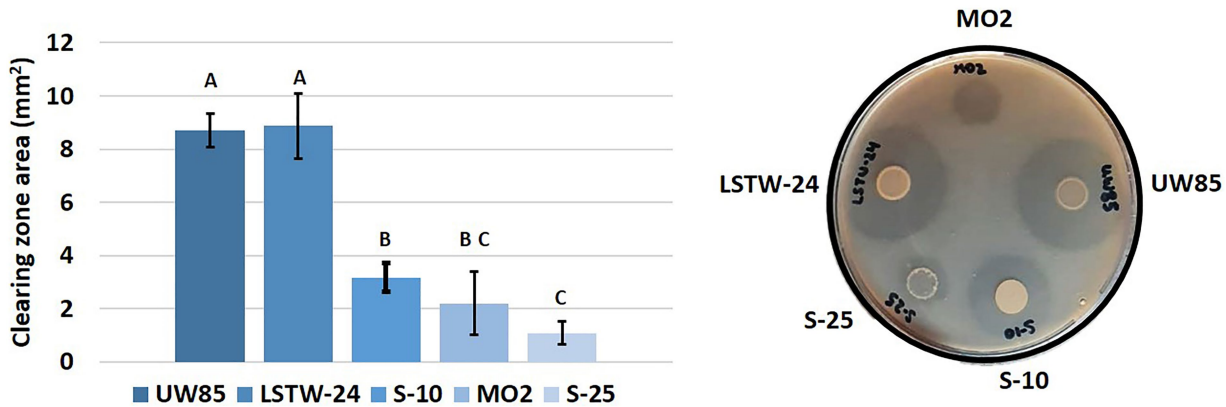

FIGURE 4
Chitinolitic activity of five Bcsl strains. Area of clearing zones indicating the different chitinolytic activity of the five Bcsl strains on M9 minimal medium containing colloidal chitin as a sole carbon source. The graph showing the mean and standard deviations of 10 independent measurements (left); and image illustrating the extracellular chitinolytic activity of the five isolates (right). Different letters indicate statistically significant differences ($p<0.05$) based on the ANOVA Tukey-HSD test ($\alpha=0.05$).

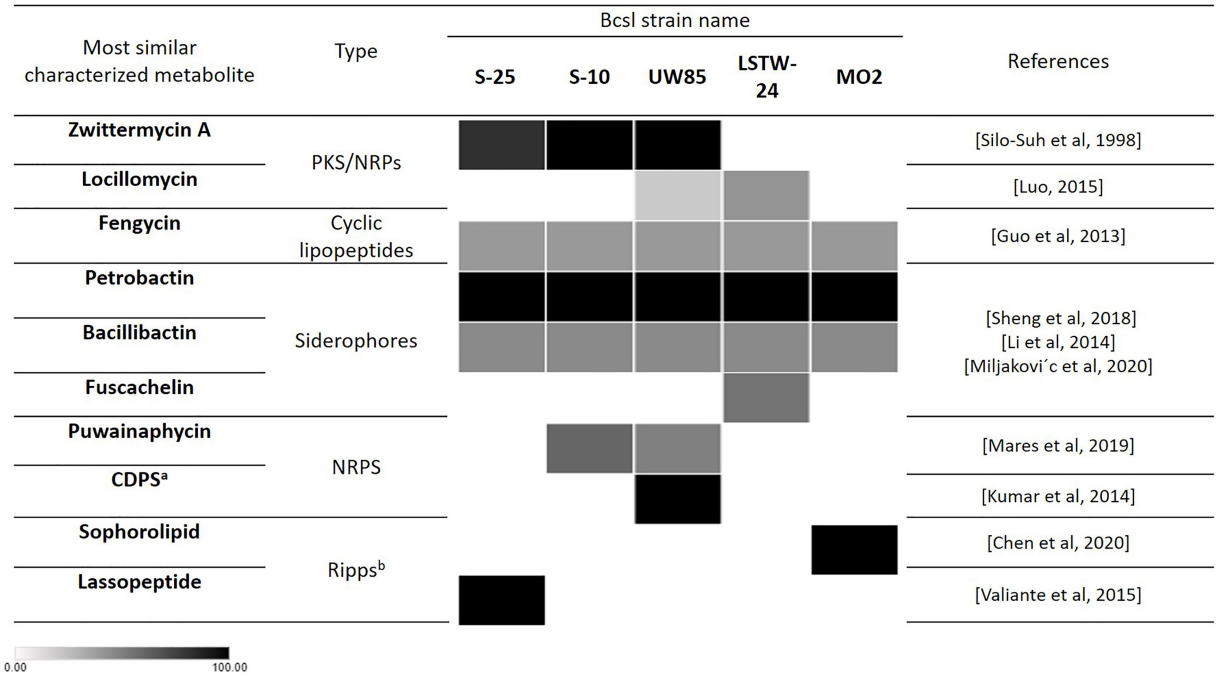

FIGURE 5
Occurrence of secondary metabolite encoding biosynthetic gene clusters with putative antifungal activity in the five analyzed Bcsl strains based on Antismash predictions. Heatmap shades represent the percentage of genes in the queried cluster that are similar to the known BGC. The darker the color the higher the percentage of similar genes in the cluster to the known BGC. [a]CDPS: cyclic dipeptides. [b]RiPPs: Ribosomally synthesized and post-translationally modified peptides.

(Raffel et al., 1996; Silo-Suh et al., 1998; Broderick et al., 2000; Zhao et al., 2007).

3.6. Comparative analysis of ZmA harboring mega-plasmids

We compared the mega-plasmid harboring the ZmA encoding BGC in UW85 to its two homologs in S-25 and S-10. The UW85, S-25 and S-10 mega-plasmids were 578,721, 436,050, and 588,156 bp, encoding for 636, 404 and 530 genes, respectively. The GC content of all of the plasmids was approximately 32%, which was slightly lower than that of the chromosomes. A total of 257, 196 and 217 genes, respectively, were functionally annotated by RAST, almost half (92) of whom were shared between the three strains (Figure 6A).

Approximately 12% of the annotated mega-plasmid genes (16% of shared genes) were predicted to be part of the ZwA BGC (Figure 6B). Common annotated genes found on the plasmid that were not part of the ZmA BGC included genes encoding for putative virulence factors and pathogenesis factors (i.e., microbial collagenase, hemolysin B, reticulocyte binding protein, and type II secretion systems), ABC transporters, tetracycline and β-lactam resistance and quorum sensing and chemotaxis mechanisms (Figure 6B). In addition, 89, 53, and 64 of the annotated genes were unique in the UW85, S-25, and S-10 mega-plasmids, respectively, representing over 50% of the unique genes reported above. The UW85 mega-plasmid contained nine genes encoding for ABC transporters that were absent in the other two strains (Supplementary Table S2). The S-25 mega-plasmid contained genes encoding for chitin binding proteins and a predicted endoglucanase, potentially involved in antifungal activity, which were absent in the other two strains. (Supplementary Figure S6; Supplementary Table S2).

3.7. Comparative analysis of ZmA BGCs

Gene synteny comparisons between UW85 ZmA BGCs and homologs from S-25 and S-10 revealed high similarity between the clusters (Figure 7), except for a group of genes predicted to encode for the antibiotic kanosamine situated within the ZmA BGCs of UW85 and S-10, but absent in the S-25 BGC. In contrast, the ZmA encoding BGC of S-25 contained genes predicted to encode for a β-lactone containing protease inhibitor located proximal to the ZmaA BGC, which was absent in the other two strains. In addition, two hypothetical protein-encoding genes were identified in the ZmA-encoding BGC of S-25, whereas a mobile element sequence proximal to the kanosamine encoding gene was detected in S-10.

4. Discussion

The five analyzed Bcsl strains described in this study displayed unique *in-vitro* antagonistic profiles against fungal and fungal-like (i.e., Ascomycota, Basidiomycota, and Oomycetes) plant pathogens as previously demonstrated for other Bcsl strains (Silo-Suh et al., 1994; Xu et al., 2014; Kumar et al., 2014b). We therefore mined their genomes to pinpoint genes and gene clusters encoding potential antifungal factors associated with the observed antagonism and performed comparative genomic analysis to identify specific factors that might explain differences in their *in-vitro* antagonistic phenotypes.

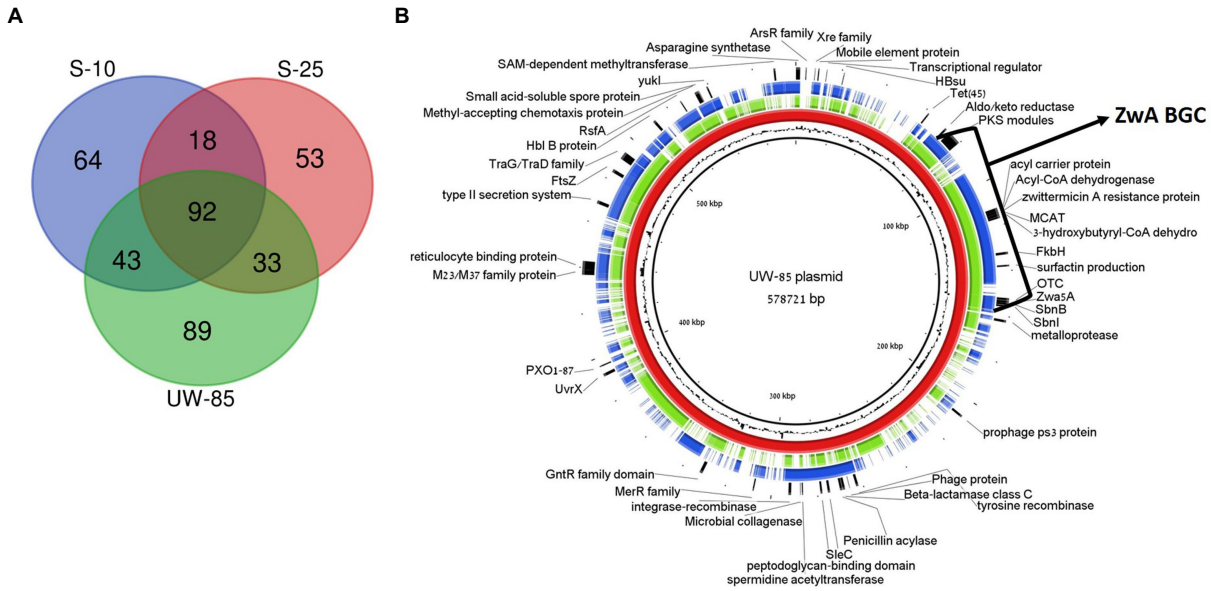

FIGURE 6
Comparative analysis of plasmids containing ZwA BGC homologues in *Bacillus cereus* spp. UW85, S-10 and S-25. **(A)** Venn-diagram showing similar and unique RAST annotated genes in the three plasmids. **(B)** Genetic map of the S-10 (green) and S-25 (blue) plasmids aligned against the UW85 reference plasmid (red) using the BRIG software package. The annotations of relevant encoded proteins from three sequenced plasmids appear in the outer black ring, and the GC content of the reference plasmid is displayed between the inner black and red rings.

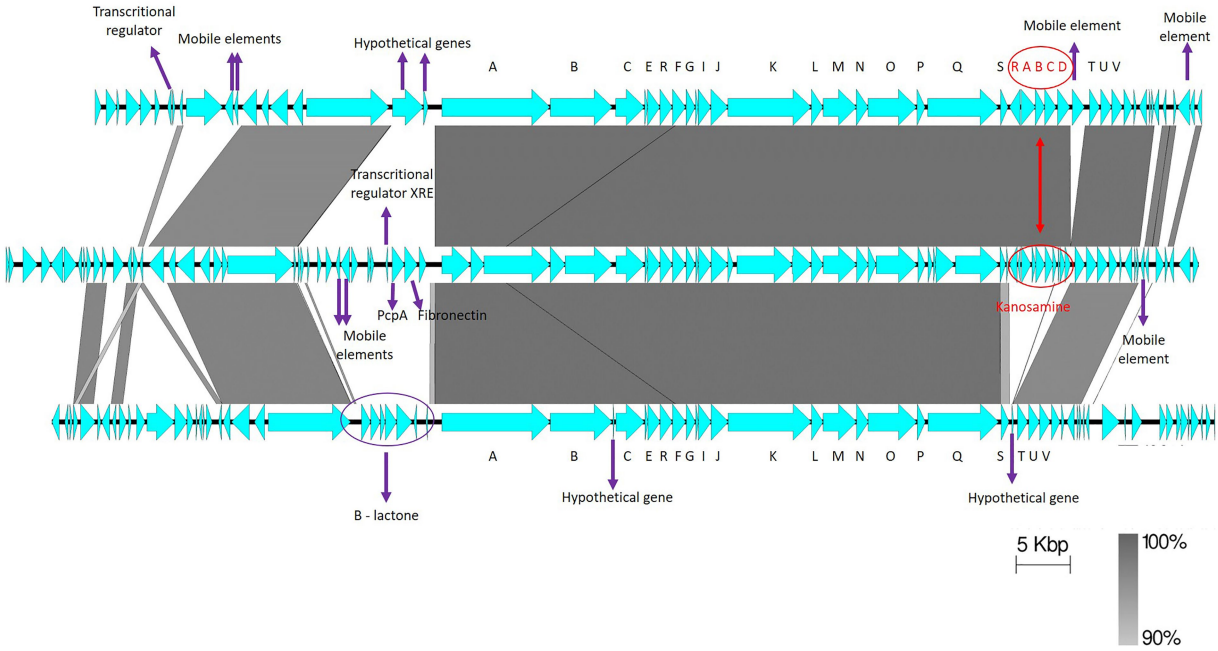

FIGURE 7
Synteny of ZmA homolog BGCs. The reference ZwA BGC of UW-85 (middle), is flanked by S-10 (top), and S-25 (bottom) homologues. The annotations of relevant encoded proteins from three BGCs are indicated by arrows. ZmA BGC genes are shown in black capital letters A–V, and kanosamine encoding genes in red capital letters. The figure was generated using Easyfig software with a cut-off of 90% gene identity.

Collectively, more unique genes were detected in UW85 and MO2 relative to the three other Bcsl strains. This increased diversity may be explained by the fact that they were isolated from plant roots in contrast to the other three strains, which were isolated from bulk soil, although it is sometimes difficult to differentiate between these two niches. Root ecosystems are considered to be more competitive than bulk soil, necessitating genes encoding specific characteristics to ensure survival (Lugtenberg and Dekkers, 1999; Zhang et al., 2016; Ling et al., 2022). An example are genes encoding for transporters which facilitate the uptake of root-associated nutrients and essential molecules, or

remove antibiotics or other toxic compounds produced by competitors in the root environment from the cell (Rees et al., 2009). The involvement of ABC transporters in biocontrol and rhizosphere competence is well established. For example, the ABC transporter abcG5 in the fungal biocontrol agent *Clonostachys rosea* was recently found to be essential for biocontrol activity against *F. graminearium*-facilitated foot rot disease (Dubey et al., 2014), and a gene encoding for a putative ABC transporter from *Erwinia chrysanthemi* was found to play a role in *in planta* fitness of the bacterium (Llama-Palacios et al., 2002). It is possible that the presence of additional ABC transporter encoding genes on the UW85 ZwA mega-plasmid may contributes to UW85 capacity to colonize and persist in the rhizosphere and therefore potentially enhances its biocontrol activity.

The presence of unique genes involved in carbohydrate and phosphate metabolism in the UW85 and MO2 genomes may also contribute to the capacity of these strains to survive in the copiotrophic plant root ecosystem. This is supported by a comparative genomic analysis of plant associated vs. non-plant-associated *B. amyloliquefaciens* and *B. subtilis* strains, which showed that plant-associated strains possess additional genes involved in utilizing plant-derived substrates, seemingly acquired through horizontal gene transfer (HGT; Zhang et al., 2016). UW85 and MO2 also contained more transposase genes, which may indicate higher occurrence of HGT events that can facilitate the acquisition of genes associated with environmental adaptation (Aminov, 2011; Raymond and Bonsall, 2013).

4.1. Linking chitinolytic activity and chitin degrading genes in Bcsl strains

Bacterial chitinases that degrade α-1,3-glucans, and β-1,3-glucans (the major components of fungal cell walls) can play a fundamental role in fungal antagonism by biocontrol strains (Swiontek Brzezinska et al., 2014). For example, *chiA* encoded chitinases in *Serratia marcescens* and *S. plymuthica* were linked to biological control of plant diseases caused by phytopathogenic fungi (Chernin et al., 1997; Downing and Thomson, 2000), and *B. thuringiensis* isolates from tomato roots only exhibited *in-vitro* antifungal activity against *Verticillium* spp. when harboring one or two putative chitinases (Hollensteiner et al., 2016; Veliz et al., 2017). Interestingly, the chitinolytic activity of the five Bcsl isolates investigated in this study correlated to their genetic potential, with higher activity documented in UW85 (which harbored almost twice as many CBPs as the other strains) and LSTW-24 (which contained more chitinases than the other strains). Previous reports have explored the genetic context of chitinase genes (Yan and Fong, 2015), the association between molecular structure, substrate specificity, the catalytic mechanisms that facilitate chitinase activity (Hamid et al., 2013), and the synergistic activity of different chitinases (Suzuki et al., 2002). The linkage between the quantity of chitin degrading genes and the chitinolytic activity of strains UW85 and LSTW-24 documented here is supported by previous studies suggesting that synergistic interactions between CBP and chitinases enhance the capacity of biocontrol agents to metabolize chitin (Purushotham et al., 2012; Manjeet et al., 2013; Veliz et al., 2017).

S-25 harbors a unique gene encoding a probable endoglucanase on its mega-plasmid. Previous studies demonstrated that endoglucanase activity antagonized *P. aphanidermatum* (Natarajan et al., 2013) and reduced disease incidence by *Pythium* on cucumber seedlings (Chet et al., 1998). Other studies reported that a b-1,3-glucanase facilitated morphological changes and growth inhibition of *R. solani* and *Fusarium* sp. (Benitez et al., 1998; Bhat, 2000). In view of these findings, we suggest further examination of this endoglucanase gene, and specifically examination of its involvement of S-25 antagonism of *P. aphanidermatum* and *R. solani*. The proximity between this endoglucanase gene and three CBPs genes may imply combined antifungal activity of these genes.

While our analyses revealed strong correlations between chitinase activity and the abundance of chitinase encoding genes, there was no correlation between extracellular chitinolitic activity, and the antifungal activity of the CFS, suggesting that either particular chitinases may be more active against specific fungi or that additional antagonistic mechanisms are also required.

4.2. Presence of secondary metabolite encoding BGCs in Bcsl strains with putative antifungal activity

Secondary metabolites play a critical role in the antagonism of phytopathogens by bacterial biocontrol agents (Vizcaino et al., 2014) and many secondary metabolites with antifungal activity have been detected in *Bacillus spp.* (Shahid et al., 2021). We therefore screened the five Bcsl genomes for secondary metabolite encoding genes and performed comparative genomic analyses to uncover the genetic basis of the observed differences in their *in-vitro* antagonistic capacity.

Shared BGCs, common to all of the five analyzed strains and having putative antifungal activity, included clusters encoding for catecholate siderophores similar to petrobactin and bacillibactin, which were previously shown to play vital roles in the antagonistic capacity of various bacterial biocontrol agents against phytopathogens (Prema and Selvarani, 2012; Li et al., 2014; Patil et al., 2014; Miljakovic et al., 2020; Sheng et al., 2020). Another shared genes cluster is similar to the antifungal lipopeptide fengycin, which was shown to inhibit *R. solani* (Guo et al., 2013) and other fungal pathogens (Ongena et al., 2005; Deleu et al., 2008; Kulimushi et al., 2017). In contrast, several unique clusters, which may contribute to the specific antifungal activity of each Bcsl strain, were also detected. These include a BGC, only detected in the UW85 and LSTW-24 genomes, having similarity (21%–42%) for the NRPs-PKs hybrid locillomycin, reported to antagonize *R. solani* and *F. oxysporum* (Luo, 2015) and a BGC found in S-10 and UW85 genomes with similarity (50–60%) to a puwainaphycin lipopeptide, which was previously shown to possess antifungal activity against members of the Ascomycota phylum (Mares et al., 2019; Hajek et al., 2021). Interestingly, in our research we did not observe inhibition of *F. oxysporum* which represent the Ascomycetes soilborne pathogen, but this predicted gene cluster similar to puwainaphycin need to be further explored for its role in the inhibition activity of these two strains against *R. solani* and *P. aphanidermatum*. Sophorolipid, only detected in MO2, is an extracellular bio-surfactant reported to inhibit mycelial growth of *R. solani* (64.3%) and *P. ultimum* (95%; de OCaretta et al., 2021), in addition to other fungal phytopathogens in both *in vitro* and *in planta* experiments (Yoo et al., 2005; Sen et al., 2017; Haque et al., 2019; Chen et al., 2020; de OCaretta et al., 2021). The presence of this antifungal encoding BGC in MO2 genome may contribute to its observed antagonistic activity against *R. solani* and *P. aphanidermatum*. In addition, S-25 carried unique BGC encoding for a lassopeptide, a group of natural products previously shown to have therapeutic effects on fungal infections, as demonstrated for the class I lassopeptide humidimycin from *Streptomyces humidus*. This compound expedited activity of fungal cell wall inhibitors that antagonized *Candida albicans* and *Aspergillus fumigatus* (Valiante et al., 2015). The different profiles of secondary metabolite encoding genes between the five Bcsl strains may partially explain their different antifungal

phenotypes against the three soilborne pathogens, but additional work is required to clarify their exact role in the observed antagonistic activity.

4.3. Comparative analysis of ZwA BGC and the ZwA harboring plasmid

S-25 and S-10 harbored homologs of the well-established antifungal hybrid NRP/PK zwittwrmicin A, a linear aminopolyol antibiotic originally isolated from UW85 (Kevany et al., 2009). ZwA has been previously shown to supress alfalfa seedlings damping off caused by the oomycete *P. medicaginis* (Handelsman et al., 1990), it has been indicated in inhibition of other fungal and bacterial growth (Silo-Suh et al., 1998) and has been shown to enhance insecticidal activity of Cry toxins in *B. thuringiensis* (Broderick et al., 2003). The expression and activity of ZwA might likely be different in the three strains, because S-25 BGC lacked the five flanking kab (kabA-kabD; kabR) genes that encode for the antifungal element kanosamine (Janiak and Milewski, 2001), and S-25 contained a flanking gene encoding for a beta-lactone containing protease inhibitor that was absent in S-10 and UW85. The contribution of flanking genes to zwittermicin activity is supported by Luo et al., who identified zmaWXY downstream of ZmA that functioned as a resistance conferring in addition to the previously characterized zmaR gene, and was found to increase the yield of ZmA (Luo et al., 2011).

The antagonistic capacity of ZwA, and the documented role of plasmids in environmental adaptation (Heuer and Smalla, 2012; Adams et al., 2014; Patino-Navarrete and Sanchis, 2016; Lechuga et al., 2020), led us to further explore the composition of the ZmA-harboring plasmids. We detected several genes on the three plasmids with putative roles in environmental adaptation. These include as methyl-accepting chemotaxis protein (MCP) which has been previously shown to be involved in chemical sensing (Salah Ud-Din and Roujeinikova, 2017), biofilm formation (Hickman et al., 2005) and production of toxins (Harkey et al., 1994), and the two-component system sensor histidine kinase. These sensory mechanisms and response regulators are believed to enhance fitness in bacteria from unstable and low nutrient environments with multiple interactions like soil (Ashby, 2004). Each of the plasmids had its own set of unique genes, which may also have an impact on the biocontrol potential of the isolate. These included increased abundance of ABC transporters on the UW85 mega-plasmid, and the presence of chitin (CBPs) and cellulose (endoglucanase) metabolizing enzyme encoding genes gathered in S-25 mega-plasmid.

Collectively, we identified both common and unique BGCs encoding for metabolites with putative antifungal activity in the five Bcsl strains, as well as chitinases with potential antifungal activity. Nonetheless, the potential link between these factors and the observed *in-vitro* antifungal capacity of the Bcsl strains that harbor them, needs to be experimentally validated by knockout (Guo et al., 2013) and/or heterologous expression (Luo et al., 2011), demonstrated for fengycin and zwittermicin, respectively. Experiments should also be conducted to determine the expression of candidate genes and BGCs following exposure to pathogens, or under different environmental conditions, as previously described for lipopeptides and bacilibactin (Li et al., 2014).

In summary, comparative genomics provided important insights into similarities and differences of mechanisms potentially linked to the antifungal activity of the five strains. Although there are several potential candidates, we were not able to specifically link genotypes to phenotypes, or pinpoint genetic factors that explain the elevated activity of the S-25 cell-free supernatant relative to the other strains. Future studies will need to follow up on these candidates in order to validate their antifungal capacity.

Data availability statement

The datasets presented in this study can be found in online repositories. The names of the repository/repositories and accession number (s) can be found at: https://www.ncbi.nlm.nih.gov/, JAKJPR000000000; https://www.ncbi.nlm.nih.gov/, JAKJPS000000000 https://www.ncbi.nlm.nih.gov/, JAKJPT000000000; https://www.ncbi.nlm.nih.gov/, JAKJPU000000000; https://www.ncbi.nlm.nih.gov/, CP091444; https://www.ncbi.nlm.nih.gov/, PRJNA784166.

Author contributions

MM: conducted experiments, data and bioinformatics analyses, wrote manuscript. CG: bioinformatics analysis. NS: genome assembly. DM: project idea, funding acquisition. EB: supervision. EC: experimental design, supervision, funding acquisition, writing and revisions. OF: participating in experimental design, supervision, funding acquisition, writing and revisions. All authors contributed to the article and approved the submitted version.

Funding

This research was funded by the Israeli Chief Scientist of the Ministry of Agriculture and Rural Development (Grant no. 20-13-0027). In addition, MM was supported by scholarships from the Israeli Ministry of Innovation, Science and Technology, and the Avi Greinstein fellowship.

Acknowledgments

The authors would like to thank Cytryn and Frenkel lab members for technical support and Barak Dror for assistance with genome assembly.

Conflict of interest

The authors declare that the research was conducted in the absence of any commercial or financial relationships that could be construed as a potential conflict of interest.

Publisher's note

Supplementary material

The Supplementary material for this article can be found online at: https://www.frontiersin.org/articles/10.3389/fmicb.2023.996287/full#supplementary-material

References

Adams, V., Li, J., Wisniewski, J. A., Uzal, F. A., Moore, R. J., McClane, B. A., et al. (2014). Virulence plasmids of spore-forming bacteria. *Microbiol. Spectr.* 2:2.6.04. doi: 10.1128/microbiolspec.PLAS-0024-2014

Alikhan, N. F., Petty, N. K., Ben Zakour, N. L., and Beatson, S. A. (2011). BLAST ring image generator (BRIG): simple prokaryote genome comparisons. *BMC Genomics* 12:402. doi: 10.1186/1471-2164-12-402

Aminov, R. (2011). Horizontal gene exchange in environmental microbiota. *Front. Microbiol.* 2:158. doi: 10.3389/fmicb.2011.00158

Arredondo-Alonso, S., Willems, R. J., van Schaik, W., and Schürch, A. C. (2017). On the (im) possibility of reconstructing plasmids from wholegenome short-read sequencing data. *Microb. Genom.* 3:e000128. doi: 10.1099/mgen.0.000128

Ashby, M. K. (2004). Survey of the number of two-component response regulator genes in the complete and annotated genome sequences of prokaryotes. *FEMS Microbiol. Lett.* 231, 277–281. doi: 10.1016/S0378-1097(04)00004-7

Aziz, R. K., Bartels, D., Best, A. A., DeJongh, M., Disz, T., Edwards, R. A., et al. (2008). The RAST server: rapid annotations using subsystems technology. *BMC Genomics* 9:75. doi: 10.1186/1471-2164-9-75

Benitez, T., Limon, C., Delgado-Jarana, J., and Rey, M. (1998). "Glucanolytic and other enzymes and their genes," in *Trichoderma & Gliocladium—Enzymes, Biological Control and Commercial Applications. Vol. 2.* eds. G. F. Harman and C. P. Kubicek (Taylor and Francis), 101–127.

Bhat, M. K. (2000). Cellulases and related enzymes in biotechnology. *Biotechnol. Adv.* 18, 355–383. doi: 10.1016/s0734-9750(00)00041-0

Bianco, A., Capozzi, L., Monno, M. R., Sambro, L. D., Manzulli, V., Pesole, G., et al. (2021). Characterization of *Bacillus cereus* group isolates from human Bacteremia by whole-genome sequencing. *Front. Microbiol.* 11:599524. doi: 10.3389/fmicb.2020.599524

Blin, K., Shaw, S., Steinke, K., Villebro, R., Ziemert, N., Lee, S. Y., et al. (2019). AntiSMASH 5.0: updates to the secondary metabolite genome mining pipeline. *Nucleic Acids Res.* 47, W81–W87. doi: 10.1093/nar/gkz310

Bolger, A. M., Lohse, M., and Usadel, B. (2014). Trimmomatic: a flexible trimmer for Illumina sequence data. *Bioinformatics* 30, 2114–2120. doi: 10.1093/bioinformatics/btu170

Braga, R. M., Dourado, M. N., and Araújo, W. L. (2016). Microbial interactions: ecology in a molecular perspective. *Braz. J. Microbiol.* 47, 86–98. doi: 10.1016/j.bjm.2016.10.005

Brettin, T., Davis, J. J., Disz, T., Edwards, R. A., Gerdes, S., Olsen, G. J., et al. (2015). RASTtk: A modular and extensible implementation of the RAST algorithm for building custom annotation pipelines and annotating batches of genomes. *Sci. Rep.* 5:8365. doi: 10.1038/srep08365

Broderick, N. A., Goodman, R. M., Raffa, K. F., and Handelsman, J. (2000). Synergy between Zwittermicin A and *Bacillus thuringiensis* subsp. kurstaki against gypsy moth (Lepidoptera-Lymantriidae). *Environ. Entomol.* 29, 101–107. doi: 10.1603/0046-225X-29.1.101

Broderick, N. A., Goodman, R. M., Handelsman, J., and Raffa, K. F. (2003). Effect of host diet and insect source on synergy of gypsy moth (Lepidoptera: Lymantriidae) mortality to *Bacillus thuringiensis* subsp. kurstaki by Zwittermicin A. *Environ. Entomol.* 32, 387–391. doi: 10.1603/0046-225X-32.2.387

Brzezinska, M. S., Jankiewicz, U., Burkowska, A., and Walczak, M. (2014). Chitinolytic microorganisms and their possible application in environmental protection. *Curr. Microbiol.* 68, 71–81. doi: 10.1007/s00284-013-0440-4

Carroll, L. M., Cheng, R. A., Wiedmann, M., and Kovac, J. (2021). Keeping up with the *Bacillus cereus* group: taxonomy through the genomics era and beyond. *Crit. Rev. Food Sci. Nutr.* 62, 7677–7702. doi: 10.1080/10408398.2021.1916735

Chen, J., Liu, X., Fu, S., An, Z., Feng, Y., Wang, R., et al. (2020). Effects of sophorolipids on fungal and oomycete pathogens in relation to pH. *J. Appl. Microbiol.* 128, 1754–1763. doi: 10.1111/jam.14594

Chernin, L. S., De la Fuente, L., and Sobolev, V. (1997). Molecular cloning structural analysis and expression in *Escherichia coli* of a chitinase gene from Enterobacter agglomeran. *Appl. Environ. Microbiol.* 63, 834–839. doi: 10.1128/aem.63.3.834-839.1997

Chet, I., Benhamou, N., and Haran, S. (1998). "Mycoparasitism and lytic enzymes" in *Trichoderma & Gliocladium–Enzymes, Biological Control and Commercial Applications. Vol. 2.* eds. G. F. Harman and C. P. Kubicek (Taylor and Francis), 327–342.

de OCaretta, T. I., Silveira, V. A., Andrade, G., Macedo, F. Jr., and Celligoi, M. A. (2021). Antimicrobial activity of sophorolipids produced by *Starmerella bombicola* against phytopathogens from cherry tomato. *J. Sci. Food Agric.* 102, 1245–1254. doi: 10.1002/jsfa.11462

Deleu, M., Paquot, M., and Nylandery, T. (2008). Effect of fengycin, a lipopeptide produced by *Bacillus subtilis*, on model biomembranes. *Biophys. J.* 94, 2667–2679. doi: 10.1529/biophysj.107.114090

Downing, K. J., and Thomson, J. A. (2000). Introduction of the Serratia marcescens chiA gene into an endophytic *Pseudomonas fluorescens* for the biocontrol of phytopathogenic fungi. *Can. J. Microbiol.* 46, 363–369. doi: 10.1139/w99-147

Drula, E., Marie-Line Garron, M. L., Dogan, S., Lombard, V., Henrissat, B., and Terrapon, N. (2022). The carbohydrate-active enzyme database: functions and literature. *Nucleic Acids Res.* 50, D571–D577. doi: 10.1093/nar/gkab1045

Dubey, M. K., Jensen, D. F., and Karlsson, M. (2014). An ATP-binding cassette pleiotropic drug transporter protein is required for xenobiotic tolerance and antagonism in the fungal biocontrol agent *Clonostachys rosea*. *Mol. Plant-Microbe Interact.* 27, 725–732. doi: 10.1094/MPMI-12-13-0365-R

Ehling-Schulz, M., Koehler, T. M., and Lereclus, D. (2019). The *Bacillus cereus* group: bacillus species with pathogenic potential. *Microbiol. Spectr.* 7, 875–902. doi: 10.1128/microbiolspec.GPP3-0032-2018

George, S., Pankhurst, L., Hubbard, A., Votintseva, A., Stoesser, N., Sheppard, A. E., et al. (2017). Resolving plasmid structures in Enterobacteriaceae using the MinION nanopore sequencer-assessment of MinION and MinION Illumina hybrid data assembly approaches. *Microb. Genom.* 3:e000118. doi: 10.1099/mgen.0.000118

Gillis, A., Fayad, N., Makart, L., Bolotin, A., Sorokin, A., Kallassy, M., et al. (2018). Role of plasmid plasticity and mobile genetic elements in the entomopathogen *Bacillus thuringiensis* serovar israelensis. *FEMS Microbiol. Rev.* 42, 829–856. doi: 10.1093/femsre/fuy034

Guinebretière, M. H., Thompson, F. L., Sorokin, A., Normand, P., Dawyndt, P., Ehling-Schulz, M., et al. (2008). Ecological diversification in the *Bacillus cereus* group. *Environ. Microbiol.* 10, 851–865. doi: 10.1111/j.1462-2920.2007.01495.x

Guo, Q., Dong, W., Li, S., Lu, X., Wang, P., Zhang, X., et al. (2013). Fengycin produced by *Bacillus subtilis* NCD-2 plays a major role in biocontrol of cotton seedling damping-off disease. *Microbiol. Res.* 169, 533–540. doi: 10.1016/j.micres.2013.12.001

Gupta, P., Samant, K., and Sahu, A. (2011). Isolation of cellulose-degrading bacteria and determination of their cellulolytic potential. *Int. J. Microbiol.* 2012:578925, 1–5. doi: 10.1155/2012/578925

Hamid, R., Khan, M. A., Ahmad, M., Ahmad, M. M., Abdin, M. Z., Musarrat, J., et al. (2013). Chitinases: an update. *J. Pharm. Bioallied Sci.* 5, 21–29. doi: 10.4103/0975-7406.106559

Handelsman, J., Raffel, S., Mester, E. H., Wunderlich, L., and Grau, C. R. (1990). Biological control of damping-off of alfalfa seedlings with *Bacillus cereus* UW85. *Appl. Environ. Microbiol.* 56, 713–718. doi: 10.1128/aem.56.3.713-718.1990

Haque, F., Verma, N. K., Alfatah, M., Bijlani, S., and Bhattacharyya, M. S. (2019). Sophorolipid exhibits antifungal activity by ROS mediated endoplasmic reticulum stress and mitochondrial dysfunction pathways in *Candida albicans*. *RSC Adv.* 9, 41639–41648. doi: 10.1039/c9ra07599b

Harkey, C. W., Everiss, K. D., and Peterson, K. M. (1994). The vibrio cholerae toxin-coregulated-pilus gene tcpI encodes a homolog of methyl-accepting chemotaxis proteins. *Infect Immun.* 62, 2669–2678. doi: 10.1128/iai.62.7.2669-2678.1994

Heuer, H., and Smalla, K. (2012). Plasmids foster diversification and adaptation of bacterial populations in soil. *FEMS Microbiol. Rev.* 36, 1083–1104. doi: 10.1111/j.1574-6976.2012.00337.x

Hickman, J. W., Tifrea, D. F., and Harwood, C. S. (2005). A chemosensory system that regulates bioflm formation through modulation of cyclic diguanylate levels. *PNAS* 102, 14422–14427. doi: 10.1073/pnas.0507170102

Hollensteiner, J., Wemheuer, F., Harting, R., Kolarzyk, A. M., Diaz Valerio, S., Poehlein, A., et al. (2016). Bacillus thuringiensis and bacillus weihenstephanensis inhibit the growth of Phytopathogenic Verticillium species. *Front. Microbiol.* 7:2171. doi: 10.3389/fmicb.2016.02171

Hoton, F. M., Andrup, L., Swiecicka, I., and Mahillon, J. (2005). The cereulide genetic determinants of emetic *Bacillus cereus* are plasmid-borne. *Microbiol. Comment.* 151, 2121–2124. doi: 10.1099/mic.0.28069-0

Janiak, A. M., and Milewski, S. (2001). Mechanism of antifungal action of kanosamine. *Med. Mycol.* 39, 401–408. doi: 10.1080/mmy.39.5.401.408

Kevany, B. M., Rasko, D. V., and Thomas, M. G. (2009). Characterization of the complete Zwittermicin A biosynthesis gene cluster from *Bacillus cereus*. *Appl. Environ. Microbiol.* 75, 1144–1155. doi: 10.1128/AEM.02518-08

Kuddus, S. M., and Ahmad, R. I. Z. (2013). Isolation of novel chitinolytic bacteria and production optimization of extracellular chitinase. *J. Gen. Eng. Biotech.* 11, 39–46. doi: 10.1016/j.jgeb.2013.03.001

Kulimushi, P. Z., Arias, A. A., Franzil, L., Steels, S., and Ongena, M. (2017). Stimulation of Fengycin-type antifungal Lipopeptides in bacillus amyloliquefaciens in the presence of the maize fungal pathogen Rhizomucor variabilis front. *Microbiol.* 8:850. doi: 10.3389/fmicb.2017.00850

Kumar, S. N., Nath, V. S., Chandran, R. P., and Nambisan, B. (2014a). Cyclic dipeptides from rhabditid entomopathogenic nematodeassociated *Bacillus cereus* have antimicrobial activities. *World J. Microbiol. Biotechnol.* 30, 439–449. doi: 10.1007/s11274-013-1461-7

Kumar, S. N., Nambisan, B., and Mohandas, C. (2014b). Purification and identification of two antifungal cyclic dipeptides from *Bacillus cereus* subsp. thuringiensis associated with a rhabditid entomopathogenic nematode especially against *Fusarium oxysporum*. *J. Enzyme Inhib. Med. Chem.* 29, 190–197. doi: 10.3109/14756366.2013.765414

Lechuga, A., Lood, C., Salas, M., van Noort, V., Lavigne, R., and Redrejo-Rodríguez, M. (2020). Completed genomic sequence of *Bacillus thuringiensis* HER1410 reveals a cry-containing chromosome, two megaplasmids, and an integrative plasmidial prophage. *G3 (Bethesda)* 10, 2927–2939. doi: 10.1534/g3.120.401361

Lee, J. Y., Passalacqua, K. D., Hanna, P. C., and Sherman, D. H. (2011). Regulation of petrobactin and bacillibactin biosynthesis in *Bacillus anthracis* under iron and oxygen variation. *PLoS One* 6:e20777. doi: 10.1371/journal.pone.0020777

Lee, I., Kim, Y. O., Park, S. C., and Chun, J. (2015). OrthoANI: An improved algorithm and software for calculating average nucleotide identity. *Int. J. Syst. Evol. Microbiol.* 66, 1100–1103. doi: 10.1099/ijsem.0.000760

Li, B., Li, Q., Xu, Z., Zhang, N., Shen, Q., and Zhang, R. (2014). Responses of beneficial bacillus amyloliquefaciens SQR9 to different soilborne fungal pathogens through the alteration of antifungal compounds production. *Front. Microbiol.* 5:636. doi: 10.3389/fmicb.2014.00636

Ling, N., Wang, T., and Kuzyakov, Y. (2022). Rhizosphere bacteriome structure and functions. *Nat. Commun.* 13:836. doi: 10.1038/s41467-022-28448-9

Llama-Palacios, A., López-Solanilla, E., and Rodríguez-Palenzuela, P. (2002). The ybiT gene of *Erwinia chrysanthemi* codes for a putative ABC transporter and is involved in competitiveness against Endophytic bacteria during infection. *Appl. Environ. Microbiol.* 68, 1624–1630. doi: 10.1128/AEM.68.4.1624-1630.2002

Lozano, G. L., Holt, J., Ravel, J., Rasko, D. A., Thomas, M. G., and Handelsman, J. (2016). Draft genome sequence of biocontrol agent *Bacillus cereus* UW85. *Genome Announc.* 4:e00910-16. doi: 10.1128/genomeA.00910-16

Lugtenberg, B. J. J., and Dekkers, L. C. (1999). What makes pseudomonas bacteria rhizosphere competent? *Environ. Microbiol.* 1, 9–13. doi: 10.1046/j.1462-2920.1999.00005.x

Luo, C. (2015). Cyclic Lipopeptide Antibiotic Locillomycin (Locillomycin-A, Locillomycin-B, Locillomycin-C) and Methods of Making and Using the Same. U.S. patent no. US20150080292A1. Washington, DC: U.S. Patent and Trademark Office.

Luo, Y., Ruan, L. F., Zhao, C. M., Wang, C. X., Peng, D. H., and Sun, M. (2011). Validation of the intact Zwittermicin A biosynthetic gene cluster and discovery of a complementary resistance mechanism in bacillus thuringiensis. *Antimicrob. Agents Chemother.* 55, 4161–4169. doi: 10.1128/AAC.00111-11

Manjeet, K., Purushotham, P., Neeraja, C., and Podile, A. R. (2013). Bacterial chitin binding proteins show differential substrate binding and synergy with chitinases. *Microbiol. Res.* 168, 461–468. doi: 10.1016/j.micres.2013.01.006

Manni, M., Berkeley, M. R., Seppey, M., and Zdobnov, E. M. (2021). BUSCO: assessing genomic data quality and beyond. *Curr. Protoc.* 1:e323. doi: 10.1002/cpz1.323

Ongena, M., Jacques, P., Touré, Y., Destain, J., Jabrane, A., and Thonart, P. (2005). Involvement of fengycin-type lipopeptides in the multifaceted biocontrol potential of Bacillus subtilis. *Appl. Microbiol. Biotechnol.* 69, 29–38. doi: 10.1007/s00253-005-1940-3

Mares, J., Hajek, J., Urajova, P., Kust, A., Jokela, J., Saurav, K., et al. (2019). Alternative biosynthetic starter units enhance the structural diversity of Cyanobacterial Lipopeptides. *Appl. Environ. Microbiol.* 85, e02675–e02618. doi: 10.1128/AEM.02675-18

Medema, M. H., Blin, K., Cimermancic, P., de Jager, V., Zakrzewski, P., Fischbach, M. A., et al. (2011). AntiSMASH: rapid identification, annotation and analysis of secondary metabolite biosynthesis gene clusters in bacterial and fungal genome sequences. *Nucleic Acids Res.* 39, W339–W346. doi: 10.1093/nar/gkr466

Miljakovic, D., Marinkovic, J., and Balešević-Tubic, S. (2020). The significance of bacillus spp. in disease suppression and growth promotion of field and vegetable crops. *Microorganisms.* 8:1037. doi: 10.3390/microorganisms8071037

Natarajan, C., Gupta, V., Kumar, K., and Prasanna, R. (2013). Molecular characterization of a fungicidal Endoglucanase from the Cyanobacterium Calothrix elenkinii. *Biochem. Genet.* 51, 766–779. doi: 10.1007/s10528-013-9605-x

Okinaka, R. T., Cloud, K., Hampton, O., Hoffmaster, A. R., Hill, K. K., Keim, P., et al. (1999). Sequence and organization of pXO1, the large bacillus anthracis plasmid harboring the anthrax toxin genes. *J. Bacteriol.* 181, 6509–6515. doi: 10.1128/JB.181.20.6509-6515.1999

Ongena, M., and Jacques, P. (2008). Bacillus lipopeptides: versatile weapons for plant disease biocontrol. *Trends Microbiol.* 16, 115–125. doi: 10.1016/j.tim.2007.12.009

Overbeek, R., Olson, R., Pusch, G. D., Olsen, G. J., Davis, J. J., Disz, T., et al. (2014). The SEED and the rapid annotation of microbial genomes using subsystems technology (RAST). *Nucleic Acids Res.* 42, D206–D214. doi: 10.1093/nar/gkt1226

Patil, S., Bheemaraddi, M. C., Shivannavar, C. T., and Gaddad, S. M. (2014). Biocontrol activity of siderophore producing Bacillus subtilis CTS-G24 against wilt and dry root rot causing fungi in chickpea. *J. Agri. Vet. Sci.* 7, 63–68. doi: 10.9790/2380-07916368

Patino-Navarrete, R., and Sanchis, V. (2016). Evolutionary processes and environmental factors underlying the genetic diversity and lifestyles of *Bacillus cereus* group bacteria. *Res. Microbiol.* 168, 309–318. doi: 10.1016/j.resmic.2016.07.002

Pieterse, C. M. J., Zamioudis, C., Berendsen, R. L., Weller, D. M., Van Wees, S. C. M., and Bakker, P. A. H. M. (2014). Induced systemic resistance by beneficial microbes. *Annu. Rev. Phytopathol.* 52, 347–375. doi: 10.1146/annurev-phyto-082712-102340

Prema, P., and Selvarani, M. (2012). Microbial Siderophore as a potent biocontrol agent for plant pathogens. *Int. J. Sci. Res.* 2, 521–523. doi: 10.15373/22778179/JULY2013/181

Purushotham, P., Arun, P. V. P. S., Prakash, J. S. S., and Podile, A. R. (2012). Chitin binding proteins act synergistically with chitinases in Serratia proteamaculans 568. *PLoS One* 7:e36714. doi: 10.1371/journal.pone.0036714

Raaijmakers, J. M., Vlami, M., and de Souza, J. T. (2002). Antibiotic production by bacterial biocontrol agents. *Antonie Van Leeuwenhoek* 81, 537–547. doi: 10.1023/a:1020501420831

Raffel, S. J., Stabb, E. V., Milner, J. L., and Handelsman, J. (1996). Genotypic and phenotypic analysis of zwittermicin A-producing strains of *Bacillus cereus*. *Microbiology* 142, 3425–3436. doi: 10.1099/13500872-142-12-3425

Raymond, B., and Bonsall, M. B. (2013). Cooperation and the evolutionary ecology of bacterial virulence: the *Bacillus cereus* group as a novel study system. *Bio Essays.* 35, 706–716. doi: 10.1002/bies.201300028

Rees, D. C., Johnson, E., and Lewinson, O. (2009). ABC transporter: the power to change. *Nat. Rev. Mol. Cell Biol.* 10, 218–227. doi: 10.1038/nrm2646

Richter, M., Rosselló-Móra, R., Glöckner, F. O., and Peplies, J. (2015). JSpeciesWS: a web server for prokaryotic species circumscription based on pairwise genome comparison. *Bioinformatics* 32, 929–931. doi: 10.1093/bioinformatics/btv681

Salah Ud-Din, A. I. M., and Roujeinikova, A. (2017). Methyl-accepting chemotaxis proteins: a core sensing element in prokaryotes and archaea. *Cell. Mol. Life Sci.* 74, 3293–3303. doi: 10.1007/s00018-017-2514-0

Sen, S., Borah, S. N., Bora, A., and Deka, S. (2017). Production, characterization, and antifungal activity of a biosurfactant produced by Rhodotorula babjevae YS3. *Microb. Cell Factories* 16:95. doi: 10.1186/s12934-017-0711-z

Shafi, J., Tian, H., and Ji, M. (2017). Bacillus species as versatile weapons for plant pathogens: a review. *Biotechnol. Biotechnol. Equip.* 31, 446–459. doi: 10.1080/13102818.2017.1286950

Shahid, I., Han, J., Hanooq, S., Malik, K. A., Borchers, C. H., and Mehnaz, S. (2021). Profiling of metabolites of *Bacillus* spp. and their application in sustainable plant growth promotion and biocontrol. *Front. Sustain. Food Syst.* 5:605195. doi: 10.3389/fsufs.2021.605195

Sheng, M., Jia, H., Zhang, G., Zeng, L., Zhang, T., Long, Y., et al. (2020). Siderophore production by Rhizosphere biological control bacteria *Brevibacillus brevis* GZDF3 of *Pinellia ternata* and its antifungal effects on *Candida albicans*. *J. Microbiol. Biotechnol.* 30, 689–699. doi: 10.4014/jmb.1910.10066

Silo-Suh, L. A., Lethbridge, B. J., Raffel, S. J., He, H., Clardy, J., and Handelsman, J. (1994). Biological activities of two fungistatic antibiotics produced by *Bacillus cereus* UW85. *Appl. Environ. Microbiol.* 60, 2023–2030. doi: 10.1128/aem.60.12.4404-4412.1994

Silo-Suh, L. A., Stabb, E. V., Raffel, S. J., and Handelsman, J. (1998). Target range of Zwittermicin A, an Aminopolyol antibiotic from *Bacillus cereus*. *Curr. Microbiol.* 37, 6–11. doi: 10.1007/s002849900328

Spadaro, D., Ciavorella, A., Dianpeng, Z., Garibaldi, A., and Gullino, M. L. (2010). Effect of culture media and pH on the biomass production and biocontrol efficacy of a *Metschnikowia pulcherrima* strain to be used as a biofungicide for postharvest disease control. *Can. J. Microbiol.* 56, 128–137. doi: 10.1139/w09-117

Stenfors Arnesen, L. P., Fagerlund, A., and Granum, P. E. (2008). From soil to gut: *Bacillus cereus* and its food poisoning toxins. *FEMS Microbiol. Rev.* 32, 579–606. doi: 10.1111/j.1574-6976.2008.00112.x

Sullivan, M. J., Petty, N. K., and Beatson, S. A. (2011). Easyfig: a genome comparison visualizer. *Bioinformatics* 27, 1009–1010. doi: 10.1093/bioinformatics/btr039

Suzuki, K., Sugawara, N., Suzuki, M., Uchiyama, T., Katouno, F., Nikaidou, N., et al. (2002). Chitinases A, B, and C1 of Serratia marcescens 2170 produced by recombinant *Escherichia coli*: enzymatic properties and synergism on chitin degradation. *Biosci. Biotechnol. Biochem.* 66, 1075–1083. doi: 10.1271/bbb.66.1075

Valiante, V., Monteiro, M. C., Martin, J., Altwasser, R., El Aouad, N., Gonzalez, I., et al. (2015). Hitting the caspofungin salvage pathway of human-pathogenic fungi with the novel lasso peptide humidimycin (MDN-0010). *Antimicrob. Agents Chemother.* 59, 5145–5153. doi: 10.1128/Aac.00683-15

Veliz, E. A., Martínez-Hidalgo, P., and Hirsch, A. M. (2017). Chitinase-producing bacteria and their role in biocontrol. *AIMS Microbiol.* 3, 689–705. doi: 10.3934/microbiol.2017.3.689

Vizcaino, M. I., Guo, X., and Crawford, J. M. (2014). Merging chemical ecology with bacterial genome mining for secondary metabolite discovery. *J. Ind. Microbiol. Biotechnol.* 41, 285–299. doi: 10.1007/s10295-013-1356-5

Wang, X., Ji, C., Song, X., Liu, Z., Liu, Y., Li, H., et al. (2021). Biocontrol of two bacterial inoculant strains and their effects on the Rhizosphere microbial Community of Field-Grown Wheat. *Biomed Res. Int.* 2021:8835275. doi: 10.1155/2021/8835275

Wick, R. R., Judd, L. M., Gorrie, C. L., and Holt, K. E. (2017). Unicycler: resolving bacterial genome assemblies from short and long sequencing reads. *PLoS Comput. Biol.* 13:e1005595. doi: 10.1371/journal.pcbi.1005595

Xu, L., Dong, Z., Fang, L., Luo, Y., Wei, Z., Guo, H., et al. (2019). OrthoVenn2: A web server for whole-genome comparison and annotation of orthologous clusters across multiple species. *Nucleic Acids Res.* 47, W52–W58. doi: 10.1093/nar/gkz333

Xu, Y. B., Chen, M., Zhang, Y., Wang, M., Wang, Y., Huang, Q. B., et al. (2014). The phosphotransferase system gene pts I in the endophytic bacterium *Bacillus cereus* is required for biofilm formation, colonization, and biocontrol against wheat sharp eyespot. *FEMS Microbiol. Lett.* 354, 142–152. doi: 10.1111/1574-6968.12438

Yan, Q., and Fong, S. S. (2015). Bacterial chitinase: nature and perspectives for sustainable bioproduction. *Bioresour. Bioprocess.* 2:31. doi: 10.1186/s40643-015-0057-5

Yoo, D. S., Lee, B. S., and Kim, E. K. (2005). Characteristics of microbial biosurfactant as an antifungal agent against plant pathogenic fungus. *J. Microbiol. Biotechnol.* 15, 1164–1169.

Yu, X., Ai, C., Xin, L., and Zhou, G. (2010). The siderophore-producing bacterium, Bacillus subtilis CAS15, has a biocontrol effect on Fusarium wilt and promotes the

growth of pepper. *Eur. J. Soil Biol.* 47, 138–145. doi: 10.1016/j.ejsobi.2010.11.001

Zhang, H., Yohe, T., Huang, L., Entwistle, S., Wu, P., Yang, Z., et al. (2018). dbCAN2: a meta server for automated carbohydrate-active enzyme annotation. *Nucleic Acids Res.* 46, W95–W101. doi: 10.1093/nar/gky418

Zhang, N., Yang, D., Kendall, J. R. A., Borriss, R., Druzhinina, I. S., Kubicek, C. P., et al. (2016). Comparative genomic analysis of bacillus amyloliquefaciens and Bacillus subtilis reveals evolutional traits for adaptation to plant-associated habitats. *Front. Microbiol.* 7:2039. doi: 10.3389/fmicb.2016.02039

Zhao, C., Zeng, H., Yu, Z., and Sun, M. (2007). N-acyl homoserine lactonase promotes prevention of Erwinia virulence with zwittermicin A-producing strain *Bacillus cereus*. *Biotechnol. Bioeng.* 100, 599–603. doi: 10.1002/bit.21794

Zheng, J., Peng, D., Ruan, L., and Sun, M. (2013). Evolution and dynamics of megaplasmids with genome sizes larger than 100 kb in the *Bacillus cereus* group. *BMC Evol. Biol.* 13:262. doi: 10.1186/1471-2148-13-262

Hajek, J., Bieringer, S., Voracova, K., Macho, M., Saurav, K., Delawska, K., et al. (2021). Semi-synthetic puwainaphycin/minutissamide cyclic lipopeptides with improved antifungal activity and limited cytotoxicity. *RSC Adv.* 11, 30873–30886. doi: 10.1039/d1ra04882a

Frontiers in Microbiology

Explores the habitable world and the potential of microbial life

The largest and most cited microbiology journal which advances our understanding of the role microbes play in addressing global challenges such as healthcare, food security, and climate change.

Discover the latest Research Topics

See more →

Frontiers

Avenue du Tribunal-Fédéral 34
1005 Lausanne, Switzerland
frontiersin.org

Contact us

+41 (0)21 510 17 00
frontiersin.org/about/contact